VOLCANIC AND HYDROTHERMAL RECONSTRUCTION OF THE PILLEY'S ISLAND VOLCANOGENIC MASSIVE SULFIDE DISTRICT, CENTRAL NEWFOUNDLAND

CONOR PATRICK McKINLEY

VOLCANIC AND HYDROTHERMAL RECONSTRUCTION OF THE PILLEY'S ISLAND VOLCANOGENIC MASSIVE SULFIDE DISTRICT, CENTRAL NEWFOUNDLAND

by

© Conor Patrick McKinley

A thesis submitted to the

School of Graduate Studies

in partial fulfillment of the requirements for the degree of

Master of Science

Department of Earth Sciences

Memorial University of Newfoundland

April 2013

St. John's Newfoundland and Labrador

ABSTRACT

Pilley's Island in the Central Mobile Belt, Newfoundland, Canada, is host to a cluster of bimodal felsic Zn-Pb-Cu-Au-Ag volcanogenic massive sulfide (VMS) deposits. In the Pilley's Island terrane, VMS-bearing felsic volcanic rocks are derived from the remelting of a hydrated, arc basalt substrate; these have been juxtaposed by thrust faulting against barren mafic volcanic rocks derived from partial melting of slab metasomatized mantle wedge within an Ordovician peri-Laurentian subduction zone.

Sulfide formation likely took place within a peri-Laurentian arc rift based on immobile element signatures. The deposits formed via sub-seafloor replacement of volcanic flows or volcaniclastic strata, with evidence including: large, gradational alteration and mineralization haloes surrounding the deposits and relict host rock fragments within the sulfide.

Zones proximal to mineralization exhibit muscovite ± illite alteration and elemental vectors to mineralization include loss of SiO_2, CaO, Na_2O and gains of Fe_2O_3, K_2O, base metals, and volatile elements (As, Sb, Tl).

ACKNOWLEDGEMENTS

This project benefitted from the help of many people. I would like to thank my supervisor, Dr. Stephen Piercey, whose expertise, mentorship, patience, and fun-loving nature were invaluable to the completion of this project and greatly appreciated. I am very grateful for the many enriching opportunities that he provided me, including attending various short courses, field trips and conferences. Also, his steady supply of caffeine and similar taste in music and humour were of great benefit to the project.

This project was supported and funded by Altius Minerals Corporation. This research was also supported by the NSERC-Altius Industrial Research Chair in the Metallogeny of Ores in Volcanic and Sedimentary Basins at Memorial University of Newfoundland, an NSERC Discovery Grant, and funds from the Industrial Research Innovation Fund (IRIF) from the Research and Development Corporation of Newfoundland and Labrador (RDCNL) to Dr. Stephen Piercey. I wish to thank the Society of Economic Geologists (SEG) and Gold Fields Exploration Inc. for their generous support in providing me with a Graduate Student Fellowship award, and the Geological Society of America for providing me with a research grant.

I would like to thank my committee member Dr. Lawrence Winter of Altius Minerals Corporation for his logistical support, expertise, and for suggesting this project. I would also like to thank Dr. J. Geoffrey Thurlow, whose previous work on Pilley's Island paved the way for this project and his expertise has been essential to both the creation and completion of this project. Dr. Derek Wilton is thanked for his research advice, mentorship and steady prodding from the office next door.

Dr. Aphrodite Indares of Memorial University of Newfoundland and Dr. Harold Gibson of Laurentian University are thanked for their thorough examination of this thesis. Their comments have greatly improved this thesis.

Lab assistance and project support from Pam King, Lakmali Hewa, Sherri Furey, and Michael Shaffer of the CREAIT Network at Memorial University of Newfoundland was greatly appreciated. Also, thanks to Dr. Greg Dunning for the utmost patience and assistance in my hunt for zircons. Field assistance from Stefanie Brueckner and Hannah Mills was greatly appreciated and their ideas and confident geological debates aided this project. I would also like to thank Stewart Cochrane and Alvin Harris of the Newfoundland and Labrador Department of Natural Resources Geological Survey's Mines Branch for providing access to core storage libraries in Springdale and Buchans, NL.

An enormous thanks goes to my good friends and colleagues Dean Courage, Matt Minnett, Stefanie Brueckner, and Stefanie Lode for many passionate geological discussions, which greatly improved this project, as well as many extra-curricular events and late nights (along with Corey, Margie, Michelle, Ryan, Hereward and more), which always improved my sanity.

I owe an immense thank you and I am greatly indebted to my brother, Seán, who inspired me to pursue a post-secondary education (twice) and a career in geology, and for giving me my first summer job in a remote bush camp long before I had ever planned on taking a course in geology. A huge thanks to the rest of my family (Mom, Dad, Kelly, John, Ella, Will, Erin and Ailish), whose endless support and motivation were integral to

my entire university studies. Finally, I would like to thank Moira, whose emotional support, inspiration and constant understanding kept me moving forward through any circumstance.

Table of Contents

List of Tables

List of Figures

List of Abbreviations

NSERC	National Science and Engineering Research Council of Canada
CREAIT	Core Research Equipment and Instrument Training Network
ICP-OES	inductively coupled plasma optical emission spectroscopy
ICP-MS	inductively coupled plasma mass spectroscopy
CV-FIMS	cold vapour flow injection mercury system
NIR-SWIR	near infrared-short wave infrared spectroscopy
VMS	volcanogenic massive sulfide
P_{H2O}	water pressure
LBOT	Lushs Bight oceanic tract
BVOT	Baie Verte oceanic tract
AAT	Annieopsquotch accretionary tract
T	metric tonne
Ma	megaannum (million years)
nm	nanometre
cm	centimetre
m	metre
ppm	parts per million
wt %	weight percent
°C	degrees Celsius
LOI	loss on ignition
LFSE	low field strength element
HFSE	high field strength element
REE	rare earth element
LREE	light rare earth element
AI	Hashimoto alteration index
CCPI	chlorite-carbonate-pyrite index
CN	chondrite-normalized
MN	primitive mantle-normalized
UCN	upper continental crustal-normalized
MORB	mid-ocean ridge basalt
N-MORB	normal mid-ocean ridge basalt
E-MORB	enriched mid-ocean ridge basalt

List of Appendices

Co-authorship Statement

This thesis represents the culmination of research with both economic and academic implications at Memorial University of Newfoundland, and has been supported by government and industry. It contains four chapters and four appendices including two papers written in collaboration with my supervisor (Dr. Stephen Piercey), supervisory committee member (Dr. Lawrence Winter), and Dr. J. Geoffrey Thurlow. The format of the thesis is as follows.

Chapter 1 serves as an introduction to the Pilley's Island volcanogenic massive sulfide district and explains the previous work completed in the area, the objectives of this project and the research methods undertaken to solve the various problems.

Chapter 2 is a re-interpretation of the volcanic stratigraphy and it's control on the alteration and mineralization in the area. It is written to be published in a peer-reviewed journal, and is co-authored by Dr. Stephen Piercey, Dr. Lawrence Winter and Dr. J. Geoffrey Thurlow.

Chapter 3 is an interpretation of the primary and alteration lithogeochemistry of the Pilley's Island terrane. It is written as a companion paper to Chapter 2, also to be published in a peer-reviewed journal, and is co-authored by Dr. Stephen Piercey, Dr. Lawrence Winter and Dr. J. Geoffrey Thurlow.

Chapter 4 summarizes the main conclusions of the thesis and provides opportunities for future research at Pilley's Island.

Appendix I consists of raw lithogeochemical (ICP-OES and ICP-MS) data and key geochemical ratios used throughout Chapter 3.

Appendix II presents the normalized, LOI-free lithogeochemical data and the equations of the fractionation curves that were used to calculate the mass change results.

Appendix III consists of geological maps with specific mass change results plotted as point data to identify spatial relationships to the massive sulfide deposits from surface.

Appendix IV consists of 3D gridded mass change data from drill core samples to identify spatial relationships to the massive sulfide deposits.

Chapter 1: An Introduction to the Pilley's Island Volcanogenic Massive Sulfide District, Notre Dame Bay Region, Central Newfoundland

1.1. Introduction and Purpose of Study

Pilley's Island in Notre Dame Bay, central Newfoundland (Fig. 1-1), is located in the Ordovician Buchans-Roberts Arm belt of the Annieopsquotch accretionary tract (AAT) and is host to a significant cluster of volcanogenic massive sulfide (VMS) deposits. The area has previously been mined including more than 500 000T of cupriferous pyrite ore production in the late 1800s, and has been explored periodically for more economic massive sulfide deposits since then (Espenshade, 1937; Thurlow, 2001). These deposits are 'bimodal felsic' or Kuroko-style Zn-Pb-Cu-Au-Ag VMS deposits that are hosted by predominantly felsic volcanic rocks of various facies. Although several of the deposits on Pilley's Island are of apparent high tonnage, base metal contents are generally low and the highest-grade base metals occur within the smallest deposits (Thurlow, 2001).

Exploration since the early 1990s by Phelps Dodge Corporation of Canada Limited and Altius Resources Inc. has provided a new geological framework for Pilley's Island, which included the discovery of three new VMS deposits and the recognition of a number of low-angle thrust faults which dissect the volcanic package (Thurlow, 2001). The identification of these faults has created a need for the re-interpretation of the district's stratigraphy, structure, hydrothermal alteration and lithogeochemistry. This thesis will use new geological mapping and lithogeochemistry to better understand and

reconstruct the volcanic stratigraphy, hydrothermal alteration, and setting of the Pilley's Island VMS district. The thesis will also apply more recent deposit models, analytical techniques and spatial visualization methods (surface and 3D gridding) to better understand the formation of the various deposits within the district.

The following chapter will serve as an introduction to the geology of the Pilley's Island VMS district, a summary of previous research and exploration projects in the area, the objectives of this thesis, the data collection methods and an overview of the thesis structure.

1.2. Geological Overview

Pilley's Island volcanogenic massive sulfide district is located in the Ordovician Buchans-Roberts Arm belt within the Notre Dame subzone in central Newfoundland (Fig. 1-1). The Notre Dame subzone extends from north-central to southwest Newfoundland, with some exposure in southern Quebec (Fig. 1-1). It consists of Cambrian to mid-Ordovician submarine volcanic rocks and ophiolitic suites overlain by non-marine Silurian overlap sequences, and is host to approximately 26 documented VMS deposits (Williams, 1979; Williams et al., 1988; Swinden, 1991; van Staal, 2007).

The Notre Dame subzone consists of numerous accreted elements, including: ophiolitic rocks; mafic plutonic and volcanic rocks; and metamorphosed, migmatized siliciclastic rocks (Williams, 1979; Williams et al., 1988). The formation of these rocks ceased in the Middle Ordovician due to the Taconic orogeny, the first of three major orogenic events that defined the geologic and tectonic evolution in the Notre Dame subzone and Pilley's Island. The Taconic orogenic cycle involved the subduction of the

eastern margin of Laurentia below the Dashwoods microcontinent and Notre Dame arc sequence, resulting in the westward accretion of continental and oceanic arcs onto the Laurentian margin (Fig. 1-2A) (Rogers and Neale, 1969; Stevens, 1970; Williams, 1975; Dunning et al., 1990). The subduction was initiated at approximately 490 Ma and had ended by approximately 468 Ma, and arc magmatism pulsing into the Notre Dame arc was prevalent during and after the closure of the Taconic Seaway (Fig. 1-2AB) (van Staal, 2007; van Staal and Barr, 2011). Eventually the subducting margin of Laurentia broke off (Fig. 1-2C), leading to: 1) additional thickening of the Notre Dame arc; 2) convergence of an Iapetan slab outboard of Dashwoods; 3) the production of back-arc magmatism (Zagorevski et al., 2006; Zagorevski et al., 2008); and 4) underplating-related accretion of the Annieopsquotch accretionary tract (AAT) onto the Iapetan slab (van Staal, 2007). Convergence terminated between 455 and 450 Ma as the leading edge of Ganderia sutured its peri-Gondwanan elements, such as the Popelogan-Victoria arc, to the peri-Laurentian AAT (van Staal and Barr, 2011).

The Penobscot orogenic cycle took place between approximately 515 and 478 Ma and overlaps with the latter part of the Taconic orogeny (van Staal, 1994; Johnson et al., 2009; Zagorevski et al., 2010). It was initiated with the onset of eastward subduction beneath the leading Ganderian margin to create the Penobscot arc (van Staal, 1994; Johnson et al., 2009; Zagorevski et al., 2010). The closure of the Penobscot back-arc resulted in high level thrusting and black shale mélange (Williams and Piasecki, 1990).

The Salinic orogenic cycle commenced as the underplated, west-dipping subduction zone below the AAT and composite Laurentia stepped back to cause

additional subduction in the back-arc basin between 447 and 430 Ma (van Staal, 1994; van Staal et al., 1998; van Staal et al., 2003a; Valverde-Vaquero et al., 2006). This event caused structures such as mélange, folds, and thrust faults (Williams et al., 1988; Elliott et al., 1991; Lafrance and Williams, 1992; Currie, 1995; Lee and Williams, 1995; O'Brien, 2003; Zagorevski et al., 2007; van staal et al., 2009). The subduction arc resulted in a third pulse of magmatism into the Notre Dame arc between 445 and 435 Ma, unconformably overlying the rocks that resulted from the second pulse of magmatism (van Staal and Barr, 2011).

The AAT is the easternmost tectonostratigraphic element within the Notre Dame subzone and consists of imbricated thrust slices of ophiolitic rocks and arc and back-arc felsic and mafic rocks (Figs. 1-1 & 1-2) (Dunning and Krogh, 1985; Swinden et al., 1997; Lissenberg et al., 2005a; Zagorevski et al., 2006). One of the largest packages within the AAT is the Roberts Arm Group, which, in the Pilley's Island area, is divided into several volcanic terranes including: the Mud Pond terrane, the Pilley's Island terrane, and the Boot Harbour terrane (Fig. 1-3). The Pilley's Island terrane is bound by the Lobster Cove strike-slip fault to the northeast, the Swimming Hole thrust fault to the northwest and the Loadabats thrust fault to the southeast (Fig. 1-4). The Mud Pond terrane is adjacent to Pilley's Island terrane and is bound by the Loadabats fault and the Little Harbour fault. In the Pilley's Island area, these faults are commonly major topographic lineaments that often imbricate altered and mineralized rocks with relatively unaltered and unmineralized units (Thurlow, 2001). Furthermore, significant thrust faulting in the area has offset

stratigraphic units and often causes difficulty in reconstruction and interpretation of the stratigraphy.

In general, the stratigraphy of the Pilley's Island area is a bimodal assemblage of basaltic volcanic rocks that are overlain and intruded by dacitic intrusive, flow and volcaniclastic rocks that host several styles of massive sulfide mineralization (Fig. 1-4). The significant thrust faulting in the area has imbricated VMS-barren mafic volcanic flow-dominated panels (Liquor Street panel and Pilley's Hills panel) against VMS-rich felsic flow- and volcaniclastic-dominated panels (Spencer's Dock panel, 3B panel and Old Mine panel; Fig. 1-4). Mafic volcanic rocks in the Pilley's Hills panel and Liquor Street panel are typically dark green to grey, finely amygdaloidal with quartz, calcite or chlorite and are commonly pillowed. Basaltic volcanic rocks in these panels are intruded by quartz diorite dikes and possibly sills. Quartz diorite intrusions are feldspar-phyric and characterized by hematite-stained phenocrysts in a sericite- and chlorite-altered matrix of quartz and plagioclase. Felsic flows in the Spencer's Dock panel are generally light green to grey and have abundant amygdules, perlitic cracking, and sparse quartz phenocrysts. Many of the flows in this panel are contorted and flow banded and are characterized, locally, by anomalous spheroidal lithophysae. Pseudofragmental textures are abundant throughout formerly vitric flows, which now contain perlitic fracturing and quench fracturing. Hyaloclastic and pyrite-clastic breccias are associated to flows especially in the Spencer's Dock panel and in the Bull Road showing. Felsic volcaniclastic units are more abundant in the 3B and Old Mine panel and include tuff, lapilli tuff, tuff breccia,

autoclastic breccias and hyaloclastite textures. These units are usually intercalated with felsic volcanic flows.

The Pilley's Island district is host to a widespread alteration system, which is characterized by sericite, chlorite, silica, pyrite, potassium feldspar and Fe-carbonate alteration, with variations in intensity and composition with proximity to mineralization. Much of the widespread alteration in the area is hosted within the felsic lavas, which were formerly highly porous and permeable due to vesicularity, quench fracturing and perlitic cracking (Thurlow, 2001). In general, quartz and carbonate alteration are the most widespread alteration facies as they occur in both mafic and felsic rocks that are structurally bound, whereas sericite and Mg- and Fe-chlorite alteration form large haloes surrounding the VMS deposits and are the main products of hydrothermal alteration. Sericite alteration is the most widespread product of hydrothermal alteration and is normally accompanied by weak quartz alteration, disseminated pyrite and low-grade, void filling sphalerite and chalcopyrite (Thurlow, 2001). Chlorite alteration is most abundant in mafic volcanic rocks (Thurlow, 2001). K-feldspar alteration is reported as an exclusively hanging wall alteration facies at the Old Mine area, and is characterized by 6-11% K_2O, despite a lack of sericite (Santaguida et al., 1992; Thurlow, 2001). In the field, carbonate alteration occurs as rusty outcrops that are devoid of pyrite, found specifically in felsic cataclasite of the Liquor Street fault (Thurlow, 2001) but also as amygdules and veins throughout the entire district. Quartz alteration occurs throughout felsic and mafic volcanic rocks and is generally pervasive and commonly associated to devitrification and sericite alteration of felsic flows (Thurlow, 2001). Disseminated pyrite alteration is

volumetrically insignificant and occurs with strong sericite alteration in the Spencer's Dock panel, and never in rocks that are carbonate- or K-feldspar-altered (Thurlow, 2001).

Most Pilley's Island VMS deposits consist of lenses of massive and semi-massive sulfide with surrounding stringer and disseminated sulfide zones. These deposits are hosted exclusively within felsic volcanic and volcaniclastic rocks of the Pilley's Island terrane. The district contains six VMS deposits of variable grade and tonnage. The Spencer's Dock panel on the west side of Pilley's Island is host to the Spencer's Dock, Jane's Cove and Rowsell's Cove deposits. The Spencer's Dock deposit is a lens of massive pyrite that ranges from 26m thick to 11.6m downdip, with only trace sphalerite and chalcopyrite and low precious metal values (Thurlow, 2001). Similarly, the Jane's Cove deposit is a thick lens of (approximately 34m) massive pyrite with trace chalcopyrite and some compositional banding between sulfides and gangue minerals (sericite, silica, carbonate, barite). In contrast to the Spencer's Dock and Jane's Cove deposits, the Rowsell's Cove deposit is composed of coarse, polylithic sulfide-clastic breccia (pyrite and trace chalcopyrite clasts) with weakly altered lithic clasts. The 3B and Bumble Bee Bight deposits are hosted within the 3B panel on the eastern side of Pilley's Island, and are stacked lenses of copper-rich (~4% Cu) pyrite and chalcopyrite with trace sphalerite and galena (Thurlow, 2001). The 3B deposit is stratigraphically higher and is a 5-10m thick lens of massive pyrite (40-80%) and chalcopyrite (3-20%) with trace sphalerite and galena. The lower Bumble Bee Bight deposit contains three, 1-2m lenses of massive pyrite and sphalerite. Lastly, the Old Mine deposit is hosted within the Old Mine panel, which structurally overlies the 3B panel and it consists of two lenses of massive

sulfide that are up to 12m thick with a strike length of 180-300m (Swinden and Kean, 1988). The upper lens consists of massive pyrite and chalcopyrite with trace sphalerite and barite hosted within felsic breccia, and the lower lens consists of massive and stringer pyrite (Swinden and Kean, 1988). These deposits have previously been interpreted to represent sub-seafloor massive pyrite replacement deposits (Spencer's Dock, Jane's Cove, and Old Mine deposits), seafloor massive sulfide deposits (3B deposit), and transported/ resedimented breccia sulfide deposits (Rowsell's Cove deposit and Bull Road showing) (Thurlow, 2001).

1.3. Previous Work

The Pilley's Island massive sulfide district was discovered in 1875 and was mined from 1881-1908, producing approximately 500 000 T of cupriferous massive pyrite (Espenshade, 1937; Thurlow, 2001). Following mine operation, intermittent and infrequent exploration took place (Frobisher Mines in the 1950s) until the late 1960s when drilling (~10,300 m), mapping, soil geochemistry, electromagnetic (VLF-EM) surveys were completed by British Newfoundland Exploration Limited (Brinex). Brinex calculated remaining reserves in the Old Mine area to be 1 159 000T at 1.23% Cu (Grimley, 1968; Thurlow, 2001). Also, in the late 1960s, Brinex discovered the Bull Road showing, and the 3B zone later in 1984 (Epp, 1984).

Exploration was substantial through the 1980s and early 1990s with several geophysical surveys (IP, radiometric and gravity) and diamond drilling (~55 holes) in the area, completed by a Brinco-Getty joint venture up to 1985 and Au Pell Resources Incorporated in 1987-1988.

Through the late 1980s and early 1990s, regional mapping (1:50,000) was completed by the Geological Survey of Canada (Bostock, 1988) and research was conducted on the alteration including a Masters thesis at the University of Waterloo and several published open-file reports and journal articles (Santaguida et al., 1993; Santaguida, 1994; Santaguida and Hannington, 1996). These studies focused on modifying the previous interpretation of the volcanic stratigraphy and environments of formation, sulfide textures and geochemistry, and they identified relationships between alteration geochemistry and likely hydrothermal fluid chemistry.

Phelps Dodge Corporation of Canada discovered a cluster of blind massive sulfide deposits between 1993 and 1996, after mapping, drill core re-logging, gravity surveys and subsequently drilling 18 holes in the Spencer's Dock area (Thurlow, 1996). Along with this discovery came the recognition of a number of low-angle southeast dipping thrust faults crosscutting the area (Liquor Street fault, Hoskin's Cove fault, Ches' Dome fault and Head's Pond fault; Fig. 1-3) (Thurlow, 1996). The work of Thurlow (1996) was the first study to recognize thrust faulting on Pilley's Island and to re-define the stratigraphy of the Spencer's Dock area.

The property was acquired by Altius Resources Inc. in 2000, where a program consisting of drill core re-logging, lithogeochemical sampling and a new geological interpretation was provided (Thurlow, 2001). Subsequent exploration and drilling by Altius and partner Inmet Mining focused on testing down dip of existing mineralization, as well as confirming the geometry of the thrust panels cross-cutting and offsetting the stratigraphy.

1.4. Location and Access

Pilley's Island is located on the northern coast of central Newfoundland and is accessible by Highway 380 from the Trans Canada Highway, which is approximately 40km away from the town of Pilley's Island.

Access to the field area is excellent, as most showings and outcrops are easily accessed from the road; however, topography is generally steep, with some bare, steep cliffs into the ocean. Vegetation is a stunted, coastal, softwood forest with several swamps and bogs at the base of fault valleys. Overall, outcrop exposure is excellent, especially along the shoreline and around most mineralized areas, despite much of the island being covered by trees and forest.

1.5. Objectives

While there have been previous studies on the volcanic stratigraphy, mineralization and hydrothermal alteration of Pilley's Island (Santaguida et al., 1992; Santaguida et al., 1993; Santaguida, 1994; Santaguida and Hannington, 1996; Thurlow, 1996; Thurlow, 2001), the district has not seen recent geological mapping, lithogeochemistry, mineralogy or metallogenic interpretation. Therefore, it is important to re-evaluate the setting of the district by: 1) creating an up to date and detailed geological map of the district; 2) applying modern lithogeochemical analyses and other analytical methods (e.g., TerraSpec); 3) reconstructing the volcanic stratigraphy in light of revised models for the setting of VMS deposits, especially in light of the recognition of the importance of faulting in the area (e.g., Thurlow, 1996; Thurlow, 2001); and 4)

integrating both surface and subsurface geology (drill core) and geochemistry within a 3D framework.

The objectives of this research are to:

1) define the VMS-hosting volcanic stratigraphy and interpret the depositional setting of VMS mineralization in the Pilley's Island VMS district;

2) determine if and how the stratigraphy and lithofacies affects hydrothermal alteration and style of VMS mineralization;

3) identify if and how the stratigraphy and deposits have been modified since sulfide deposition by post-VMS deformation;

4) interpret the 'primary lithogeochemistry' of the Pilley's Island terrane with respect to the petrogenesis of the mafic and felsic volcanic rocks, as well as the tectonic setting in which they were deposited;

5) document the hydrothermal fluid-rock interactions related to VMS-formation by analyzing 'alteration lithogeochemistry';

6) geochemically document zones of hydrothermal alteration and element mobility proximal and distal to sulfide mineralization;

7) interpret the volcanic stratigraphy and use information on proximal and distal alteration signatures, using geochemical and spectral data, to identify useful vectors towards VMS mineralization at Pilley's Island; and

8) assess the exploration potential of Pilley's Island and offer suggestions for continued exploration and research in the area and within the Roberts Arm Group.

1.6. Methodology

1.6.1. Geological Mapping and Sampling

Fieldwork was carried out over the summer months of 2010 and 2011 and involved geological, stratigraphic, and alteration mapping at surface and at depth using diamond drill core. Field mapping was completed at 1:2500 scale to document volcanic stratigraphy and lithofacies relationships, to record structural measurements and test current structural and geological interpretations and to identify alteration zonation associated to the VMS deposits.

Two hundred and eighty five representative samples were collected from outcrops and drill core archives for a record of lithology, alteration, sulfide mineralization and veining styles. Many of these samples were used for petrography, infrared spectroscopy and lithogeochemistry.

1.6.2. Petrography

Of the 285 representative samples, 63 representative samples were made into polished thin section. Polished thin sections were made at Vancouver Petrographic following the summer field seasons in 2010 and 2011. Polished thin sections were made for samples if: they had unique textures and/or mineralogy that could not be determined by the naked eye; they were representative samples for lithology or alteration type; or if they contained sulfide mineralization.

Samples were analyzed using plane, transmitted and reflected light to define mineralogy, primary and secondary (alteration) textures and sulfide mineralization, as well as micro-scale volcanic textures (e.g., perlitic cracking, lithophysae, spherulites).

1.6.3. Lithogeochemistry

Two hundred and eight samples from outcrop and drill core were analyzed for a complete suite of major and trace elements. These samples were chosen for analysis to: 1) determine primary lithologies; 2) identify element mobility in different lithofacies; and 3) compare the geochemistry of rocks close to the mineralized zones versus those farther away. Lithogeochemical samples have been analyzed for major and trace elements by using inductively coupled plasma optical emission spectroscopy (ICP-OES) at ActLabs (Ancaster, Ontario) and by inductively coupled plasma mass spectroscopy (ICP-MS) and x-ray fluorescence (XRF) at Memorial University of Newfoundland (St. John's, Newfoundland and Labrador). Details on the methodology of these analytical techniques are outlined in Chapter 3.

1.6.4. U-Pb Geochronology

Several attempts were made to obtain an age for the Pilley's Island terrane using U-Pb radiometric dating. Despite collecting and processing six samples, no minerals suitable for U-Pb dating (e.g. zircon, titanite) were procured from the felsic volcanic outcrops with the highest zirconium values at Pilley's Island. Samples were processed using a hydraulic splitter, jaw crusher, disk mill, Wilfley table, methylene iodide heavy

liquid separation, Frantz magnetic separator and no significant amounts of zircon, titanite or rutile were available for dating.

1.6.5. Near Infrared-Short Wave Infrared Spectroscopy

All representative samples have been analyzed by near infrared-short wave infrared spectroscopy (NIR-SWIR) using a TerraSpec Infrared Spectrometer at Memorial University of Newfoundland. Details on the methodology for the use of this instrument are outlined in Chapter 3.

1.7. Thesis Presentation

Following this introductory chapter are two chapters consisting of individual research manuscripts to be submitted to an international scientific journal followed by a summary chapter and four appendices with supplementary data, maps and figures. The contents of the chapters and appendices are outlined below.

Chapter 2 contains the results of geological mapping and drill core logging of the Pilley's Island VMS district. Chapter 2 provides both a reconstruction of the volcanic stratigraphy of the district, including the identification of key mineralized lenses, alteration facies, and geological relationships associated with mineralization. Chapter 2 demonstrates: 1) how the volcanic stratigraphy of the area reflects the depositional setting of VMS mineralization in the Pilley's Island VMS district; 2) how the stratigraphy and lithofacies control the hydrothermal alteration and style of VMS mineralization; 3) how the stratigraphy and deposits have been modified since sulfide deposition by post-VMS deformation; and 4) how the volcanic stratigraphy has implications for exploration and

delineation of VMS and other hydrothermal deposits elsewhere in the Appalachians and in other orogenic belts globally.

Chapter 3 contains the results of an integrated field, lithogeochemical, and NIR-SWIR study of volcanic rocks in the Pilley's Island VMS district and is a companion manuscript to Chapter 2. Chapter 3 demonstrates: 1) how the primary lithogeochemistry of the Pilley's Island terrane can be used to understand the petrogenesis and tectonic setting of mafic and felsic magmas within the terrane; 2) how alteration lithogeochemistry can be used to identify zones of element mobility proximal and distal to sulfide mineralization; 3) how the identification of proximal and distal alteration signatures can be used to identify useful vectors towards sulfide mineralization. The results have implications for exploration and delineation of VMS and other hydrothermal deposits in the Appalachians and similar orogenic belts worldwide.

Key conclusions of the thesis are summarized in Chapter 4. This chapter also identifies existing knowledge gaps and potential directions for future research and exploration.

Appendix I includes all raw lithogeochemical (ICP-OES and ICP-MS) data used in this project. Appendix II consists of normalized, LOI-free lithogeochemical data, equations of the fractionation curves that were determined using least altered samples to calculate the mass change data via the Maclean (1990) multiple precursor method. Appendix III consists of supplementary maps illustrating mass change data, for a variety of elements, from outcrop samples. Appendix IV consists of 3D gridded mass change

data from drill core samples to identify spatial relationships to the massive sulfide deposits.

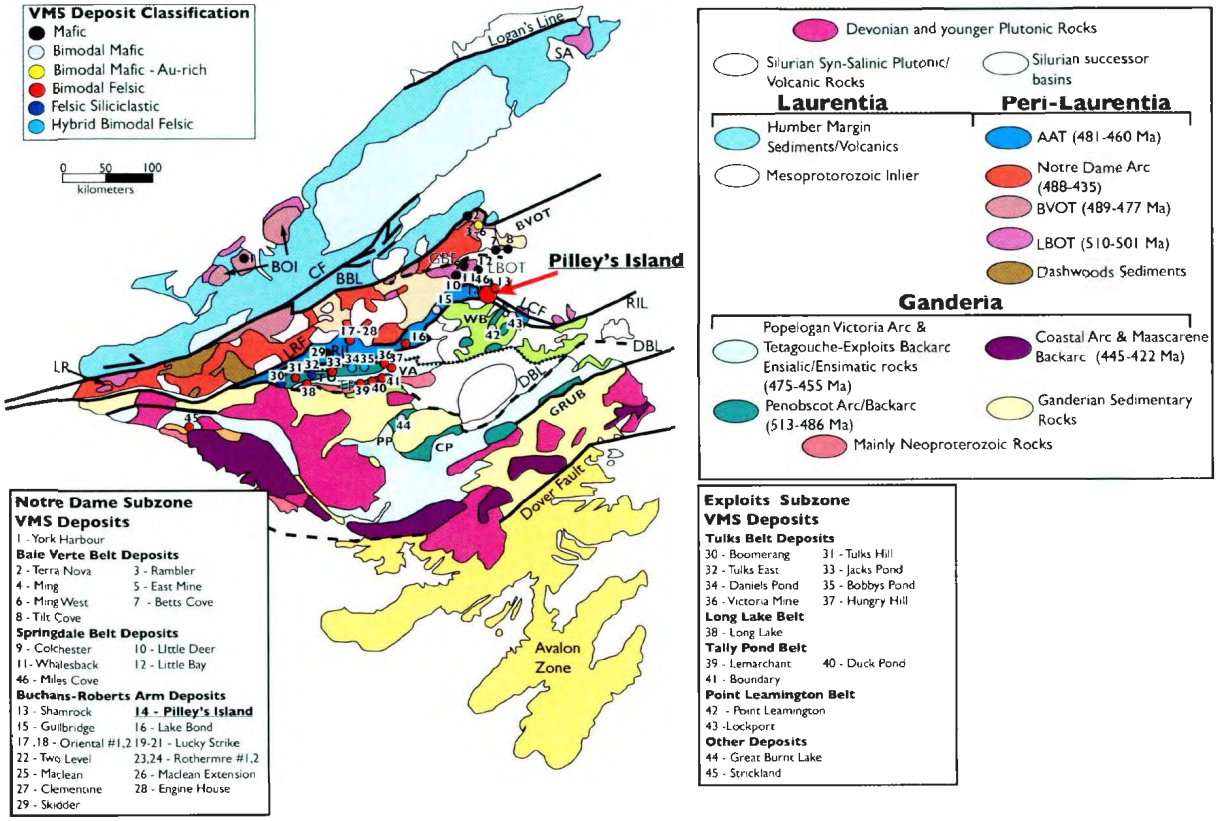

Figure 1-1 Geological map of the Newfoundland Appalachians with tectonostratigraphic zones, accretionary tracts, VMS deposits their classifications and associated belts. Map tectonostratigraphy modified from van Staal (2007) and van Staal and Barr (2011). Volcanogenic massive sulfide (VMS) deposit classification from Piercey (2007c) and Hinchey (2011). Abbreviations: BBL Baie Verte Brompton Line; BOI - Bay of Islands; BVOT = Baie Verte Oceanic Tract; CF = Cabot Fault; CP = Coy Pond Complex; DBL = Dog Bay Line; GBF = Green Bay Fault; GRUB = Gander River Ultramafic Belt; LBOT = Lushs Bight Oceanic Tract; LCF = Lobster Cove Fault; LR = Long Range; LRF - Lloyds River Fault; PP = Pipestone Pond Complex; RIL = Red Indian Line; SA - St. Anthony; TP = Tally Pond Belt; TU = Tulks Volcanic Belt; VA = Victoria Arc; WB = Wild Bight Group.

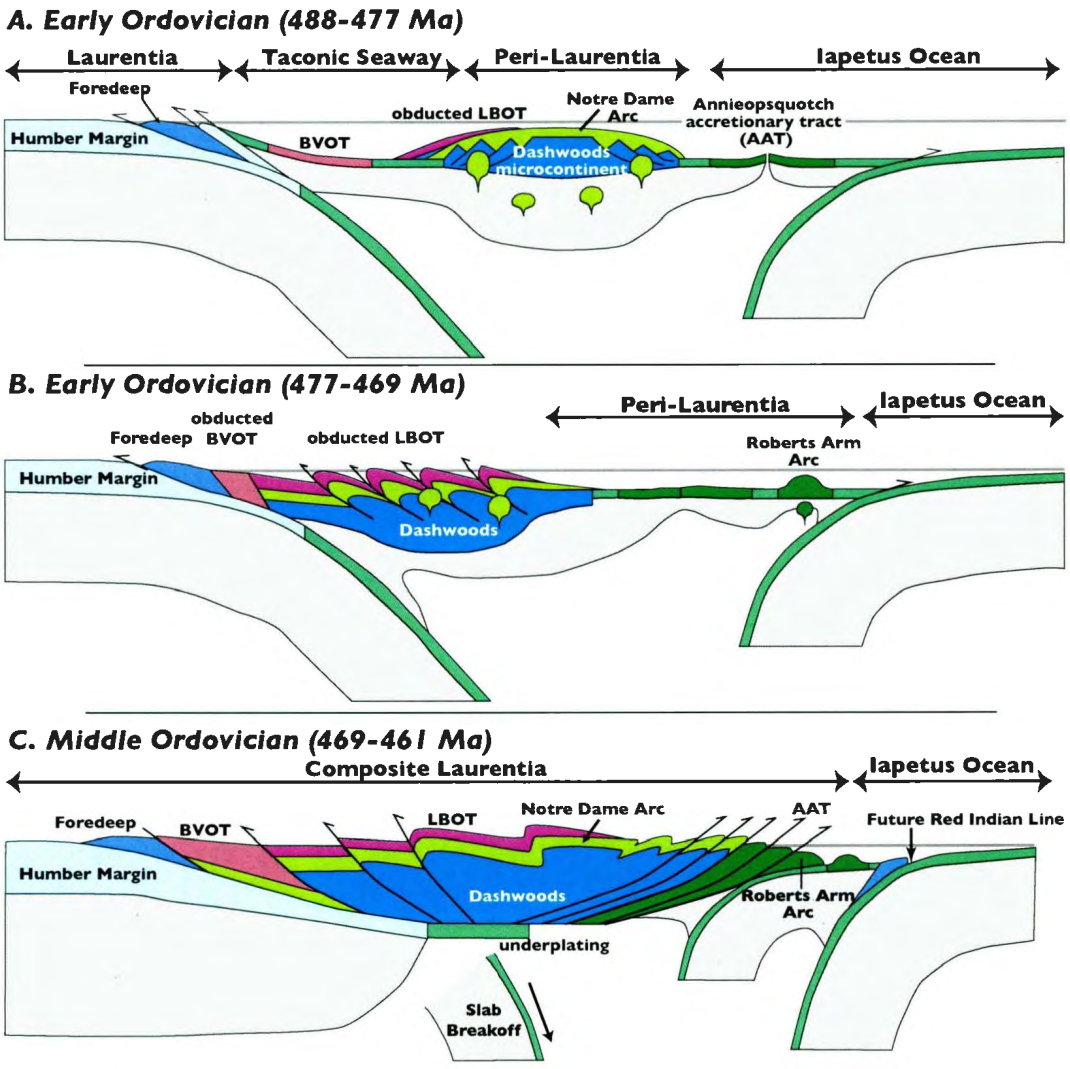

Figure 1-2 Tectonic evolution of the Notre Dame subzone (A) Start of Taconic 2 orogeny and initiation of subduction outboard of the Dashwoods microcontinent (b) Taconic 2 collision of Dashwoods with the Humber margin and subduction initiation west of Dashwoods, responsible for formation and extension of the Annieopsquotch ophiolite belt; (C) Peak of Taconic 2 orogeny resulting in thickening of the Notre Dame arc, the accretion of the Annieopsquotch ophiolite belt and narrowing of the Iapetus Ocean (from van Staal and Barr, 2011)

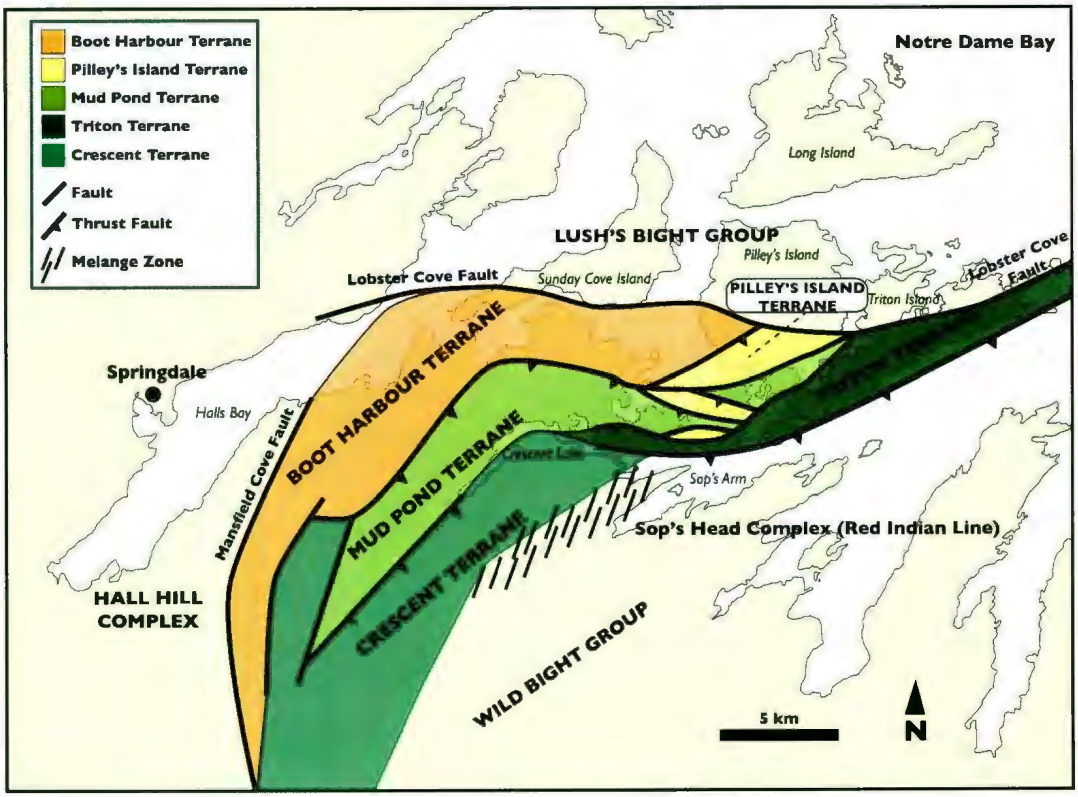

Figure 1-3 Simplified geological map of the northern Roberts Arm Group showing the location of Pilley's Island terrane and adjacent terranes that have been imbricated due to faulting. Modified from Kerr (1996).

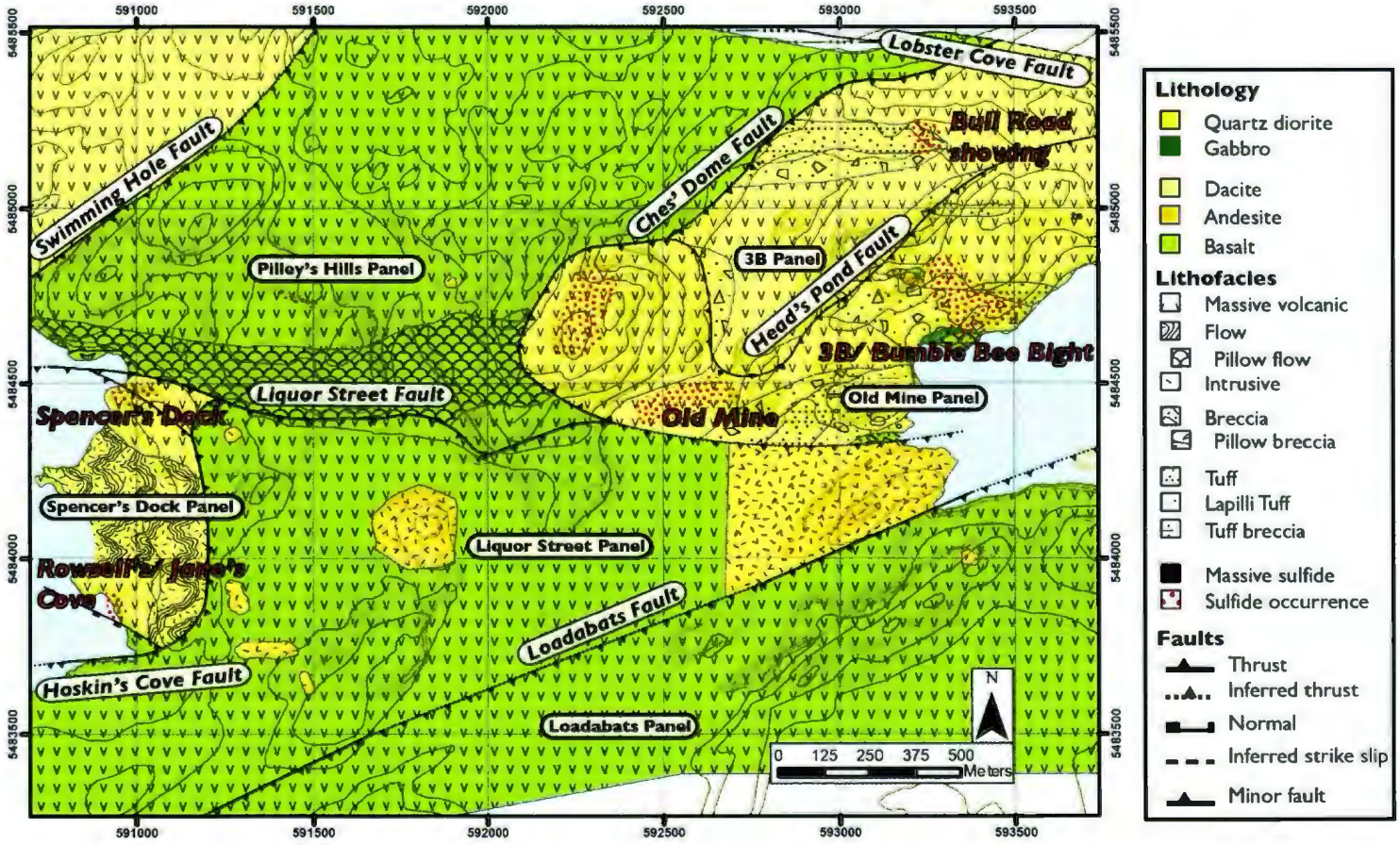

Figure 1-4 Surface map of the Pilley's Island VMS district showing the distribution of different lithologies and lithofacies, as well as the thrust faults that juxtapose different units in the area.

Chapter 2: The Pilley's Island Volcanogenic Massive Sulfide District, Central Newfoundland: Part 1. Geological Setting and Volcanic Reconstruction

2.1. Abstract

Pilley's Island in the Central Mobile Belt of Newfoundland, Canada, is host to a cluster of 'bimodal felsic' Zn-Pb-Cu-Au-Ag volcanogenic massive sulfide (VMS) deposits within the Ordovician Annieopsquotch accretionary tract (AAT). Several southeast dipping thrust faults have been discovered that imbricate the stratigraphic succession, therefore necessitating a re-interpretation of the district's stratigraphy, structure, hydrothermal alteration and mineralization. Detailed mapping and drill core logging have allowed a reconstruction of the volcanic stratigraphy and the interpretation of the stratigraphic control on alteration and VMS mineralization. An understanding of the stratigraphy, lithofacies, alteration, and deformation history within the Pilley's Island VMS district provides a new understanding of the role of primary lithofacies control on mineralization and alteration style, and the effects of post-depositional thrust faulting on the localization of mineralization within this imbricated VMS-hosting belt.

The district contains six VMS deposits that range in style from massive pyrite deposits, polymetallic sulfide deposits, and high-grade polymetallic breccia sulfide deposits. The deposits are hosted within three felsic volcanic-dominated (Spencer's Dock panel) and felsic volcaniclastic-dominated thrust panels (3B panel and Old Mine panel), which are imbricated between several mafic volcanic panels that lack significant sulfide

mineralization (Liquor Street panel, Pilley's Hills panel). The Spencer's Dock panel hosts the Spencer's Dock and Jane's Cove deposits, which are thick lenses of massive pyrite within expansive hydrothermal alteration zones with stringer to trace sulfide mineralization. It also hosts the Rowsell's Cove deposit; a 15m thick layer of coarse, polylithic sulfide breccia with polylithic volcanic clasts. The 3B panel hosts the 3B and Bumble Bee Bight deposit, which are stacked lenses of high-grade (4% Cu) pyrite and chalcopyrite (± sphalerite and galena). The Old Mine panel hosts the Old Mine deposit, with former production of over 500 000 T of ore. It contains two lenses of massive chalcopyrite and pyrite and is hosted by strongly altered felsic volcaniclastic rocks with disseminated and stringer sulfides.

The Spencer's Dock panel, 3B panel and Old Mine panel consist of a variety of felsic volcanic flows and volcaniclastic rocks. The relative abundance and distribution of flows and volcaniclastic rocks in each panel has implications for the deposition of massive sulfide and hydrothermal activity and fluid flow. The Spencer's Dock panel is dominated by massive and flow banded dacite with intervals of polylithic sulfide breccia. It represents a proximal lobe-hyaloclastite facies resulting episodic endogenous flow-dome growth; migrating dacitic flows; and associated hyaloclastite formation along the flow margins within a deep-water extensional fissure system or perhaps part of a larger subsidence structure. The 3B panel is dominated by graded, felsic volcaniclastic rocks with dacitic flows surrounding the volcaniclastic package. The 3B panel stratigraphy represents alternating periods of lava eruption and waning volcanism involving volcaniclastic deposition. The Old Mine panel contains thinly bedded and intercalated

volcaniclastic rocks and volcanic flows. These are attributed to episodic eruptive activity with periods of volcanic activity that form large blankets of volcanic and volcaniclastic material, some of which may also be redeposited from other sources. The overall stratigraphy of these panels represents a transition from flow-dominated to volcaniclastic-dominated lithofacies and represents either: 1) a shallowing basin environment with variable periods of lava outpouring and pyroclastic volcanism or debris flow; or 2) a transition from flow and dome extrusion in a more vent proximal environment and volcaniclastic-dominated facies in a more distal environment because they are more easily transported and resedimented.

Alteration assemblages depend on the composition of host lithofacies and the size and intensity of the alteration is controlled by the permeability and porosity of the host rock. The Spencer's Dock panel contains widespread quartz and sericite alteration that increases in intensity near mineralized zones, but is laterally restricted to fractures and permeable zones in the volcanic flows. In the 3B and Old Mine panels, quartz and sericite alteration is abundant but less widespread and is more intense in volcaniclastic facies, especially those proximal to the mineralized zones.

Mineralization style at Pilley's Island is also controlled by host lithofacies, and most have evidence for sub-seafloor replacement, including: large, gradational alteration and mineralization haloes in the hanging wall and footwall; relicts of host rocks in sulfide zones (quartz crystals, fine tuff to lapilli tuff, and interstitial sericite). Conversely, sulfide breccia deposits form by either: 1) resedimentation of unconsolidated debris (volcanic

and sulfide composition) from a volcanic dome causing collection downslope; or 2) pyroclastic volcanism along the flanks of the volcanic dome.

2.2. Introduction

A major challenge in many ancient volcanogenic massive sulfide (VMS) districts is reconstructing the stratigraphic and structural setting of mineralization (e.g. Allen, 1992; Gibson et al., 1993; DeWolfe et al., 2009). In many post-Archean VMS districts, notably those in Phanerozoic orogenic belts, regional metamorphism and deformation have caused the imbrication of stratigraphic packages, and the obscuring of primary stratigraphic and volcanic facies relationships (e.g. Buchans, Newfoundland; Bathurst, New Brunswick; Iberian Pyrite Belt, Spain) (Calon and Green, 1987; van Staal et al., 2003a; van Staal et al., 2003b; Castroviejo et al., 2011). In many cases, deformation and metamorphism result in the imbrication and juxtaposition of VMS-bearing and barren thrust panels, and difficulty in interpretation arises because of adjacent panels often have very little difference in stratigraphy, volcanic facies, and hydrothermal alteration across faults. Reconstructing such environments requires detailed geological mapping, stratigraphic and volcanic facies analysis, and correlation of alteration zones (Gibson et al., 1983; Cas et al., 1990; Gibson and Watkinson, 1990; Allen, 1992; McPhie and Allen, 1992; Allen et al., 1996; Doyle and Huston, 1999; Gibson et al., 2000; McPhie and Allen, 2003). However, this type of work is often difficult in many ancient districts due to extensive cover by post-VMS rocks and/or extensive surficial cover materials (e.g., soil, till).

The Central Mobile Belt of the Newfoundland Appalachians contains numerous Cambrian to Ordovician VMS deposits that have been variably affected by accretionary tectonics in the Ordovician and Silurian (Fig. 2-1) (e.g., van Staal, 2007). In some belts, deciphering the stratigraphy and effects of subsequent deformation and metamorphism are very difficult due to extensive cover (e.g., Tally Pond belt). In contrast, in some areas, particularly near coastal regions, there is outstanding exposure, topography, and textural preservation, allowing one to understand the primary stratigraphic and alteration relationships, as well as the subsequent effects of deformation and tectonic imbrication. Furthermore, in many locations where advanced exploration has occurred, there is abundant drill core from numerous drill holes allowing reconstruction of these environments in the third dimension, such as at Pilley's Island (Fig. 2-1).

The Pilley's Island district is host to a cluster of bimodal felsic Zn-Pb-Cu-Au-Ag VMS deposits within the Ordovician Buchans-Roberts Arm belt in the Annieopsquotch accretionary tract (AAT) of the Newfoundland Appalachians, Canada. The Pilley's Island terrane of the Roberts Arm Group is dominated by altered, formerly vitric, dacitic breccia and volcaniclastic rocks intercalated with lesser flow banded dacite and mafic pillow lava and pillow breccia, which are interpreted to have originated within a peri-Laurentian volcanic arc/back-arc complex in the western Iapetus Ocean (Thurlow, 1996; Swinden et al., 1997; Thurlow, 2001). The district contains six VMS deposits within a relatively small area (~6km^2). The deposits vary in sulfide composition and mineralization style from massive pyrite, polymetallic sulfide, and polymetallic breccia sulfide, each of which is hosted within distinct stratigraphic assemblages and structural panels. Within the

various thrust panels the host rocks have been immaculately preserved with low grade, prenhite-pumpellyite facies metamorphism (Zagorevski et al., 2009) and no penetrative metamorphic fabrics. Furthermore, the high level of coastal surface rock exposure, coupled with archived diamond drill core, allows one to map the stratigraphic and structural setting of mineralization in three dimensions, a feature not possible in many VMS camps in the Appalachians and globally.

This manuscript provides the results of detailed 1:2500 scale geological mapping, drill core logging, lithofacies analysis, and alteration facies documentation in the Pilley's Island VMS district, and provides both a reconstruction of the volcanic stratigraphy of the district, including the identification of key mineralized intervals, alteration facies, and lithofacies that host VMS mineralization. The ultimate goals of this manuscript are to: 1) identify if and how the volcanic stratigraphy of the area reflects the depositional setting of VMS mineralization in the Pilley's Island VMS district; 2) identify if and how the stratigraphy and lithofacies controls hydrothermal alteration and style of VMS mineralization; 3) identify how the stratigraphy and deposits have been modified since sulfide deposition via subsequent deformation; and 4) provide implications for exploration and delineation of VMS and other hydrothermal deposits elsewhere in the Appalachians and in other similar orogenic belts globally.

2.3. Regional Geological and Tectonic Setting

The Canadian Appalachians are divided into four tectonostratigraphic zones (Williams, 1979; Williams et al., 1988; Williams, 1995; Williams and Grant, 1998): the Humber, Dunnage, Gander and Avalon zones, from west to east (Fig. 2-1). These zones

were juxtaposed during the closing of the Iapetus Ocean in the early to mid-Paleozoic (Williams, 1979; Dunning et al., 1991; O'Brien et al., 1997; van Staal, 2007; van Staal et al., 2007). The Dunnage Zone hosts the majority of VMS deposits in the northern Appalachians. This zone, along with the microcontinents Ganderia, Avalonia and Meguma (Gander, Avalon and Meguma zones) were sequentially accreted to the continental margin of Laurentia, the Humber Zone, throughout the Middle Paleozoic (450-380 Ma) during the closure of the Iapetus Ocean (Williams et al., 1988; van Staal, 2007).

The Dunnage Zone consists predominantly of Cambro-Ordovician volcanic and sedimentary rocks, and is divided into two subzones: the Notre Dame subzone, which formed proximal to Laurentia (peri-Laurentian), and the Exploits subzone, which formed proximal to Gondwana (peri-Gondwanan) (O'Brien et al., 1997; Swinden et al., 1997; Thurlow, 2001; van Staal, 2007). The Pilley's Island VMS district lies within the Notre Dame subzone, which consists of four, Cambrian to Middle Ordovician assemblages, including: the Lushs Bight oceanic tract (LBOT, 510-501 Ma), the Baie Verte oceanic tract (BVOT, 489-477 Ma), Annieopsquotch accretionary tract (AAT, 481-460 Ma) and the Notre Dame magmatic arc (488-435 Ma) (Elliott et al., 1991; Williams, 1992; van Staal et al., 1998; Ramezani et al., 2002; van Staal et al., 2007). The Lushs Bight oceanic tract consists of pillow basalts, sheeted dikes, gabbro and rare ultramafic rocks (Kean et al., 1995; van Staal et al., 1998). The BVOT consists of ophiolitic rocks of mafic to ultramafic composition (Hibbard, 1983; van Staal and Barr, 2011). The AAT consists of 'ophiolitic' rocks, but differs from the BVOT in that ultramafic rocks are relatively rare

and it contains thrust slices of mafic and felsic volcanic rocks (Dunning and Krogh, 1985; Swinden et al., 1997; Lissenberg et al., 2005a; Zagorevski et al., 2006). Lastly, the Notre Dame magmatic arc consists of three igneous populations including: granodiorite to diorite plutons and associated volcanic rocks; tonalite plutons; and, gabbro to granodiorite plutons that were built atop these assemblages (Szybinski, 1995; van Staal, 2007).

The continental and oceanic arc, back-arc, and ophiolitic terranes were episodically accreted to the Laurentian margin in the Ordovician through Silurian (Swinden et al., 1997; Thurlow, 2001; van Staal, 2007). The accretion of the peri-Laurentian elements to the Laurentian margin occurred during the Taconic orogeny occurred in three diachronous events (Taconic 1, 2, and 3) (van Staal et al., 2007). Taconic 1 consisted of the obduction of the Lushs Bight oceanic tract onto the Dashwoods microcontinent and the stepping back of subduction to allow the first phase of Notre Dame arc magmatism and the subduction of the Baie Verte oceanic tract (Lissenberg et al., 2005b; van Staal, 2007). Taconic 2 included the deceleration of convergence between the Humber margin and the Dashwoods block that allowed a new westward dipping subduction zone in the Iapetus Ocean (~481Ma) (van Staal et al., 2007), and the accretion of the AAT to the Dashwoods block (Lissenberg et al., 2005a). The arc-arc collision of the AAT with the peri-Gondwanan Popelogan-Victoria arc was the terminal event of the Taconic orogeny and resulted in the suturing of the peri-Laurentian and peri-Gondwanan elements along the Red Indian Line (Fig. 2-1) (van Staal et al., 1998). The AAT (Fig. 2-1) is the youngest oceanic terrane in the Notre Dame subzone and, in Newfoundland, is a collage of infant arc ophiolite, arc and back-arc

terranes (e.g., the Buchans-Roberts Arm arc) (Swinden et al., 1997; Lissenberg et al., 2005b; Zagorevski et al., 2006). The Pilley's Island VMS district is hosted within the Roberts Arm Group in the northern Buchans-Roberts Arm belt that formed during the onset of westward subduction at ~481 Ma, beneath the Dashwoods microcontinent (Swinden and Dunsworth, 1995; Zagorevski et al., 2006).

The Roberts Arm Group consists of a Lower Ordovician (473-456 Ma; O'Brien and Dunning, 2008) mature island-arc sequence (Swinden et al., 1997) and is divided into four different southeast dipping thrust-fault-bound terranes: the Mud Pond terrane, the Pilley's Island terrane, the Boot Harbour terrane, and the Triton terrane (Fig. 2-2) (Bostock, 1988; Kerr, 1996; Williams et al., 1988). The Mud Pond, Pilley's Island and Boot Harbour terranes are unconformably overlain by the Middle Silurian Springdale Group (Kerr, 1996). The Roberts Arm Group and Springdale Group are bound to the north by the Lobster Cove fault, where overturned Roberts Arm Group volcanic rocks are in contact with upright Cambrian mafic volcanic rocks of the Lushs Bight Group (Dean and Strong, 1977; Kean et al., 1995). To the south, the Roberts Arm Group is bound by the Sops Head Complex, which is a regional scale mélange associated with the Red Indian Line (Williams et al., 1988). This study focuses on the Pilley's Island terrane, and parts of the Boot Harbour or Mud Pond terrane that are closest to Pilley's Island (Fig. 2-2).

2.4. Stratigraphy and Setting of the Pilley's Island VMS District

The Pilley's Island massive sulfide deposits are hosted by variably altered felsic volcanic and volcaniclastic rocks. The area of study consists of three tectonic terranes,

including: the Mud Pond terrane, the Pilley's Island terrane and the Boot Harbour terrane (Fig. 2-2). The terranes are bound by southeast dipping thrust faults (Bostock, 1988; Kerr, 1996). The Loadabats thrust fault juxtaposes the Mud Pond terrane upon the Pilley's Island terrane, which is subsequently juxtaposed upon the Boot Harbour terrane by the Swimming Hole thrust fault (Figs. 2-3 & 2-4). Pilley's Island terrane is also crosscut, internally, by several southeast dipping thrust faults. This study focuses upon the Pilley's Island terrane as well as the units directly adjacent to it, in the Mud Pond terrane and Boot Harbour terrane (Figs. 2-2 to 2-4)

The Pilley's Island terrane is divided into 5 thrust panels (units 2-6), which have been subdivided into specific lithofacies based on 1:2500 scale geological mapping and detailed diamond drill core logging. While the Pilley's Island terrane is the host to mineralization, several units from the Boot Harbour terrane and Mud Pond terrane are also described, including the adjacent Swimming Hole panel (unit 1) and Loadabats panel (unit 7), respectively (Figs. 2-2 & 2-4). The various panels have been distinguished by the identification or inference of thrust faults. Thurlow (1996) first identified the thrust faults based on their shallow dip and lithological contrast. Thrust faults in this study are identified by major topographic lineaments, shear zones in outcrop, abrupt lithological changes, and abrupt variations in the intensity of hydrothermal alteration. In drill core, faults are identified by zones of strong shearing, broken core, fault gouge and cataclasite in combination with sharp changes in lithology, lithofacies, and alteration. Carbonate shear veining commonly occurs with thrust fault movement but is not diagnostic.

Slickensides are often observed in non-oriented drill core and therefore are not kinematic indicators. No other kinematic indicators were observed in fault zones.

The thrust panels and individual units are described and numbered accordingly, in order from lowest to highest, structurally, which is approximately from northwest to southeast (Figs. 2-2 & 2-3). Some panels have been more subdivided into units than others, which is generally a result of better surface exposure or higher recognition of stratigraphic 'marker' units and higher quantity of drill holes in specific panels (e.g., panels with VMS mineralization, such as Spencer's Dock, 3B and Old Mine panels, have better geological control than barren mafic panels, such as the Loadabats and Pilley's Hills panels).

Each lithofacies in the area has been defined based on volcanic textures and field relationships. Textural relationships and contact characteristics of the coherent volcanic and intrusive lithofacies are summarized in Table 2-1. Volcaniclastic lithofacies have been subdivided using the granulometric classification of Fisher (1961), which is used in a non-genetic sense as proposed by White and Houghton (2006). The term volcaniclastic is used herein to describe deposits that consist of particles that were mobilized directly by explosive or effusive volcanism. These rocks are assigned names based on their relative abundance of: tuff (<2mm particles), lapilli (2-64mm particles), and blocks and bombs (>64mm particles) (Fisher, 1961). An exception is the term hyaloclastite, which is frequently used to describe the a deposit formed during effusive volcanism when extruding magma or a lava flow is chilled and fragments due to contact with water, and continued lava extrusion influences the deposition of the fragments (Fisher, 1961).

2.4.1. Swimming Hole Panel

The Swimming Hole panel (unit 1) is the highest structural thrust panel of the Boot Harbour terrane (Figs. 2-3 & 2-4) and is bound by the Swimming Hole thrust fault to the south, the Lobster Cove strike-slip fault to the north and is unconstrained at depth. Two geological units are present at surface. Massive coherent dacite (unit 1.1) is most abundant in this panel, along with lesser felsic tuff (unit 1.2); contacts between the two units are inferred (Table 2-1). Unit 1.1 (Figs. 2-4 & 2-5A) consists of massive coherent dacite with thin, slightly contorted alteration (possibly flow-related) bands that are quartz- and chlorite-amygdaloidal locally. The unit is strongly quartz-altered and mineral banding is defined by moderate chlorite and sericite alteration. Unit 1.2 (Figs. 2-4 & 2-5B) consists of dacitic tuff with strong quartz and hematite alteration causing pink colouration in the rock. Lithic clasts in the tuff have undergone weak, selective sericite alteration. No sulfide mineralization is observed within either of these units.

2.4.2. Pilley's Hills Panel

The Pilley's Hills panel (unit 2) is the lowest structural thrust panel of the Pilley's Island terrane (Fig. 2-4). The inferred thickness of the panel is approximately 500m, based on surface geology and thrust fault dip angles. It is juxtaposed upon the Swimming Hole panel by the Swimming Hole thrust fault and is constrained by the Ches' Dome thrust fault above (Figs. 2-3A & 2-4). The Swimming Hole thrust is identified at surface by a sharp change in lithology between dacitic and basaltic flows, a long linear ridge from southwest to northeast, and shear zones present in outcrop. Unit 2 consists of

undifferentiated massive and pillowed basalt flows and pillow breccias. There are no distinct 'marker' units identified in this panel (Figs. 2-3 & 2-4).

Basaltic flows are quartz-, carbonate-, and chlorite-amygdaloidal (Fig. 2-5C) with bleached and altered pillow margins (Table 2-1). 'Pillow breccias' are matrix supported and characterized by large (~3cm), angular clasts of basalt in a chlorite-, quartz-, and carbonate-rich matrix (Fig. 2-5D). Moderate chlorite alteration is generally pervasive throughout the panel. Disseminated, blebby fine-grained pyrite occurs within several pillow flows and interpillow massive pyrite and sphalerite occurs rarely (Fig. 2-5E). A 9m thick zone of bright red jasper, massive pyrite, and sphalerite occurs in one pillow basalt unit between flows (Fig. 2-5E).

2.4.3. 3B Panel

The 3B panel (unit 3) contains five stratigraphic units and ranges in thickness from approximately 100m in the southeast to 200m in the northwest (Figs. 2-3CD & 2-4). It is juxtaposed upon the Pilley's Hills panel by the Ches' Dome fault and is constrained by the Head's Pond fault above (Figs. 2-3 & 2-4). The Ches' Dome fault is identified by a sharp lithological contact between felsic and mafic volcanic rocks, which are separated by quartz-carbonate shear veins and fault gouge. It is also a major topographic lineament marked by several shear zones where outcrop is available. The panel pinches out down-dip to the southeast. The 3B panel is a package of southeast dipping (slightly steeper than the southeast dipping panel itself) felsic volcanic flows and volcaniclastic rocks (Fig. 2-3CD). The lowest stratigraphic unit consists of dacitic flows (unit 3.1), overlain by monolithic dacitic lapilli tuff (unit 3.2), which grades into dacitic tuff (unit 3.3), and is

overlain by another dacitic flow (unit 3.4) (Figs. 2-3CD & 2-4). Multiple mafic dikes (unit 3.5) crosscut units 3.1, 3.2 and 3.3 (Figs. 2-3C & 2-4). Where undercut by the Ches' Dome fault, units 3.1 to 3.4 are juxtaposed upon unit 2 mafic volcanic rocks (Figs. 2-3CD & 2-4).

Unit 3.1 consists of dacitic flows and is approximately 100m thick (Fig. 2-4). Contacts between flows often contain clast-rotated breccia and lesser hyaloclastite (Table 2-1). Elongate and flow-foliated quartz amygdules are abundant throughout. Flows are moderately altered by sericite and chlorite, both of which define perlitic and pseudofragmental textures (Fig. 2-6A). Sericite alteration also forms networks along fractures. This unit contains only trace pyrite and chalcopyrite, with sphalerite disseminated throughout and amygdules filled by galena, locally. Veining consists of quartz and chlorite ± jasper and crosscut the unit at various orientations.

Unit 3.2 consists of polylithic lapilli tuff and has a sharp contact with unit 3.1 dacitic flows (Fig. 2-4). This unit has thickness ranging from approximately 30m updip to ~200m downdip (Fig. 2-3CD). Lapilli are mostly composed of dacite, although some mafic clasts are recognized. Clasts are mm- to cm-scale, subangular fragments and supported in a tuffaceous, silica-rich matrix (Fig. 2-6BC). Lapilli are altered to K-feldspar, chlorite, sericite, and/or hematite with a variety of alteration intensities. This unit is host to the Bull Road showing (updip, northwest) and the 3B massive sulfide deposit (downdip) (Fig. 2-3CD & 2-6D).

Unit 3.3 consists of felsic tuff and is normally graded and conformably overlies unit 3.2 (Fig. 2-4). The tuff is approximately 80-90m thick. The unit contains numerous

fine, formerly glass shards, now chlorite and sericite, and has minor bedding/clast deformation. The felsic tuff is dominated by quartz and sericite alteration with local chlorite alteration (Fig. 2-E). The alteration is commonly intense and destroys primary textures. This unit is host to the Bumble Bee Bight deposit.

Unit 3.4 consists of dacitic flows and is approximately 100m thick and forms a sharp contact with the underlying volcaniclastic units (Figs. 2-3D & 2-4). In-situ brecciation is observed on the lower contact of unit 3.4, and the upper contact is truncated by the Head's Pond fault (Table 2-1). Dacitic flows are quartz- and carbonate-amygdaloidal. Flow banding is defined by alternating bands of moderate to strong sericite and chlorite alteration (Fig. 2-6G). Trace flecks of disseminated and void-filling pyrite, sphalerite and galena (up to 5%) are observed throughout this unit.

Unit 3.5 represents a group of mafic dikes that cut through units 3.1, 3.2 and 3.3 at various locations (Figs. 2-3C & 2-4) and contain bleached and chilled margins in drill core (Table 2-1). The dikes range in size from several metres width to upwards of 20m. The dikes are coarsely crystalline with pyroxene and plagioclase phenocrysts that are mostly altered to chlorite and sericite, respectively (Fig. 2-6H). The matrix of the intrusions is strongly altered by sericite. Mineralization was not observed in the dikes.

2.4.4. Old Mine Panel

Old Mine panel (unit 4) contains six stratigraphic units and the entire panel ranges in thickness from approximately 200m at surface to 400m at depth (Figs. 2-3CD & 2-4). The panel is juxtaposed upon the 3B panel by the Head's Pond fault and is constrained by the Liquor Street fault above (Figs. 2-3ACD & 2-4). The Head's Pond fault is very subtle

and is identified by strong shear zones and topographic lineaments at surface, and zones of sheared, broken rock and fault gouge in drill core. The panel consists of southeast-dipping, intercalated dacitic flows and felsic volcaniclastic rocks overlying mafic flows (Figs. 2-3ACD & 2-4). The lowest stratigraphic unit consists of massive to pillowed basalt (unit 4.1), overlain by dacitic flows (unit 4.2), dacitic tuff (unit 4.3), dacitic flows (unit 4.4), felsic hyaloclastite (unit 4.5) and a variety of dacitic flows (units 4.6a-c) (Figs. 2-3CD & 2-4). Where undercut by the Head's Pond fault, each unit in the panel (4.1-4.6) is in contact with unit 3, and primarily volcaniclastic units 4.2 and 4.3 (Figs. 2-3CD & 2-4).

Unit 4.1 consists of massive to pillowed basalt, marked by a sharp, fault contact with unit 3.2 below. The unit is approximately 80-100m thick. Basaltic flows contain round to elongate, quartz-, chlorite- and sparse sulfide-filled amygdules. The top of this unit consists of a hyaloclastite breccia. Zones of brecciation contain strong sericite and quartz alteration. Sulfide mineralization in unit 4.1 is focused along pillow margins and consists of massive sulfide (pyrite > chalcopyrite + sphalerite) and bright red jasper (Fig. 2-7A).

Unit 4.2 consists of dacitic flows, which form a sharp contact with unit 4.1 below, as well as units 3.2 and 3.3 of the 3B panel (Fig. 2-3C). The unit is approximately 40m thick. The upper and lower contacts are brecciated, and some internal flow margins contain clast-rotated breccia intervals (Table 2-1). Directly below the Old Mine deposit, the dacite is strongly chlorite-altered and moderately sericite-altered. Sericite alteration

intensity decreases with depth. Dacitic flows contain up to 5% blebby pyrite and sphalerite.

Unit 4.3 consists of dacitic tuff to lapilli tuff, which overlie unit 4.2 dacitic flows (Figs. 2-3C & 2-4). The unit is approximately 100m thick. The dacitic tuff is fine grained with chlorite-rich olive-green fragments hosted in a very fine-grained quartz-sericite-chlorite matrix (Fig. 2-7B). The fragments were glass, now mainly chlorite and sericite, and have been flattened and deformed. They exhibit a parallelism to a weak foliation observed throughout the rock. Lapilli are sometimes mineralogically zoned with strongly sericite-altered rims and weakly chlorite-altered cores, and are hosted within a chlorite-rich matrix. Many of the lapilli appear to be deformed, altered dacitic glass shards. Sericite alteration increases towards sulfide mineralization, and has destroyed primary textures (e.g. tuff grains, bedding) in proximity to massive sulfide. This unit is host to the Old Mine deposit. There is a lithofacies change in proximity to the Old Mine VMS deposit, which is hosted in finer-grained, more tuffaceous strata. The Old Mine deposit contains two massive sulfide lenses that are up to 12m thick (Fig. 2-7C) (Swinden and Kean, 1988).

Unit 4.4 consists of dacitic flows that unconformably overlie units 4.2 and 4.3 (Figs. 2-3CD & 2-4). The unit is approximately 20-30m thick. Clast-rotated breccia is observed along the lower contact of the unit and its upper contact exhibits perlitic textures (Table 2-1). Dacitic flows are quartz-, carbonate- and chlorite-amygdaloidal. Flows are characterized by contorted, concentric flow bands, which are defined by sericite and chlorite (Fig. 2-7D). Disseminated sulfides (pyrite > sphalerite > chalcopyrite > galena)

also form as bands and coarse masses throughout the flow and within the amygdules (Fig. 2-7E).

Unit 4.5 consists of dacitic hyaloclastite, which overlies unit 4.4 with an obscured contact margin (Figs. 2-3CD & 2-4). The unit is approximately 5m thick. Clasts have distinct ragged margins, range in size from 1mm up to 3-4cm and exhibit a weakly interlocking, jigsaw fit texture, typical of hyaloclastite, in some sections of the unit (Fig. 2-7F). The clasts are altered by chlorite, quartz and hematite, and are hosted within a strongly silicified matrix. Disseminated pyrite blebs and bright red jasper occur throughout the matrix, locally.

Unit 4.6 is divided into three, albeit similar, subunits based on volcanic textures and field relationships (units 4.6a, 4.6b and 4.6c from bottom to top, respectively) (Figs. 2-3CD, 2-4). The thickness of the three subunits form a thick volcanic is unknown due to surface erosion. The subunits have an obscured, poorly defined contact with the underlying unit 4.5, and they are eroded at surface. Unit 4.6a is composed of dark grey massive dacite that contains quartz- and chlorite-filled amygdules. It is quartz, hematite, and sericite-altered. Fractures in this unit are locally filled by hematite or jasper with disseminated pyrite. Unit 4.6b consists of dacitic flows that have contorted and undulating flow bands (Fig. 2-7G). The dacite contains numerous thin, mm-scale bands of alternating chlorite- and sericite-rich alteration, and can be flow brecciated with some parts containing deformed clasts in a silica-rich matrix (Fig. 2-7G). Along contacts within the unit, breccia are clast rotated and individual clasts exhibit the characteristic flow banding of the surrounding subunits (Fig. 2-7H). Unit 4.6c is the highest stratigraphic unit in the

panel and consists of dark grey, massive dacite and contains large (up to 1cm) rounded amygdules that are filled with quartz ± concentric Fe-carbonate.

2.4.5. Spencer's Dock Panel

The geology of the Spencer's Dock panel has been reconstructed through archived drill logs (re-logged by J. Geoffrey Thurlow, 1994) (Fig. 2-3B) coupled with results from surface mapping. The Spencer's Dock panel contains six stratigraphic units and ranges from approximately 300m thick to over 700m downdip in the panel (Fig. 2-3B). The panel is juxtaposed upon the Pilley's Hills panel along the Liquor Street fault (Figs. 2-3AB & 2-4). The units pinch out towards the northeast of the panel where the Hoskin's Cove fault merges with the Liquor Street fault (Fig. 2-3A). The Liquor Street fault is recognized by the sharp lithological change between hanging wall dacitic flows and footwall basaltic flows, a thick mélange zone with fault gouge and cataclasite, and a major topographic lineament at surface. The Hoskin's Cove fault is identified by lithological change at surface and in drill core, and does not contain significant fault gouge or significant zones of broken core. The panel is dissected by three minor thrust faults and is subdivided into the Lower panel, Rowsell's Cove panel, and Upper panel (Fig 2-3B) (Thurlow, 1996). The Lower panel consists of massive coherent dacite (unit 5.1), most of which is mineralized, and has some occurrences of breccia and one mafic intrusion (Figs. 2-3B & 2-4). The Rowsell's Cove panel consists of mafic volcanic rocks (unit 5.2) with a large gabbro intrusion (unit 5.3), which is overlain by felsic volcaniclastic rocks (unit 5.4) and dacitic flows (unit 5.5). The Upper panel consists of massive coherent dacite (unit 5.6) (Figs. 2-3B & 2-4). Two major faults, defined by

gouge, are recognized within the Spencer's Dock panel. The Lower panel thins towards the surface and is characterized by an upper fault/shear zone within strongly sheared, soft, friable gouge and sericite-rich matrix. The Lower panel is underlain by a mélange, characterized by litheness supported by a dark grey pyrite-sericite-rich cataclasite.

Unit 5.1 consists of massive coherent dacite that is juxtaposed upon unit 2 basaltic volcanic rocks by the Liquor Street thrust fault and is truncated above by a minor fault (Figs. 2-3B & 2-4). The massive dacite is locally quartz-amygdaloidal and contain polylithic breccia between coherent units (Table 2-1). The panel contains several intervals of polylithic breccia, which are composed of lithic clasts and altered vitriclasts in siliceous matrix. Moderate to strong sericite alteration is abundant throughout. Unit 5.1 contains abundant sulfide mineralization and hosts both the Jane's Cove and Spencer's Dock deposits (Figs. 2-3B & 2-4). The Jane's Cove deposit is approximately 35m thick, consisting of massive pyrite with trace chalcopyrite, sphalerite and galena and transitions outwards into zones of 3-20% disseminated sulfides replacing quench-fractured dacite. Abundant pseudofragmental alteration textures (e.g. pseudobreccia, perlitic cracks) characterize the volcanic rocks in proximity to the Jane's Cove deposit. The polylithic breccia between the deposits consists of approximately 5-10m of massive sulfide clasts and variably altered lithic clasts in a silica rich matrix (overall approx. 30-40% pyrite). Breccia is locally supported by sulfide in place of a silica-rich matrix. The Spencer's Dock deposit is a 20-25m thick lens of massive to semi-massive, medium to coarse grained pyrite with trace sphalerite, which transitions outwards into zones of disseminated and veinlet sulfide mineralization.

Unit 5.2, the lowest unit of the Rowsell's Cove panel, consists of basaltic flows and associated breccia, which are juxtaposed upon unit 5.1 by a minor fault (Figs. 2-3B & 2-4). The unit is approximately 120m thick, including up to 50m of basaltic breccia along its lower contact (Table 2-1). Breccia clasts contain leucocratic rims and are supported by a siliceous matrix. The unit contains moderate to strong chlorite and sericite alteration. Flows contain disseminated pyrite (2%, up to 20% locally) and trace, veinlet-hosted chalcopyrite and sphalerite. Basalt breccia contains 5-10% disseminated sulfide and minor massive pyrite clasts locally.

Unit 5.3 is a large gabbro intrusion (Figs. 2-3B & 2-4), which cuts units 5.2, 5.4 and 5.5, and is in contact with unit 5.1 felsic volcanic rocks due to fault offset. The intrusion, where observed, is approximately 50m thick. Intrusive contacts are weakly sheared and are locally brecciated with coarse pyrite-silica-calcite matrix (Table 2-1). Weak to strong chlorite, weak to strong epidote and weak sericite are pervasive throughout the gabbro. The intrusion contains disseminated and veinlet pyrite (1-3%) with trace sphalerite and chalcopyrite.

Unit 5.4 consists of felsic hyaloclastite and volcaniclastic rocks that have been intruded by unit 5.3. It is bound updip by unit 5.5 dacitic flows and above by a minor fault (Figs. 2-3B & 2-4). The unit is approximately 100m thick. Volcaniclastic intervals are dominantly tuffaceous and have poorly defined bedding. Felsic breccia contains angular, melanocratic fragments in a silica-rich matrix. Moderate to strong quartz, sericite and pyrite alteration is pervasive throughout the unit. This unit is host to the Rowsell's Cove deposit, which is a 15-20m thick lens of coarse sulfide breccia with massive sulfide

clasts, of approximately 10cm diameter (max. 65cm), and lesser lithic clasts. Disseminated and minor stringer pyrite (1-5%) and trace chalcopyrite and sphalerite occur throughout the breccia interval.

Unit 5.5 is the highest unit of the Rowsell's Cove panel, consisting of dacitic flows and sparse mafic intrusions, and is approximately 100m thick (Figs. 2-3B & 2-4). Unit 5.5 forms a poorly defined contact with unit 5.4 downdip, and is separated from units 5.1 (below) and 5.6 (above) by minor faults (Figs. 2-3B & 2-4). Contacts between flows contain autobreccia with randomly oriented, flow-banded fragments (Table 2-1). Dacitic flows contain 2-20cm spheroidal lithophysae, most of which are composed of radiating acicular crystals surrounding hollow or quartz-carbonate (± pyrite, sphalerite) cores (Fig. 2-8A). The unit is dominated by moderate sericite, and weak quartz and carbonate alteration (Fig. 2-8B). Alteration along perlitic cracks results in pseudofragmental textures. Sulfide mineralization in unit 5.5 consists of very sparse, disseminated pyrite and sphalerite.

Unit 5.6 is the only unit within the Upper panel of the Spencer's Docks panel (Figs. 2-3B & 2-4). It consists of massive coherent dacite and is separated from units 5.4 and 5.5 by a minor fault and is bound by the Hoskin's Cove thrust fault above (Figs. 2-3B & 2-4; Table 2-1). The unit ranges from approximately 110m to 170m in thickness. The massive dacite is amygdaloidal with small, quartz-pyrite filled amygdules and contains abundant perlitic fracturing (Fig. 2-8C). Alteration banding is contorted and defined by sericite and chlorite. The unit contains moderate to strong sericite alteration, and weak chlorite, quartz and carbonate alteration. Alteration defines a pseudofragmental 'alligator-

skin' texture. Sulfide mineralization consists of 1-5% disseminated and veinlet-filling pyrite throughout, with sparse flecks of sphalerite and chalcopyrite (Fig. 2-8D).

2.4.6. Liquor Street Panel

The Liquor Street panel is the highest structural thrust panel of the Pilley's Island terrane and is juxtaposed upon the Spencer's Dock panel, Pilley's Hills panel and Old Mine panel by the Liquor Street fault below and is bound by the Loadabats fault above (Fig. 2-3A & 2-4). The panel consists of undifferentiated massive and pillow basalt flows (unit 6.1), which are crosscut by quartz diorite dikes and possibly sills (unit 6.2) (Fig. 2-4; Table 2-1).

Unit 6.1 consists of pillowed basalt flows that contain quartz, carbonate, and/or chlorite filled amygdules (Fig. 2-8E). It often has hematite alteration of the groundmass. No sulfide mineralization has been observed in this unit.

Quartz diorite (unit 6.2) intrudes unit 6.1 with irregular contact margins. The intrusions have a fine quartz-plagioclase pilotaxitic groundmass with coarse euhedral plagioclase phenocrysts. They are locally quartz- and chlorite-amygdaloidal. The intrusions are feldspar-phyric with salmon pink, hematite-stained plagioclase phenocrysts, in a sericite- and chlorite-altered matrix (Fig. 2-8F). The intrusions contain sparse, bleached and hematite-rich basalt xenoliths (Table 2-1). Rutile is a common accessory mineral throughout the intrusions. Much of the plagioclase in the intrusion has been altered to sericite, which is manifested as a spotty network throughout the plagioclase grains.

2.4.7. Loadabats Panel

The Loadabats panel (unit 7) is the lowest structural thrust panel of the Mud Pond terrane (Fig. 2-3A & 2-4). It is bound by the Loadabats fault below, and is unconstrained above (Fig. 2-4). Two geological units are observed at surface and in drill core, including massive and pillowed basalt flows (unit 7.1), and gabbro intrusions (unit 7.2). Unit 7.1 predominates throughout the panel and unit 7.2 gabbro intrusions are only observed in drill core.

Unit 7.1 consists of massive to pillowed basalt flows with associated breccia units and is quartz-, calcite-, and chlorite-amygdaloidal (Fig. 2-8G; Table 2-1). The basalt is quartz-, chlorite-, hematite- and locally epidote-altered. Pillow breccia is infilled, locally, by bright red hematitic jasper.

Gabbro intrusions (unit 7.2) cut Loadabats panel basalt and are characterized by a bright green groundmass with olive green pyroxene phenocrysts (Fig. 2-8H). They have irregular, chilled and glassy margins (Table 2-1). Pyroxene phenocrysts and groundmass are commonly replaced by chlorite, and few plagioclase laths remain as most have been altered to sericite.

2.5. Volcanogenic Massive Sulfide Deposits of the Pilley's Island District

The Pilley's Island VMS deposits are massive to semi-massive sulfide lenses and breccia sulfide occurrences with associated stringer sulfide veins and disseminated sulfides. Felsic volcanic and volcaniclastic rocks of the Pilley's Island terrane host numerous massive sulfide deposits that represent different styles of deposition. The Pilley's Island District is host to six VMS deposits of variable grade and tonnage,

including: Spencer's Dock deposit (low grade with trace base/ precious metal, up to 26m drill intersection); Jane's Cove deposit (not delineated, up to 35m massive pyrite intersection); Rowsell's Cove deposit (not delineated, intersection 0.34% Cu over 14.6m in breccia sulfide); 3B deposit (~200 000T, 3.5% Cu); Bumble Bee Bight deposit (not delineated, 4.42m intersection of 4.42% Cu); and Old Mine deposit (approximately 500 000T past production and approximately 1 159 000T remaining, 1.23% Cu) (Grimley, 1968; Appleyard and Bowles, 1978; Thurlow, 1996; Thurlow, 2001).

The deposits of the Pilley's Island district are hosted within 3 different thrust panels: Spencer's Dock panel, 3B panel and Old Mine panel. The Spencer's Dock panel is host to the Spencer's Dock, Jane's Cove and Rowsell's Cove deposits, which are the largest and lowest grade massive sulfide deposits on Pilley's Island (Thurlow, 2001), the 3B panel hosts the 3B and Bumble Bee Bight deposits, and the Old Mine panel hosts the Old Mine deposit.

The Spencer's Dock deposit is a lens of massive, coarse pyrite that ranges from 26m thick to 11.6m downdip, with only trace sphalerite and chalcopyrite and low precious metal values (Thurlow, 2001). Massive pyrite in the Spencer's Dock deposit is generally granular and contains upwards of 10% interstitial gangue minerals (sericite, silica, carbonate, barite) and local angular volcanic clasts. The deposit is surrounded by expansive, gradational zones of semi-massive to stringer pyrite and sphalerite (up to 50% sulfide) with trace chalcopyrite veinlets. Mineralized zones are hosted by felsic flows that have been almost entirely altered to sericite.

The Jane's Cove deposit is a thick lens of massive, coarse pyrite with trace chalcopyrite and some compositional banding between mineralization and gangue minerals (sericite, silica, carbonate, barite). Strongly altered felsic volcanic rocks surround the massive sulfide zone, which consists of semi-massive to 'peppery' disseminated and stringer pyrite (up to 10cm width) and interstitial chalcopyrite and sphalerite. Most sulfide textures have been destroyed by brittle-ductile deformation resulting in extensive development of friable core.

The Rowsell's Cove deposit is structurally higher than the Jane's Cove deposit and is composed of coarse, polylithic sulfide breccia tightly packed with less altered volcanic clasts. Clasts are composed of pyrite and trace chalcopyrite, are generally 10cm in diameter, and range upwards of 65cm. Pyrite-rich breccia flanks a dacitic flow/dome with interbedded hyaloclastic breccia (Thurlow, 2001).

The Bull Road showing is a Zn-Pb-Cu-Au-Ag–rich prospect that contains massive pyrite clasts, up to 1m in size, as well as massive pyrite-sphalerite matrix, hosted within polylithic lapilli tuff (Santaguida, 1994; Thurlow, 2001). Massive sulfide mineralization extends over 20m downdip in the 3B panel. Several massive sphalerite intervals have compositional banding between chalcopyrite and pyrite, and envelop other felsic lapilli clasts (Santaguida, 1994).

The 3B and Bumble Bee Bight deposits are stacked lenses of Cu-rich (4% Cu), disaggregated pyrite and chalcopyrite with trace sphalerite and galena (Thurlow 2001). The 3B deposit is stratigraphically higher and is a 5-10m thick lens of massive pyrite (40-80%) and chalcopyrite (3-20%) with finely granular, trace sphalerite and galena and

contains interstitial sericite and quartz (Fig. 2-6D). The deposit is surrounded by large zones of disseminated and veinlet pyrite and chalcopyrite. Massive sulfide contains lithic-fragment-rich zones with variable clast compositions (Fig. 2-6C). The lower Bumble Bee Bight deposit is less constrained, but contains three, 1-2m lenses of massive pyrite and sphalerite. Pyrite and sphalerite are disseminated throughout the tuff (1-5%) and fill dendritic fractures, extending over 100m into the surrounding rock (Fig. 2-6F).

The Old Mine panel hosts the Old Mine deposit, which is a former producing mine, having shipped over 500 000 T of ore (Espenshade, 1937). It consists of two lenses of massive sulfide that are up to 12m thick with a strike length of 180-300m (Swinden and Kean, 1988). The upper lens consists of massive pyrite and chalcopyrite with trace sphalerite and barite hosted within felsic breccia, and the lower lens consists of massive and stringer pyrite in a dacitic flow (Swinden and Kean, 1988). The massive pyrite in each lens is granular and contains interstitial quartz and barite and fragments of felsic lapilli and tuff. Mineralization occurs throughout the hanging wall and footwall and consists of up to 5% pyrite and chalcopyrite in disseminated stringers.

2.6. Discussion

This study examines the volcanic stratigraphy, alteration, and deformation history within the Pilley's Island VMS district. It suggests a primary lithofacies control on mineralization and alteration style and illustrates the secondary effects of post-depositional thrust faulting on VMS mineralization within an imbricated volcanic succession. The results herein illustrate how each thrust panel in the district provides a wide variety of volcanic textures, lithofacies and alteration assemblages that reflect

different zones within a VMS hydrothermal environment. Furthermore, the detailed mapping and drill core reconstructions provide discrimination criteria for barren and mineralized thrust panels.

2.6.1. Depositional Setting

Pilley's Island VMS district consists of basaltic volcanic rocks that are overlain and intruded by dacitic dike, flow and volcaniclastic rocks. Thrust faulting has complicated the reconstruction of the stratigraphy by imbricating felsic- and mafic-volcanic-dominated panels. In the Pilley's Island terrane, the Liquor Street panel and Pilley's Hills panel are dominated by mafic volcanic rocks and consist of massive and pillowed basalt flows with associated breccias. These panels are relatively devoid of sulfide mineralization, with the exception of a 9m thick lens of red hematitic jasper, with massive pyrite and sphalerite in the Pilley's Hills panel. The majority of basalts were emplaced as seafloor lava flows, with alternating pillow flows and pillow breccia with local jigsaw-fit texture.

The Spencer's Dock panel, 3B panel and Old Mine panel are dominated by felsic volcanic rocks and consist of a variety of flows and volcaniclastic rocks. The relative abundance and distribution of flows and volcaniclastic rocks in each panel has implications on the deposition of massive sulfide and hydrothermal activity/ fluid flow.

The Spencer's Dock panel is dominated by massive and flow banded dacite with several occurrences of polylithic sulfide breccia and few mafic intrusions and flows. Felsic flows were emplaced as a group of lobe-hyaloclastite felsic flows and as three specific flow facies: massive; lobe-hyaloclastite; and breccia (e.g., Gibson et al., 1999).

The massive flow facies includes parts of unit 5.1, 5.5 and 5.6 where flows are massive to flow banded, without significant hyaloclastite (Fig. 2-3B). Despite being subaqueous flows, this facies contains little hyaloclastite and could result from internal pulses of magma into the interior of the flow during endogenous growth (Gibson et al., 1999). Unit 5.1 and 5.6 dacitic flows and massive coherent units are locally amygdaloidal and contain highly contorted flow bands which may indicate that they formed near the margins of the dacite lobes (Gibson et al., 1999).

The lobe-hyaloclastite facies consists of massive lava with brecciated, flow-banded lava and hyaloclastite. Unit 5.5 contains zones of autobreccia with randomly oriented, flow-banded fragments derived from the margins of the flow. It also contains large lithophysae that consist of radiating, acicular needles around a hollow core, suggesting that these flows have undergone high temperature devitrification (Fig. 2-8A) (e.g. Lipman, 1965; Anderson, 1969; Lofgren, 1971; Bigger and Hanson, 1992; McArthur et al., 1998).

The breccia facies is the least abundant facies and it consists of: carapace breccias containing massive or flow-banded fragments of the lobe that are supported by a hyaloclastite matrix; or flank breccias, which are framework-supported beds of coarse lobe fragments in a fine hyaloclastite matrix. Unit 5.4 and parts of unit 5.1 contain poorly sorted polylithic breccia. Hyaloclastite hosted along the sides of the massive flows is framework supported flank breccia and results from spalling and mass flow from the migrating dacite lobes (Gibson et al., 1999).

Although lobe-hyaloclastite flows are not governed by water depth constraints, an abundance of reworked, bedded hyaloclastite usually represents shallower water depth (<500m) above storm-wave base (Gibson et al., 1999). Since the Spencer's Dock panel contains little hyaloclastite relative to the abundant volcanic flows, it is possible that it formed in deeper water, within an extensional fissure system that may be part of a larger subsidence structure (Gibson et al., 1999). The flow-dominated stratigraphy present in the Spencer's Dock panel is similar to the footwall of the Ansil, Vauze and Norbec deposits in the summit caldera of the Central Noranda Volcanic Complex and suggests a potentially analogous environment of formation (Gibson, 1990; Gibson and Watkinson, 1990).

The 3B panel is dominated by graded, felsic volcaniclastic rocks with dacitic flows surrounding the volcaniclastic package (Figs. 2-3CD, 2-4 & 2-6). Specifically, the panel consists of massive dacitic flows with abundant pseudofragmental textures (unit 3.1; Fig. 2-6A); polylithic lapilli tuff with some mineralogically zoned clasts (unit 3.2); altered, felsic tuff (unit 3.3, Fig. 2-6EF); and dacitic flows (unit 3.4, Fig. 2-6G). This succession is interpreted to represent a period of effusive dacitic lava eruption, followed by a period of (possibly waning) volcanism involving syn-eruptive volcaniclastic deposition followed by another period of dacitic lava eruption. Evidence for this representing a syn-eruptive volcaniclastic unit includes (Gibson et al., 1999; McPhie and Allen, 2003): 1) volcaniclastic units with a sharp base; 2) coarser, graded to massive lapilli tuff basal unit; 3) finer, thinly stratified upper unit; 4) devitrification of glassy components to fine-grained quartz-feldspar-phyllosilicate-carbonate assemblages; 5) clast

shapes still well preserved in lower, coarse clasts; and 6) bedding-parallel foliation defined by diagenetically compacted glass shards in upper, finer levels (e.g., McPhie and Allen, 2003). Similar to volcaniclastic units described for the Mount Read Volcanics, clasts and shards in the volcaniclastic units of the 3B panel lack evidence of hot emplacement (i.e., welding) and are uncompacted (Allen and Cas, 1997; Gifkins and Allen, 2001). Furthermore, the large thickness of the felsic volcaniclastic deposits within the 3B panel suggests vent proximal deposition and association with a submarine silicic eruption (McPhie and Allen, 2003). The volcaniclastic-dominated stratigraphy is similar to the stratigraphy that hosts the Rosebery and Hercules deposits, which consists of thick (200m) massive to graded pumice breccia (Allen et al., 1996; Large et al., 2001c).

The Old Mine panel consists of more thinly bedded and intercalated felsic volcaniclastic rocks and dacitic flows. The alternating, intercalated strata can be attributed to episodic eruptive activity (Gibson et al., 1999). Certain episodes were effusive and erupted dacitic flows onto the seafloor (units 4.2, 4.4, 4.6), with local flow banding and hyaloclastite and various breccia styles (unit 4.5), whereas other eruptive episodes may have been either: pyroclastic eruptions that formed large blankets of volcaniclastic material (Gibson et al., 1999), or more likely, due to the lack of evidence for pyroclastic volcanism, the volcaniclastic material may be debris flows redeposited from other sources.

Felsic lava flows are more likely to be intercalated with primary and redeposited volcaniclastic material in shallower water environments (Gibson et al., 1999). In the Old Mine panel, dacitic flows are very thin and less abundant than volcaniclastic material.

This may represent increased resedimentation of finer, volcaniclastic rocks. The intercalated volcaniclastic-dominated stratigraphy observed in the Old Mine panel is similar to that of the Hercules and Rosebery deposits, where the stratigraphy consists of intercalated crystal- and/or pumice-rich volcaniclastic rocks and massive dacite and autoclastic breccia (Large et al., 2001c).

The felsic volcanic-dominated thrust panels are considered to be lateral equivalents that formed in close spatial proximity to one another, and were subsequently imbricated against mafic volcanic-dominated panels due to thrust faulting. Their current proximity to each other, as well as their similar lithogeochemistry and alteration, support this interpretation. A direct correlation of volcanic lithofacies and structural reconstruction is not possible because unique 'marker' units are not recognized in the area. The broadly similar volcanic strata across the felsic volcanic lithofacies of the Pilley's Island terrane is consistent with formation within a felsic volcanic centre located within a fissure-fed extensional setting, perhaps within a larger subsidence structure (Dimroth et al., 1985; Gibson, 1990; Gibson and Watkinson, 1990; Morton et al., 1991; Gibson et al., 1999). The Spencer's Dock panel stratigraphy may indicate a deeper depositional setting, with the 3B and Old Mine panels representing a shallower, submarine or near-sealevel setting. Therefore, it may be interpreted that the felsic volcanic edifice was built on a submarine basaltic floor and the transition from flow-dominated to volcaniclastic-dominated lithofacies represents a progressively shallowing basin environment, with variable periods of lava outpouring and volcaniclastic deposition (Fig. 2-9). Alternatively, the change in lithofacies may reflect different parts of the basin,

such that flows and domes represent a proximal, near-vent facies, and volcaniclastic lithofacies a more distal facies as they are more easily transported and then resedimented (Gibson et al., 1999).

2.6.2. Stratigraphic Control on Alteration and Mineralization

Alteration assemblages depend in part on the lithofacies present as the geometry and size of the alteration zones are largely controlled by the permeability and porosity of the host rock (e.g. Gibson, 2005). In the Pilley's Island district, the lithology and lithofacies strongly control VMS-related alteration and mineralization. In the mafic volcanic-dominated Pilley's Hills and Liquor Street panels, alteration assemblages are predominantly chlorite, with lesser sericite, hematite, and (±Fe)-carbonate. In contrast, in the felsic-dominated panels (e.g. Spencer's Dock, 3B and Old Mine panels), the alteration is dominated by sericite, quartz, with lesser chlorite, and carbonate. Given the predominance of mineralization within felsic panels, the remaining discussion is concentrated on the nature of alteration and mineralization within the felsic panels.

As illustrated above, the Spencer's Dock panel consists predominantly of flows with less abundant volcaniclastic rocks, whereas the 3B and Old Mine panels consist of predominantly volcaniclastic rocks (Fig. 2-3ACD & 2-4). The Spencer's Dock panel is characterized by restricted alteration related to focused fluid flow that causes increased alteration intensity near mineralized zones (disseminated into stringer and massive sulfide), but is laterally restricted by fractures and permeable zones in the coherent volcanic flows. This is particularly so proximal to perlitic cracks in the flows, in hyaloclastite and in breccias (Fig. 2-3B), in which primary fractures are interpreted to

have facilitated fluid flow. In the 3B and Old Mine panels, alteration is localized and is more intense in the volcaniclastic intervals, particularly so proximal to the mineralized zones. Quartz and sericite alteration in volcaniclastic intervals is intense and pervasive and commonly occurs with disseminated to stringer sulfide mineralization (Fig. 2-6EF). In contrast, the quartz and sericite alteration of dacitic flows is generally weak and occurs with weak chlorite alteration locally (Fig. 2-6G), and is often associated with fractures as in the Spencer's Dock panel.

The mineralization styles at Pilley's Island are also controlled by host lithofacies. The two main processes by which VMS deposits form, include: 1) seafloor exhalative activity; and 2) sub-seafloor replacement (Franklin et al., 1981; Lydon, 1988; Doyle and Allen, 2003; Franklin et al., 2005). While there is minor exhalative sulfide (hematitic jasper with abundant stringer and massive sulfide) in the basaltic rocks associated with the Pilley's Hills panel (Fig. 2-5F), the vast majority of deposits in the Pilley's Island district have features suggestive of replacement. However, the nature of the replacement varies as a function of lithofacies.

Doyle and Allen (2003) outlined numerous textures that are indicative of sub-seafloor replacement, many of which are found in the various deposits at Pilley's Island. Their criteria for replacement include: 1) mineralization hosted within rapidly emplaced volcanic or volcaniclastic facies; 2) relicts of host volcanic rocks within mineralization; and 3) gradational replacement fronts between host lithofacies and mineralization. Additional evidence for sub-seafloor sulfide replacement include: 1) massive sulfide deposits discordant to bedding; and 2) continuous strong hydrothermal alteration into the

hanging wall without a break in alteration intensity, although these two criteria alone are not diagnostic. Most Pilley's Island VMS deposits have several characteristics of sub-seafloor replacement.

In the Spencer's Dock and Jane's Cove deposits, the alteration and mineralization is focused along fractures in the dacitic flow-dominated facies resulting in deposits with elongate, stratabound morphologies (Fig. 2-3A) and the deposits have gradational boundaries from massive pyrite outwards into semi-massive to disseminated stringer sulfides in perlitic-fractured dacite. This gradational boundary also occurs within a large halo of strong hydrothermal alteration (Fig. 2-3A). The massive pyrite lenses contain approximately 10% sericite, which likely represents resistant relict host rock that was not replaced.

The 3B, Bumble Bee Bight and Old Mine deposits are hosted within porous volcaniclastic rocks and the sulfides contain abundant relicts of host rocks, including quartz crystals, fine tuff and lapilli (Fig. 2-6BC). The deposits also have distinctive hanging wall and footwall alteration haloes (Fig. 2-3ACD), and massive to stringer and disseminated sulfide mineralization occurs throughout both the hanging wall and footwall strata (Fig. 2-3B). Replacement-style deposits in volcaniclastic-dominated successions have also been described at Duck Pond, Boundary and the Tulks volcanic belt deposits in central Newfoundland (Squires et al., 2001; Squires and Moore, 2004; Hinchey, 2007) as well as the aforementioned Rosebery and Hercules deposits in Tasmania (Large et al., 2001c).

The Rowsell's Cove deposit and Bull Road showing are not controlled by the host lithofacies and represent slumped and transported clastic sulfide deposits (e.g. Thurlow et al., 1975; Gibson and Watkinson, 1990). It is likely that these deposits formed by either: 1) resedimentation/ slumping of unconsolidated debris (e.g. collapse breccia of volcanic and sulfide composition) from a volcanic flow or dome, resulting in downslope debris flows; or 2) pyroclastic volcanism along the flanks of the volcanic dome hosting a VMS deposit (Thurlow et al., 1975). Evidence for pyroclastic eruption is lacking in both panels; therefore, it is likely that they formed by resedimentation/ slumping of unconsolidated debris. These deposits are very similar to the transported Maclean orebodies in the Buchans VMS district, central Newfoundland (Thurlow et al., 1975; Stewart, 1987).

2.6.3. Post-mineralization Modification

The stratigraphy of Pilley's Island has been complicated by multiple faulting events, which have been interpreted based on their crosscutting relationships and orientations (Fig. 2-3 & 2-4). Imbricate thrust faults were caused by pre-Middle Silurian collision with the Ganderian margin during the closure of the Iapetus Ocean (Kerr, 1996; van Staal and Barr, 2011). The first event produced north to northwestward-directed thrust faulting, which formed the Mud Pond, Pilley's Island and Boot Harbour terrane boundaries (Fig. 2-2 & 2-4) (Kerr, 1996). Secondary intraterrane faulting occurred within the Pilley's Island terrane to produce the Hoskin's Cove and Ches' Dome faults, which have broadly northwestward thrust direction and are arcuate in plan view due to topographic relief (Fig. 2-3 & 2-4). The secondary faults are crosscut by the Liquor Street fault, which has northward thrust direction (Fig. 2-3 & 2-4). The final event of faulting

produced the dextral strike-slip Lobster Cove fault, which forms the northern boundary of the Roberts Arm Group and Springdale Group and truncates all previous faults (Fig. 2-3) (Calon and Szybinski, 1988; Kerr, 1996).

Although the stratigraphy is very well preserved (i.e., no penetrative metamorphic fabrics or local brittle shearing), the southeast dipping, imbricate thrust faulting within the district often truncates zones of alteration and mineralization. Specifically, footwall rocks of the Spencer's Dock and Jane's Cove have been almost entirely truncated by the Liquor Street fault (Fig. 2-3B) and the Bumble Bee Bight and Old Mine deposit both occur within 10s of metres of underlying thrust faults (Fig. 2-3D). The quantification of offset across the various thrust faults is difficult due to lack of marker units in each panel. Nevertheless, the other felsic panels at Pilley's Island, and throughout the region, merit additional exploration to test for offset alteration and mineralization in different locations and at different depths in the panels.

2.6.4. Exploration Implications

The stratigraphic reconstruction of Pilley's Island indicates that favourable zones of mineralization lie within felsic volcanic intervals that are flow-dominated or volcaniclastic-dominated. Massive sulfide deposits in flow-dominated facies host much larger deposits, although they are much lower in grade (e.g. Jane's Cove and Spencer's Dock deposits). Conversely, massive sulfide deposits in volcaniclastic facies are smaller, but higher grade (e.g. Old Mine and 3B deposit). This result is expected because sub-seafloor replacement is considered to be a more efficient process than sulfide accumulation within seafloor sulfide mounds below black smokers, or within fractured

volcanic flows, because it traps a higher quantity of the overall metal budget from exhaling hydrothermal fluids (Doyle and Allen, 2003). This indicates how the host lithofacies can have major control on grade and tonnage.

Difficulty arises in targeting sulfide deposits because most of the rocks in the felsic panels have undergone strong hydrothermal alteration and alteration mineralogy alone does not provide sufficient indication of the presence of mineralization. For more effective exploration of VMS deposits in imbricated successions, more closely spaced drilling is required to better understand the geometry of felsic volcanic-dominated thrust panels. Additionally, the stratigraphy needs to be integrated with lithogeochemistry and advanced geophysical modeling for a better understanding of the location of VMS deposits in imbricated terranes.

The complicated stratigraphy at Pilley's Island is mainly a result of thrust faulting and imbrication of mineralized and barren panels. This is a widespread problem in Phanerozoic VMS districts in orogenic belts (e.g. Buchans, Newfoundland; Bathurst, New Brunswick; Iberian Pyrite Belt, Spain) (Calon and Green, 1987; van Staal et al., 2003a; van Staal et al., 2003b; Castroviejo et al., 2011) and the recognition of thrust faults and understanding their geometry and panel juxtaposition is essential to the reconstruction of a VMS deposit or district.

2.7. Conclusions

The Pilley's Island VMS district contains 6 VMS deposits that are hosted within imbricate thrust panels consisting of predominantly felsic volcanic lithofacies. These panels are juxtaposed between barren mafic volcanic panels. Detailed mapping and drill

core logging have allowed a reconstruction of the volcanic stratigraphy and has improved the understanding of the role of primary lithofacies control on mineralization and alteration style, and the effects of post-depositional thrust faulting on VMS mineralization within a thrust imbricated volcanic succession.

Lithofacies analysis has allowed an interpretation of the depositional setting of the VMS deposits. Felsic flow-dominated stratigraphy in the Spencer's Dock panel represents lobe-hyaloclastite facies resulting from episodic endogenous flow-dome growth, migrating dacitic flows and associated hyaloclastite formation along the flow margins within a deep-water extensional fissure system. Conversely, volcaniclastic-dominated stratigraphy of the 3B and Old Mine panels formed under different depositional settings, involving alternating episodes of lava eruption and volcaniclastic deposition. These likely formed in a shallowing, subaqueous environment or a transition from flow and dome extrusion in a vent proximal environment to a more distal volcaniclastic-dominated facies, which are more easily transported and resedimented.

Lithofacies analysis also allows an interpretation of the stratigraphic control on alteration and mineralization. Alteration assemblages depend on the composition of host lithofacies and the size and intensity of the alteration is controlled by the permeability and porosity of the host lithofacies. The less porous and less permeable, flow-dominated lithofacies of the Spencer's Dock panel results in alteration that is localized laterally along fractures and more permeable zones such as perlitic cracks, breccia intervals, and in hyaloclastite. Volcaniclastic-dominated lithofacies in the 3B and Old Mine panels are

more porous and permeable resulting in the localization of more intense and pervasive quartz and sericite alteration along tuff and lapilli tuff intervals.

Most deposits in the Pilley's Island VMS district show evidence for sub-seafloor replacement. For example, the Spencer's Dock and Jane's Cove deposits are characterized by gradational boundaries between massive sulfide and perlitic-fractured dacite. This transition also coincides with a large halo of strong hydrothermal alteration. Massive pyrite lenses also contain approximately 10% sericite, which may represent a relict host rock component that was not replaced. Deposits in the 3B and Old Mine panels have similar replacement features with large, gradational alteration and mineralization haloes throughout more permeable strata. The 3B and Old Mine deposits also contain relicts of host rocks (quartz crystals, fine tuff and lapilli, and interstitial sericite) suggestive of sub-seafloor sulfide replacement.

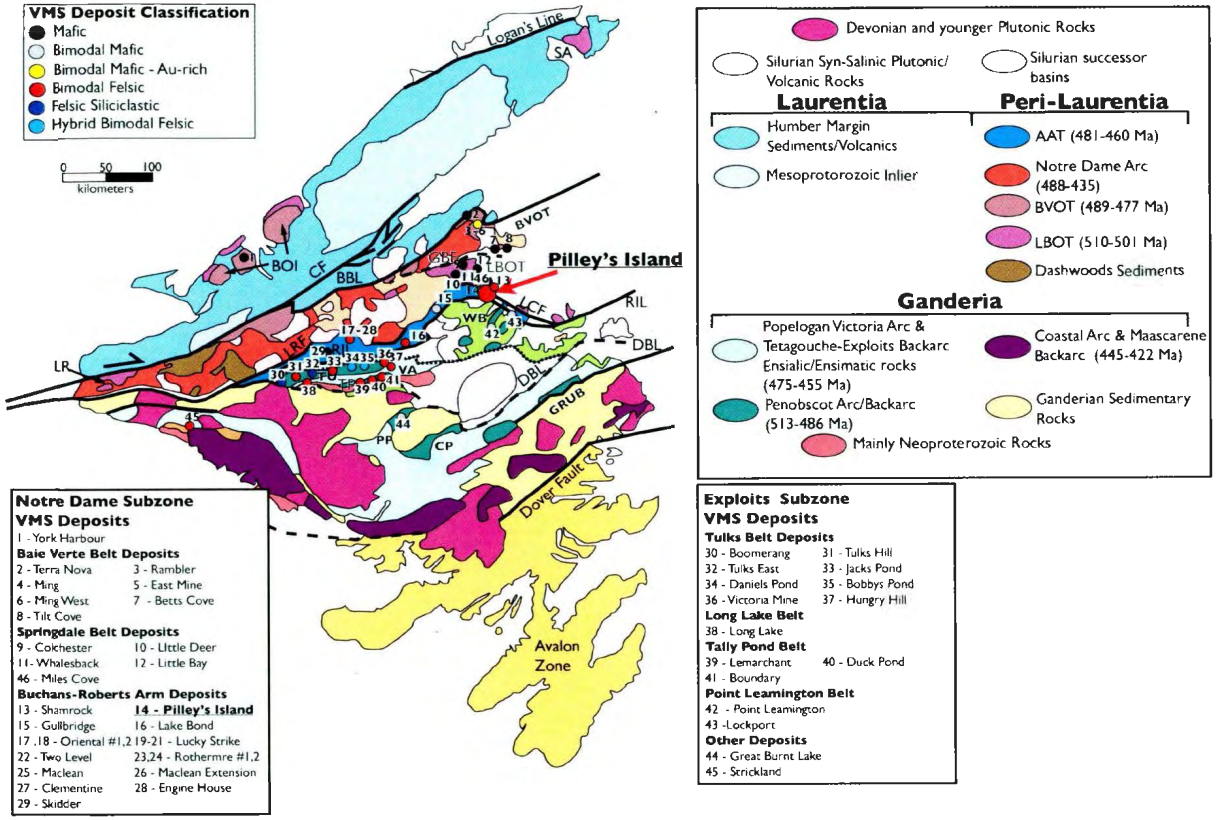

Figure 2-1 Geological map of the Newfoundland Appalachians with tectonostratigraphic zones, accretionary tracts, VMS deposits their classifications and associated belts. Map tectonostratigraphy modified from van Staal (2007) and van Staal and Barr (2011). Volcanogenic massive sulfide (VMS) deposit classification from Piercey (2007c) and Hinchey (2011). Abbreviations: BBL Baie Verte Brompton Line; BOI - Bay of Islands; BVOT = Baie Verte Oceanic Tract; CF = Cabot Fault; CP = Coy Pond Complex; DBL = Dog Bay Line; GBF = Green Bay Fault; GRUB = Gander River Ultramafic Belt; LBOT = Lushs Bight Oceanic Tract; LCF = Lobster Cove Fault; LR = Long Range; LRF - Lloyds River Fault; PP = Pipestone Pond Complex; RIL = Red Indian Line; SA - St. Anthony; TP = Tally Pond Belt; TU = Tulks Volcanic Belt; VA = Victoria Arc; WB = Wild Bight Group.

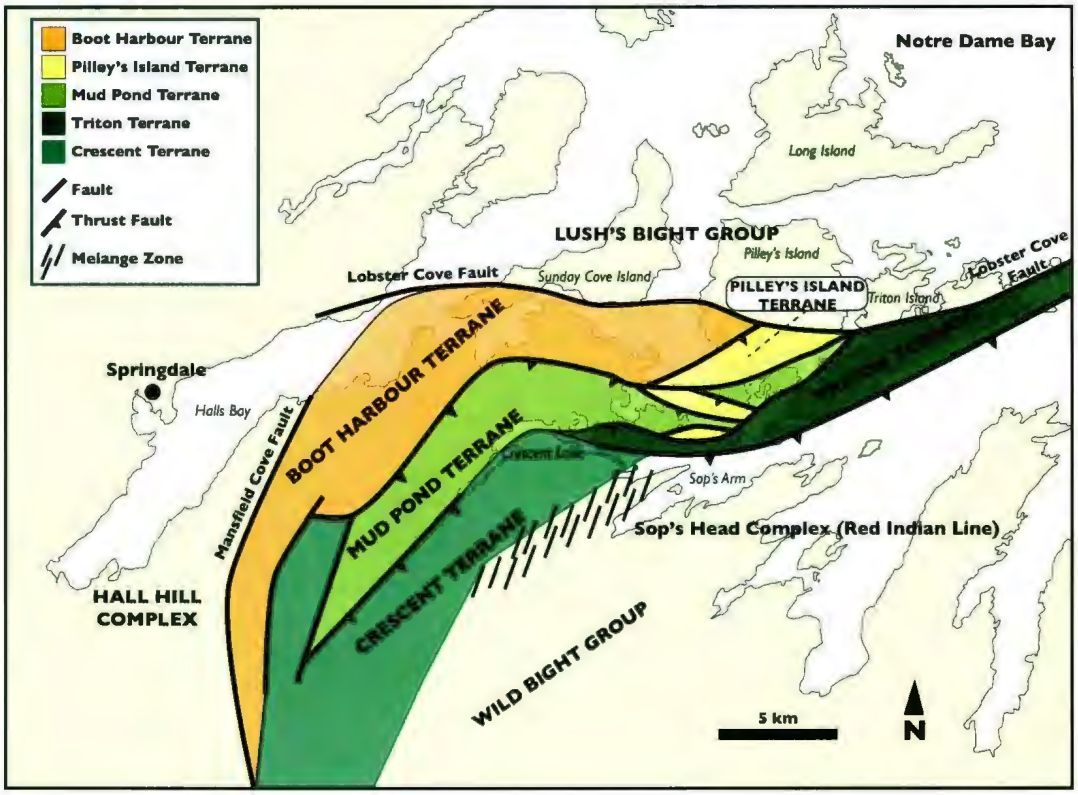

Figure 2-2 Simplified geological map of the northern Roberts Arm Group showing the location of Pilley's Island terrane and adjacent terranes that have been imbricated due to faulting. Modified from Kerr (1996)

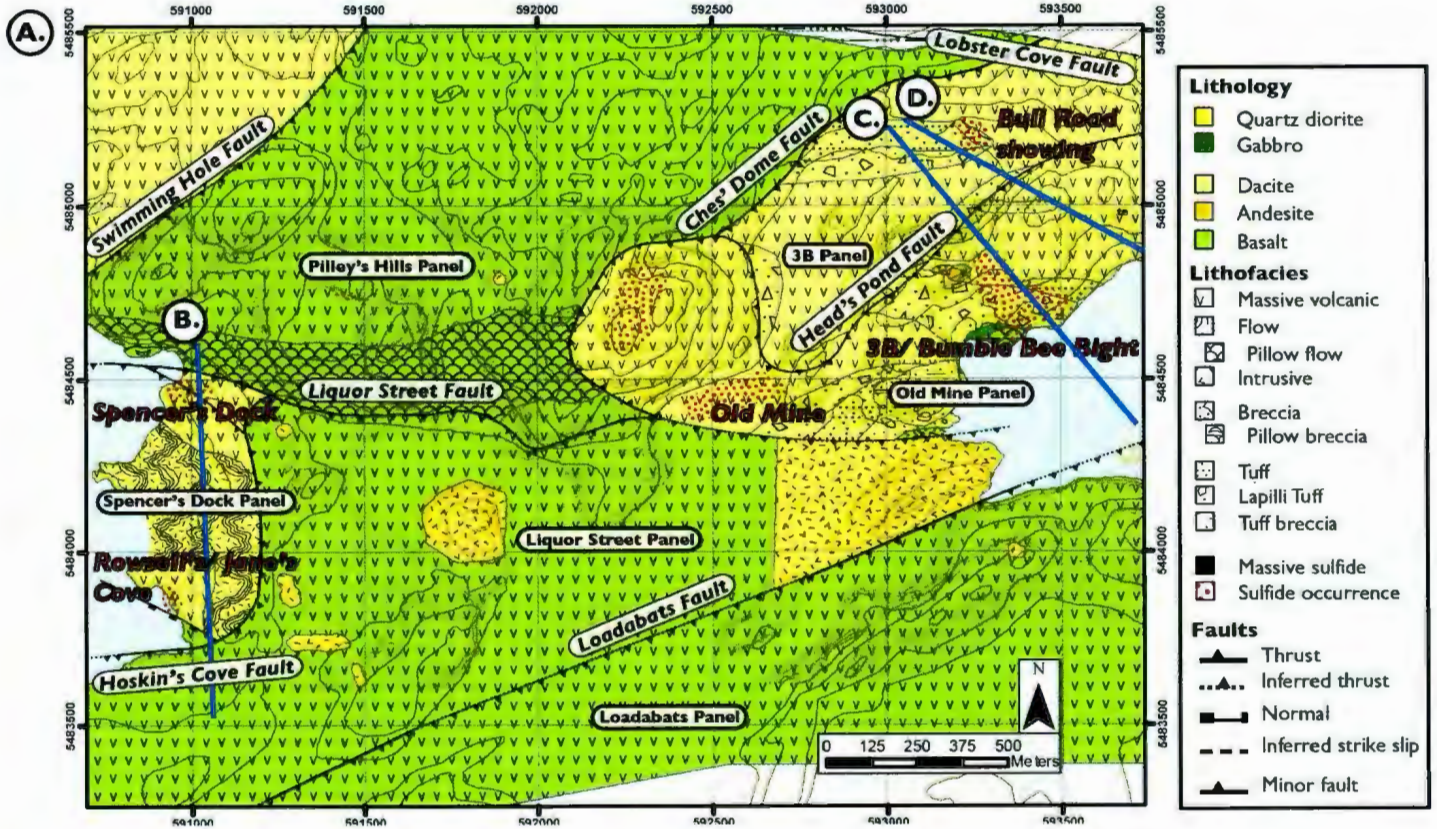

Figure 2-3 Geological map of the Pilley's Island VMS district and representative cross sections through the deposits (next page) A. Surface map of the Pilley's Island VMS district showing the distribution of different lithologies and lithofacies in the area, as well as the thrust faults that juxtapose different units in the area. (Continued on next page)

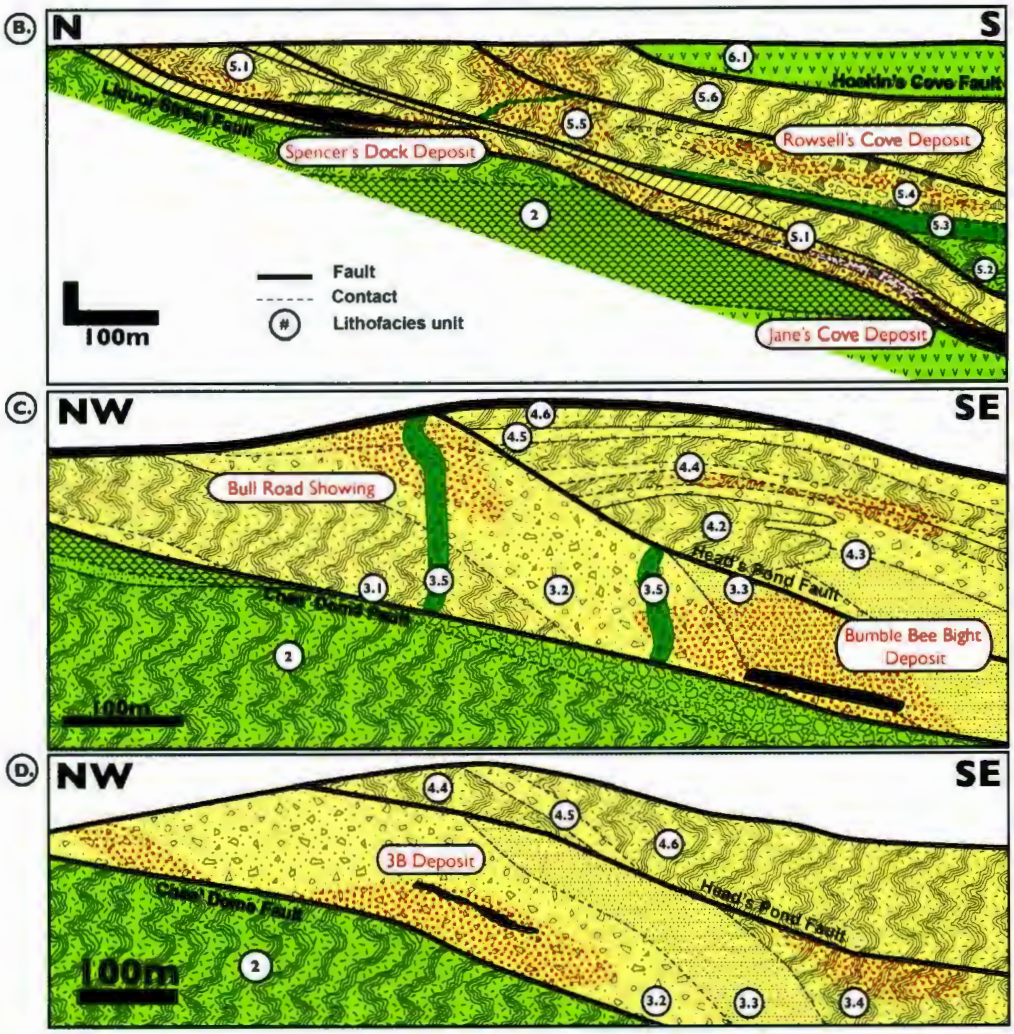

Figure 2-3 ***cont'd.*** **B. Cross section through the Spencer's Dock panel, showing the three different deposits at different stratigraphic levels. C. Cross section through portions of the 3B and Old Mine panels and the host lithofacies of the Bull Road showing and Bumble Bee Bight deposit. D. Cross section through the 3B and Old Mine panels, including the 3B deposit. Legend in Fig. 2-3A.**

Table 2-1 Summary of the main textures and contact relationships of the coherent volcanic lithofacies in the Pilley's Island VMS district.

Terrane	Thrust Panel	Unit	Approximate thickness	Lithofacies/ Emplacement	Textures	Contacts
Boot Harbour	Swimming Hole	1.1	Unknown	Massive coherent dacite	Massive; alteration (possibly flow) banding	Inferred
Pilley's Island	Pilley's Hills	2	500m	Undifferentiated pillowed and massive basaltic flow	Pillow margins	Bleached and altered pillow margins; pillow breccia; chert and jasper void replacement
	3B	3.1	100m	Dacitic flows	Clast-rotated breccia and hyaloclastite	Lower contact faulted (Liquor Street), sharp against 3.2 above
		3.4	100m	Dacitic flows	Flow banded; quartz-, carbonate- amygdaloidal	In-situ brecciation against 3.3 tuff below, faulted above (Head's Pond)
		3.5	20m	Mafic dikes	Coarsely crystalline plagioclase, pyroxene	Bleached and chilled margins; cross-cuts multiple units
	Old Mine	4.1	80-100m	Massive to pillowed basalt flows	Pillow margins; chert and jasper void replacement; quartz-, chlorite-amygdaloidal	Lower contact faulted (Head's Pond); sharp, brecciated upper contact
		4.2	40m	Dacitic flows	Amygdaloidal, flow banded and clast-rotated breccia	Brecciated upper and lower contacts, clast-rotated breccia between flows
		4.4	20-30m	Dacitic flows	Amygdaloidal; contorted flow banding	Perlitic, devitrified at upper contact; clast-rotated breccia on lower contact
		4.6	Unknown; eroded at surface	Dacitic flows	Contorted flow banding; quartz-, chlorite-amygdaloidal	Flow-banded, clast-rotated breccia between subunits and at top erosional contact; obscured lower contact
	Spencer's Dock	5.1	50-100m	Massive coherent dacite with resedimented breccia clasts	Quartz-amygdaloidal; polylithic breccia ± massive sulfide clasts	Faulted lower contact (Liquor Street); minor fault truncates upper contact
		5.2	120m	Basaltic flows	Breccia with siliceous matrix, leucocratic rims on some breccia clasts	Thick basaltic breccia (47m) below basalt, lower contact faulted
		5.3	50m	Gabbro intrusion	Locally brecciated with coarse pyrite-silica-calcite matrix filling.	Weakly sheared contacts
		5.5	100m	Dacitic flows	Spheroidal lithophysae; flow banding	Faulted lower contact, eroded at surface; autobreccia with randomly oriented and flow-banded fragments between flows
		5.6	110-170m	Massive coherent dacite	Quartz-, pyrite- amygdaloidal; perlitic fracturing	Faulted upper and lower contact
	Liquor Street	6.1	Unknown	Undifferentiated pillowed and massive basaltic flows	Quartz-, carbonate-, chlorite- amygdaloidal; pillow margins	Pillow breccias between flows; upper and lower contacts faulted (Liquor Street and Loadabats, respectively)
		6.2	Unknown	Quartz diorite intrusions	Feldspar-phyric	Bleached basalt xenoliths (unit 6.1)
Mud Pond	Loadabats	7.1	Unknown	Basaltic flows	Quartz-, calcite-, chlorite- amygdaloidal; pillow margins	Pillow breccia and jasper between flows; upper and lower contacts not observed.
		7.2	Unknown	Gabbro intrusions	Coarse grained chlorite replacing pyroxene; sericite replacing plagioclase laths	Hematite/carbonate shear zones; chilled margins

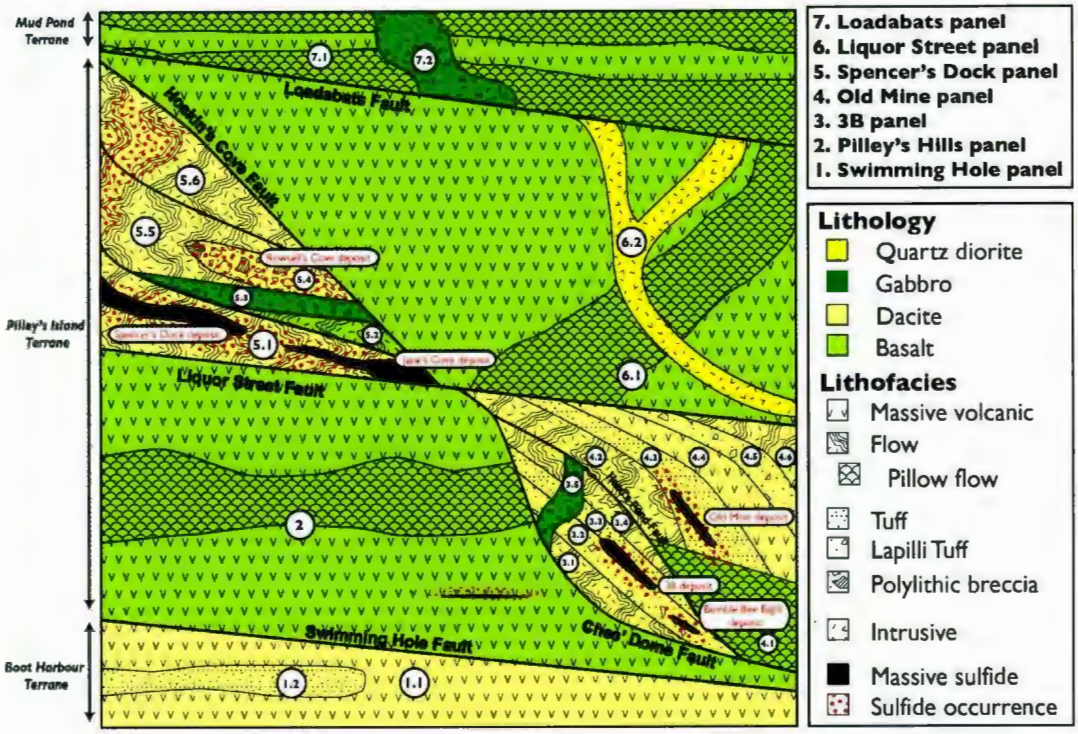

Figure 2-4 Schematic illustration (not to scale) of the volcanic stratigraphy within each panel and field relationships between stratigraphic units and VMS deposits within the Pilley's Island terrane, including juxtaposition by thrust faults.

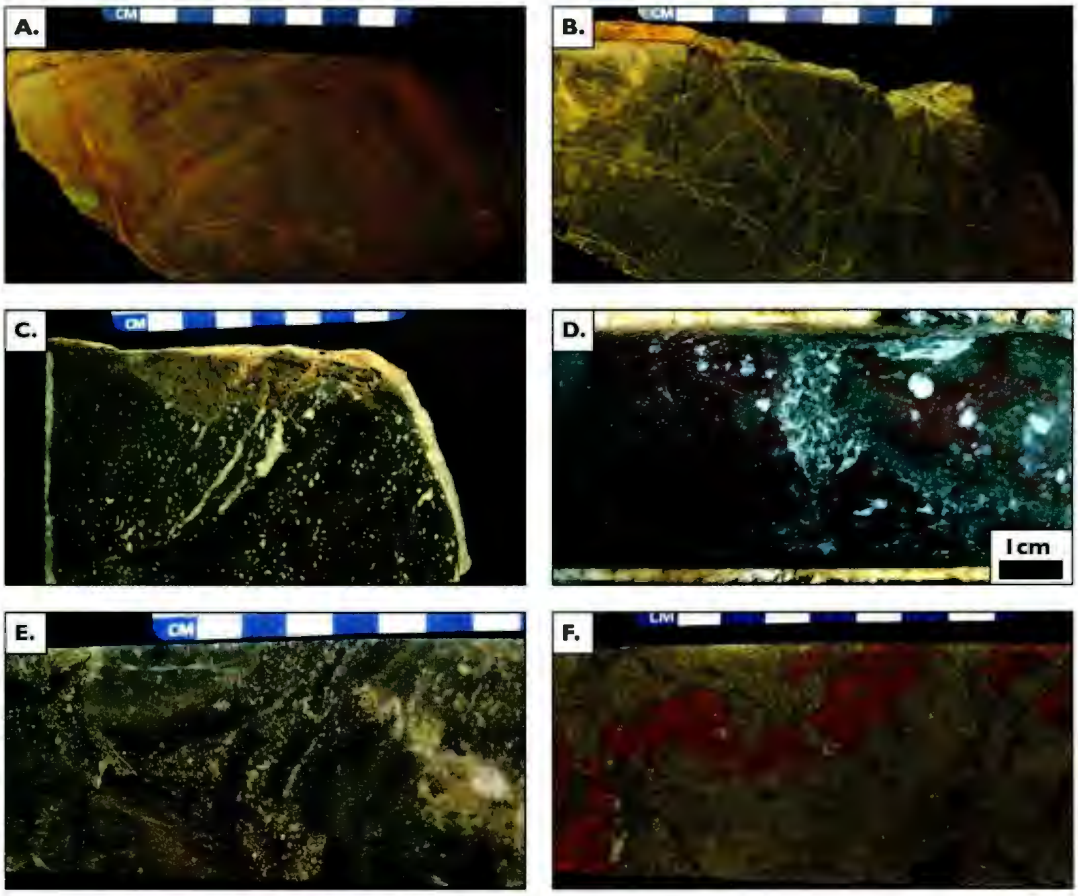

Figure 2-5 Representative samples from the Swimming Hole panel and Pilley's Hills panel. A. Fine felsic tuff with strong hematite alteration in unit 1.2. B. Example of chlorite and sericite defining flow banding in dacitic flow constituting unit 1.2. C. Massive, quartz- and carbonate-amygdaloidal basaltic flow in unit 2. D. Basalt pillow breccia with angular hematite-altered clasts hosted within a chlorite-, quartz-, and carbonate-rich matrix in unit 2. E. Disseminated, blebby pyrite between pillow margins in pillow basalt flow of unit 2. F. A rare zone of massive sulfide mineralization in unit 2, with abundant bright red hematitic jasper within massive pyrite and sphalerite.

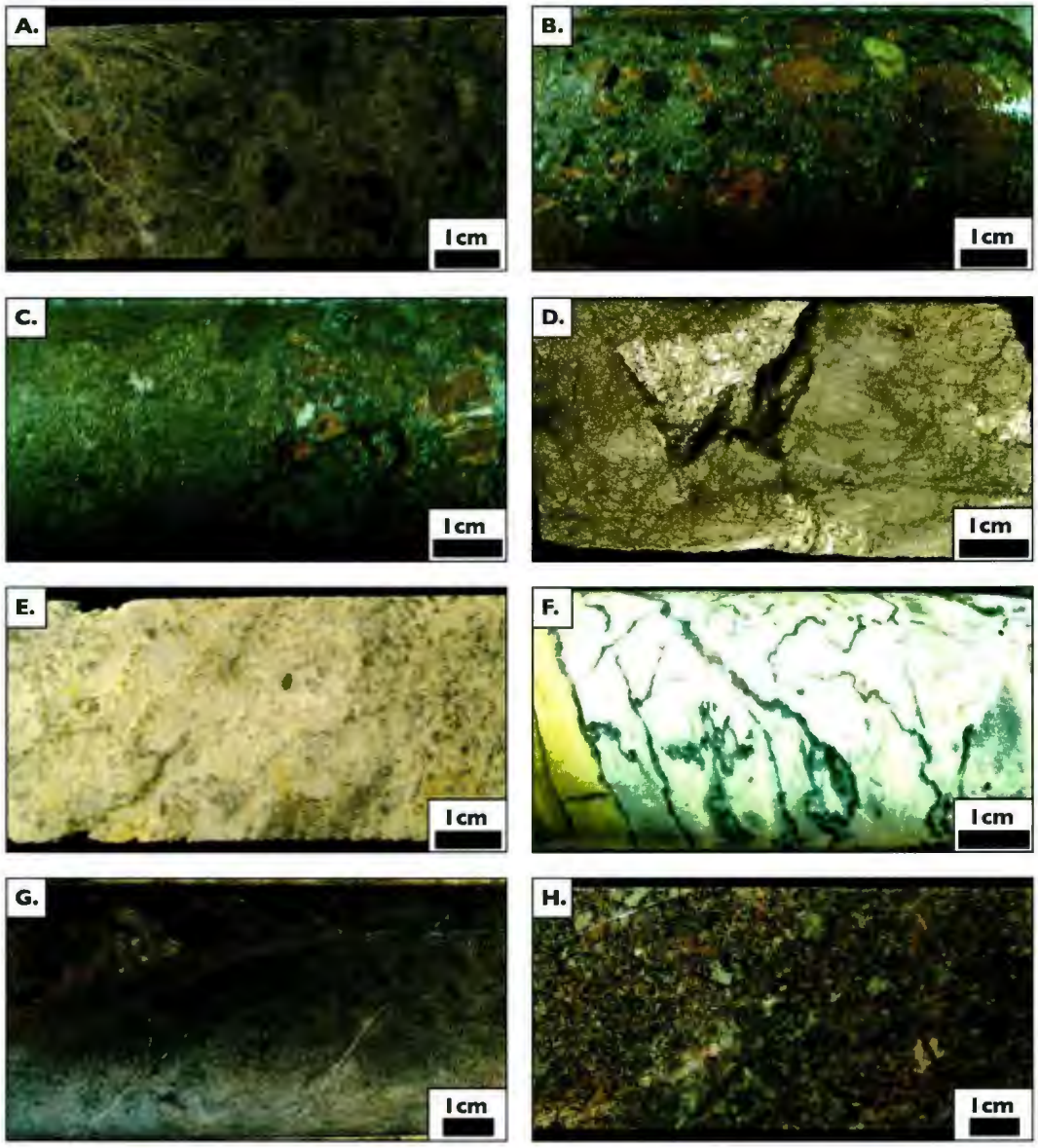

Figure 2-6 Representative samples from the 3B panel. A. Perlitic, pseudofragmental texture defined by sericite and chlorite alteration, characteristic of dacitic flows in unit 3.1. B. Polylithic lapilli tuff comprised of both mafic and felsic clasts with variable alteration (chlorite, K-feldspar, sericite). C. Fragment-rich sulfide zone from the 3B deposit in unit 3.2, with pyrite hosting potassium feldspar-altered lapilli and other fine volcaniclastic particles. D. Massive pyrite and chalcopyrite with trace sphalerite and galena with interstitial sericite and quartz from the 3B deposit in unit 3.2. E. Mineralized and intensely sericite- and quartz-altered felsic tuff (unit 3.3) with minor bedding/ clast deformation. F. Pyrite and sphalerite filling deformed fractures throughout unit 3.3, intensely quartz- and sericite-altered felsic tuff. G. Chlorite- and sericite-altered flow banding in dacite (unit 3.4). H. Coarsely crystalline mafic dike with pyroxene and plagioclase phenocrysts are mostly altered to chlorite and sericite, respectively, and characteristic of unit 3.5.

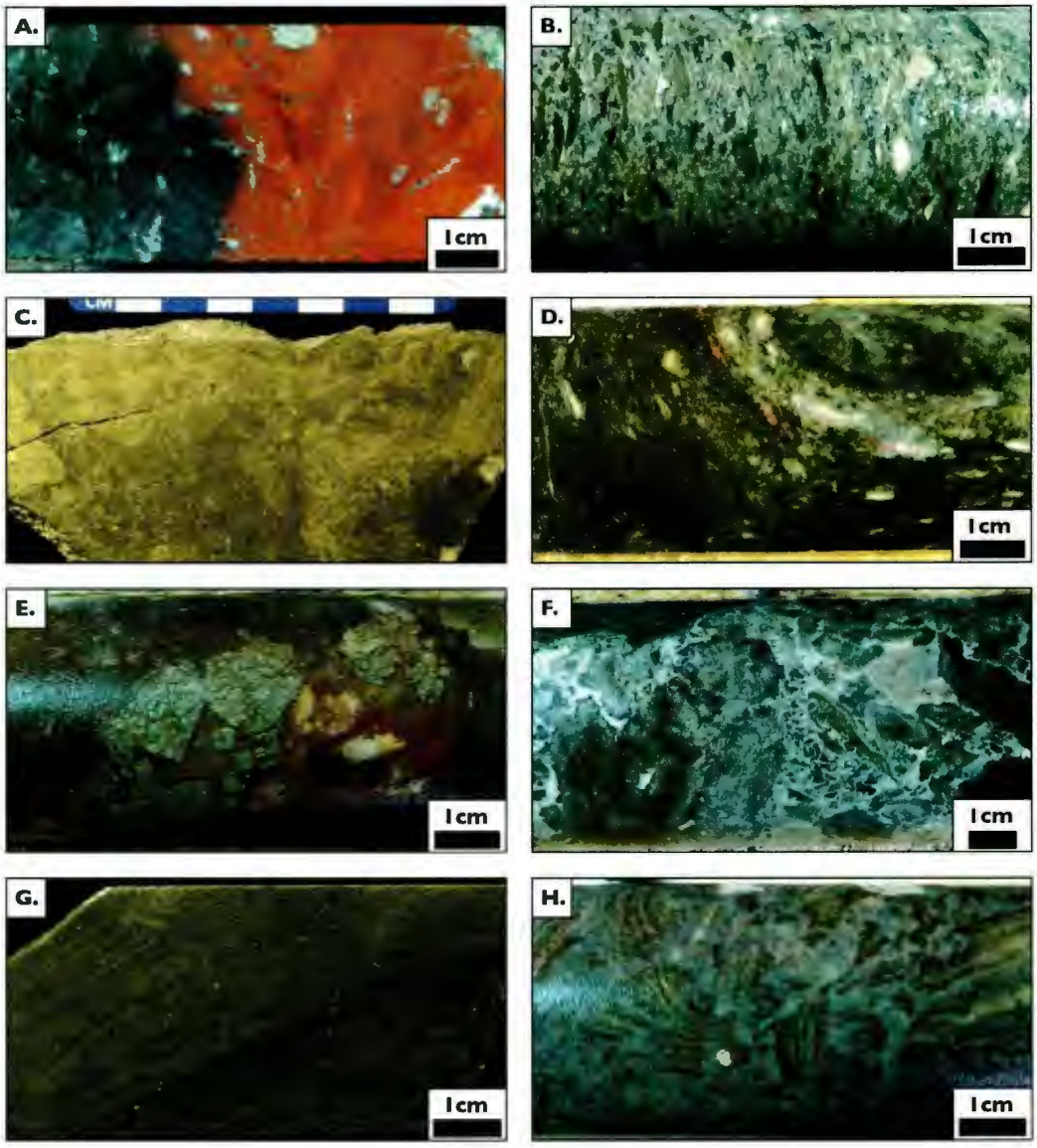

Figure 2-7 Representative samples from the Old Mine panel. A. Pyrite mineralization within interpillow hematitic jasper in unit 4.1 pillow basalt. B. Lapilli tuff with formerly glassy, deformed, slightly foliated clasts in quartz- and sericite-altered matrix (unit 3.2). C. Massive pyrite and chalcopyrite (with trace sphalerite) from the Old Mine deposit in unit 4.3. D. Unit 4.4 quartz- and carbonate-amygdaloidal dacitic flow, characterized by contorted flow banding with variable sericite and chlorite alteration. E. Coarse subhedral pyrite and sphalerite in unit 4.4 dacitic flow with hematitic jasper. F. Dacitic hyaloclastite with intense quartz alteration in the matrix and weakly interlocking dark chlorite- and sericite-altered clasts. G. Undulating flow banding defined by sericite- and chlorite-alteration within a dacitic flow in unit 4.6b. H. Dacitic breccia (unit 4.6c) with blocky, tabular, flow banded and rotated clasts exhibiting variable orientation in a strongly quartz-altered matrix.

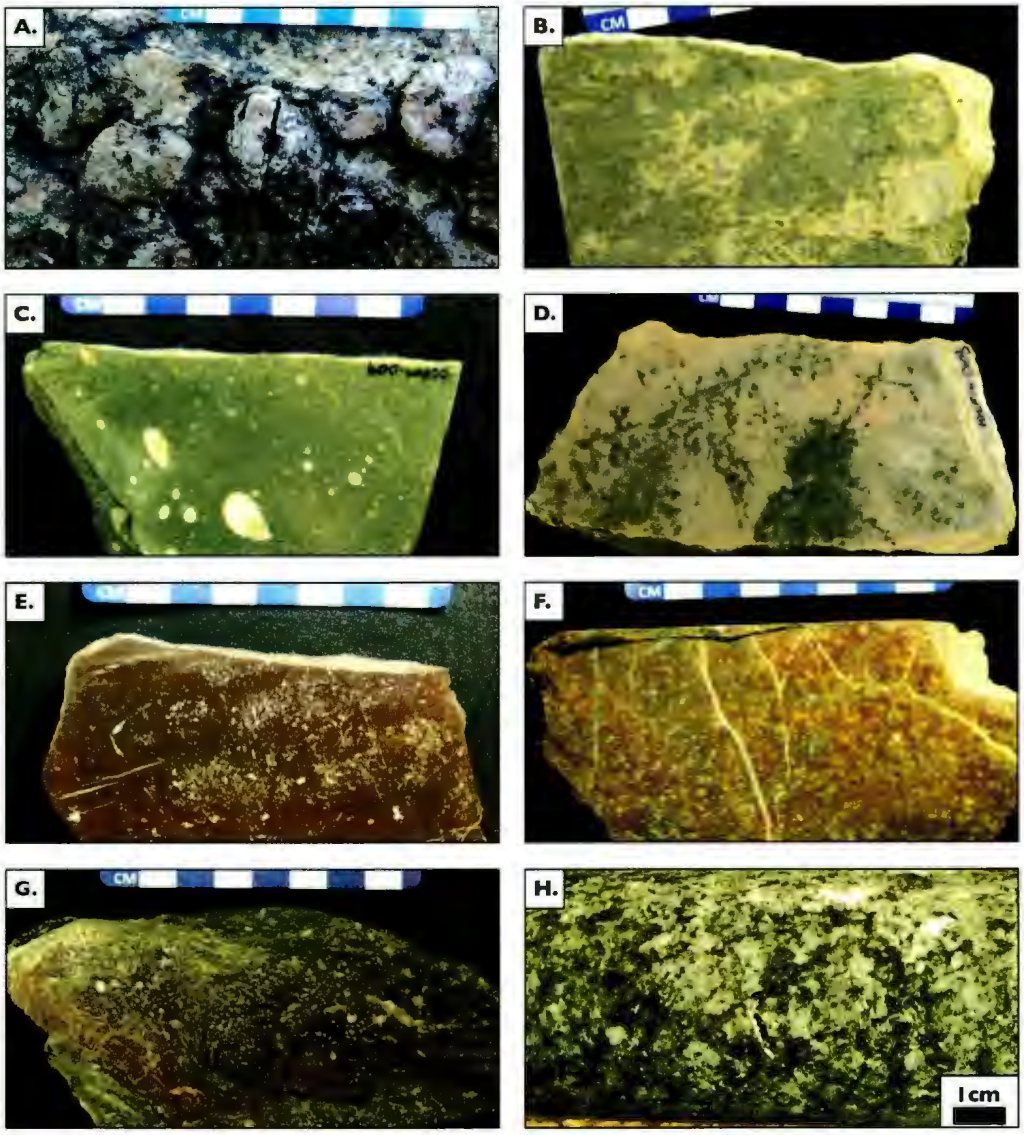

Figure 2-8 Representative samples from the Spencer's Dock panel, Liquor Street panel and Loadabats panel. A. Spheroidal lithophysae, with hollow cores, in devitrified dacitic flow (unit 5.5). B. Characteristic strong quartz-sericite alteration of dacitic flows associated with zones surrounding sulfide mineralization in unit 5.5. C. Lenticular quartz-carbonate amygdules in massive dacite, which have been partially replaced by euhedral pyrite (unit 5.6). D. Disseminated and veinlet pyrite, with sparse flecks of sphalerite and chalcopyrite, in massive dacite above the Jane's Cove deposit (unit 5.6). E. Representative sample from Liquor Street panel, consisting of massive hematitic and quartz-amygdaloidal basalt from unit 6.1. F. Quartz diorite intrusion (unit 6.2) characterized by hematite stained, coarse and euhedral plagioclase phenocrysts, commonly with sericite alteration, in a sericite- and chlorite-altered matrix. G. Massive quartz- and carbonate-amygdaloidal basaltic flow with bands of strong hematite and chlorite alteration, characteristic of unit 7.1. H. Gabbro intrusion (unit 7.2) characterized by coarse, subhedral, olive green pyroxene and lighter plagioclase phenocrysts.

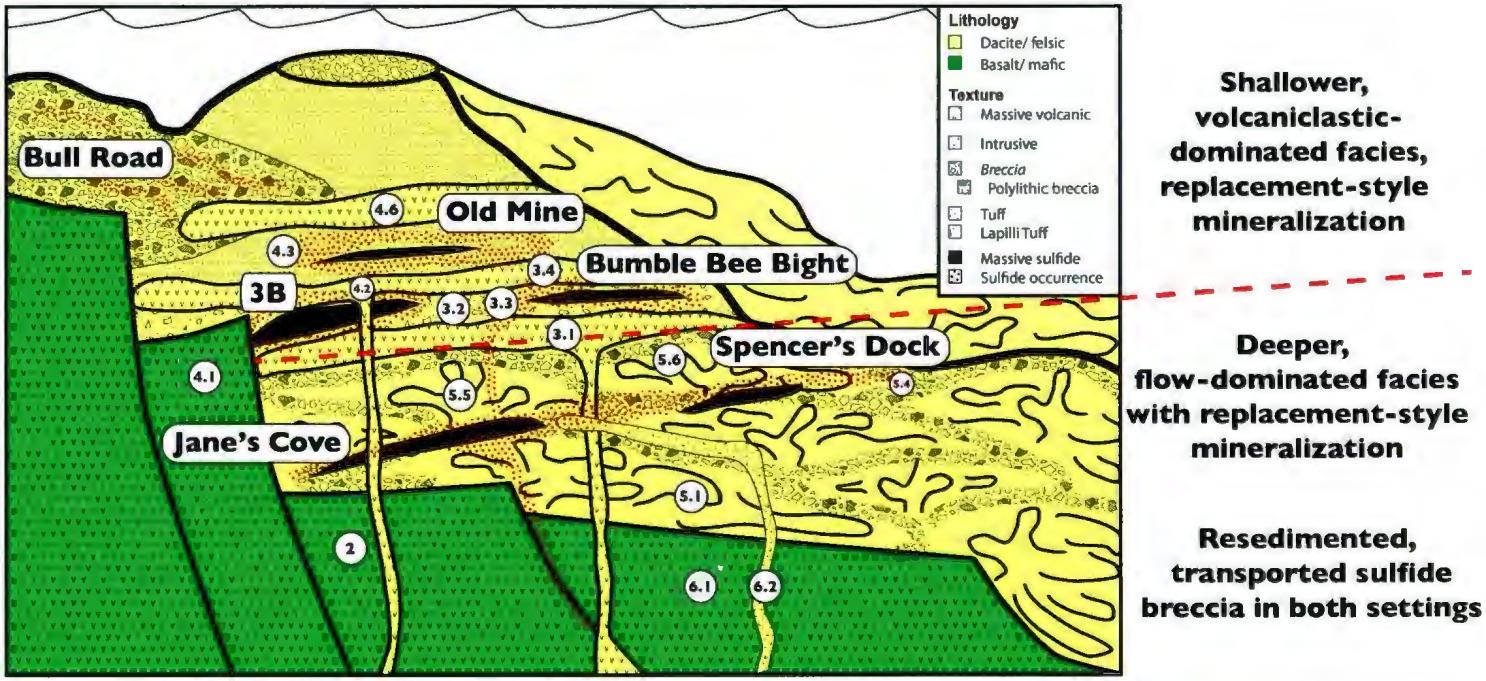

Figure 2-9 Schematic section illustrating a possible depositional environment for the Pilley's Island deposits within either flow-dominated or volcaniclastic-dominated stratigraphy. This proposed depositional setting is a combination of the sub-seafloor replacement models presented in Doyle and Allen (2003) and lobe-hyaloclastite volcanic successions presented in Gibson et al. (1999) and Gibson and Watkinson (1990). In this depositional model, the VMS mineralization is controlled by either the exploitation of porous and permeable fluid pathways (between flows and via fracturing, or in volcaniclastic layers) and subsequent sub-seafloor replacement, or by the transport of sulfide and volcanics as breccia clasts. An alternative to this depositional environment may be that the change in lithofacies reflects different parts of the basin, such that flows and domes are more abundant in environments more proximal to the vent, and volcaniclastic dominated facies are more distal to the vent as they are more easily transported and then resedimented (Gibson et al., 1999).

Chapter 3: The Pilley's Island Volcanogenic Massive Sulfide District, Central Newfoundland: Part 2. Lithogeochemistry, Petrogenesis, Tectonic Setting, and Hydrothermal Reconstruction

3.1. Abstract

Pilley's Island in the Central Mobile Belt of Newfoundland, Canada, hosts a cluster of bimodal felsic Zn-Pb-Cu-Au-Ag volcanogenic massive sulfide (VMS) deposits within the Ordovician Annieopsquotch accretionary tract (AAT). Primary, immobile element lithogeochemistry has been used at Pilley's Island to identify potential tectonic environments of formation, and to help determine the petrogenesis of the volcanic rocks associated with mineralization. Hydrothermal alteration using secondary, or mobile element, lithogeochemistry is also evaluated. Collectively, a spatial analysis of the results provides potential tools to vector towards mineralization.

The Pilley's Island district contains six VMS deposits that vary in style and are hosted within imbricate thrust panels. Some deposits are hosted within felsic volcanic- and volcaniclastic-dominated thrust panels (Spencer's Dock panel, 3B panel and Old Mine panel), which are juxtaposed between mafic volcanic panels that lack significant sulfide mineralization (Liquor Street panel, Pilley's Hills panel). The mafic volcanic rocks of the Pilley's Island terrane are calc-alkalic to transitional arc rocks that were derived from a slab metasomatized, weakly depleted to weakly enriched mantle wedge within an Ordovician peri-Laurentian subduction zone. Given the broad similarities in the trace element signatures between the felsic rocks and their mafic counterparts, the felsic

volcanic rocks formed via remelting of a hydrated, arc basalt substrate. The felsic rocks are interpreted to have formed during arc rifting and extensional geodynamic activity. Magma upwelling produced an elevated geothermal gradient, increased fracture permeability and porosity and produced fluid conduits that allowed for the convective recharge and discharge required to form the VMS deposits of the district.

Hydrothermal alteration at Pilley's Island is extensive and varies depending on the dominant lithofacies within the thrust panel. In porous volcaniclastic-rich stratigraphy alteration is dominated by sericite and lesser chlorite that is unfocused and widespread rather than pipe-like in geometry. Sericite alteration zones have been subdivided using near infrared-short wave infrared (NIR-SWIR) spectroscopy into phengite, illitic phengite, muscovite and illitic muscovite zones. Phengite and illitic phengite form large (>500m) haloes surrounding the deposits and show a marked increase in abundance proximal to mineralization. Illitic muscovite and muscovite are the most proximal alteration assemblages and form small (<50m) haloes surrounding the deposits. Chlorite alteration is less abundant around the deposits, ubiquitous in mafic volcanic-dominated thrust panels, and although it is not immediately associated with mineralization, it does occur regionally due to low grade, prenhite-pumpellyite facies metamorphism.

Each alteration assemblage has unique mass change trends in 2D and 3D space. Illitic phengite and phengite alteration zones are characterized by losses in SiO_2, CaO and Na_2O, and gains in MgO, Fe_2O_3, K_2O, base metals (Cu, Pb, Zn), LFSE (Rb, Sr, Ba) and volatile elements (As, Sb and Tl). Proximal muscovite alteration zones are characterized by the same elemental gains and losses, except for MgO and LFSE. The elemental

signatures related to muscovite alteration are the most useful vectors to mineralization in the Pilley's Island district.

3.2. Introduction

Lithogeochemistry is very useful in the exploration for VMS deposits. Primary, immobile element lithogeochemical signatures provide new information on the roles that tectonics, petrogenesis, and heat flow play in the localization of VMS mineralization (e.g. Lesher et al., 1986; Barrie et al., 1993; Lentz, 1998; Piercey, 2011, and references therein). Alteration lithogeochemistry adds further information on chemical changes associated with hydrothermal fluid-rock interaction during VMS formation. In particular, gains and losses of different mobile elements (e.g. Mg, Na, Ca, Si, K, Fe) can identify the various parts of the VMS hydrothermal environment and proximity (or distance) to VMS mineralization. The mobile element lithogeochemical signatures are proportional to the alteration mineralogy associated with VMS mineralization (e.g., sericite, chlorite, quartz) and therefore show a distinct zonation within the VMS environment (e.g., Huston, 1993; Barrett and MacLean, 1994a, b; Barrett and MacLean, 1999; Large et al., 2001a; Large et al., 2001b). Similarly, near infrared-short wave infrared spectroscopy (NIR-SWIR) can be utilized to not only identify hydrous minerals associated with VMS-related mineralization (e.g., muscovite, chlorite), but also to determine mineralogical compositional variations (e.g., Thompson et al., 1999; Herrmann et al., 2001; Jones et al., 2005). Taken together, the utilization of lithogeochemistry with NIR-SWIR can provide considerable information on the extent and variability of hydrothermal alteration associated with VMS mineralization and provide potential vectors to mineralization.

The Central Mobile Belt of the Newfoundland Appalachians contains numerous Cambrian to Ordovician VMS deposits, which are hosted within volcanic-arc, arc-rift, and back-arc basin assemblages (Swinden, 1991; Evans and Kean, 2002). The deposits have varying host lithostratigraphic assemblages, metal contents, and deposit styles (e.g., Piercey, 2007; Hinchey, 2011; Piercey and Hinchey, 2012), but have not been the subject of extensive modern lithogeochemical research. The relationships of mafic volcanic rocks to VMS mineralization in the Central Mineral Belt has been studied in detail (Swinden, 1991), with minor research on felsic volcanic rocks (e.g. Winter and Wilton, 2001; Squires and Moore, 2004); however, very little modern work has been undertaken on integrated lithogeochemical-NIR-SWIR studies in Newfoundland and much of the northern Appalachians outside of the Bathurst Mining Camp (e.g., Lentz and Goodfellow, 1996; Winter, 2000; Yang et al., 2003; Mireku and Stanley, 2006; Hinchey, 2011).

The Pilley's Island VMS district in Notre Dame Bay, central Newfoundland (Fig. 3-1) is an ideal location to study the petrogenesis of volcanic rocks and lithogeochemistry associated with alteration in a VMS environment. The district contains six VMS deposits within a relatively small area (~6km^2). The deposits vary in sulfide composition and mineralization style from massive pyrite, polymetallic sulfide, and polymetallic breccia sulfide, each of which is hosted within distinct stratigraphic assemblages and structural panels. Within the various thrust panels, the host rocks have been immaculately preserved with low grade, prenhite-pumpellyite facies metamorphism (Zagorevski et al., 2009) and no penetrative metamorphic fabric. Additionally, the level of coastal surface rock exposure (~60-70%) and abundance of archived diamond drill core allows for the

collection of lithogeochemical samples with reasonable distribution at surface and at depth. This allows one to confidently identify and compare different stratigraphic units and structural panels. Furthermore, the 2D and 3D stratigraphic and structural control allows for 2D-3D visualizations of the alteration lithogeochemistry, elemental mass changes, and variations in NIR-SWIR signatures in alteration minerals, which is not possible in many VMS districts.

This manuscript provides an integrated field, lithogeochemical, and NIR-SWIR study of volcanic rocks in the Pilley's Island VMS district and is a companion manuscript to Chapter 2. The ultimate goals of this manuscript are to: 1) document the primary, immobile element lithogeochemistry of the Pilley's Island terrane to understand the petrogenesis and tectonic setting of mafic and felsic magmas; 2) document the VMS-related hydrothermal alteration lithogeochemistry and element mobility proximal and distal to sulfide mineralization; and 3) use lithogeochemical and NIR-SWIR data from proximal and distal alteration assemblages to identify vectors towards sulfide mineralization. The results have implications for exploration for VMS in the Appalachians and similar orogenic belts worldwide.

3.3. Geological Setting

The Pilley's Island VMS district is host to a cluster of bimodal felsic Zn-Pb-Cu-Au-Ag volcanogenic massive sulfide (VMS) deposits within the Ordovician Buchans-Roberts Arm belt, which is part of the Annieopsquotch accretionary tract (AAT) of the Newfoundland Appalachians, Canada (Swinden and Dunsworth, 1995; Thurlow, 1996; van Staal, 2007). The Buchans-Roberts Arm belt consists of a Lower Ordovician (473-

456 Ma) (O'Brien and Dunning, 2008) mature island-arc sequence (Swinden et al., 1997) and is divided into four different thrust-fault-bound terranes: the Mud Pond terrane, the Pilley's Island terrane, the Boot Harbour terrane, and the Triton terrane (Fig. 3-2) (Bostock, 1988; Williams et al., 1988). The Pilley's Island terrane consists predominantly of calc-alkaline to transitional mafic rocks and calc-alkaline to transitional felsic rocks (Thurlow, 1996; Swinden et al., 1997). The Pilley's Island terrane is divided into five volcanic-dominated thrust panels: Liquor Street panel; Spencer's Dock panel; Old Mine panel; 3B panel; and Pilley's Hills panel (Thurlow, 1996; Thurlow, 2001). The thrust faults juxtapose felsic-dominated VMS-bearing panels against mafic volcanic-dominated panels that are VMS barren (Figs. 3-3 & 3-4). The Liquor Street panel and Pilley's Hills panel are dominated by basaltic flows that have strong chlorite and hematite alteration; these panels also contain several quartz diorite intrusions (Figs. 3-3 & 3-4). The Spencer's Dock panel is dominated by dacitic flows that can contain flow banding and lithophysae, much less felsic volcaniclastic rock, and minor basaltic flows and gabbro intrusions (Figs. 3-3 & 3-4). The Old Mine and 3B panel consist of intercalated, felsic volcanic and volcaniclastic rocks that are predominantly dacitic in composition (Figs. 3-3 & 3-4).

The Pilley's Island VMS district is hosted within the Roberts Arm Group in the northern Buchans-Roberts Arm belt that formed following the 481Ma onset of westward subduction beneath the Dashwoods microcontinent (Swinden and Dunsworth, 1995; Zagorevski et al., 2006). The Buchans-Roberts Arm belt is interpreted to have originated within an Ordovician peri-Laurentian volcanic arc/back-arc complex in the western

Iapetus Ocean (Swinden et al., 1997; van Staal, 2007; van Staal and Barr, 2011). The Roberts Arm Group and associated Pilley's Island terrane has previously been interpreted to represent elongate shield volcanoes that were intruded by contemporaneous felsic magmas (Bostock, 1988; Waldie et al., 1991; Swinden, 1992). These different lithologies were subsequently juxtaposed upon each other by imbricate thrust faulting caused by pre-Middle Silurian collision with the Ganderian margin during the closure of the Iapetus Ocean (Kerr, 1996; van Staal and Barr, 2011).

3.4. Pilley's Island Stratigraphy and Mineralization

The stratigraphy of Pilley's Island is crosscut, internally, by several southeast dipping thrust faults, forming structural panels, including: the 3B, Old Mine, and Spencer's Dock panels, which host VMS deposits; and the Pilley's Hills and Liquor Street panels, which are barren. All of these panels are part of the Pilley's Island terrane and their stratigraphy and lithofacies are described in a companion paper (Chapter 2); a condensed summary is given here.

The thrust panels have been distinguished by the identification or inference of thrust faults, using surface mapping and drill core. Thurlow (1996) first identified the thrust faults based on their shallow dip and lithological contrast. Thrust faults in this study are identified by major topographic lineaments, shear zones in outcrop, abrupt lithological changes, and abrupt variations in the intensity of hydrothermal alteration. In drill core, where faults are identified by zones of strong shearing, broken core, fault gouge and cataclasite in combination with sharp changes in lithology, lithofacies, and alteration. Carbonate shear veining commonly occurs with thrust fault movement but is

not diagnostic. Slickensides are often observed in non-oriented drill core and therefore are not kinematic indicators. No other kinematic indicators were observed in fault zones.

The Pilley's Hills panel is composed of undifferentiated massive and pillowed basalt flows and breccia intervals with sparse, small occurrences of massive sulfide mineralization with hematitic jasper (unit 2; Figs. 3-3 & 3-4). The 3B panel consists of dacitic flows (unit 3.1), overlain by dacitic lapilli tuff (unit 3.2), which grades into dacitic tuff (unit 3.3), and is overlain by additional dacitic flows (unit 3.4; Figs. 3-3CD & 3-4). Multiple mafic dikes (unit 3.4) crosscut units 3.1, 3.2 and 3.3. The Old Mine panel consists of massive to pillowed basalt (unit 4.1), overlain by dacitic flows (unit 4.2), dacitic tuff (unit 4.3), dacitic flows (unit 4.4), felsic hyaloclastite (unit 4.5) and a variety of dacitic flows (units 4.6a-c; Figs. 3-3CD & 3-4). The Spencer's Dock panel is cut by three minor thrust faults and is subdivided into the Lower panel, Rowsell's Cove panel, and Upper panel (Thurlow, 1996) (Figs. 3-3B & 3-4). The Lower panel consists of massive coherent dacite and associated breccia (unit 5.1), most of which are mineralized, and have one observed mafic intrusion (Figs. 3-3B & 3-4). The Rowsell's Cove panel consists of basalt flows (unit 5.2) including a large gabbro intrusion (unit 5.3), which is in contact with felsic volcaniclastic rocks (unit 5.4) and dacitic flows (unit 5.5; Figs. 3-3B & 3-4). The upper panel consists of massive coherent dacite (unit 5.6; Figs. 3-3B & 3-4). The Liquor Street panel consists of undifferentiated massive and pillow basalt flows (unit 6.1), which are crosscut by quartz diorite dikes and possibly sills (unit 6.2; Figs. 3-3B, 3-4).

The Pilley's Island VMS deposits consist of lenses of massive and semi-massive sulfide with surrounding stringer and disseminated sulfide zones. These deposits are hosted exclusively within felsic volcanic and volcaniclastic rocks of the Pilley's Island terrane (Figs. 3-3 & 3-4). The district contains six VMS deposits of variable grade and tonnage. The Spencer's Dock panel on the west side of Pilley's Island is host to the Spencer's Dock deposit, Jane's Cove deposit and Rowsell's Cove deposit (Figs. 3-3AB & 3-4). The Spencer's Dock deposit is a lens of massive pyrite that thins from 26m thick to 11.6m downdip, with only trace sphalerite and chalcopyrite and precious metals (Thurlow, 2001). Similarly, the Jane's Cove deposit is a thick lens of massive pyrite with trace chalcopyrite and interbanded sericite, quartz, carbonate, and barite gangue. In contrast to the Spencer's Dock and Jane's Cove deposits, the Rowsell's Cove deposit is composed of coarse, polylithic sulfide breccia (pyrite and trace chalcopyrite clasts) with less altered lithic clasts. The 3B and Bumble Bee Bight deposits are hosted within the 3B panel, on the eastern side of Pilley's Island, and they are stacked lenses of Cu-rich (~4% Cu) pyrite and chalcopyrite with trace sphalerite and galena (Thurlow 2001) (Figs. 3-3ACD & 3-4). The 3B deposit is higher stratigraphically and is a 5-10m thick lens of massive pyrite (40-80%) and chalcopyrite (3-20%) with trace sphalerite and galena. The lower Bumble Bee Bight deposit contains three, 1-2m lenses of massive pyrite and sphalerite. Lastly, the Old Mine deposit is hosted within the Old Mine panel, which structurally overlies the 3B panel and the deposit consists of two lenses of massive sulfide that are up to 12m thick with a strike length of 180-300m (Swinden and Kean, 1988) (Figs. 3-3ACD & 3-4). The upper lens consists of massive pyrite and chalcopyrite with

trace sphalerite and barite hosted within felsic breccia, and the lower lens consists of massive and stringer pyrite (Swinden and Kean, 1988).

Each of the Pilley's Island VMS deposits are surrounded by extensive zones of hydrothermal alteration and stringer and disseminated sulfide mineralization throughout the footwall and hanging wall (Figs. 3-3 & 3-4). Evidence supporting an origin through sub-seafloor replacement is outlined in Chapter 2.

3.4.1. Pilley's Island Mineralization and Alteration

The alteration of specific stratigraphic units within the Pilley's Island terrane is described in a companion paper (Chapter 2), and a condensed summary of the alteration is given here.

The dominant alteration minerals in the Pilley's Island terrane include sericite, chlorite, quartz and Fe-carbonate. Sparse occurrences of K-feldspar and epidote alteration are also observed. Sericite, chlorite and quartz alteration represent VMS-related alteration, with quartz and sericite alteration forming proximal to mineralization and chlorite alteration occurring distal to mineralization, predominantly within basaltic rocks. The intensity of VMS-related alteration is generally controlled by the primary permeability and porosity of the lithofacies. For example, felsic volcaniclastic lithofacies are often more intensely altered than basaltic flows or dacitic flows. Conversely, carbonate alteration occurs proximal to faults and shear zones and associated fractures and is likely related to post-mineralization faulting rather than VMS alteration. K-feldspar and epidote alteration do not form continuous or widespread alteration zones; therefore, their association to VMS mineralization cannot be determined.

Sericite alteration is the most abundant alteration facies and forms large alteration haloes within predominantly felsic volcanic rocks. It is commonly associated with quartz alteration, which is also widespread and is pervasive to void filling in both mafic and felsic volcanic rocks. Zones of strong sericite and quartz alteration surround the massive sulfide lenses within the Spencer's Dock panel (i.e., the Spencer's Dock and Jane's Cove deposits) (Fig. 3-3B), and the intensity of alteration increases near mineralized zones and particularly so in perlitic cracks, hyaloclastite, or in volcanic breccias. The deposits within the 3B and Old Mine panel (3B, Bumble Bee Bight and Old Mine deposits; Fig. 3-3CD) are hosted within volcaniclastic facies and strong sericite and quartz alteration is localized, and more intense, proximal to the mineralized zones.

Chlorite alteration is most abundant within pillowed and massive basaltic flows and various mafic intrusions in the Pilley's Island terrane. It is generally pervasive throughout the mafic volcanic rocks and fills amygdules and veins locally; however, chlorite forms with lesser sericite within felsic volcanic and volcaniclastic units that are distal to mineralization. In the 3B panel, chlorite and sericite commonly occur in perlitic-fractured dacitic flows distal to mineralization, and minor chlorite forms in felsic volcaniclastic units. In the Old Mine panel, flow units distal to mineralization have chlorite-defined perlitic cracks; however, proximal to mineralization in the Old Mine deposit, the volcaniclastic units are altered to sericite and quartz with minor chlorite.

3.5. Near Infrared-Short Wave Infrared (NIR-SWIR) Spectroscopy

3.5.1. Methods and Background Information

Near infrared-short wave infrared (NIR-SWIR) spectroscopy was used in this study to determine the distribution, intensity and speciation of hydrothermal white mica and chlorite surrounding VMS deposits in the Pilley's Island VMS district. The goal is to determine potential variations in the typology of phases proximal versus distal to mineralization.

Representative samples were analyzed using a TerraSpec mineral spectrometer using a Hi-Brite Muglight on flat surfaces of clean, dust-free outcrop and drill core samples. Spectra were collected using RS^3 Spectral Acquisition software. To minimize instrument drift, an automated instrument optimization was completed and a white reference was taken every 10 analyses, as were two internal mineral standards of pyrophyllite and talc. The rock sample reflectance was measured within the SWIR band (1300-2500nm). Each sample was analyzed for approximately two to four minutes, and a cumulative average of the spectra was saved once the live spectral reading was stabilized. The RS^3 software saves a cumulative spectra and not the most recently acquired spectrum to assure and maintain the most accurate data collection. Spectral data was processed using a splice correction in ViewSpec Pro™ v.6.0 software by ASD Inc. Mineral identification and relative mineral abundances were identified using "The Spectral Geologist™ Professional, v.7.1" spectral analysis software (Merry and Pontual, 2011), which calculates the relative mineral abundances based on white mica and chlorite absorption features. Error in the individual spectra is calculated using a "goodness of fit"

between unknown spectra and known reference values, and is determined by calculating the standardized residual sum of squares for each spectra (Pontual et al., 2008). In determining AlOH absorption features, only spectra attributed to dominantly white mica were used (e.g. muscovite, illitic muscovite, phengite and illitic phengite having >50% abundance relative to the next most abundant mineral determined by SWIR). Likewise, in determining FeOH and MgOH absorption features, only spectra attributed to chlorite were used (e.g. Fe-, Fe,Mg-, and Mg-chlorite).

Short wave infrared spectroscopy is based on the premise that certain mineral phases absorb light of specific wavelength. Diagnostic hulls in the SWIR spectra are caused by absorption by OH, H_2O, CO_3, NH_4, AlOH, FeOH, and MgOH bonds (Fig. 3-5) (Thompson et al., 1999). The identification of absorption hulls allows the identification of different alteration minerals in the sample, such as phyllosilicates, carbonates, OH-bearing silicates and sulfates. For example, white mica has a sharp, well-defined AlOH absorption feature between 2190 and 2288nm and a slight feature near 2344nm and 2440nm (Fig. 3-5). Variations in the AlOH absorption wavelength identify different proportions of octahedral Al in the crystal lattice (Jones et al., 2005) and can lead to the identification of the following minerals: 1) Na-bearing white micas (2190-2195nm); 2) muscovite (normal potassic mica, 2200-2208nm); and 3) phengite (2216-2228nm) (Post and Noble, 1993; Herrmann et al., 2001). Wavelengths that do not fall within these ranges represent multiple mica phases. Similarly, variations in the MgOH and FeOH absorption wavelength (2235-2255nm for MgOH and 2320-2360nm for FeOH) identify different proportions of Fe-OH and Mg-OH bonds in the crystal lattice, and lower wavelengths are

indicative of Mg-rich chlorites, as opposed to Fe-rich chlorites at higher wavelengths (Pontual, 2008). These absorption phenomena are especially useful in the VMS environment because the main hydrothermal alteration mineral assemblages often have distinct mineralogical and mineral chemical variations as a function of proximity to mineralization (e.g., Huston, 1999; Thompson et al., 1999; Herrmann et al., 2001; Pontual, 2008), and NIR-SWIR can be used to identify and discriminate the phases and their chemical variations. This is particularly useful in areas like Pilley's Island that have rather simple yet widespread alteration minerals proximal and distal to mineralization.

3.5.2. Results

The dominant white mica compositions at Pilley's Island include illitic muscovite, muscovite, illitic phengite and phengite, and the dominant chlorite compositions include Fe-, Fe,Mg-, and Mg-chlorite; both mica and chlorite species have unique spectra and specific AlOH, FeOH and MgOH absorption features (Fig. 3-5; Table 3-1). The distribution of these minerals and their AlOH and FeOH absorption features are presented on a geological map of the area in Figure 3-6A, and on a cross section through the Bumble Bee Bight deposit in Figure 3-6B.

In the Pilley's Island VMS district, AlOH absorption features in SWIR spectra are the most practical data to analyze spatially because white mica alteration is more abundant than chlorite alteration (Fig. 3-6 & Table 3-1); chlorite-rich samples are also included and categorized by their FeOH absorption features for comparison (Fig. 3-6A & Table 3-1).

In felsic-dominated panels, illitic phengite with AlOH absorption >2220nm predominates and is associated with lesser Fe,Mg-chlorite (Fig. 3-6A). The mafic-dominated panels are less altered, but are dominated by Fe,Mg-chlorite alteration with less abundant Mg-chlorite (Fig. 6A). Mafic volcanic rocks are commonly intruded by quartz diorite, most of which contain illitic phengite and minor illitic muscovite and muscovite alteration (Fig. 3-6A).

In cross-sectional view through two mineralized alteration zones in the 3B area the felsic panels are dominated by illitic phengite ± illitic muscovite, muscovite, and phengite alteration with very little chlorite, and the underlying mafic volcanic rocks are dominated by Fe,Mg- and Mg-chlorite (Fig. 3-6B). Throughout the felsic panel, AlOH absorption feature wavelengths are high (>2200nm) due to abundant phengite and illitic phengite alteration (Fig. 3-6A); however, lower wavelength AlOH absorption features (2200-2210nm), associated with muscovite and illitic muscovite, are restricted to alteration zones proximal to stringer and massive sulfide mineralization (Fig. 3-6B).

3.6. Lithogeochemistry

3.6.1. Sampling and Analytical Methods

Major, trace, and rare earth elements were obtained on 203 samples from surface and drill core. All samples were analyzed at Activation Laboratories in Ancaster, Ontario, and the Department of Earth Sciences, Memorial University of Newfoundland. Prior to shipment, field samples were sawn to reduce size, to retain a representative sample, and to remove all weathered surfaces. Each sample and the saw were washed between cutting

to avoid cross-contamination and samples were individually bagged for shipment. Samples were crushed and pulverized using mild steel at Activation Laboratories.

Major elements and select trace elements were analyzed at Activation Laboratories using a pre-analysis lithium metaborate/ tetraborate fusion, dissolution of the fused bead in nitric acid, and subsequent analysis using inductively coupled plasma optical emission spectroscopy (ICP-OES). Mercury analyses were also undertaken at Activation Laboratories using a cold vapour flow injection mercury system (CV-FIMS) where a sample is digested with aqua regia to leach out soluble compounds and then analyzed using CV-FIMS. Other trace elements, including the rare earth elements, high field strength elements, and volatile elements were obtained at Memorial University using high-pressure bomb dissolution with subsequent analyses of solutions on an inductively coupled plasma mass spectrometer (ICP-MS). Precision and accuracy of the various methods have been previously reported in Piercey and Colpron (2009) for Actlabs, and by Jenner et al. (1990) and Diegor et al. (2001) for Memorial University.

3.6.2. Element Mobility

Although the majority of the rocks from Pilley's Island have undergone low grade, prenhite-pumpellyite facies metamorphism (Zagorevski et al., 2009), most exhibit widespread hydrothermal alteration, especially those associated with mineralized strata. This limits what elements can be utilized to understand the primary petrological signatures in a unit. In deciphering the primary lithogeochemistry of altered rocks, it is essential to use elements that are resistant to hydrothermal alteration and metamorphism (e.g., MacLean and Kranidiotis, 1987; MacLean, 1988; Richards et al., 1989; MacLean,

1990; Barrett and MacLean, 1991; Elliott-Meadows and Appleyard, 1991; MacLean and Barrett, 1993).

Hydrothermal alteration reactions in the VMS environment commonly result in the destruction of glass, ferromagnesian minerals and feldspars (e.g., Munhá et al., 1980; Saeki and Date, 1980; Hajash and Chandler, 1981; Lentz, 1999; Large et al., 2001b), which results in the mobilization of specific elements. Feldspar and glass destruction is accompanied by Na, Ca and Si losses as sericite is produced (Ishikawa et al., 1976; Spitz and Darling, 1978; Munhá et al., 1980; Saeki and Date, 1980). The formation of chlorite from both feldspars and sericite results in the incorporation of Mg (±Fe) from the fluids, or mafic rocks, to produce chlorite and cause Fe (±Mg) gains in the rock (Saeki and Date, 1980; Hajash and Chandler, 1981; Date et al., 1983; Lentz, 1999). In light of the above common VMS reactions, is assumed that these elements (alkalis, silica and Fe-Mg are mobile throughout the Pilley's Island stratigraphy. Conversely, Al_2O_3 and TiO_2 are assumed to be immobile (Whitford et al., 1989; Barrett and MacLean, 1999). The low field strength elements (LFSE) behave like the alkalis and therefore are commonly mobile during hydrothermal alteration (MacLean, 1990; Lentz, 1999), and this is assumed for the rocks of the Pilley's Island terrane. Rare earth elements (REE) are assumed to have little mobility in the Pilley's Island rocks because they have not been subject to the extreme temperatures and reactions that are necessary to mobilize them. An exception to this assumption is Eu, which is easily mobilized during hydrothermal alteration; however, some REE mobility does occur in highly altered samples (Sverjensky, 1984; Whitford et al., 1988; Peter et al., 1994; Wood and Williams-Jones, 1994), which is the case for some

samples in the Pilley's Island area. High field strength elements (HFSE) are assumed to be immobile and this is widely accepted (e.g., Whitford et al., 1989; MacLean, 1990; Barrett and MacLean, 1999; Lentz, 1999) although some exceptions exist (e.g., Finlow-Bates and Stumpfl, 1981). Lastly, metals (Cu, Zn, Pb) and volatile elements (Sn, As, Tl) are considered to be mobile (e.g., Large et al., 2001a).

In addition to using elements that are relatively immobile, the samples have been screened to select a least altered sample suite for mass change calculations. The least altered samples were chosen based on several criteria including: low metal contents of the samples (Cu, Zn, Pb < 100ppm), $Al_2O_3/Na_2O < 10$, low LOI values (<7% for mafic rocks, <5% for felsic rocks), major element concentrations (Na_2O = 2-5%) and mineralogical composition (i.e., low alteration mineral abundance in thin section and NIR-SWIR data with aspectral absorption signatures). These least altered criteria were decided upon through an iterative process of evaluating the lithogeochemical data set and culling the data set with successive iterations. The least altered samples are compared to, and plotted with, altered samples throughout the manuscript.

3.6.3. Primary Immobile Element Lithogeochemistry

3.6.3.1. Pilley's Hills Panel

Unit 2 rocks of the Pilley's Hills panel have geochemical signatures of calk-alkaline basalt (CAB) with Zr/TiO_2 and Nb/Y ratios typical of subalkalic andesite/basalt (Fig. 3-7A). Unit 2 has high TiO_2 and HFSE contents, and Th-Yb ratios consistent with a calc-alkaline to slightly transitional magmatic affinity (Fig. 3-7B). Unit 2 has primitive

mantle-normalized patterns with LREE enrichment (La/Sm_{MN} = 1.1-3.6), a distinct negative Nb anomaly (Nb/Th_{MN} = 0.11-0.42) and slightly negative Zr, Eu and Sc anomalies (Fig. 3-8 & Table A1-1). Least altered samples have less variable LREE enrichment (La/Sm_{MN} = 1.4-2.0) and negative Nb anomalies (Nb/Th_{MN} = 0.13-0.20) (Table A1-1).

3.6.3.2. 3B Panel

Felsic volcanic rocks in units 3.1-3.4 have geochemical signatures of calc-alkaline, volcanic arc dacite. The samples show considerable scatter in the andesite, dacite and trachyandesite fields in Zr/TiO_2-Nb/Y space (Fig. 3-7A); this scatter is partially attributed to the mobility of Y (e.g., Murphy and Hynes, 1986; Bau, 1996) as the least altered samples have lower Nb/Y ratios (Nb/Y = 0.47-0.66), are subalkalic, and plot in the rhyodacite/ dacite field (Fig. 3-7A & Table A1-1). Units 3.1-3.4, with very rare exceptions, have calc-alkaline (Th/Yb > 0.8) (Fig. 3-7B & Table A1-1), volcanic arc (I-type) affinities (Fig. 3-7C). Felsic flows (unit 3.1 and 3.4) have FII to FIIIa chondrite-normalized $(La/Yb)_{CN}$-Yb_{CN} ratios (Fig. 3-7D) (Lesher et al., 1986; Hart et al., 2004). The least altered dacite samples have LREE-enriched (La/Sm_{MN} = 2.19-2.86) primitive mantle-normalized patterns with negative Nb anomalies (Nb/Th_{MN} = 0.21-0.28) (Fig. 3-9AB & Table A1-1). Altered samples have greater scatter in all REE values, some HFSE (e.g., Th, V), and have a wider range of La/Sm_{MN} ratios (La/Sm_{MN} = 0.52-3.89) and Nb/Th_{MN} ratios (0.09-1.06) (Fig. 3-9AB & Table A1-1).

The trace element geochemical attributes of unit 3.5 mafic intrusions are similar to calc-alkaline basalt (CAB). Unit 3.5 samples have significant scatter in Zr/TiO_2-Nb/Y

space in the subalkaline andesite/basalt to subalkaline basalt fields (Fig. 3-7A), and have a calc-alkaline magmatic affinity (Th/Yb > 0.8) (Fig. 3-7B & Table A1-1). Unit 3.5 is similar to unit 2 basalt and is LREE-enriched (La/Sm_{MN} = 0.94-2.30) and has negative Nb anomalies (Nb/Th_{MN} = 0.11-0.23) (Fig. 3-8B & Table A1-1). Unit 3.5 differs from unit 2 in that it contains positive Eu anomalies in most samples and displays slight HREE depletion (Fig. 3-8B).

3.6.3.3. Old Mine Panel

Unit 4.1 mafic volcanic rocks have geochemical signatures of calc-alkaline basalt (CAB), but with elevated Hf and Zr contents (Fig. 3-8C). This unit has highly variable Zr/TiO_2 and Nb/Y ratios, plotting in andesite, basalt, and basanite/ nephelinite fields (Fig. 3-7A). This scatter is partially attributed to the mobility of Y, as discussed previously. The HFSE contents and Th/Yb ratios are similar to unit 2 and 3.5 and are calc-alkaline (Fig. 3-7B & Table A1-1). Unit 4.1 samples are LREE-enriched (La/Sm_{MN} = 1.6-2.9) and have negative Nb anomalies (Nb/Th_{MN} = 0.5-0.8) on primitive mantle-normalized plots (Fig. 3-8C & Table A1-1).

The geochemical attributes of units 4.2-4.6 are similar to calc-alkaline volcanic arc dacite. The rocks have Zr/TiO_2 and Nb/Y ratios that plot with significant scatter throughout andesite, rhyodacite/ dacite, trachyandesite and (few) in basanite/ nephelinite and alkaline basalt fields; however, least altered samples plot as trachyandesite (Fig. 3-8A). Th/Yb ratios are more variable in this panel (Th/Yb = 0.36-3.33) and have transitional to calc-alkaline magmatic affinities (Fig. 3-8B & Table A1-1). As with felsic units of the 3B panel (units 3.1-3.4), these units also have Nb/Y ratios indicative of a

volcanic arc (I-type) affinity (Fig. 3-8C), and least altered felsic flows plot as FII to FIIIa felsic volcanic rocks (Fig. 3-8D). Units 4.2-4.6 are LREE-enriched (La/Sm_{MN} = 0.92-2.57 in least altered samples) and with negative Nb anomalies (Nb/Th_{MN} = 0.33-0.82 in least altered samples), and slightly negative Y anomalies on primitive mantle-normalized plots (Fig. 3-9CD & Table A1-1). These samples have similar Zr- and Hf-enrichment as in unit 3 felsic units. Altered felsic samples in the Old Mine panel have significant scatter in all REE values, and some HFSE (e.g., Th, V, Sc), and have a wider range of La/Sm_{MN} ratios (0.88-3.32) and Nb/Th_{MN} ratios (0.09-4.57) (Fig. 3-9CD & Table A1-1).

3.6.3.4. Spencer's Dock Panel

Unit 5.5 and 5.6 have geochemical signatures of calc-alkaline volcanic arc dacite. The samples have Zr/TiO_2 and Nb/Y ratios that plot within rhyodacite/ dacite and trachyandesite fields, and the only least altered sample plots within the rhyodacite/ dacite field (Fig. 3-7A). These units have calc-alkaline Th-Yb systematics (Th/Yb >0.8) (Fig. 3-7B) and they have similar Nb/Y ratios to felsic units in the 3B and Old Mine panels, which indicate a volcanic arc (I-type) affinity (Fig. 3-7C). The least altered sample from unit 5.5 has an FII signature, and altered samples scatter between FII, FIIIa and FIV fields (Fig. 3-7D). Units 5.5 and 5.6 are characterized by LREE-enrichment (La/Sm_{MN} = 2.82 in least altered sample) and negative Nb anomalies (Nb/Th_{MN} = 0.25 in least altered sample) (Fig. 3-9EF & Table A1-1). The La/Sm_{MN} and Nb/Th_{MN} values are highly variable in more altered samples (e.g. La/Sm_{MN} = 1.88-3.13 and Nb/Th_{MN} = 0.21-2.69) (Fig. 3-9EF & Table A1-1).

3.6.3.5. Liquor Street Panel

Unit 6.1 mafic volcanic rocks have geochemical signatures of calc-alkaline basalts (CAB). One least altered sample has a Zr/TiO_2-Nb/Y ratio that plots as andesite/basalt; whereas, altered samples show more scatter (Fig. 3-7A). Ratios of Th-Yb indicate that most rocks are slightly transitional to calc-alkaline (Fig. 3-7B). The least altered sample from unit 6.1 has LREE-enrichment (La/Sm_{MN} = 1.37) and a negative Nb anomaly (Nb/Th_{MN} = 0.24) (Fig. 3-8D & Table A1-1). The Nb/Th_{MN} and La/Sm_{MN} ratios are variable in more altered samples (e.g. La/Sm_{MN} = 1.10-2.91 and Nb/Th_{MN} = 0.12-0.46) (Fig. 3-8D & Table A1-1).

Unit 6.2 quartz diorite intrusions are similar to volcanic arc granites. Least altered samples have rhyodacite/dacite Zr/TiO_2-Nb/Y ratios; more altered samples show scatter (Fig. 3-7A). This unit has mostly calc-alkalic Th-Yb ratios with Nb-Y ratios indicative of volcanic arc affinity (Fig. 7BC). Least altered samples display LREE-enrichment (La/Sm_{MN} = 2.76-3.19), negative Nb anomalies (Nb/Th_{MN} = 0.19-0.21), and slightly negative Y anomalies on primitive mantle-normalized plots (Fig. 3-9GH & Table A1-1). Similar to other felsic stratigraphic units, the REE and Nb anomalies are more variable in more altered samples (e.g. La/Sm_{MN} = 0.70-3.19 and Nb/Th_{MN} = 0.18-1.96) (Fig. 3-9GH & Table A1-1).

3.6.4. Mobile Element Lithogeochemistry

3.6.4.1. General Mobile Element Variations

Samples from the Pilley's Island terrane contain a wide variety of Na_2O and K_2O values. In the Hughes (1973) diagram, many samples exhibit K-metasomatism and mafic volcanic rocks (unit 2, unit 6.1) have very low $Na_2O + K_2O$, indicating significant alkali loss, and samples that cluster toward the right side of the plot have strong sericite (potassic) alteration (Fig. 3-10A). A similar distribution is illustrated in the plot of Spitz-Darling index (Al_2O_3/Na_2O) (Spitz and Darling, 1978) against Na_2O (Fig. 3-10B). Many samples have high Spitz-Darling index values ($Al_2O_3/Na_2O>10$), and these samples are predominantly felsic volcanic rocks with strong sericite alteration (Fig. 3-10B). Conversely, mafic volcanic rocks tend to have lower Spitz-Darling index values (especially unit 2 and unit 6.1), indicating that they are largely unaltered and/or have undergone albite alteration (Fig. 3-10B).

Samples that are strongly altered as indicated by a high Spitz-Darling index also have high chlorite-carbonate-pyrite index (CCPI) (Large et al., 2001b) and high Hashimoto alteration index (AI; Fig. 3-10C) (Ishikawa et al., 1976). Most mafic volcanic rocks (unit 2, unit 3.5, unit 4.1 and unit 6.1) plot at higher CCPI values and tend to form a trend toward the chlorite/pyrite node, illustrating the variable AI values of these rocks and their predominant chlorite alteration despite little pyrite content (Fig. 3-10C). In contrast, the felsic volcanic rocks (all other units) plot with significant scatter, but have predominantly chlorite, pyrite, sericite, and/or K-feldspar alteration (Fig. 3-10C).

3.6.4.2. Mass Balance Calculations

Although plotting raw lithogeochemical data illustrate trends in elemental changes associated with alteration, the absolute gains and losses of elements during the alteration process cannot be determined due to volume change and mass change during alteration (Gresens, 1967; Grant, 1986; MacLean, 1990). Because the Pilley's Island volcanic rocks are bimodal and form a heterogeneous series on immobile element plots (Fig. 3-11), a single precursor method (e.g., Gresens, 1967; Grant, 1986) is not appropriate for correcting mass/volume change and determining absolute elemental gains and losses. Consequently, the multiple precursor method of MacLean (1990) is utilized. The multiple precursor method uses immobile elements to define different rock types (e.g. mafic, felsic) by plotting an immobile, compatible element on the Y-axis (e.g. Al_2O_3, TiO_2) versus an immobile, incompatible element on the X-axis (e.g. Zr, Nb) (Fig. 3-11). For the different rock types, this immobile-compatible versus immobile-incompatible plot defines alteration lines in X-Y space with defined Y/X ratios that go through the origin (Fig. 3-11) (MacLean, 1990; MacLean and Barrett, 1993). For example, mafic rocks have high Al_2O_3/Zr ratios and felsic rocks have lower Al_2O_3/Zr ratios (Fig. 3-11). An estimate of a magmatic fractionation line is created by fitting a polynomial or exponential curve to least altered samples, although a linear regression is typically used in Al_2O_3-Zr space (MacLean, 1990; MacLean and Barrett, 1993).

Alteration lines have specific Al_2O_3/Zr ratios dependent on the rock type and plot through the origin (Fig. 3-11). Samples that fall along the alteration line, but lie above the least altered fractionation curve have had residual increases in element concentrations due

to mass loss (Fig. 3-11). Conversely, data that lie below the fractionation line have had residual decrease in element concentrations due to mass gains and element dilution (Fig. 3-11). The precursor composition of each rock type (e.g. Al and Zr contents in unaltered rock) occurs where the alteration line intersects the least altered fractionation line, and these intersection points can be determined graphically or algebraically (Fig. 3-11). These lines are used to determine the precursor Zr contents of a rock suite (Fig. 3-11). An enrichment factor (EF) is then calculated by comparing the Zr concentration in the precursor to that of the altered rock:

$$EF = Zr_{precursor}/Zr_{altered\ rock} \quad (1)$$

The enrichment factor corrects for change in the size of the system (e.g. mass gain or loss) due to alteration by multiplying any given element concentration (i) in the altered rock by the enrichment factor to yield the reconstructed composition for each element (RC_i):

$$RC_i = EF \times [i]_{altered\ rock} \quad (2)$$

The reconstructed composition (RC) is compared to the precursor composition (PC) to calculate the elemental mass change (MC) for any element (i) during alteration:

$$MC_i = RC_i - PC_i \quad (3)$$

To find the precursor composition of a given element i, a series of plots (i versus Zr) are made and an exponential curve is fitted to each (Fig. 3-11). The $Zr_{precursor}$ value calculated previously via (1) is then substituted into that curve to determine the given element's precursor composition.

It is important to note that the introduction of an estimated fractionation line introduces some error to the mass change calculation. Firstly, a least altered regression (fractionation) line is ideally fit to igneous rocks series that exhibit chemical continuity between fractionated units (MacLean, 1990). However, the volcanic rocks in the Pilley's Island stratigraphy are bimodal (as are most VMS districts worldwide). They consist of dacitic and basaltic volcanic rocks and do not form a continuous series of fractionated rocks due to the lack of intermediate andesitic volcanic rocks. Overall, the method herein is considered to remain valid because the line is fit to both felsic and mafic end members (Fig. 3-11), and the line should remain unchanged despite missing andesitic rocks in between. Secondly, the dacitic and mafic rocks at Pilley's Island are not considered to be related by fractionation (discussed in section 3.7.1). However, the regression line fit to selected least altered samples (Fig. 3-11) still reflects Al_2O_3 , SiO_2, and Fe_2O_3 (including all other elements, not illustrated; Table A2-1) fractionation trends that would be expected from a continuous series of fractionated rocks (MacLean and Barrett, 1993). Lastly, with a relatively small data set, least altered sample data used to fit the fractionation lines have some scatter, and the line fits are approximate. However, the approximated lines are superior to having no guiding fractionation trends whatsoever. With additional exploration and lithogeochemical sampling of least altered units, the line

fit of the lines should improve (MacLean and Barrett, 1993). Overall, the MacLean (1990) multiple precursor method is widely accepted and is considered to be the best possible method to calculate mass change on Pilley's Island volcanic rocks.

3.6.4.3. Results: Mass Balance Calculations

Results of the mass change calculations have been summarized and subdivided by dominant alteration minerals (Table A2-3). Mass change is subdivided in this manner because elements have a different susceptibility to mobilization depending on the alteration process and reaction.

Mass balance was calculated for all lithogeochemical samples. It is best to calculate mass balance on coherent volcanic rocks to minimize variations due to heterogeneity; however, samples from select volcaniclastic lithofacies have been included herein for a more widespread sample distribution and to approximate mobile element trends through volcaniclastic lithofacies. Heterogeneous samples with obvious or questionable polylithic content were excluded. Additionally, the majority of samples plot on immobile element discrimination diagrams in or around their expected fields (Fig. 3-7) to support that they contain negligible polylithic content.

SiO_2. Gains and losses in SiO_2 are the main causes of mass/volume change in the altered rocks and they mirror the total mass change in the altered rocks (Table A2-3). Most altered samples have undergone SiO_2 loss, but it does not appear to be associated with any dominant mineral assemblage or lithofacies (Table 3-2 & A2-3). Nevertheless, samples in the 3B panel have undergone greater SiO_2 depletion than the Spencer's Dock or Old Mine panel (Table 3-2 & A2-3).

Na_2O, CaO. Sodium and calcium depletion occurs in the majority of altered felsic rocks (Table 3-2 & A2-3). All chlorite-altered samples have variable Na_2O and CaO mass change, and some have very high gains and losses in CaO (±8%) and Na_2O (±4%) (Table 3-2 & A2-3). Most illitic phengite and samples with any white mica-dominated alteration have undergone both CaO and Na_2O losses (most 1-5%, some >10% CaO loss) (Table 3-2 & A2-3). Samples from the 3B and Old Mine panels (units 3 and 4) have the strongest depletion in alkali elements (Table 3-2 & A2-3). Some rocks, despite having obvious white mica alteration, have contradictory mass change data such as gains in Na_2O and CaO. This can be attributed to carbonate alteration (Ca addition), albite alteration (Na addition), and heterogeneous samples (e.g. amygdules, carbonate veinlets).

K_2O. Most Mg-chlorite-altered samples have K_2O loss (variable, up to 1.4% loss), whereas Fe,Mg-chlorite samples have both K_2O gains and losses (Table 3-2 & A2-3). Illitic phengite-altered samples have variable mass change in K_2O (most between 2% loss to 5% gain), although most phengite-, muscovite- and illitic muscovite-altered samples have undergone K_2O gains upwards of 7% (Table 3-2 & A2-3).

MgO, Fe_2O_3. The majority of Mg- and Fe,Mg-chlorite-altered samples have gains in both Fe_2O_3 and MgO (Table 3-2 & A2-3). Some samples have mass change data that contradict their end member chemistry and have mass loss of MgO or Fe_2O_3 and this is attributed to inherent error within the mass calculation method and fractionation curve estimation. These losses are highest in mafic volcanic rocks. Most muscovite- and illitic muscovite-altered samples have Fe_2O_3 gains (upwards of 15% gain), whereas phengite and illitic phengite-rich samples have smaller gains in Fe_2O_3 (upwards of 5%) with

variable gains and losses in MgO (Table 3-2 & A2-3). Such high Fe_2O_3 gains can be attributed to pyrite addition within the samples, which is likely to be more prevalent in muscovite and illitic muscovite-altered samples as they have the highest gains.

Transition Metals (Sc, Ti, V, Mn, Co, Ni): The most significant mass changes in transition metals are gains and losses in V and Ni, and the others remain relatively unchanged with only slight depletion locally (Table 3-2 & A2-3). Notable values in V and Ni mass change include: gains up to 100ppm V in Fe,Mg-chlorite rich rocks; over 200ppm Ni gains in Mg-chlorite-rich rocks; up to 100ppm V gains in illitic phengite-altered rocks; and ~60-80ppm loss of Ni and V, respectively, in muscovite-altered rocks (Table 3-2 & A2-3). Titanium, MnO, Sc, and Co have minimal changes in all alteration assemblages (Table 3-2 & A2-3).

Base Metals (Cu, Zn, Pb): Chlorite-altered samples have gains in Cu and Zn, with negligible mass change in Pb (Table 3-2 & A2-3). Samples with white mica alteration have gains in Cu and Zn, with the highest base metal gains in muscovite-altered samples (Table 3-2 & A2-3).

Other LFSE (Li, Rb, Sr, Ba, Th, U): Lithium, Th, and U do not have significant mass changes in hydrothermally altered rocks (Table 3-2 & A2-3). Most chlorite-altered samples have gains in Rb and Sr and highly variable gains and losses in Ba (Table 3-2 & A2-3). Similar gains are observed in white mica-altered rocks, but with greater Ba gains in most phengite-altered samples, and notably less Sr change in muscovite- and illitic muscovite-altered rocks (Table 3-2 & A2-3). Strong enrichment of Sr occurs in almost all illitic phengite-altered rocks (up to 179ppm gain; Table 3-2 & A2-3).

HFSE (Y, Nb, Hf, Ta): Yttrium is the only HFSE with significant mass gain or loss. Chlorite-altered rocks have variable Y mass change (Table 3-2 & A2-3). Most Fe-chlorite-altered rocks contain Y gains up to 12ppm (Table 3-2 & A2-3). White mica-altered rocks exhibit variable changes in Y, with approximately 10ppm in several muscovite and illitic muscovite-altered samples, and ranging from over 7ppm loss to over 10ppm gains in phengite- and illitic phengite-altered samples (Table 3-2 & A2-3). Generally, Nb, Hf and Ta change by less than 1ppm (Table 3-2 & A2-3).

Volatile Elements (As, Sb, Tl): Volatile elements As, Sb and Tl have a wide range of mass change values depending on the dominant alteration mineralogy of the rocks (Table 3-2 & A2-3). In chlorite-altered samples, Sb and Tl do not have significant mass change, whereas As has major mass gains in Mg-chlorite-altered samples (e.g. ~10-40ppm gains) (Table 3-2 & A2-3). Mass change in As is also present in Fe,Mg-chlorite altered rocks, but with <10ppm gains (Table 3-2 & A2-3). Both mass gains and losses of As (up 10ppm gain or loss) occur in Fe-chlorite-altered rocks (Table 3-2 & A2-3). Volatile elements have mass gains of several ppm in the majority of samples with white mica alteration (Table 3-2 & A2-3). These gains are especially evident in muscovite- and phengite- altered rocks, most of which have As gains of ~10-50ppm (Table 3-2 & A2-3). Most white mica altered samples contain Tl gains of over 1ppm (upwards of 12ppm gains) (Table 3-2 & A2-3).

REE (La to Lu): In most alteration assemblages, REE have little mass change (Table 3-2 & A2-3). Notable mass change in REE include: 1) several chlorite-altered samples with >10ppm gains and losses in La, Ca and Nd; 2) variable loss or gain of La,

Ce and Nd in most white mica-altered rocks; and 3) losses of La, Ce and Nd (~ 5-10ppm) in most Fe,Mg-chlorite-altered samples (Table 3-2 & A2-3).

3.6.4.4. Results: Spatial Distribution of Alteration and Mass Change: 2D and 3D Distributions

While the results above provide general characteristics of the elements associated with alteration, a spatial analysis of the data provide information on spatial relationships to mineralization, which has implications for exploration and deposit targeting.

On a map of the Pilley's Island study area, Na_2O is lost in zones of alteration surrounding mineralization in felsic volcanic-dominated panels (Spencer's Dock panel, 3B panel and Old Mine panel) (Fig. 3-12A), typical of most VMS environments (e.g., Galley, 1993; Barrett and MacLean, 1994a; Goodfellow et al., 1994; Large et al., 2001a; Large et al., 2001b). The Spencer's Dock panel has undergone ubiquitous Na_2O loss, whereas the 3B and Old Mine panels have Na_2O loss proximal (~200m) to mineralization only (Fig. 3-12A). This spatially limited alteration in the latter panels is likely due to the fact that the deposits are farther apart from one another with more focused hydrothermal fluid in the 3B and Old Mine panels as compared to the Spencer's Dock panel due to lithofacies differences (Fig. 3-12A). Outside of the mineralized zones in the 3B and Old Mine panel, felsic volcanic and volcaniclastic lithofacies are characterized by Na_2O mass gain (generally up to ~ 2% addition) (Fig. 3-12A). Mafic volcanic-dominated panels (Pilley's Hills and Liquor Street panel) have variable Na_2O mass change, ranging from 4.5% loss to 5% gain, but most of the rocks have 1-3% Na_2O gain and do not form any distinct spatial trends (Fig. 3-12A). Rocks that have Na_2O loss also have enrichments in

base metals (Cu, Zn, Pb), gains in LFSE (Rb, Sr, Ba) and enrichments in volatile elements (As, Sb, Tl) (Table A2-3).

In the felsic volcanic-dominated panels, K_2O shows mass gain proximal to mineralization (Fig. 3-12B). In the Spencer's Dock panel, K_2O gain is ubiquitous with up to 8% gain (Fig. 3-12B). In the Old Mine panel, K_2O gain is associated with Na_2O loss surrounding zones of mineralization (and up to 150m away) (Fig. 3-12AB). Conversely, rocks outside of the mineralized zones have up to 5.5% K_2O loss (Fig. 3-12B). Mafic volcanic-dominated panels have undergone widespread K_2O loss (up to 5.5%), although most rocks within the panels have <3% loss. Such widespread K_2O loss in mafic volcanic rocks is likely related to metasomatic Na_2O alteration from chemical exchange between the rock and low temperature seawater (Franklin et al., 2005). Rocks that exhibit K_2O gains also have losses in Na_2O, gains in base metals (Cu, Zn, Pb), gains in LFSE (Rb, Sr, Ba), and enrichments in volatile elements (As, Sb, Tl) (Table A2-3).

These trends in Na_2O and K_2O mass change are shown in 3D perspectives of the 3B and Bumble Bee Bight area (Fig. 3-12CD). This area was chosen for 3D modeling for its abundant archived drill core and its variety of alteration styles and multiple VMS deposits; such drilling data does not exist for the Spencer's Dock area. In the 3D models, mass change data is plotted as clouds surrounding the drillhole traces and a wireframe of raw Cu data is included to identify zones with Cu concentrations over 400ppm (Fig. 3-12CD). The upper wireframe represents the Bull Road showing and the lower wireframe is associated to the 3B deposit (Fig. 3-12CD). The 3D model illustrates the widespread Na_2O loss throughout the 3B and Old Mine panels, with most rocks exhibiting up to 2%

Na_2O loss and some >4.2% loss (Fig. 3-12C). Loss of Na_2O is increased surrounding the deposits (2-3%) and these haloes extend for several hundred metres, as seen surrounding the Bull Road showing (Fig. 3-12C). Concentration of Cu is higher (>400ppm) in alteration zones with 1-3% Na_2O loss.

The 3D model of K_2O mass change illustrates K_2O addition throughout the stratigraphy (Fig 12D). The Old Mine panel has undergone the most K_2O addition with the majority of rocks containing over 5% K_2O addition, most of which have been altered to phengite, illitic phengite, Fe,Mg-chlorite and/or potassium feldspar (Fig 12D). The 3B panel does not contain as high K_2O addition and most rocks exhibit 3-4% addition (Fig. 3-12D). Mass change in K_2O is minimal in the mafic volcanic rocks of the Pilley's Hills panel (0.6-3%) (Fig. 3-12D). Concentration of Cu is highest (>400ppm) in rocks with 3.4-4.4% K_2O addition (Fig. 3-12D).

Other major elements also show trends in mass change throughout the stratigraphy (Appendix III & IV). For example, SiO_2 is depleted throughout the 3B and Old Mine panels (6-15% SiO_2 loss), but exhibits addition in the Pilley's Hills panel, likely due to solidification of basalts (Appendix IV). Conversely, some elements exhibit unique mass change depending on the lithofacies. Most felsic volcanic flows have CaO addition (up to 5%), whereas volcaniclastic strata and mineralized intervals generally have up to 2.5% CaO loss; likely due to the transformation of Ca-feldspars (e.g. zoisite, andesine) to sericite due to alteration (Riverin and Hodgson, 1980). The mafic volcanic rocks in the Pilley's Hills panel have CaO addition up to 5.8% (Appendix IV). Since pervasive carbonate alteration is rarely observed in the basalts, CaO addition is likely due to

inhomogeneous sampling, including either carbonate veins/veinlets or, more likely, carbonate filled amygdules. The 3B and Old Mine panels also have gains in both MgO (up to 2.7%) and Fe_2O_3 (up to 4.3%) but with no observed correlation to host lithofacies. Mineralized zones are characterized by MgO gains (<1.3%), possibly due to Mg-chlorite chlorite), and high Fe_2O_3 addition (>2.0%), which is likely a result of trace to disseminated sulfides in the rock (Appendix IV).

Transition metals (V, Ni) and HFSE (Y, Nb) with significant mass change do not have any correlation to sulfide mineralization, lithology or lithofacies. Conversely, base metals (Cu, Zn, Pb) show correlations, such as: 1) high base metal gains in felsic volcaniclastic lithofacies (>200ppm Cu, >700ppm Zn, >50ppm Pb); and 2) base metal gains (mean 71.7ppm Cu gain, 56.1ppm Zn gain) in the Pilley's Hills panel mafic volcanic rocks, with the exception of Pb, which exhibits variable mass change throughout the samples (Appendix III & IV).

Mass change data for volatile elements (As, Sb, Tl) also has unique trends, including: 1) highest mass gains (>18ppm As, >2ppm Tl) in volcaniclastic strata and low change or losses in volcanic flows; 2) spatial association between high volatile gains and mineralized zones and high base metal concentrations; and 3) low volatile element change outside of mineralized and altered zones (Appendix III & IV).

3.7. Discussion

Primary and alteration lithogeochemistry provides information on the petrogenesis, hydrothermal alteration and element mobility for the rocks in the Pilley's Island terrane. These results provide information on the evolution of the magmas, heat

flow within the volcanic assemblages and the tectonic setting in which they formed. Furthermore, analysis of the alteration lithogeochemistry and element mass change in the volcanic rocks aid the interpretation of the hydrothermal environment in which the Pilley's Island deposits formed.

3.7.1. Petrogenesis of the Pilley's Island Terrane Volcanic Rocks

3.7.1.1. Mafic volcanic rocks

Mafic volcanic rocks of the Pilley's Island terrane (unit 2, unit 3.1 & unit 6.1) are LREE-enriched and have variable HFSE contents with negative primitive mantle-normalized Nb anomalies, and a geochemical signature similar to calc-alkaline arc basalts (Pearce, 1983; Shinjo et al., 2000). Negative Nb anomalies are characteristic of rocks associated with subduction zones and back-arc basins, because the subducting slab causes an increase in LFSE (e.g., Th) in mantle source regions relative to the HFSE (Pearce, 1983; Hawkins, 1995; Pearce and Peate, 1995; Shinjo, 1999); however, these signatures are also characteristic of bulk and upper continental crust and can be caused by contamination by continental crust (Taylor and McLennan, 1995; McLennan, 2001). Various element plots can be used to understand the relative contributions of mantle and crust/slab in the genesis of basalts. The mantle sources of basalts can be interpreted using the normalized concentrations of Zr, Nb, Th and Yb (Pearce, 1983; Pearce and Peate, 1995; Piercey et al., 2002). These elements are extremely useful as they are strongly incompatible during partial melting and fractional crystallization (Pearce, 1983; Pearce and Peate, 1995; Piercey et al., 2002), and are resistant to mobility during hydrothermal

alteration and therefore remain relatively unaffected by element mass change (e.g. MacLean, 1990; MacLean and Barrett, 1993; Barrett and MacLean, 1999). Furthermore, plots of Zr/Yb and Nb/Yb are insensitive to effects of Th addition either due to slab metasomatism or crustal contamination, therefore providing information on the nature of the mantle source (e.g., depleted vs. enriched), whereas ratios of Th/Yb provide insight into crustal contamination and/or slab metasomatism (Pearce and Peate, 1995).

In Zr/Yb - Nb/Yb space (Fig. 3-13A) most samples have Nb/Yb ratios higher than N-MORB, towards E-MORB, which suggests that the basalts are derived from a variable, weakly depleted to weakly enriched mantle (Sun and McDonough, 1989; Pearce and Peate, 1995). Some samples have higher Zr content relative to the MORB fields, however, suggesting that another process, or processes, have increased the Zr content of the basalt.

In Th/Yb-Nb/Yb space (Fig. 3-13B) samples have elevated Th/Yb and plot far above N-MORB and E-MORB fields also suggesting that another process has influenced the Th concentration in the basalt (Sun and McDonough, 1989). Elevated Th relative to the HFSE (i.e., high Th/Nb) may be a result of the addition of Th to the mantle wedge from the subducting slab or by crustal contamination (Pearce, 1983; Brenan et al., 1995; Pearce and Peate, 1995). Deciphering whether this signature is related to slab metasomatism requires negating the potential effects of crustal contamination (or arc crustal contamination).

In Th/Nb-La/Sm space, crustal contamination typically shows a hyperbolic mixing array from mantle towards crustal values (Fig. 3-13C). Given that the data array shows a

vertical trend that is not hyperbolic suggests that the high Th/Nb in the basalts arises from slab metasomatism and is an "arc" signature. This is also consistent with additional data from the felsic volcanic rocks, the stratigraphy, and Pb isotope systematics from the VMS deposits in the area (Swinden and Thorpe, 1984), all of which point to minimal contamination in the Pilley's Island volcanic rocks. The data suggest that the basalts represent typical, calc-alkalic arc basalts formed via partial melting of slab metasomatized mantle wedge within an Ordovician peri-Laurentian subduction zone (e.g., Swinden et al., 1997).

3.7.1.2. Felsic volcanic rocks

Felsic magmas can form by two methods, including: 1) via fractional crystallization of a basaltic magma (Geist et al., 1995); or 2) via partial melting of oceanic or continental crust due to underplating of basaltic magma (Huppert and Sparks, 1988; Barrie et al., 1993). It is unlikely that the felsic volcanic rocks in the Pilley's Island terrane formed via fractional crystallization because the volcanic assemblage is distinctly bimodal with basalt and felsic volcanic rocks, and does not have a continuous igneous spectrum from basalt to rhyolite (Syme and Bailes, 1993; Hart et al., 2004). This suggests that the rocks formed via partial melting of a crustal substrate; however, the conditions and nature of melting and the substrate are uncertain.

In some VMS districts, the melting of continental crust (or hydrated mafic crust) via basaltic underplating during rifting yields rhyolites with FII to FIII signatures, and this can also lead to the negative Nb anomalies present in many calc-alkalic felsic volcanic rocks (e.g. Lentz, 1998; Piercey et al., 2001; Hart et al., 2004; Piercey, 2011). The

potential role for continental crustal assimilation is tested in Figure 3-14 using incompatible element ratios of Nb, Th, La, Sm, and U. Niobium, Th, and U are immobile during alteration, as are the REE, for the most part. Furthermore, these elements are incompatible during melting, therefore identifying potential crustal sources of the felsic rocks. Notably, Nb/Th and Nb/U ratios in the Pilley's Island felsic rocks are higher than the upper continental crust control line, and below the upper crustal control line in La/Sm space, and is inconsistent with derivation from continental crust, therefore requiring derivation from sources more depleted than continental crust (e.g., hydrated mafic arc crust; Barrie et al., 1993; Barrie, 1995).

The broad similarities in the trace element signatures between the felsic rocks and their mafic counterparts, yet a bimodal assemblage, points to the likelihood that the signatures present in the dacite were inherited from the remelting of an arc basaltic substrate (e.g., Barrie et al., 1993; Barrie, 1995). It is well established that remelting of hydrated basalt can lead to the generation of felsic rocks and the formation of bimodal mafic-felsic assemblages (e.g., Barrie et al., 1993; Barrie, 1995; Bindeman et al., 2008; Wanless et al., 2010; Elders et al., 2011; Bindeman et al., 2012). Furthermore, melting of hydrated basaltic crust often results in the transfer of the "arc" signature from the mafic crust to the associated felsic melts (e.g., Shukuno et al., 2006; Piercey, 2011). Therefore, given the bimodal nature of the Pilley's Island district and strong similarities between the felsic rocks and the mafic rocks, it is inferred that the Pilley's Island dacitic rocks formed via the remelting of hydrated mafic arc rocks. This is also supported by the primitive, low μ Pb isotopic values present in sulfides hosted by felsic rocks at Pilley's Island (Swinden

and Thorpe, 1984), suggesting that they leached Pb from primitive sources (i.e., primitive basalt and rhyolite).

While it is likely that the felsic rocks from Pilley's Island originated via melting of mafic crust, their physicochemical conditions of formation are not well established. While exhaustive thermodynamic modeling is not possible in these rocks due to their altered nature, some information can be obtained from their primitive mantle-normalized signatures and HFSE systematics. Most of the felsic rocks from Pilley's Island have FII to FIIIa signatures (Lesher et al., 1986; Hart et al., 2004) with gently sloping to flat REE patterns ($[La/Yb]_{CN}$ = 2-6 to ~1) with slightly negative Eu anomalies and intermediate HFSE abundance, and transitional to calc-alkalic Zr/Y ratios (Figs. 3-8, 3-9 & 3-10; Table A1-1). Using published experimental data for melt experiments on basalts, Hart et al. (2004) argued that FII-FIIIa rhyolite-dacite volcanic rocks form at lower pressure (<1.0Gpa), high P_{H2O} and high temperature (>750°C-1100°C) at moderate to shallow depth (10-15km). Under such conditions melting of hydrated basalt would yield a residue that contains amphibole as a residual phase, resulting in a melt that is weakly depleted in HREE and Y and has moderate Zr/Y and $[La/Yb]_{CN}$ ratios (e.g., Fig. 3-7D). Furthermore, this type of melt would have plagioclase as a residual phase leading to Eu depletions in the associated melts (Hart et al., 2004), something present in the Pilley's Island felsic rocks (Fig. 3-9); however, Eu can be mobile during alteration (e.g., Sverjensky, 1984) and therefore this signature may in part be due to alteration. Regardless, the trace element signatures of the Pilley's Island felsic rocks are consistent with generation at moderate depths in the crust via remelting of hydrated arc basement, likely during arc rifting.

3.7.2. Tectonic Setting and Implications for VMS Formation

The tectonic setting of the Buchans-Roberts Arm belt, and associated Pilley's Island district, has been variously interpreted. Swinden et al. (1997) argued that the tholeiitic portions of the belt might represent formation within intra-oceanic island arcs, whereas the bimodal sections likely represented arc magmatism built upon a continental substrate. Zagorevski et al. (2006) argued that the belt represents continental arc magmatism within the AAT, where juvenile and evolved blocks were juxtaposed against one another due to strike-slip motions within a broadly peri-Laurentian continental arc environment. The results presented within this manuscript are broadly supportive of these interpretations, albeit with modifications that are unique to the Pilley's Island area. The mafic units have lithogeochemical signatures that are very similar to units found in modern intra-oceanic and continental arcs (e.g., Stoltz et al., 1990; Pearce et al., 1995; Shinjo, 1999). Furthermore, the calc-alkalic dacite have similar signatures and trace element systematics to rocks found in ancient intra-oceanic to continental arcs (e.g., Hildreth and Moorbath, 1988; Lentz, 1998; Piercey, 2011, and references therein). While there is certainly evidence for continental crustal influence in parts of the Buchans-Roberts Arm belt (e.g., Swinden et al., 1997; Zagorevski et al., 2006), the lithogeochemical signatures for the felsic rocks are inconsistent with derivation from a continental crustal substrate (Fig. 3-14). Furthermore, this is also consistent with Pb isotopic data for dacite-hosted VMS mineralization in the district, which have low μ Pb isotopic signatures, consistent with leaching from a juvenile substrate (Swinden and Thorpe, 1984). This suggests that the crust upon which the rocks from which Pilley's

Island and the Buchans-Roberts Arm belt formed was likely transitional in nature, with some areas having juvenile crust underlying and other areas floored by continental crust (e.g., Swinden et al., 1997; Zagorevski et al., 2006).

Despite formation within a peri-Laurentian "arc" system in the broadest sense, the immediate environment of massive sulfide formation at Pilley's Island is likely within a peri-Laurentian arc rift. In particular, the distinctly bimodal assemblage of rocks, indicative of an extensional environment (e.g., Lentz, 1998; Piercey, 2011), contrasts with the typical continuous fractionation sequence from basalt, through andesite, dacite, and rhyolite found in most arcs (e.g., Arculus, 1994), arguing against formation during arc construction. Furthermore, as argued above, the similarity in trace element patterns between felsic rocks and associated basaltic rocks suggests that the former were derived from the latter, and it is envisioned that basaltic underplating associated with rifting resulted in extension and remelting of hydrated mafic arc crust resulting in the formation of associated dacitic rocks.

These tectonic and geochemical features are very common in many bimodal VMS belts (e.g. Lentz, 1998; Piercey, 2011, and references therein). In particular, VMS belts are invariably associated with extensional geodynamic activity as rifting increases fracture permeability and porosity, which creates fluid conduits to generate the convective cell and associated recharge and discharge in the hydrothermal system necessary to form VMS deposits (Swinden, 1991; Lentz, 1998; Hart et al., 2004; Piercey, 2011). Also, additional accommodation space in the crust allows metal-rich fluids to flow into chemical and physical traps to precipitate massive sulfide (Piercey, 2011). Furthermore,

the upwelling of mantle beneath the rifted arc provides anomalous heat flow elevating the geothermal gradient that increases the rigor and longevity of hydrothermal convection (Hart et al., 2004; Piercey, 2011).

3.7.3. Hydrothermal Alteration and Chemical Changes

The effect of hydrothermal alteration in the Pilley's Island district is widespread, but varies as a function of thrust panel (i.e., felsic volcanic-dominated versus mafic volcanic-dominated), and unlike many VMS districts, alteration is not restricted to a pipe, but is rather widespread (e.g., Fig. 3-6). It is interpreted that the widespread alteration is a product of upflow associated with VMS deposit formation (i.e., discordant alteration; e.g., Riverin and Hodgson, 1980; Gemmell and Large, 1992; Franklin et al., 2005), rather than semi-conformable alteration associated with hydrothermal recharge (e.g., Galley, 1993; Skirrow and Franklin, 1994; Franklin et al., 2005), and its geometry is a function of unfocused discharge into relatively unconsolidated and porous volcaniclastic-rich stratigraphy (Gibson, 2005). Flow-dominated environments form different alteration patterns because alteration and fluid flow are restricted by the surrounding impermeable strata (e.g., Riverin and Hodgson, 1980; Gemmell and Large, 1992; Gemmell and Fulton, 2001).

The hydrothermal alteration in the Pilley's Island district is dominated by white mica alteration (i.e., >60% of sampled rocks in the district). Furthermore, many chlorite-altered samples also have sericite alteration (84% of the altered rock samples). The formation of sericite results from the reaction of existing feldspars (e.g., albite) and volcanic glass with VMS-forming fluids (Barrett and MacLean, 1994b):

(R.1) $3NaAlSi_3O_8 + K^+_{(aq)} + 2H^+_{(aq)} = KAl_3Si_3O_{10}(OH)_2 + 6SiO_{2(aq)} + 3Na^+_{(aq)}$

albite muscovite quartz

Sericite can also form via the transformation of zoisite or andesine (Ca-feldspar) via interaction with hydrothermal fluids (Riverin and Hodgson, 1980):

(R.2) $Ca_2Al_2Si_3O_{12}(OH) + K^+_{(aq)} + 2H^+_{(aq)} = KAl_3Si_3O_{10}(OH)_2 + 2Ca^{2+}_{(aq)} + OH^-_{(aq)}$

zoisite muscovite

(R.3) $2Ca_{0.5}Na_{0.5}Al_{1.5}Si_{2.5}O_8 + 4.48Al(OH)_4^-_{(aq)} + 1.16K^+_{(aq)} + 2.23H^+_{(aq)} = 1.16KAl_3Si_3O_{10}(OH)_2 + 1.5SiO_{2(aq)} + Na^+_{(aq)} + Ca^{2+}_{(aq)}$

andesine sericite quartz

These reactions generally result in the addition of K_2O and losses in SiO_2, CaO and Na_2O. The mass balance results illustrate losses in Na_2O, CaO and SiO_2 associated with gains in K_2O (Fig. 3-15); however, numerous samples do have coincident gains in K_2O and SiO_2, consistent with field observations where there is coincident quartz alteration addition with pervasive sericite alteration. Furthermore, some samples have enrichments in CaO (predominantly mafic volcanic rocks; units 2, 4.1, 6.1), consistent with addition of calcite (or other carbonates) likely by seafloor diagenesis or semicomformable alteration (Fig. 3-15E) (Alt, 1995, 1999).

Coincident with enrichments in K_2O are general enrichments in Rb, Ba, and Tl, consistent with their substitution within the sericite structure (e.g., MacLean and Hoy, 1991; Large et al., 2001a). Similarly, Sr behaves like CaO and is depleted in samples with

low K_2O, and enriched in samples with high CaO, consistent with depletions associated with losses during feldspar destruction, and gains when associated with carbonate.

Chlorite is present in lesser abundance than sericite, but is present with a variety of chemical compositions (e.g., Mg-, Fe-, Fe,Mg-chlorite). Chlorite alteration in these samples is either due to the chloritization of existing white micas, particularly in felsic rocks, or the chloritization of mafic phases in the mafic rocks (e.g., Riverin and Hodgson, 1980; Knuckey et al., 1982):

(R.4) $K_2Fe^{2+}Al_3Si_7AlO_{20}(OH)_4 + 9FeCl_{2(aq)} + 16H_2O = Fe^{2+}{}_{10}Al_2Si_6Al_2O_{20}(OH)_{16} + H_4SiO_{4(aq)} + 2KCl_{(aq)} + 16HCl_{(aq)}$

Phengite — Fe-rich chlorite

(R.5) $2KAl_3Si_3O_{10}(OH)_2 + 3H_4SiO_{4(aq)} + 9Fe^{2+}{}_{(aq)} + 6Mg^{2+}{}_{(aq)} + 18H_2O = 3Mg_2Fe_3Al_2Si_3O_{10}(OH)_8 + 2K^{+}{}_{(aq)} + 28H^{+}{}_{(aq)}$

Muscovite — Chlorite

(R.6) $2Ca(Mg,Fe)Si_2O_6 + 0.58Al(OH)_4^{-}{}_{(aq)} + 0.58H^{+}{}_{(aq)} = 0.29(Mg,Fe)_5Al_2Si_3O_{10}(OH)_8 + 3.3SiO_{2(aq)} + 2Ca^{2+}{}_{(aq)} + 0.55(Fe,Mg)2^{+}{}_{(aq)} + 2.84H_2O$

Diopside — Chlorite — Quartz

In the reactions above, there is a net gain in Fe_2O_3 and MgO during the chloritization of white micas and diopside, with net losses in alkalis, and in the case of the chloritization of muscovite there is a net loss in silica. The losses of alkalis with increased Fe_2O_3+MgO are observed in the mass balance results, and those with higher alkali content and low Fe_2O_3+MgO have CaO and Na_2O gained by carbonate and albite alteration (Table A2-3). There is also a coincident loss in SiO_2 in the more Fe_2O_3-MgO-enriched rocks, consistent with chlorite-(pyrite) addition and destruction of muscovite or mafic minerals (Fig. 3-

16A). However, some samples have both high Fe_2O_3+MgO and SiO_2, consistent with quartz-chlorite-pyrite formation, found in some samples (Fig. 3-16A).

While most samples with enrichments in Fe_2O_3+MgO are associated with chlorite alteration, the samples with significant gains in Fe_2O_3 and loss in MgO are associated with sulfide addition (Fig. 3-16B). These samples also have gains in base metals (Cu, Zn, Pb), As, and Tl, consistent with the occurrence of various sulfide phases in the mineralization (Fig. 3-16C).

The HFSE and REE are plotted in Figures 3-17 and 3-18 against Fe_2O_3 (proxy for chlorite alteration and sulfides), CaO (proxy for calcite alteration), and Na_2O and K_2O (proxies for sericite alteration). For the Th, U, Nb, Ta, and Hf there are gains and losses in elements but they do not show any systematic relationship to the proxies above, this argues that these gains and losses are due to the natural variations between the altered rocks and the precursor(s) (i.e., errors inherent in assumptions made with the multiple precursor method; Fig. 3-17). An exception to the latter is Y, which does show a positive correlation with changes in CaO, suggesting that it has been mobile, potentially due to mobilization by carbonate-rich fluids (e.g., Murphy and Hynes, 1986; Bau, 1996). The REE also show scattered patterns with no trends against the proxies above, suggesting they are likely immobile, for the most extent; however, some samples show positive trends with changes in CaO, particularly so for the basaltic samples, suggesting the potential for minor remobilization associated with carbonate alteration in some of the samples at Pilley's Island (Fig. 3-18) (Bau and Möller, 1992). Mobilization of REE may

also explain some of the spiky patterns in the primitive mantle normalized diagrams shown in Figures 3-8 and 3-9.

3.7.4. Distribution of Hydrothermal Alteration and Exploration Vectors

The thrust panels within the Pilley's Island terrane contain a variety of different hydrothermal alteration assemblages, some that are found more proximal to mineralization (i.e., muscovite and illitic muscovite alteration), and some that are distal to mineralization (i.e., chlorite alteration). Mafic volcanic-dominated thrust panels (Pilley's Hills and Liquor Street panels) are characterized by widespread and pervasive Mg- to Fe,Mg-chlorite alteration. In the felsic-dominated and mineralized thrust panels (Spencer's Dock, 3B and Old Mine panels) chlorite alteration is not immediately associated with mineralization, but does occurs regionally. In particular, distal to the deposits there is Fe,Mg-chlorite with mid-range FeOH spectral absorption (2252-2255nm; Fig. 3-6).

Phengite and illitic phengite form interchangeably within large alteration haloes (over 500m) surrounding the Pilley's Island VMS deposits, and have increasing alteration intensity more proximal to mineralization (Fig. 3-6). The size of the phengitic alteration halo is evident in the Spencer's Dock panel surface geology and in cross section through the 3B and Old Mine panels (Fig. 3-6). Illitic phengite- and phengite-altered rocks can be differentiated from other white mica-altered rocks because they have moderate to high wavelength AlOH absorption features (average 2223.0 and 2221.4nm, respectively) (Fig. 3-6, Table 3-1). Illitic muscovite and muscovite are the most proximal hydrothermal alteration product surrounding mineralization, and they form fairly small haloes

surrounding the deposits (less than 50m) (Fig. 3-6B). The occurrence of muscovite minerals proximal to mineralization is evident in cross section through the Bull Road showing and Bumble Bee Bight deposits (Fig. 3-6B). Muscovite and illitic muscovite alteration are infrequently observed at surface because the majority of the deposits exist at depth. Illitic muscovite and muscovite can be differentiated from other white mica because they have moderate to low wavelength AlOH absorption features (average 2208.9 and 2208.8, respectively) (Fig. 3-6B; Table 3-1).

Each alteration phase has unique elemental associations and mass change trends. For example, illitic phengite and phengite alteration zones are characterized by losses in SiO_2, CaO and Na_2O, and gains in MgO, Fe_2O_3, K_2O, base metals (Cu, Pb, Zn), LFSE (Rb, Sr, Ba) and volatile elements (As, Sb and Tl) (Table 3-2). Similarly, muscovite alteration zones are also characterized by loss of SiO_2, CaO, Na_2O and gains of Fe_2O_3, K_2O, base metals, and volatile elements (Table 3-2). Illitic muscovite differs from the other alteration assemblages because it exhibits loss of MgO and Ba (Table 3-2).

3.7.5. Implications for Exploration

Although lithogeochemistry alone cannot predict the presence of ore mineralization, it is a useful tool to select areas favourable for VMS deposits (permissive environments) and to map a larger scale footprint to potentially vector towards less obvious deposits. The primary and alteration lithogeochemistry of Pilley's Island terrane indicate that favourable zones of mineralization have very specific lithogeochemical attributes. These zones include: 1) FII-FIIIa felsic volcanic rocks; 2) muscovite and illitic muscovite alteration zones; 3) AlOH absorption features close to 2208nm, and less than

2215nm; 4) major element mass change involving Na_2O, CaO, SiO_2 loss and K_2O, Fe_2O_3 addition; 5) base metal (Cu, Pb, Zn) gains; and 6) volatile element mass change including As, Sb, and Tl gains.

3.8. Conclusions

The Pilley's Island VMS district contains six VMS deposits that are hosted within imbricate thrust panels consisting of predominantly felsic volcanic rocks. These panels are imbricated with barren mafic volcanic panels. Primary, immobile element lithogeochemistry has been used to indicate the possible tectonic environments and provide information on the petrogenesis of the volcanic rocks associated with the deposits. Furthermore, alteration lithogeochemistry has been used to identify later modifications to the primary petrochemistry associated with hydrothermal alteration of the host units in the VMS environment. The integration of primary lithogeochemistry and alteration lithogeochemistry in both 2D and 3D space have provided an understanding of the geochemistry of the rocks involved in the formation, duration and later modifications of the VMS system, providing potential vectors towards prospective intervals and mineralization.

A. The mafic volcanic rocks of the Pilley's Island terrane are derived from a variable, weakly depleted to weakly enriched mantle source, and have been enriched in Th due to slab metasomatism. The mafic volcanic rocks represent typical, calc-alkalic arc basalts formed via partial melting of a slab metasomatized mantle wedge within an Ordovician peri-Laurentian subduction zone (e.g., Swinden et al., 1997).

B. The broad similarities in the trace element signatures between the felsic rocks and their mafic counterparts indicate that the felsic volcanic rocks of the Pilley's Island terrane likely formed via the remelting of a hydrated, arc basalt substrate.

C. The lithogeochemical signatures of the mafic units are similar to those found in modern intra-oceanic and continental arcs and the felsic units are similar to those found in ancient intra-oceanic to continental arcs. However, low μ Pb isotopic signatures suggest that the rocks from which the Pilley's Island terrane formed were likely transitional in nature, with some areas having juvenile crust underlying and other areas floored by continental crust. Massive sulfide formation at Pilley's Island likely took place within a peri-Laurentian arc rift.

D. Widespread, unfocussed alteration hosted in volcaniclastic-dominated stratigraphy has caused extensive sericite alteration and results from the reaction of feldspars (e.g., albite, zoisite, andesine) and glass with hydrothermal fluids. Sericite alteration is also often coincident with quartz or calcite (or other carbonates) addition. Quartz and calcite addition likely represents seafloor diagenesis or semi-comformable alteration. Chlorite alteration is less abundant, commonly forms Fe- to Mg-rich chemical end members, and is the result of the destruction of muscovite or mafic minerals. Chlorite alteration is common in mafic volcanic-dominated thrust panels and is not immediately associated with mineralization, but does occur regionally. Phengite and illitic phengite alteration form large (>500m) haloes surrounding the VMS deposits and have higher alteration intensity proximal to mineralization. Illitic muscovite and muscovite alteration are the most proximal alteration assemblage and form small (<50m) haloes surrounding

the VMS deposits. They are most easily identified using NIR-SWIR and locating them by their low to moderate AlOH absorption features averaging 2208.9nm (illitic phengite) and 2208.8nm (phengite).

E. Element vectoring can also be used to indicate proximity to VMS mineralization because each alteration assemblage has unique mass change trends. For example, illitic phengite and phengite alteration zones are characterized by losses in SiO_2, CaO and Na_2O, and gains in MgO, Fe_2O_3, K_2O, base metals (Cu, Pb, Zn), LFSE (Rb, Sr, Ba) and volatile elements (As, Sb and Tl). Also, muscovite alteration zones are characterized by loss of SiO_2, CaO, Na_2O and gains of Fe_2O_3, K_2O, base metals, and volatile elements. The most useful element vectors in the Pilley's Island district include those that are most mobile during VMS formation, including: 1) major elements (Na_2O, CaO, SiO_2 loss and K_2O, Fe_2O_3 addition); 2) base metals (Cu, Pb, Zn); and volatile elements (As, Sb, Tl).

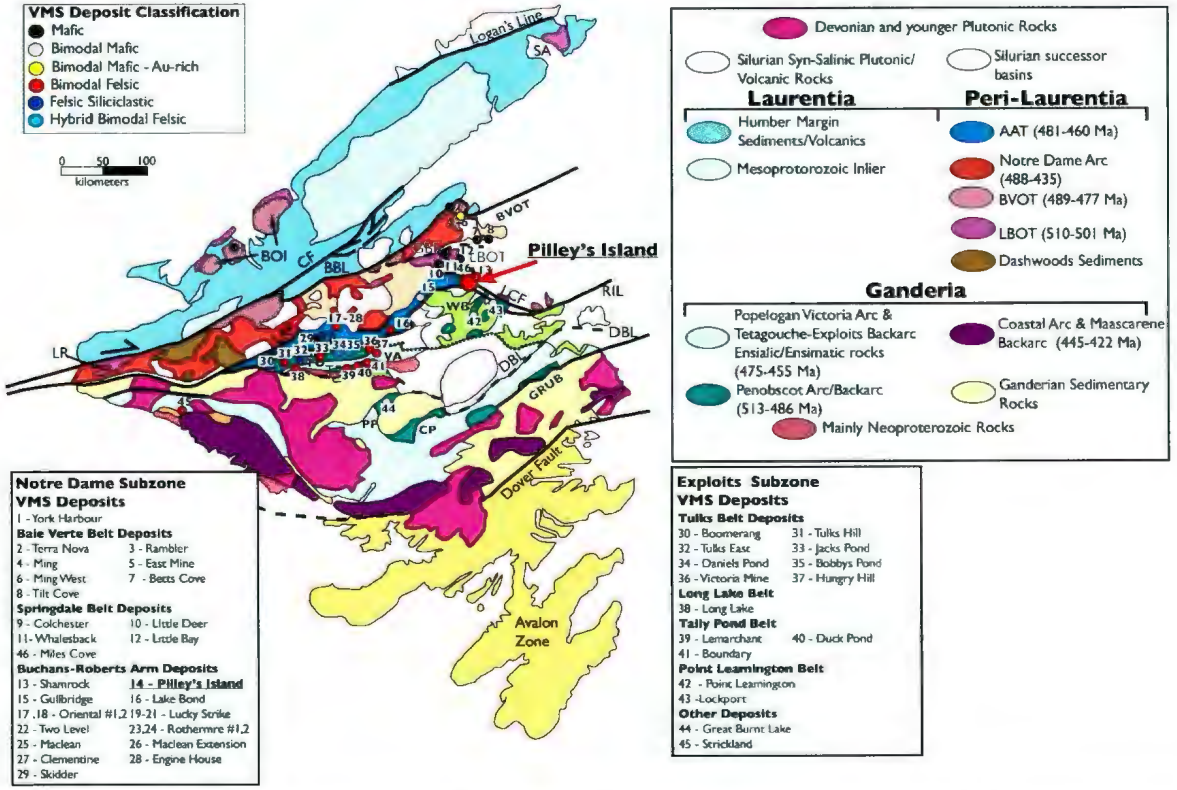

Figure 3-1 Geological map of the Newfoundland Appalachians with tectonostratigraphic zones, accretionary tracts, VMS deposits their classifications and associated belts. Map tectonostratigraphy modified from van Staal (2007) and van Staal and Barr (2011). Volcanogenic massive sulfide (VMS) deposit classification from Piercey (2007c) and Hinchey (2011). Abbreviations: BBL Baie Verte Brompton Line; BOI - Bay of Islands; BVOT = Baie Verte Oceanic Tract; CF = Cabot Fault; CP = Coy Pond Complex; DBL = Dog Bay Line; GBF = Green Bay Fault; GRUB = Gander River Ultramafic Belt; LBOT = Lushs Bight Oceanic Tract; LCF = Lobster Cove Fault; LR = Long Range; LRF - Lloyds River Fault; PP = Pipestone Pond Complex; RIL = Red Indian Line; SA - St. Anthony; TP = Tally Pond Belt; TU = Tulks Volcanic Belt; VA = Victoria Arc; WB = Wild Bight Group.

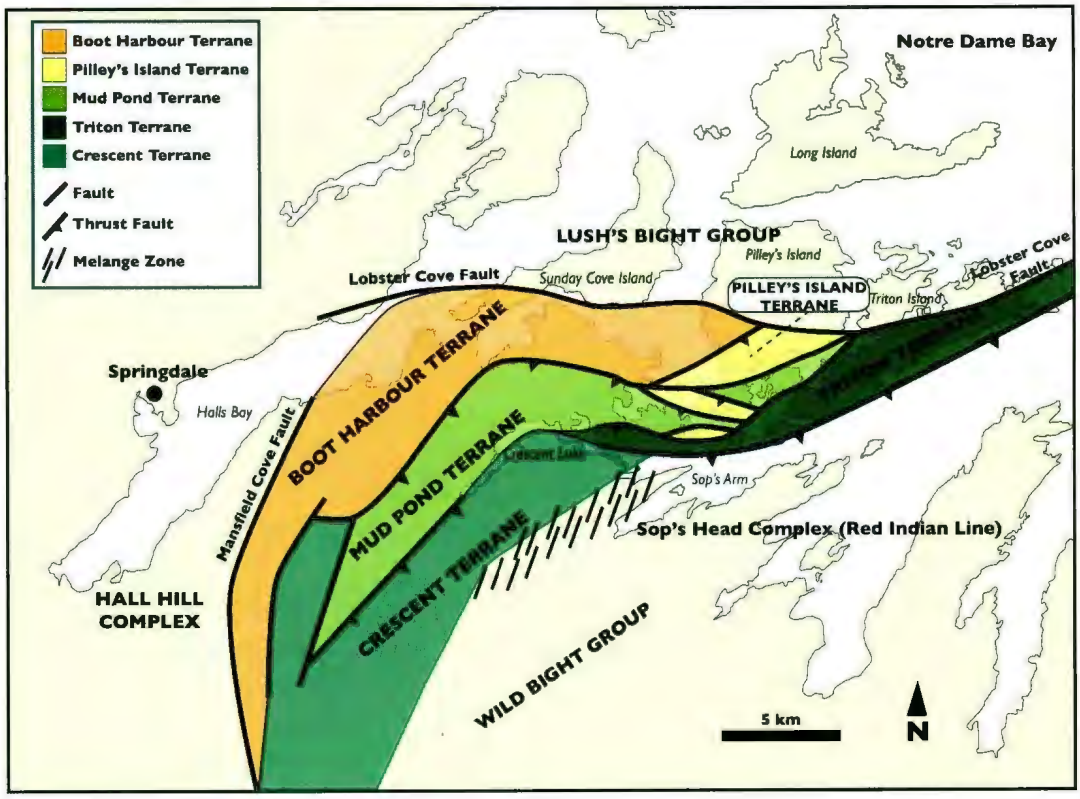

Figure 3-2 Simplified geological map of the northern Roberts Arm Group showing the location of Pilley's Island terrane and adjacent terranes that have been imbricated due to faulting. Modified from Kerr (1996)

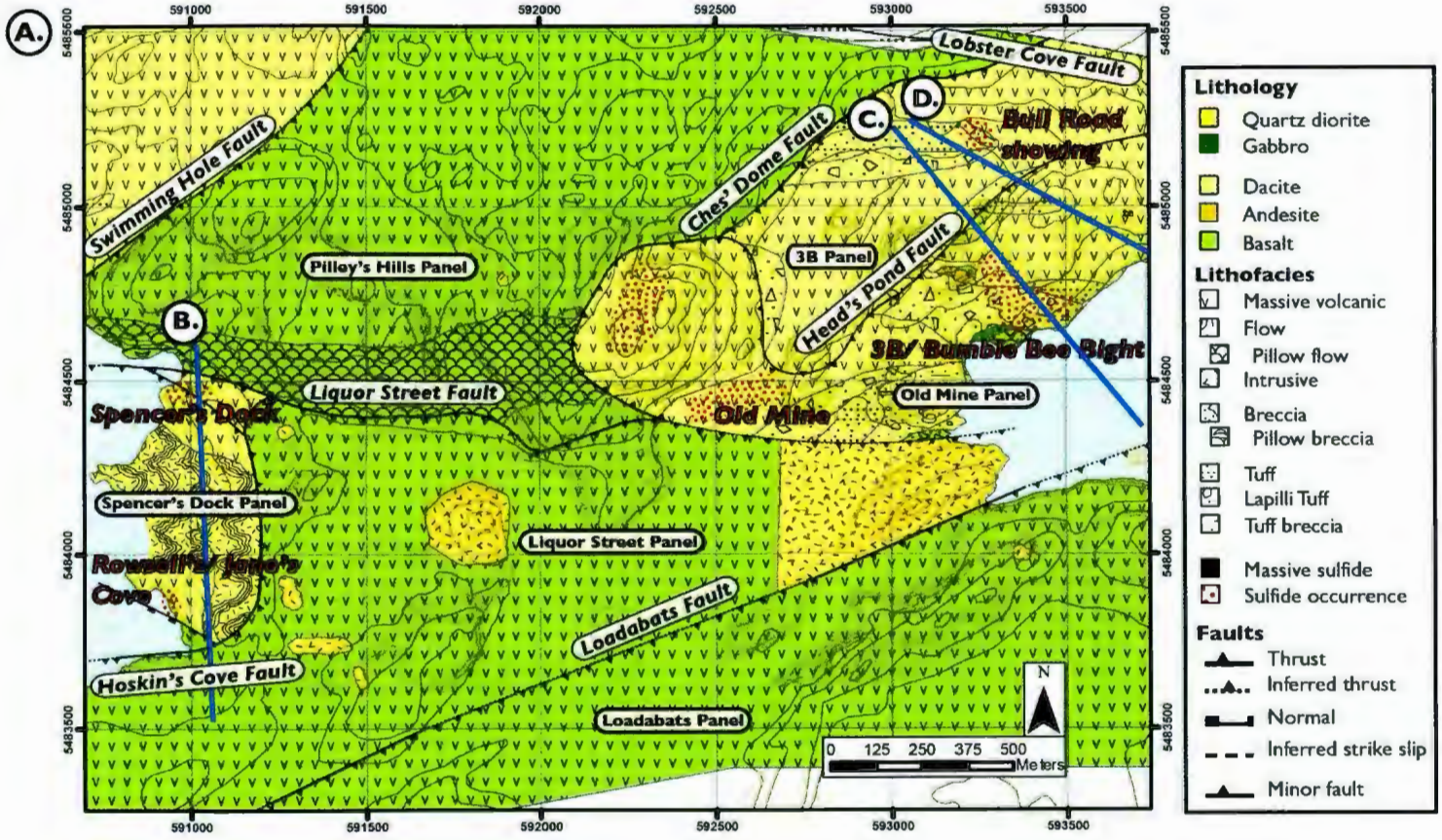

Figure 3-3 Geological map of the Pilley's Island VMS district and representative cross sections through the deposits (next page). A. Surface map of the Pilley's Island VMS district showing the distribution of different lithologies and lithofacies in the area, as well as the thrust faults that juxtapose different units in the area. Continued on next page.

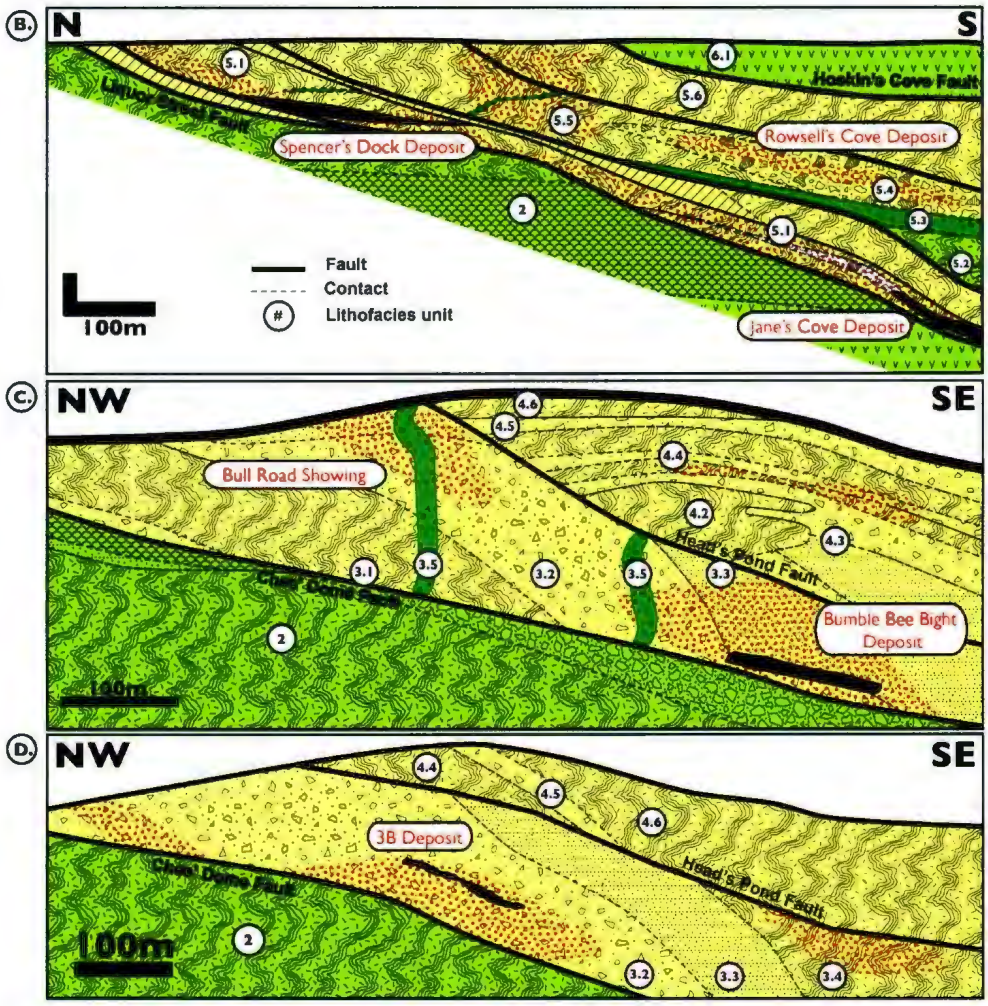

Figure 3-3 *cont'd.* B. Cross section through the Spencer's Dock panel, showing the three different deposits at different stratigraphic levels. C. Cross section through portions of the 3B and Old Mine panels and the host lithofacies of the Bull Road showing and Bumble Bee Bight deposit. D. Cross section through the 3B and Old Mine panels, including the 3B deposit. Legend in Figure 3-3A.

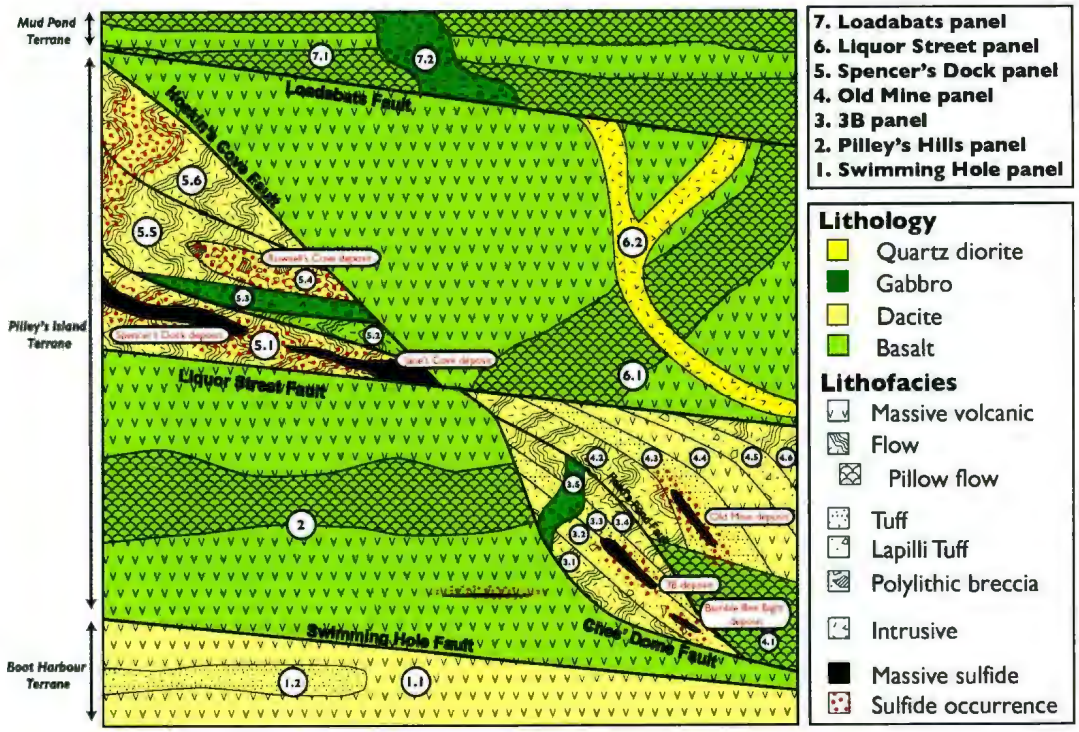

Figure 3-4 Schematic illustration (not to scale) of the volcanic stratigraphy within each panel and field relationships between stratigraphic units and VMS deposits within the Pilley's Island terrane, including juxtaposition by thrust faults.

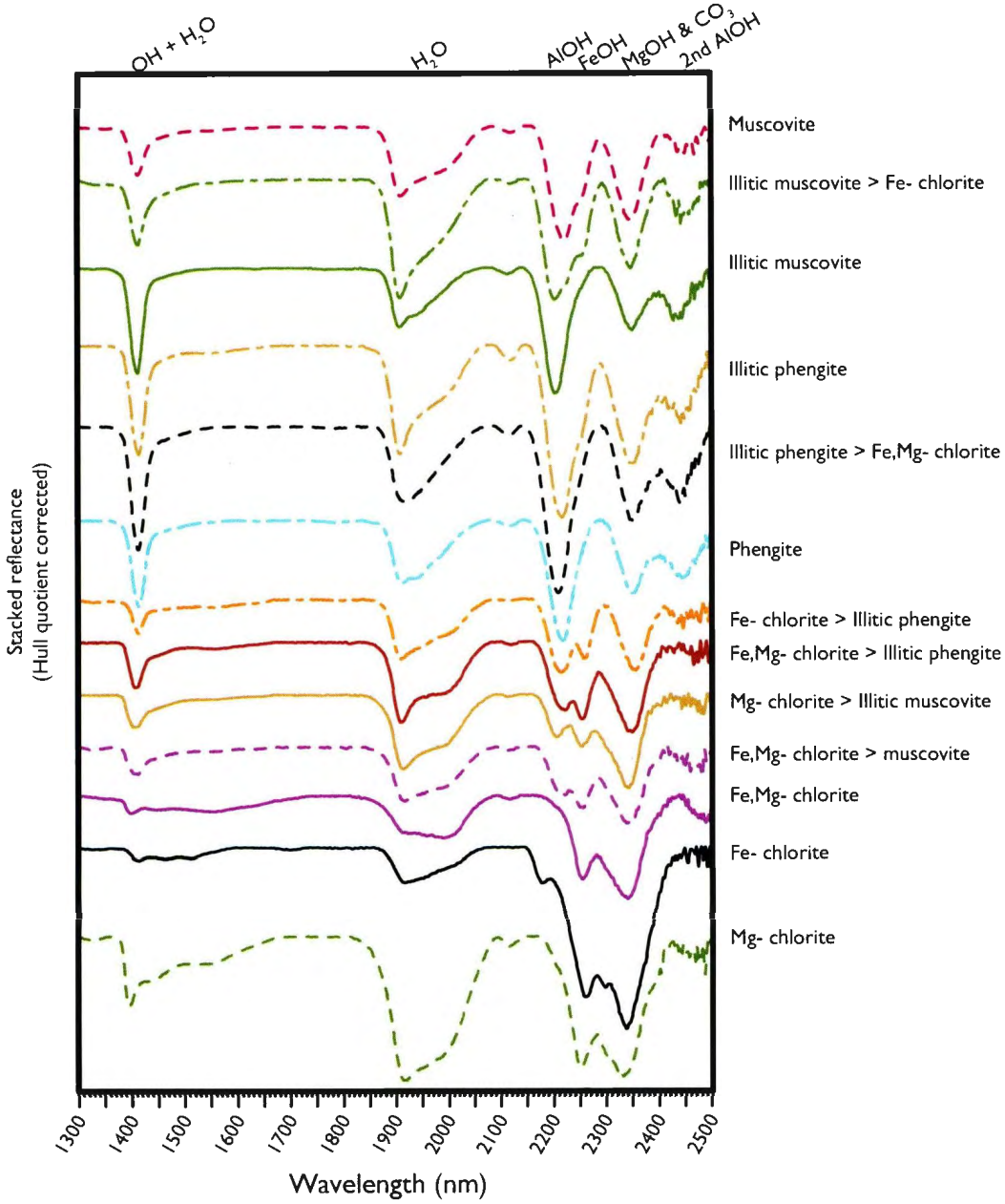

Figure 3-5 Typical SWIR absorption spectra (Hull quotient corrected) from the Pilley's Island VMS district, including: white mica (phengite, illitic phengite, muscovite and illitic muscovite), chlorite (Fe-chlorite, Fe,Mg-chlorite, Mg-chlorite), and combinations of these phyllosilicates.

Table 3-1 Summary of AlOH, FeOH and MgOH absorption features in SWIR spectra for different alteration minerals from the Pilley's Island VMS district.

Dominant alteration mineral	Wavelength of white mica AlOH feature (nm)	Wavelength of chlorite FeOH feature (nm)	Wavelength of chlorite MgOH Feature (nm)
Fe-chlorite	N/A	2252-2255 (avg. 2254.6)	2345-2352 (avg. 2349.7)
Fe,Mg-chlorite	N/A	2248-2255 (avg. 2253.7)	2332-2355 (avg. 2345.7)
Mg-chlorite	N/A	2247-2255 (avg. 2251.8)	2325-2347 (avg. 2339.7)
Muscovite	2208-2215 (avg. 2208.8)	N/A	N/A
Illitic muscovite	2200-2225 (avg. 2208.9)	N/A	N/A
Phengite	2215-2226 (avg. 2221.4)	N/A	N/A
Illitic phengite	2214-2228 (avg. 2223.0)	N/A	N/A

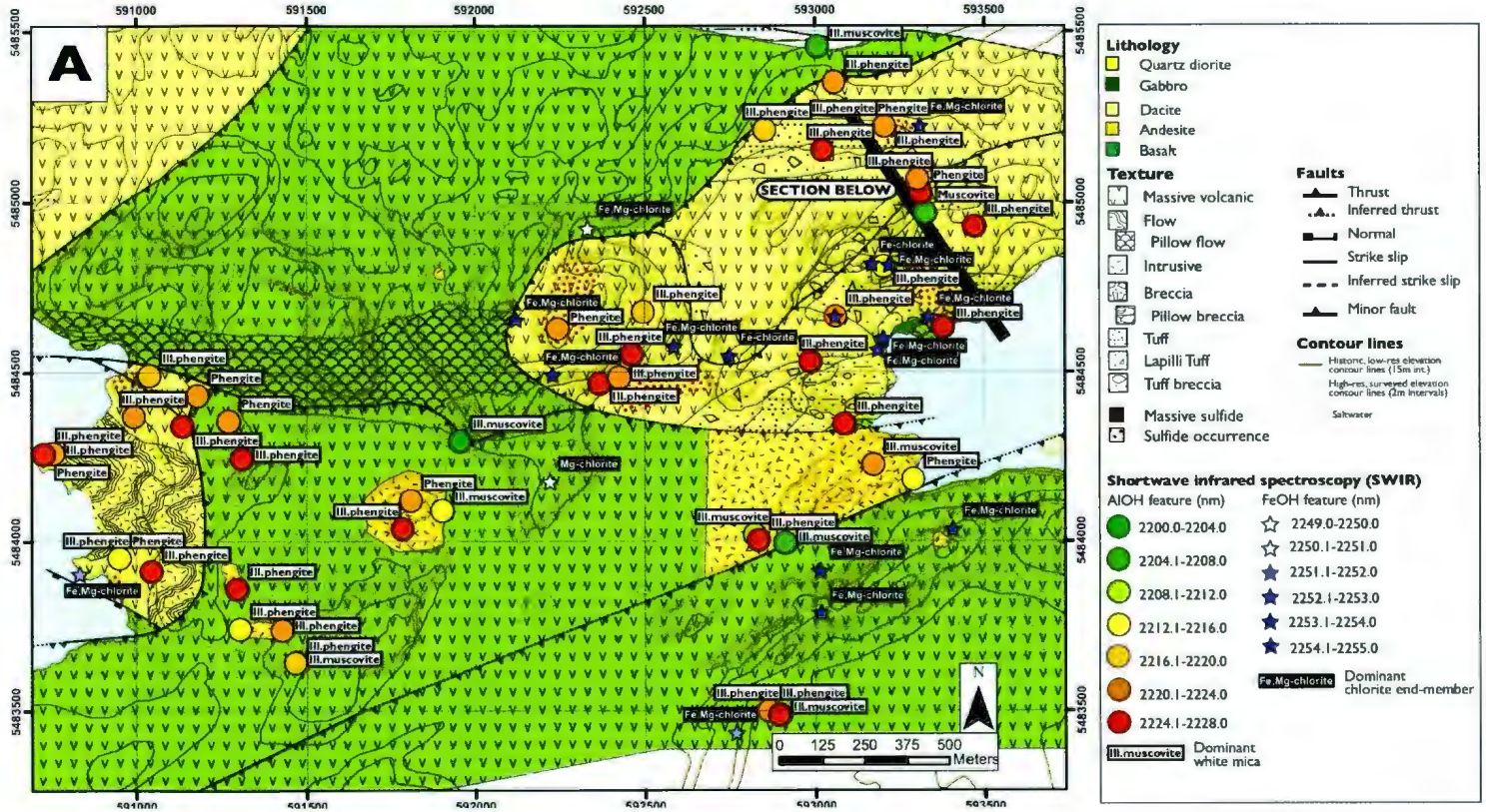

Figure 3-6 Spatial distributions of white mica and chlorite alteration minerals in the Pilley's Island VMS district as determined by SWIR. A. Geological map of the Pilley's Island VMS district with sample locations symbolized based on AlOH or FeOH absorption features and labeled by the dominant alteration mineral. Continued on next page.

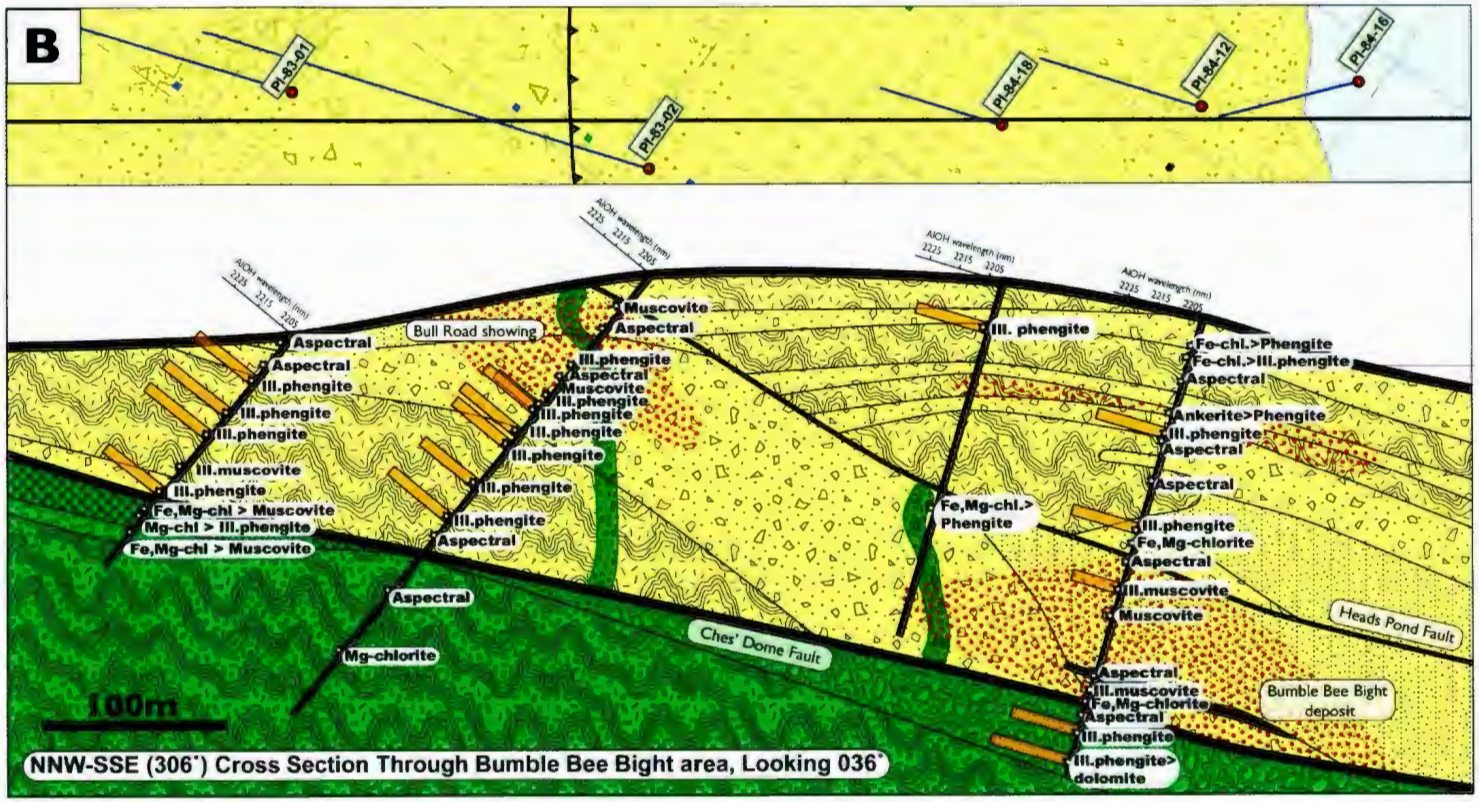

Figure 3-6 *cont'd* B. Cross section through the 3B and Old Mine panels illustrating the AlOH absorption features from SWIR spectra and dominant alteration minerals. Legend in Figure 3-6A.

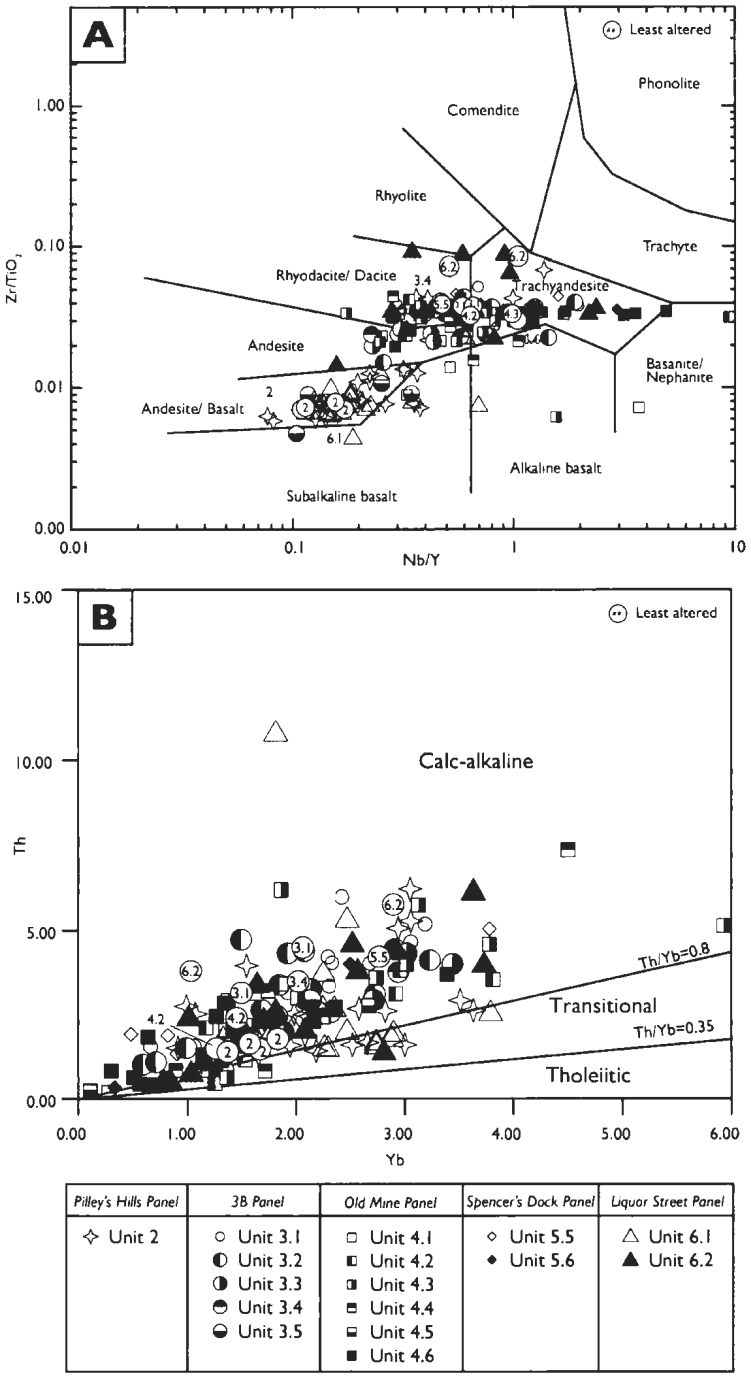

Pilley's Hills Panel	3B Panel	Old Mine Panel	Spencer's Dock Panel	Liquor Street Panel
✧ Unit 2	○ Unit 3.1	□ Unit 4.1	◇ Unit 5.5	△ Unit 6.1
	◐ Unit 3.2	◧ Unit 4.2	◆ Unit 5.6	▲ Unit 6.2
	◑ Unit 3.3	◨ Unit 4.3		
	◓ Unit 3.4	▣ Unit 4.4		
	◒ Unit 3.5	▤ Unit 4.5		
		■ Unit 4.6		

Figure 3-7 Major and trace element plots of the stratigraphic units in the Pilley's Island terrane. A. Zr/TiO_2 vs Nb/Y discrimination diagram from Winchester and Floyd (1977). B. Th vs. Yb plot of tholeiitic vs. calc-alkaline affinity of the volcanic rocks from the Pilley's Island terrane from Barrett and Maclean (1999) and Ross and Bedard (2009). Continued on next page.

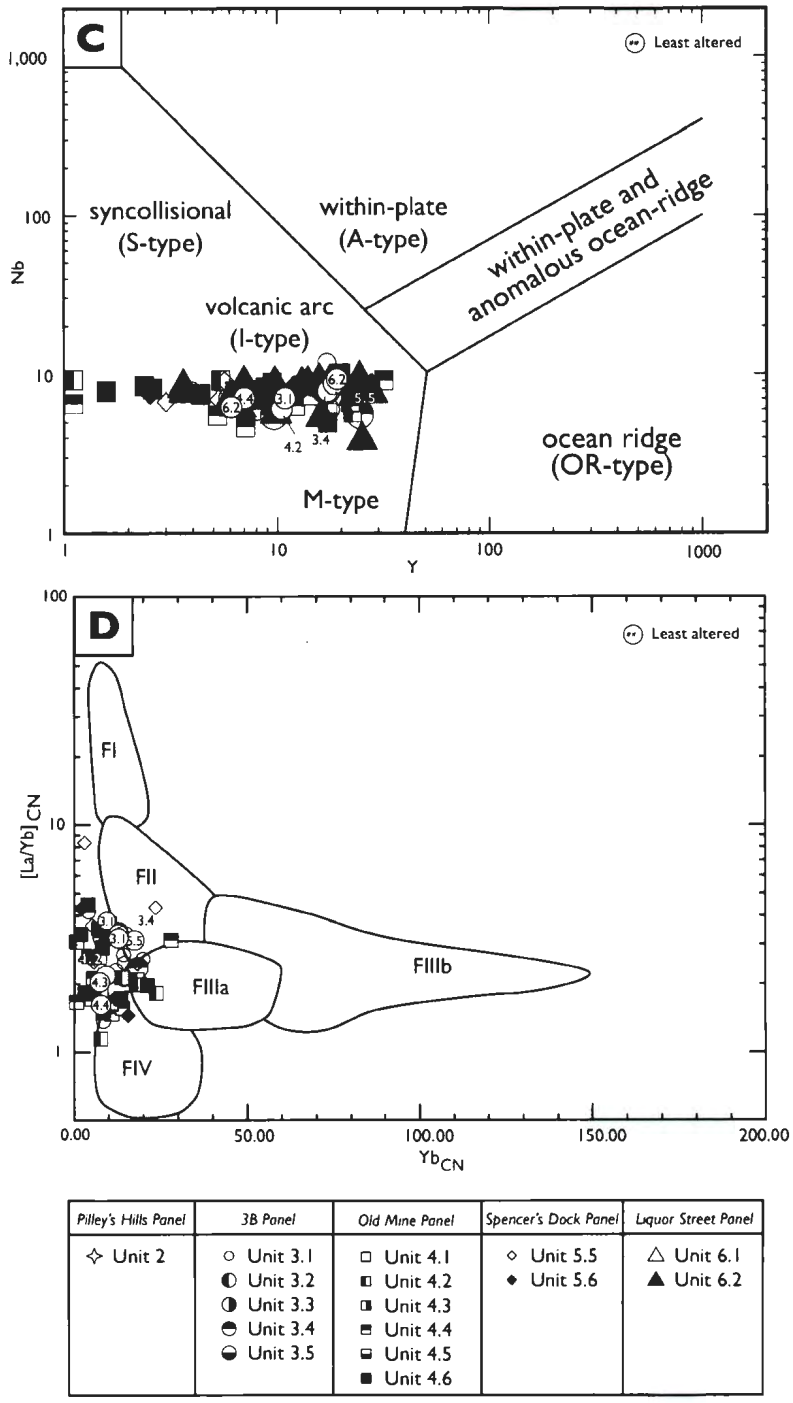

Figure 3-7 *cont'd* C. Nb vs. Y tectonic discrimination diagram of Pearce et al. (1984) showing the felsic flow units from the Pilley's Island terrane. D. La/Yb_{CN} vs. Yb_{CN} (CN= chondrite normalized) plot with fields for FI-FIV felsic volcanic rocks from Lesher et al. (1986) and Hart et al. (2004).

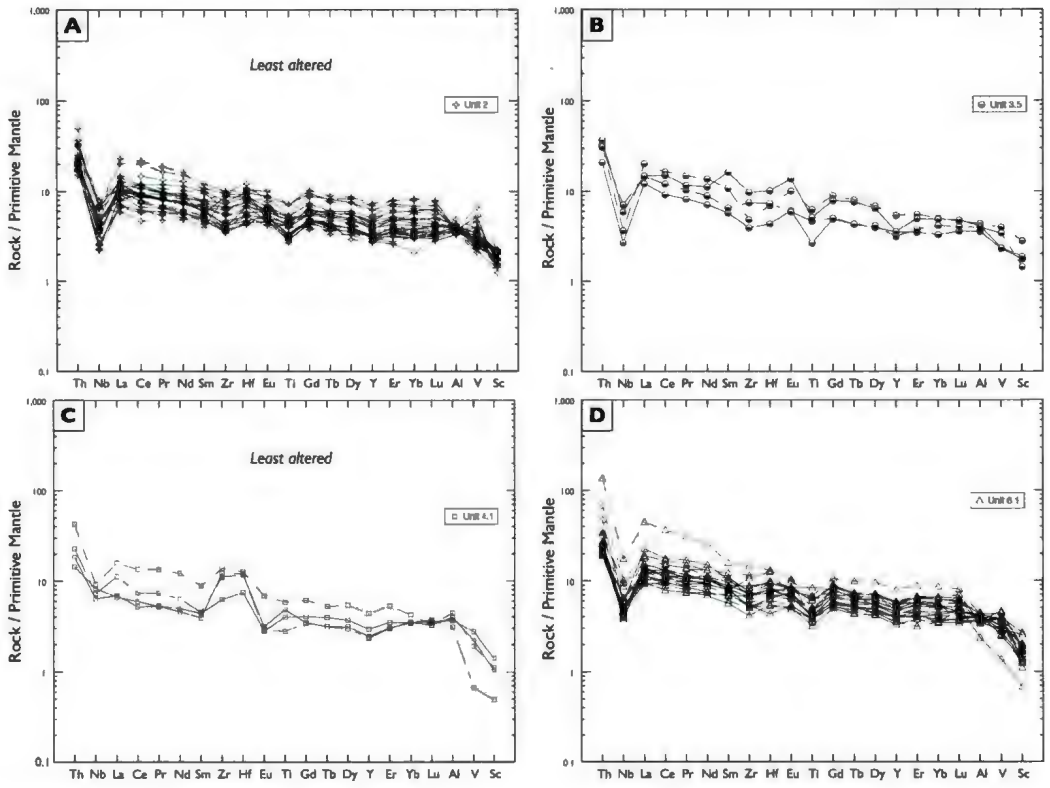

Figure 3-8 Primitive mantle-normalized trace element plots for mafic rocks from the Pilley's Island terrane. Normalization values from Sun and McDonough (1989). A. Trace element signatures for Pilley's Hills panel rocks. B. Trace element signatures for unit 3.5 mafic intrusions in the 3B panel. C. Trace element signatures for unit 4.1 basaltic flows in the Old Mine panel. D. Trace element signatures for unit 6.1 basaltic flows in the Liquor Street panel.

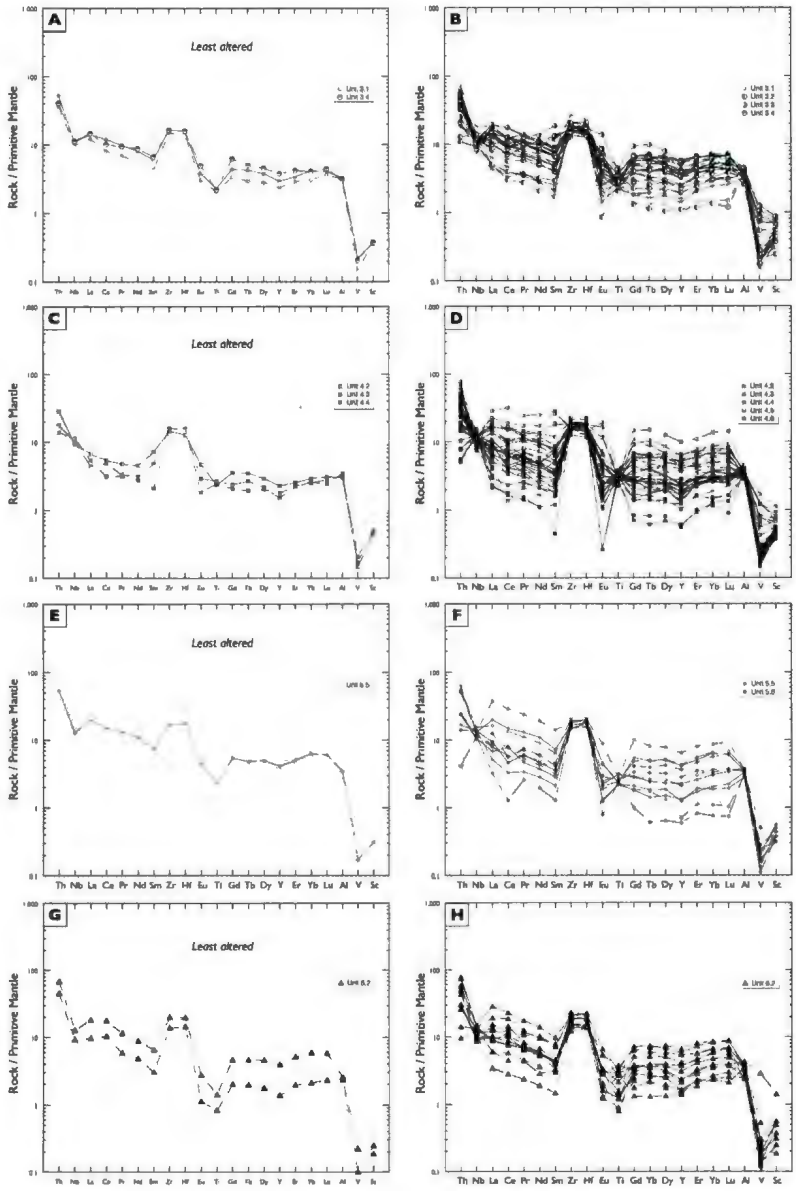

Figure 3-9 Primitive mantle-normalized trace element plots for felsic rocks from the Pilley's Island terrane. Normalization values from Sun and McDonough (1989). A. Trace element signatures for least altered rocks from the 3B panel. B. Trace element signatures for hydrothermally altered rocks of the 3B panel. C. Trace element signatures for least altered rocks from the Old Mine panel. D. Trace element signatures for hydrothermally altered sample from the Old Mine panel. E. Trace element signatures for least altered rocks from the Spencer's Dock panel. F. Trace element signatures for hydrothermally altered rocks from the Spencer's Dock panel. G. Trace element signatures for least altered samples from unit 6.2 quartz diorite intrusions in the Liquor Street panel. H. Trace element signatures for hydrothermally altered samples from unit 6.2 felsic intrusions in the Liquor Street panel.

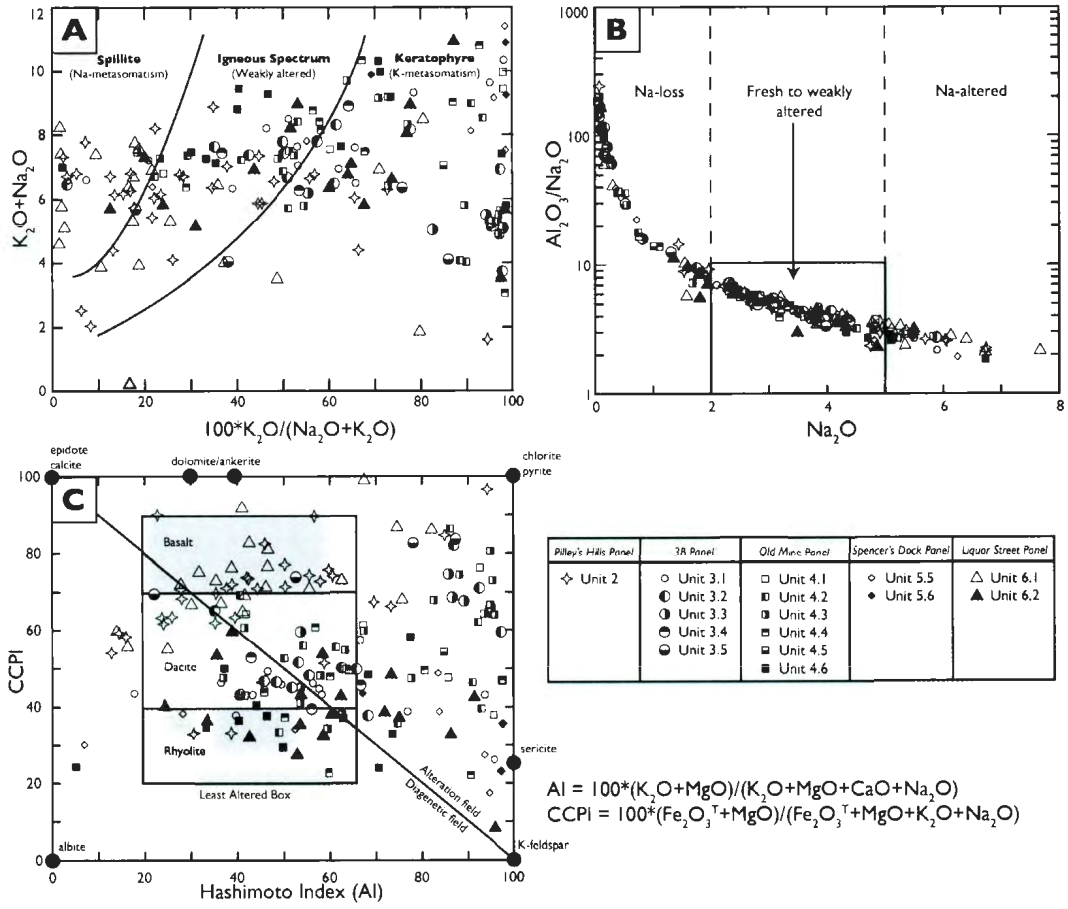

Figure 3-10 Alteration lithogeochemical plots of the stratigraphic units in the Pilley's Island terrane. A. Hughes (1973) diagram illustrating fresh, spilitized (Na-altered), and keratophyric (K-altered) igneous rocks. B. Spitz-Darling index (Spitz and Darling, 1978) (Al_2O_3/Na_2O) versus Na_2O differentiating fresh rocks versus those with Na-gain (spillite) and Na-loss. C. Alteration box plot from Large et al. (2001b) of the Hashimoto alteration index (AI) and chlorite-carbonate-pyrite index (CCPI).

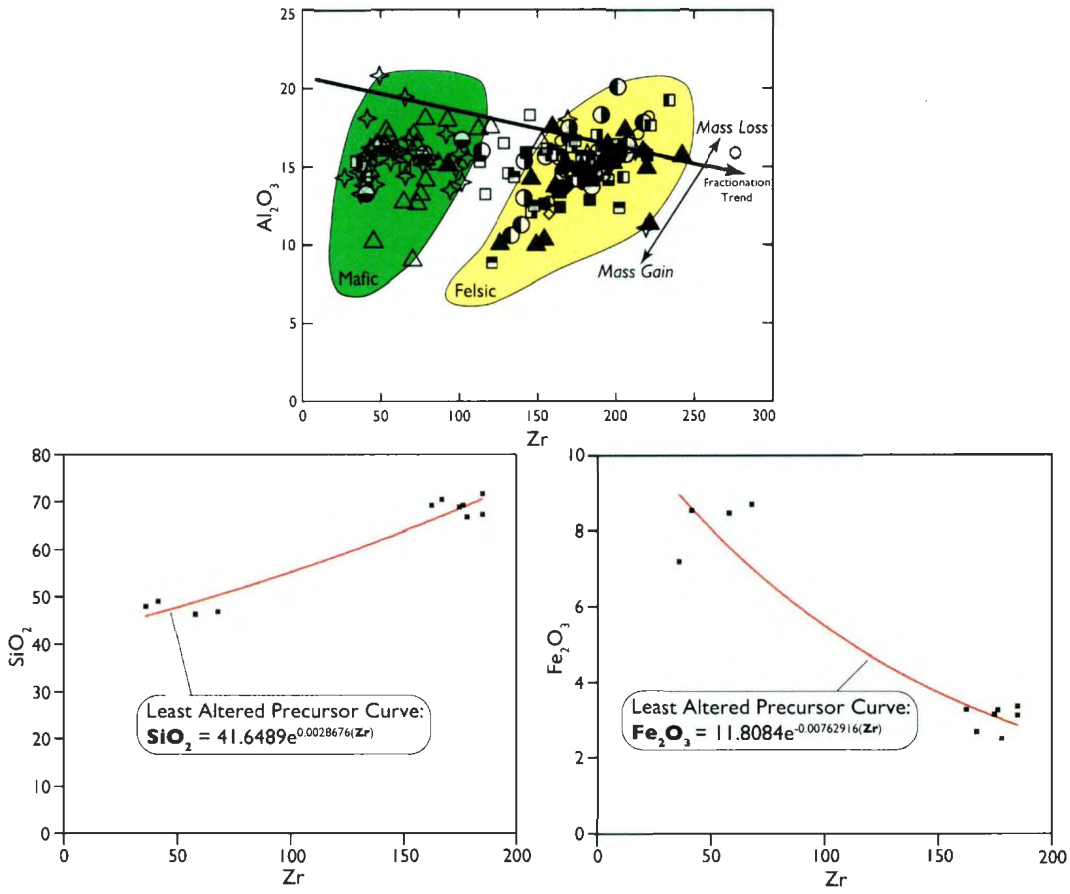

Figure 3-11 Immobile element mass balance diagrams. A. Al_2O_3 - Zr plot with least altered fractionation curve and mass gain and mass loss trends associated to mafic and felsic rock types. B. Exponential fit of the SiO_2 concentrations from the least altered sample suite against their Zr concentrations. C. Exponential fit of the Fe_2O_3 concentrations from the least altered sample suite against their Zr concentrations.

Table 3-2 Summary of element mobility for each dominant alteration mineralogy.

Dominant alteration mineral	Majors elements gained	Majors elements lost	Majors elements immobile	Trace elements gained	Trace elements lost	Trace elements immobile (<5 ppm change)
Fe-chlorite	FeO	SiO_2, MgO, Na_2O	Al_2O_3, MnO, TiO_2, P_2O_5	Cu, Zn, Rb, Sr, Ba, La, Ce, Nd, Y, La, Ce, Nd	-	Sc, V, Co, Ni, Li, Th, U, Zr, Nb, Hf, Ta, Sb, Tl, other REE
Fe,Mg-chlorite	MgO, Fe_2O_3	SiO_2, CaO, Na_2O	Al_2O_3, MnO, TiO_2, P_2O_5	Cu, Zn, V, Rb, Sr, Ba, Y	As, La, Ce, Nd	Sc, Co, Li, Th, U, Zr, Nb, Hf, Ta, Sb, Tl, other REE
Mg-chlorite	Fe_2O_3, MgO	SiO_2, K_2O	Al_2O_3, MnO, TiO_2, P_2O_5	Cu, Zn, Rb, Sr, As, La, Ce, Nd	Ba, Y	Sc, Li, Th, U, Zr, Nb, Hf, Ta, Sb, Tl, other REE
Muscovite	Fe_2O_3, K_2O	SiO_2, MgO, CaO, Na_2O	Al_2O_3, MnO, TiO_2, P_2O_5	Cu, Zn, Pb, Rb, Ba, As, Sb, Tl	V, Ni, Y, La, Ce, Nd	Sc, Co, Th, U, Zr, Nb, Hf, Ta, other REE
Illitic muscovite	Fe_2O_3, K_2O	SiO_2, MgO, CaO, Na_2O	Al_2O_3, MnO, TiO_2, P_2O_5	Cu, Zn, Pb, Rb, As, Sb, Tl, La, Ce, Nd	Ni, Ba, Y	Sc, Co, Th, U, Zr, Nb, Hf, Ta, other REE
Phengite	Fe_2O_3, K_2O	SiO_2, CaO, Na_2O	Al_2O_3, MnO, TiO_2, P_2O_5	Cu, Zn, Pb, V, Rb, Sr, Ba, As, Tl	Y, La, Ce, Nd	Sc, Co, Ni, Li, Th, U, Zr, Nb, Hf, Ta, other REE
Illitic phengite	Fe_2O_3, MgO	SiO_2, CaO, Na_2O	Al_2O_3, MnO, TiO_2, P_2O_5	Cu, Zn, Pb, V, Rb, Sr, Ba, Y, As, Sb, Tl	-	Sc, Co, Ni, Li, Th, U, Zr Nb, Hf, Ta, other REE

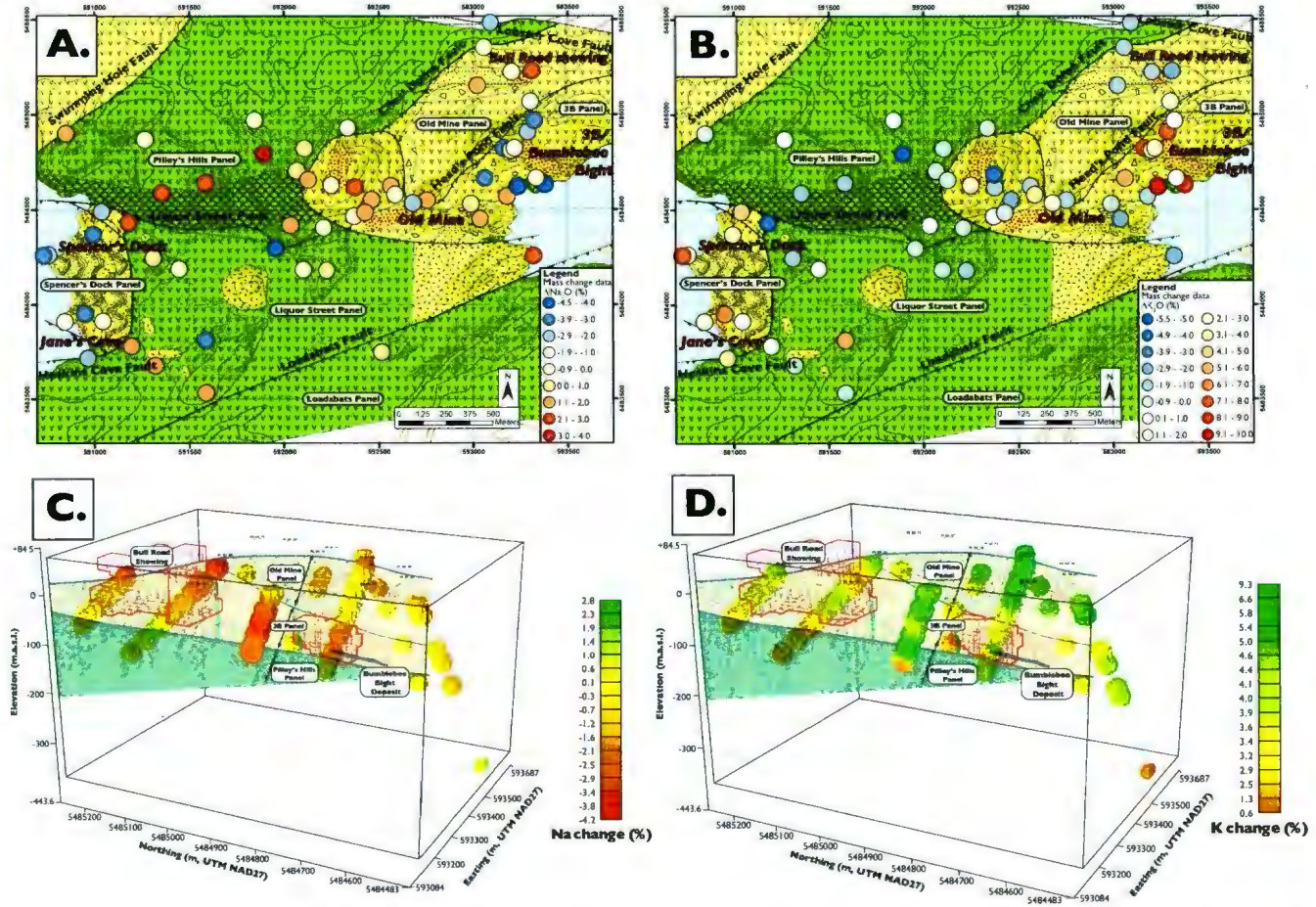

Figure 3-12 Spatial distribution of Na_2O and K_2O (highly mobile elements) mass change data in 2D and 3D. Surface map with A. Na_2O and B. K_2O mass change data for outcrop samples. 3D gridding of kriged C. Na_2O and D. K_2O mass change data from drill core samples throughout and surrounding the Bull Road showing and the Bumble Bee Bight deposit on Pilley's Island. Red wireframes represent raw, kriged Cu values greater than 400ppm. Legend for geological features in Figure 3-6A.

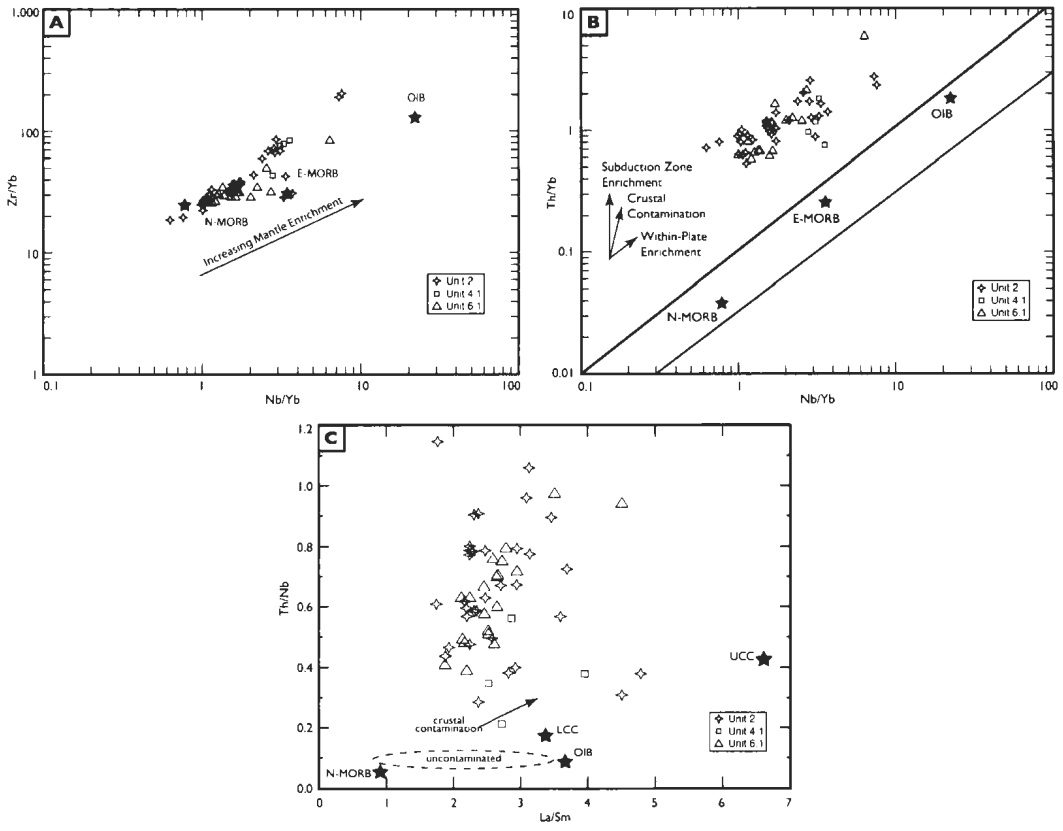

Figure 3-13 Immobile high-field strength element ratio plots. A. Zr/Yb vs. Nb/Yb, B. Th/Yb vs. Nb/Yb, and C. Th/Nb vs. La/Sm. Modified from Pearce (1983), Pearce and Peate (1995) and Stern et al. (1995). N-MORB, normal mid-ocean-ridge basalt; OIB, ocean-island basalt (Sun and McDonough 1989); LCC, BCC, and UCC, lower, bulk, and upper continental crust, respectively (Taylor and McLennan 1985).

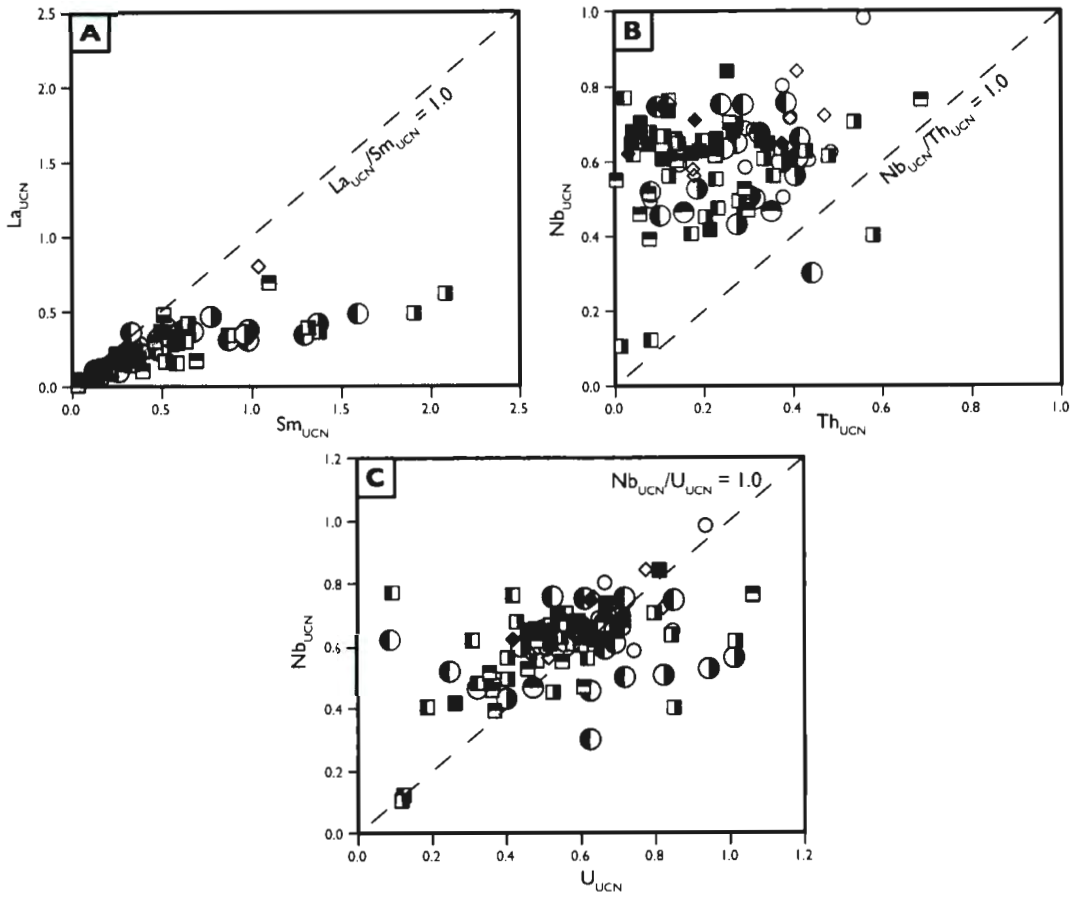

Figure 3-14 Upper continental crustal-normalized incompatible element ratios of Nb, Th, La, Sm and U for felsic volcanic and volcaniclastic rocks in the Pilley's Island terrane. Symbology of different stratigraphic units are consistent with previous figures. A. La_{UCN} vs. Sm_{UCN}. B. Nb_{UCN} vs. Th_{UCN}. C. Nb_{UCN} vs. U_{UCN}. Symbols in Figure 3-7.

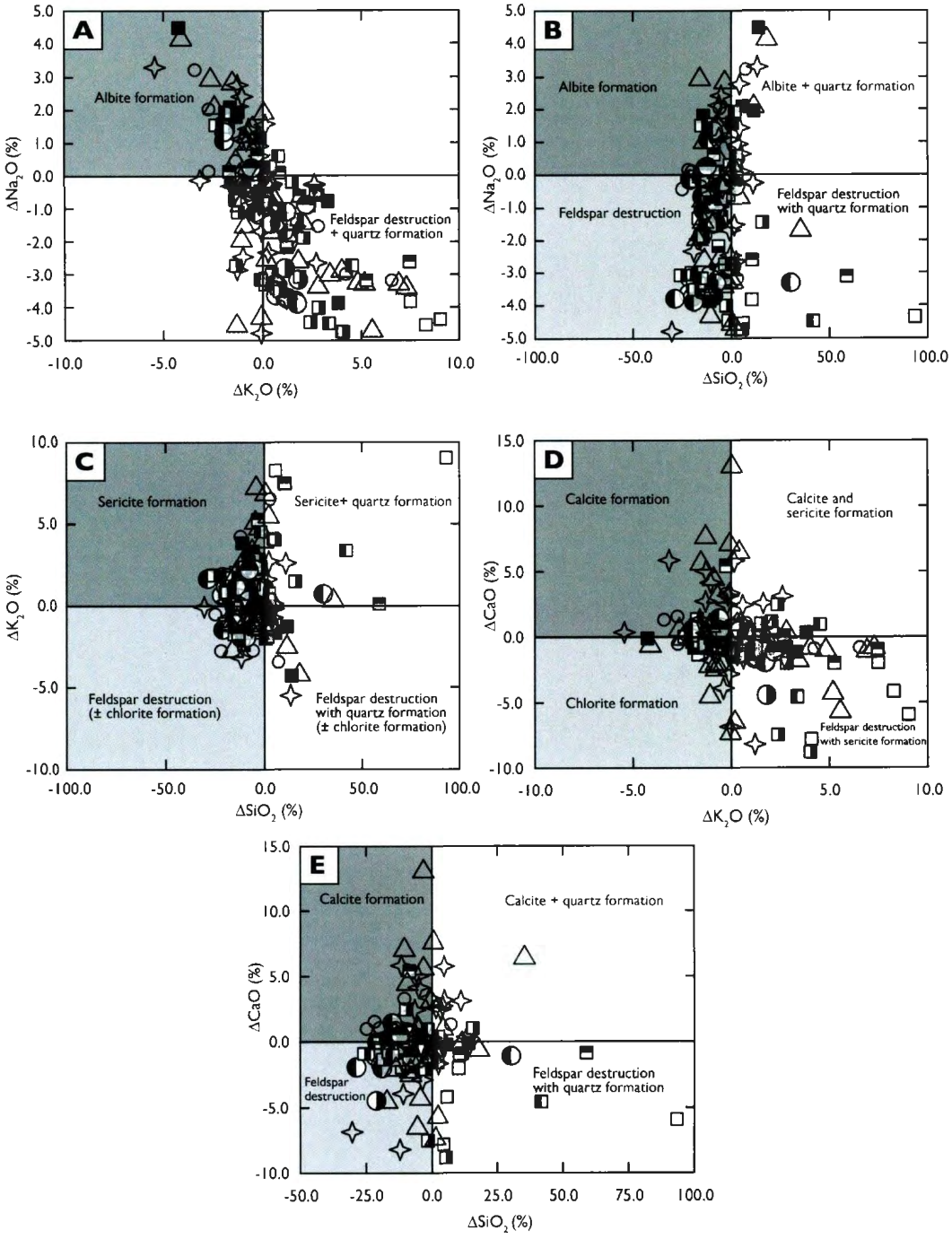

Figure 3-15 Mass change plots for the Pilley's Island terrane stratigraphic units. A. ΔNa_2O-ΔK_2O. B. ΔNa_2O-ΔSiO_2. C. ΔK_2O-ΔSiO_2. D. ΔCaO-ΔK_2O. E. ΔCaO-ΔSiO_2. Symbols in Figure 3-7.

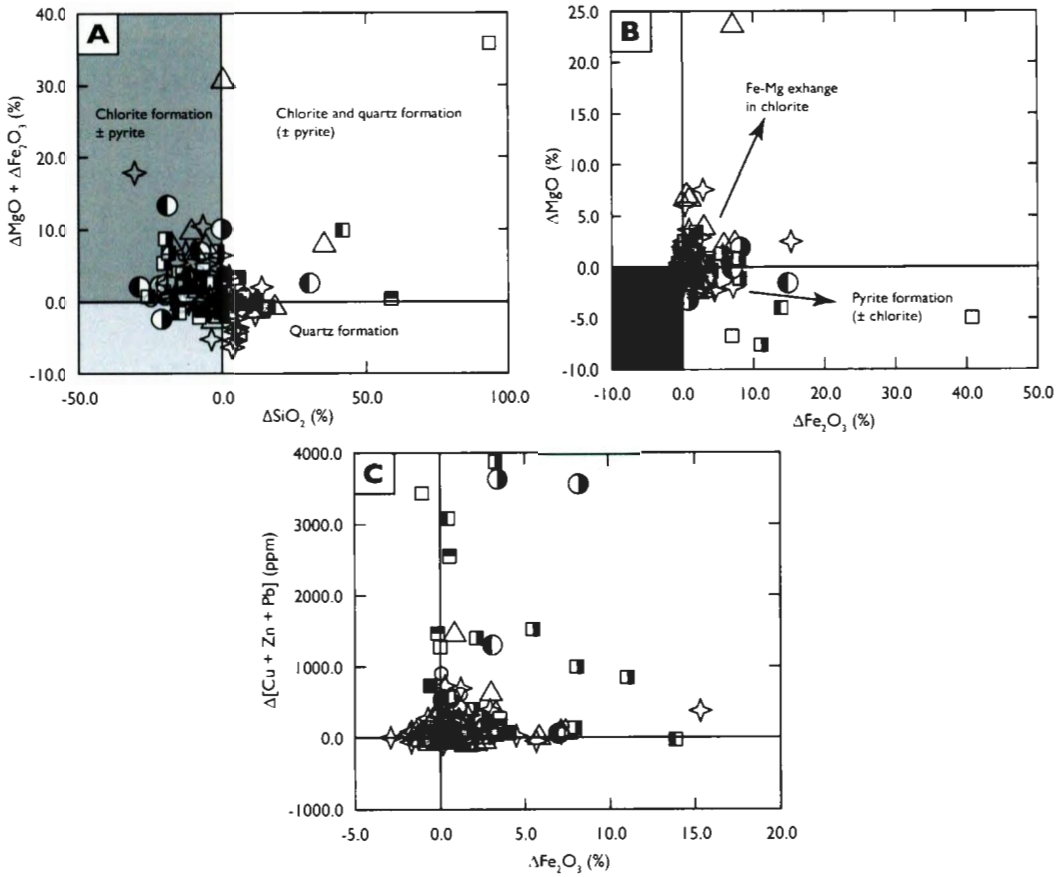

Figure 3-16 Mass change plots for the Pilley's Island terrane stratigraphic units. A. [ΔMgO+ΔFeO]-ΔSiO_2. B. ΔMgO-ΔFe_2O_3. C. Δ[Cu+Zn+Pb]-ΔFe_2O_3. Symbols in Figure 3-7.

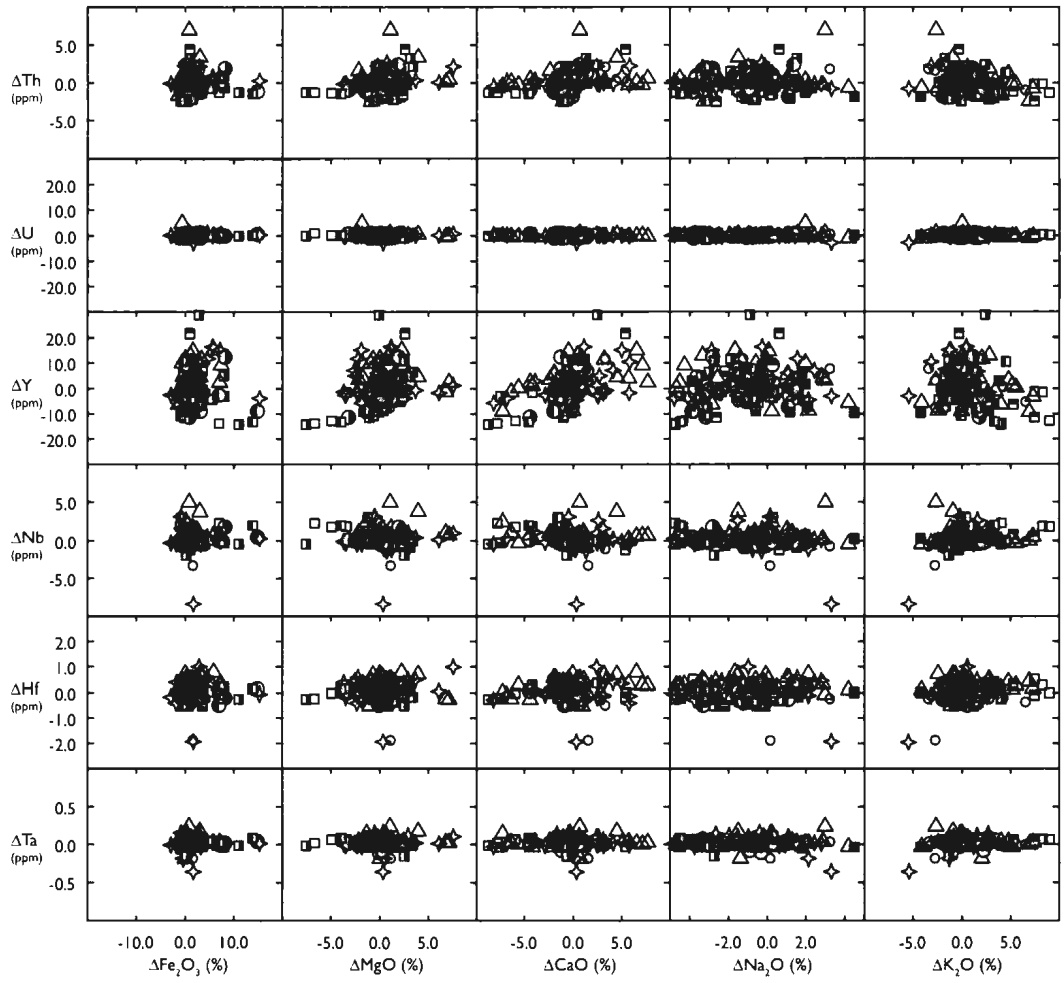

Figure 3-17 Data array testing the relationships between the mobility of HFSE and Fe_2O_3 (proxy for chlorite alteration and sulfides), CaO (proxy for calcite alteration), and Na_2O and K_2O (proxies for sericite alteration). Symbols in Figure 3-7.

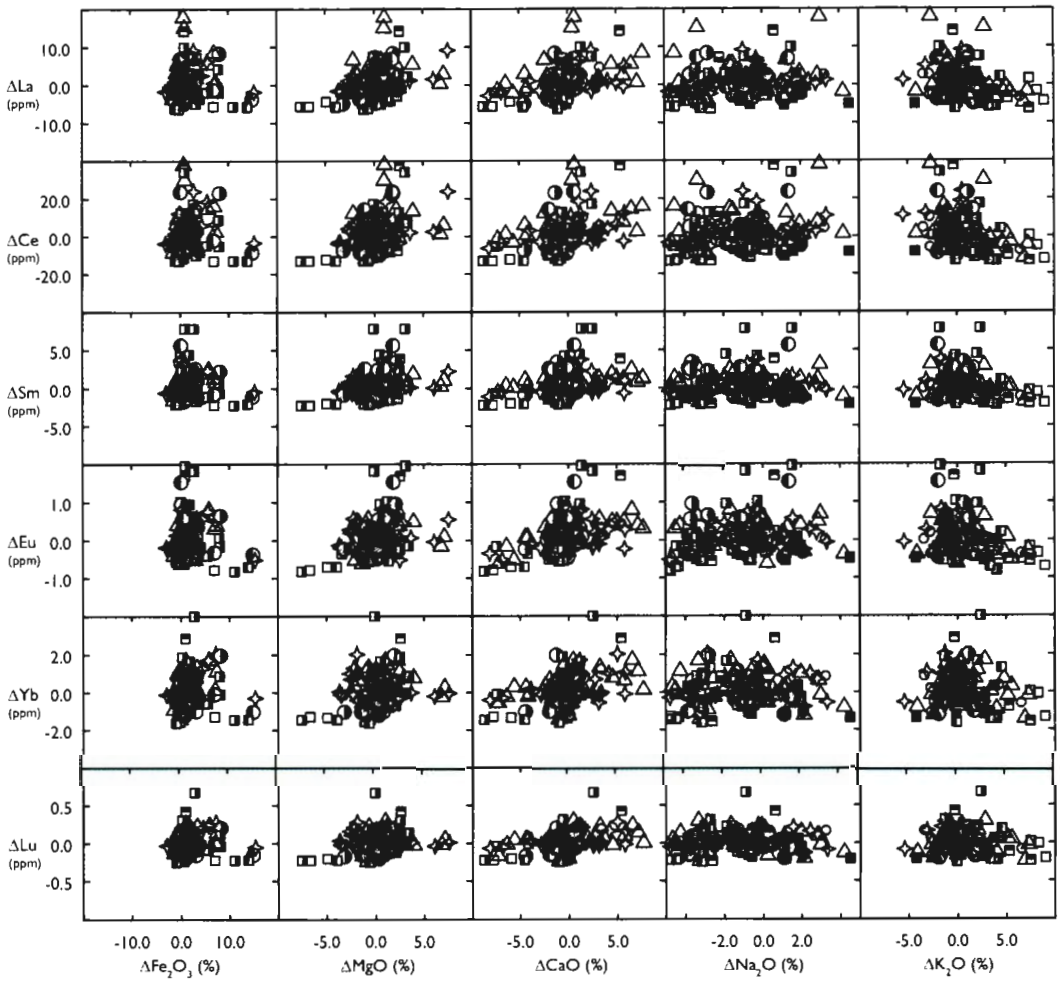

Figure 3-18 Data array testing the relationships between the mobility of REE and Fe_2O_3 (proxies for chlorite alteration and sulfides), CaO (proxy for calcite alteration), and Na_2O and K_2O (proxies for sericite alteration). Symbols in Figure 3-7.

Chapter 4: Summary and Direction for Future Research

4.1. Summary

The Pilley's Island district, Central Mobile Belt of Newfoundland, Canada, records a Lower Ordovician magmatic, tectonic and metallogenic event within a rifted arc environment. The integration of field and geochemical results produced throughout this study has generated a new interpretation of the magmatic, tectonic, stratigraphic and metallogenic evolution in the Pilley's Island terrane. Key conclusions of this study include:

1) The mafic volcanic rocks of the Pilley's Island terrane are derived from a variable, weakly depleted to weakly enriched mantle source, and have been enriched in Th due to slab metasomatism (Chapter 3). The mafic volcanic rocks represent typical, calc-alkalic arc basalts formed via partial melting of slab metasomatized mantle wedge within an Ordovician peri-Laurentian subduction zone (e.g., Swinden et al., 1997). The felsic volcanic rocks of the Pilley's Island terrane likely formed via the remelting of a hydrated, arc basalt substrate as they have similar trace element signatures to their mafic counterparts. The lithogeochemical signatures of the mafic units are similar to those found in modern intra-oceanic and continental arcs and the felsic units are similar to those found in ancient intra-oceanic to continental arcs (e.g., Hildreth and Moorbath, 1988; Lentz, 1998; Piercey, 2011, and references therein). Low μ Pb isotopic signatures suggest that the rocks from which the Pilley's Island terrane formed were likely transitional in nature, with some areas having juvenile crust underlying and other areas floored by

continental crust. Massive sulfide formation at Pilley's Island likely took place within a peri-Laurentian arc rift.

3) The VMS deposits in Pilley's Island are hosted within both volcaniclastic-dominated and flow-dominated stratigraphy, each of which reflect different depositional settings (Chapter 2). Felsic flow-dominated stratigraphy in the Spencer's Dock panel represents lobe-hyaloclastite facies (e.g. Gibson et al., 1999) resulting from episodic endogenous flow-dome growth, migrating dacitic flows and associated hyaloclastite formation along the flow margins within a deep water extensional fissure system that may be part of a larger subsidence structure. Conversely, volcaniclastic-dominated stratigraphy of the 3B and Old Mine panels formed under different depositional settings, involving alternating periods of lava eruption and waning volcanism involving volcaniclastic deposition. These likely formed in a shallowing, basin environment or a transition from flow and dome extrusion in vent proximal environments to volcaniclastic-dominated facies, which are more easily transported and resedimented in distal environments.

4) The permeability and porosity of the volcanic strata has strong control on the hydrothermal alteration (Chapter 2). The less porous and less permeable, flow-dominated stratigraphy of the Spencer's Dock panel results in alteration being focussed laterally along fractures and more permeable zones such as perlitic cracks, breccia intervals, and in hyaloclastite. Volcaniclastic-dominated stratigraphy in the 3B and Old Mine panels are more porous and permeable resulting in the localization of more intense and pervasive quartz and sericite alteration along tuff and lapilli tuff intervals.

5) The stratigraphy of the Pilley's Island VMS district has undergone widespread hydrothermal alteration, and distinctive alteration haloes (based on mineralogy and alteration intensity) surrounding the massive sulfide deposits can be used as exploration vectors (Chapter 3). The alteration is a product of fluid upflow, associated to VMS deposit formation, and emplacement into unconsolidated and porous volcaniclastic-rich stratigraphy, therefore allowing widespread, unfocussed alteration, rather than typical pipe-like alteration. Sericite alteration is the most abundant and results from the reaction of feldspars (e.g., albite, zoisite, andesine) and glass with hydrothermal fluids. Chlorite alteration is less abundant, commonly forms Fe- to Mg-rich chemical end members, and is the result of the destruction of muscovite or mafic minerals. Phengite and illitic phengite alteration form large (>500m) haloes surrounding the VMS deposits and have higher alteration intensity proximal to mineralization. Illitic muscovite and muscovite alteration are the most proximal alteration assemblage and form small (<50m) haloes surrounding the VMS deposits.

6) Most Pilley's Island VMS deposits show evidence of sub-seafloor replacement (e.g. Franklin et al., 1981; Lydon, 1988; Doyle and Allen, 2003; Franklin et al., 2005) (Chapter 2). The Spencer's Dock and Jane's Cove deposits are characterized by large gradational boundaries from massive pyrite outwards into semi-massive to disseminated stringer sulfides in perlitic-fractured dacite, which occur within a large halo of strong hydrothermal alteration. Massive pyrite lenses also contain upwards of 10% sericite, which likely represents a resistant relict host rock component that was not replaced. Deposits in the 3B and Old Mine panels display similar replacement features with large,

gradational alteration and mineralization haloes throughout the more permeable strata. The 3B and Old Mine deposits also contain relicts of host rocks (quartz crystals, fine tuff, lapilli, and interstitial sericite) suggesting sub-seafloor sulfide replacement.

7) Element vectoring can be used to identify proximity to VMS mineralization because each alteration assemblage has unique mass change trends (Chapter 3). Illitic phengite and phengite alteration zones are characterized by losses in SiO_2, CaO and Na_2O, and gains in MgO, Fe_2O_3, K_2O, base metals (Cu, Pb, Zn), LFSE (Rb, Sr, Ba) and volatile elements (As, Sb and Tl). Also, muscovite alteration zones are characterized by loss of SiO_2, CaO, Na_2O and gains of Fe_2O_3, K_2O, base metals, and volatile elements. The most useful element vectors in the Pilley's Island district include those that are most mobile during VMS formation, including: 1) major elements (Na_2O, CaO, SiO_2 loss and K_2O, Fe_2O_3 addition); 2) base metals (Cu, Pb, Zn gains); and 3) volatile elements (As, Sb, Tl gains).

4.2. Potential Directions for Future Research

Although this thesis has contributed to the understanding of the magmatism, tectonics, volcanic stratigraphy, hydrothermal alteration and mineralization and lithogeochemistry of the Pilley's Island VMS district, several knowledge gaps still exist and present potential future research directions.

Efforts to acquire a geochronological U-Pb age for the Pilley's Island terrane were unsuccessful. Zircons were not procured from the felsic volcanic rocks presumably because zirconium did not saturate and crystallize in the felsic magmas. However, efforts could be made to obtain a U-Pb age of the rocks using other minerals (e.g. rutile, titanite).

An accurate U-Pb age of the terrane would provide information on the tectonic evolution of the Annieopsquotch accretionary tract and related arc rifting, which is the interpreted depositional environment of the Pilley's Island terrane.

Secondly, Pilley's Island is somewhat anomalous because despite having significant tonnages in some deposits, grades are generally low and only reach ore grade in some of the smaller deposits (e.g. 3B deposit, Bumble Bee Bight deposit). A potential research avenue would be to understand the geological processes that cause the largest massive sulfide deposits to have lower grade and vice versa.

Another potential research avenue would be to use additional modern analytical methods in the field (e.g. portable infrared mineral analyzer, portable x-ray fluorescence device) in efforts to constrain additional chemical and mineralogical vectors towards sulfide mineralization. These techniques provide low-cost, real-time data for the researcher or explorationist in the field that could aid in the interpretation of the district.

Lastly, additional and closer-spaced drilling is required in the area to better constrain and model the element haloes and the VMS deposits themselves. Continued drilling and use of 3D modeling in the district could provide genetic relationships between the deposits and reveal additional deposits and/or drill targets.

Regarding more widespread implications within this thesis, similar integrated volcanic stratigraphic – lithogeochemical studies should be used in other prospective and existing VMS districts within the Appalachians and orogenic belts worldwide. Lithogeochemistry is most useful in identifying the different parts of the VMS system

and, when integrated with mapping, drill core logging, and lithofacies analysis, can provide new exploration models and drill targets.

Bibliography

Allen, R. L., 1992, Reconstruction of the tectonic, volcanic, and sedimentary setting of strongly deformed Zn-Cu massive sulfide deposits at Benambra, Victoria: Economic Geology, v. 87, p. 825-854.

Allen, R. L., and Cas, R. A. F., 1997, The Rosebery controversy: distinguishing prospective submarine ignimbrite-like units from true subaerial ignimbrites in the Rosebery-Hercules Zn-Cu-Pb massive sulfide district, Tasmania: Geological Society of Australia Abstracts, v. 25, p. 1022-1053.

Allen, R. L., Lundstrom, I., Ripa, M., and Christofferson, H., 1996, Facies analysis of a 1.9 Ga, continental margin, back-arc, felsic caldera province with diverse Zn-Pb-Ag-(Cu-Au) sulfide and Fe oxide deposits, Bergslagen region, Sweden: Economic Geology, v. 91, p. 979-1008.

Alt, J. C., 1995, Subseafloor processes in mid-ocean ridge hydrothermal systems: Geophysical Monograph, v. 91, p. 85-114.

Alt, J. C., 1999, Hydrothermal alteration and mineralization of oceanic crust; mineralogy, geochemistry, and processes: Reviews in Economic Geology, v. 8, p. 133-155.

Anderson, J. E., 1969, Development of a snowflake texture in a welded tuff, Davis Mountains, Texas: Geological Society of America Bulletin, v. 80.

Appleyard, E. C., and Bowles, E. G., 1978, The geology of the West Mine, Pilley's Island, Newfoundland, Geological Survey of Canada, p. 199-203.

Arculus, R. J., 1994, Aspects of magma genesis in arcs: Lithos, v. 33, p. 189-208.

Barrett, T. J., and MacLean, W. H., 1991, Chemical, mass, and oxygen isotope changes during extreme hydrothermal alteration of an Archean rhyolite, Noranda, Quebec: Economic Geology and the Bulletin of the Society of Economic Geologists, April, v. 86, p. 406-414.

Barrett, T. J., and MacLean, W. H., 1994a, Chemostratigraphy and hydrothermal alteration in exploration for VHMS deposits in greenstones and younger rocks, *in* Lentz, D. R., ed., Alteration and Alteration Processes Associated with Ore-Forming Systems, Short Course Notes Volume 11, Geological Association of Canada, p. 433-467.

Barrett, T. J., and MacLean, W. H., 1994b, Mass changes in hydrothermal alteration zones associated with VMS deposits of the Noranda area: Exploration and Mining Geology, v. 3, p. 131-160.

Barrett, T. J., and MacLean, W. H., 1999, Volcanic sequences, lithogeochemistry, and hydrothermal alteration in some bimodal volcanic-associated massive sulfide systems, *in* Barrie, C. T., and Hannington, M. D., eds., Volcanic-Associated Massive Sulfide Deposits: Processes and Examples in Modern and Ancient Environments, Reviews in Economic Geology 8, Society of Economic Geologists, p. 101-131.

Barrie, C. T., 1995, Zircon thermometry of high-temperature rhyolites near volcanic-associated massive sulfide deposits. Abitibi subprovince, Canada: Geology, v. 23, p. 169-172.

Barrie, C. T., Ludden, J. N., and Green, T. H., 1993, Geochemistry of volcanic rocks associated with Cu-Zn and Ni-Cu deposits in the Abitibi Subprovince: Economic Geology, v. 88, p. 1341-1358.

Bau, M., 1996, Controls on the fractionation of isovalent trace elements in magmatic and aqueous systems; evidence from Y/Ho, Zr/Hf, and lanthanide tetrad effect: Contributions to Mineralogy and Petrology, v. 123, p. 323-333.

Bau, M., and Möller, P., 1992, Rare earth element fractionation in metamorphogenic hydrothermal calcite, magnesite and siderite: Mineralogy and Petrology, v. 45, p. 231-246.

Bigger, S. E., and Hanson, R. E., 1992, Devitrification textures and related features in the Carlton Rhyolite in the Blue Creek Canyon area, Wichita Mountains, southwestern Oklahoma: Oklahoma Geology Notes, v. 52, p. 124-142.

Bindeman, I., Gurenko, A., Carley, T., Miller, C., Martin, E., and Sigmarsson, O., 2012, Silicic magma petrogenesis in Iceland by remelting of hydrothermally altered crust based on oxygen isotope diversity and disequilibria between zircon and magma with implications for MORB: Terra Nova, v. 24, p. 227-232.

Bindeman, I. N., Fu, B., Kita, N. T., and Valley, J. W., 2008, Origin and Evolution of Silicic Magmatism at Yellowstone Based on Ion Microprobe Analysis of Isotopically Zoned Zircons: J. Petrology, v. 49, p. 163-193.

Bostock, H. H., 1988, Geology and petrochemistry of the Ordovician volcano-plutonic Roberts-Arm Group, Notre Dame Bay, Newfoundland., 66, Geological Survey of Canada, Bulletin 369, p. 1196-1230.

Brenan, J. M., Shaw, H. F., Ryerson, F. J., and Phinney, D., 1995, Mineral-aqueous fluid partitioning of trace elements at 900 C at 2.0 Gpa: constraints on the trace element chemistry of mantle and deep crustal fluids: Geochimica et Cosmochimica Acta, v. 59, p. 3331-3350.

Calon, T. J., and Green, F. K., 1987, Preliminary results of a detailed structural analysis of the Buchans Mine area: Paper - Geological Survey of Canada, v. 86-24, p. 273-288.

Calon, T. J., and Szybinski, Z. A., 1988, Lobster Cove Fault: Dextral strike-slip fault system: Geological Assocation of Canada/ Mineralogical Association of Canada/ Canadian Society of Petroleum Geologists Joint Annual Meeting, St. John's, Newfoundland, 1988, GAC/MAC/CSPG Program with Abstracts, p. A17.

Cas, R. A. F., Allen, R. L., Bull, S. W., Clifford, B. A., and Wright, J. V., 1990, Subaqueous, rhyolitic dome-top tuff cones: a model based on the Devonian Bunga Beds, southeastern Australia and a modern analogue: Bulletin of Volcanology, v. 52, p. 159-174.

Castroviejo, R., Quesada, C., and Soler, M., 2011, Post-depositional tectonic modification of VMS deposits in Iberia and its economic significance: Mineralium Deposita, v. 46, p. 615-637.

Currie, K. L., 1995, The Northeastern End of the Dunnage Zone in Newfoundland: Atlantic Geology, v. 31, p. 25-38.

Date, J., Watanabe, Y., and Saeki, Y., 1983, Zonal alteration around the Fukazawa Kuroko deposits, Akita Prefecture, northern Japan., *in* Ohmoto, H., and Skinner, B. J., eds., Kuroko and Related Volcanogenic Massive Sulfide Deposits, Economic Geology Monograph 5, p. 365-386.

Dean, P. L., and Strong, D. F., 1977, Folded thrust faults in Notre Dame Bay, central Newfoundland: American Journal of Science, v. 277, p. 97-108.

DeWolfe, Y. M., Gibson, H. L., Lafrance, B., and Bailes, A. H., 2009, Volcanic reconstruction of Paleoproterozoic arc volcanoes: the Hidden and Louis formations, Flin Flon, Manitoba, Canada: Canadian Journal of Earth Sciences, v. 46, p. 481-508.

Diegor, W., Longerich, H., Abrajano, T., and Horn, I., 2001, Applicability of a high pressure digestion technique to the analysis of sediment and soil samples by inductively coupled plasma-mass spectrometry: Analytica Chimica Acta, v. 431, p. 195-207.

Dimroth, E., Rocheleau, M., and Archambault, G., 1985, Archean wrench fault tectonics and structural evolution of the Blake River Group, Abitibi Belt, Quebec; discussions: Canadian Journal of Earth Sciences, v. 22, p. 941-945.

Doyle, M. G., and Allen, R. L., 2003, Subsea-floor replacement in volcanic-hosted massive sulfide deposits: Ore Geology Reviews, v. 23, p. 183-222.

Doyle, M. G., and Huston, D. L., 1999, The subseafloor replacement origin of the Ordovician Highway-Reward volcanic-associated massive sulfide deposit, Mount Windsor Subprovince, Australia: Economic Geology, v. 94, p. 825-844.

Dunning, G. R., and Krogh, T. E., 1985, Geochronology of ophiolites of the Newfoundland Appalachians: Canadian Journal of Earth Sciences, v. 22, p. 1659-1670.

Dunning, G. R., O'Brien, S. J., Colman-Sadd, S. P., Blackwood, R. F., Dickson, W. L., O'Neill, P. P., and Krogh, T. E., 1990, Silurian Orogeny in the Newfoundland Appalachians: Journal of Geology, v. 98, p. 895-913.

Dunning, G. R., Swinden, H. S., Kean, B. F., Evans, D. T. W., and Jenner, G. A., 1991, A Cambrian island arc in Iapetus; geochronology and geochemistry of the Lake Ambrose volcanic belt, Newfoundland Appalachians: Geological Magazine, v. 128, p. 1-17.

Elders, W. A., Fridleifsson, G., Zierenberg, R. A., Pope, E. C., Mortensen, A. K., Gudmundsson, A., Lowenstern, J. B., Marks, N. E., Owens, L., Bird, D. K., Reed, M., Olsen, N. J., and Schiffman, P., 2011, Origin of a rhyolite that intruded a geothermal well while drilling at the Krafla volcano, Iceland: Geology.

Elliott, C. G., Dunning, G. R., and Williams, P. F., 1991, New U/Pb zircon age constraints on the timing of deformation in north-central Newfoundland and implications for early Paleozoic Appalachian orogenesis: Geological Society of America Bulletin, v. 103, p. 125-135.

Elliott-Meadows, S. R., and Appleyard, E. C., 1991, The alteration geochemistry and petrology of the Lar Cu-Zn deposit, Lynn Lake area, Manitoba, Canada: Economic Geology, v. 86, p. 486-505.

Epp, W. R., 1984, Brinco Mining Ltd., Brinco-Getty Joint Venture, Dawes Pond Project, Pilley's Island 1984 Diamond Drilling Report, Blast Furnace Option, C.B. 2400, Lic. 2240, v. Brinco Report #640, p. 1-34.

Espenshade, G. H., 1937, Geology and mineral deposits of the Pilley's Island area., Newfoundland Department of Natural Resources, Bulletin #6, p. 56.

Evans, D. T. W., and Kean, B. F., 2002, The Victoria Lake Supergroup, central Newfoundland - its definition, setting and volcanogenic massive sulphide mineralization, Newfoundland and Labroador Department of Mines and Energy, Geological Survey, Open File NFLD/2790, p. 68.

Finlow-Bates, T., and Stumpfl, E. F., 1981, The behaviour of so-called immobile elements in hydrothermally altered rocks associated with volcanogenic submarine-exhalative ore deposits: Mineralium Deposita, v. 16, p. 319-328.

Fisher, R. V., 1961, Proposed Classification Of Volcaniclastic Sediments And Rocks: Geological Society of America Bulletin, v. 72, p. 1409-1414.

Franklin, J. M., Gibson, H. L., Galley, A. G., and Jonasson, I. R., 2005, Volcanogenic Massive Sulfide Deposits, *in* Hedenquist, J. W., Thompson, J. F. H., Goldfarb, R. J., and Richards, J. P., eds., Economic Geology 100th Anniversary Volume: Littleton, CO, Society of Economic Geologists, p. 523-560.

Franklin, J. M., Sangster, D. M., and Lydon, J. W., 1981, Volcanic-associated massive sulfide deposits, *in* Skinner, B. J., ed., Economic Geology Seventy-Fifth Anniversary Volume, Society of Economic Geologists, p. 485-627.

Galley, A. G., 1993, Characteristics of semi-conformable alteration zones associated with volcanogenic massive sulphide districts: Journal of Geochemical Exploration, v. 48, p. 175-200.

Geist, D., Howard, K. A., and Larson, P., 1995, The generation of oceanic rhyolites by crystal fractionation; the basalt-rhyolite association at Volcan Alcedo, Galapagos Archipelago: Journal of Petrology, v. 36, p. 965-982.

Gemmell, J. B., and Fulton, R., 2001, Geology, genesis, and exploration implications of the footwall and hanging-wall alteration associated with the Hellyer volcanic-hosted massive sulphide deposit, Tasmania, Australia.: Economic Geology, v. 96, p. 1003-1036.

Gemmell, J. B., and Large, R. R., 1992, Stringer system and alteration zones underlying the Hellyer volcanic-hosted massive sulfide deposit, Tasmania, Australia: Economic Geology, v. 87, p. 620-649.

Gibson, H. L., 1990, The mine sequence of the Central Noranda Volcanic Complex: Geology, alteration, massive sulfide deposits and volcanological reconstruction: Unpub. Unpublished PhD thesis, Carleton University, 800 p.

Gibson, H. L., 2005, Volcanic-hosted ore deposits, *in* Marti, J., and Ernst, G. G. J., eds., Volcanoes in the Environment: New York, NY, USA, Cambridge University Press, p. 332-386.

Gibson, H. L., Kerr, D. J., and Cattalani, S., 2000, The Horne Mine; geology, history, influence on genetic models, and a comparison to the Kidd Creek Mine: Exploration and Mining Geology, v. 9, p. 91-111.

Gibson, H. L., Morton, R. L., and Hudak, G. J., 1999, Submarine volcanic processes, deposits, and environments favorable for the location of volcanic-associated massive sulfide deposits, *in* Barrie, C. T., and Hannington, M. D., eds., Volcanic-Associated Massive Sulfide Deposits: Processes and Examples in Modern and Ancient Environments, Reviews in Economic Geology v.8, p. 13-51.

Gibson, H. L., and Watkinson, D. H., 1990, Volcanogenic massive sulphide deposits of the Noranda cauldron and shield volcano, Québec., *in* Rive, M., Verpaelst, P., Gagnon, Y., Lulin, J.-M., Riverin, G., and Simard, A., eds., The Northwestern Québec Polymetallic Belt: A summary of 60 years of mining exploration, 43. Special Volume: Rouyn-Noranda, Canadian Institute of Mining and Metallurgy, p. 119-132.

Gibson, H. L., Watkinson, D. H., and Comba, C. D. A., 1983, Silicification: Hydrothermal alteration in an Archean geothermal system within the Amulet Rhyolite Formation, Noranda, Quebec: Economic Geology, v. 78, p. 954-971.

Gibson, H. L., Watkinson, D. H., Watkins, J. J., Labrie, M., and Doiron, G., 1993, Vocanological reconstruction of the Corbet breccia pile, and Cu-Zn massive sulfide deposit, Noranda, Québec.: Exploration and Mining Geology, v. 2, p. 1-16.

Gifkins, C. C., and Allen, R. L., 2001, Textural and Chemical Characteristics of Diagenetic and Hydrothermal Alteration in Glassy Volcanic Rocks: Examples from the Mount Read Volcanics, Tasmania: Economic Geology, v. 96, p. 973-1002.

Goodfellow, W. D., Peter, J. M., Mottl, M. J., Davis, E. E., Fisher, A. T., Baker, P. A., Becker, K., Boni, M., Boulegue, J. J., Brunner, C. A., Duckworth, R. C., Franklin, J. M., Goodfellow, W. D., Groeschel-Becker, H. M., Kinoshita, M., Konyukhov, B. A., Koerner, U., Krasnov, S. G., Langseth, M. G., Mao, S., Marchig, V., Marumo, K., Oda, H., Rigsby, C. A., Simoneit, B. R. T., Stakes, D. S., Villinger, H. W., Wheat, C. G., Whelan, J. K., and Zierenberg, R. A., 1994, Geochemistry of hydrothermally altered sediment, Middle Valley, northern Juan de Fuca Ridge: Proceedings of the Ocean Drilling Program, Scientific Results, v. 139, p. 207-289.

Grant, J. A., 1986, The isocon diagram: A simple solution to Gresens' equation for metasomatic alteration: Economic Geology, v. 81, p. 1976-1982.

Gresens, R. L., 1967, Composition-volume relationships of metasomatism: Chemical Geology, v. 2, p. 47-65.

Grimley, P. H., 1968, Geological and other notes on Pilley's Island, Brinex Report G68026, p. 1-34.

Hajash, A., and Chandler, G. W., 1981, An experimental investigation of high-temperature interactions between seawater and rhyolite, andesite, basalt and peridotite: Contributions to Mineralogy and Petrology, v. 78, p. 240-254.

Hart, T. R., Gibson, H. L., and Lesher, C. M., 2004, Trace element geochemistry and petrogenesis of felsic volcanic rocks associated with volcanogenic massive Cu-Zn-Pb sulfide deposits: Economic Geology, v. 99, p. 1003-1013.

Hawkins, J. W., 1995, Evolution of the Lau Basin - Insights from ODP Leg 135, *in* Taylor, B., and Natland, J., eds., Active Margins and Marginal Basins of the Western Pacific, 88. American Geophysical Union Geophysical Monograph, American Geophysical Union, p. 125-173.

Herrmann, W., Blake, M., Doyle, M., Huston, D., Kamprad, J., Merry, N., and Pontual, S., 2001, Short Wavelength Infrared (SWIR) Spectral Analysis of Hydrothermal Alteration Zones Associated with Base Metal Sulfide Deposits at Rosebery and Western Tharsis, Tasmania, and Highway-Reward, Queensland: Economic Geology, v. 96, p. 939-955.

Hibbard, J., 1983, Geology of the Baie Verte Peninsula, Newfoundland. Memoir - Government of Newfoundland and Labrador, Department of Mines and Energy, Mineral Development Division, Vol. 2, 279 p.

Hildreth, W., and Moorbath, S., 1988, Crustal contribution to arc magmatism in the Andes of Central Chile: Contributions to Mineralogy and Petrology, v. 98, p. 455-489.

Hinchey, J. G., 2007, Volcanogenic massive sulphides of the southern Tulks Volcanic Belt, central Newfoundland: Preliminary findings and overview of styles and environments of mineralization, *in* Pereira, C. P. G., and Walsh, D. G., eds., Current Research, Report 07-1: St. John's, NL, Geological Survey Branch, p. 117-143.

Hinchey, J. G., 2011, The Tulks Volcanic Belt, Victoria Lake supergroup, central Newfoundland - geology, tectonic setting, and volcanogenic massive sulfide mineralization., Newfoundland and Labrador Department of Natural Resources, Geological Survey, p. 167.

Hughes, C. J., 1973, Spilites, keratophyres, and the igneous spectrum: Geological Magazine, v. 109, p. 513-527.

Huppert, H., and Sparks, R. S. J., 1988, The generation of granitic magmas by intrusion of basalt into continental crust: Journal of Petrology, v. 29, p. 599-624.

Huston, D. L., 1993, The effect of alteration and metamorphism on wall rocks to the Balcooma and Dry River South volcanic-hosted massive sulfide deposits, Queensland, Australia: Journal of Geochemical Exploration, v. 48, p. 277-307.

Huston, D. L., 1999, Definition of high-temperature alteration zones with PIMA; an example from the Panorama VHMS district, central Pilbara Craton, *in* Kamprad, J., and Brauhart, C., eds., AGSO Research Newsletter, 30: Australia, Australian Geological Survey Organisation : Canberra, A.C.T., Australia, p. 10-12.

Ishikawa, Y., Sawaguchi, T., Ywaya, S., and Horiuchi, M., 1976, Delineation of prospecting targets for Kuroko deposits based on modes of volcanism of underlying dacite and alteration haloes: Mining Geology, v. 26, p. 105-117.

Jenner, G. A., Longerich, H. P., Jackson, S. E., and Fryer, B. J., 1990, ICP-MS - A powerful tool for high-precision trace element analysis in Earth sciences: Evidence from analysis of selected U.S.G.S. reference samples: Chemical Geology, v. 83, p. 133-148.

Johnson, S. C., McLeod, M. J., Fyffe, L. R., and Dunning, G. R., 2009, Stratigraphy, geochemistry, and geochronology of the Annidale and New River belts, and the development of the Penobscot arc in southern New Brunswick, *in* Martin, G. L., ed., Geological Investigations in New Brunswick for 2008., Mineral Resource Report 2009-2, New Brunswick Department for Natural Resources, Minerals, Policy, and Planning Division, p. 141-218.

Jones, S., Herrmann, W., and Gemmell, J. B., 2005, Short Wavelength Infrared Spectral Characteristics of the HW Horizon: Implications for Exploration in the Myra Falls Volcanic-Hosted Massive Sulfide Camp, Vancouver Island, British Columbia, Canada: Economic Geology, v. 100, p. 273-294.

Kean, B. F., Evans, D. T. W., and Jenner, G. A., 1995, Geology and Mineralization of the Lushs Bight Group, Report 95-02: St. John's, NL, Canada, Geological Survey of Newfoundland and Labrador, Newfoundland Department of Natural Resources, p. 204.

Kerr, A., 1996, New perspectives on the stratigraphy, volcanology, and structure of island-arc volcanic rocks in the Ordovician Roberts Arm Group, Notre Dame Bay, *in* Pereira, C. P. G., and Walsh, D. G., eds., Current Research Report, Report: 96-1: St. John's, NL, Canada, Geological Survey of Newfoundland and Labradoor, p. 283-310.

Knuckey, M. J., Comba, C. D. A., and Riverin, G., 1982, Structure, metal zoning and alteration at the Millenbach Deposit, Noranda, Quebec: Special Paper - Geological Association of Canada, v. 25, p. 255-295.

Lafrance, B., and Williams, P. F., 1992, Silurian Deformation in Eastern Notre-Dame Bay, Newfoundland: Canadian Journal of Earth Sciences, v. 29, p. 1899-1914.

Large, R. R., Allen, R. L., Blake, M. D., and Herrmann, W., 2001a, Hydrothermal alteration and volatile element haloes for the Rosebery K Lens volcanic-hosted massive sulfide deposit, western Tasmania: Economic Geology, v. 96, p. 1055-1072.

Large, R. R., Gemmell, J. B., Paulick, H., and Huston, D. L., 2001b, The alteration box plot: a simple approach to understanding the relationships between alteration mineralogy and lithogeochemistry associated with VHMS deposits: Economic Geology, v. 96, p. 957-971.

Large, R. R., McPhie, J., Gemmell, J. B., Herrmann, W., and Davidson, G. J., 2001c, The spectrum of ore deposit types, volcanic environments, alteration halos, and related exploration vectors in submarine volcanic successions: some examples from Australia: Economic Geology, v. 96, p. 913-938.

Lee, C. B., and Williams, H., 1995, The Teakettle and Carmanville mélanges in the Exploits Subzone of northeast Newfoundland: recycling and diapiric emplacement in an accretionary prism, *in* Hibbard, J., Cawood, P., Colman-Sadd, S., and van Staal, C., eds., New Perspectives in the Appalachian Orogen, Geological Association of Canada Special Paper 41, p. 147-160.

Lentz, D. R., 1998, Petrogenetic evolution of felsic volcanic sequences associated with Phanerozoic volcanic-hosted massive sulfide systems: the role of extensional geodynamics: Ore Geology Reviews, v. 12, p. 289-327.

Lentz, D. R., 1999, Petrology, geochemistry and oxygen isotopic interpretation of felsic volcanic and related rocks hosting the Brunswick 6 and 12 massive sulfide deposits (Brunswick Belt), Bathurst Mining Camp, New Brunswick, Canada: Economic Geology, v. 94, p. 57-86.

Lentz, D. R., and Goodfellow, W. D., 1996, Intense silicification of footwall sedimentary rocks in the stockwork alteration zone beneath the Brunswick No. 12 massive sulphide deposit, Bathurst, New Brunswick: Canadian Journal of Earth Sciences, v. 33, p. 284-302.

Lesher, C. M., Goodwin, A. M., Campbell, I. H., and Gorton, M. P., 1986, Trace element geochemistry of ore-associated and barren felsic metavolcanic rocks in the Superior province, Canada: Canadian Journal of Earth Sciences, v. 23, p. 222-237.

Lipman, P. W., 1965, Chemical comparison of glassy and crystalline volcanic rocks: US Bulletin, v. 1201-D, p. 24.

Lissenberg, C. J., van Staal, C. R., Bedard, J. H., and Zagorevski, A., 2005a, Geochemical constraints on the origin of the Annieopsquotch ophiolite belt, Newfoundland Appalachians: Geological Society of America Bulletin, v. 117, p. 1413-1426.

Lissenberg, C. J., Zagorevski, A., McNicoll, V. J., van Staal, C. R., and Whalen, J. B., 2005b, Assembly of the Annieopsquotch accretionary tract, Newfoundland Appalachians: age and geodynamic constraints from syn-kinematic intrusions: Journal of Geology, v. 113, p. 553-570.

Lofgren, G., 1971, Experimentally produced devitrification textures in natural rhyolitic glass: Geological Society of America Bulletin, v. 82.

Lydon, J. W., 1988, Volcanogenic massive sulphide deposits; Part 2, Genetic models: Geoscience Canada, v. 15, p. 43-65.

MacLean, W. H., 1988, Rare earth element mobility at constant inter-REE ratios in the alteration zone at the Phelps Dodge massive sulphide deposit, Matagami, Quebec: Mineralium Deposita, v. 23, p. 231-238.

MacLean, W. H., 1990, Mass change calculations in altered rock series: Mineralium Deposita, v. 25, p. 44-49.

MacLean, W. H., and Barrett, T. J., 1993, Lithogeochemical techniques using immobile elements: Journal of Geochemical Exploration, v. 48, p. 109-133.

MacLean, W. H., and Hoy, L. D., 1991, Geochemistry of hydrothermally altered rocks at the Horne Mine, Noranda, Quebec: Economic Geology and the Bulletin of the Society of Economic Geologists, May, v. 86, p. 506-528.

MacLean, W. H., and Kranidiotis, P., 1987, Immobile elements as monitors of mass transfer in hydrothermal alteration; Phelps Dodge massive sulfide deposit, Matagami, Quebec: Economic Geology and the Bulletin of the Society of Economic Geologists, July, v. 82, p. 951-962.

McArthur, A. N., Cas, R. A. E., and Orton, G. J., 1998, Distribution and significance of crystalline, perlitic and vesicular textures in the Ordovician Garth Tuff (Wales): Bulletin of Volcanology, v. 60, p. 260-285.

McLennan, S. M., 2001, Relationships between the trace element composition of sedimentary rocks and upper continental crust: Geochemistry, Geophysics, Geosystems, v. 2, p. Paper 2000GC000109.

McPhie, J., and Allen, R. L., 1992, Facies architecture of mineralised submarine volcanic sequences: Cambrian Mount Read Volcanics, western Tasmania: Economic Geology, v. 87, p. 587-596.

McPhie, J., and Allen, R. L., 2003, Submarine, silicic, syn-eruptive pyroclastic units in the Mount Read Volcanics, western Tasmania; influence of vent setting and proximity on lithofacies characteristics, *in* White, J. D. L., Smellie, J. L., and Clague, D. A., eds., Explosive subaqueous volcanism, Geophysical Monograph 140: San Francisco, American Geophysical Union, p. 245-258.

Merry, N. J., and Pontual, S., 2011, The Spectral Geologist, v. 7 User's manual: Kew, Victoria 3101, Australia, Ausspec International Pty. Ltd, 43 p.

Mireku, L. K., and Stanley, C. R., 2006, Lithogeochemistry and Hydrothermal Alteration at the Halfmile Lake South Deep Zone, a Volcanic-Hosted Massive Sulfide Deposit, Bathurst Mining Camp, New Brunswick: Exploration and Mining Geology, v. 15, p. 177-199.

Morton, R. L., Walker, J. S., Hudak, G. J., and Franklin, J. M., 1991, The early development of an Archean submarine caldera complex with emphasis on the Mattabi ash-flow tuff and the relationship to the Mattabi massive sulfide deposit: Economic Geology, v. 86, p. 1002-1011.

Munhá, J., Fyffe, W. S., and Kerrich, R., 1980, Adularia, the characteristic mineral of felsic spilites: Contributions to Mineralogy and Petrology., v. 75, p. 15-19.

Murphy, J. B., and Hynes, A. J., 1986, Contrasting secondary mobility of Ti, P, Zr, Nb, and Y in two metabasaltic suites in the Appalachians: Canadian Journal of Earth Sciences, v. 23, p. 1138-1144.

O'Brien, B., Swinden, H. S., Dunning, G. R., Williams, S. H., and O'Brien, F. H. C., 1997, A peri-Gondwanan arc-back arc complex in Iapetus; Early-Mid Ordovician evolution of the Exploits Group, Newfoundland: American Journal of Science, v. 297, p. 220-272.

O'Brien, B. H., 2003, Geology of the central Notre Dame Bay region (parts of NTS areas 2E/3,6,11), northeastern Newfoundland, Government of Newfoundland and Labrador, Department of Mines and Energy.

O'Brien, B. H., and Dunning, G. R., 2008, Late darriwilian - early Caradocian felsic volcanism and coeval migmatization in a peri-Gondwanan island arc complex, Newfoundland Appalachians: The 22nd International Geological Congress, Oslo, Norway, 2008.

Pearce, J. A., 1983, Role of sub-continental lithosphere in magma genesis at active continental Margins., *in* Hawkesworth, C. J., and Norry, M. J., eds., Continental Basalts and Mantle Xenoliths: Nantwich, U.K., Shivan, p. 230-249.

Pearce, J. A., Baker, P. E., Harvey, P. K., and Luff, I. W., 1995, Geochemical Evidence for Subduction Fluxes, Mantle Melting and Fractional Crystallization Beneath the South Sandwich Island Arc: J. Petrology, v. 36, p. 1073-1109.

Pearce, J. A., and Peate, D. W., 1995, Tectonic implications of the composition of volcanic arc magmas: Annual Reviews of Earth and Planetary Science, v. 23, p. 251-285.

Peter, J. M., Goodfellow, W. D., Leybourne, M. I., Mottl, M. J., Davis, E. E., Fisher, A. T., Baker, P. A., Becker, K., Boni, M., Boulegue, J. J., Brunner, C. A., Duckworth, R. C., Franklin, J. M., Goodfellow, W. D., Groeschel-Becker, H. M., Kinoshita, M., Konyukhov, B. A., Koerner, U., Krasnov, S. G., Langseth, M. G., Mao, S., Marchig, V., Marumo, K., Oda, H., Rigsby, C. A., Simoneit, B. R. T., Stakes, D. S., Villinger, H. W., Wheat, C. G., Whelan, J. K., and Zierenberg, R. A., 1994, Fluid inclusion petrography and microthermometry of the Middle Valley hydrothermal system, northern Juan de Fuca Ridge: Proceedings of the Ocean Drilling Program, Scientific Results, v. 139, p. 411-428.

Piercey, S., 2011, The setting, style, and role of magmatism in the formation of volcanogenic massive sulfide deposits: Mineralium Deposita, v. 46, p. 449-471.

Piercey, S. J., 2007, Volcanogenic massive sulphide (VMS) deposits of the Newfoundland Appalachians: An overview of their setting, classification, grade-tonnage data, and unresolved questions, *in* Pereira, C. P. G., and Walsh, D. G., eds., Current Research, Report 07-01: St. John's, NL, Geological Survey Branch, p. 169-178.

Piercey, S. J., and Colpron, M., 2009, Composition and provenance of the Snowcap assemblage, basement to the Yukon-Tanana terrane, northern Cordillera: Implications for Cordilleran crustal growth: Geosphere, v. 5, p. 439-464.

Piercey, S. J., and Hinchey, J. G., 2012, Volcanogenic Massive Sulphide (VMS) Deposits of the Central Mineral Belt, Newfoundland (2012 GAC-MAC Field Trip Guidebook B4), Newfoundland and Labrador Department of Natural Resources, Geological Survey.

Piercey, S. J., Murphy, D. C., Mortensen, J. K., Paradis, S., and Creaser, R. A., 2002, Geochemistry and tectonic significance of alkalic mafic magmatism in the Yukon-Tanana Terrane, Finlayson Lake Region, Yukon: Canadian Journal of Earth Sciences., v. 39, p. 1729-1744.

Piercey, S. J., Paradis, S., Murphy, D. C., and Mortensen, J. K., 2001, Geochemistry and paleotectonic setting of felsic volcanic rocks in the Finlayson Lake volcanic-hosted massive sulfide (VHMS) district, Yukon, Canada: Economic Geology, v. 96, p. 1877-1905.

Pontual, S., 2008, G-Mex Vol. 7, Volcanic-hosted massive sulfide systems: Victoria, Australia, Ausspec International Pty. Ltd., 44 p.

Pontual, S., Merry, N., and Gamson, P., 2008, G-Mex Vol. 1, Spectral interpretation field manual: Kew, Victoria 3101, Australia, Ausspec International Pty. Ltd, 169 p.

Post, J. L., and Noble, P. L., 1993, The near-infrared combination band frequencies of dioctohedral smectites, micas and illites: Clays and Clay Minerals, v. 41, p. 639-644.

Ramezani, J., Dunning, G. R., and Wilson, M. R., 2002, Geologic setting, geochemistry of alteration, and U-Pb age of hydrothermal zircon from the Silurian Stog'er Tight gold prospect, Newfoundland Appalachians, Canada: Exploration and Mining Geology, v. 9, p. 171-188.

Richards, H. G., Cann, J. R., and Jensenius, J., 1989, Mineralogical zonation and metasomatism of the alteration pipes of Cyprus sulfide deposits: Economic Geology, v. 84, p. 91-115.

Riverin, G., and Hodgson, C. J., 1980, Wall-rock alteration at the Millenbach Cu-Zn mine, Noranda, Quebec: Economic Geology, v. 75, p. 424-444.

Rogers, J., and Neale, E. R. W., 1969, Possible "taconic" klippen in western Newfoundland: American Journal of Science, v. 261, p. 713-730.

Ross, P.-S., and Bedard, J. H., 2009, Magmatic affinity of modern and ancient subalkaline volcanic rocks determined from trace-element discriminant diagrams: Canadian Journal of Earth Sciences, v. 46, p. 823-839.

Saeki, Y., and Date, J., 1980, Computer application to the alteration data of the footwall dacite lava at the Ezuri Kuroko deposits, Akito Prefecture: Mining Geology, v. 30, p. 241-250.

Santaguida, F., 1994, Volcanic stratigraphy, mineralization, and hydrothermal alteration of the Pilley's Island massive sulphides, Newfoundland. Unpublished M.Sc. Thesis., University of Waterloo, 239 p.

Santaguida, F., Hannington, M., and Jowett, C., 1992, An alteration and sulphur isotope study of the Pilley's Island massive sulphides, central Newfoundland, Geological Survey of Canada, Report 92-01D, p. 265-274.

Santaguida, F., and Hannington, M. D., 1996, Characteristics of gold mineralization in volcanogenic massive sulphide deposits of the Notre Dame Bay area, central Newfoundland: Canadian Journal of Earth Sciences, v. 33, p. 316-334.

Santaguida, F., Hannington, M. D., and Jowett, E. C., 1993, Volume and mass-balance constraints on hydrothermal alteration at the Pilley's Island massive-sulfide deposits, central Newfoundland: Exploration and Mining Geology, v. 2, p. 429.

Shinjo, R., 1999, Geochemistry of high Mg andesites and the tectonic evolution of the Okinawa Trough-Ryukyu arc system: Chemical Geology, v. 157, p. 69-88.

Shinjo, R., Woodhead, J. D., and Hergt, J. M., 2000, Geochemical variation within the northern Ryukyu Arc; magma source compositions and geodynamic implications: Contributions to Mineralogy and Petrology, v. 140, p. 263-282.

Shukuno, H., Tamura, Y., Tani, K., Chang, Q., Suzuki, T., and Fiske, R. S., 2006, Origin of silicic magmas and the compositional gap at Sumisu submarine caldera, Izu-Bonin arc, Japan: Journal of Volcanology and Geothermal Research, v. 156, p. 187-216.

Skirrow, R. G., and Franklin, J. M., 1994, Silicification and metal leaching in semiconformable alteration beneath the Chisel Lake massive sulfide deposit, Snow Lake, Manitoba: Economic Geology and the Bulletin of the Society of Economic Geologists, v. 89, p. 31-50.

Spitz, G., and Darling, R., 1978, Major and minor element lithogeochemical anomalies surrounding the Louvem copper deposit, Val d'Or, Quebec: Canadian Journal of Earth Sciences, v. 15, p. 1161-1169.

Squires, G. C., Brace, T. D., and Hussey. A. M., 2001, Newfoundland's polymetallic Duck Pond deposit: Earliest Iapetan VMS mineralization formed within a sub-seafloor, carbonate-rich alteration system., *in* Evans, D. T. W., and Kerr, A., eds., Geology and Mineral Deposits of the Northern Dunnage Zone, Newfoundland Appalachians, Field Trip Guide A2: St. John's, NL, Geological Association of Canada/Mineralogical Association of Canada, p. 167-187.

Squires, G. C., and Moore, P. J., 2004, Volcanogenic massive sulphide environments of the Tally Pond Volcanics and adjacent area; geological, lithogeochemical and geochronological results, *in* Pereira, C. P. G., Walsh, D. G., and Kean, B. F., eds., Current Research, Report 04-1: St. John's, NL, Geological Survey Branch, p. 63-91.

Stern, R. A., Syme, E. C., Bailes, A. H., and Lucas, S. B., 1995, Paleoproterozoic (1.90-1.86 Ga) arc volcanism in the Flin Flon Belt, Trans-Hudson Orogen, Canada: Contributions to Mineralogy and Petrology, v. 119, p. 117-141.

Stevens, R. K., 1970, Cambro-Ordovician sedimentation and tectonics in western Newfoundland and their possible bearing on a proto-Atlantic ocean: Geological Association of Canada Special Paper, v. 7, p. 165-177.

Stewart, P. W., 1987, Geology and genesis of granitoid clasts in the MacLean Extension transported orebody: Paper - Geological Survey of Canada, v. 86-24, p. 149-176.

Stoltz, A. J., Varne, R., Davies, G. R., Wheller, G. E., and Foden, J. D., 1990, Magma source components in an arc-continent collision zone: The Flores-Lembata sector, Sunda Arc, Indonesia: Contributions to Mineralogy and Petrology, v. 105, p. 585-601.

Sun, S.-s., and McDonough, W. F., 1989, Chemical and isotopic systematics of oceanic basalts: implications for mantle composition and processes, *in* Saunders, A. D., and Norry, M. J., eds., Magmatism in the Ocean Basins, Geological Society Special Publication 42, p. 313-345.

Sverjensky, D. A., 1984, Europium redox equilibria in aqueous solutions: Earth and Planetary Science Letters, v. 67, p. 70-78.

Swinden, H. S., 1991, Paleotectonic settings of volcanogenic massive sulphide deposits in the Dunnage Zone, Newfoundland Appalachians: Canadian Institute of Mining and Metallurgy Bulletin, v. 84, p. 59-89.

Swinden, H. S., 1992, Bipartite massive sulphide metallogeny in the Buchans-Roberts Arm Belt, Central Newfoundland, indicated by whole rock geochemistry.: Geological Association of Canada - Mineralogical Association of Canada Joint Annual Meeting, 1992, Abstracts Volume, p. 106.

Swinden, H. S., and Dunsworth, S. M., 1995, Metallogeny, *in* Williams, H., ed., The Appalachian/Caledonian Orogen: Canada and Greenland: Geological Survey of Canada, Geology of Canada, No. 6, p. 681-814.

Swinden, H. S., Jenner, G. A., and Szybinski, Z. A., 1997, Magmatic and tectonic evolution of the Cambrian-Ordovician Laurentian margin of Iapetus: Geochemical and isotopic constraints from the Notre Dame subzone, Newfoundland, *in* Sinha, A. K., Whalen, J. B., and Hogan, J. P., eds., The Nature of Magmatism in the Appalachian Orogen, Memoir 191, Geological Society of America, p. 337-365.

Swinden, H. S., and Kean, B. F., 1988, Volcanogenic Sulphide Districts of Central Newfoundland, Mineral Deposits Division, Geological Association of Canada, 250 p.

Swinden, H. S., and Thorpe, R. I., 1984, Variations in style of volcanism and massive sulfide deposition in Early to Middle Ordovician island-arc sequences of the Newfoundland Central Mobile Belt: Economic Geology, v. 79, p. 1596-1619.

Syme, E. C., and Bailes, A. H., 1993, Stratigraphy and tectonic setting of Early Proterozoic volcanogenic massive sulphide deposits, Flin Flon, Manitoba: Economic Geology, v. 88, p. 566-589.

Szybinski, Z. A., 1995, Paleotectonic and Structural Setting of the Western Notre Dame Bay Area, Newfoundland Appalachians: Unpub. Ph.D. thesis, Memorial University of Newfoundland, 481 p.

Taylor, S. R., and McLennan, S. M., 1995, The geochemical evolution of the continental crust: Reviews of Geophysics, v. 33, p. 241-265.

Thompson, A. J., Hauff, B., and Robitaille, P. L., 1999, Alteration mapping in exploration: Application of short-wave infrared (SWIR) spectroscopy: Society of Economic Geologists Newsletter, v. 39.

Thurlow, J. G., 1996, Geology of a newly discovered cluster of blind massive-sulphide deposits, Pilley's Island, central Newfoundland, *in* Pereira, C. P. G., and Walsh, D. G., eds., Current Research Report, Report: 96-1: St. John's, NL, Geological Survey of Newfoundland and Labrador, p. 181-189.

Thurlow, J. G., 2001, Report on Diamond Drilling and Downhole Time domain EM Surveys on Mineral Licence 7528M, Pilley's Island, Notre Dame Bay (2E/12), Central Newfoundland. A report by VMS Consultants Inc. for Inmet Mining and Altius Resources Inc.

Thurlow, J. G., Swanson, E. A., and Strong, D. F., 1975, Geology and lithogeochemistry of the Buchans polymetallic sulfide deposits, Newfoundland: Economic Geology, v. 70, p. 130-144.

Valverde-Vaquero, P., van Staal, C. R., McNicoll, V., and Dunning, G. R., 2006, Mid-Late Ordovician magmatism and metamorphism along the Gander margin in central Newfoundland: Journal of the Geological Society of London, v. 163, p. 347-362.

van Staal, C., 1994, Brunswick subduction complex in the Canadian Appalachians: Record of the Late Ordovician to Late Silurian collision between Laurentia and the Gander margin of Avalon: Tectonics, v. 13, p. 946-962.

van Staal, C. R., 2007, Pre-Carboniferous tectonic evolution and metallogeny of the Canadian Appalachians, *in* Goodfellow, W. D., ed., Mineral Deposits of Canada: A Synthesis of Major Deposit-types, District Metallogeny, the Evolution of Geological Provinces, and Exploration Methods, Special Publication 5, Mineral Deposits Division, Geological Association of Canada, p. 793-818.

van Staal, C. R., and Barr, S. M., 2011, Lithospheric Architecture and Tectonic Evolution of the Canadian Appalachians and Associated Atlantic Margin, *in* J.A. Percival, F. A. C., and R.M. Clowes, ed., Tectonic Styles in Canada: the LITHOPROBE Perspective, Geological Association of Canada.

van Staal, C. R., Dewey, J. F., Niocaill, C. M., and McKerrow, W. S., 1998, The Cambrian-Silurian tectonic evolution of the northern Appalachians and British Caledonides: history of a complex, west and southwest Pacific-type segment of Iapetus: Geological Society, London, Special Publications, v. 143, p. 197-242.

van Staal, C. R., Whalen, J. B., McNicoll, V. J., Pehrsson, S., Lissenberg, C. J., Zagorevski, A., van Breemen, O., and Jenner, G. A., 2007, The Notre Dame Arc and the Taconic Orogeny in Newfoundland: Memoir - Geological Society of America, v. 200, p. 511-552.

van staal, C. R., Whalen, J. B., Valverde-Vaquero, P., Zagorevski, A., and Rogers, N., 2009, Pre-Carboniferous, episodic accretion-related, orogenesis along the Laurentian margin of the northern Appalachians, *in* Murphy, J. B., Keppie, J. D., and Hynes, A. J., eds., Ancient Orogens and Modern Analogues, Special Publication 327, Geological Society of London, p. 271-316.

van Staal, C. R., Wilson, R. A., Rogers, N., Fyfee, L. R., Langton, J. P., McCutcheon, S. R., McNicoll, V., and Ravenhurst, C. E., 2003a, Geology and tectonic history of the Bathurst Supergroup, Bathurst mining camp, and its relationships to coeval rocks in southwestern New Brunswick and adjacent mine; a synthesis, *in* Goodfellow, W. D., McCutcheon, S. R., and Peter, J. M., eds., Massive Sulfide Deposits of the Bathurst Mining Camp, New Brunswick, and Northern Maine, Monograph 11: Littleton, CO, USA, Society of Economic Geologists, p. 37-60.

van Staal, C. R., Wilson, R. A., Rogers, N., Fyffe, L. R., Gower, S. J., Langton, J. P., McCutcheon, S. R., and Walker, J. A., 2003b, A new geologic map of the Bathurst mining camp and surrounding areas; a product of integrated geological, geochemical, and geophysical data, *in* Goodfellow, W. D., McCutcheon, S. R., and Peter, J. M., eds., Massive Sulfide Deposits of the Bathurst Mining Camp, New Brunswick, and Northern Maine, Monograph 11: Littleton, CO, USA, Society of Economic Geologists, p. 61-64.

Waldie, C. J., Jowett, E. C., and Swinden, H. S., 1991, The Crescent Lake copper deposit, Central Newfoundland: deep levels of a volcanogenical hydrothermal system?: Atlantic Geology, v. 27, p. 1-13.

Wanless, V. D., Perfit, M. R., Ridley, W. I., and Klein, E., 2010, Dacite Petrogenesis on Mid-Ocean Ridges: Evidence for Oceanic Crustal Melting and Assimilation: Journal of Petrology, v. 51, p. 2377-2410.

White, J. D. L., and Houghton, B. F., 2006, Primary volcaniclastic rocks: Geology, v. 34, p. 677-680.

Whitford, D. J., Korsch, M. J., Porritt, P. M., and Craven, S. J., 1988, Rare-earth element mobility around the volcanogenic polymetallic massive sulfide deposit at Que River, Tasmania, Australia: Chemical Geology, v. 68, p. 105-119.

Whitford, D. J., McPherson, W. P. A., and Wallace, D. B., 1989, Geochemistry of the host rocks of the volcanogenic massive sulfide deposit at Que River, Tasmania: Economic Geology, v. 84, p. 1-21.

Williams, H., 1975, Sturctural succession, nomenclature, and interpretation of transported rocks in western Newfoundland: Canadian Journal of Earth Sciences, v. 16, p. 792-807.

Williams, H., 1979, Appalachian Orogen in Canada: Canadian Journal of Earth Sciences, v. 16, p. 792-807.

Williams, H., 1992, Lower Ordovician (Arenig-Llanvirn) graptolites from the Notre Dame subzone, central Newfoundland: Canadian Journal of Earth Sciences, v. 29, p. 1717-1733.

Williams, H., 1995, Geology of the Appalachian-Caledonian Orogen in Canada and Greenland, Geological Survey of Canada.

Williams, H., Colman-Sadd, S. P., and Swinden, H. S., 1988, Tectonostratigraphic subdivisions of central Newfoundland., Current Research, Part B, Paper 88-1B: Ottawa, ON, Canada, Geological Survey of Canada, p. 91-98.

Williams, H., and Grant, A. C., 1998, Tectonic Assemblages, Atlantic Region, Canada: Geological Survey of Canada, Open File 3657.

Williams, H., and Piasecki, M. A. J., 1990, The Cold Spring Melange and a possible model for Dunnage-Gander zone interaction in central Newfoundland: Canadian Journal of Earth Sciences, v. 27, p. 1126-1134.

Winter, L. S., 2000, Derivation of base-line geochemistry, petrography, and isotopic data for the host rocks to the Lucky Strike Deposit and comparison with data from other alteration zones, Buchans mining camp, Newfoundland: Unpub. M.Sc. thesis, Memorial University of Newfoundland and Labrador.

Winter, L. S., and Wilton, D. H. C., 2001, Fingerprinting volcanic rocks and hydrothermal systems with lithogeochemistry and Pb-isotopes from the Buchans VMS Camp, Newfoundland: Geological Assocation of Canada/Mineralogical Association of Canada Annual Meeting, St. John's, NL, 2001, Program with Abstracts

Wood, S. A., and Williams-Jones, A. E., 1994, The aqueous geochemistry of rare-earth elements and yttrium. Part 4. Monazite solubility and REE mobility in exhalative massive sulfide-depositing environments: Chemical Geology, v. 115, p. 135-162.

Yang, K., Scott, S. D., and Goodfellow, W. D., 2003, Footwall alteration associated with some massive sulfide deposits in the Bathurst mining camp, New Brunswick; implication for sea-floor hydrothermal mining processes: Economic Geology Monographs, v. 11, p. 435-456.

Zagorevski, A., Lissenberg, C. J., and van Staal, C. R., 2009, Dynamics of accretion of arc and backarc crust to continental margins: Inferences from the Annieopsquotch accretionary tract, Newfoundland Appalachians: Tectonophysics, v. 479, p. 150-164.

Zagorevski, A., Rogers, N., van Staal, C. R., McNicoll, V., Lissenberg, C. J., and Valverde-Vaquero, P., 2006, Lower to Middle Ordovician evolution of peri-Laurentian arc and backarc complexes in Iapetus; constraints from the Annieopsquotch accretionary tract, central Newfoundland: Geological Society of America Bulletin, v. 118, p. 324-342.

Zagorevski, A., van Staal, C. R., McNicoll, V., Rogers, N., and Valverde-Vaquero, P., 2008, Tectonic architecture of an arc-arc collision zone, Newfoundland Appalachians, *in* Draut, A. E., Clift, P. D., and Scholl, D. W., eds., Formation and Applications of the Sedimentary Record in Arc Collision Zones, Geological Society of America Special Paper 436: Boulder, CO, USA, Geological Society of America, p. 309-333.

Zagorevski, A., van Staal, C. R., and McNicoll, V. J., 2007, Distinct Taconic, Salinic, and Acadian deformation along the Iapetus suture zone, Newfoundland Appalachians: Canadian Journal of Earth Sciences, v. 44, p. 1567-1585.

Zagorevski, A., van Staal, C. R., Rogers, N., McNicoll, V., Dunning, G. R., and Pollock, J. C., 2010, Middle Cambrian to Ordovician arc-backarc development on the leading edge of Ganderia, Newfoundland Appalachians, *in* Tollo, R. P., Batholomew, M. J., Hibbard, J. P., and Karabinos, P. M., eds., From Rodinia to Pangea: The Lithotectonic Record of the Appalachian Region, Memoir 206, Geological Society of America, p. 367-396.

Appendix I: Lithogeochemical Data

Table A1-1 Major and trace lithogeochemical data for outcrop and drill core samples from Pilley's Island VMS district.

Sample ID	Det. Limit	10CPM-004a	10CPM-004b	10CPM-005	10CPM-009	10CPM-010a	10CPM-010b	10CPM-012	10CPM-021	10CPM-023
Easting [1]		590759	590759	590731	590845	590950	590950	590967	591045	591196
Northing [1]		5484262	5484262	5484259	5483909	5483950	5483950	5483714	5483911	5483778
Drillhole ID		-	-	-	-	-	-	-	-	-
From (m)		-	-	-	-	-	-	-	-	-
To (m)		-	-	-	-	-	-	-	-	-
Strat. unit		5.5	5.5	5.5	5.6	5.6	5.6	6.1	5.6	6.1
SiO_2 *	0.01	69.04	66.27	66.27	64.09	67.74	68.67	45.02	68.14	42.56
Al_2O_3 *	0.01	14.92	16.12	14.70	16.26	14.12	13.83	16.18	14.99	12.89
Fe_2O_3 *	0.01	3.17	3.35	3.31	3.79	3.24	2.99	9.55	3.88	5.64
MnO *	0.001	0.12	0.10	0.11	0.07	0.04	0.01	0.17	0.06	0.14
MgO *	0.01	0.78	1.62	0.91	2.37	1.68	0.19	8.04	1.83	2.70
CaO *	0.01	1.11	0.98	0.64	0.56	0.13	0.15	5.67	0.41	15.01
Na_2O *	0.01	3.40	0.72	0.18	2.97	0.12	0.15	1.86	2.77	5.34
K_2O *	0.01	4.19	7.15	10.98	6.68	8.79	10.41	4.54	4.66	1.24
TiO_2 *	0.001	0.45	0.47	0.62	0.61	0.46	0.47	0.70	0.49	0.79
P_2O_5 *	0.01	0.10	0.10	0.15	0.15	0.11	0.09	0.30	0.12	0.45
LOI *		3.43	3.75	2.14	2.41	2.24	2.33	7.86	2.95	12.88
TOTAL *		100.70	100.70	100.00	99.95	98.68	99.29	99.86	100.30	99.63
Cr^{52} #	3.65	22.94	6.64	12.75	6.11	8.97	16.35	56.78	8.13	-
Cr^{53} #	12.85	26.75	-	13.41	-	-	17.14	65.01	-	-
Ni #	5.14	6.43	-	-	-	-	-	43.68	-	11.26
Co #	0.26	3.24	2.21	2.57	2.29	3.24	4.71	36.54	4.53	27.90
Sc #	1.00	5.00	6.00	9.00	9.00	7.00	7.00	28.00	7.00	18.00
V #	3.42	10.97	11.49	12.26	15.59	37.66	8.47	221.93	18.81	303.22
Cu #	3.94	-	-	345.99	-	11.07	-	45.02	-	-
Pb #	0.25	13.42	10.33	20.10	6.20	45.42	21.99	6.07	4.77	8.53
Zn #	8.16	56.55	60.86	19.29	16.68	19.98	-	45.06	13.13	18.81
Bi #	0.06	0.13	0.10	-	-	0.11	0.59	0.07	-	-
Cd #	0.99	-	-	-	-	-	1.20	-	-	-
Sn #	0.12	1.22	1.55	0.36	1.18	0.99	0.55	0.57	0.87	0.44
Mo #	0.63	2.01	1.85	2.92	2.16	3.55	2.44	-	2.12	-
As #	1.33	4.72	1.85	1.85	-	2.69	10.16	5.51	3.32	15.73
Sb #	0.20	0.40	0.58	-	-	0.21	-	-	0.31	0.30
Ag #	0.23	0.81	0.72	0.61	0.52	0.81	0.68	0.34	0.39	0.26
Li #	0.79	1.86	1.93	1.65	3.76	4.88	0.96	54.43	4.77	8.96
Rb #	0.76	118.31	221.58	162.43	75.30	184.27	201.83	104.41	104.87	50.21
Cs #	0.08	0.49	1.06	0.24	0.25	0.28	0.23	0.81	0.46	0.28
Ba #	0.80	1125.90	1140.96	2496.76	1627.75	3553.99	1544.75	1223.66	1085.55	588.09
Sr #	4.16	70.52	27.49	46.91	37.50	37.37	-	266.24	33.87	215.93
Tl #	0.08	1.15	2.53	1.49	0.89	1.04	1.46	0.39	0.67	0.17
Ta #	0.04	0.49	0.52	0.39	0.46	0.45	0.38	0.15	0.46	0.15
Nb #	0.08	8.58	10.10	7.52	8.97	7.79	7.46	2.71	8.53	2.85
Hf #	0.21	5.04	5.93	4.52	5.54	5.31	5.01	1.72	5.44	2.03
Zr #	0.14	174.53	218.63	166.40	202.60	179.86	170.06	52.12	195.59	64.69
Y #	0.08	17.81	18.40	9.13	9.63	15.48	2.55	15.14	12.01	22.84
Th #	0.08	4.22	4.38	1.92	1.12	4.01	0.33	2.06	1.93	2.01
U #	0.09	1.93	2.17	1.65	1.75	1.47	1.17	1.04	1.86	5.49

Table A1-1 (continued) Major and trace lithogeochemical data for outcrop and drill core samples from Pilley's Island VMS district.

Sample ID	Det. Limit	10CPM-004a	10CPM-004b	10CPM-005	10CPM-009	10CPM-010a	10CPM-010b	10CPM-012	10CPM-021	10CPM-023
La #	0.09	12.84	10.64	5.13	6.08	5.35	2.09	6.47	8.09	9.04
Ce #	0.13	24.74	22.34	9.46	7.72	9.62	2.15	14.76	9.40	19.30
Pr #	0.06	3.32	2.81	1.47	1.53	1.80	0.65	2.04	1.89	2.80
Nd #	0.50	13.54	11.23	6.14	5.73	7.29	2.42	9.50	7.49	12.84
Sm #	0.36	2.94	2.58	1.44	1.45	1.84	0.52	2.50	1.67	3.39
Eu #	0.08	0.69	0.67	0.37	0.34	0.32	0.12	0.81	0.45	1.11
Gd #	0.16	2.96	2.63	1.55	1.53	2.24	0.54	2.95	1.81	4.25
Tb #	0.03	0.48	0.50	0.26	0.24	0.39	0.06	0.43	0.32	0.64
Dy #	0.13	3.39	3.47	1.73	1.55	2.85	0.43	2.82	2.15	4.23
Ho #	0.03	0.72	0.74	0.39	0.34	0.63	0.09	0.61	0.46	0.88
Er #	0.14	2.23	2.42	1.32	1.12	2.05	0.36	1.73	1.53	2.61
Tm #	0.04	0.39	0.42	0.23	0.23	0.36	0.09	0.34	0.23	0.41
Yb #	0.21	2.77	2.93	1.59	1.34	2.50	0.33	1.79	1.46	2.47
Lu #	0.05	0.41	0.46	0.25	0.23	0.41	0.05	0.27	0.25	0.38
Sericite Index[2]		50.00	55.20	90.85	98.39	69.22	98.65	98.58	70.94	62.72
Al_2O_3/Na_2O		4.39	22.39	81.67	5.47	117.67	92.20	8.70	5.41	2.41
CCPI[3]		34.23	38.71	27.44	38.96	35.57	23.14	73.32	43.46	55.90
AI[4]		52.43	83.76	93.55	71.94	97.67	97.25	62.56	67.11	16.22
Zn/TiO_2*10000		17.45	0.05	0.04	0.03	0.03	0.04	0.01	0.03	0.01
Nb/Y		0.48	0.55	0.82	0.93	0.50	2.93	0.18	0.71	0.12
Th/Yb		1.52	1.49	1.21	0.84	1.60	1.00	1.15	1.32	0.82
$[La/Yb]_{CN}$[5]		3.15	2.47	2.20	3.09	1.45	4.25	2.45	3.77	2.49
$[La/Sm]_{MN}$[6]		2.82	2.66	2.30	2.71	1.88	2.60	1.67	3.13	1.72
$[Nb/Th]_{MN}$[6]		0.25	0.28	0.47	0.97	0.23	2.69	0.16	0.54	0.17
Zr/Yb		0.67	63.00	74.64	104.81	151.65	71.88	508.33	29.11	134.16
Nb/Yb		3.10	3.45	4.73	6.71	3.11	22.30	1.51	5.85	1.15
Th/Nb		0.49	0.43	0.26	0.12	0.51	0.04	0.76	0.23	0.71
La/Sm		4.36	4.12	3.57	4.20	2.91	4.02	2.59	4.84	2.66

* wt%; ICP-OES

ppm; ICP-MS

LOI Loss On Ignition

[1] Universal Transverse Mercator, North American Datum 27 (UTM NAD27)

[2] Sericite Index = $100*K_2O/Na_2O+K_2O$

[3] CCPI = $100*(Fe_2O_3^T+MgO)/(Fe_2O_3^T+MgO+K_2O+Na_2O)$

[4] AI = $100*(K_2O+MgO)/(K_2O+MgO+CaO+Na_2O)$

[5] CN = chondrite normalized

[6] MN = primitive mantle normalized

\- < Limit of Detection

N.D. Not Detected

Table A1-1 (continued) Major and trace lithogeochemical data for outcrop and drill core samples from Pilley's Island VMS district.

Sample ID	Det. Limit	10CPM-025	10CPM-029	10CPM-032	10CPM-036a	10CPM-036b	10CPM-037a	10CPM-037b	10CPM-038	10CPM-039
Easting [1]		590994	591355	591585	591311	591311	591271	591271	591267	591296
Northing [1]		5484368	5484586	5484638	5484244	5484244	5484354	5484354	5484868	5483858
Drillhole ID		-	-	-	-	-	-	-	-	-
From (m)		-	-	-	-	-	-	-	-	-
To (m)		-	-	-	-	-	-	-	-	-
Strat. unit		5.5	2	2	6.2	6.1	6.2	6.2	2	6.2
SiO_2 *	0.01	62.87	49.78	54.43	68.54	51.61	64.89	67.67	49.35	65.04
Al_2O_3 *	0.01	15.05	15.23	14.47	14.55	17.66	16.55	13.90	15.63	15.50
Fe_2O_3 *	0.01	4.55	8.43	7.10	4.67	8.74	1.10	3.99	11.86	4.50
MnO *	0.001	0.07	0.13	0.11	0.08	0.17	0.02	0.28	0.20	0.11
MgO *	0.01	2.20	2.12	2.53	1.95	5.09	0.17	1.22	4.57	0.73
CaO *	0.01	1.72	8.91	7.55	1.69	3.52	0.34	0.72	4.78	0.25
Na_2O *	0.01	0.10	6.74	6.73	4.33	5.06	0.24	1.94	4.15	1.36
K_2O *	0.01	6.99	0.52	0.17	1.37	1.00	13.45	6.78	2.52	9.32
TiO_2 *	0.001	0.52	0.98	0.88	0.52	1.29	0.56	0.55	1.36	0.51
P_2O_5 *	0.01	0.11	0.33	0.29	0.13	0.56	0.12	0.17	0.45	0.12
LOI *		6.38	7.48	6.47	2.71	4.44	1.24	2.11	3.96	2.38
TOTAL *		100.60	100.60	100.70	100.50	99.14	98.68	99.32	98.84	99.83
Cr^{52} #	3.65	3.95	11.08	28.26	3.91	-	16.97	6.90	8.21	-
Cr^{53} #	12.85	-	13.71	31.27	-	-	18.70	-	-	-
Ni #	5.14	-	27.79	26.20	-	7.42	-	-	12.99	238.56
Co #	0.26	4.61	26.66	17.95	4.26	22.33	4.07	3.86	31.45	2.39
Sc #	1.00	8.00	28.00	24.00	8.00	23.00	9.00	8.00	27.00	8.00
V #	3.42	8.55	292.63	276.52	15.04	212.76	13.21	18.56	361.39	8.48
Cu #	3.94	-	-	-	-	-	50.19	-	-	11.23
Pb #	0.25	72.34	5.08	3.45	21.38	7.90	24.22	27.41	5.94	9.55
Zn #	8.16	112.47	42.63	-	78.21	29.49	1012.09	67.99	23.58	112.48
Bi #	0.06	0.10	-	-	0.08	-	0.06	0.08	-	0.08
Cd #	0.99	1.54	-	-	1.08	-	5.62	-	-	1.12
Sn #	0.12	1.63	0.38	0.47	1.02	0.71	1.85	1.06	0.32	1.19
Mo #	0.63	10.90	-	-	-	-	2.25	1.19	0.70	0.70
As #	1.33	36.97	11.93	21.00	7.08	21.50	85.50	11.23	66.93	9.47
Sb #	0.20	0.71	0.23	-	0.34	0.28	2.96	0.24	-	0.93
Ag #	0.23	0.80	0.53	-	0.54	0.33	1.34	0.54	0.36	0.50
Li #	0.79	2.60	4.73	6.30	19.66	43.47	-	7.45	23.75	5.56
Rb #	0.76	200.16	12.32	27.65	47.90	43.55	403.22	109.38	72.58	835.33
Cs #	0.08	0.76	0.09	-	1.00	0.87	0.42	0.36	0.36	1.03
Ba #	0.80	496.67	68.04	78.94	467.48	553.82	1269.94	1011.65	1779.49	1651.09
Sr #	4.16	92.19	112.17	136.09	346.14	322.92	22.92	47.85	213.11	7.16
Tl #	0.08	1.51	0.17	0.13	0.34	0.18	3.15	1.60	0.33	1.54
Ta #	0.04	0.49	0.16	0.13	0.44	0.31	0.47	0.42	0.22	0.33
Nb #	0.08	8.67	2.85	2.43	7.93	6.27	8.91	7.21	4.34	8.57
Hf #	0.21	5.58	2.44	2.22	5.14	3.62	5.64	4.42	2.92	5.14
Zr #	0.14	187.54	76.83	65.97	184.22	120.28	194.72	161.55	105.24	191.78
Y #	0.08	27.66	21.60	18.37	28.10	34.05	13.91	6.00	31.38	3.63
Th #	0.08	5.04	1.67	1.42	4.00	2.57	2.61	0.76	2.91	0.53
U #	0.09	2.30	0.89	0.61	1.50	1.20	1.67	1.38	0.66	0.73

Table A1-1 (continued) Major and trace lithogeochemical data for outcrop and drill core samples from Pilley's Island VMS district.

Sample ID	Det. Limit	10CPM-025	10CPM-029	10CPM-032	10CPM-036a	10CPM-036b	10CPM-037a	10CPM-037b	10CPM-038	10CPM-039
La #	0.09	24.15	7.47	6.15	9.79	9.22	9.41	2.19	13.17	1.55
Ce #	0.13	48.11	18.35	15.78	21.86	25.68	15.06	4.67	34.07	3.01
Pr #	0.06	6.06	2.51	2.11	2.99	3.42	2.41	0.59	4.16	0.52
Nd #	0.50	23.86	11.71	9.62	11.96	16.38	10.14	2.34	18.93	2.35
Sm #	0.36	5.70	3.19	2.67	3.16	4.93	2.51	0.60	4.86	0.69
Eu #	0.08	1.36	1.05	0.92	0.82	1.54	0.72	0.19	1.56	0.23
Gd #	0.16	5.46	3.98	3.32	3.39	5.75	2.61	0.72	5.55	0.40
Tb #	0.03	0.80	0.59	0.56	0.68	0.98	0.42	0.13	0.88	0.09
Dy #	0.13	5.24	4.02	3.75	5.01	6.50	2.82	0.90	5.81	0.59
Ho #	0.03	1.11	0.86	0.74	1.08	1.31	0.57	0.23	1.18	0.12
Er #	0.14	3.52	2.56	2.12	3.51	3.84	1.77	0.81	3.47	0.59
Tm #	0.04	0.58	0.45	0.34	0.56	0.58	0.27	0.17	0.55	0.16
Yb #	0.21	3.78	2.66	2.18	3.73	3.79	1.81	1.03	3.51	0.78
Lu #	0.05	0.63	0.42	0.34	0.59	0.54	0.29	0.17	0.52	0.13
Sericite Index[2]		18.84	98.59	7.16	2.46	24.04	16.50	98.25	77.75	37.78
Al_2O_3/Na_2O		150.50	2.26	2.15	3.36	3.49	68.96	7.16	3.77	11.40
CCPI[3]		48.77	59.24	58.26	53.73	69.53	8.49	37.40	71.13	32.87
AI[4]		83.47	14.43	15.90	35.55	41.51	95.92	75.05	44.26	86.19
$Zn/TiO_2*10000$		0.02	0.01	0.01	0.02	0.02	0.02	0.03	0.02	0.01
Nb/Y		0.31	0.13	0.13	0.28	0.18	0.64	1.20	0.14	2.36
Th/Yb		1.33	0.63	0.65	1.07	0.68	1.44	0.74	0.83	0.67
$[La/Yb]_{CN}$[5]		4.34	1.91	1.92	1.78	1.65	3.53	1.44	2.55	1.35
$[La/Sm]_{MN}$[6]		2.74	1.51	1.49	2.00	1.21	2.42	2.36	1.75	1.44
$[Nb/Th]_{MN}$[6]		0.21	0.21	0.21	0.24	0.29	0.41	1.14	0.18	1.96
Zr/Yb		26.21	49.60	28.87	30.31	49.43	31.73	107.60	156.60	29.98
Nb/Yb		2.29	1.07	1.12	2.13	1.65	4.92	6.99	1.24	10.96
Th/Nb		0.58	0.58	0.58	0.50	0.41	0.29	0.11	0.67	0.06
La/Sm		4.24	2.34	2.31	3.09	1.87	3.75	3.66	2.71	2.23

* wt%; ICP-OES

\# ppm; ICP-MS

LOI Loss On Ignition

[1] Universal Transverse Mercator, North American Datum 27 (UTM NAD27)

[2] Sericite Index = $100*K_2O/Na_2O + K_2O$

[3] CCPI = $100*(Fe_2O_3^T+MgO)/(Fe_2O_3^T+MgO+K_2O+Na_2O)$

[4] AI = $100*(K_2O+MgO)/(K_2O+MgO+CaO+Na_2O)$

[5] CN = chondrite normalized

[6] MN = primitive mantle normalized

\- < Limit of Detection

N.D. Not Detected

Table A1-1 (continued) Major and trace lithogeochemical data for outcrop and drill core samples from Pilley's Island VMS district.

Sample ID	Det. Limit	10CPM-040	10CPM-041	10CPM-044	10CPM-049	10CPM-052	10CPM-053	10CPM-059	10CPM-062	10CPM-064
Easting [1]		591427	591587	591446	591903	591843	591785	591892	592104	592066
Northing [1]		5483738	5483809	5484186	5484090	5484969	5484035	5484792	5484821	5484703
Drillhole ID		-	-	-	-	-	-	-	-	-
From (m)		-	-	-	-	-	-	-	-	-
To (m)		-	-	-	-	-	-	-	-	-
Strat. unit		6.2	6.1	6.1	6.2	6.1	6.2	2	2	2
SiO_2 *	0.01	75.14	48.32	51.89	68.46	50.23	67.01	75.06	48.23	50.08
Al_2O_3 *	0.01	10.22	16.18	15.33	16.08	14.86	15.42	11.16	14.76	15.61
Fe_2O_3 *	0.01	1.78	10.39	9.28	2.48	8.30	3.80	2.73	7.19	6.04
MnO *	0.001	0.06	0.11	0.13	0.20	0.15	0.11	0.07	0.14	0.12
MgO *	0.01	0.93	6.63	3.24	1.56	8.85	1.17	0.52	5.20	4.19
CaO *	0.01	1.51	2.64	5.55	0.55	7.94	1.02	0.55	10.49	10.27
Na_2O *	0.01	1.81	1.55	3.86	0.10	3.81	1.80	4.75	4.91	5.48
K_2O *	0.01	3.77	6.41	2.16	5.34	1.31	6.03	1.81	0.77	0.79
TiO_2 *	0.001	0.41	0.91	1.12	0.62	0.61	0.55	0.32	0.52	0.54
P_2O_5 *	0.01	0.13	0.39	0.62	0.15	0.21	0.12	0.04	0.19	0.17
LOI *		3.14	5.81	6.12	4.36	3.63	3.37	0.99	6.85	6.09
TOTAL *		98.89	99.34	99.30	99.90	99.90	100.40	98.01	99.24	99.39
Cr^{52} #	3.65	13.62	12.13	-	-	351.11	4.31	28.35	209.99	187.10
Cr^{53} #	12.85	-	-	-	-	356.25	-	32.11	221.22	193.43
Ni #	5.14	-	46.60	-	5.16	103.55	-	-	63.36	78.83
Co #	0.26	2.33	28.43	29.76	2.66	36.43	3.00	2.14	21.39	24.97
Sc #	1.00	6.00	31.00	22.00	9.00	41.00	9.00	6.00	27.00	25.00
V #	3.42	12.43	273.02	292.64	20.66	212.63	12.61	5.05	202.61	184.02
Cu #	3.94	-	91.56	-	19.60	102.38	13.59	-	66.39	68.37
Pb #	0.25	7.63	5.58	8.64	5.68	3.88	8.18	18.05	6.23	7.21
Zn #	8.16	20.43	106.66	40.19	58.87	34.12	57.13	47.95	45.89	32.87
Bi #	0.06	-	-	-	-	-	0.07	0.07	-	-
Cd #	0.99	-	-	-	-	-	-	-	-	-
Sn #	0.12	0.58	0.68	0.46	1.39	0.26	2.42	1.51	0.58	-
Mo #	0.63	-	-	1.25	2.16	-	-	-	0.81	0.89
As #	1.33	7.51	7.80	24.47	15.50	17.97	6.79	4.09	8.56	3.65
Sb #	0.20	1.05	0.27	0.73	1.48	0.24	1.58	0.35	-	-
Ag #	0.23	0.53	-	0.23	0.67	-	0.72	0.75	-	-
Li #	0.79	0.97	41.74	19.25	1.63	37.82	1.23	-	12.53	7.12
Rb #	0.76	123.32	1005.60	103.22	173.72	40.14	150.01	59.73	28.11	13.56
Cs #	0.08	0.67	2.16	0.95	0.65	0.49	2.31	0.11	0.48	-
Ba #	0.80	1338.69	516.00	537.12	569.32	597.93	481.50	983.01	326.22	437.22
Sr #	4.16	72.87	139.20	308.63	27.53	429.33	71.61	108.35	325.97	283.56
Tl #	0.08	0.67	0.93	0.41	2.16	0.20	1.00	0.26	0.11	0.11
Ta #	0.04	0.34	0.10	0.22	0.56	0.15	0.46	0.44	0.07	0.09
Nb #	0.08	5.92	2.60	3.99	9.68	3.03	8.80	8.12	1.45	1.50
Hf #	0.21	3.85	1.93	2.77	6.14	1.51	5.31	6.33	1.26	1.27
Zr #	0.14	126.01	58.54	86.64	217.24	43.35	198.03	219.06	36.23	39.84
Y #	0.08	9.88	17.12	25.18	24.46	14.05	13.08	5.93	13.44	12.59
Th #	0.08	2.35	1.64	1.97	6.16	1.82	2.06	2.51	1.39	1.36
U #	0.09	1.22	0.69	1.04	2.22	0.39	1.59	1.32	0.28	0.42

Table A1-1 (continued) Major and trace lithogeochemical data for outcrop and drill core samples from Pilley's Island VMS district.

Sample ID	Det. Limit	10CPM-040	10CPM-041	10CPM-044	10CPM-049	10CPM-052	10CPM-053	10CPM-059	10CPM-062	10CPM-064
La #	0.09	6.30	6.00	8.30	18.39	6.18	5.63	7.20	6.00	4.42
Ce #	0.13	14.52	16.04	22.40	38.52	13.15	12.55	20.68	11.22	10.04
Pr #	0.06	1.75	1.86	2.95	4.44	1.89	1.72	1.77	1.64	1.44
Nd #	0.50	7.19	9.37	13.85	17.41	8.59	7.08	7.46	7.20	6.85
Sm #	0.36	1.76	2.84	3.90	3.90	2.33	1.77	1.60	1.94	1.87
Eu #	0.08	0.51	0.96	1.27	1.01	0.78	0.47	0.37	0.71	0.65
Gd #	0.16	2.05	3.13	4.75	3.87	2.68	1.94	1.54	2.44	2.37
Tb #	0.03	0.34	0.53	0.73	0.72	0.42	0.35	0.25	0.37	0.38
Dy #	0.13	2.11	3.05	4.78	4.56	2.78	2.47	1.73	2.41	2.52
Ho #	0.03	0.43	0.72	0.97	0.99	0.55	0.54	0.36	0.52	0.51
Er #	0.14	1.32	1.83	2.94	3.19	1.62	1.78	1.02	1.56	1.56
Tm #	0.04	0.23	0.35	0.46	0.54	0.28	0.31	0.16	0.26	0.24
Yb #	0.21	1.70	1.52	2.90	3.63	1.50	2.08	1.07	1.38	1.47
Lu #	0.05	0.26	0.32	0.43	0.58	0.23	0.33	0.17	0.23	0.22
Sericite Index[2]		87.27	67.56	80.53	35.88	98.16	25.59	77.01	27.59	13.56
Al_2O_3/Na_2O		5.65	10.44	3.97	160.80	3.90	8.57	2.35	3.01	2.85
CCPI[3]		32.69	68.13	67.53	42.62	77.01	38.83	33.13	68.57	62.00
AI[4]		58.60	75.68	36.46	91.39	46.37	71.86	30.54	27.94	24.02
$Zn/TiO_2*10000$		0.02	0.01	0.01	0.02	0.01	0.03	0.04	0.01	0.01
Nb/Y		0.60	0.15	0.16	0.40	0.22	0.67	1.37	0.11	0.12
Th/Yb		1.39	1.08	0.68	1.70	1.22	0.99	2.36	1.01	0.93
$[La/Yb]_{CN}$[5]		2.53	2.67	1.94	3.44	2.81	1.84	4.58	2.95	2.05
$[La/Sm]_{MN}$[6]		2.31	1.37	1.37	3.05	1.71	2.06	2.91	1.99	1.53
$[Nb/Th]_{MN}$[6]		0.30	0.19	0.24	0.19	0.20	0.52	0.39	0.13	0.13
Zr/Yb		245.17	74.34	38.44	29.87	59.83	28.99	95.30	205.26	26.24
Nb/Yb		3.49	1.71	1.38	2.67	2.03	4.23	7.60	1.05	1.02
Th/Nb		0.40	0.63	0.49	0.64	0.60	0.23	0.31	0.96	0.90
La/Sm		3.58	2.11	2.13	4.72	2.65	3.19	4.50	3.09	2.36

* wt%; ICP-OES

ppm; ICP-MS

LOI Loss On Ignition

[1] Universal Transverse Mercator, North American Datum 27 (UTM NAD27)

[2] Sericite Index = $100*K_2O/Na_2O+K_2O$

[3] CCPI = $100*(Fe_2O_3{}^1+MgO)/(Fe_2O_3{}^1+MgO+K_2O+Na_2O)$

[4] AI = $100*(K_2O+MgO)/(K_2O+MgO+CaO+Na_2O)$

[5] CN = chondrite normalized

[6] MN = primitive mantle normalized

- < Limit of Detection

N.D. Not Detected

Table A1-1 (continued) Major and trace lithogeochemical data for outcrop and drill core samples from Pilley's Island VMS district.

Sample ID	Det. Limit	10CPM-065	10CPM-069	10CPM-071	10CPM-073	10CPM-074	10CPM-075	10CPM-076	10CPM-078	10CPM-083
Easting [1]		592124	592207	592224	592099	592463	592374	592247	592337	592564
Northing [1]		5484655	5484403	5484178	5484182	5484551	5484616	5484628	5484928	5484623
Drillhole ID		-	-	-	-	-	-	-	-	-
From (m)		-	-	-	-	-	-	-	-	-
To (m)		-	-	-	-	-	-	-	-	-
Strat. unit		4.6	2	6.1	6.1	4.6	4.6	4.6	2	4.6
SiO_2 *	0.01	65.88	49.33	50.83	48.41	66.58	71.51	68.93	43.17	72.36
Al_2O_3 *	0.01	14.90	18.15	16.53	13.40	12.95	13.45	14.49	13.93	12.70
Fe_2O_3 *	0.01	4.61	8.53	9.13	8.86	6.27	3.08	2.63	8.24	3.06
MnO *	0.001	0.10	0.13	0.19	0.32	0.04	0.11	0.09	0.22	0.05
MgO *	0.01	1.14	5.22	5.92	3.30	0.44	0.79	0.46	9.10	1.01
CaO *	0.01	0.66	6.48	5.70	6.85	0.45	0.88	0.29	9.19	0.26
Na_2O *	0.01	5.08	4.91	5.36	3.83	4.33	5.10	2.79	2.69	4.70
K_2O *	0.01	3.40	1.00	0.11	0.81	2.38	2.20	6.92	0.95	2.35
TiO_2 *	0.001	0.53	0.58	0.80	1.13	0.51	0.47	0.55	0.59	0.43
P_2O_5 *	0.01	0.14	0.17	0.21	0.29	0.08	0.13	0.13	0.32	0.10
LOI *		2.82	5.57	4.52	11.54	4.58	1.38	2.20	10.95	1.96
TOTAL *		99.27	100.10	99.28	98.73	98.60	99.12	99.48	99.34	98.99
Cr^{52} #	3.65	16.79	120.51	79.90	13.62	5.95	21.77	12.83	863.44	22.81
Cr^{53} #	12.85	19.65	120.84	81.31	17.35	-	24.06	14.18	879.22	26.66
Ni #	5.14	-	56.44	46.71	19.24	-	-	-	372.96	-
Co #	0.26	3.61	29.80	24.93	18.71	2.96	3.07	3.04	50.70	2.24
Sc #	1.00	7.00	34.00	32.00	25.00	6.00	6.00	7.00	33.00	7.00
V #	3.42	17.74	197.93	243.22	289.03	16.17	12.69	18.53	241.72	10.71
Cu #	3.94	28.45	-	24.64	45.43	9.64	-	16.47	88.36	15.48
Pb #	0.25	10.11	8.49	2.72	9.52	89.22	11.25	14.45	3.97	49.19
Zn #	8.16	227.11	47.45	353.80	375.03	26.72	31.79	792.74	53.72	355.29
Bi #	0.06	0.07	-	0.07	-	0.09	0.08	-	-	0.06
Cd #	0.99	-	-	-	1.05	-	-	1.82	-	1.41
Sn #	0.12	1.13	0.34	0.47	0.63	1.30	0.94	0.74	0.25	0.99
Mo #	0.63	3.18	1.13	1.02	0.83	21.25	1.04	2.57	-	3.30
As #	1.33	28.09	24.71	7.17	11.44	127.36	25.26	7.51	7.32	5.65
Sb #	0.20	0.41	-	0.25	0.79	32.47	3.86	0.23	0.28	0.51
Ag #	0.23	0.95	-	-	-	28.40	0.65	0.74	-	0.89
Li #	0.79	3.17	13.59	18.77	16.78	2.02	4.14	1.67	20.02	5.40
Rb #	0.76	55.20	34.84	3.28	38.18	75.09	44.92	103.98	42.23	44.35
Cs #	0.08	0.20	0.66	0.38	0.53	0.26	0.19	0.48	0.52	0.13
Ba #	0.80	1154.67	359.14	80.44	1261.92	8770.80	1027.92	1393.88	347.22	704.44
Sr #	4.16	67.67	310.41	212.94	96.93	184.59	167.16	17.86	208.07	53.57
Tl #	0.08	1.05	0.14	0.15	0.21	20.11	1.87	1.10	0.32	0.70
Ta #	0.04	0.43	0.09	0.17	0.17	0.46	0.38	0.43	0.12	0.38
Nb #	0.08	7.92	1.65	3.13	2.87	8.20	7.48	8.16	2.27	7.30
Hf #	0.21	5.10	1.51	2.26	2.66	4.98	4.63	4.88	1.97	4.29
Zr #	0.14	178.57	41.68	72.94	75.68	183.49	164.83	181.40	46.79	154.55
Y #	0.08	8.01	14.55	16.84	24.98	8.76	4.37	2.60	13.42	11.96
Th #	0.08	2.44	1.49	2.09	1.81	2.85	1.83	0.44	1.80	1.15
U #	0.09	1.72	0.22	0.52	0.66	2.00	1.83	1.66	0.57	1.45

Table A1-1 (continued) Major and trace lithogeochemical data for outcrop and drill core samples from Pilley's Island VMS district.

Sample ID	Det. Limit	10CPM-065	10CPM-069	10CPM-071	10CPM-073	10CPM-074	10CPM-075	10CPM-076	10CPM-078	10CPM-083
La #	0.09	6.46	5.16	6.80	8.08	2.95	4.22	1.50	7.08	5.61
Ce #	0.13	11.90	12.65	16.19	17.76	4.88	9.13	2.76	15.46	7.57
Pr #	0.06	1.56	1.69	2.16	2.49	0.77	1.12	0.36	2.11	1.37
Nd #	0.50	6.02	7.51	9.45	12.11	3.02	4.07	1.40	9.47	5.42
Sm #	0.36	1.36	2.24	2.78	3.61	0.83	1.00	-	2.40	1.34
Eu #	0.08	0.39	0.74	1.00	1.29	0.38	0.25	-	0.84	0.40
Gd #	0.16	1.43	2.54	3.11	4.60	1.06	0.92	0.38	2.69	1.56
Tb #	0.03	0.25	0.46	0.50	0.70	0.20	0.16	0.06	0.42	0.28
Dy #	0.13	1.56	2.85	3.23	4.85	1.48	0.97	0.46	2.68	1.83
Ho #	0.03	0.34	0.58	0.66	1.03	0.34	0.22	0.10	0.54	0.39
Er #	0.14	1.05	1.77	1.99	2.89	1.12	0.70	0.40	1.55	1.24
Tm #	0.04	0.17	0.29	0.32	0.45	0.22	0.15	0.10	0.25	0.21
Yb #	0.21	1.26	1.67	1.97	2.88	1.34	0.64	0.56	1.50	1.31
Lu #	0.05	0.19	0.26	0.31	0.47	0.24	0.11	0.09	0.24	0.20
Sericite Index[2]		12.60	40.09	16.92	2.01	17.46	35.47	30.14	71.27	26.10
Al_2O_3/Na_2O		2.93	3.70	3.08	3.50	2.99	2.64	5.19	5.18	2.70
CCPI[3]		40.41	69.94	73.34	72.38	50.00	34.65	24.14	82.65	36.60
AI[4]		44.16	35.32	35.28	27.79	37.11	33.33	70.55	45.83	40.38
Zn/TiO_2*10000		0.03	0.01	0.01	0.01	0.02	0.03	0.04	0.01	0.03
Nb/Y		0.99	0.11	0.19	0.11	0.94	1.71	3.14	0.17	0.61
Th/Yb		1.93	0.89	1.06	0.63	2.12	2.86	0.78	1.20	0.88
$[La/Yb]_{CN}$[5]		3.47	2.10	2.34	1.90	1.49	4.49	1.83	3.20	2.90
$[La/Sm]_{MN}$[6]		3.07	1.49	1.58	1.45	2.30	2.72	-	1.91	2.70
$[Nb/Th]_{MN}$[6]		0.39	0.13	0.18	0.19	0.35	0.49	2.26	0.15	0.77
Zr/Yb		27.16	141.47	24.96	36.98	26.25	136.64	257.83	325.44	31.18
Nb/Yb		6.27	0.99	1.59	1.00	6.11	11.69	14.63	1.52	5.56
Th/Nb		0.31	0.91	0.67	0.63	0.35	0.24	0.05	0.79	0.16
La/Sm		4.74	2.31	2.44	2.24	3.56	4.20	-	2.95	4.17

* wt%; ICP-OES

\# ppm; ICP-MS

LOI Loss On Ignition

[1] Universal Transverse Mercator, North American Datum 27 (UTM NAD27)

[2] Sericite Index = $100*K_2O/Na_2O + K_2O$

[3] CCPI = $100*(Fe_2O_3^T+MgO)/(Fe_2O_3^T+MgO+K_2O+Na_2O)$

[4] AI = $100*(K_2O+MgO)/(K_2O+MgO+CaO+Na_2O)$

[5] CN = chondrite normalized

[6] MN = primitive mantle normalized

\- < Limit of Detection

N.D. Not Detected

Table A1-1 (continued) Major and trace lithogeochemical data for outcrop and drill core samples from Pilley's Island VMS district.

Sample ID	Det. Limit	10CPM-084	10CPM-086	10CPM-090	10CPM-093	10CPM-095	10CPM-098b	10CPM-102	10CPM-105	10CPM-106
Easting [1]		592587	592753	592371	593037	592988	593061	593164	593203	593221
Northing [1]		5484579	5484549	5484685	5484450	5484530	5484664	5484822	5484811	5484823
Drillhole ID		-	-	-	-	-	-	-	-	-
From (m)		-	-	-	-	-	-	-	-	-
To (m)		-	-	-	-	-	-	-	-	-
Strat. unit		4.6	4.6	4.6	4.3	4.3	4.4	4.1	4.4	4.1
SiO_2 *	0.01	66.02	65.18	75.37	65.32	69.30	59.73	67.50	62.75	56.57
Al_2O_3 *	0.01	15.14	15.78	12.49	15.65	14.20	15.42	13.34	14.43	16.57
Fe_2O_3 *	0.01	3.17	3.97	1.98	4.08	3.29	6.32	4.30	5.26	7.53
MnO *	0.001	0.09	0.08	0.04	0.10	0.10	0.64	0.28	0.59	0.67
MgO *	0.01	1.75	1.63	0.24	2.29	1.62	2.10	1.27	1.82	3.86
CaO *	0.01	0.25	0.72	0.74	1.32	0.77	1.19	0.30	0.99	1.14
Na_2O *	0.01	2.92	5.48	6.73	5.38	3.61	1.11	0.17	3.21	2.85
K_2O *	0.01	7.09	3.73	0.16	1.64	3.44	7.46	8.97	4.48	4.32
TiO_2 *	0.001	0.55	0.56	0.47	0.55	0.52	0.72	0.54	0.63	0.92
P_2O_5 *	0.01	0.13	0.14	0.12	0.17	0.11	0.35	0.28	0.29	0.40
LOI *		1.59	1.62	0.78	2.12	2.05	3.30	2.08	5.39	4.25
TOTAL *		98.69	98.89	99.12	98.62	99.00	98.34	99.02	99.85	99.09
Cr^{52} #	3.65	9.22	13.06	25.08	3.96	5.86	-	N.D.	N.D.	N.D.
Cr^{53} #	12.85	-	17.09	26.83	-	-	-	18.48	20.33	-
Ni #	5.14	-	-	-	-	-	-	-	20.05	15.75
Co #	0.26	2.14	4.35	1.26	4.91	2.57	10.15	4.37	4.81	31.29
Sc #	1.00	8.00	8.00	6.00	8.00	8.00	11.00	8.00	9.00	17.00
V #	3.42	14.07	15.90	11.92	32.51	14.05	94.33	50.31	59.47	170.39
Cu #	3.94	-	-	-	6.94	-	60.60	24.72	-	-
Pb #	0.25	2.35	12.49	6.80	14.47	14.13	328.53	925.48	25.64	36.14
Zn #	8.16	159.60	63.67	26.40	46.25	56.52	2360.28	266.20	144.71	255.78
Bi #	0.06	-	0.08	0.08	0.07	-	-	-	-	0.12
Cd #	0.99	-	-	-	-	-	5.20	-	-	-
Sn #	0.12	1.51	1.59	1.07	1.31	1.17	0.61	0.74	0.77	1.11
Mo #	0.63	0.83	-	-	-	-	0.99	1.16	-	0.74
As #	1.33	4.13	4.95	2.06	7.20	6.14	7.44	35.03	10.27	12.04
Sb #	0.20	0.24	-	-	-	-	-	0.52	1.11	0.22
Ag #	0.23	0.68	0.90	0.54	0.65	0.64	0.60	0.76	0.64	0.84
Li #	0.79	7.05	4.24	1.46	11.18	5.84	10.54	6.04	2.53	8.06
Rb #	0.76	45.17	110.93	3.64	58.36	87.92	57.47	170.12	45.09	40.38
Cs #	0.08	-	0.15	-	0.70	0.79	0.56	0.21	0.49	0.41
Ba #	0.80	484.88	1537.94	77.40	647.90	857.80	1754.83	3416.05	562.79	1280.32
Sr #	4.16	16.60	102.80	49.78	202.33	96.08	34.60	36.30	41.54	49.58
Tl #	0.08	0.85	0.63	-	0.47	0.65	1.07	1.95	0.81	1.05
Ta #	0.04	0.38	0.48	0.35	0.45	0.39	0.27	0.28	0.32	0.29
Nb #	0.08	7.81	10.09	7.77	8.41	8.02	4.70	4.77	5.51	5.43
Hf #	0.21	4.80	6.25	4.54	5.23	4.91	3.09	3.33	3.62	3.39
Zr #	0.14	169.24	219.92	164.34	189.81	176.03	113.02	116.74	135.23	128.80
Y #	0.08	6.33	19.91	1.59	7.96	8.06	7.12	10.16	5.24	10.49
Th #	0.08	0.41	2.70	0.82	2.91	1.18	0.83	1.81	0.60	1.15
U #	0.09	1.28	2.27	1.95	1.99	1.57	1.03	0.91	1.01	1.50

Table A1-1 (continued) Major and trace lithogeochemical data for outcrop and drill core samples from Pilley's Island VMS district.

Sample ID	Det. Limit	10CPM-084	10CPM-086	10CPM-090	10CPM-093	10CPM-095	10CPM-098b	10CPM-102	10CPM-105	10CPM-106
La #	0.09	2.64	11.08	1.47	5.12	3.73	2.79	7.24	2.05	4.30
Ce #	0.13	2.79	15.36	4.48	14.96	5.61	3.88	12.41	2.25	9.94
Pr #	0.06	0.64	2.65	0.37	1.56	0.87	0.73	1.88	0.54	1.32
Nd #	0.50	2.65	10.70	1.75	6.02	3.76	2.82	7.90	2.02	5.72
Sm #	0.36	0.66	2.71	-	1.41	0.94	0.85	1.83	0.63	1.58
Eu #	0.08	0.17	0.74	0.09	0.36	0.31	0.21	0.44	0.21	0.48
Gd #	0.16	0.78	3.20	0.32	1.45	1.22	0.95	1.85	0.75	1.88
Tb #	0.03	0.14	0.54	0.05	0.26	0.21	0.18	0.31	0.14	0.31
Dy #	0.13	0.91	3.41	0.37	1.66	1.49	1.16	1.99	0.84	2.10
Ho #	0.03	0.21	0.73	0.08	0.37	0.34	0.25	0.44	0.20	0.43
Er #	0.14	0.71	2.17	0.26	1.19	1.10	0.82	1.31	0.70	1.32
Tm #	0.04	0.14	0.35	0.08	0.25	0.19	0.16	0.22	0.16	0.25
Yb #	0.21	0.67	2.36	0.30	1.37	1.24	0.89	1.54	0.81	1.53
Lu #	0.05	0.11	0.37	0.05	0.21	0.21	0.14	0.25	0.15	0.22
Sericite Index[2]		33.33	70.83	40.50	2.32	23.36	48.79	87.05	98.14	58.26
Al_2O_3/Na_2O		5.18	2.88	1.86	2.91	3.93	13.89	78.47	4.50	5.81
CCPI[3]		32.95	37.81	24.37	47.57	41.05	49.56	37.87	47.94	61.37
AI[4]		73.61	46.37	5.08	36.97	53.60	80.61	95.61	60.00	67.21
$Zn/TiO_2*10000$		0.04	0.04	0.03	0.04	0.03	0.02	0.02	0.03	0.02
Nb/Y		1.24	0.51	4.89	1.06	0.99	0.66	0.47	1.05	0.52
Th/Yb		0.61	1.14	2.73	2.12	0.95	0.94	1.17	0.75	0.75
$[La/Yb]_{CN}$[5]		2.66	3.18	3.35	2.54	2.04	2.13	3.18	1.72	1.90
$[La/Sm]_{MN}$[6]		2.56	2.64	-	2.34	2.57	2.13	2.56	2.10	1.75
$[Nb/Th]_{MN}$[6]		2.28	0.45	1.15	0.35	0.82	0.68	0.32	1.10	0.57
Zr/Yb		117.64	251.05	92.99	550.50	138.46	141.86	127.02	75.57	167.12
Nb/Yb		11.59	4.27	26.04	6.13	6.46	5.28	3.08	6.81	3.54
Th/Nb		0.05	0.27	0.10	0.35	0.15	0.18	0.38	0.11	0.21
La/Sm		3.97	4.08	-	3.63	3.97	3.30	3.95	3.24	2.72

* wt%; ICP-OES
# ppm; ICP-MS
LOI Loss On Ignition
[1] Universal Transverse Mercator, North American Datum 27 (UTM NAD27)
[2] Sericite Index = $100*K_2O/Na_2O+K_2O$
[3] CCPI = $100*(Fe_2O_3^T+MgO)/(Fe_2O_3^T+MgO+K_2O+Na_2O)$
[4] AI = $100*(K_2O+MgO)/(K_2O+MgO+CaO+Na_2O)$
[5] CN = chondrite normalized
[6] MN = primitive mantle normalized
- < Limit of Detection
N.D. Not Detected

Table A1-1 (continued) Major and trace lithogeochemical data for outcrop and drill core samples from Pilley's Island VMS district.

Sample ID	Det. Limit	10CPM-108	10CPM-109	10CPM-113b	10CPM-114	10CPM-116a	10CPM-116c	10CPM-116e	10CPM-120	10CPM-121
Easting [1]		593380	593337	593291	593327	593471	593859	593859	593859	593323
Northing [1]		5484631	5484665	5484907	5484968	5484928	5484912	5484912	5484912	5484255
Drillhole ID		-	-	-	-	-	-	-	-	-
From (m)		-	-	-	-	-	-	-	-	-
To (m)		-	-	-	-	-	-	-	-	-
Strat. unit		4.1	4.3	4.4	4.4	4.3	4.3	4.3	6.1	6.2
SiO_2 *	0.01	57.17	62.31	70.08	82.13	13.80	76.98	62.58	55.73	78.31
Al_2O_3 *	0.01	15.04	16.32	12.57	8.93	0.63	8.45	16.30	16.68	10.49
Fe_2O_3 *	0.01	6.41	5.93	2.89	2.31	53.29	5.31	4.65	6.20	2.44
MnO *	0.001	0.28	0.17	0.01	0.01	0.04	0.01	0.11	0.15	0.03
MgO *	0.01	1.98	2.70	0.07	0.29	0.08	0.49	3.10	3.48	0.48
CaO *	0.01	1.66	0.35	0.26	0.03	0.10	0.09	1.72	3.23	0.58
Na_2O *	0.01	0.19	3.36	0.76	0.05	0.14	0.11	3.92	7.67	3.49
K_2O *	0.01	9.05	3.70	9.70	2.91	0.11	2.51	2.06	0.13	1.57
TiO_2 *	0.001	0.74	0.69	0.44	0.28	0.02	0.34	0.65	0.67	0.18
P_2O_5 *	0.01	0.31	0.21	0.10	0.01	0.02	0.08	0.18	0.47	0.06
LOI *		4.91	2.79	1.94	2.23	28.67	4.36	3.80	4.00	1.88
TOTAL *		97.75	98.52	98.82	99.17	96.90	98.73	99.07	98.41	99.50
Cr^{52} #	3.65	N.D.	N.D.	N.D.	N.D.	N.D.	N.D.	N.D.	N.D.	N.D.
Cr^{53} #	12.85	74.50	13.28	18.71	-	-	-	-	43.98	21.74
Ni #	5.14	25.85	-	-	-	8.07	-	-	24.49	6.16
Co #	0.26	23.09	6.21	2.78	0.57	1.18	2.73	4.75	15.32	2.18
Sc #	1.00	23.00	11.00	5.00	3.00	-	5.00	9.00	21.00	3.00
V #	3.42	214.08	53.20	7.74	3.68	-	14.37	24.10	194.71	15.74
Cu #	3.94	205.94	-	1340.28	63.71	5056.49	81.40	45.08	38.37	7.38
Pb #	0.25	37.88	4.42	11.89	5.09	798.50	37.07	33.94	6.25	7.21
Zn #	8.16	3298.43	80.36	-	149.78	1450.57	29.97	177.24	34.35	19.29
Bi #	0.06	0.18	-	0.53	0.08	27.27	0.69	0.18	-	-
Cd #	0.99	8.88	-	-	-	4.88	-	-	-	-
Sn #	0.12	0.47	1.04	0.87	2.00	1.54	1.36	1.28	0.85	0.47
Mo #	0.63	9.10	-	8.35	1.78	29.66	3.27	1.19	-	-
As #	1.33	45.07	2.43	23.17	5.40	1169.79	20.84	19.58	13.33	4.31
Sb #	0.20	1.09	-	0.44	0.80	19.24	0.89	0.68	1.35	0.47
Ag #	0.23	0.82	0.72	1.00	1.00	9.14	0.67	0.90	0.68	0.64
Li #	0.79	4.15	8.32	-	1.91	1.04	3.45	20.55	12.29	1.26
Rb #	0.76	174.67	82.12	190.13	221.89	6.47	73.77	188.90	13.59	143.90
Cs #	0.08	0.37	0.33	0.15	0.24	-	0.77	1.71	0.10	0.98
Ba #	0.80	3782.60	588.39	4250.04	274.22	2342.19	2221.05	580.12	211.61	294.29
Sr #	4.16	34.42	29.05	4.87	-	73.23	30.72	201.58	148.97	71.01
Tl #	0.08	2.54	0.80	2.41	1.00	22.40	2.50	2.14	-	0.35
Ta #	0.04	0.20	0.37	0.34	0.29	-	0.22	0.47	0.58	0.38
Nb #	0.08	4.20	6.75	6.61	5.64	0.41	4.64	8.82	11.49	6.54
Hf #	0.21	2.11	4.35	3.77	3.60	-	2.88	5.93	3.70	4.45
Zr #	0.14	65.69	171.69	147.95	120.84	6.63	103.65	188.92	152.97	154.52
Y #	0.08	12.69	9.28	0.27	9.77	0.89	7.14	31.28	18.86	6.31
Th #	0.08	1.46	1.30	-	3.20	0.21	1.46	6.04	10.82	3.81
U #	0.09	0.84	1.13	1.54	1.70	0.32	1.68	2.22	2.87	1.80

Table A1-1 (continued) Major and trace lithogeochemical data for outcrop and drill core samples from Pilley's Island VMS district.

Sample ID	Det. Limit	10CPM-108	10CPM-109	10CPM-113b	10CPM-114	10CPM-116a	10CPM-116c	10CPM-116e	10CPM-120	10CPM-121
La *	0.09	4.49	6.14	0.27	3.79	0.86	4.10	20.09	28.78	6.61
Ce #	0.13	8.68	7.71	0.18	8.25	1.41	7.62	42.67	60.99	18.29
Pr #	0.06	1.35	1.61	0.13	1.06	0.22	1.15	5.48	7.79	1.60
Nd #	0.50	6.20	6.45	-	4.12	0.81	4.47	23.06	32.13	6.50
Sm #	0.36	1.78	1.35	-	1.13	-	1.26	5.50	6.39	1.34
Eu #	0.08	0.43	0.38	-	0.19	-	0.34	1.46	1.60	0.19
Gd #	0.16	2.19	1.54	-	1.07	-	1.01	5.64	4.98	1.19
Tb #	0.03	0.39	0.24	-	0.24	-	0.19	0.93	0.66	0.21
Dy #	0.13	2.48	1.67	-	1.81	0.18	1.41	6.16	3.74	1.30
Ho #	0.03	0.50	0.34	-	0.41	0.04	0.31	1.26	0.67	0.27
Er #	0.14	1.52	1.20	-	1.35	-	1.15	3.93	1.99	0.93
Tm #	0.04	0.23	0.22	0.07	0.25	0.06	0.25	0.67	0.31	0.16
Yb #	0.21	1.51	1.34	-	1.74	-	1.31	4.32	1.81	1.03
Lu #	0.05	0.24	0.21	-	0.29	-	0.22	0.70	0.29	0.17
Sericite Index[2]		60.25	97.94	52.41	92.73	98.31	44.00	95.80	34.45	1.67
Al_2O_3/Na_2O		79.16	4.86	16.54	178.60	4.50	76.82	4.16	2.17	3.01
CCPI[3]		47.59	55.00	22.06	46.76	99.53	68.88	56.45	55.38	36.59
AI[4]		85.64	63.30	90.55	97.56	44.19	93.75	47.78	24.88	33.50
Zn/TiO_2*10000		0.01	0.02	0.02	0.03	0.00	0.47	0.06	0.02	0.02
Nb/Y		0.33	0.73	24.34	0.58	0.46	0.65	0.28	0.61	1.04
Th/Yb		0.97	0.97	-	1.84	-	1.12	1.40	5.98	3.71
$[La/Yb]_{CN}$[5]		2.02	3.10	-	1.48	-	2.13	3.16	10.81	4.36
$[La/Sm]_{MN}$[6]		1.63	2.94	-	2.17	-	2.10	2.36	2.91	3.19
$[Nb/Th]_{MN}$[6]		0.35	0.63	-	0.21	0.24	0.38	0.18	0.13	0.21
Zr/Yb		83.95	43.43	127.69	-	69.50	-	79.25	43.72	84.59
Nb/Yb		2.78	5.02	-	3.24	-	3.55	2.04	6.35	6.35
Th/Nb		0.35	0.19	-	0.57	0.51	0.32	0.69	0.94	0.58
La/Sm		2.53	4.55	-	3.36	-	3.24	3.65	4.51	4.93

* wt%; ICP-OES

\# ppm; ICP-MS

LOI Loss On Ignition

[1] Universal Transverse Mercator, North American Datum 27 (UTM NAD27)

[2] Sericite Index = $100*K_2O/Na_2O+K_2O$

[3] CCPI = $100*(Fe_2O_3{}^T+MgO)/(Fe_2O_3{}^T+MgO+K_2O+Na_2O)$

[4] AI = $100*(K_2O+MgO)/(K_2O+MgO+CaO+Na_2O)$

[5] CN = chondrite normalized

[6] MN = primitive mantle normalized

\- < Limit of Detection

N.D. Not Detected

Table A1-1 (continued) Major and trace lithogeochemical data for outcrop and drill core samples from Pilley's Island VMS district.

Sample ID	Det. Limit	10CPM-124	10CPM-125a	10CPM-127	10CPM-128	10CPM-129	10CPM-131b	10CPM-131C	10CPM-136	10CPM-137
Easting [1]		592823	592835	593009	591639	591588	591468	591468	593008	593093
Northing [1]		5484018	5484001	5484063	5483441	5483531	5483641	5483641	5485455	5485481
Drillhole ID		-	-	-	-	-	-	-	-	-
From (m)		-	-	-	-	-	-	-	-	-
To (m)		-	-	-	-	-	-	-	-	-
Strat. unit		6.2	6.2	6.2	7.1	6.1	6.2	6.2	2	2
SiO_2 *	0.01	65.92	75.32	54.54	35.86	49.88	68.88	58.13	79.26	48.93
Al_2O_3 *	0.01	14.40	11.49	17.68	13.80	17.18	15.26	15.43	10.27	15.67
Fe_2O_3 *	0.01	2.44	2.52	6.37	8.09	10.73	2.54	4.59	2.53	14.55
MnO *	0.001	0.06	0.03	0.16	0.09	0.21	0.04	0.11	0.01	0.14
MgO *	0.01	2.12	1.25	4.01	2.61	3.75	0.64	2.56	0.30	3.49
CaO *	0.01	2.54	1.16	3.00	17.54	3.93	1.01	3.41	0.25	10.57
Na_2O *	0.01	2.39	4.86	5.50	3.55	6.40	3.75	1.60	0.52	1.81
K_2O *	0.01	3.59	0.70	1.38	1.58	0.68	2.91	4.47	2.25	0.16
TiO_2 *	0.001	0.22	0.30	0.70	0.79	1.60	0.63	0.64	0.69	1.07
P_2O_5 *	0.01	0.05	0.06	0.49	0.21	0.81	0.23	0.24	0.16	0.15
LOI *		5.36	1.96	4.71	14.51	4.85	2.84	8.09	2.29	2.89
TOTAL *		99.11	99.64	98.53	98.63	100.00	98.72	99.26	98.52	99.42
Cr^{52} #	3.65	N.D.	N.D.	N.D.	N.D.	N.D.	N.D.	4.44	N.D.	N.D.
Cr^{53} #	12.85	-	21.14	50.91	469.43	71.34	-	-	159.97	34.37
Ni #	5.14	30.74	-	27.10	169.48	21.33	-	41.99	23.81	13.46
Co #	0.26	2.74	2.11	17.77	33.14	21.25	3.37	9.11	2.65	27.24
Sc #	1.00	4.00	4.00	23.00	29.00	22.00	8.00	9.00	8.00	35.00
V #	3.42	11.34	6.77	221.88	147.75	193.91	40.36	42.33	52.40	497.90
Cu #	3.94	30.67	4.95	38.36	21.88	-	86.50	41.03	9.65	122.94
Pb #	0.25	7.42	16.31	10.07	8.64	5.34	4.36	6.44	8.42	5.80
Zn #	8.16	34.55	37.88	31.93	12.48	24.57	-	111.25	-	28.18
Bi #	0.06	-	0.10	-	-	-	-	-	0.09	-
Cd #	0.99	-	-	-	-	-	-	-	-	-
Sn #	0.12	1.16	0.76	0.99	0.35	0.60	0.97	1.07	1.34	0.32
Mo #	0.63	-	-	-	-	-	-	-	-	-
As #	1.33	5.92	5.40	5.35	27.68	4.85	6.48	15.09	9.80	12.68
Sb #	0.20	-	-	-	1.77	0.22	1.14	2.76	0.66	0.63
Ag #	0.23	1.10	0.70	0.80	0.31	0.42	0.68	0.64	1.74	0.40
Li #	0.79	-	3.16	4.54	37.55	23.18	8.91	4.57	6.29	7.49
Rb #	0.76	116.43	120.42	32.91	109.06	71.29	27.90	292.44	150.02	16.32
Cs #	0.08	1.28	1.30	0.52	1.20	1.80	0.27	1.58	1.78	0.16
Ba #	0.80	248.67	490.15	1238.50	194.13	295.96	109.34	127.72	199.85	108.98
Sr #	4.16	35.13	96.70	199.60	120.77	228.49	124.40	34.14	249.56	307.84
Tl #	0.08	0.33	0.84	0.16	0.41	0.19	0.12	0.56	0.56	-
Ta #	0.04	0.28	0.53	0.38	0.62	0.20	0.22	0.40	1.01	0.16
Nb #	0.08	6.48	9.13	7.27	12.42	3.85	3.99	7.59	14.70	2.28
Hf #	0.21	3.92	6.09	4.29	4.60	2.10	2.69	4.01	11.47	2.20
Zr #	0.14	146.02	221.49	159.70	165.20	71.23	92.94	167.59	384.17	67.41
Y #	0.08	6.73	17.74	8.89	14.70	20.46	25.16	23.06	6.96	29.64
Th #	0.08	2.43	5.80	3.41	7.03	3.75	1.40	4.41	5.52	2.61
U #	0.09	1.55	1.61	1.50	3.35	0.50	0.82	1.64	2.01	0.57

Table A1-1 (continued) Major and trace lithogeochemical data for outcrop and drill core samples from Pilley's Island VMS district.

Sample ID	Det. Limit	10CPM-124	10CPM-125a	10CPM-127	10CPM-128	10CPM-129	10CPM-131b	10CPM-131C	10CPM-136	10CPM-137
La #	0.09	6.12	12.37	8.00	15.32	14.70	4.31	8.81	15.59	6.83
Ce #	0.13	16.86	31.13	23.97	45.67	29.69	16.37	19.45	46.55	20.24
Pr #	0.06	1.63	3.17	2.08	4.96	4.30	2.23	2.69	3.92	2.73
Nd #	0.50	6.81	11.87	8.26	20.63	18.69	11.83	12.67	14.74	12.78
Sm #	0.36	1.67	2.89	1.83	4.44	4.19	3.98	3.09	2.77	3.88
Eu #	0.08	0.47	0.46	0.42	1.21	1.28	1.39	0.83	0.57	1.31
Gd #	0.16	1.54	2.75	1.73	3.77	4.29	5.01	3.47	2.26	4.81
Tb #	0.03	0.26	0.50	0.29	0.54	0.64	0.81	0.58	0.34	0.81
Dy #	0.13	1.66	3.35	2.04	3.12	3.99	4.97	3.90	1.92	5.54
Ho #	0.03	0.33	0.74	0.44	0.58	0.81	0.99	0.83	0.35	1.15
Er #	0.14	0.98	2.43	1.44	1.60	2.28	2.78	2.48	1.04	3.44
Tm #	0.04	0.14	0.45	0.26	0.24	0.39	0.43	0.50	0.17	0.55
Yb #	0.21	1.01	2.90	1.64	1.57	2.25	2.81	2.93	1.02	3.63
Lu #	0.05	0.14	0.43	0.26	0.24	0.31	0.41	0.46	0.16	0.53
Sericite Index[2]		31.03	60.03	12.59	20.06	30.80	9.60	43.69	73.64	81.23
Al_2O_3/Na_2O		6.03	2.36	3.21	3.89	2.68	4.07	9.64	19.75	8.66
CCPI[3]		43.26	40.41	60.14	67.59	67.16	32.32	54.08	50.54	90.15
AI[4]		53.67	24.47	38.80	16.57	30.01	42.72	58.39	76.81	22.77
$Zn/TiO_2*10000$		0.08	0.10	0.05	0.02	0.01	0.01	0.03	0.06	0.01
Nb/Y		0.96	0.51	0.82	0.84	0.19	0.16	0.33	2.11	0.08
Th/Yb		2.39	2.00	2.08	4.47	1.67	0.50	1.51	5.39	0.72
$[La/Yb]_{CN}$[5]		4.10	2.90	3.31	6.62	4.44	1.04	2.04	10.34	1.28
$[La/Sm]_{MN}$[6]		2.37	2.76	2.82	2.23	2.27	0.70	1.84	3.64	1.14
$[Nb/Th]_{MN}$[6]		0.32	0.19	0.26	0.21	0.12	0.34	0.21	0.32	0.11
Zr/Yb		150.11	143.92	76.40	97.18	105.07	31.65	33.04	57.26	375.13
Nb/Yb		6.38	3.15	4.42	7.90	1.71	1.42	2.59	14.36	0.63
Th/Nb		0.38	0.64	0.47	0.57	0.97	0.35	0.58	0.38	1.15
La/Sm		3.67	4.28	4.36	3.45	3.51	1.08	2.85	5.63	1.76

* wt%; ICP-OES

\# ppm; ICP-MS

LOI Loss On Ignition

[1] Universal Transverse Mercator, North American Datum 27 (UTM NAD27)

[2] Sericite Index = $100*K_2O/Na_2O+K_2O$

[3] CCPI = $100*(Fe_2O_3^T+MgO)/(Fe_2O_3^T+MgO+K_2O+Na_2O)$

[4] AI = $100*(K_2O+MgO)/(K_2O+MgO+CaO+Na_2O)$

[5] CN = chondrite normalized

[6] MN = primitive mantle normalized

\- < Limit of Detection

N.D. Not Detected

Table A1-1 (continued) Major and trace lithogeochemical data for outcrop and drill core samples from Pilley's Island VMS district.

Sample ID	Det. Limit	10CPM-139	10CPM-140a	10CPM-140d	10CPM-140e	10CPM-140f	10CPM-141	10CPM-146	10CPM-150	10CPM-156
Easting [1]		593057	593207	593207	593207	593207	593023	590531	591810	592033
Northing [1]		5485351	5485222	5485222	5485222	5485222	5485151	5483389	5484120	5484416
Drillhole ID		-	-	-	-	-	-	-	-	-
From (m)		-	-	-	-	-	-	-	-	-
To (m)		-	-	-	-	-	-	-	-	-
Strat. unit		3.4	3.2	3.2	3.2	3.2	3.2	6.1	6.2	2
SiO_2 *	0.01	71.85	74.69	9.69	22.13	61.52	66.63	49.74	70.61	50.44
Al_2O_3 *	0.01	13.79	10.69	1.03	0.78	17.88	15.87	18.10	15.12	15.62
Fe_2O_3 *	0.01	3.15	4.28	53.55	42.16	4.35	4.29	11.05	2.99	11.46
MnO *	0.001	0.07	0.01	0.02	0.02	0.06	0.11	0.12	0.09	0.14
MgO *	0.01	0.82	0.90	0.13	0.04	3.25	1.37	5.91	0.44	2.30
CaO *	0.01	0.38	0.04	0.05	0.05	1.45	1.01	3.36	0.45	5.54
Na_2O *	0.01	2.81	0.08	0.07	0.29	4.07	4.82	5.25	4.18	6.06
K_2O *	0.01	3.25	3.45	0.26	0.09	3.03	2.62	1.45	4.75	1.75
TiO_2 *	0.001	0.46	0.39	0.02	0.01	0.49	0.51	1.17	0.52	1.36
P_2O_5 *	0.01	0.10	0.01	0.05	0.05	0.12	0.13	0.75	0.11	0.46
LOI *		2.40	4.13	27.73	24.08	3.39	2.58	3.73	1.54	4.78
TOTAL *		99.07	98.69	92.60	89.72	99.59	99.95	100.60	100.80	99.92
Cr^{52} #	3.65	N.D.	7.02	-	5.71	47.78	-	-	7.58	7.72
Cr^{53} #	12.85	-	N.D.	N.D.	N.D.	N.D.	N.D.	N.D.	N.D.	N.D.
Ni #	5.14	-	-	-	-	14.10	5.59	9.48	-	14.30
Co #	0.26	2.36	4.59	0.83	0.87	7.82	4.66	32.39	2.66	29.06
Sc #	1.00	6.00	4.00	-	-	9.00	6.00	23.00	8.00	25.00
V #	3.42	13.69	17.82	7.86	-	43.98	20.96	288.09	10.21	394.42
Cu #	3.94	-	40.83	40403.67	53515.54	413.93	59.80	83.12	27.12	67.95
Pb #	0.25	7.83	36.63	339.95	897.35	24.42	12.15	8.70	11.80	7.07
Zn #	8.16	32.53	73.91	2617.79	8355.17	330.12	79.88	44.80	40.99	40.96
Bi #	0.06	0.07	3.01	42.08	114.82	0.83	0.20	0.10	0.12	0.07
Cd #	0.99	-	-	3.48	22.83	-	-	-	-	-
Sn #	0.12	0.99	2.40	3.12	6.99	1.37	1.37	0.80	1.51	0.57
Mo #	0.63	-	3.67	10.26	11.62	-	-	0.76	-	0.94
As #	1.33	7.69	19.33	319.62	464.14	37.07	10.07	17.19	10.58	9.40
Sb #	0.20	1.79	2.41	7.14	7.28	2.61	0.67	0.21	1.46	-
Ag #	0.23	0.78	0.60	14.85	18.02	0.96	0.79	0.23	0.64	-
Li #	0.79	1.27	2.77	-	-	13.45	6.14	27.83	1.65	3.85
Rb #	0.76	130.25	140.93	8.81	2.09	75.62	77.08	42.50	175.23	39.63
Cs #	0.08	0.97	0.71	0.19	-	1.77	0.93	1.18	0.90	0.24
Ba #	0.80	203.04	3376.76	1002.45	2855.79	887.34	516.73	478.07	1714.18	451.46
Sr #	4.16	94.12	42.03	148.92	207.01	148.90	128.76	428.14	60.14	145.73
Tl #	0.08	0.78	3.92	36.62	16.33	2.89	0.73	0.23	0.86	0.28
Ta #	0.04	0.32	0.35	-	-	0.50	0.50	0.23	0.40	0.18
Nb #	0.08	8.11	6.00	0.36	0.43	9.03	8.96	4.34	8.02	3.37
Hf #	0.21	4.92	3.87	-	-	5.87	5.34	2.66	5.56	2.71
Zr #	0.14	184.68	133.46	7.18	5.70	217.34	206.20	92.69	177.91	81.79
Y #	0.08	17.16	10.57	1.12	0.60	15.13	4.74	23.94	3.67	26.59
Th #	0.08	3.48	3.37	0.29	0.17	2.56	1.02	1.70	0.53	1.60
U #	0.09	1.86	2.01	2.25	0.41	2.01	2.38	0.97	1.65	1.86

Table A1-1 (continued) Major and trace lithogeochemical data for outcrop and drill core samples from Pilley's Island VMS district.

Sample ID	Det. Limit	10CPM-139	10CPM-140a	10CPM-140d	10CPM-140e	10CPM-140f	10CPM-141	10CPM-146	10CPM-150	10CPM-156
La #	0.09	10.03	10.84	2.22	0.69	5.26	3.18	7.93	1.03	9.01
Ce #	0.13	18.00	19.86	3.53	1.16	9.38	4.97	20.96	1.31	20.12
Pr #	0.06	2.61	2.49	0.45	0.17	1.46	0.69	2.76	0.38	3.04
Nd #	0.50	11.92	9.80	1.61	-	6.10	2.55	12.87	1.52	14.24
Sm #	0.36	2.96	1.80	0.38	-	1.68	0.69	3.61	0.55	4.02
Eu #	0.08	0.83	0.42	-	-	0.53	0.13	1.26	0.15	1.36
Gd #	0.16	3.71	1.61	0.22	-	2.16	0.70	4.69	0.63	5.11
Tb #	0.03	0.54	0.25	0.05	-	0.41	0.11	0.70	0.13	0.80
Dy #	0.13	3.37	1.81	0.25	-	2.71	0.69	4.69	0.90	5.04
Ho #	0.03	0.69	0.44	0.04	-	0.58	0.15	0.97	0.20	1.05
Er #	0.14	2.02	1.50	0.16	-	2.00	0.51	2.84	0.70	3.16
Tm #	0.04	0.33	0.26	0.06	0.05	0.33	0.11	0.46	0.13	0.53
Yb #	0.21	2.01	1.84	-	-	2.32	0.59	2.74	0.84	3.00
Lu #	0.05	0.33	0.30	-	-	0.37	0.08	0.41	0.14	0.47
Sericite Index[2]		8.12	53.63	97.73	78.79	23.68	42.68	35.22	21.64	53.19
Al_2O_3/Na_2O		4.91	133.63	14.71	2.69	4.39	3.29	3.45	3.62	2.58
CCPI[3]		39.58	59.47	99.39	99.11	51.70	43.21	71.68	27.75	63.79
AI[4]		56.06	97.32	76.47	27.66	53.22	40.63	46.09	52.85	25.88
$Zn/TiO_2*10000$		0.02	0.03	0.00	0.02	1.55	0.04	0.02	0.02	0.02
Nb/Y		0.47	0.57	0.32	0.71	0.60	1.89	0.18	2.18	0.13
Th/Yb		1.73	1.84	-	-	1.10	1.72	0.62	0.64	0.53
$[La/Yb]_{CN}$[5]		3.38	4.01	-	-	1.54	3.65	1.97	0.84	2.04
$[La/Sm]_{MN}$[6]		2.19	3.89	3.78	-	2.03	2.98	1.42	1.20	1.45
$[Nb/Th]_{MN}$[6]		0.28	0.22	0.15	0.30	0.43	1.06	0.31	1.82	0.26
Zr/Yb		18.58	91.68	72.71	-	-	93.71	348.63	33.82	212.89
Nb/Yb		4.02	3.27	-	-	3.89	15.14	1.58	9.60	1.12
Th/Nb		0.43	0.56	0.82	0.40	0.28	0.11	0.39	0.07	0.47
La/Sm		3.39	6.03	5.84	-	3.13	4.61	2.20	1.85	2.24

* wt%; ICP-OES

\# ppm; ICP-MS

LOI Loss On Ignition

[1] Universal Transverse Mercator, North American Datum 27 (UTM NAD27)

[2] Sericite Index = $100*K_2O/Na_2O+K_2O$

[3] CCPI = $100*(Fe_2O_3{}^1+MgO)/(Fe_2O_3{}^1+MgO+K_2O+Na_2O)$

[4] AI = $100*(K_2O+MgO)/(K_2O+MgO+CaO+Na_2O)$

[5] CN = chondrite normalized

[6] MN = primitive mantle normalized

\- < Limit of Detection

N.D. Not Detected

Table A1-1 (continued) Major and trace lithogeochemical data for outcrop and drill core samples from Pilley's Island VMS district.

Sample ID	Det. Limit	10CPM-159	10CPM-163a	10CPM-163b	10CPM-166a	10CPM-166b	10CPM-167	10CPM-168a	10CPM-172	10CPM-174
Easting [1]		591039	591181	591181	591956	591956	592370	592428	593182	593172
Northing [1]		5484489	5484430	5484430	5484295	5484295	5484464	5484484	5484569	5484226
Drillhole ID		-	-	-	-	-	-	-	-	-
From (m)		-	-	-	-	-	-	-	-	-
To (m)		-	-	-	-	-	-	-	-	-
Strat. unit		5.5	5.5	5.5	6.1	6.1	4.6	4.6	4.2	6.2
SiO_2 *	0.01	72.41	72.11	76.03	57.83	37.27	64.04	67.88	71.76	78.24
Al_2O_3 *	0.01	14.41	12.64	12.06	9.17	12.79	16.15	15.30	14.15	10.16
Fe_2O_3 *	0.01	1.46	2.90	2.54	6.95	11.86	4.55	2.83	3.80	1.94
MnO *	0.001	0.02	0.07	0.04	0.15	0.52	0.20	0.08	0.07	0.05
MgO *	0.01	0.44	0.95	0.26	3.20	5.89	2.36	0.97	1.73	1.32
CaO *	0.01	0.15	1.01	0.36	5.88	9.92	0.48	0.44	0.27	1.62
Na_2O *	0.01	0.36	4.82	6.25	1.58	0.31	2.75	4.80	5.20	0.09
K_2O *	0.01	8.65	1.34	0.23	1.50	1.21	4.59	4.22	2.16	3.37
TiO_2 *	0.001	0.43	0.44	0.43	0.70	1.10	0.61	0.57	0.51	0.16
P_2O_5 *	0.01	0.09	0.08	0.09	0.37	0.26	0.15	0.15	0.13	0.04
LOI *		1.56	2.08	0.62	12.14	18.61	3.29	2.05	-1.33	1.56
TOTAL *		99.99	98.44	98.90	99.48	99.72	99.17	99.29	98.46	98.55
Cr^{52} #	3.65	11.21	11.50	25.96	10.11	8.78	4.34	9.53	12.11	13.92
Cr^{53} #	12.85	N.D.	N.D.	N.D.	N.D.	N.D.	N.D.	N.D.	N.D.	N.D.
Ni #	5.14	-	-	-	-	25.89	-	-	-	9.81
Co #	0.26	0.80	2.32	2.17	13.38	43.99	2.74	2.49	3.03	3.33
Sc #	1.00	5.00	6.00	6.00	11.00	27.00	8.00	8.00	7.00	3.00
V #	3.42	17.65	9.65	8.51	111.96	363.14	18.88	15.50	9.18	10.13
Cu #	3.94	19.29	13.86	6.67	14.39	35.53	28.64	141.43	5.28	16.29
Pb #	0.25	43.57	10.30	12.49	3.59	12.51	662.91	11.86	15.77	7.03
Zn #	8.16	83.08	41.68	38.33	46.85	133.60	1089.48	23.73	58.08	24.72
Bi #	0.06	0.11	0.07	0.09	-	-	0.12	-	0.07	0.11
Cd #	0.99	-	-	-	-	1.12	2.73	-	-	-
Sn #	0.12	1.38	1.28	1.42	0.49	0.54	1.09	0.18	0.97	0.80
Mo #	0.63	-	-	-	-	3.47	2.68	-	0.99	-
As #	1.33	20.03	5.25	6.53	8.70	95.37	10.32	5.22	4.58	19.13
Sb #	0.20	1.50	0.34	0.33	2.36	7.59	0.30	-	-	0.29
Ag #	0.23	0.78	0.66	0.53	0.25	-	0.83	0.68	0.67	0.47
Li #	0.79	1.21	3.97	-	17.12	25.92	6.86	-	2.74	3.03
Rb #	0.76	252.03	73.80	8.43	66.16	40.91	94.84	33.20	35.89	145.41
Cs #	0.08	0.39	0.53	0.08	0.84	0.66	0.29	0.24	0.27	1.74
Ba #	0.80	1484.17	980.32	183.82	1205.81	1000.60	573.43	2701.66	530.19	201.93
Sr #	4.16	21.55	162.10	131.77	105.49	83.43	36.11	37.77	68.10	33.41
Tl #	0.08	1.91	0.38	-	0.53	0.25	0.80	0.62	0.38	0.72
Ta #	0.04	0.51	0.37	0.35	0.15	0.16	0.51	0.46	0.41	0.33
Nb #	0.08	9.05	6.75	6.95	2.90	3.32	8.82	8.45	7.88	5.62
Hf #	0.21	5.59	4.84	4.45	2.28	2.28	5.32	5.17	4.80	4.29
Zr #	0.14	192.78	155.43	157.46	70.36	73.36	203.08	192.07	172.21	149.34
Y #	0.08	5.68	3.01	5.33	19.50	23.41	9.48	2.38	6.68	16.11
Th #	0.08	1.33	1.91	1.88	1.51	1.60	1.29	0.62	2.10	3.82
U #	0.09	1.78	1.44	1.29	0.69	1.06	1.87	1.51	1.81	1.47

Table A1-1 (continued) Major and trace lithogeochemical data for outcrop and drill core samples from Pilley's Island VMS district.

Sample ID	Det. Limit	10CPM-159	10CPM-163a	10CPM-163b	10CPM-166a	10CPM-166b	10CPM-167	10CPM-168a	10CPM-172	10CPM-174
La #	0.09	3.33	5.93	4.39	8.21	7.09	5.93	1.38	4.55	8.24
Ce #	0.13	5.52	13.45	12.99	19.35	16.49	6.92	3.01	13.18	17.47
Pr #	0.06	0.85	1.34	1.19	2.61	2.45	1.27	0.39	1.20	1.97
Nd #	0.50	3.53	5.35	4.66	11.45	11.73	5.44	1.37	5.13	7.26
Sm #	0.36	0.86	1.26	1.15	3.27	3.28	1.33	0.48	1.35	1.68
Eu #	0.08	0.19	0.29	0.20	1.03	1.17	0.28	-	0.29	0.31
Gd #	0.16	0.98	1.01	1.14	3.68	4.00	1.52	0.45	1.35	1.84
Tb #	0.03	0.14	0.17	0.18	0.59	0.69	0.24	0.08	0.23	0.38
Dy #	0.13	1.01	0.89	1.25	3.62	4.54	1.64	0.54	1.58	2.55
Ho #	0.03	0.23	0.18	0.26	0.80	0.92	0.34	0.11	0.34	0.55
Er #	0.14	0.75	0.49	0.84	2.41	2.79	1.05	0.44	1.06	2.01
Tm #	0.04	0.14	0.08	0.17	0.38	0.45	0.18	0.10	0.20	0.36
Yb #	0.21	0.90	0.48	0.82	2.29	2.74	1.14	0.51	1.17	2.57
Lu #	0.05	0.15	0.07	0.13	0.34	0.39	0.17	0.06	0.16	0.38
Sericite Index[2]		22.41	96.00	21.75	3.55	48.70	79.61	62.53	46.78	29.35
Al_2O_3/Na_2O		40.03	2.62	1.93	5.80	41.26	5.87	3.19	2.72	112.89
CCPI[3]		17.42	38.46	30.17	76.72	92.11	48.49	29.64	42.90	48.51
AI[4]		94.69	28.20	6.90	38.65	40.97	68.27	49.76	41.56	73.28
$Zn/TiO_2*10000$		0.01	0.04	0.04	0.02	0.01	0.02	0.03	0.03	0.03
Nb/Y		1.59	2.24	1.30	0.15	0.14	0.93	3.55	1.18	0.35
Th/Yb		1.49	3.99	2.29	0.66	0.59	1.13	1.22	1.79	1.48
$[La/Yb]_{CN}$[5]		2.53	8.43	3.64	2.44	1.76	3.53	1.85	2.63	2.18
$[La/Sm]_{MN}$[6]		2.49	3.03	2.47	1.62	1.40	2.88	1.84	2.18	3.18
$[Nb/Th]_{MN}$[6]		0.82	0.43	0.45	0.23	0.25	0.83	1.66	0.45	0.18
Zr/Yb		27.22	215.05	325.43	192.22	30.78	26.78	177.78	379.60	146.75
Nb/Yb		10.10	14.13	8.48	1.27	1.21	7.72	16.71	6.71	2.18
Th/Nb		0.15	0.28	0.27	0.52	0.48	0.15	0.07	0.27	0.68
La/Sm		3.86	4.69	3.83	2.51	2.16	4.46	2.84	3.37	4.91

* wt%; ICP-OES
# ppm; ICP-MS
LOI Loss On Ignition
[1] Universal Transverse Mercator, North American Datum 27 (UTM NAD27)
[2] Sericite Index = $100*K_2O/Na_2O+K_2O$
[3] CCPI = $100*(Fe_2O_3^T+MgO)/(Fe_2O_3^T+MgO+K_2O+Na_2O)$
[4] AI = $100*(K_2O+MgO)/(K_2O+MgO+CaO+Na_2O)$
[5] CN = chondrite normalized
[6] MN = primitive mantle normalized
- < Limit of Detection
N.D. Not Detected

Table A1-1 (continued) Major and trace lithogeochemical data for outcrop and drill core samples from Pilley's Island VMS district.

Sample ID	Det. Limit	10CPM-175	10CPM-176	10CPM-178	10CPM-181	10CPM-185	10CPM-190	10CPM-191	10CPM-193	10CPM-194
Easting [1]		593368	593143	593015	592767	593410	593305	593313	593793	593957
Northing [1]		5484001	5483828	5483914	5483435	5484037	5485067	5485228	5484020	5484120
Drillhole ID		-	-	-	-	-	-	-	-	-
From (m)		-	-	-	-	-	-	-	-	-
To (m)		-	-	-	-	-	-	-	-	-
Strat. unit		7.1	7.1	7.1	7.1	7.1	3.2	3.1	7.1	7.1
SiO_2 *	0.01	68.34	45.01	47.11	47.62	46.24	64.43	67.22	46.05	45.74
Al_2O_3 *	0.01	14.48	14.40	16.34	14.57	15.44	16.43	14.76	16.51	14.77
Fe_2O_3 *	0.01	4.22	7.74	8.55	9.31	8.90	3.54	3.96	8.70	10.44
MnO *	0.001	0.14	0.19	0.16	0.14	0.16	0.11	0.15	0.19	0.15
MgO *	0.01	1.13	8.32	7.76	9.52	5.51	1.21	2.03	7.39	6.63
CaO *	0.01	0.45	11.63	8.64	8.00	13.47	1.65	0.58	8.34	9.91
Na_2O *	0.01	4.29	2.48	2.29	3.19	1.44	1.75	5.50	2.80	2.94
K_2O *	0.01	3.46	1.19	0.23	0.30	0.09	6.09	1.45	2.12	1.20
TiO_2 *	0.001	0.54	0.84	0.98	0.85	0.78	0.62	0.49	0.87	0.74
P_2O_5 *	0.01	0.11	0.24	0.24	0.20	0.15	0.13	0.13	0.18	0.15
LOI *		2.04	8.82	7.53	5.83	7.73	3.71	2.40	6.27	7.99
TOTAL *		99.19	100.90	99.81	99.53	99.90	99.66	98.68	99.43	100.70
Cr^{52} #	3.65	6.49	306.61	283.38	501.72	62.52	4.57	7.54	75.33	155.77
Cr^{53} #	12.85	N.D.	N.D.	N.D.	N.D.	N.D.	N.D.	N.D.	N.D.	N.D.
Ni #	5.14	-	109.30	147.20	106.20	41.55	-	5.27	60.21	67.22
Co #	0.26	3.54	37.50	33.18	36.83	29.74	2.28	3.83	38.53	30.24
Sc #	1.00	8.00	39.00	32.00	40.00	35.00	9.00	6.00	40.00	35.00
V #	3.42	15.88	270.84	251.41	285.96	275.40	15.69	16.15	314.20	282.55
Cu #	3.94	7.29	98.57	76.21	133.23	104.80	5.48	42.54	113.39	175.75
Pb #	0.25	14.21	6.30	4.10	4.23	3.94	9.47	23.94	4.74	4.50
Zn #	8.16	68.24	43.94	34.82	25.29	35.15	39.25	557.51	41.12	30.99
Bi #	0.06	0.09	0.09	-	-	-	0.09	0.16	-	-
Cd #	0.99	-	-	-	-	-	-	3.00	-	-
Sn #	0.12	1.20	0.67	0.56	0.37	0.80	1.55	1.12	0.69	0.66
Mo #	0.63	0.79	-	2.76	-	-	1.83	3.37	-	-
As #	1.33	5.02	12.51	19.59	29.71	46.96	2.76	21.92	14.01	20.31
Sb #	0.20	0.20	0.27	-	1.27	0.98	-	0.99	0.29	-
Ag #	0.23	0.68	-	0.50	0.44	-	0.62	0.70	-	-
Li #	0.79	4.02	36.12	58.39	32.52	29.68	3.52	5.90	42.01	36.74
Rb #	0.76	72.05	41.05	30.33	18.82	10.50	133.31	25.49	97.76	48.19
Cs #	0.08	0.37	0.89	0.50	0.50	-	1.70	0.36	1.00	0.77
Ba #	0.80	568.88	215.96	72.83	206.28	63.96	913.62	1274.78	379.15	142.96
Sr #	4.16	43.85	338.01	357.71	424.95	117.29	22.21	69.77	323.37	390.85
Tl #	0.08	0.69	0.15	0.10	0.16	-	1.42	0.48	0.29	0.15
Ta #	0.04	0.38	0.28	0.35	0.29	0.16	0.49	0.46	0.15	0.11
Nb #	0.08	7.73	5.83	6.09	5.58	2.90	9.02	7.79	2.84	1.90
Hf #	0.21	4.91	2.39	4.25	2.48	2.23	5.72	5.07	2.35	1.47
Zr #	0.14	173.00	76.22	121.76	80.48	55.02	207.35	187.81	63.03	44.60
Y #	0.08	7.53	16.66	19.91	14.98	18.49	15.89	3.97	16.75	14.31
Th #	0.08	1.02	5.26	4.76	4.07	3.27	3.09	1.54	2.69	1.83
U #	0.09	1.36	1.87	1.20	1.29	0.65	1.71	2.37	1.12	0.59

Table A1-1 (continued) Major and trace lithogeochemical data for outcrop and drill core samples from Pilley's Island VMS district.

Sample ID	Det. Limit	10CPM-175	10CPM-176	10CPM-178	10CPM-181	10CPM-185	10CPM-190	10CPM-191	10CPM-193	10CPM-194
La #	0.09	4.18	11.72	15.51	14.13	12.94	7.27	4.06	10.41	7.98
Ce #	0.13	5.29	26.70	35.45	31.81	26.17	10.97	7.69	23.23	17.14
Pr #	0.06	1.16	3.85	4.63	4.41	3.67	2.38	0.94	3.13	2.32
Nd #	0.50	4.38	16.71	19.25	19.44	14.93	10.65	3.45	13.29	10.21
Sm #	0.36	1.04	3.83	4.34	4.02	3.46	2.63	0.82	3.25	2.50
Eu #	0.08	0.32	1.07	1.29	1.13	1.06	0.69	0.22	1.02	0.86
Gd #	0.16	1.23	3.60	4.22	3.53	3.55	2.77	0.73	3.24	2.69
Tb #	0.03	0.22	0.55	0.60	0.49	0.56	0.43	0.13	0.52	0.42
Dy #	0.13	1.44	3.45	3.84	3.13	3.54	2.90	0.91	3.39	2.89
Ho #	0.03	0.32	0.68	0.80	0.59	0.73	0.66	0.20	0.69	0.58
Er #	0.14	1.01	1.91	2.27	1.74	2.09	2.31	0.62	2.01	1.70
Tm #	0.04	0.19	0.33	0.36	0.29	0.30	0.39	0.13	0.30	0.27
Yb #	0.21	1.03	1.89	2.17	1.57	2.04	2.73	0.66	2.06	1.60
Lu #	0.05	0.17	0.27	0.36	0.26	0.32	0.46	0.10	0.29	0.23
Sericite Index[2]		97.40	44.65	32.43	9.13	8.60	5.88	77.68	20.86	43.09
Al_2O_3/Na_2O		3.38	5.81	7.14	4.57	10.72	9.39	2.68	5.90	5.02
CCPI[3]		40.84	81.40	86.62	84.36	90.40	37.73	46.29	76.58	80.48
AI[4]		49.20	40.26	42.23	46.74	27.30	68.22	36.40	46.05	37.86
$Zn/TiO_2*10000$		0.11	0.01	0.01	0.01	0.01	0.03	0.03	0.01	0.01
Nb/Y		1.03	0.35	0.31	0.37	0.16	0.57	1.96	0.17	0.13
Th/Yb		0.99	2.79	2.19	2.60	1.61	1.13	2.34	1.30	1.15
$[La/Yb]_{CN}$[5]		2.76	4.22	4.85	6.13	4.32	1.81	4.20	3.43	3.39
$[La/Sm]_{MN}$[6]		2.59	1.98	2.31	2.27	2.42	1.79	3.20	2.07	2.06
$[Nb/Th]_{MN}$[6]		0.92	0.13	0.15	0.17	0.11	0.35	0.61	0.13	0.12
Zr/Yb		58.04	168.09	40.42	56.08	51.35	27.02	75.87	286.14	30.57
Nb/Yb		7.51	3.09	2.80	3.56	1.43	3.30	11.86	1.38	1.18
Th/Nb		0.13	0.90	0.78	0.73	1.13	0.34	0.20	0.95	0.97
La/Sm		4.00	3.06	3.57	3.51	3.74	2.77	4.96	3.20	3.19

* wt%; ICP-OES

\# ppm; ICP-MS

LOI Loss On Ignition

[1] Universal Transverse Mercator, North American Datum 27 (UTM NAD27)

[2] Sericite Index = $100*K_2O/Na_2O+K_2O$

[3] CCPI = $100*(Fe_2O_3{}^1+MgO)/(Fe_2O_3{}^1+MgO+K_2O+Na_2O)$

[4] AI = $100*(K_2O+MgO)/(K_2O+MgO+CaO+Na_2O)$

[5] CN = chondrite normalized

[6] MN = primitive mantle normalized

\- < Limit of Detection

N.D. Not Detected

Table A1-1 (continued) Major and trace lithogeochemical data for outcrop and drill core samples from Pilley's Island VMS district.

Sample ID	Det. Limit	10CPM-195	10CPM-198	10CPM-199	10CPM-200	10CPM-202b	10CPM-203	10CPM-205	10CPM-206	10CPM-207
Easting [1]		593760	590850	590580	590611	590627	590361	590317	593240	592681
Northing [1]		5484074	5484900	5484991	5484839	5484737	5482132	5482163	5484620	5484534
Drillhole ID		-	-	-	-	-	-	-	-	-
From (m)		-	-	-	-	-	-	-	-	-
To (m)		-	-	-	-	-	-	-	-	-
Strat. unit		7.1	2	1.2	1.1	2	8	8	4.1	4.3
SiO_2 *	0.01	37.80	51.84	65.05	63.79	51.24	62.25	48.97	57.46	17.56
Al_2O_3 *	0.01	12.85	15.82	15.39	15.98	14.11	15.96	15.11	6.27	0.13
Fe_2O_3 *	0.01	5.61	7.23	3.34	3.04	7.94	4.70	11.76	18.91	49.85
MnO *	0.001	0.11	0.11	0.09	0.09	0.18	0.13	0.30	0.02	0.03
MgO *	0.01	4.18	3.91	1.02	0.80	9.68	2.68	4.55	0.33	0.03
CaO *	0.01	17.90	7.62	0.44	1.13	5.22	3.03	5.14	0.11	0.06
Na_2O *	0.01	3.77	6.04	2.61	3.55	3.05	3.85	5.17	0.16	0.02
K_2O *	0.01	0.73	0.34	7.20	6.33	2.52	3.11	0.64	4.04	0.03
TiO_2 *	0.001	0.71	0.59	0.35	0.34	0.75	0.66	1.46	0.30	0.01
P_2O_5 *	0.01	0.18	0.22	0.08	0.11	0.18	0.16	0.64	0.03	0.01
LOI *		15.97	5.41	3.04	3.31	4.31	2.79	5.46	10.55	27.69
TOTAL *		99.83	99.13	98.63	98.47	99.18	99.32	99.20	98.17	95.43
Cr^{52} #	3.65	306.73	44.89	7.03	7.36	543.23	165.36	12.71	28.28	4.28
Cr^{53} #	12.85	N.D.	N.D.	N.D.	N.D.	N.D.	N.D.	N.D.	N.D.	N.D.
Ni #	5.14	151.63	33.37	-	-	230.77	27.31	11.14	16.91	-
Co #	0.26	25.29	22.14	2.73	2.41	36.84	7.48	28.70	46.88	46.34
Sc #	1.00	28.00	28.00	5.00	4.00	23.00	13.00	25.00	8.00	2.00
V #	3.42	217.45	215.92	13.53	10.39	151.82	42.92	318.78	81.82	-
Cu #	3.94	27.35	168.16	6.69	5.58	81.12	19.00	31.84	103.95	1184.57
Pb #	0.25	1.87	3.77	9.38	13.67	9.79	10.84	28.73	86.06	2637.72
Zn #	8.16	23.94	26.21	60.58	43.50	46.12	56.02	128.74	56.45	225.22
Bi #	0.06	-	-	0.07	0.10	0.10	-	-	2.20	31.10
Cd #	0.99	-	-	-	-	-	-	-	-	-
Sn #	0.12	0.48	0.32	1.41	1.50	0.74	1.56	0.81	0.59	0.89
Mo #	0.63	-	1.02	-	-	-	-	0.83	6.14	9.30
As #	1.33	7.51	52.14	13.11	8.52	47.69	17.05	9.28	120.68	904.61
Sb #	0.20	0.23	-	0.45	0.85	0.25	-	0.48	2.79	40.32
Ag #	0.23	-	-	0.76	0.73	0.32	0.48	0.50	2.61	7.83
Li #	0.79	26.41	9.99	1.81	-	31.88	8.27	15.58	1.82	-
Rb #	0.76	24.85	26.12	234.93	162.89	106.42	44.36	31.77	75.93	5.49
Cs #	0.08	0.88	0.13	0.71	0.67	0.34	0.62	0.38	0.24	-
Ba #	0.80	140.88	155.34	1027.75	1183.91	1748.18	947.35	1401.99	3471.25	11239.24
Sr #	4.16	219.89	111.56	38.21	71.97	198.41	153.63	183.97	25.36	103.75
Tl #	0.08	0.12	0.12	1.28	0.93	0.55	0.51	0.45	8.61	5.66
Ta #	0.04	0.13	0.11	0.57	0.56	0.28	0.51	0.21	0.08	-
Nb #	0.08	2.38	1.71	9.28	8.93	4.42	8.28	3.57	1.80	0.15
Hf #	0.21	1.77	1.90	6.61	6.40	3.43	6.69	2.48	0.76	-
Zr #	0.14	55.96	41.59	241.42	230.53	101.90	225.67	82.74	27.58	1.11
Y #	0.08	15.03	13.92	5.39	3.15	13.88	32.72	26.75	0.68	0.41
Th #	0.08	2.61	1.32	1.24	0.94	3.95	3.58	1.38	0.12	0.09
U #	0.09	2.07	0.32	1.99	2.17	1.40	1.53	0.56	0.27	0.14

Table A1-1 (continued) Major and trace lithogeochemical data for outcrop and drill core samples from Pilley's Island VMS district.

Sample ID	Det. Limit	10CPM-195	10CPM-198	10CPM-199	10CPM-200	10CPM-202b	10CPM-203	10CPM-205	10CPM-206	10CPM-207
La #	0.09	8.40	4.59	3.87	2.15	14.95	10.81	8.56	0.80	0.29
Ce #	0.13	18.39	10.28	4.48	3.96	35.92	25.71	23.66	0.62	0.61
Pr #	0.06	2.51	1.51	1.04	0.52	4.74	3.81	3.16	0.40	0.07
Nd #	0.50	11.30	7.10	4.02	1.99	20.41	17.02	15.69	3.78	-
Sm #	0.36	2.69	2.05	0.92	0.43	4.32	4.70	4.54	-	-
Eu #	0.08	0.92	0.72	0.21	0.08	1.19	1.19	1.60	-	-
Gd #	0.16	3.05	2.54	0.87	0.48	3.71	5.21	5.25	-	-
Tb #	0.03	0.47	0.40	0.14	0.08	0.52	0.92	0.83	-	-
Dy #	0.13	2.95	2.67	1.01	0.58	3.03	6.06	5.34	0.27	-
Ho #	0.03	0.60	0.57	0.23	0.12	0.55	1.32	1.13	-	-
Er #	0.14	1.67	1.69	0.77	0.51	1.58	4.07	3.16	-	-
Tm #	0.04	0.26	0.26	0.15	0.10	0.23	0.67	0.49	0.04	-
Yb #	0.21	1.68	1.65	1.00	0.64	1.54	4.57	2.86	-	-
Lu #	0.05	0.24	0.28	0.14	0.10	0.25	0.74	0.43	-	-
Sericite Index[2]		28.99	16.22	5.33	73.39	64.07	45.24	44.68	11.02	96.19
Al_2O_3/Na_2O		3.41	2.62	5.90	4.50	4.63	4.15	2.92	39.19	6.50
CCPI[3]		68.51	63.58	30.77	27.99	75.98	51.46	73.73	82.08	99.90
AI[4]		18.47	23.73	72.94	60.37	59.60	45.70	33.48	94.18	42.86
Zn/TiO_2*10000		0.01	0.01	0.04	0.07	0.03	0.03	0.01	0.00	0.00
Nb/Y		0.16	0.12	1.72	2.84	0.32	0.25	0.13	2.66	0.37
Th/Yb		1.56	0.80	1.24	1.46	2.56	0.78	0.48	-	-
$[La/Yb]_{CN}$[5]		3.40	1.89	2.63	2.27	6.58	1.61	2.04	-	-
$[La/Sm]_{MN}$[6]		2.02	1.45	2.73	3.22	2.24	1.49	1.22	-	-
$[Nb/Th]_{MN}$[6]		0.11	0.16	0.91	1.15	0.14	0.28	0.31	1.83	0.22
Zr/Yb		27.85	33.35	25.21	241.65	357.89	66.00	49.39	28.95	-
Nb/Yb		1.42	1.04	9.29	13.86	2.86	1.81	1.25	-	-
Th/Nb		1.10	0.77	0.13	0.11	0.89	0.43	0.39	0.07	0.56
La/Sm		3.12	2.24	4.23	4.98	3.46	2.30	1.89	-	-

* wt%; ICP-OES

\# ppm; ICP-MS

LOI Loss On Ignition

[1] Universal Transverse Mercator, North American Datum 27 (UTM NAD27)

[2] Sericite Index = $100*K_2O/Na_2O - K_2O$

[3] CCPI = $100*(Fe_2O_3{}^1-MgO)/(Fe_2O_3{}^1+MgO+K_2O+Na_2O)$

[4] AI = $100*(K_2O+MgO)/(K_2O+MgO+CaO+Na_2O)$

[5] CN – chondrite normalized

[6] MN = primitive mantle normalized

\- < Limit of Detection

N.D. Not Detected

Table A1-1 (continued) Major and trace lithogeochemical data for outcrop and drill core samples from Pilley's Island VMS district.

Sample ID	Det. Limit	10CPM-208	10CPM-209b	11CPM-003	11CPM-004	11CPM-006	11CPM-007	11CPM-008	11CPM-009	11CPM-010
Easting [1]		591391	591262	-	-	-	-	-	-	-
Northing [1]		5485362	5483227	-	-	-	-	-	-	-
Drillhole ID		-	-	84-11	83-01	83-01	83-01	83-01	83-01	83-01
From (m)		-	-	75.80	6.70	33.50	58.30	75.70	101.00	119.70
To (m)		-	-	76.70	7.30	34.00	59.20	76.20	101.40	120.10
Strat. unit		1.1	6.1	3.2	3.3	3.1	3.1	3.1	3.1	3.1
SiO_2 *	0.01	76.82	49.61	64.01	60.68	56.83	67.44	63.04	70.63	60.97
Al_2O_3 *	0.01	12.56	14.30	15.13	13.10	18.24	14.60	16.04	13.75	15.88
Fe_2O_3 *	0.01	2.52	7.75	4.51	10.79	4.67	3.39	4.06	2.71	4.18
MnO *	0.001	0.03	0.10	0.11	0.04	0.13	0.08	0.10	0.07	0.11
MgO *	0.01	0.43	2.48	1.65	3.08	1.66	1.68	1.79	0.99	1.83
CaO *	0.01	0.19	9.47	2.04	0.34	2.90	1.66	2.32	1.38	2.39
Na_2O *	0.01	0.06	6.72	3.52	0.82	3.86	2.53	2.49	3.71	3.33
K_2O *	0.01	1.39	0.13	3.56	3.88	4.05	4.15	4.76	2.37	3.78
TiO_2 *	0.001	0.25	1.18	0.55	0.54	0.62	0.48	0.53	0.44	0.53
P_2O_5 *	0.01	0.06	0.32	0.10	0.13	0.16	0.06	0.08	0.07	0.07
LOI *		5.07	8.01	4.37	5.14	5.81	3.91	5.69	4.07	6.30
TOTAL *		99.38	100.10	99.54	98.53	98.91	99.98	100.90	100.20	99.38
Cr^{52} #	3.65	7.37	7.40	15.25	7.80	5.18	8.07	5.36	14.44	6.77
Cr^{53} #	12.85	N.D.	N.D.	18.44	14.63	-	-	-	20.54	-
Ni #	5.14	5.82	8.82	-	23.58	345.16	-	-	9.70	-
Co #	0.26	2.56	12.53	3.09	9.94	4.61	2.93	3.17	2.83	3.64
Sc #	1.00	3.00	21.00	8.00	8.00	8.00	6.00	7.00	6.00	7.00
V #	3.42	9.84	233.36	12.13	71.67	24.02	17.34	18.26	14.06	18.95
Cu #	3.94	23.95	-	10.35	1580.81	17.94	11.75	10.30	29.61	8.11
Pb #	0.25	27.43	5.60	8.69	160.60	9.01	7.48	7.12	11.46	12.17
Zn #	8.16	25.41	-	50.21	1689.06	87.77	53.78	56.80	78.99	61.10
Bi #	0.06	0.29	-	-	4.61	0.11	-	0.11	0.12	0.09
Cd #	0.99	-	-	-	2.04	1.19	-	-	-	-
Sn #	0.12	1.06	0.92	1.73	1.85	1.50	1.11	1.00	1.25	1.31
Mo #	0.63	-	-	-	1.57	-	0.77	0.68	-	-
As #	1.33	58.90	4.10	1.62	324.94	15.67	8.31	7.18	14.44	11.92
Sb #	0.20	7.12	0.47	0.26	117.20	0.93	0.26	0.28	3.28	1.04
Ag #	0.23	0.67	-	0.54	0.61	0.55	0.57	0.65	0.33	0.51
Li #	0.79	19.64	4.05	6.97	11.46	6.02	3.48	0.90	1.12	-
Rb #	0.76	81.92	6.52	74.78	89.13	54.96	113.92	82.02	29.37	163.82
Cs #	0.08	0.48	-	0.39	3.94	1.42	1.91	1.78	1.19	1.51
Ba #	0.80	3696.01	66.49	347.37	1703.41	212.46	562.65	463.02	300.03	299.71
Sr #	4.16	278.68	161.98	34.79	47.79	67.75	120.24	162.43	137.79	209.25
Tl #	0.08	0.60	-	0.78	4.39	1.28	0.81	0.87	0.33	0.93
Ta #	0.04	0.40	0.19	0.40	0.30	0.42	0.41	0.46	0.37	0.55
Nb #	0.08	6.82	3.04	9.08	7.19	9.62	7.88	8.60	7.02	11.80
Hf #	0.21	4.91	2.39	4.89	3.37	5.38	4.92	5.02	4.39	6.48
Zr #	0.14	181.44	78.74	186.17	141.49	220.84	184.67	198.56	166.78	276.24
Y #	0.08	6.97	18.03	22.84	23.26	18.44	13.34	16.39	10.71	17.06
Th #	0.08	2.93	1.55	4.12	4.01	4.03	4.49	4.22	3.14	5.98
U #	0.09	1.77	0.68	1.47	1.23	1.86	2.00	1.93	2.08	2.62

Table A1-1 (continued) Major and trace lithogeochemical data for outcrop and drill core samples from Pilley's Island VMS district.

Sample ID	Det. Limit	10CPM-208	10CPM-209b	11CPM-003	11CPM-004	11CPM-006	11CPM-007	11CPM-008	11CPM-009	11CPM-010
La #	0.09	7.20	8.81	10.96	14.00	9.08	9.71	9.14	8.40	11.91
Ce #	0.13	15.96	21.30	21.04	34.51	15.58	21.46	20.99	14.36	28.73
Pr #	0.06	1.84	2.85	3.27	3.91	2.55	2.73	2.56	1.90	3.31
Nd #	0.50	7.30	13.55	13.98	16.29	9.96	10.98	10.48	7.69	13.30
Sm #	0.36	1.52	3.50	3.69	4.24	2.66	2.68	2.63	1.90	3.36
Eu #	0.08	0.29	1.24	0.97	1.20	0.65	0.64	0.69	0.51	0.88
Gd #	0.16	1.29	3.61	3.67	4.21	2.78	2.61	2.77	2.01	3.41
Tb #	0.03	0.22	0.55	0.69	0.80	0.51	0.46	0.47	0.32	0.56
Dy #	0.13	1.49	3.59	4.45	4.62	3.37	2.80	3.22	2.08	3.50
Ho #	0.03	0.31	0.70	0.91	1.03	0.72	0.56	0.63	0.43	0.76
Er #	0.14	0.96	2.14	2.90	2.95	2.33	1.63	2.08	1.39	2.22
Tm #	0.04	0.20	0.35	0.47	0.48	0.42	0.29	0.38	0.27	0.36
Yb #	0.21	1.11	2.26	3.23	3.44	2.68	2.06	2.29	1.50	2.42
Lu #	0.05	0.18	0.35	0.50	0.44	0.41	0.30	0.36	0.27	0.40
Sericite Index[2]		60.00	95.86	1.90	50.28	82.55	51.20	62.13	65.66	38.98
Al_2O_3/Na_2O		209.33	2.13	4.30	15.98	4.73	5.77	6.44	3.71	4.77
CCPI[3]		67.05	59.89	46.53	74.69	44.45	43.15	44.66	37.83	45.81
AI[4]		87.92	13.88	48.38	85.71	45.79	58.18	57.66	39.76	49.51
$Zn/TiO_2*10000$		3.02	0.03	0.02	0.03	0.04	0.03	0.04	0.03	0.06
Nb/Y		0.98	0.17	0.40	0.31	0.52	0.59	0.52	0.66	0.69
Th/Yb		2.65	0.69	1.27	1.17	1.50	2.18	1.84	2.09	2.47
$[La/Yb]_{CN}$[5]		4.42	2.64	2.30	2.77	2.30	3.20	2.71	3.80	3.34
$[La/Sm]_{MN}$[6]		3.06	1.62	1.92	2.13	2.20	2.34	2.24	2.86	2.29
$[Nb/Th]_{MN}$[6]		0.28	0.24	0.27	0.22	0.29	0.21	0.25	0.27	0.24
Zr/Yb		-	164.00	34.80	57.57	41.16	82.30	89.67	86.75	110.98
Nb/Yb		6.16	1.35	2.81	2.09	3.58	3.82	3.76	4.67	4.87
Th/Nb		0.43	0.51	0.45	0.56	0.42	0.57	0.49	0.45	0.51
La/Sm		4.74	2.51	2.97	3.30	3.41	3.63	3.47	4.42	3.54

* wt%; ICP-OES

\# ppm; ICP-MS

LOI Loss On Ignition

[1] Universal Transverse Mercator, North American Datum 27 (UTM NAD27)

[2] Sericite Index = $100*K_2O/Na_2O+K_2O$

[3] CCPI = $100*(Fe_2O_3^T+MgO)/(Fe_2O_3^T+MgO+K_2O+Na_2O)$

[4] AI = $100*(K_2O+MgO)/(K_2O+MgO+CaO+Na_2O)$

[5] CN = chondrite normalized

[6] MN = primitive mantle normalized

\- < Limit of Detection

N.D. Not Detected

Table A1-1 (continued) Major and trace lithogeochemical data for outcrop and drill core samples from Pilley's Island VMS district.

Sample ID	Det. Limit	11CPM-011	11CPM-012	11CPM-013	11CPM-014	11CPM-015	11CPM-016	11CPM-017	11CPM-018	11CPM-019
Easting [1]		-	-	-	-	-	-	-	-	-
Northing [1]		-	-	-	-	-	-	-	-	-
Drillhole ID		83-01	83-01	83-01	84-03	84-03	84-03	84-03	84-03	84-03
From (m)		133.90	138.70	150.80	12.10	19.00	50.60	73.00	80.00	99.20
To (m)		134.40	139.20	151.30	12.60	19.40	51.60	74.00	81.00	99.70
Strat. unit		2	2	2	4.4	4.4	4.3	4.3	4.2	3.2
SiO_2 *	0.01	47.55	44.00	41.02	57.62	63.93	60.78	55.14	42.96	61.55
Al_2O_3 *	0.01	15.97	15.84	13.34	12.43	14.55	14.66	16.02	15.11	14.12
Fe_2O_3 *	0.01	8.06	9.25	7.67	3.02	5.25	7.98	5.94	15.99	10.06
MnO *	0.001	0.15	0.13	0.15	0.63	0.47	0.25	0.19	0.50	0.03
MgO *	0.01	7.34	6.97	6.25	2.86	1.76	1.63	5.06	6.56	1.01
CaO *	0.01	4.62	5.00	8.94	5.41	1.38	0.41	1.50	1.15	0.31
Na_2O *	0.01	4.37	2.58	2.70	3.18	2.31	0.07	0.55	0.41	0.13
K_2O *	0.01	1.74	3.41	2.17	4.39	4.83	5.25	4.65	3.12	4.38
TiO_2 *	0.001	0.88	0.91	0.49	0.45	0.61	0.61	0.53	0.65	0.48
P_2O_5 *	0.01	0.25	0.22	0.13	0.09	0.19	0.13	0.07	0.12	0.06
LOI *		9.80	11.40	16.15	9.09	4.24	6.15	10.03	11.97	7.36
TOTAL *		100.70	99.72	99.01	99.18	99.50	97.91	99.68	98.55	99.49
Cr^{52} #	3.65	120.75	130.50	31.86	9.10	6.28	29.72	12.09	133.88	16.55
Cr^{53} #	12.85	127.27	147.26	32.88	17.47	-	27.62	18.00	142.57	18.26
Ni #	5.14	55.21	39.78	33.88	-	-	14.45	-	62.71	-
Co #	0.26	32.73	26.95	28.75	4.07	6.68	12.87	4.00	40.68	5.69
Sc #	1.00	36.00	36.00	27.00	6.00	8.00	13.00	6.00	40.00	6.00
V #	3.42	237.74	262.83	195.64	15.61	46.40	89.58	22.40	208.04	16.40
Cu #	3.94	100.04	114.78	144.45	11.52	33.68	220.60	30.33	862.67	77.77
Pb #	0.25	10.67	7.25	4.89	41.80	11.76	387.51	24.00	26.28	7.20
Zn #	8.16	78.62	69.99	54.67	66.50	102.28	3541.18	511.66	269.52	42.44
Bi #	0.06	-	0.09	-	0.12	0.06	0.39	0.51	0.80	0.78
Cd #	0.99	1.37	-	-	-	-	9.89	1.16	-	1.38
Sn #	0.12	0.74	0.72	0.67	1.17	1.14	0.98	1.57	0.68	2.88
Mo #	0.63	-	2.65	0.67	2.73	1.05	3.98	2.53	0.83	4.13
As #	1.33	14.03	14.53	16.93	9.41	8.58	41.06	12.27	14.42	31.07
Sb #	0.20	0.36	0.96	1.90	0.27	-	0.80	0.34	0.45	5.10
Ag #	0.23	-	-	-	0.97	0.37	1.11	0.83	0.66	0.79
Li #	0.79	32.74	28.96	16.77	5.00	2.57	4.72	7.95	8.16	1.76
Rb #	0.76	63.04	194.33	95.44	108.38	128.98	72.93	203.18	92.65	60.15
Cs #	0.08	1.19	3.08	2.44	0.70	0.73	0.57	0.54	0.66	0.42
Ba #	0.80	286.46	495.56	78.65	587.47	445.17	656.46	1602.93	592.33	631.96
Sr #	4.16	218.36	163.56	151.18	351.11	62.18	12.48	30.88	33.15	10.66
Tl #	0.08	0.40	1.05	0.46	1.27	1.64	2.66	1.80	1.70	1.10
Ta #	0.04	0.16	0.32	0.19	0.49	0.32	0.28	0.43	0.06	0.39
Nb #	0.08	3.38	4.58	4.27	9.16	6.33	5.43	8.46	1.46	7.62
Hf #	0.21	1.94	3.06	1.22	5.83	3.92	3.28	5.09	1.23	4.22
Zr #	0.14	71.14	99.89	37.48	201.86	164.62	131.56	203.20	38.08	179.55
Y #	0.08	16.26	23.19	11.95	31.90	12.18	9.79	22.23	12.80	9.55
Th #	0.08	1.57	2.60	1.71	7.35	3.12	2.18	5.74	0.86	2.63
U #	0.09	0.80	1.23	0.53	2.97	1.28	1.47	2.23	0.34	1.68

Table A1-1 (continued) Major and trace lithogeochemical data for outcrop and drill core samples from Pilley's Island VMS district.

Sample ID	Det. Limit	11CPM-011	11CPM-012	11CPM-013	11CPM-014	11CPM-015	11CPM-016	11CPM-017	11CPM-018	11CPM-019
La #	0.09	5.31	9.49	6.17	20.78	8.90	5.12	10.87	4.37	5.70
Ce #	0.13	15.24	24.81	12.96	49.84	17.44	11.38	25.32	9.13	11.81
Pr #	0.06	2.11	3.41	1.76	6.05	2.57	1.50	3.06	1.34	1.63
Nd #	0.50	9.34	16.11	7.79	24.03	10.67	6.23	12.27	6.05	6.28
Sm #	0.36	2.75	4.33	2.11	6.03	2.53	1.59	3.14	1.82	1.57
Eu #	0.08	0.91	1.35	0.70	2.20	0.82	0.35	0.55	0.72	0.29
Gd #	0.16	3.04	4.73	2.33	6.65	2.63	1.63	3.12	2.31	1.46
Tb #	0.03	0.54	0.75	0.40	1.07	0.42	0.32	0.58	0.38	0.30
Dy #	0.13	3.32	5.05	2.38	6.63	2.56	2.18	4.14	2.49	1.97
Ho #	0.03	0.72	1.00	0.46	1.29	0.53	0.44	0.89	0.52	0.44
Er #	0.14	2.10	2.99	1.36	4.21	1.69	1.51	2.87	1.60	1.45
Tm #	0.04	0.35	0.52	0.22	0.72	0.37	0.29	0.47	0.28	0.29
Yb #	0.21	1.94	2.82	1.31	4.50	1.63	1.59	3.13	1.54	1.68
Lu #	0.05	0.29	0.41	0.22	0.68	0.26	0.23	0.50	0.21	0.27
Sericite Index[2]		53.16	28.48	56.93	44.56	57.99	67.65	98.68	89.42	88.39
Al_2O_3/Na_2O		3.65	6.14	4.94	3.91	6.30	209.43	29.13	36.85	108.62
CCPI[3]		71.59	73.03	74.08	43.72	49.54	64.37	67.90	86.46	71.05
AI[4]		50.25	57.80	41.97	45.77	64.11	93.48	82.57	86.12	92.45
$Zn/TiO_2*10000$		0.01	0.01	0.00	0.04	0.04	0.02	0.03	0.01	0.03
Nb/Y		0.21	0.20	0.36	0.29	0.52	0.55	0.38	0.11	0.80
Th/Yb		0.81	0.92	1.31	1.63	1.92	1.37	1.83	0.55	1.57
$[La/Yb]_{CN}$[5]		1.86	2.28	3.21	3.14	3.72	2.19	2.36	1.92	2.31
$[La/Sm]_{MN}$[6]		1.25	1.42	1.89	2.23	2.27	2.08	2.24	1.55	2.35
$[Nb/Th]_{MN}$[6]		0.26	0.21	0.30	0.15	0.25	0.30	0.18	0.21	0.35
Zr/Yb		114.05	36.71	35.37	28.70	44.88	101.24	82.67	64.95	24.65
Nb/Yb		1.74	1.62	3.27	2.04	3.89	3.41	2.70	0.95	4.54
Th/Nb		0.46	0.57	0.40	0.80	0.49	0.40	0.68	0.58	0.35
La/Sm		1.93	2.19	2.92	3.45	3.51	3.21	3.46	2.40	3.63

* wt%; ICP-OES

\# ppm; ICP-MS

LOI Loss On Ignition

[1] Universal Transverse Mercator, North American Datum 27 (UTM NAD27)

[2] Sericite Index = $100*K_2O/Na_2O + K_2O$

[3] CCPI = $100*(Fe_2O_3^T+MgO)/(Fe_2O_3^T+MgO+K_2O+Na_2O)$

[4] AI = $100*(K_2O+MgO)/(K_2O+MgO+CaO+Na_2O)$

[5] CN = chondrite normalized

[6] MN = primitive mantle normalized

\- < Limit of Detection

N.D. Not Detected

Table A1-1 (continued) Major and trace lithogeochemical data for outcrop and drill core samples from Pilley's Island VMS district.

Sample ID	Det. Limit	11CPM-020	11CPM-021	11CPM-022	11CPM-023	11CPM-024	11CPM-025	11CPM-026	11CPM-027	11CPM-028
Easting [1]		-	-	-	-	-	-	-	-	-
Northing [1]		-	-	-	-	-	-	-	-	-
Drillhole ID		84-03	84-03	84-03	84-03	84-12	84-12	84-12	84-12	84-12
From (m)		126.50	131.50	140.20	155.80	12.50	20.10	37.20	52.30	64.00
To (m)		127.00	132.00	140.70	156.30	13.00	20.60	37.70	52.90	64.50
Strat. unit		3.1	3.1	3.1	3.5	4.5	4.4	4.4	4.3	4.3
SiO_2 *	0.01	65.71	70.09	63.68	38.73	65.73	65.68	66.86	59.19	59.46
Al_2O_3 *	0.01	14.99	13.63	15.61	13.35	14.23	14.99	15.75	14.14	15.70
Fe_2O_3 *	0.01	4.56	3.11	4.84	6.16	6.37	4.39	2.52	6.00	5.91
MnO *	0.001	0.10	0.06	0.17	0.14	0.21	0.11	0.07	0.14	0.20
MgO *	0.01	1.17	0.51	2.18	5.01	1.70	0.64	0.45	1.04	1.93
CaO *	0.01	0.54	0.28	0.29	16.83	0.32	1.70	1.60	3.61	2.78
Na_2O *	0.01	1.94	0.19	0.46	3.98	1.02	3.68	3.32	2.50	1.81
K_2O *	0.01	7.08	9.99	8.84	0.88	5.75	4.78	6.82	6.05	6.07
TiO_2 *	0.001	0.50	0.45	0.56	0.46	0.53	0.55	0.58	0.52	0.58
P_2O_5 *	0.01	0.09	0.10	0.09	0.10	0.07	0.10	0.09	0.24	0.09
LOI *		3.94	2.46	2.70	12.70	2.73	2.73	2.49	5.87	4.83
TOTAL *		100.60	100.90	99.43	98.35	98.68	99.35	100.60	99.31	99.34
Cr^{52} #	3.65	13.11	15.11	14.78	113.95	9.16	-	10.42	11.62	10.81
Cr^{53} #	12.85	15.06	14.80	13.90	120.49	-	-	-	-	-
Ni #	5.14	6.69	-	6.66	34.88	9.19	-	-	-	-
Co #	0.26	3.74	3.24	4.93	19.49	2.14	-	0.44	14.26	3.40
Sc #	1.00	6.00	6.00	8.00	28.00	8.00	8.00	8.00	7.00	8.00
V #	3.42	17.17	14.39	36.61	172.92	10.88	-	12.41	11.94	13.35
Cu #	3.94	23.72	37.92	44.16	95.81	63.88	6.00	8.20	97.50	11.50
Pb #	0.25	172.80	402.42	25.74	9.56	45.24	5.87	3.63	40.67	4.32
Zn #	8.16	333.55	489.59	680.64	53.36	239.56	-	25.40	50.94	61.93
Bi #	0.06	0.13	0.17	0.10	0.08	0.31	0.08	0.07	0.68	0.15
Cd #	0.99	-	-	1.38	-	-	-	-	-	-
Sn #	0.12	1.15	0.86	0.71	0.14	2.15	-	0.58	0.80	1.74
Mo #	0.63	3.11	3.58	1.21	-	2.20	0.88	3.13	5.11	2.19
As #	1.33	29.90	50.88	13.44	14.25	16.94	-	5.62	7.16	1.38
Sb #	0.20	1.51	1.22	0.37	-	0.21	-	0.34	0.48	0.21
Ag #	0.23	1.39	0.75	0.62	0.45	0.30	-	0.56	0.70	0.63
Li #	0.79	1.04	0.99	6.46	68.47	10.13	4.93	2.40	3.11	5.73
Rb #	0.76	311.51	242.47	147.95	172.64	358.00	153.91	155.32	120.94	199.41
Cs #	0.08	0.38	0.44	0.70	0.29	0.36	0.45	0.51	0.55	0.47
Ba #	0.80	1513.35	2334.55	3259.33	400.80	719.28	947.10	1264.40	2909.94	1110.30
Sr #	4.16	19.21	20.46	47.20	477.31	37.77	20.98	27.34	71.76	46.87
Tl #	0.08	3.23	3.14	1.74	0.40	1.15	0.91	0.99	1.04	1.22
Ta #	0.04	0.39	0.37	0.41	0.10	0.43	0.41	0.40	0.44	0.39
Nb #	0.08	7.90	7.10	8.21	1.75	8.45	7.39	7.24	7.38	7.54
Hf #	0.21	4.69	4.11	4.86	1.22	4.90	4.94	4.77	5.00	4.53
Zr #	0.14	185.54	166.87	191.70	40.89	195.27	177.24	177.83	175.31	182.01
Y #	0.08	6.69	5.87	13.48	14.96	18.97	14.49	6.90	42.08	26.48
Th #	0.08	1.45	1.56	3.33	1.66	2.76	2.42	1.50	5.13	4.58
U #	0.09	1.41	1.42	1.87	0.60	1.57	1.35	1.68	2.84	1.54

Table A1-1 (continued) Major and trace lithogeochemical data for outcrop and drill core samples from Pilley's Island VMS district.

Sample ID	Det. Limit	11CPM-020	11CPM-021	11CPM-022	11CPM-023	11CPM-024	11CPM-025	11CPM-026	11CPM-027	11CPM-028
La #	0.09	3.31	3.16	7.11	7.86	14.39	5.16	3.08	14.60	10.91
Ce #	0.13	6.61	5.49	15.72	15.30	27.33	10.78	8.81	31.72	25.48
Pr #	0.06	0.87	0.96	2.06	2.08	3.26	1.60	0.91	4.40	3.33
Nd #	0.50	3.45	3.56	8.16	8.80	12.71	8.14	4.27	21.38	16.68
Sm #	0.36	0.85	1.03	2.16	2.31	2.80	3.79	2.15	10.47	7.55
Eu #	0.08	0.32	0.22	0.41	0.93	0.66	1.08	0.49	2.50	1.77
Gd #	0.16	0.97	0.97	2.00	2.64	2.98	2.87	1.42	7.88	4.86
Tb #	0.03	0.19	0.16	0.34	0.42	0.48	0.53	0.29	1.48	1.03
Dy #	0.13	1.27	1.18	2.55	2.64	3.41	3.16	1.60	8.41	5.69
Ho #	0.03	0.29	0.27	0.58	0.58	0.69	0.67	0.33	1.64	1.14
Er #	0.14	0.90	0.88	1.93	1.52	2.14	1.94	1.06	4.76	3.33
Tm #	0.04	0.19	0.20	0.40	0.28	0.39	0.35	0.23	0.85	0.55
Yb #	0.21	1.26	1.06	2.30	1.44	2.67	2.24	1.29	5.93	3.78
Lu #	0.05	0.21	0.17	0.36	0.24	0.37	0.38	0.18	0.97	0.55
Sericite Index[2]		97.12	78.49	98.13	95.05	18.11	84.93	56.50	67.26	70.76
Al_2O_3/Na_2O		7.73	71.74	33.93	3.35	13.95	4.07	4.74	5.66	8.67
CCPI[3]		38.85	26.23	43.01	69.68	54.38	37.29	22.65	45.16	49.87
AI[4]		76.89	95.72	93.63	22.06	84.76	50.19	59.64	53.71	63.54
Zn/TiO_2*10000		0.04	0.03	0.04	0.01	0.04	0.03	0.03	0.03	0.04
Nb/Y		1.18	1.21	0.61	0.12	0.45	0.51	1.05	0.18	0.28
Th/Yb		1.14	1.47	1.45	1.15	1.03	1.08	1.16	0.86	1.21
$[La/Yb]_{CN}$[5]		1.78	2.02	2.10	3.70	3.65	1.56	1.62	1.67	1.96
$[La/Sm]_{MN}$[6]		2.52	1.98	2.13	2.20	3.32	0.88	0.92	0.90	0.93
$[Nb/Th]_{MN}$[6]		0.66	0.55	0.30	0.13	0.37	0.37	0.58	0.17	0.20
Zr/Yb		107.03	146.85	157.14	83.21	28.34	73.01	79.08	137.37	29.54
Nb/Yb		6.25	6.68	3.56	1.21	3.16	3.30	5.59	1.24	2.00
Th/Nb		0.18	0.22	0.41	0.95	0.33	0.33	0.21	0.69	0.61
La/Sm		3.89	3.06	3.29	3.41	5.13	1.36	1.43	1.39	1.44

* wt%; ICP-OES

\# ppm; ICP-MS

LOI Loss On Ignition

[1] Universal Transverse Mercator, North American Datum 27 (UTM NAD27)

[2] Sericite Index = $100*K_2O/Na_2O+K_2O$

[3] CCPI = $100*(Fe_2O_3{}^{t}+MgO)/(Fe_2O_3{}^{t}+MgO+K_2O+Na_2O)$

[4] AI = $100*(K_2O+MgO)/(K_2O+MgO+CaO+Na_2O)$

[5] CN = chondrite normalized

[6] MN = primitive mantle normalized

\- < Limit of Detection

N.D. Not Detected

Table A1-1 (continued) Major and trace lithogeochemical data for outcrop and drill core samples from Pilley's Island VMS district.

Sample ID	Det. Limit	11CPM-029	11CPM-030	11CPM-031	11CPM-032	11CPM-033	11CPM-034	11CPM-035	11CPM-037	11CPM-038
Easting [1]		-	-	-	-	-	-	-	-	-
Northing [1]		-	-	-	-	-	-	-	-	-
Drillhole ID		84-12	84-12	84-12	84-12	84-12	84-12	84-12	84-12	84-12
From (m)		68.30	94.20	119.70	127.30	138.80	154.60	169.80	212.70	219.90
To (m)		68.80	94.70	120.20	127.80	139.30	155.10	170.80	213.20	220.30
Strat. unit		4.2	4.3	4.3	4.3	3.3	3.3	3.3	3.2	3.2
SiO_2 *	0.01	69.31	65.25	64.48	56.49	47.79	57.19	54.65	51.67	55.16
Al_2O_3 *	0.01	13.76	15.56	15.66	16.21	21.31	18.36	17.53	20.14	16.06
Fe_2O_3 *	0.01	3.30	4.26	3.98	5.83	11.01	5.50	9.46	10.25	6.29
MnO *	0.001	0.12	0.15	0.12	0.13	0.10	0.23	0.06	0.03	0.17
MgO *	0.01	0.83	1.58	2.73	5.39	2.38	4.65	1.33	1.23	5.21
CaO *	0.01	1.58	1.15	1.15	3.65	1.19	0.92	0.64	0.22	4.16
Na_2O *	0.01	3.84	3.43	3.52	5.83	2.01	0.22	0.29	0.17	5.88
K_2O *	0.01	4.37	6.08	3.70	1.32	4.48	4.64	4.64	6.11	0.20
TiO_2 *	0.001	0.50	0.57	0.69	0.74	1.19	0.79	0.80	0.88	0.75
P_2O_5 *	0.01	0.08	0.08	0.11	0.19	0.04	0.16	0.42	0.09	0.17
LOI *		2.79	2.55	3.67	3.78	7.67	6.13	8.52	7.97	5.84
TOTAL *		100.50	100.70	99.80	99.57	99.15	98.79	98.32	98.76	99.89
Cr^{52} #	3.65	23.47	9.13	16.82	126.94	48.54	14.40	15.18	25.32	30.39
Cr^{53} #	12.85	20.82	-	18.57	124.13	44.32	-	14.34	23.73	28.19
Ni #	5.14	-	-	15.27	38.12	35.14	-	7.93	15.57	12.17
Co #	0.26	1.18	1.02	3.84	21.22	30.51	7.13	10.74	14.67	8.06
Sc #	1.00	7.00	8.00	9.00	18.00	39.00	13.00	14.00	15.00	20.00
V #	3.42	9.64	15.04	16.24	130.54	94.14	78.01	91.13	33.79	124.16
Cu #	3.94	14.80	7.10	9.60	38.26	85.51	13.32	1895.64	1737.56	8.01
Pb #	0.25	2.68	3.12	7.72	10.85	43.79	19.99	569.61	38.71	7.03
Zn #	8.16	53.25	45.93	44.40	77.27	131.35	175.29	2320.23	243.32	67.51
Bi #	0.06	-	-	0.19	0.13	0.08	0.08	1.14	1.98	0.15
Cd #	0.99	-	-	-	-	-	-	8.07	-	-
Sn #	0.12	0.65	0.79	1.19	0.72	0.71	1.32	1.27	1.43	0.97
Mo #	0.63	3.42	1.35	1.08	-	0.99	1.59	7.27	1.07	1.27
As #	1.33	1.45	2.51	3.02	19.17	20.89	12.63	47.83	29.84	3.42
Sb #	0.20	0.23	-	-	0.46	0.97	1.02	2.18	1.02	0.38
Ag #	0.23	0.49	0.56	0.66	0.41	0.33	1.64	6.50	0.98	0.50
Li #	0.79	2.94	4.62	6.27	16.34	6.91	12.68	3.87	2.57	19.24
Rb #	0.76	92.03	107.31	268.84	73.70	129.47	357.90	230.15	578.81	5.88
Cs #	0.08	0.22	0.36	0.45	0.51	1.34	0.84	0.63	0.71	0.34
Ba #	0.80	1726.56	1422.45	645.43	4580.11	483.35	620.02	1275.04	460.86	530.03
Sr #	4.16	47.30	35.83	29.00	471.07	15.30	24.68	17.01	4.93	393.14
Tl #	0.08	0.62	0.76	0.97	0.38	5.29	3.94	5.65	2.43	-
Ta #	0.04	0.35	0.40	0.40	0.30	0.23	0.37	0.34	0.45	0.24
Nb #	0.08	6.64	7.79	7.29	4.82	3.92	6.75	6.33	7.45	3.62
Hf #	0.21	3.95	4.74	5.11	4.04	2.89	4.83	4.42	5.11	3.15
Zr #	0.14	162.22	194.15	178.52	156.03	106.78	190.68	170.22	201.05	114.41
Y #	0.08	10.42	10.28	21.19	19.35	3.86	22.43	14.53	5.17	14.00
Th #	0.08	2.43	1.53	3.58	6.19	1.15	4.33	1.98	1.51	4.73
U #	0.09	1.35	1.68	1.62	2.38	1.78	2.83	2.64	0.24	1.75

Table A1-1 (continued) Major and trace lithogeochemical data for outcrop and drill core samples from Pilley's Island VMS district.

Sample ID	Det. Limit	11CPM-029	11CPM-030	11CPM-031	11CPM-032	11CPM-033	11CPM-034	11CPM-035	11CPM-037	11CPM-038
La #	0.09	4.65	5.03	11.75	18.57	1.76	12.55	11.30	10.34	14.63
Ce #	0.13	9.81	10.74	25.06	53.69	9.03	29.31	21.43	40.99	40.87
Pr #	0.06	1.33	1.30	3.17	6.16	0.77	3.50	2.76	3.48	4.98
Nd #	0.50	6.27	6.18	14.93	30.90	3.73	16.70	13.17	15.49	23.44
Sm #	0.36	3.20	2.85	7.22	11.43	2.18	7.52	5.39	7.10	8.76
Eu #	0.08	0.80	0.66	1.81	2.94	0.78	2.11	1.29	1.11	2.46
Gd #	0.16	2.14	1.88	4.95	5.87	1.48	5.01	3.35	3.32	4.95
Tb #	0.03	0.38	0.40	0.86	0.89	0.29	0.97	0.61	0.48	0.69
Dy #	0.13	2.16	2.18	4.53	4.40	1.55	5.28	3.22	2.11	3.45
Ho #	0.03	0.42	0.45	0.87	0.73	0.27	1.02	0.62	0.35	0.60
Er #	0.14	1.22	1.29	2.49	1.94	0.75	2.83	1.61	0.95	1.61
Tm #	0.04	0.24	0.28	0.40	0.34	0.15	0.48	0.34	0.29	0.32
Yb #	0.21	1.45	1.64	2.74	1.86	0.84	3.02	1.88	0.99	1.49
Lu #	0.05	0.23	0.23	0.42	0.28	0.11	0.47	0.31	0.16	0.21
Sericite Index[2]		77.03	53.23	63.93	51.25	18.46	69.03	95.47	94.12	97.29
Al_2O_3/Na_2O		3.58	4.54	4.45	2.78	10.60	83.45	60.45	118.47	2.73
CCPI[3]		33.47	38.05	48.17	61.08	67.35	67.62	68.64	64.64	65.42
AI[4]		48.96	62.58	57.93	41.45	68.19	89.07	86.52	94.95	35.02
$Zn/TiO_2*10000$		0.03	0.04	0.03	0.02	0.01	0.02	0.02	0.03	0.01
Nb/Y		0.64	0.76	0.34	0.25	1.02	0.30	0.44	1.44	0.26
Th/Yb		1.68	0.93	1.31	3.33	1.37	1.43	1.05	1.52	3.18
$[La/Yb]_{CN}$[5]		2.18	2.09	2.92	6.78	1.42	2.82	4.08	7.08	6.68
$[La/Sm]_{MN}$[6]		0.94	1.14	1.05	1.05	0.52	1.08	1.35	0.94	1.08
$[Nb/Th]_{MN}$[6]		0.33	0.62	0.25	0.09	0.41	0.19	0.39	0.60	0.09
Zr/Yb		48.20	111.87	118.48	65.25	83.81	126.63	63.04	90.43	202.49
Nb/Yb		4.58	4.75	2.67	2.59	4.65	2.23	3.36	7.51	2.44
Th/Nb		0.37	0.20	0.49	1.28	0.29	0.64	0.31	0.20	1.31
La/Sm		1.45	1.77	1.63	1.62	0.81	1.67	2.10	1.46	1.67

* wt%; ICP-OES

\# ppm; ICP-MS

LOI Loss On Ignition

[1] Universal Transverse Mercator, North American Datum 27 (UTM NAD27)

[2] Sericite Index = $100*K_2O/Na_2O + K_2O$

[3] CCPI = $100*(Fe_2O_3^T+MgO)/(Fe_2O_3^T+MgO+K_2O+Na_2O)$

[4] AI = $100*(K_2O+MgO)/(K_2O+MgO+CaO+Na_2O)$

[5] CN = chondrite normalized

[6] MN = primitive mantle normalized

\- < Limit of Detection

N.D. Not Detected

Table A1-1 (continued) Major and trace lithogeochemical data for outcrop and drill core samples from Pilley's Island VMS district.

Sample ID	Det. Limit	11CPM-039	11CPM-040	11CPM-041	11CPM-042	11CPM-043	11CPM-044	11CPM-045	11CPM-046	11CPM-047
Easting [1]		-	-	-	-	-	-	-	-	-
Northing [1]		-	-	-	-	-	-	-	-	-
Drillhole ID		84-12	84-12	84-12	83-02	83-02	83-02	83-02	83-02	83-02
From (m)		222.30	237.30	254.70	23.00	38.00	69.00	77.90	90.30	99.30
To (m)		222.80	237.80	255.20	23.50	39.00	69.50	78.40	90.80	99.80
Strat. unit		2	2	2	3.3	3.5	3.2	3.2	3.2	3.2
SiO_2 *	0.01	57.21	65.23	66.13	62.11	51.99	65.86	65.01	34.72	59.64
Al_2O_3 *	0.01	18.08	16.09	16.00	15.67	16.78	14.62	14.93	11.37	15.50
Fe_2O_3 *	0.01	6.92	4.44	3.67	6.99	9.65	3.92	4.06	14.87	4.48
MnO *	0.001	0.07	0.06	0.09	0.07	0.88	0.39	0.16	0.04	0.11
MgO *	0.01	4.29	2.37	1.83	2.10	8.28	1.98	2.10	0.64	1.80
CaO *	0.01	0.97	1.33	2.59	0.27	0.40	1.07	1.12	0.42	2.79
Na_2O *	0.01	1.96	2.84	3.31	0.09	2.32	3.10	2.37	0.16	3.59
K_2O *	0.01	3.73	3.58	3.06	4.63	1.43	3.22	3.74	3.23	3.58
TiO_2 *	0.001	0.78	0.49	0.48	0.68	0.95	0.50	0.53	0.37	0.56
P_2O_5 *	0.01	0.10	0.12	0.07	0.14	0.05	0.07	0.08	0.08	0.07
LOI *		5.76	3.51	3.19	6.18	7.20	4.10	4.45	12.77	6.79
TOTAL *		99.87	100.10	100.40	98.92	99.93	98.81	98.56	78.68	98.92
Cr^{52} #	3.65	189.59	12.69	13.48	19.72	40.62	9.76	15.52	10.43	26.54
Cr^{53} #	12.85	181.60	-	-	17.42	33.60	-	-	-	28.54
Ni #	5.14	52.22	-	-	8.38	15.40	-	5.45	-	-
Co #	0.26	24.98	3.73	3.72	10.27	17.76	3.58	4.20	3.35	2.99
Sc #	1.00	22.00	6.00	6.00	10.00	30.00	6.00	7.00	5.00	7.00
V #	3.42	144.38	19.98	20.31	54.30	174.34	19.23	22.37	14.89	13.22
Cu #	3.94	48.36	37.21	16.36	270.45	42.48	20.68	13.78	8153.45	11.85
Pb #	0.25	9.51	4.16	16.64	17.18	92.65	40.85	15.09	982.87	10.99
Zn #	8.16	92.96	68.55	75.91	74.72	395.71	93.42	73.89	98856.15	218.52
Bi #	0.06	0.09	0.09	0.13	0.16	0.08	0.07	0.09	0.17	0.08
Cd #	0.99	-	-	-	-	-	-	-	339.10	-
Sn #	0.12	0.76	1.43	1.50	1.28	0.60	1.62	1.17	11.09	1.82
Mo #	0.63	-	-	0.66	4.89	3.07	2.63	3.29	4.37	0.64
As #	1.33	18.30	6.52	7.70	47.35	16.18	15.30	25.45	445.59	11.70
Sb #	0.20	1.09	0.26	0.29	1.47	0.69	0.56	0.96	12.29	2.19
Ag #	0.23	0.56	0.70	0.79	0.65	0.86	0.79	0.57	12.74	0.72
Li #	0.79	17.22	7.48	8.27	1.99	15.66	5.26	6.92	1.66	3.70
Rb #	0.76	476.05	235.73	212.27	3067.57	580.91	1311.00	7848.07	2106.18	264.58
Cs #	0.08	2.09	1.47	1.04	0.42	0.73	0.72	1.28	0.53	1.01
Ba #	0.80	1000.82	1150.05	375.81	648.84	358.70	1312.56	1809.72	11335.56	2025.55
Sr #	4.16	72.10	136.34	144.65	6.38	47.20	41.75	78.99	22.29	89.03
Tl #	0.08	1.47	1.25	1.21	13.69	0.66	1.99	5.46	5.27	1.82
Ta #	0.04	0.34	0.48	0.48	0.34	0.23	0.41	0.43	0.30	0.44
Nb #	0.08	5.77	8.31	7.91	6.08	3.86	7.10	7.32	5.47	7.94
Hf #	0.21	4.74	5.37	5.51	4.13	2.84	4.44	4.61	3.55	5.10
Zr #	0.14	169.37	212.14	209.22	164.36	101.86	182.48	189.29	139.90	198.43
Y #	0.08	13.95	20.28	21.72	14.34	15.20	14.70	16.58	4.38	21.58
Th #	0.08	2.52	5.06	6.20	3.25	2.93	4.32	4.40	1.09	4.45
U #	0.09	0.92	1.76	2.52	2.30	1.12	1.86	1.94	1.75	1.68

Table A1-1 (continued) Major and trace lithogeochemical data for outcrop and drill core samples from Pilley's Island VMS district.

Sample ID	Det. Limit	11CPM-039	11CPM-040	11CPM-041	11CPM-042	11CPM-043	11CPM-044	11CPM-045	11CPM-046	11CPM-047
La #	0.09	8.14	10.90	15.59	10.35	9.60	9.30	9.17	3.00	8.49
Ce #	0.13	17.49	22.69	28.67	21.00	25.05	20.90	20.90	5.47	14.75
Pr #	0.06	2.09	3.04	3.77	2.69	2.93	2.42	2.43	0.77	2.47
Nd #	0.50	9.58	13.23	17.31	13.17	13.91	11.02	10.88	2.97	10.62
Sm #	0.36	4.34	6.24	6.84	5.27	6.58	4.78	5.38	1.42	2.80
Eu #	0.08	1.32	1.53	1.59	1.33	2.10	1.12	1.29	0.34	0.79
Gd #	0.16	3.40	4.22	4.80	3.57	4.26	3.09	3.53	0.83	3.12
Tb #	0.03	0.60	0.78	0.83	0.68	0.75	0.58	0.67	0.16	0.55
Dy #	0.13	3.50	4.54	4.64	3.45	4.32	3.16	3.58	0.86	3.73
Ho #	0.03	0.66	0.89	0.90	0.70	0.75	0.59	0.69	0.17	0.79
Er #	0.14	1.85	2.58	2.70	1.92	2.16	1.76	1.90	0.63	2.46
Tm #	0.04	0.32	0.49	0.51	0.34	0.45	0.37	0.35	0.18	0.43
Yb #	0.21	1.98	2.94	3.05	2.13	2.13	1.92	2.07	0.71	2.91
Lu #	0.05	0.33	0.48	0.55	0.35	0.32	0.30	0.35	0.12	0.45
Sericite Index[2]		3.29	65.55	55.76	48.04	98.09	38.13	50.95	61.21	95.28
Al_2O_3/Na_2O		9.22	5.67	4.83	174.11	7.23	4.72	6.30	71.06	4.32
CCPI[3]		66.33	51.47	46.34	65.82	82.70	48.28	50.20	82.06	46.69
AI[4]		73.24	58.79	45.32	94.92	78.12	55.50	62.59	86.97	45.75
Zn/TiO_2*10000		0.02	0.03	0.04	0.03	0.02	0.02	0.04	0.03	0.05
Nb/Y		0.41	0.41	0.36	0.42	0.25	0.48	0.44	1.25	0.37
Th/Yb		1.27	1.72	2.03	1.53	1.38	2.25	2.13	1.52	1.53
$[La/Yb]_{CN}$[5]		2.79	2.52	3.47	3.30	3.07	3.29	3.01	2.86	1.98
$[La/Sm]_{MN}$[6]		1.21	1.13	1.47	1.27	0.94	1.26	1.10	1.36	1.96
$[Nb/Th]_{MN}$[6]		0.28	0.20	0.15	0.23	0.16	0.20	0.20	0.61	0.22
Zr/Yb		76.92	85.46	72.26	68.51	77.06	47.92	95.07	91.58	196.56
Nb/Yb		2.91	2.83	2.59	2.85	1.81	3.70	3.54	7.68	2.72
Th/Nb		0.44	0.61	0.78	0.54	0.76	0.61	0.60	0.20	0.56
La/Sm		1.87	1.75	2.28	1.96	1.46	1.94	1.70	2.11	3.03

* wt%; ICP-OES

\# ppm; ICP-MS

LOI Loss On Ignition

[1] Universal Transverse Mercator, North American Datum 27 (UTM NAD27)

[2] Sericite Index = $100*K_2O/Na_2O + K_2O$

[3] CCPI = $100*(Fe_2O_3^T+MgO)/(Fe_2O_3^T+MgO+K_2O+Na_2O)$

[4] AI = $100*(K_2O+MgO)/(K_2O+MgO+CaO+Na_2O)$

[5] CN = chondrite normalized

[6] MN = primitive mantle normalized

\- < Limit of Detection

N.D. Not Detected

Table A1-1 (continued) Major and trace lithogeochemical data for outcrop and drill core samples from Pilley's Island VMS district.

Sample ID	Det. Limit	11CPM-048	11CPM-050	11CPM-051	11CPM-052	11CPM-053	11CPM-054	11CPM-055	11CPM-056	11CPM-057
Easting [1]		-	-	-	-	-	-	-	-	-
Northing [1]		-	-	-	-	-	-	-	-	-
Drillhole ID		83-02	83-02	83-02	83-02	83-02	83-02	83-02	83-05	83-05
From (m)		100.80	128.00	158.70	184.70	205.90	242.90	287.50	13.80	27.20
To (m)		101.30	128.50	159.20	185.20	206.40	243.40	288.00	14.30	27.70
Strat. unit		3.2	3.1	3.1	3.1	3.1	2	2	4.3	4.3
SiO_2 *	0.01	62.53	61.77	60.37	62.50	69.39	47.09	44.64	63.36	55.42
Al_2O_3 *	0.01	16.29	16.11	17.14	14.71	12.85	16.82	14.37	15.62	16.10
Fe_2O_3 *	0.01	4.65	4.47	4.26	4.32	3.61	8.69	6.93	5.23	12.72
MnO *	0.001	0.11	0.11	0.12	0.14	0.07	0.15	0.17	0.19	0.23
MgO *	0.01	1.45	1.61	1.61	1.66	1.27	8.77	5.79	2.91	2.28
CaO *	0.01	2.16	2.71	2.65	4.46	2.22	4.82	13.21	0.38	0.82
Na_2O *	0.01	3.16	2.27	4.16	2.10	5.89	3.89	4.29	2.47	0.16
K_2O *	0.01	4.27	4.82	3.60	4.05	0.47	2.06	0.93	2.97	4.98
TiO_2 *	0.001	0.59	0.55	0.57	0.50	0.43	0.97	0.47	0.67	0.61
P_2O_5 *	0.01	0.06	0.09	0.10	0.12	0.09	0.34	0.21	0.16	0.11
LOI *		5.62	6.17	5.64	6.38	2.65	6.59	8.09	6.17	5.64
TOTAL *		100.90	100.70	100.20	100.90	98.94	100.20	99.12	100.10	99.06
Cr^{52} #	3.65	4.62	5.08	4.84	-	15.70	92.10	124.91	8.21	11.42
Cr^{53} #	12.85	-	-	-	-	17.06	91.44	127.49	-	-
Ni #	5.14	-	-	-	-	-	43.79	50.02	8.45	-
Co #	0.26	2.58	3.51	4.09	3.58	3.66	30.49	22.06	3.37	3.98
Sc #	1.00	7.00	6.00	7.00	6.00	5.00	32.00	29.00	9.00	9.00
V #	3.42	15.13	18.37	19.42	17.71	14.21	235.18	188.63	18.36	12.45
Cu #	3.94	5.84	6.18	6.54	7.34	15.80	99.91	93.68	240.96	42.88
Pb #	0.25	8.75	9.88	11.02	9.14	10.18	5.40	4.41	18.92	42.80
Zn #	8.16	180.42	68.61	70.45	65.55	76.18	81.77	54.20	72.22	148.86
Bi #	0.06	0.08	0.08	0.10	0.10	0.07	-	-	0.25	1.03
Cd #	0.99	-	-	-	-	-	-	-	-	-
Sn #	0.12	1.75	1.55	1.69	1.47	1.39	0.63	0.64	1.29	1.46
Mo #	0.63	-	-	-	-	-	0.66	-	2.49	4.25
As #	1.33	11.73	14.32	10.44	6.42	7.09	16.22	28.86	13.89	52.96
Sb #	0.20	2.37	2.97	2.02	1.48	0.77	-	-	0.37	1.05
Ag #	0.23	0.67	0.57	0.66	0.63	0.53	0.28	-	0.77	1.64
Li #	0.79	2.34	2.37	4.16	15.58	5.42	21.89	9.07	4.74	3.78
Rb #	0.76	200.85	163.39	411.52	205.91	25.42	318.41	91.97	70.93	474.63
Cs #	0.08	0.97	1.10	1.00	1.16	0.13	0.61	0.24	0.24	0.57
Ba #	0.80	1158.85	385.10	252.77	248.94	184.75	369.05	267.47	268.59	1288.68
Sr #	4.16	68.03	52.78	67.97	64.31	67.63	223.30	224.04	24.80	7.02
Tl #	0.08	1.66	0.85	0.91	0.71	-	0.51	0.11	0.78	3.30
Ta #	0.04	0.42	0.39	0.46	0.42	0.37	0.18	0.07	0.42	0.42
Nb #	0.08	7.81	7.25	8.26	7.50	6.05	2.90	1.05	8.01	7.62
Hf #	0.21	4.68	4.41	5.42	4.73	3.95	2.14	0.86	4.91	5.19
Zr #	0.14	196.69	187.47	214.19	193.80	157.46	68.01	27.37	198.50	190.60
Y #	0.08	15.93	23.54	15.10	25.20	17.82	16.79	12.84	8.07	19.85
Th #	0.08	2.94	4.66	3.15	5.19	4.04	1.79	1.11	0.63	3.99
U #	0.09	1.40	1.55	1.81	1.63	2.00	0.73	0.29	1.45	2.36

Table A1-1 (continued) Major and trace lithogeochemical data for outcrop and drill core samples from Pilley's Island VMS district.

Sample ID	Det. Limit	11CPM-048	11CPM-050	11CPM-051	11CPM-052	11CPM-053	11CPM-054	11CPM-055	11CPM-056	11CPM-057
La #	0.09	6.54	9.31	6.54	12.17	8.55	6.60	5.26	2.78	12.66
Ce #	0.13	12.16	16.65	18.45	20.58	16.37	16.35	10.66	5.96	25.85
Pr #	0.06	1.74	2.86	1.77	3.50	2.14	2.34	1.42	0.78	3.54
Nd #	0.50	7.13	12.04	7.61	14.24	8.78	10.83	6.27	3.22	14.81
Sm #	0.36	1.96	3.04	1.92	3.46	2.09	3.05	1.68	0.86	3.54
Eu #	0.08	0.56	0.83	0.57	0.96	0.56	0.96	0.59	0.22	0.79
Gd #	0.16	2.19	3.36	2.23	3.71	2.26	2.92	2.01	1.00	3.49
Tb #	0.03	0.40	0.61	0.39	0.64	0.42	0.52	0.35	0.18	0.62
Dy #	0.13	2.70	4.17	2.47	4.34	2.78	3.21	2.26	1.30	3.92
Ho #	0.03	0.58	0.90	0.51	0.90	0.60	0.66	0.47	0.29	0.84
Er #	0.14	1.89	2.76	1.69	2.77	1.97	1.87	1.46	0.99	2.67
Tm #	0.04	0.32	0.44	0.28	0.51	0.35	0.27	0.25	0.19	0.44
Yb #	0.21	2.09	3.06	1.92	3.19	2.33	1.83	1.39	1.36	3.02
Lu #	0.05	0.31	0.47	0.31	0.49	0.39	0.27	0.21	0.20	0.44
Sericite Index[2]		49.93	57.47	67.98	46.39	65.85	7.39	34.62	17.82	54.60
Al_2O_3/Na_2O		5.16	7.10	4.12	7.00	2.18	4.32	3.35	6.32	100.63
CCPI[3]		45.08	46.17	43.07	49.30	43.42	74.58	70.90	59.94	74.48
AI[4]		51.81	56.35	43.34	46.54	17.66	55.42	27.75	67.35	88.11
Zn/TiO_2*10000		0.03	0.03	0.04	0.03	0.03	0.02	0.00	0.04	0.03
Nb/Y		0.49	0.31	0.55	0.30	0.34	0.17	0.08	0.99	0.38
Th/Yb		1.41	1.52	1.64	1.63	1.73	0.98	0.80	0.47	1.32
$[La/Yb]_{CN}$[5]		2.13	2.07	2.32	2.59	2.49	2.45	2.56	1.39	2.85
$[La/Sm]_{MN}$[6]		2.16	1.98	2.21	2.27	2.64	1.40	2.02	2.10	2.31
$[Nb/Th]_{MN}$[6]		0.32	0.19	0.32	0.17	0.18	0.20	0.11	1.53	0.23
Zr/Yb		68.11	94.33	61.24	111.67	60.81	67.46	37.21	19.64	146.35
Nb/Yb		3.74	2.37	4.31	2.35	2.59	1.58	0.75	5.90	2.52
Th/Nb		0.38	0.64	0.38	0.69	0.67	0.62	1.06	0.08	0.52
La/Sm		3.34	3.07	3.41	3.51	4.09	2.17	3.13	3.25	3.57

* wt%; ICP-OES

ppm; ICP-MS

LOI Loss On Ignition

[1] Universal Transverse Mercator, North American Datum 27 (UTM NAD27)

[2] Sericite Index = $100*K_2O/Na_2O+K_2O$

[3] CCPI = $100*(Fe_2O_3{}^{1}+MgO)/(Fe_2O_3{}^{1}+MgO+K_2O+Na_2O)$

[4] AI = $100*(K_2O+MgO)/(K_2O+MgO+CaO+Na_2O)$

[5] CN = chondrite normalized

[6] MN = primitive mantle normalized

\- < Limit of Detection

N.D. Not Detected

Table A1-1 (continued) Major and trace lithogeochemical data for outcrop and drill core samples from Pilley's Island VMS district.

Sample ID	Det. Limit	11CPM-058	11CPM-059	11CPM-060	11CPM-062	11CPM-063	11CPM-065	11CPM-066	11CPM-067	11CPM-077
Easting [1]		-	-	-	-	-	-	-	-	-
Northing [1]		-	-	-	-	-	-	-	-	-
Drillhole ID		83-05	83-05	83-05	83-05	83-05	83-05	83-05	83-05	84-18
From (m)		50.60	77.40	87.90	123.50	132.20	155.50	164.00	172.80	129.20
To (m)		51.60	77.80	88.40	124.00	132.70	156.00	164.50	173.30	129.70
Strat. unit		4.3	4.3	4.3	4.3	2	2	2	2	3.5
SiO_2 *	0.01	62.81	58.68	62.08	49.81	46.76	25.61	47.12	46.64	49.77
Al_2O_3 *	0.01	15.23	17.07	15.76	15.38	20.87	19.52	15.26	16.03	15.88
Fe_2O_3 *	0.01	5.89	10.79	7.27	19.06	15.87	28.72	8.64	8.46	13.05
MnO *	0.001	0.08	0.05	0.04	0.02	0.19	0.28	0.33	0.17	0.88
MgO *	0.01	2.55	3.13	1.80	0.82	7.85	11.34	12.42	8.41	6.28
CaO *	0.01	0.21	0.23	0.20	0.15	0.45	0.70	7.44	5.57	0.86
Na_2O *	0.01	0.10	0.16	0.14	0.15	1.44	0.08	2.23	3.87	0.53
K_2O *	0.01	4.64	4.97	4.39	4.64	2.84	1.34	0.15	1.07	3.24
TiO_2 *	0.001	0.55	0.63	0.58	0.56	0.82	0.80	0.64	0.73	0.85
P_2O_5 *	0.01	0.12	0.13	0.13	0.06	0.21	0.47	0.24	0.41	0.34
LOI *		6.38	2.65	6.59	8.09	3.41	9.44	5.98	7.68	6.52
TOTAL *		98.54	98.48	98.98	98.76	100.70	98.31	100.50	99.03	98.19
Cr^{52} #	3.65	12.26	13.42	15.05	87.04	114.21	239.50	798.25	369.63	32.26
Cr^{53} #	12.85	14.35	13.68	16.49	85.17	113.55	238.80	785.75	372.42	31.22
Ni #	5.14	-	-	-	40.39	39.54	111.09	276.32	148.85	14.99
Co #	0.26	3.54	3.57	4.92	27.15	28.35	25.06	37.68	32.23	29.47
Sc #	1.00	7.00	8.00	8.00	33.00	32.00	36.00	36.00	34.00	23.00
V #	3.42	16.28	16.99	17.11	223.48	267.34	251.02	201.65	224.40	252.24
Cu #	3.94	678.67	1607.51	81.69	835.18	189.68	462.69	9.14	98.97	531.81
Pb #	0.25	25.08	14.90	6.61	33.02	3.20	11.60	2.04	3.62	8.45
Zn #	8.16	946.57	287.86	33.11	107.67	53.55	162.50	137.50	78.88	221.04
Bi #	0.06	0.50	0.75	0.78	1.01	0.66	2.63	-	-	0.42
Cd #	0.99	3.11	1.14	-	-	-	-	-	-	-
Sn #	0.12	1.51	1.84	1.29	0.41	0.82	0.33	0.40	0.53	1.15
Mo #	0.63	4.18	1.50	2.84	1.30	0.65	3.76	-	-	1.30
As #	1.33	25.44	21.33	20.45	57.65	3.24	28.73	1.65	5.95	9.94
Sb #	0.20	0.56	0.49	2.01	1.15	-	-	-	0.30	0.39
Ag #	0.23	0.93	0.79	0.79	1.42	-	0.32	-	0.29	0.37
Li #	0.79	2.85	1.87	2.19	1.05	5.80	12.49	16.88	13.93	11.97
Rb #	0.76	137.25	306.05	121.74	520.41	157.40	99.28	120.39	223.10	241.38
Cs #	0.08	0.23	0.19	0.20	0.23	0.27	0.29	0.27	0.63	0.91
Ba #	0.80	1089.84	1122.95	1411.04	437.45	1332.16	312.97	196.98	448.57	2055.84
Sr #	4.16	6.38	-	-	-	11.01	9.49	92.97	198.75	39.46
Tl #	0.08	1.30	1.55	0.89	3.91	0.42	0.30	0.15	0.53	1.28
Ta #	0.04	0.41	0.43	0.43	0.07	0.09	0.16	0.11	0.13	0.24
Nb #	0.08	7.44	7.56	7.92	1.26	1.69	2.96	2.00	2.44	4.63
Hf #	0.21	4.65	4.83	4.99	1.14	1.47	2.00	1.55	1.64	2.05
Zr #	0.14	186.60	187.55	200.16	34.89	49.42	65.71	45.18	58.05	77.73
Y #	0.08	8.97	9.17	5.90	0.81	11.97	14.59	12.76	15.59	13.35
Th #	0.08	2.41	2.04	1.46	0.14	1.33	2.37	1.55	1.64	2.46
U #	0.09	1.72	1.53	1.71	0.33	1.07	0.92	0.49	0.85	0.75

Table A1-1 (continued) Major and trace lithogeochemical data for outcrop and drill core samples from Pilley's Island VMS district.

Sample ID	Det. Limit	11CPM-058	11CPM-059	11CPM-060	11CPM-062	11CPM-063	11CPM-065	11CPM-066	11CPM-067	11CPM-077
La #	0.09	5.16	5.57	1.92	0.38	4.29	5.80	7.57	7.96	9.40
Ce #	0.13	11.32	10.15	3.91	0.65	9.75	13.73	16.00	18.09	20.15
Pr #	0.06	1.56	1.48	0.66	0.14	1.38	2.18	2.15	2.46	2.61
Nd #	0.50	6.45	5.86	2.63	0.56	6.36	10.01	9.36	11.15	11.07
Sm #	0.36	1.54	1.41	0.74	-	1.74	2.59	2.41	2.70	2.64
Eu #	0.08	0.48	0.27	0.16	-	0.65	0.40	0.77	0.92	0.90
Gd #	0.16	1.64	1.47	0.80	0.18	2.16	3.00	2.60	3.03	2.71
Tb #	0.03	0.28	0.25	0.17	0.04	0.36	0.41	0.41	0.49	0.42
Dy #	0.13	1.89	1.74	1.32	0.22	2.37	2.70	2.59	2.93	2.77
Ho #	0.03	0.39	0.38	0.30	0.05	0.51	0.54	0.49	0.60	0.55
Er #	0.14	1.29	1.27	1.06	0.20	1.48	1.72	1.39	1.65	1.64
Tm #	0.04	0.25	0.25	0.21	0.04	0.28	0.29	0.22	0.26	0.28
Yb #	0.21	1.42	1.35	1.30	-	1.48	1.70	1.33	1.58	1.82
Lu #	0.05	0.21	0.21	0.19	-	0.22	0.26	0.20	0.23	0.27
Sericite Index[2]		96.89	97.89	96.88	96.91	96.87	66.36	94.37	6.30	21.66
Al_2O_3/Na_2O		152.30	106.69	112.57	102.53	14.49	244.00	6.84	4.14	29.96
CCPI[3]		64.04	73.07	66.69	80.58	84.71	96.58	89.85	77.35	83.68
AI[4]		95.87	95.41	94.79	94.79	84.98	94.21	56.52	50.11	87.26
$Zn/TiO_2*10000$		0.03	0.03	0.03	0.01	0.01	0.01	0.01	0.01	0.01
Nb/Y		0.83	0.82	1.34	1.56	0.14	0.20	0.16	0.16	0.35
Th/Yb		1.70	1.51	1.12	-	0.90	1.40	1.17	1.04	1.35
$[La/Yb]_{CN}$[5]		2.48	2.80	1.01	-	1.97	2.32	3.87	3.42	3.50
$[La/Sm]_{MN}$[6]		2.17	2.55	1.69	-	1.59	1.45	2.03	1.91	2.30
$[Nb/Th]_{MN}$[6]		0.37	0.45	0.66	1.10	0.15	0.15	0.16	0.18	0.23
Zr/Yb		63.15	131.86	138.93	153.95	-	33.49	38.70	34.02	36.73
Nb/Yb		5.26	5.60	6.09	-	1.14	1.75	1.51	1.55	2.54
Th/Nb		0.32	0.27	0.18	0.11	0.79	0.80	0.77	0.67	0.53
La/Sm		3.36	3.94	2.62	-	2.46	2.24	3.14	2.95	3.55

* wt%; ICP-OES

\# ppm; ICP-MS

LOI Loss On Ignition

[1] Universal Transverse Mercator, North American Datum 27 (UTM NAD27)

[2] Sericite Index = $100*K_2O/Na_2O + K_2O$

[3] CCPI = $100*(Fe_2O_3^T+MgO)/(Fe_2O_3^T+MgO+K_2O+Na_2O)$

[4] AI = $100*(K_2O+MgO)/(K_2O+MgO+CaO+Na_2O)$

[5] CN = chondrite normalized

[6] MN = primitive mantle normalized

\- < Limit of Detection

N.D. Not Detected

Table A1-1 (continued) Major and trace lithogeochemical data for outcrop and drill core samples from Pilley's Island VMS district.

Sample ID	Det. Limit	11CPM-078	11CPM-080	11CPM-084	11CPM-087	11CPM-088	11CPM-089	11CPM-090	11CPM-091	11CPM-092
Easting [1]		-	-	-	-	-	-	-	-	-
Northing [1]		-	-	-	-	-	-	-	-	-
Drillhole ID		84-14	84-14	84-14	PI-01-01	PI-01-01	PI-01-01	PI-01-01	PI-01-01	PI-01-01
From (m)		57.30	90.30	230.40	54.50	76.20	157.60	188.60	242.30	261.30
To (m)		58.30	90.80	230.70	55.00	76.40	158.00	189.00	242.80	261.80
Strat. unit		4.2	3.3	2	4.3	4.3	4.2	3.2	3.1	3.5
SiO_2 *	0.01	63.57	59.77	63.58	72.32	61.64	62.95	61.43	62.53	37.70
Al_2O_3 *	0.01	13.53	15.43	15.90	12.16	16.48	15.81	16.87	16.69	16.41
Fe_2O_3 *	0.01	3.74	5.62	3.90	2.51	4.38	4.92	5.10	5.49	8.84
MnO *	0.001	0.27	0.20	0.12	0.09	0.19	0.18	0.15	0.21	0.63
MgO *	0.01	0.90	3.07	1.13	0.73	3.62	2.85	2.87	3.78	6.78
CaO *	0.01	2.14	2.86	7.81	1.90	0.49	1.57	0.99	0.53	8.56
Na_2O *	0.01	0.75	2.59	3.72	1.68	2.40	4.10	3.07	3.20	1.31
K_2O *	0.01	7.62	3.21	0.56	4.50	6.45	2.85	4.93	3.65	4.14
TiO_2 *	0.001	0.49	0.72	0.55	0.45	0.60	0.68	0.71	0.71	1.07
P_2O_5 *	0.01	0.12	0.22	0.11	0.11	0.15	0.22	0.21	0.22	0.34
LOI *		4.79	7.17	2.91	3.46	3.14	3.70	3.62	3.58	13.63
TOTAL *		97.90	100.80	100.30	99.91	99.53	99.82	99.93	100.60	99.41
Cr^{52} #	3.65	9.29	17.28	21.52	-	-	6.23	6.33	6.07	290.69
Cr^{53} #	12.85	-	17.38	22.44	-	-	-	-	-	288.99
Ni #	5.14	-	5.15	-	-	-	-	-	-	121.80
Co #	0.26	3.95	10.32	3.27	2.00	3.67	6.54	6.12	6.71	38.53
Sc #	1.00	7.00	14.00	7.00	6.00	8.00	11.00	11.00	11.00	45.00
V #	3.42	13.12	88.55	20.43	14.80	18.68	96.58	54.35	56.18	300.29
Cu #	3.94	93.34	5.87	15.44	202.62	70.17	-	-	-	105.67
Pb #	0.25	24.07	12.70	15.27	4.86	6.46	6.91	11.00	17.30	6.97
Zn #	8.16	3005.80	150.68	81.18	24.13	164.80	109.76	132.02	175.75	225.47
Bi #	0.06	0.62	0.09	0.07	0.14	-	-	0.07	0.09	-
Cd #	0.99	10.51	-	1.29	-	16.07	-	-	-	-
Sn #	0.12	1.06	1.03	1.51	1.25	1.85	1.33	1.39	1.19	0.81
Mo #	0.63	9.98	-	0.69	1.16	-	-	-	-	-
As #	1.33	10.31	1.75	12.91	1.35	2.11	1.47	5.58	3.70	28.10
Sb #	0.20	0.70	0.23	0.51	0.27	0.25	-	-	-	-
Ag #	0.23	0.85	0.48	0.78	0.52	0.60	0.52	0.64	0.58	0.68
Li #	0.79	4.39	9.22	3.26	2.32	7.77	5.15	4.97	6.76	24.24
Rb #	0.76	927.76	208.24	184.67	280.69	158.26	402.26	233.82	89.29	809.43
Cs #	0.08	0.41	0.93	0.34	0.48	0.25	0.39	0.49	0.39	1.76
Ba #	0.80	1142.99	121.32	102.80	1702.01	1518.82	1581.49	334.90	286.76	573.17
Sr #	4.16	29.03	30.61	165.12	23.02	54.62	63.64	18.84	53.52	138.73
Tl #	0.08	1.71	0.63	0.32	0.92	0.81	0.65	0.89	0.66	1.17
Ta #	0.04	0.32	0.31	0.40	0.31	0.43	0.32	0.36	0.34	0.12
Nb #	0.08	6.74	5.18	7.28	5.94	8.13	5.70	6.23	5.93	2.39
Hf #	0.21	4.34	3.53	4.57	3.55	4.86	3.99	4.21	3.94	1.95
Zr #	0.14	162.78	141.71	181.84	145.98	200.81	159.54	170.60	164.82	50.76
Y #	0.08	22.17	22.46	24.97	15.79	7.66	17.28	8.31	8.03	22.95
Th #	0.08	3.81	2.93	5.28	2.98	0.84	2.48	0.86	0.86	2.60
U #	0.09	1.73	1.12	1.89	1.13	1.20	1.02	0.69	1.05	0.62

Table A1-1 (continued) Major and trace lithogeochemical data for outcrop and drill core samples from Pilley's Island VMS district.

Sample ID	Det. Limit	11CPM-078	11CPM-080	11CPM-084	11CPM-087	11CPM-088	11CPM-089	11CPM-090	11CPM-091	11CPM-092
La #	0.09	8.68	9.13	13.00	5.64	4.30	6.96	3.30	2.75	13.05
Ce #	0.13	17.21	14.57	28.61	12.57	8.86	10.65	6.52	6.57	27.39
Pr #	0.06	2.72	2.76	3.37	1.80	1.16	2.03	0.90	0.85	3.77
Nd #	0.50	11.99	12.08	13.68	7.33	4.61	8.97	3.98	3.52	17.01
Sm #	0.36	3.20	3.14	3.52	1.99	1.12	2.15	1.18	0.93	4.34
Eu #	0.08	0.81	0.97	0.99	0.61	0.28	0.73	0.37	0.26	1.54
Gd #	0.16	3.25	3.56	3.83	2.19	1.15	2.56	1.21	1.01	4.82
Tb #	0.03	0.58	0.59	0.67	0.39	0.21	0.47	0.22	0.19	0.79
Dy #	0.13	3.81	3.97	4.37	2.82	1.41	2.95	1.46	1.49	4.58
Ho #	0.03	0.86	0.83	0.94	0.59	0.32	0.63	0.32	0.33	0.92
Er #	0.14	2.64	2.58	2.88	1.83	1.07	2.02	1.05	1.09	2.41
Tm #	0.04	0.45	0.43	0.46	0.30	0.20	0.33	0.20	0.22	0.36
Yb #	0.21	2.96	2.71	3.06	2.01	1.19	2.21	1.33	1.36	2.19
Lu #	0.05	0.45	0.43	0.47	0.31	0.17	0.35	0.20	0.21	0.31
Sericite Index[2]		85.94	91.04	55.34	13.08	72.82	72.88	41.01	61.63	53.28
Al_2O_3/Na_2O		18.04	5.96	4.27	7.24	6.87	3.86	5.50	5.22	12.53
CCPI[3]		35.66	59.97	54.03	34.39	47.48	52.79	49.91	57.51	74.13
AI[4]		74.67	53.54	12.78	59.36	77.70	50.13	65.77	66.58	52.53
$Zn/TiO_2*10000$		0.02	0.03	0.03	0.03	0.04	0.03	0.03	0.02	0.01
Nb/Y		0.30	0.23	0.29	0.38	1.06	0.33	0.75	0.74	0.10
Th/Yb		1.28	1.08	1.73	1.48	0.71	1.12	0.65	0.64	1.19
$[La/Yb]_{CN}$[5]		1.99	2.29	2.89	1.91	2.44	2.14	1.69	1.37	4.04
$[La/Sm]_{MN}$[6]		1.75	1.88	2.39	1.83	2.49	2.09	1.80	1.91	1.94
$[Nb/Th]_{MN}$[6]		0.21	0.21	0.17	0.24	1.16	0.28	0.87	0.83	0.11
Zr/Yb		42.68	54.91	52.24	59.44	72.60	168.21	72.31	128.70	121.48
Nb/Yb		2.27	1.91	2.38	2.95	6.81	2.58	4.70	4.37	1.09
Th/Nb		0.57	0.57	0.73	0.50	0.10	0.44	0.14	0.15	1.09
La/Sm		2.71	2.91	3.69	2.83	3.85	3.23	2.79	2.96	3.01

* wt%; ICP-OES

\# ppm; ICP-MS

LOI Loss On Ignition

[1] Universal Transverse Mercator, North American Datum 27 (UTM NAD27)

[2] Sericite Index = $100*K_2O/Na_2O+K_2O$

[3] CCPI = $100*(Fe_2O_3^T+MgO)/(Fe_2O_3^T+MgO+K_2O+Na_2O)$

[4] AI = $100*(K_2O+MgO)/(K_2O+MgO+CaO+Na_2O)$

[5] CN = chondrite normalized

[6] MN = primitive mantle normalized

\- < Limit of Detection

N.D. Not Detected

Table A1-1 (continued) Major and trace lithogeochemical data for outcrop and drill core samples from Pilley's Island VMS district.

Sample ID	Det. Limit	11CPM-095	11CPM-096	11CPM-097	11CPM-099	11CPM-101	11CPM-102	11CPM-103	11CPM-104	11CPM-105
Easting [1]		-	-	-	-	-	-	-	-	-
Northing [1]		-	-	-	-	-	-	-	-	-
Drillhole ID		PI-01-01	PI-01-04	PI-01-04	PI-01-04	PI-01-04	PI-01-04	PI-01-04	PI-01-04	PI-01-04
From (m)		438.70	22.50	60.70	115.10	234.90	295.80	321.20	346.30	379.80
To (m)		439.10	22.90	61.10	115.50	235.30	296.20	321.60	346.60	380.10
Strat. unit		2	6.2	6.1	4.2	4.2	4.4	4.1	4.2	4.2
SiO_2 *	0.01	48.98	65.84	35.04	59.60	59.98	62.49	51.50	62.07	45.76
Al_2O_3 *	0.01	16.27	15.85	10.36	19.29	15.83	16.70	15.56	9.98	14.45
Fe_2O_3 *	0.01	8.25	2.95	9.77	4.63	5.15	5.24	15.22	13.26	7.42
MnO *	0.001	0.13	0.06	0.20	0.06	0.20	0.21	0.02	0.01	0.46
MgO *	0.01	7.03	1.89	18.99	2.40	3.07	4.41	0.94	0.53	5.79
CaO *	0.01	7.58	1.33	9.01	0.47	2.11	0.38	0.34	0.37	5.89
Na_2O *	0.01	4.95	2.31	0.17	0.53	3.21	4.36	0.13	0.11	4.51
K_2O *	0.01	0.90	4.12	0.03	7.61	3.22	1.78	4.89	3.10	1.29
TiO_2 *	0.001	0.61	0.27	0.62	0.70	0.68	0.69	0.61	0.56	0.55
P_2O_5 *	0.01	0.26	0.07	0.14	0.16	0.22	0.21	0.25	0.26	0.24
LOI *		5.83	4.53	15.02	4.43	4.47	3.61	10.29	8.49	12.35
TOTAL *		100.80	99.21	99.35	99.87	98.12	100.10	99.76	98.73	98.73
Cr^{52} #	3.65	49.33	20.48	2025.57	4.39	8.27	5.13	38.53	15.47	40.27
Cr^{53} #	12.85	46.04	17.34	1975.00	-	-	-	37.35	17.02	39.65
Ni #	5.14	52.63	7.10	801.03	-	5.67	-	47.60	13.68	44.93
Co #	0.26	34.11	3.80	72.44	3.19	7.08	6.44	34.82	50.90	32.35
Sc #	1.00	33.00	5.00	28.00	11.00	12.00	11.00	33.00	15.00	29.00
V #	3.42	213.78	20.30	172.91	15.16	63.24	55.66	249.24	174.44	197.77
Cu #	3.94	125.48	13.71	55.49	5.07	634.49	-	80.74	16.15	128.77
Pb #	0.25	4.54	9.52	6.34	17.96	7.08	2.67	11.03	4.26	31.27
Zn #	8.16	65.92	55.93	81.45	110.21	83.86	142.10	70.44	17.59	94.28
Bi #	0.06	-	0.11	-	0.13	-	0.08	2.87	0.66	0.07
Cd #	0.99	-	-	-	-	-	-	-	-	-
Sn #	0.12	0.69	1.73	0.40	2.00	0.74	1.14	1.70	0.75	0.38
Mo #	0.63	-	-	-	2.12	-	-	5.43	3.00	0.92
As #	1.33	10.85	2.78	11.11	3.09	1.65	1.47	122.94	15.38	26.80
Sb #	0.20	-	1.08	-	0.71	0.23	-	2.37	-	0.90
Ag #	0.23	0.23	0.82	0.23	0.92	0.54	0.58	4.09	0.29	0.51
Li #	0.79	32.98	6.02	68.77	3.78	3.94	5.13	0.84	1.69	10.05
Rb #	0.76	119.08	276.65	58.80	566.61	372.14	114.28	583.79	193.60	131.52
Cs #	0.08	0.17	1.88	0.96	1.18	0.58	0.57	0.34	0.35	0.64
Ba #	0.80	475.02	335.66	66.03	103.48	539.29	481.12	455.91	391.84	283.48
Sr #	4.16	399.99	36.30	62.90	7.62	31.91	58.55	-	-	145.61
Tl #	0.08	-	0.66	-	1.60	1.12	0.26	13.72	0.34	1.29
Ta #	0.04	0.26	0.50	0.12	0.49	0.32	0.36	0.13	0.15	0.22
Nb #	0.08	5.19	8.91	2.27	9.15	5.78	6.18	4.30	3.20	4.87
Hf #	0.21	1.33	6.05	1.56	5.89	3.89	4.29	1.29	1.46	1.25
Zr #	0.14	43.63	241.91	45.73	233.89	158.96	174.29	43.93	52.38	40.93
Y #	0.08	13.72	9.77	13.17	5.44	22.69	9.97	1.17	0.60	13.62
Th #	0.08	1.98	2.04	1.81	1.30	3.10	0.82	0.17	0.17	1.83
U #	0.09	0.74	1.19	0.42	1.17	0.90	0.99	1.41	0.44	0.52

Table A1-1 (continued) Major and trace lithogeochemical data for outcrop and drill core samples from Pilley's Island VMS district.

Sample ID	Det. Limit	11CPM-095	11CPM-096	11CPM-097	11CPM-099	11CPM-101	11CPM-102	11CPM-103	11CPM-104	11CPM-105
La #	0.09	7.00	3.82	11.29	2.08	9.04	4.14	0.44	0.26	7.15
Ce #	0.13	15.08	9.55	22.94	6.26	15.04	6.86	0.85	0.35	15.02
Pr #	0.06	2.05	1.14	2.82	0.79	2.98	1.01	0.16	0.13	2.15
Nd #	0.50	9.16	4.46	12.10	3.50	13.15	4.14	0.70	-	9.33
Sm #	0.36	2.48	1.19	2.84	0.88	3.47	1.07	-	-	2.54
Eu #	0.08	0.82	0.20	0.85	0.21	1.09	0.35	-	-	0.85
Gd #	0.16	2.67	1.32	2.85	1.00	3.63	1.33	0.26	-	2.76
Tb #	0.03	0.43	0.25	0.45	0.21	0.61	0.24	0.05	-	0.43
Dy #	0.13	2.57	1.73	2.61	1.32	3.96	1.65	0.36	-	2.55
Ho #	0.03	0.52	0.37	0.50	0.29	0.84	0.37	0.09	-	0.53
Er #	0.14	1.47	1.22	1.45	1.02	2.62	1.25	0.25	0.16	1.57
Tm #	0.04	0.24	0.23	0.22	0.18	0.51	0.26	0.05	0.07	0.29
Yb #	0.21	1.40	1.51	1.33	1.23	2.92	1.71	0.28	-	1.43
Lu #	0.05	0.21	0.25	0.20	0.19	0.43	0.26	-	-	0.20
Sericite Index[2]		75.96	15.38	64.07	15.00	93.49	50.08	28.99	97.41	96.57
Al_2O_3/Na_2O		3.29	6.86	60.94	36.40	4.93	3.83	119.69	90.73	3.20
CCPI[3]		72.31	42.95	99.31	46.34	56.11	61.11	76.30	81.12	69.49
AI[4]		38.76	62.28	67.45	90.92	54.18	56.63	92.54	88.32	40.50
Zn/TiO_2*10000		0.00	0.04	0.02	0.04	0.02	0.03	0.01	0.01	0.01
Nb/Y		0.38	0.91	0.17	1.68	0.25	0.62	3.66	5.30	0.36
Th/Yb		1.42	1.35	1.36	1.06	1.06	0.48	0.61	-	1.28
$[La/Yb]_{CN}$[5]		3.40	1.72	5.77	1.15	2.11	1.64	1.08	-	3.40
$[La/Sm]_{MN}$[6]		1.83	2.08	2.57	1.52	1.68	2.50	-	-	1.82
$[Nb/Th]_{MN}$[6]		0.32	0.53	0.15	0.85	0.23	0.91	3.05	2.32	0.32
Zr/Yb		23.15	31.24	160.53	34.36	190.71	54.52	101.84	158.66	-
Nb/Yb		3.72	5.91	1.70	7.46	1.98	3.61	15.51	-	3.40
Th/Nb		0.38	0.23	0.80	0.14	0.54	0.13	0.04	0.05	0.38
La/Sm		2.82	3.22	3.98	2.36	2.61	3.86	-	-	2.82

* wt%; ICP-OES

ppm; ICP-MS

LOI Loss On Ignition

[1] Universal Transverse Mercator, North American Datum 27 (UTM NAD27)

[2] Sericite Index = 100*K_2O/Na_2O +K_2O

[3] CCPI = 100*(Fe_2O_3[1] +MgO)/(Fe_2O_3[1] +MgO+K_2O+Na_2O)

[4] AI = 100*(K_2O+MgO)/(K_2O+MgO+CaO+Na_2O)

[5] CN = chondrite normalized

[6] MN = primitive mantle normalized

- < Limit of Detection

N.D. Not Detected

Table A1-1 (continued) Major and trace lithogeochemical data for outcrop and drill core samples from Pilley's Island VMS district.

Sample ID	Det. Limit	11CPM-106	11CPM-108	11CPM-110	11CPM-111	11CPM-114	11CPM-116	11CPM-119	11CPM-121	11CPM-122
Easting [1]		-	-	-	-	-	-	-	-	-
Northing [1]		-	-	-	-	-	-	-	-	-
Drillhole ID		PI-01-04	PI-01-02	PI-01-02	PI-01-02	PI-01-02	PI-01-02	PI-02-01	PI-02-01	PI-02-01
From (m)		391.40	5.70	80.60	132.20	222.70	314.80	338.70	472.70	555.40
To (m)		391.80	6.10	81.00	132.60	223.10	315.20	339.10	473.00	555.70
Strat. unit		2	4.6	4.6	3.4	3.4	2	6.2	4.2	4.2
SiO_2 *	0.01	68.30	63.23	58.15	63.54	58.90	52.30	67.77	67.66	70.79
Al_2O_3 *	0.01	15.04	16.39	15.99	15.74	15.96	13.87	15.07	14.75	14.39
Fe_2O_3 *	0.01	2.89	3.95	6.55	5.22	5.00	7.00	2.74	4.50	3.01
MnO *	0.001	0.05	0.22	0.35	0.50	0.12	0.13	0.07	0.08	0.04
MgO *	0.01	1.46	1.32	3.27	2.05	2.78	5.36	1.50	2.41	3.34
CaO *	0.01	1.42	2.29	2.80	0.72	2.69	9.24	1.50	0.60	0.19
Na_2O *	0.01	5.69	2.37	0.16	3.10	4.39	3.88	2.40	2.69	0.39
K_2O *	0.01	3.05	6.56	6.90	5.58	2.56	3.16	4.44	2.81	3.48
TiO_2 *	0.001	0.44	0.59	0.73	0.67	0.66	0.51	0.24	0.64	0.48
P_2O_5 *	0.01	0.12	0.17	0.21	0.22	0.20	0.20	0.06	0.17	0.12
LOI *		2.47	3.90	5.13	2.44	5.96	3.39	3.57	3.74	3.49
TOTAL *		100.90	101.00	100.20	99.78	99.22	99.06	99.36	100.00	99.72
Cr^{52} #	3.65	-	-	11.24	6.74	5.34	44.30	7.55	-	-
Cr^{53} #	12.85	-	-	-	-	-	41.88	-	-	-
Ni #	5.14	-	-	7.51	-	5.55	76.95	11.79	18.76	-
Co #	0.26	3.56	2.93	4.35	4.93	7.39	25.74	3.95	6.29	2.47
Sc #	1.00	5.00	9.00	15.00	12.00	11.00	29.00	5.00	11.00	7.00
V #	3.42	17.84	12.84	89.49	68.54	65.82	189.15	14.85	41.54	21.05
Cu #	3.94	22.51	20.23	-	-	-	132.19	9.29	11.29	5.02
Pb #	0.25	15.44	22.01	9.67	16.78	8.98	3.42	8.72	4.11	0.79
Zn #	8.16	51.73	80.83	167.48	142.35	106.88	192.96	53.90	122.68	28.49
Bi #	0.06	0.17	0.09	-	-	0.06	-	-	0.25	-
Cd #	0.99	-	-	-	-	-	1.73	-	-	1.22
Sn #	0.12	1.45	1.33	0.53	1.09	0.94	0.66	1.43	1.05	0.86
Mo #	0.63	3.04	3.23	-	-	-	-	0.84	2.52	7.37
As #	1.33	15.18	15.87	1.53	4.77	1.77	28.44	5.08	4.00	3.42
Sb #	0.20	0.48	0.36	-	0.23	0.33	0.22	-	0.26	-
Ag #	0.23	0.71	0.70	0.49	0.54	0.51	-	0.78	1.03	0.70
Li #	0.79	2.74	3.20	5.51	4.93	5.85	-	-	-	-
Rb #	0.76	506.21	540.78	345.70	1124.04	280.18	893.87	357.03	116.99	1377.67
Cs #	0.08	0.10	0.48	0.79	0.30	0.47	0.09	2.34	0.44	0.40
Ba #	0.80	750.70	1048.24	1127.76	915.11	218.91	470.92	282.36	417.95	609.12
Sr #	4.16	56.55	31.77	35.45	34.10	49.40	182.15	33.72	19.05	9.22
Tl #	0.08	0.71	1.26	1.23	1.56	0.55	0.70	0.82	0.32	0.83
Ta #	0.04	0.23	0.21	0.28	0.22	0.31	0.14	0.47	0.38	0.33
Nb #	0.08	7.20	7.79	5.01	5.57	5.60	3.05	9.29	7.43	7.87
Hf #	0.21	5.00	5.05	3.69	3.90	3.83	1.21	6.31	4.69	5.29
Zr #	0.14	188.96	191.87	142.83	155.14	158.71	39.27	219.62	187.71	204.67
Y #	0.08	7.25	27.69	17.20	9.65	24.53	11.56	15.78	7.37	23.22
Th #	0.08	2.73	3.69	2.29	1.66	3.76	1.51	4.62	0.45	3.53
U #	0.09	1.74	1.39	0.73	0.90	1.32	0.53	1.33	0.86	1.34

Table A1-1 (continued) Major and trace lithogeochemical data for outcrop and drill core samples from Pilley's Island VMS district.

Sample ID	Det. Limit	11CPM-106	11CPM-108	11CPM-110	11CPM-111	11CPM-114	11CPM-116	11CPM-119	11CPM-121	11CPM-122
La #	0.09	6.03	9.86	5.50	6.43	10.26	6.31	5.77	3.34	10.25
Ce #	0.13	12.91	17.68	9.79	11.79	14.14	13.48	12.65	7.06	27.30
Pr #	0.06	1.46	2.93	1.73	1.60	3.18	1.80	1.85	0.93	3.66
Nd #	0.50	5.38	11.63	7.37	6.49	13.48	9.57	7.16	3.02	16.67
Sm #	0.36	1.26	3.13	2.02	1.60	3.46	2.45	1.59	0.72	4.77
Eu #	0.08	0.35	1.01	0.72	0.51	1.02	0.85	0.25	-	0.33
Gd #	0.16	1.28	3.67	2.35	1.52	3.67	2.52	1.90	1.47	3.21
Tb #	0.03	0.23	0.63	0.41	0.29	0.65	0.33	0.38	0.20	0.65
Dy #	0.13	1.33	4.41	2.95	1.76	4.13	2.20	2.63	1.26	4.18
Ho #	0.03	0.28	0.93	0.61	0.38	0.90	0.45	0.65	0.27	0.98
Er #	0.14	0.78	3.05	1.99	1.18	2.87	1.13	1.98	0.96	3.04
Tm #	0.04	0.17	0.52	0.35	0.21	0.50	0.20	0.46	0.18	0.57
Yb #	0.21	0.99	3.39	2.16	1.35	2.94	0.91	2.52	1.25	3.81
Lu #	0.05	0.15	0.52	0.35	0.22	0.46	0.19	0.46	0.18	0.61
Sericite Index[2]		22.24	34.90	73.46	97.73	64.29	36.83	44.89	64.91	51.09
Al_2O_3/Na_2O		2.64	6.92	99.94	5.08	3.64	3.57	6.28	5.48	36.90
CCPI[3]		33.23	37.11	58.18	45.58	52.82	63.71	38.27	55.68	62.13
AI[4]		38.81	62.84	77.46	66.64	43.00	39.37	60.37	61.34	92.16
$Zn/TiO_2*10000$		0.03	0.04	0.02	0.02	0.02	0.01	0.04	0.08	0.03
Nb/Y		0.99	0.28	0.29	0.58	0.23	0.26	0.59	1.01	0.34
Th/Yb		2.75	1.09	1.06	1.23	1.28	1.66	1.83	0.36	0.93
$[La/Yb]_{CN}$[5]		4.13	1.98	1.73	3.23	2.37	4.70	1.55	1.82	1.83
$[La/Sm]_{MN}$[6]		3.10	2.03	1.76	2.59	1.92	1.66	2.34	3.00	1.39
$[Nb/Th]_{MN}$[6]		0.32	0.25	0.26	0.41	0.18	0.24	0.24	1.97	0.27
Zr/Yb		28.63	190.39	56.64	65.98	114.70	53.91	43.05	87.12	150.47
Nb/Yb		7.25	2.30	2.31	4.12	1.90	3.35	3.69	5.95	2.06
Th/Nb		0.38	0.47	0.46	0.30	0.67	0.50	0.50	0.06	0.45
La/Sm		4.79	3.15	2.73	4.01	2.97	2.57	3.62	4.65	2.15

* wt%; ICP-OES
\# ppm; ICP-MS
LOI Loss On Ignition
[1] Universal Transverse Mercator, North American Datum 27 (UTM NAD27)
[2] Sericite Index = $100*K_2O/Na_2O + K_2O$
[3] CCPI = $100*(Fe_2O_3^T+MgO)/(Fe_2O_3^T+MgO+K_2O+Na_2O)$
[4] AI = $100*(K_2O+MgO)/(K_2O+MgO+CaO+Na_2O)$
[5] CN = chondrite normalized
[6] MN = primitive mantle normalized
\- < Limit of Detection
N.D. Not Detected

Table A1-1 (continued) Major and trace lithogeochemical data for outcrop and drill core samples from Pilley's Island VMS district.

Sample ID	Det. Limit	11CPM-123	11CPM-124	11CPM-128	11CPM-130	11CPM-131	11CPM-133	11CPM-134	11CPM-136	11CPM-137
Easting [1]		-	-	-	-	-	-	-	-	-
Northing [1]		-	-	-	-	-	-	-	-	-
Drillhole ID		PI-02-01	PI-02-01	PI-03-02	PI-03-02	PI-03-02	PI-03-02	PI-03-02	PI-03-02	PI-03-02
From (m)		580.10	595.70	53.20	120.60	203.40	357.40	443.00	554.90	578.10
To (m)		580.50	596.10	53.60	121.00	203.70	357.70	443.40	555.50	578.50
Strat. unit		4.2	4.1	7.2	7.1	7.1	6.1	6.1	6.1	6.1
SiO_2 *	0.01	68.80	52.31	43.10	52.46	52.54	47.40	48.97	54.47	42.84
Al_2O_3 *	0.01	17.67	18.36	16.61	16.87	15.73	15.66	17.07	15.74	18.21
Fe_2O_3 *	0.01	2.83	7.19	6.74	10.39	8.87	10.12	9.14	10.95	9.65
MnO *	0.001	0.01	0.13	0.11	0.18	0.10	0.15	0.14	0.53	0.20
MgO *	0.01	0.51	4.40	5.34	4.30	2.11	8.54	6.06	3.95	14.46
CaO *	0.01	0.14	3.42	11.82	3.84	6.99	9.40	8.56	0.93	1.85
Na_2O *	0.01	0.27	4.83	2.06	5.13	5.06	3.09	4.78	0.12	3.20
K_2O *	0.01	4.84	1.53	2.10	0.53	1.50	0.71	0.13	6.66	0.38
TiO_2 *	0.001	0.70	1.10	0.55	1.35	1.39	0.99	0.72	0.87	0.88
P_2O_5 *	0.01	0.10	0.19	0.06	0.41	0.73	0.25	0.28	0.18	0.33
LOI *		3.88	6.17	12.08	3.92	4.89	4.25	4.61	5.15	7.43
TOTAL *		99.75	99.61	100.60	99.35	99.91	100.60	100.50	99.55	99.43
Cr^{52} #	3.65	4.47	14.65	216.15	10.78	5.27	108.62	62.62	8.05	32.94
Cr^{53} #	12.85	-	-	233.36	-	-	111.47	63.25	-	30.71
Ni #	5.14	27.24	24.61	154.57	25.54	56.88	72.81	128.04	75.87	40.49
Co #	0.26	2.15	21.64	28.46	25.84	12.98	38.69	29.23	22.68	24.79
Sc #	1.00	11.00	18.00	35.00	23.00	21.00	43.00	33.00	31.00	29.00
V #	3.42	17.24	142.77	240.89	277.14	301.75	290.33	242.34	283.32	294.72
Cu #	3.94	10.22	22.51	64.78	32.53	36.19	125.52	195.04	389.85	56.42
Pb #	0.25	0.91	2.24	2.84	6.58	8.06	9.22	4.62	11.94	49.73
Zn #	8.16	33.88	81.65	145.42	124.50	125.18	90.29	340.24	356.49	142.78
Bi #	0.06	1.40	-	-	-	0.07	0.11	-	0.45	0.17
Cd #	0.99	-	-	1.36	-	1.14	1.21	-	1.20	-
Sn #	0.12	2.26	0.90	0.48	0.68	0.65	0.79	0.63	0.41	0.48
Mo #	0.63	5.85	-	1.85	-	1.38	-	-	3.05	1.62
As #	1.33	3.67	4.17	27.26	51.58	43.60	20.05	13.90	21.22	5.06
Sb #	0.20	0.34	-	1.41	0.25	-	1.60	0.96	-	0.23
Ag #	0.23	0.56	0.57	-	0.43	0.53	0.55	-	0.76	0.23
Li #	0.79	380.54	8.13	15.35	14.86	7.15	27.38	14.72	12.74	27.26
Rb #	0.76	535.41	263.63	1122.59	155.69	362.02	533.00	45.78	937.40	33.27
Cs #	0.08	0.45	1.20	3.04	0.63	1.26	0.42	0.24	0.64	0.73
Ba #	0.80	251.23	2838.54	279.68	169.66	265.08	234.55	36.45	3105.86	74.81
Sr #	4.16	-	335.11	216.39	382.68	289.58	136.61	185.04	30.17	160.03
Tl #	0.08	0.67	0.22	0.69	-	0.43	0.48	-	1.60	0.10
Ta #	0.04	0.45	0.29	0.09	0.17	0.16	0.34	0.10	0.14	0.20
Nb #	0.08	9.24	6.06	1.50	4.39	3.95	6.71	2.46	2.03	3.87
Hf #	0.21	6.04	3.61	1.23	2.38	1.96	2.82	1.22	2.08	1.91
Zr #	0.14	222.04	145.29	29.19	99.96	76.39	78.93	55.28	59.96	78.66
Y #	0.08	0.96	18.77	9.54	28.04	30.55	19.32	16.98	15.72	21.08
Th #	0.08	0.24	3.40	1.48	2.15	1.89	5.34	1.85	1.54	2.71
U #	0.09	0.26	1.25	0.19	0.79	3.57	1.46	0.61	0.51	1.01

Table A1-1 (continued) Major and trace lithogeochemical data for outcrop and drill core samples from Pilley's Island VMS district.

Sample ID	Det. Limit	11CPM-123	11CPM-124	11CPM-128	11CPM-130	11CPM-131	11CPM-133	11CPM-134	11CPM-136	11CPM-137
La #	0.09	0.50	10.30	4.62	10.53	11.94	12.29	8.83	4.43	11.51
Ce #	0.13	0.74	22.58	10.71	26.78	28.55	28.19	18.62	11.31	24.98
Pr #	0.06	0.15	3.42	1.58	3.46	3.68	3.80	2.34	1.83	3.51
Nd #	0.50	1.01	15.25	6.01	16.27	18.17	16.27	11.61	6.44	14.19
Sm #	0.36	-	3.59	1.70	4.99	5.12	4.41	3.24	2.62	4.35
Eu #	0.08	-	1.06	0.74	1.31	1.67	1.30	0.82	0.31	1.09
Gd #	0.16	0.42	3.35	1.96	4.34	5.23	3.75	2.93	2.47	4.42
Tb #	0.03	0.12	0.52	0.42	0.80	0.83	0.64	0.51	0.50	0.61
Dy #	0.13	0.54	3.64	2.00	5.44	6.16	3.60	3.28	3.10	4.23
Ho #	0.03	0.06	0.76	0.42	1.09	1.08	0.79	0.70	0.70	0.72
Er #	0.14	0.28	2.31	1.28	2.59	3.07	2.43	1.79	2.12	2.55
Tm #	0.04	0.16	0.46	0.15	0.54	0.48	0.37	0.35	0.44	0.37
Yb #	0.21	-	1.86	1.10	3.27	2.65	2.47	1.62	2.00	2.35
Lu #	0.05	-	0.22	0.11	0.40	0.39	0.24	0.25	0.31	0.39
Sericite Index[2]		89.92	94.72	24.06	50.48	9.36	22.87	18.68	2.65	98.23
Al_2O_3/Na_2O		65.44	3.80	8.06	3.29	3.11	5.07	3.57	131.17	5.69
CCPI[3]		39.53	64.57	74.38	72.19	62.60	83.08	75.58	68.73	87.07
AI[4]		92.88	41.82	34.90	35.00	23.05	42.55	31.69	90.99	74.61
$Zn/TiO_2*10000$		0.05	0.02	0.00	0.02	0.01	0.01	0.01	0.01	0.01
Nb/Y		9.64	0.32	0.16	0.16	0.13	0.35	0.14	0.13	0.18
Th/Yb		-	1.83	1.35	0.66	0.71	2.16	1.14	0.77	1.15
$[La/Yb]_{CN}$[5]		-	3.77	2.85	2.19	3.06	3.38	3.70	1.51	3.32
$[La/Sm]_{MN}$[6]		-	1.85	1.76	1.36	1.51	1.80	1.76	1.10	1.71
$[Nb/Th]_{MN}$[6]		4.57	0.22	0.12	0.25	0.25	0.15	0.16	0.16	0.17
Zr/Yb		53.66	-	78.27	26.54	30.61	28.81	31.97	34.12	29.96
Nb/Yb		-	3.26	1.36	1.34	1.49	2.72	1.52	1.02	1.65
Th/Nb		0.03	0.56	0.99	0.49	0.48	0.80	0.75	0.76	0.70
La/Sm		-	2.87	2.72	2.11	2.33	2.79	2.72	1.70	2.65

* wt%; ICP-OES

\# ppm; ICP-MS

LOI Loss On Ignition

[1] Universal Transverse Mercator, North American Datum 27 (UTM NAD27)

[2] Sericite Index = $100*K_2O/Na_2O + K_2O$

[3] CCPI = $100*(Fe_2O_3^T+MgO)/(Fe_2O_3^T+MgO+K_2O+Na_2O)$

[4] AI = $100*(K_2O+MgO)/(K_2O+MgO+CaO+Na_2O)$

[5] CN = chondrite normalized

[6] MN = primitive mantle normalized

\- < Limit of Detection

N.D. Not Detected

Table A1-1 (continued) Major and trace lithogeochemical data for outcrop and drill core samples from Pilley's Island VMS district.

Sample ID	Det. Limit	11CPM-138	11CPM-139	11CPM-141	11CPM-143	11CPM-144	11CPM-145	11CPM-146	11CPM-147	11CPM-148
Easting [1]		-	-	-	-	-	-	-	-	591320
Northing [1]		-	-	-	-	-	-	-	-	5483676
Drillhole ID		PI-03-02	PI-03-02	PI-03-02	PI-03-02	PI-03-02	PI-03-02	PI-03-02	PI-03-02	-
From (m)		662.30	695.20	763.20	852.50	866.90	886.20	960.00	1008.50	-
To (m)		662.70	695.50	763.60	852.90	867.20	886.60	960.40	1008.90	-
Strat. unit		6.1	6.1	6.1	2	2	2	2	2	6.1
SiO_2 *	0.01	52.06	45.98	46.73	55.38	50.62	57.38	46.64	45.75	53.23
Al_2O_3 *	0.01	16.51	17.44	16.51	13.58	17.13	14.94	16.17	15.41	17.55
Fe_2O_3 *	0.01	9.25	10.25	9.87	8.00	9.49	7.20	8.69	8.48	9.69
MnO *	0.001	0.46	0.24	0.43	0.32	0.32	0.31	0.54	0.14	0.21
MgO *	0.01	6.15	8.68	13.86	3.65	7.00	3.24	6.41	6.56	4.40
CaO *	0.01	0.71	5.80	0.98	1.85	1.09	2.71	5.06	6.36	2.10
Na_2O *	0.01	5.11	4.26	2.35	1.54	4.34	5.26	5.89	4.18	6.13
K_2O *	0.01	1.09	0.07	1.40	4.09	1.34	1.08	0.20	1.18	1.34
TiO_2 *	0.001	0.63	0.72	0.71	0.74	0.82	0.77	0.78	0.76	0.88
P_2O_5 *	0.01	0.27	0.34	0.20	0.20	0.26	0.25	0.21	0.17	0.49
LOI *		7.11	6.62	7.61	9.59	6.68	6.63	9.15	11.11	4.16
TOTAL *		99.35	100.40	100.70	98.95	99.10	99.76	99.73	100.10	100.20
Cr^{52} #	3.65	33.08	45.12	64.49	11.07	26.02	45.41	49.84	67.48	6.49
Cr^{53} #	12.85	26.83	43.02	62.93	-	22.29	44.71	47.90	61.84	-
Ni #	5.14	54.89	99.39	97.39	124.83	46.70	28.83	36.41	64.36	48.91
Co #	0.26	30.01	28.79	26.38	16.97	23.89	20.82	29.81	29.09	26.47
Sc #	1.00	31.00	31.00	33.00	20.00	27.00	24.00	33.00	32.00	20.00
V #	3.42	226.12	364.41	238.65	172.33	217.66	191.45	243.91	239.26	208.48
Cu #	3.94	18.65	31.30	58.51	82.78	52.72	123.68	107.66	75.85	75.66
Pb #	0.25	28.55	7.52	6.87	74.48	11.69	13.62	19.28	5.78	5.20
Zn #	8.16	350.71	154.20	307.17	303.38	404.14	657.86	775.92	106.67	134.80
Bi #	0.06	0.08	0.24	0.45	0.07	0.13	0.26	-	0.10	0.08
Cd #	0.99	-	-	-	-	1.01	2.92	1.91	-	-
Sn #	0.12	0.62	0.51	0.74	0.54	0.73	0.51	0.83	0.32	0.95
Mo #	0.63	1.75	1.05	1.17	2.27	-	2.89	1.44	2.26	1.95
As #	1.33	23.03	7.53	12.53	54.46	10.77	12.34	10.86	5.18	14.02
Sb #	0.20	-	0.20	0.27	7.33	0.85	1.70	0.79	3.20	0.43
Ag #	0.23	-	0.56	-	0.58	0.60	0.52	0.32	0.25	0.56
Li #	0.79	11.51	12.98	26.20	8.02	15.53	12.22	16.80	12.04	23.78
Rb #	0.76	728.73	21.17	265.67	984.31	188.37	129.63	361.30	424.60	372.18
Cs #	0.08	0.55	0.38	0.47	1.59	0.71	0.94	0.75	0.66	0.25
Ba #	0.80	187.32	309.12	1380.82	745.97	359.18	596.75	51.66	63.56	622.77
Sr #	4.16	85.64	180.38	97.71	111.15	90.61	131.44	162.33	148.90	214.70
Tl #	0.08	0.62	-	0.80	2.44	0.30	1.31	0.47	0.50	0.33
Ta #	0.04	0.28	0.10	0.16	0.31	0.23	0.28	0.17	0.29	0.24
Nb #	0.08	4.83	2.99	3.38	4.24	4.39	4.48	2.39	2.54	5.68
Hf #	0.21	1.66	1.78	1.48	2.81	2.45	2.59	2.47	1.66	3.48
Zr #	0.14	47.54	53.71	53.75	94.17	91.73	97.97	60.23	56.34	112.19
Y #	0.08	6.96	16.98	14.90	11.52	19.48	19.98	17.84	17.91	22.60
Th #	0.08	1.26	2.15	1.95	1.21	2.49	2.67	1.88	1.60	2.71
U #	0.09	0.78	0.86	0.56	0.47	0.76	1.02	0.74	0.34	1.14

Table A1-1 (continued) Major and trace lithogeochemical data for outcrop and drill core samples from Pilley's Island VMS district.

Sample ID	Det. Limit	11CPM-138	11CPM-139	11CPM-141	11CPM-143	11CPM-144	11CPM-145	11CPM-146	11CPM-147	11CPM-148
La #	0.09	5.43	9.88	7.35	3.81	8.37	7.15	6.49	6.61	8.35
Ce #	0.13	14.40	22.05	16.88	7.83	19.56	15.80	14.85	14.71	18.51
Pr #	0.06	1.45	2.95	2.22	1.21	2.54	2.23	2.18	2.07	2.73
Nd #	0.50	6.72	12.79	10.71	6.06	10.99	10.36	9.21	9.16	13.32
Sm #	0.36	2.16	3.35	2.99	1.61	2.33	3.27	2.90	2.68	3.20
Eu #	0.08	0.25	1.15	0.74	0.72	0.77	0.84	1.08	1.02	1.09
Gd #	0.16	1.45	3.23	2.76	2.03	3.41	3.28	3.13	3.10	3.75
Tb #	0.03	0.33	0.50	0.47	0.42	0.56	0.60	0.59	0.52	0.67
Dy #	0.13	1.81	2.96	2.96	1.96	3.73	3.79	3.43	3.17	4.32
Ho #	0.03	0.28	0.70	0.58	0.49	0.76	0.82	0.67	0.71	0.87
Er #	0.14	1.13	1.74	1.37	1.21	2.27	2.68	2.19	2.01	2.49
Tm #	0.04	0.18	0.27	0.28	0.23	0.37	0.48	0.41	0.42	0.39
Yb #	0.21	1.17	1.84	1.53	1.37	2.08	2.58	2.08	2.52	2.24
Lu #	0.05	0.10	0.31	0.26	0.23	0.34	0.37	0.34	0.30	0.38
Sericite Index[2]		10.61	17.58	1.62	37.33	72.65	23.59	17.03	3.28	22.01
Al_2O_3/Na_2O		3.23	4.09	7.03	8.82	3.95	2.84	2.75	3.69	2.86
CCPI[3]		71.30	81.38	86.35	67.42	74.38	62.22	71.26	73.73	65.35
AI[4]		55.44	46.52	82.09	69.54	60.57	35.15	37.64	42.34	41.09
$Zn/TiO_2*10000$		0.01	0.01	0.01	0.01	0.01	0.01	0.01	0.01	0.01
Nb/Y		0.70	0.18	0.23	0.37	0.23	0.22	0.13	0.14	0.25
Th/Yb		1.07	1.17	1.27	0.89	1.20	1.03	0.91	0.63	1.21
$[La/Yb]_{CN}$[5]		3.14	3.65	3.26	1.89	2.74	1.88	2.12	1.78	2.54
$[La/Sm]_{MN}$[6]		1.63	1.90	1.59	1.53	2.32	1.41	1.45	1.59	1.69
$[Nb/Th]_{MN}$[6]		0.46	0.17	0.21	0.42	0.21	0.20	0.15	0.19	0.25
Zr/Yb		33.42	40.55	29.24	35.13	68.89	44.17	37.91	29.01	22.32
Nb/Yb		4.12	1.63	2.21	3.10	2.11	1.74	1.15	1.00	2.54
Th/Nb		0.26	0.72	0.58	0.29	0.57	0.60	0.79	0.63	0.48
La/Sm		2.52	2.95	2.45	2.37	3.59	2.18	2.24	2.46	2.61

* wt%; ICP-OES

\# ppm; ICP-MS

LOI Loss On Ignition

[1] Universal Transverse Mercator, North American Datum 27 (UTM NAD27)

[2] Sericite Index = $100*K_2O/Na_2O+K_2O$

[3] CCPI = $100*(Fe_2O_3^T+MgO)/(Fe_2O_3^T+MgO+K_2O+Na_2O)$

[4] AI = $100*(K_2O+MgO)/(K_2O+MgO+CaO+Na_2O)$

[5] CN = chondrite normalized

[6] MN = primitive mantle normalized

\- < Limit of Detection

N.D. Not Detected

Table A1-1 (continued) Major and trace lithogeochemical data for outcrop and drill core samples from Pilley's Island VMS district.

Sample ID	Det. Limit	11CPM-149
Easting [1]		591303
Northing [1]		5483741
Drillhole ID		-
From (m)		-
To (m)		-
Strat. unit		6.2
SiO_2 *	0.01	65.17
Al_2O_3 *	0.01	17.45
Fe_2O_3 *	0.01	3.58
MnO *	0.001	0.07
MgO *	0.01	0.78
CaO *	0.01	0.41
Na_2O *	0.01	3.82
K_2O *	0.01	4.09
TiO_2 *	0.001	0.56
P_2O_5 *	0.01	0.13
LOI *		2.60
TOTAL *		98.66
Cr^{52} #	3.65	-
Cr^{53} #	12.85	-
Ni #	5.14	-
Co #	0.26	2.97
Sc #	1.00	9.00
V #	3.42	9.08
Cu #	3.94	10.31
Pb #	0.25	7.42
Zn #	8.16	79.34
Bi #	0.06	0.06
Cd #	0.99	-
Sn #	0.12	1.57
Mo #	0.63	0.79
As #	1.33	10.68
Sb #	0.20	5.06
Ag #	0.23	0.44
Li #	0.79	3.17
Rb #	0.76	408.35
Cs #	0.08	1.72
Ba #	0.80	90.54
Sr #	4.16	42.72
Tl #	0.08	0.82
Ta #	0.04	0.29
Nb #	0.08	8.97
Hf #	0.21	5.35
Zr #	0.14	205.76
Y #	0.08	6.99
Th #	0.08	1.12
U #	0.09	1.20

Table A1-1 (continued) Major and trace lithogeochemical data for outcrop and drill core samples from Pilley's Island VMS district.

Sample ID	Det. Limit	11CPM-149
La #	0.09	3.87
Ce #	0.13	7.39
Pr #	0.06	1.11
Nd #	0.50	3.52
Sm #	0.36	1.30
Eu #	0.08	0.29
Gd #	0.16	0.95
Tb #	0.03	0.21
Dy #	0.13	1.18
Ho #	0.03	0.30
Er #	0.14	0.98
Tm #	0.04	0.16
Yb #	0.21	1.16
Lu #	0.05	0.20

Sericite Index[2]	17.94
Al_2O_3/Na_2O	4.57
CCPI[3]	35.53
AI[4]	53.52
$Zn/TiO_2*10000$	0.02
Nb/Y	1.28
Th/Yb	0.96
$[La/Yb]_{CN}$[5]	2.26
$[La/Sm]_{MN}$[6]	1.92
$[Nb/Th]_{MN}$[6]	0.97
Zr/Yb	50.13
Nb/Yb	7.71
Th/Nb	0.12
La/Sm	2.98

* wt%; ICP-OES

\# ppm; ICP-MS

LOI Loss On Ignition

[1] Universal Transverse Mercator, North American Datum 27 (UTM NAD27)

[2] Sericite Index = $100*K_2O/Na_2O+K_2O$

[3] CCPI = $100*(Fe_2O_3{}^1+MgO)/(Fe_2O_3{}^1+MgO+K_2O+Na_2O)$

[4] AI = $100*(K_2O+MgO)/(K_2O+MgO+CaO+Na_2O)$

[5] CN = chondrite normalized

[6] MN = primitive mantle normalized

\- < Limit of Detection

N.D. Not Detected

Appendix II: Mass Change Data

Table A2-1 LOI-free major and trace element abundances used in multiple precursor mass change calculations (Maclean, 1990) with least altered samples indicated by shading. Values below the detection limit have been replaced with a value equal to half of the detection limit.

Sample ID	10CPM-004a	10CPM-004b	10CPM-005	10CPM-009	10CPM-010a	10CPM-010b	10CPM-012	10CPM-021	10CPM-023
SWIR Min.[1]	Ill.pheng.	Ill.pheng.	FeMgChl	Ill.pheng.	Phengite	Aspectral	Ill.pheng.	Aspectral	Ill.pheng.
Strat. unit	5.5	5.5	5.5	5.6	5.6	5.6	6.1	5.6	6.1
SiO_2 *	70.97	68.40	67.71	65.70	70.25	70.82	48.92	69.99	49.05
Al_2O_3 *	15.34	16.64	15.02	16.67	14.64	14.26	17.58	15.40	14.86
Fe_2O_3 *	3.26	3.46	3.38	3.89	3.36	3.08	10.38	3.99	6.50
MnO *	0.12	0.10	0.11	0.07	0.04	0.01	0.18	0.06	0.16
MgO *	0.80	1.67	0.93	2.43	1.74	0.20	8.74	1.88	3.11
CaO *	1.14	1.01	0.65	0.57	0.13	0.15	6.16	0.42	17.30
Na_2O *	3.50	0.74	0.18	3.04	0.12	0.15	2.02	2.85	6.15
K_2O *	4.31	7.38	11.22	6.85	9.12	10.74	4.93	4.79	1.43
TiO_2 *	0.46	0.49	0.63	0.63	0.48	0.48	0.76	0.50	0.91
P_2O_5 *	0.10	0.10	0.15	0.15	0.11	0.09	0.33	0.12	0.52
TOTAL *	100	100	100	100	100	100	100	100	100
Ni #	6.43	2.57	2.57	2.57	2.57	2.57	43.68	2.57	11.26
Co #	3.24	2.21	2.57	2.29	3.24	4.71	36.54	4.53	27.90
Sc #	5.00	6.00	9.00	9.00	7.00	7.00	28.00	7.00	18.00
V #	10.97	11.49	12.26	15.59	37.66	8.47	221.93	18.81	303.22
Cu #	1.97	1.97	345.99	1.97	11.07	1.97	45.02	1.97	1.97
Pb #	13.42	10.33	20.10	6.20	45.42	21.99	6.07	4.77	8.53
Zn #	56.55	60.86	19.29	16.68	19.98	4.08	45.06	13.13	18.81
As #	4.72	1.85	1.85	0.67	2.69	10.16	5.51	3.32	15.73
Sb #	0.40	0.58	0.10	0.10	0.21	0.10	0.10	0.31	0.30
Li #	1.86	1.93	1.65	3.76	4.88	0.96	54.43	4.77	8.96
Rb #	118.31	221.58	162.43	75.30	184.27	201.83	104.41	104.87	50.21
Ba #	1125.90	1140.96	2496.76	1627.75	3553.99	1544.75	1223.66	1085.55	588.09
Sr #	70.52	27.49	46.91	37.50	37.37	2.08	266.24	33.87	215.93
Tl #	1.15	2.53	1.49	0.89	1.04	1.46	0.39	0.67	0.17
Ta #	0.49	0.52	0.39	0.46	0.45	0.38	0.15	0.46	0.15
Nb #	8.58	10.10	7.52	8.97	7.79	7.46	2.71	8.53	2.85
Hf #	5.04	5.93	4.52	5.54	5.31	5.01	1.72	5.44	2.03
Zr #	174.53	218.63	166.40	202.60	179.86	170.06	52.12	195.59	64.69
Y #	17.81	18.40	9.13	9.63	15.48	2.55	15.14	12.01	22.84
Th #	4.22	4.38	1.92	1.12	4.01	0.33	2.06	1.93	2.01
U #	1.93	2.17	1.65	1.75	1.47	1.17	1.04	1.86	5.49
La #	12.84	10.64	5.13	6.08	5.35	2.09	6.47	8.09	9.04
Ce #	24.74	22.34	9.46	7.72	9.62	2.15	14.76	9.40	19.30
Pr #	3.32	2.81	1.47	1.53	1.80	0.65	2.04	1.89	2.80
Nd #	13.54	11.23	6.14	5.73	7.29	2.42	9.50	7.49	12.84
Sm #	2.94	2.58	1.44	1.45	1.84	0.52	2.50	1.67	3.39
Eu #	0.69	0.67	0.37	0.34	0.32	0.12	0.81	0.45	1.11
Gd #	2.96	2.63	1.55	1.53	2.24	0.54	2.95	1.81	4.25
Tb #	0.48	0.50	0.26	0.24	0.39	0.06	0.43	0.32	0.64
Dy #	3.39	3.47	1.73	1.55	2.85	0.43	2.82	2.15	4.23
Ho #	0.72	0.74	0.39	0.34	0.63	0.09	0.61	0.46	0.88
Er #	2.23	2.42	1.32	1.12	2.05	0.36	1.73	1.53	2.61
Tm #	0.39	0.42	0.23	0.23	0.36	0.09	0.34	0.23	0.41
Yb #	2.77	2.93	1.59	1.34	2.50	0.33	1.79	1.46	2.47
Lu #	0.41	0.46	0.25	0.23	0.41	0.05	0.27	0.25	0.38

[1] Dominant alteration mineral identified by near infrared-short wave infrared (NIR-SWIR) spectroscopy.

* wt%; ICP-OES

\# ppm; ICP-MS Least altered sample used to fit an approximate fractionation curve

Table A2-1 (continued) LOI-free major and trace element abundances used in multiple precursor mass change calculations (Maclean, 1990) with least altered samples indicated by shading. Values below the detection limit have been replaced with a value equal to half of the detection limit.

Sample ID	10CPM-025	10CPM-029	10CPM-032	10CPM-036b	10CPM-038	10CPM-041	10CPM-044	10CPM-052	10CPM-059	10CPM-062
SWIR Min.[1]	Aspectral	Aspectral	Ill.pheng.	Phengite	Ill.pheng.	Aspectral	Ill.musc.	Ill.pheng.	MgChl	Aspectral
Strat. unit	5.5	2	2	6.1	2	6.1	6.1	6.1	2	2
SiO_2 *	66.76	53.43	57.74	54.50	52.02	51.66	55.69	52.18	77.37	52.20
Al_2O_3 *	15.98	16.35	15.35	18.65	16.48	17.30	16.45	15.44	11.50	15.97
Fe_2O_3 *	4.83	9.05	7.53	9.23	12.50	11.11	9.96	8.62	2.81	7.78
MnO *	0.07	0.14	0.12	0.18	0.21	0.12	0.14	0.16	0.07	0.15
MgO *	2.34	2.28	2.68	5.37	4.82	7.09	3.48	9.19	0.54	5.63
CaO *	1.83	9.56	8.01	3.72	5.04	2.82	5.96	8.25	0.57	11.35
Na_2O *	0.11	7.23	7.14	5.34	4.37	1.66	4.14	3.96	4.90	5.31
K_2O *	7.42	0.56	0.18	1.06	2.66	6.85	2.32	1.36	1.87	0.83
TiO_2 *	0.55	1.05	0.93	1.36	1.43	0.97	1.20	0.63	0.33	0.56
P_2O_5 *	0.12	0.35	0.31	0.59	0.47	0.42	0.67	0.22	0.04	0.21
TOTAL *	100	100	100	100	100	100	100	100	100	100
Ni #	2.57	27.79	26.20	7.42	12.99	46.60	2.57	103.55	2.57	63.36
Co #	4.61	26.66	17.95	22.33	31.45	28.43	29.76	36.43	2.14	21.39
Sc #	8.00	28.00	24.00	23.00	27.00	31.00	22.00	41.00	6.00	27.00
V #	8.55	292.63	276.52	212.76	361.39	273.02	292.64	212.63	5.05	202.61
Cu #	1.97	1.97	1.97	1.97	1.97	91.56	1.97	102.38	1.97	66.39
Pb #	72.34	5.08	3.45	7.90	5.94	5.58	8.64	3.88	18.05	6.23
Zn #	112.47	42.63	4.08	29.49	23.58	106.66	40.19	34.12	47.95	45.89
As #	36.97	11.93	21.00	21.50	66.93	7.80	24.47	17.97	4.09	8.56
Sb #	0.71	0.23	0.10	0.28	0.10	0.27	0.73	0.24	0.35	0.10
Li #	2.60	4.73	6.30	43.47	23.75	41.74	19.25	37.82	0.39	12.53
Rb #	200.16	12.32	27.65	43.55	72.58	1005.60	103.22	40.14	59.73	28.11
Ba #	496.67	68.04	78.94	553.82	1779.49	516.00	537.12	597.93	983.01	326.22
Sr #	92.19	112.17	136.09	322.92	213.11	139.20	308.63	429.33	108.35	325.97
Tl #	1.51	0.17	0.13	0.18	0.33	0.93	0.41	0.20	0.26	0.11
Ta #	0.49	0.16	0.13	0.31	0.22	0.10	0.22	0.15	0.44	0.07
Nb #	8.67	2.85	2.43	6.27	4.34	2.60	3.99	3.03	8.12	1.45
Hf #	5.58	2.44	2.22	3.62	2.92	1.93	2.77	1.51	6.33	1.26
Zr #	187.54	76.83	65.97	120.28	105.24	58.54	86.64	43.35	219.06	36.23
Y #	27.66	21.60	18.37	34.05	31.38	17.12	25.18	14.05	5.93	13.44
Th #	5.04	1.67	1.42	2.57	2.91	1.64	1.97	1.82	2.51	1.39
U #	2.30	0.89	0.61	1.20	0.66	0.69	1.04	0.39	1.32	0.28
La #	24.15	7.47	6.15	9.22	13.17	6.00	8.30	6.18	7.20	6.00
Ce #	48.11	18.35	15.78	25.68	34.07	16.04	22.40	13.15	20.68	11.22
Pr #	6.06	2.51	2.11	3.42	4.16	1.86	2.95	1.89	1.77	1.64
Nd #	23.86	11.71	9.62	16.38	18.93	9.37	13.85	8.59	7.46	7.20
Sm #	5.70	3.19	2.67	4.93	4.86	2.84	3.90	2.33	1.60	1.94
Eu #	1.36	1.05	0.92	1.54	1.56	0.96	1.27	0.78	0.37	0.71
Gd #	5.46	3.98	3.32	5.75	5.55	3.13	4.75	2.68	1.54	2.44
Tb #	0.80	0.59	0.56	0.98	0.88	0.53	0.73	0.42	0.25	0.37
Dy #	5.24	4.02	3.75	6.50	5.81	3.05	4.78	2.78	1.73	2.41
Ho #	1.11	0.86	0.74	1.31	1.18	0.72	0.97	0.55	0.36	0.52
Er #	3.52	2.56	2.12	3.84	3.47	1.83	2.94	1.62	1.02	1.56
Tm #	0.58	0.45	0.34	0.58	0.55	0.35	0.46	0.28	0.16	0.26
Yb #	3.78	2.66	2.18	3.79	3.51	1.52	2.90	1.50	1.07	1.38
Lu #	0.63	0.42	0.34	0.54	0.52	0.32	0.43	0.23	0.17	0.23

[1] Dominant alteration mineral identified by near infrared-short wave infrared (NIR-SWIR) spectroscopy.

* wt%; ICP-OES

\# ppm; ICP-MS Least altered sample used to fit an approximate fractionation curve

Table A2-1 (continued) LOI-free major and trace element abundances used in multiple precursor mass change calculations (Maclean, 1990) with least altered samples indicated by shading. Values below the detection limit have been replaced with a value equal to half of the detection limit.

Sample ID	10CPM-064	10CPM-065	10CPM-069	10CPM-071	10CPM-073	10CPM-074	10CPM-075	10CPM-076	10CPM-078	10CPM-083
SWIR Min.[1]	FeMgChl	FeMgChl	MgChl	MgChl	Ill.pheng.	FeMgChl	Phengite	FeMgChl	Ill.pheng.	FeMgChl
Strat. unit	2	4.6	2	6.1	6.1	4.6	4.6	4.6	2	4.6
SiO_2 *	53.68	68.31	52.20	53.63	55.52	70.81	73.18	70.86	48.83	74.58
Al_2O_3 *	16.73	15.45	19.21	17.44	15.37	13.77	13.76	14.90	15.76	13.09
Fe_2O_3 *	6.47	4.78	9.03	9.63	10.16	6.67	3.15	2.70	9.32	3.15
MnO *	0.13	0.10	0.14	0.20	0.37	0.04	0.11	0.09	0.25	0.05
MgO *	4.49	1.18	5.52	6.25	3.78	0.47	0.81	0.47	10.29	1.04
CaO *	11.01	0.68	6.86	6.01	7.86	0.48	0.90	0.30	10.40	0.27
Na_2O *	5.87	5.27	5.20	5.66	4.39	4.60	5.22	2.87	3.04	4.84
K_2O *	0.85	3.53	1.06	0.12	0.93	2.53	2.25	7.11	1.07	2.42
TiO_2 *	0.58	0.55	0.61	0.84	1.30	0.54	0.48	0.57	0.67	0.44
P_2O_5 *	0.18	0.15	0.18	0.22	0.33	0.09	0.13	0.13	0.36	0.10
TOTAL *	100	100	100	100	100	100	100	100	100	100
Ni #	78.83	2.57	56.44	46.71	19.24	2.57	2.57	2.57	372.96	2.57
Co #	24.97	3.61	29.80	24.93	18.71	2.96	3.07	3.04	50.70	2.24
Sc #	25.00	7.00	34.00	32.00	25.00	6.00	6.00	7.00	33.00	7.00
V #	184.02	17.74	197.93	243.22	289.03	16.17	12.69	18.53	241.72	10.71
Cu #	68.37	28.45	1.97	24.64	45.43	9.64	1.97	16.47	88.36	15.48
Pb #	7.21	10.11	8.49	2.72	9.52	89.22	11.25	14.45	3.97	49.19
Zn #	32.87	227.11	47.45	353.80	375.03	26.72	31.79	792.74	53.72	355.29
As #	3.65	28.09	24.71	7.17	11.44	127.36	25.26	7.51	7.32	5.65
Sb #	0.10	0.41	0.10	0.25	0.79	32.47	3.86	0.23	0.28	0.51
Li #	7.12	3.17	13.59	18.77	16.78	2.02	4.14	1.67	20.02	5.40
Rb #	13.56	55.20	34.84	3.28	38.18	75.09	44.92	103.98	42.23	44.35
Ba #	437.22	1154.67	359.14	80.44	1261.92	8770.80	1027.92	1393.88	347.22	704.44
Sr #	283.56	67.67	310.41	212.94	96.93	184.59	167.16	17.86	208.07	53.57
Tl #	0.11	1.05	0.14	0.15	0.21	20.11	1.87	1.10	0.32	0.70
Ta #	0.09	0.43	0.09	0.17	0.17	0.46	0.38	0.43	0.12	0.38
Nb #	1.50	7.92	1.65	3.13	2.87	8.20	7.48	8.16	2.27	7.30
Hf #	1.27	5.10	1.51	2.26	2.66	4.98	4.63	4.88	1.97	4.29
Zr #	39.84	178.57	41.68	72.94	75.68	183.49	164.83	181.40	46.79	154.55
Y #	12.59	8.01	14.55	16.84	24.98	8.76	4.37	2.60	13.42	11.96
Th #	1.36	2.44	1.49	2.09	1.81	2.85	1.83	0.44	1.80	1.15
U #	0.42	1.72	0.22	0.52	0.66	2.00	1.83	1.66	0.57	1.45
La #	4.42	6.46	5.16	6.80	8.08	2.95	4.22	1.50	7.08	5.61
Ce #	10.04	11.90	12.65	16.19	17.76	4.88	9.13	2.76	15.46	7.57
Pr #	1.44	1.56	1.69	2.16	2.49	0.77	1.12	0.36	2.11	1.37
Nd #	6.85	6.02	7.51	9.45	12.11	3.02	4.07	1.40	9.47	5.42
Sm #	1.87	1.36	2.24	2.78	3.61	0.83	1.00	0.18	2.40	1.34
Eu #	0.65	0.39	0.74	1.00	1.29	0.38	0.25	0.04	0.84	0.40
Gd #	2.37	1.43	2.54	3.11	4.60	1.06	0.92	0.38	2.69	1.56
Tb #	0.38	0.25	0.46	0.50	0.70	0.20	0.16	0.06	0.42	0.28
Dy #	2.52	1.56	2.85	3.23	4.85	1.48	0.97	0.46	2.68	1.83
Ho #	0.51	0.34	0.58	0.66	1.03	0.34	0.22	0.10	0.54	0.39
Er #	1.56	1.05	1.77	1.99	2.89	1.12	0.70	0.40	1.55	1.24
Tm #	0.24	0.17	0.29	0.32	0.45	0.22	0.15	0.10	0.25	0.21
Yb #	1.47	1.26	1.67	1.97	2.88	1.34	0.64	0.56	1.50	1.31
Lu #	0.22	0.19	0.26	0.31	0.47	0.24	0.11	0.09	0.24	0.20

[1] Dominant alteration mineral identified by near infrared-short wave infrared (NIR-SWIR) spectroscopy.

* wt%; ICP-OES

\# ppm; ICP-MS Least altered sample used to fit an approximate fractionation curve

Table A2-1 (continued) LOI-free major and trace element abundances used in multiple precursor mass change calculations (Maclean, 1990) with least altered samples indicated by shading. Values below the detection limit have been replaced with a value equal to half of the detection limit.

Sample ID	10CPM-084	10CPM-086	10CPM-090	10CPM-093	10CPM-095	10CPM-098b	10CPM-102	10CPM-105	10CPM-106	10CPM-108
SWIR Min.[1]	FeChl	Aspectral	Aspectral	Ill.pheng.	Ill.pheng.	FeChl	Ill.pheng.	FeMgChl	Ill.pheng.	FeMgChl
Strat. unit	4.6	4.6	4.6	4.3	4.3	4.4	4.1	4.4	4.1	4.1
SiO_2 *	67.98	67.01	76.64	67.69	71.47	62.85	69.62	66.44	59.65	61.59
Al_2O_3 *	15.59	16.22	12.70	16.22	14.65	16.22	13.76	15.28	17.47	16.20
Fe_2O_3 *	3.26	4.08	2.01	4.23	3.39	6.65	4.44	5.57	7.94	6.91
MnO *	0.09	0.08	0.04	0.10	0.10	0.67	0.29	0.62	0.71	0.30
MgO *	1.80	1.68	0.24	2.37	1.67	2.21	1.31	1.93	4.07	2.13
CaO *	0.26	0.74	0.75	1.37	0.79	1.25	0.31	1.05	1.20	1.79
Na_2O *	3.01	5.63	6.84	5.58	3.72	1.17	0.18	3.40	3.01	0.20
K_2O *	7.30	3.83	0.16	1.70	3.55	7.85	9.25	4.74	4.56	9.75
TiO_2 *	0.57	0.58	0.48	0.57	0.54	0.76	0.56	0.67	0.97	0.80
P_2O_5 *	0.13	0.14	0.12	0.18	0.11	0.37	0.29	0.31	0.42	0.33
TOTAL *	100	100	100	100	100	100	100	100	100	100
Ni #	2.57	2.57	2.57	2.57	2.57	2.57	2.57	20.05	15.75	25.85
Co #	2.14	4.35	1.26	4.91	2.57	10.15	4.37	4.81	31.29	23.09
Sc #	8.00	8.00	6.00	8.00	8.00	11.00	8.00	9.00	17.00	23.00
V #	14.07	15.90	11.92	32.51	14.05	94.33	50.31	59.47	170.39	214.08
Cu #	1.97	1.97	1.97	6.94	1.97	60.60	24.72	1.97	1.97	205.94
Pb #	2.35	12.49	6.80	14.47	14.13	328.53	925.48	25.64	36.14	37.88
Zn #	159.60	63.67	26.40	46.25	56.52	2360.28	266.20	144.71	255.78	3298.43
As #	4.13	4.95	2.06	7.20	6.14	7.44	35.03	10.27	12.04	45.07
Sb #	0.24	0.10	0.10	0.10	0.10	0.10	0.52	1.11	0.22	1.09
Li #	7.05	4.24	1.46	11.18	5.84	10.54	6.04	2.53	8.06	4.15
Rb #	45.17	110.93	3.64	58.36	87.92	57.47	170.12	45.09	40.38	174.67
Ba #	484.88	1537.94	77.40	647.90	857.80	1754.83	3416.05	562.79	1280.32	3782.60
Sr #	16.60	102.80	49.78	202.33	96.08	34.60	36.30	41.54	49.58	34.42
Tl #	0.85	0.63	0.04	0.47	0.65	1.07	1.95	0.81	1.05	2.54
Ta #	0.38	0.48	0.35	0.45	0.39	0.27	0.28	0.32	0.29	0.20
Nb #	7.81	10.09	7.77	8.41	8.02	4.70	4.77	5.51	5.43	4.20
Hf #	4.80	6.25	4.54	5.23	4.91	3.09	3.33	3.62	3.39	2.11
Zr #	169.24	219.92	164.34	189.81	176.03	113.02	116.74	135.23	128.80	65.69
Y #	6.33	19.91	1.59	7.96	8.06	7.12	10.16	5.24	10.49	12.69
Th #	0.41	2.70	0.82	2.91	1.18	0.83	1.81	0.60	1.15	1.46
U #	1.28	2.27	1.95	1.99	1.57	1.03	0.91	1.01	1.50	0.84
La #	2.64	11.08	1.47	5.12	3.73	2.79	7.24	2.05	4.30	4.49
Ce #	2.79	15.36	4.48	14.96	5.61	3.88	12.41	2.25	9.94	8.68
Pr #	0.64	2.65	0.37	1.56	0.87	0.73	1.88	0.54	1.32	1.35
Nd #	2.65	10.70	1.75	6.02	3.76	2.82	7.90	2.02	5.72	6.20
Sm #	0.66	2.71	0.18	1.41	0.94	0.85	1.83	0.63	1.58	1.78
Eu #	0.17	0.74	0.09	0.36	0.31	0.21	0.44	0.21	0.48	0.43
Gd #	0.78	3.20	0.32	1.45	1.22	0.95	1.85	0.75	1.88	2.19
Tb #	0.14	0.54	0.05	0.26	0.21	0.18	0.31	0.14	0.31	0.39
Dy #	0.91	3.41	0.37	1.66	1.49	1.16	1.99	0.84	2.10	2.48
Ho #	0.21	0.73	0.08	0.37	0.34	0.25	0.44	0.20	0.43	0.50
Er #	0.71	2.17	0.26	1.19	1.10	0.82	1.31	0.70	1.32	1.52
Tm #	0.14	0.35	0.08	0.25	0.19	0.16	0.22	0.16	0.25	0.23
Yb #	0.67	2.36	0.30	1.37	1.24	0.89	1.54	0.81	1.53	1.51
Lu #	0.11	0.37	0.05	0.21	0.21	0.14	0.25	0.15	0.22	0.24

[1] Dominant alteration mineral identified by near infrared-short wave infrared (NIR-SWIR) spectroscopy.

* wt%; ICP-OES

\# ppm; ICP-MS Least altered sample used to fit an approximate fractionation curve

Table A2-1 (continued) LOI-free major and trace element abundances used in multiple precursor mass change calculations (Maclean, 1990) with least altered samples indicated by shading. Values below the detection limit have been replaced with a value equal to half of the detection limit.

Sample ID	10CPM-109	10CPM-113b	10CPM-114	10CPM-116a	10CPM-120	10CPM-128	10CPM-129	10CPM-137	10CPM-139
SWIR Min.[1]	FeMgChl	Muscovite	Ill.pheng.	Phengite	Phengite	Aspectral	FeMgChl	Ill.pheng.	Ill.pheng.
Strat. unit	4.3	4.4	4.4	4.3	6.1	7.1	6.1	2	3.4
SiO_2 *	65.08	72.34	84.71	**20.23**	**59.03**	42.63	52.41	50.68	**74.32**
Al_2O_3 *	17.05	12.97	9.21	**0.92**	**17.67**	16.41	18.05	16.23	**14.26**
Fe_2O_3 *	6.19	2.98	2.38	**78.10**	**6.57**	9.62	11.27	15.07	**3.26**
MnO *	0.18	0.01	0.01	**0.06**	**0.16**	0.11	0.22	0.15	**0.07**
MgO *	2.82	0.07	0.30	**0.12**	**3.69**	3.10	3.94	3.62	**0.85**
CaO *	0.37	0.27	0.03	**0.15**	**3.42**	20.85	4.13	10.95	**0.39**
Na_2O *	3.51	0.78	0.05	**0.21**	**8.12**	4.22	6.72	1.87	**2.91**
K_2O *	3.86	10.01	3.00	**0.16**	**0.14**	1.88	0.71	0.17	**3.36**
TiO_2 *	0.72	0.45	0.29	**0.03**	**0.71**	0.94	1.68	1.11	**0.48**
P_2O_5 *	0.22	0.10	0.01	**0.03**	**0.50**	0.25	0.85	0.16	**0.10**
TOTAL *	100	100	100	**100**	**100**	100	100	100	**100**
Ni #	2.57	2.57	2.57	**8.07**	**24.49**	169.48	21.33	13.46	**2.57**
Co #	6.21	2.78	0.57	**1.18**	**15.32**	33.14	21.25	27.24	**2.36**
Sc #	11.00	5.00	3.00	**0.50**	**21.00**	29.00	22.00	35.00	**6.00**
V #	53.20	7.74	3.68	**1.71**	**194.71**	147.75	193.91	497.90	**13.69**
Cu #	1.97	1340.28	63.71	**5056.49**	**38.37**	21.88	1.97	122.94	**1.97**
Pb #	4.42	11.89	5.09	**798.50**	**6.25**	8.64	5.34	5.80	**7.83**
Zn #	80.36	4.08	149.78	**1450.57**	**34.35**	12.48	24.57	28.18	**32.53**
As #	2.43	23.17	5.40	**1169.79**	**13.33**	27.68	4.85	12.68	**7.69**
Sb #	0.10	0.44	0.80	**19.24**	**1.35**	1.77	0.22	0.63	**1.79**
Li #	8.32	0.39	1.91	**1.04**	**12.29**	37.55	23.18	7.49	**1.27**
Rb #	82.12	190.13	221.89	**6.47**	**13.59**	109.06	71.29	16.32	**130.25**
Ba #	588.39	4250.04	274.22	**2342.19**	**211.61**	194.13	295.96	108.98	**203.04**
Sr #	29.05	4.87	2.08	**73.23**	**148.97**	120.77	228.49	307.84	**94.12**
Tl #	0.80	2.41	1.00	**22.40**	**0.04**	0.41	0.19	0.04	**0.78**
Ta #	0.37	0.34	0.29	**0.02**	**0.58**	0.62	0.20	0.16	**0.32**
Nb #	6.75	6.61	5.64	**0.41**	**11.49**	12.42	3.85	2.28	**8.11**
Hf #	4.35	3.77	3.60	**0.11**	**3.70**	4.60	2.10	2.20	**4.92**
Zr #	171.69	147.95	120.84	**6.63**	**152.97**	165.20	71.23	67.41	**184.68**
Y #	9.28	0.27	9.77	**0.89**	**18.86**	14.70	20.46	29.64	**17.16**
Th #	1.30	0.04	3.20	**0.21**	**10.82**	7.03	3.75	2.61	**3.48**
U #	1.13	1.54	1.70	**0.32**	**2.87**	3.35	0.50	0.57	**1.86**
La #	6.14	0.27	3.79	**0.86**	**28.78**	15.32	14.70	6.83	**10.03**
Ce #	7.71	0.18	8.25	**1.41**	**60.99**	45.67	29.69	20.24	**18.00**
Pr #	1.61	0.13	1.06	**0.22**	**7.79**	4.96	4.30	2.73	**2.61**
Nd #	6.45	0.25	4.12	**0.81**	**32.13**	20.63	18.69	12.78	**11.92**
Sm #	1.35	0.18	1.13	**0.18**	**6.39**	4.44	4.19	3.88	**2.96**
Eu #	0.38	0.04	0.19	**0.04**	**1.60**	1.21	1.28	1.31	**0.83**
Gd #	1.54	0.08	1.07	**0.08**	**4.98**	3.77	4.29	4.81	**3.71**
Tb #	0.24	0.02	0.24	**0.02**	**0.66**	0.54	0.64	0.81	**0.54**
Dy #	1.67	0.07	1.81	**0.18**	**3.74**	3.12	3.99	5.54	**3.37**
Ho #	0.34	0.02	0.41	**0.04**	**0.67**	0.58	0.81	1.15	**0.69**
Er #	1.20	0.07	1.35	**0.07**	**1.99**	1.60	2.28	3.44	**2.02**
Tm #	0.22	0.07	0.25	**0.06**	**0.31**	0.24	0.39	0.55	**0.33**
Yb #	1.34	0.11	1.74	**0.11**	**1.81**	1.57	2.25	3.63	**2.01**
Lu #	0.21	0.02	0.29	**0.02**	**0.29**	0.24	0.31	0.53	**0.33**

[1] Dominant alteration mineral identified by near infrared-short wave infrared (NIR-SWIR) spectroscopy.

* wt%; ICP-OES

\# ppm; ICP-MS Least altered sample used to fit an approximate fractionation curve

Table A2-1 (continued) LOI-free major and trace element abundances used in multiple precursor mass change calculations (Maclean, 1990) with least altered samples indicated by shading. Values below the detection limit have been replaced with a value equal to half of the detection limit.

Sample ID	10CPM-140a	10CPM-140d	10CPM-140e	10CPM-140f	10CPM-141	10CPM-146	10CPM-156	10CPM-159	10CPM-163a
SWIR Min.[1]	Phengite	Aspectral	Ill.pheng.	Ill.pheng.	Aspectral	Phengite	Ill.pheng.	Phengite	Aspectral
Strat. unit	3.2	3.2	3.2	3.2	3.2	6.1	2	5.5	5.5
SiO_2 *	79.00	14.94	33.72	63.94	68.44	51.33	53.02	73.57	74.83
Al_2O_3 *	11.31	1.59	1.19	18.58	16.30	18.68	16.42	14.64	13.12
Fe_2O_3 *	4.53	82.55	64.25	4.52	4.41	11.40	12.05	1.48	3.01
MnO *	0.01	0.03	0.03	0.06	0.11	0.12	0.15	0.02	0.07
MgO *	0.95	0.20	0.06	3.38	1.41	6.10	2.42	0.45	0.99
CaO *	0.04	0.08	0.08	1.51	1.04	3.47	5.82	0.15	1.05
Na_2O *	0.08	0.11	0.44	4.23	4.95	5.42	6.37	0.37	5.00
K_2O *	3.65	0.40	0.14	3.15	2.69	1.50	1.84	8.79	1.39
TiO_2 *	0.41	0.03	0.02	0.51	0.52	1.21	1.43	0.44	0.46
P_2O_5 *	0.01	0.08	0.08	0.12	0.13	0.77	0.48	0.09	0.08
TOTAL *	100	100	100	100	100	100	100	100	100
Ni #	2.57	2.57	2.57	14.10	5.59	9.48	14.30	2.57	2.57
Co #	4.59	0.83	0.87	7.82	4.66	32.39	29.06	0.80	2.32
Sc #	4.00	0.50	0.50	9.00	6.00	23.00	25.00	5.00	6.00
V #	17.82	7.86	1.71	43.98	20.96	288.09	394.42	17.65	9.65
Cu #	40.83	40403.67	53515.54	413.93	59.80	83.12	67.95	19.29	13.86
Pb #	36.63	339.95	897.35	24.42	12.15	8.70	7.07	43.57	10.30
Zn #	73.91	2617.79	8355.17	330.12	79.88	44.80	40.96	83.08	41.68
As #	19.33	319.62	464.14	37.07	10.07	17.19	9.40	20.03	5.25
Sb #	2.41	7.14	7.28	2.61	0.67	0.21	0.10	1.50	0.34
Li #	2.77	0.39	0.39	13.45	6.14	27.83	3.85	1.21	3.97
Rb #	140.93	8.81	2.09	75.62	77.08	42.50	39.63	252.03	73.80
Ba #	3376.76	1002.45	2855.79	887.34	516.73	478.07	451.46	1484.17	980.32
Sr #	42.03	148.92	207.01	148.90	128.76	428.14	145.73	21.55	162.10
Tl #	3.92	36.62	16.33	2.89	0.73	0.23	0.28	1.91	0.38
Ta #	0.35	0.02	0.02	0.50	0.50	0.23	0.18	0.51	0.37
Nb #	6.00	0.36	0.43	9.03	8.96	4.34	3.37	9.05	6.75
Hf #	3.87	0.11	0.11	5.87	5.34	2.66	2.71	5.59	4.84
Zr #	133.46	7.18	5.70	217.34	206.20	92.69	81.79	192.78	155.43
Y #	10.57	1.12	0.60	15.13	4.74	23.94	26.59	5.68	3.01
Th #	3.37	0.29	0.17	2.56	1.02	1.70	1.60	1.33	1.91
U #	2.01	2.25	0.41	2.01	2.38	0.97	1.86	1.78	1.44
La #	10.84	2.22	0.69	5.26	3.18	7.93	9.01	3.33	5.93
Ce #	19.86	3.53	1.16	9.38	4.97	20.96	20.12	5.52	13.45
Pr #	2.49	0.45	0.17	1.46	0.69	2.76	3.04	0.85	1.34
Nd #	9.80	1.61	0.25	6.10	2.55	12.87	14.24	3.53	5.35
Sm #	1.80	0.38	0.18	1.68	0.69	3.61	4.02	0.86	1.26
Eu #	0.42	0.04	0.04	0.53	0.13	1.26	1.36	0.19	0.29
Gd #	1.61	0.22	0.08	2.16	0.70	4.69	5.11	0.98	1.01
Tb #	0.25	0.05	0.02	0.41	0.11	0.70	0.80	0.14	0.17
Dy #	1.81	0.25	0.07	2.71	0.69	4.69	5.04	1.01	0.89
Ho #	0.44	0.04	0.02	0.58	0.15	0.97	1.05	0.23	0.18
Er #	1.50	0.16	0.07	2.00	0.51	2.84	3.16	0.75	0.49
Tm #	0.26	0.06	0.05	0.33	0.11	0.46	0.53	0.14	0.08
Yb #	1.84	0.11	0.11	2.32	0.59	2.74	3.00	0.90	0.48
Lu #	0.30	0.02	0.02	0.37	0.08	0.41	0.47	0.15	0.07

[1] Dominant alteration mineral identified by near infrared-short wave infrared (NIR-SWIR) spectroscopy.

* wt%; ICP-OES

\# ppm; ICP-MS Least altered sample used to fit an approximate fractionation curve

Table A2-1 (continued) LOI-free major and trace element abundances used in multiple precursor mass change calculations (Maclean, 1990) with least altered samples indicated by shading. Values below the detection limit have been replaced with a value equal to half of the detection limit.

Sample ID	10CPM-163b	10CPM-166a	10CPM-166b	10CPM-167	10CPM-168a	10CPM-172	10CPM-175	10CPM-176	10CPM-178
SWIR Min.[1]	Phengite	Kaolinite	Ill.pheng.	Ill.pheng.	Phengite	FeMgChl	FeMgChl	FeMgChl	FeMgChl
Strat. unit	5.5	6.1	6.1	4.6	4.6	4.2	7.1	7.1	7.1
SiO_2 *	77.35	66.22	45.94	66.79	69.81	71.92	70.34	48.90	51.04
Al_2O_3 *	12.27	10.50	15.76	16.84	15.73	14.18	14.90	15.65	17.70
Fe_2O_3 *	2.58	7.96	14.62	4.75	2.91	3.81	4.34	8.41	9.26
MnO *	0.04	0.17	0.64	0.21	0.08	0.07	0.14	0.21	0.17
MgO *	0.26	3.66	7.26	2.46	1.00	1.73	1.16	9.04	8.41
CaO *	0.37	6.73	12.23	0.50	0.45	0.27	0.46	12.64	9.36
Na_2O *	6.36	1.81	0.38	2.87	4.94	5.21	4.42	2.69	2.48
K_2O *	0.23	1.72	1.49	4.79	4.34	2.16	3.56	1.29	0.25
TiO_2 *	0.44	0.80	1.36	0.64	0.59	0.51	0.56	0.91	1.06
P_2O_5 *	0.09	0.42	0.32	0.16	0.15	0.13	0.11	0.26	0.26
TOTAL *	100	100	100	100	100	100	100	100	100
Ni #	2.57	2.57	25.89	2.57	2.57	2.57	2.57	109.30	147.20
Co #	2.17	13.38	43.99	2.74	2.49	3.03	3.54	37.50	33.18
Sc #	6.00	11.00	27.00	8.00	8.00	7.00	8.00	39.00	32.00
V #	8.51	111.96	363.14	18.88	15.50	9.18	15.88	270.84	251.41
Cu #	6.67	14.39	35.53	28.64	141.43	5.28	7.29	98.57	76.21
Pb #	12.49	3.59	12.51	662.91	11.86	15.77	14.21	6.30	4.10
Zn #	38.33	46.85	133.60	1089.48	23.73	58.08	68.24	43.94	34.82
As #	6.53	8.70	95.37	10.32	5.22	4.58	5.02	12.51	19.59
Sb #	0.33	2.36	7.59	0.30	0.10	0.10	0.20	0.27	0.10
Li #	0.39	17.12	25.92	6.86	0.39	2.74	4.02	36.12	58.39
Rb #	8.43	66.16	40.91	94.84	33.20	35.89	72.05	41.05	30.33
Ba #	183.82	1205.81	1000.60	573.43	2701.66	530.19	568.88	215.96	72.83
Sr #	131.77	105.49	83.43	36.11	37.77	68.10	43.85	338.01	357.71
Tl #	0.04	0.53	0.25	0.80	0.62	0.38	0.69	0.15	0.10
Ta #	0.35	0.15	0.16	0.51	0.46	0.41	0.38	0.28	0.35
Nb #	6.95	2.90	3.32	8.82	8.45	7.88	7.73	5.83	6.09
Hf #	4.45	2.28	2.28	5.32	5.17	4.80	4.91	2.39	4.25
Zr #	157.46	70.36	73.36	203.08	192.07	172.21	173.00	76.22	121.76
Y #	5.33	19.50	23.41	9.48	2.38	6.68	7.53	16.66	19.91
Th #	1.88	1.51	1.60	1.29	0.62	2.10	1.02	5.26	4.76
U #	1.29	0.69	1.06	1.87	1.51	1.81	1.36	1.87	1.20
La #	4.39	8.21	7.09	5.93	1.38	4.55	4.18	11.72	15.51
Ce #	12.99	19.35	16.49	6.92	3.01	13.18	5.29	26.70	35.45
Pr #	1.19	2.61	2.45	1.27	0.39	1.20	1.16	3.85	4.63
Nd #	4.66	11.45	11.73	5.44	1.37	5.13	4.38	16.71	19.25
Sm #	1.15	3.27	3.28	1.33	0.48	1.35	1.04	3.83	4.34
Eu #	0.20	1.03	1.17	0.28	0.04	0.29	0.32	1.07	1.29
Gd #	1.14	3.68	4.00	1.52	0.45	1.35	1.23	3.60	4.22
Tb #	0.18	0.59	0.69	0.24	0.08	0.23	0.22	0.55	0.60
Dy #	1.25	3.62	4.54	1.64	0.54	1.58	1.44	3.45	3.84
Ho #	0.26	0.80	0.92	0.34	0.11	0.34	0.32	0.68	0.80
Er #	0.84	2.41	2.79	1.05	0.44	1.06	1.01	1.91	2.27
Tm #	0.17	0.38	0.45	0.18	0.10	0.20	0.19	0.33	0.36
Yb #	0.82	2.29	2.74	1.14	0.51	1.17	1.03	1.89	2.17
Lu #	0.13	0.34	0.39	0.17	0.06	0.16	0.17	0.27	0.36

[1] Dominant alteration mineral identified by near infrared-short wave infrared (NIR-SWIR) spectroscopy.

* wt%; ICP-OES

\# ppm; ICP-MS Least altered sample used to fit an approximate fractionation curve

Table A2-1 (continued) LOI-free major and trace element abundances used in multiple precursor mass change calculations (Maclean, 1990) with least altered samples indicated by shading. Values below the detection limit have been replaced with a value equal to half of the detection limit.

Sample ID	10CPM-181	10CPM-185	10CPM-190	10CPM-191	10CPM-193	10CPM-194	10CPM-195	10CPM-198	10CPM-199	10CPM-200
SWIR Min.[1]	Ill.pheng.	Phengite	Ill.pheng.	FeMgChl	Aspectral	MgChl	MgChl	MgChl	Ill.pheng.	Ill.pheng.
Strat. unit	7.1	7.1	3.2	3.1	7.1	7.1	7.1	2	1.2	1.1
SiO_2 *	50.82	50.16	67.14	69.82	49.44	49.36	45.09	55.31	68.07	67.03
Al_2O_3 *	15.55	16.75	17.12	15.33	17.72	15.94	15.33	16.88	16.10	16.79
Fe_2O_3 *	9.94	9.66	3.69	4.11	9.34	11.27	6.69	7.71	3.49	3.19
MnO *	0.15	0.17	0.11	0.16	0.20	0.16	0.13	0.12	0.09	0.09
MgO *	10.16	5.98	1.26	2.11	7.93	7.15	4.99	4.17	1.07	0.84
CaO *	8.54	14.61	1.72	0.60	8.95	10.69	21.35	8.13	0.46	1.19
Na_2O *	3.40	1.56	1.82	5.71	3.01	3.17	4.50	6.44	2.73	3.73
K_2O *	0.32	0.10	6.35	1.51	2.28	1.29	0.87	0.36	7.53	6.65
TiO_2 *	0.91	0.85	0.65	0.51	0.93	0.80	0.85	0.63	0.37	0.36
P_2O_5 *	0.21	0.16	0.14	0.14	0.19	0.16	0.21	0.23	0.08	0.12
TOTAL *	100	100	100	100	100	100	100	100	100	100
Ni #	106.20	41.55	2.57	5.27	60.21	67.22	151.63	33.37	2.57	2.57
Co #	36.83	29.74	2.28	3.83	38.53	30.24	25.29	22.14	2.73	2.41
Sc #	40.00	35.00	9.00	6.00	40.00	35.00	28.00	28.00	5.00	4.00
V #	285.96	275.40	15.69	16.15	314.20	282.55	217.45	215.92	13.53	10.39
Cu #	133.23	104.80	5.48	42.54	113.39	175.75	27.35	168.16	6.69	5.58
Pb #	4.23	3.94	9.47	23.94	4.74	4.50	1.87	3.77	9.38	13.67
Zn #	25.29	35.15	39.25	557.51	41.12	30.99	23.94	26.21	60.58	43.50
As #	29.71	46.96	2.76	21.92	14.01	20.31	7.51	52.14	13.11	8.52
Sb #	1.27	0.98	0.10	0.99	0.29	0.10	0.23	0.10	0.45	0.85
Li #	32.52	29.68	3.52	5.90	42.01	36.74	26.41	9.99	1.81	0.39
Rb #	18.82	10.50	133.31	25.49	97.76	48.19	24.85	26.12	234.93	162.89
Ba #	206.28	63.96	913.62	1274.78	379.15	142.96	140.88	155.34	1027.75	1183.91
Sr #	424.95	117.29	22.21	69.77	323.37	390.85	219.89	111.56	38.21	71.97
Tl #	0.16	0.04	1.42	0.48	0.29	0.15	0.12	0.12	1.28	0.93
Ta #	0.29	0.16	0.49	0.46	0.15	0.11	0.13	0.11	0.57	0.56
Nb #	5.58	2.90	9.02	7.79	2.84	1.90	2.38	1.71	9.28	8.93
Hf #	2.48	2.23	5.72	5.07	2.35	1.47	1.77	1.90	6.61	6.40
Zr #	80.48	55.02	207.35	187.81	63.03	44.60	55.96	41.59	241.42	230.53
Y #	14.98	18.49	15.89	3.97	16.75	14.31	15.03	13.92	5.39	3.15
Th #	4.07	3.27	3.09	1.54	2.69	1.83	2.61	1.32	1.24	0.94
U #	1.29	0.65	1.71	2.37	1.12	0.59	2.07	0.32	1.99	2.17
La #	14.13	12.94	7.27	4.06	10.41	7.98	8.40	4.59	3.87	2.15
Ce #	31.81	26.17	10.97	7.69	23.23	17.14	18.39	10.28	4.48	3.96
Pr #	4.41	3.67	2.38	0.94	3.13	2.32	2.51	1.51	1.04	0.52
Nd #	19.44	14.93	10.65	3.45	13.29	10.21	11.30	7.10	4.02	1.99
Sm #	4.02	3.46	2.63	0.82	3.25	2.50	2.69	2.05	0.92	0.43
Eu #	1.13	1.06	0.69	0.22	1.02	0.86	0.92	0.72	0.21	0.08
Gd #	3.53	3.55	2.77	0.73	3.24	2.69	3.05	2.54	0.87	0.48
Tb #	0.49	0.56	0.43	0.13	0.52	0.42	0.47	0.40	0.14	0.08
Dy #	3.13	3.54	2.90	0.91	3.39	2.89	2.95	2.67	1.01	0.58
Ho #	0.59	0.73	0.66	0.20	0.69	0.58	0.60	0.57	0.23	0.12
Er #	1.74	2.09	2.31	0.62	2.01	1.70	1.67	1.69	0.77	0.51
Tm #	0.29	0.30	0.39	0.13	0.30	0.27	0.26	0.26	0.15	0.10
Yb #	1.57	2.04	2.73	0.66	2.06	1.60	1.68	1.65	1.00	0.64
Lu #	0.26	0.32	0.46	0.10	0.29	0.23	0.24	0.28	0.14	0.10

[1] Dominant alteration mineral identified by near infrared-short wave infrared (NIR-SWIR) spectroscopy.

* wt%; ICP-OES

\# ppm; ICP-MS Least altered sample used to fit an approximate fractionation curve

Table A2-1 (continued) LOI-free major and trace element abundances used in multiple precursor mass change calculations (Maclean, 1990) with least altered samples indicated by shading. Values below the detection limit have been replaced with a value equal to half of the detection limit.

Sample ID	10CPM-202b	10CPM-206	10CPM-207	10CPM-208	10CPM-209b	11CPM-003	11CPM-004	11CPM-006	11CPM-007
SWIR Min.[1]	MgChl	Aspectral	Aspectral	Kaolinite	Aspectral	Phengite	Aspectral	Ill.pheng.	Ill.pheng.
Strat. unit	2	4.1	4.3	1.1	6.1	3.2	3.3	3.1	3.1
SiO_2 *	54.01	65.57	25.93	81.45	53.89	67.26	64.97	61.03	70.21
Al_2O_3 *	14.87	7.16	0.19	13.32	15.53	15.90	14.03	19.59	15.20
Fe_2O_3 *	8.37	21.58	73.60	2.67	8.42	4.74	11.55	5.02	3.53
MnO *	0.19	0.02	0.04	0.03	0.11	0.11	0.04	0.14	0.07
MgO *	10.20	0.38	0.04	0.46	2.69	1.73	3.30	1.78	1.75
CaO *	5.50	0.13	0.09	0.20	10.29	2.14	0.36	3.11	1.73
Na_2O *	3.21	0.18	0.03	0.06	7.30	3.70	0.88	4.15	2.63
K_2O *	2.66	4.61	0.04	1.47	0.14	3.74	4.15	4.35	4.32
TiO_2 *	0.79	0.34	0.01	0.27	1.28	0.58	0.58	0.67	0.50
P_2O_5 *	0.19	0.03	0.01	0.06	0.35	0.11	0.14	0.17	0.06
TOTAL *	100	100	100	100	100	100	100	100	100
Ni #	230.77	16.91	2.57	5.82	8.82	2.57	23.58	345.16	2.57
Co #	36.84	46.88	46.34	2.56	12.53	3.09	9.94	4.61	2.93
Sc #	23.00	8.00	2.00	3.00	21.00	8.00	8.00	8.00	6.00
V #	151.82	81.82	1.71	9.84	233.36	12.13	71.67	24.02	17.34
Cu #	81.12	103.95	1184.57	23.95	1.97	10.35	1580.81	17.94	11.75
Pb #	9.79	86.06	2637.72	27.43	5.60	8.69	160.60	9.01	7.48
Zn #	46.12	56.45	225.22	25.41	4.08	50.21	1689.06	87.77	53.78
As #	47.69	120.68	904.61	58.90	4.10	1.62	324.94	15.67	8.31
Sb #	0.25	2.79	40.32	7.12	0.47	0.26	117.20	0.93	0.26
Li #	31.88	1.82	0.39	19.64	4.05	6.97	11.46	6.02	3.48
Rb #	106.42	75.93	5.49	81.92	6.52	74.78	89.13	54.96	113.92
Ba #	1748.18	3471.25	11239.24	3696.01	66.49	347.37	1703.41	212.46	562.65
Sr #	198.41	25.36	103.75	278.68	161.98	34.79	47.79	67.75	120.24
Tl #	0.55	8.61	5.66	0.60	0.04	0.78	4.39	1.28	0.81
Ta #	0.28	0.08	0.02	0.40	0.19	0.40	0.30	0.42	0.41
Nb #	4.42	1.80	0.15	6.82	3.04	9.08	7.19	9.62	7.88
Hf #	3.43	0.76	0.11	4.91	2.39	4.89	3.37	5.38	4.92
Zr #	101.90	27.58	1.11	181.44	78.74	186.17	141.49	220.84	184.67
Y #	13.88	0.68	0.41	6.97	18.03	22.84	23.26	18.44	13.34
Th #	3.95	0.12	0.09	2.93	1.55	4.12	4.01	4.03	4.49
U #	1.40	0.27	0.14	1.77	0.68	1.47	1.23	1.86	2.00
La #	14.95	0.80	0.29	7.20	8.81	10.96	14.00	9.08	9.71
Ce #	35.92	0.62	0.61	15.96	21.30	21.04	34.51	15.58	21.46
Pr #	4.74	0.40	0.07	1.84	2.85	3.27	3.91	2.55	2.73
Nd #	20.41	3.78	0.25	7.30	13.55	13.98	16.29	9.96	10.98
Sm #	4.32	0.18	0.18	1.52	3.50	3.69	4.24	2.66	2.68
Eu #	1.19	0.04	0.04	0.29	1.24	0.97	1.20	0.65	0.64
Gd #	3.71	0.08	0.08	1.29	3.61	3.67	4.21	2.78	2.61
Tb #	0.52	0.02	0.02	0.22	0.55	0.69	0.80	0.51	0.46
Dy #	3.03	0.27	0.07	1.49	3.59	4.45	4.62	3.37	2.80
Ho #	0.55	0.02	0.02	0.31	0.70	0.91	1.03	0.72	0.56
Er #	1.58	0.07	0.07	0.96	2.14	2.90	2.95	2.33	1.63
Tm #	0.23	0.04	0.02	0.20	0.35	0.47	0.48	0.42	0.29
Yb #	1.54	0.11	0.11	1.11	2.26	3.23	3.44	2.68	2.06
Lu #	0.25	0.02	0.02	0.18	0.35	0.50	0.44	0.41	0.30

[1] Dominant alteration mineral identified by near infrared-short wave infrared (NIR-SWIR) spectroscopy.

* wt%; ICP-OES

\# ppm; ICP-MS Least altered sample used to fit an approximate fractionation curve

Table A2-1 (continued) LOI-free major and trace element abundances used in multiple precursor mass change calculations (Maclean, 1990) with least altered samples indicated by shading. Values below the detection limit have been replaced with a value equal to half of the detection limit.

Sample ID	11CPM-008	11CPM-009	11CPM-010	11CPM-011	11CPM-012	11CPM-013	11CPM-014	11CPM-015	11CPM-016	11CPM-017
SWIR Min.[1]	Ill.pheng.	Ill.musc.	Ill.pheng.	FeMgChl	MgChl	FeMgChl	Phengite	Ill.pheng.	Phengite	Phengite
Strat. unit	3.1	3.1	3.1	2	2	2	4.4	4.4	4.3	4.3
SiO_2 *	66.21	73.49	65.51	52.29	49.82	49.51	63.97	67.10	66.23	61.51
Al_2O_3 *	16.85	14.31	17.06	17.56	17.94	16.10	13.80	15.27	15.97	17.87
Fe_2O_3 *	4.26	2.82	4.49	8.86	10.47	9.26	3.35	5.51	8.70	6.63
MnO *	0.11	0.07	0.12	0.16	0.15	0.18	0.70	0.49	0.27	0.21
MgO *	1.88	1.03	1.97	8.07	7.89	7.54	3.17	1.85	1.78	5.64
CaO *	2.44	1.44	2.57	5.08	5.66	10.79	6.01	1.45	0.45	1.67
Na_2O *	2.62	3.86	3.58	4.81	2.92	3.26	3.53	2.42	0.08	0.61
K_2O *	5.00	2.47	4.06	1.91	3.86	2.62	4.87	5.07	5.72	5.19
TiO_2 *	0.56	0.45	0.57	0.97	1.03	0.59	0.50	0.63	0.66	0.59
P_2O_5 *	0.08	0.07	0.08	0.27	0.25	0.16	0.10	0.20	0.14	0.08
TOTAL *	100	100	100	100	100	100	100	100	100	100
Ni #	2.57	9.70	2.57	55.21	39.78	33.88	2.57	2.57	14.45	2.57
Co #	3.17	2.83	3.64	32.73	26.95	28.75	4.07	6.68	12.87	4.00
Sc #	7.00	6.00	7.00	36.00	36.00	27.00	6.00	8.00	13.00	6.00
V #	18.26	14.06	18.95	237.74	262.83	195.64	15.61	46.40	89.58	22.40
Cu #	10.30	29.61	8.11	100.04	114.78	144.45	11.52	33.68	220.60	30.33
Pb #	7.12	11.46	12.17	10.67	7.25	4.89	41.80	11.76	387.51	24.00
Zn #	56.80	78.99	61.10	78.62	69.99	54.67	66.50	102.28	3541.18	511.66
As #	7.18	14.44	11.92	14.03	14.53	16.93	9.41	8.58	41.06	12.27
Sb #	0.28	3.28	1.04	0.36	0.96	1.90	0.27	0.10	0.80	0.34
Li #	0.90	1.12	0.39	32.74	28.96	16.77	5.00	2.57	4.72	7.95
Rb #	82.02	29.37	163.82	63.04	194.33	95.44	108.38	128.98	72.93	203.18
Ba #	463.02	300.03	299.71	286.46	495.56	78.65	587.47	445.17	656.46	1602.93
Sr #	162.43	137.79	209.25	218.36	163.56	151.18	351.11	62.18	12.48	30.88
Tl #	0.87	0.33	0.93	0.40	1.05	0.46	1.27	1.64	2.66	1.80
Ta #	0.46	0.37	0.55	0.16	0.32	0.19	0.49	0.32	0.28	0.43
Nb #	8.60	7.02	11.80	3.38	4.58	4.27	9.16	6.33	5.43	8.46
Hf #	5.02	4.39	6.48	1.94	3.06	1.22	5.83	3.92	3.28	5.09
Zr #	198.56	166.78	276.24	71.14	99.89	37.48	201.86	164.62	131.56	203.20
Y #	16.39	10.71	17.06	16.26	23.19	11.95	31.90	12.18	9.79	22.23
Th #	4.22	3.14	5.98	1.57	2.60	1.71	7.35	3.12	2.18	5.74
U #	1.93	2.08	2.62	0.80	1.23	0.53	2.97	1.28	1.47	2.23
La #	9.14	8.40	11.91	5.31	9.49	6.17	20.78	8.90	5.12	10.87
Ce #	20.99	14.36	28.73	15.24	24.81	12.96	49.84	17.44	11.38	25.32
Pr #	2.56	1.90	3.31	2.11	3.41	1.76	6.05	2.57	1.50	3.06
Nd #	10.48	7.69	13.30	9.34	16.11	7.79	24.03	10.67	6.23	12.27
Sm #	2.63	1.90	3.36	2.75	4.33	2.11	6.03	2.53	1.59	3.14
Eu #	0.69	0.51	0.88	0.91	1.35	0.70	2.20	0.82	0.35	0.55
Gd #	2.77	2.01	3.41	3.04	4.73	2.33	6.65	2.63	1.63	3.12
Tb #	0.47	0.32	0.56	0.54	0.75	0.40	1.07	0.42	0.32	0.58
Dy #	3.22	2.08	3.50	3.32	5.05	2.38	6.63	2.56	2.18	4.14
Ho #	0.63	0.43	0.76	0.72	1.00	0.46	1.29	0.53	0.44	0.89
Er #	2.08	1.39	2.22	2.10	2.99	1.36	4.21	1.69	1.51	2.87
Tm #	0.38	0.27	0.36	0.35	0.52	0.22	0.72	0.37	0.29	0.47
Yb #	2.29	1.50	2.42	1.94	2.82	1.31	4.50	1.63	1.59	3.13
Lu #	0.36	0.27	0.40	0.29	0.41	0.22	0.68	0.26	0.23	0.50

[1] Dominant alteration mineral identified by near infrared-short wave infrared (NIR-SWIR) spectroscopy.

* wt%; ICP-OES

\# ppm; ICP-MS

Least altered sample used to fit an approximate fractionation curve

Table A2-1 (continued) LOI-free major and trace element abundances used in multiple precursor mass change calculations (Maclean, 1990) with least altered samples indicated by shading. Values below the detection limit have been replaced with a value equal to half of the detection limit.

Sample ID	11CPM-018	11CPM-019	11CPM-020	11CPM-021	11CPM-022	11CPM-024	11CPM-025	11CPM-026	11CPM-027	11CPM-028
SWIR Min.[1]	Muscovite	Ill.musc.	Phengite	Phengite	Phengite	FeChl	FeChl	Aspectral	Ankerite	Ill.pheng.
Strat. unit	4.2	3.2	3.1	3.1	3.1	4.5	4.4	4.4	4.3	4.3
SiO_2 *	49.62	66.81	67.97	71.22	65.84	68.52	67.98	68.18	63.35	62.90
Al_2O_3 *	17.45	15.33	15.50	13.85	16.14	14.83	15.51	16.06	15.13	16.61
Fe_2O_3 *	18.47	10.92	4.72	3.16	5.00	6.64	4.54	2.57	6.42	6.25
MnO *	0.58	0.03	0.10	0.06	0.18	0.22	0.11	0.07	0.15	0.21
MgO *	7.58	1.10	1.21	0.52	2.25	1.77	0.66	0.46	1.11	2.04
CaO *	1.33	0.34	0.56	0.28	0.30	0.33	1.76	1.63	3.86	2.94
Na_2O *	0.47	0.14	2.01	0.19	0.48	1.06	3.81	3.39	2.68	1.91
K_2O *	3.60	4.75	7.32	10.15	9.14	5.99	4.95	6.95	6.48	6.42
TiO_2 *	0.75	0.52	0.52	0.46	0.58	0.55	0.57	0.59	0.56	0.61
P_2O_5 *	0.14	0.07	0.09	0.10	0.09	0.07	0.10	0.09	0.26	0.10
TOTAL *	100	100	100	100	100	100	100	100	100	100
Ni #	62.71	2.57	6.69	2.57	6.66	9.19	2.57	2.57	2.57	2.57
Co #	40.68	5.69	3.74	3.24	4.93	2.14	0.13	0.44	14.26	3.40
Sc #	40.00	6.00	6.00	6.00	8.00	8.00	8.00	8.00	7.00	8.00
V #	208.04	16.40	17.17	14.39	36.61	10.88	1.71	12.41	11.94	13.35
Cu #	862.67	77.77	23.72	37.92	44.16	63.88	6.00	8.20	97.50	11.50
Pb #	26.28	7.20	172.80	402.42	25.74	45.24	5.87	3.63	40.67	4.32
Zn #	269.52	42.44	333.55	489.59	680.64	239.56	4.08	25.40	50.94	61.93
As #	14.42	31.07	29.90	50.88	13.44	16.94	0.67	5.62	7.16	1.38
Sb #	0.45	5.10	1.51	1.22	0.37	0.21	0.10	0.34	0.48	0.21
Li #	8.16	1.76	1.04	0.99	6.46	10.13	4.93	2.40	3.11	5.73
Rb #	92.65	60.15	311.51	242.47	147.95	358.00	153.91	155.32	120.94	199.41
Ba #	592.33	631.96	1513.35	2334.55	3259.33	719.28	947.10	1264.40	2909.94	1110.30
Sr #	33.15	10.66	19.21	20.46	47.20	37.77	20.98	27.34	71.76	46.87
Tl #	1.70	1.10	3.23	3.14	1.74	1.15	0.91	0.99	1.04	1.22
Ta #	0.06	0.39	0.39	0.37	0.41	0.43	0.41	0.40	0.44	0.39
Nb #	1.46	7.62	7.90	7.10	8.21	8.45	7.39	7.24	7.38	7.54
Hf #	1.23	4.22	4.69	4.11	4.86	4.90	4.94	4.77	5.00	4.53
Zr #	38.08	179.55	185.54	166.87	191.70	195.27	177.24	177.83	175.31	182.01
Y #	12.80	9.55	6.69	5.87	13.48	18.97	14.49	6.90	42.08	26.48
Th #	0.86	2.63	1.45	1.56	3.33	2.76	2.42	1.50	5.13	4.58
U #	0.34	1.68	1.41	1.42	1.87	1.57	1.35	1.68	2.84	1.54
La #	4.37	5.70	3.31	3.16	7.11	14.39	5.16	3.08	14.60	10.91
Ce #	9.13	11.81	6.61	5.49	15.72	27.33	10.78	8.81	31.72	25.48
Pr #	1.34	1.63	0.87	0.96	2.06	3.26	1.60	0.91	4.40	3.33
Nd #	6.05	6.28	3.45	3.56	8.16	12.71	8.14	4.27	21.38	16.68
Sm #	1.82	1.57	0.85	1.03	2.16	2.80	3.79	2.15	10.47	7.55
Eu #	0.72	0.29	0.32	0.22	0.41	0.66	1.08	0.49	2.50	1.77
Gd #	2.31	1.46	0.97	0.97	2.00	2.98	2.87	1.42	7.88	4.86
Tb #	0.38	0.30	0.19	0.16	0.34	0.48	0.53	0.29	1.48	1.03
Dy #	2.49	1.97	1.27	1.18	2.55	3.41	3.16	1.60	8.41	5.69
Ho #	0.52	0.44	0.29	0.27	0.58	0.69	0.67	0.33	1.64	1.14
Er #	1.60	1.45	0.90	0.88	1.93	2.14	1.94	1.06	4.76	3.33
Tm #	0.28	0.29	0.19	0.20	0.40	0.39	0.35	0.23	0.85	0.55
Yb #	1.54	1.68	1.26	1.06	2.30	2.67	2.24	1.29	5.93	3.78
Lu #	0.21	0.27	0.21	0.17	0.36	0.37	0.38	0.18	0.97	0.55

[1] Dominant alteration mineral identified by near infrared-short wave infrared (NIR-SWIR) spectroscopy.

* wt%; ICP-OES

\# ppm; ICP-MS Least altered sample used to fit an approximate fractionation curve

Table A2-1 (continued) LOI-free major and trace element abundances used in multiple precursor mass change calculations (Maclean, 1990) with least altered samples indicated by shading. Values below the detection limit have been replaced with a value equal to half of the detection limit.

Sample ID	11CPM-029	11CPM-030	11CPM-031	11CPM-032	11CPM-033	11CPM-034	11CPM-035	11CPM-037	11CPM-038	11CPM-039
SWIR Min.[1]	NULL	Aspectral	Ill.pheng.	FeMgChl	NULL	Ill.musc.	Muscovite	Ill.musc.	FeMgChl	Aspectral
Strat. unit	4.2	4.3	4.3	4.3	3.3	3.3	3.3	3.2	3.2	2
SiO_2 *	70.96	66.51	67.07	58.98	52.23	61.72	60.84	56.91	58.65	60.79
Al_2O_3 *	14.09	15.86	16.29	16.92	23.29	19.81	19.52	22.18	17.08	19.21
Fe_2O_3 *	3.38	4.34	4.14	6.09	12.03	5.94	10.53	11.29	6.69	7.35
MnO *	0.12	0.15	0.12	0.14	0.11	0.25	0.07	0.03	0.18	0.07
MgO *	0.85	1.61	2.84	5.63	2.60	5.02	1.48	1.35	5.54	4.56
CaO *	1.62	1.17	1.20	3.81	1.30	0.99	0.71	0.24	4.42	1.03
Na_2O *	3.93	3.50	3.66	6.09	2.20	0.24	0.32	0.19	6.25	2.08
K_2O *	4.47	6.20	3.85	1.38	4.90	5.01	5.17	6.73	0.21	3.96
TiO_2 *	0.50	0.58	0.72	0.77	1.30	0.85	0.89	0.97	0.80	0.83
P_2O_5 *	0.08	0.08	0.11	0.20	0.04	0.17	0.47	0.10	0.18	0.11
TOTAL *	100	100	100	100	100	100	100	100	100	100
Ni #	2.57	2.57	15.27	38.12	35.14	2.57	7.93	15.57	12.17	52.22
Co #	1.18	1.02	3.84	21.22	30.51	7.13	10.74	14.67	8.06	24.98
Sc #	7.00	8.00	9.00	18.00	39.00	13.00	14.00	15.00	20.00	22.00
V #	9.64	15.04	16.24	130.54	94.14	78.01	91.13	33.79	124.16	144.38
Cu #	14.80	7.10	9.60	38.26	85.51	13.32	1895.64	1737.56	8.01	48.36
Pb #	2.68	3.12	7.72	10.85	43.79	19.99	569.61	38.71	7.03	9.51
Zn #	53.25	45.93	44.40	77.27	131.35	175.29	2320.23	243.32	67.51	92.96
As #	1.45	2.51	3.02	19.17	20.89	12.63	47.83	29.84	3.42	18.30
Sb #	0.23	0.10	0.10	0.46	0.97	1.02	2.18	1.02	0.38	1.09
Li #	2.94	4.62	6.27	16.34	6.91	12.68	3.87	2.57	19.24	17.22
Rb #	92.03	107.31	268.84	73.70	129.47	357.90	230.15	578.81	5.88	476.05
Ba #	1726.56	1422.45	645.43	4580.11	483.35	620.02	1275.04	460.86	530.03	1000.82
Sr #	47.30	35.83	29.00	471.07	15.30	24.68	17.01	4.93	393.14	72.10
Tl #	0.62	0.76	0.97	0.38	5.29	3.94	5.65	2.43	0.04	1.47
Ta #	0.35	0.40	0.40	0.30	0.23	0.37	0.34	0.45	0.24	0.34
Nb #	6.64	7.79	7.29	4.82	3.92	6.75	6.33	7.45	3.62	5.77
Hf #	3.95	4.74	5.11	4.04	2.89	4.83	4.42	5.11	3.15	4.74
Zr #	162.22	194.15	178.52	156.03	106.78	190.68	170.22	201.05	114.41	169.37
Y #	10.42	10.28	21.19	19.35	3.86	22.43	14.53	5.17	14.00	13.95
Th #	2.43	1.53	3.58	6.19	1.15	4.33	1.98	1.51	4.73	2.52
U #	1.35	1.68	1.62	2.38	1.78	2.83	2.64	0.24	1.75	0.92
La #	4.65	5.03	11.75	18.57	1.76	12.55	11.30	10.34	14.63	8.14
Ce #	9.81	10.74	25.06	53.69	9.03	29.31	21.43	40.99	40.87	17.49
Pr #	1.33	1.30	3.17	6.16	0.77	3.50	2.76	3.48	4.98	2.09
Nd #	6.27	6.18	14.93	30.90	3.73	16.70	13.17	15.49	23.44	9.58
Sm #	3.20	2.85	7.22	11.43	2.18	7.52	5.39	7.10	8.76	4.34
Eu #	0.80	0.66	1.81	2.94	0.78	2.11	1.29	1.11	2.46	1.32
Gd #	2.14	1.88	4.95	5.87	1.48	5.01	3.35	3.32	4.95	3.40
Tb #	0.38	0.40	0.86	0.89	0.29	0.97	0.61	0.48	0.69	0.60
Dy #	2.16	2.18	4.53	4.40	1.55	5.28	3.22	2.11	3.45	3.50
Ho #	0.42	0.45	0.87	0.73	0.27	1.02	0.62	0.35	0.60	0.66
Er #	1.22	1.29	2.49	1.94	0.75	2.83	1.61	0.95	1.61	1.85
Tm #	0.24	0.28	0.40	0.34	0.15	0.48	0.34	0.29	0.32	0.32
Yb #	1.45	1.64	2.74	1.86	0.84	3.02	1.88	0.99	1.49	1.98
Lu #	0.23	0.23	0.42	0.28	0.11	0.47	0.31	0.16	0.21	0.33

[1] Dominant alteration mineral identified by near infrared-short wave infrared (NIR-SWIR) spectroscopy.

* wt%; ICP-OES

\# ppm; ICP-MS Least altered sample used to fit an approximate fractionation curve

Table A2-1 (continued) LOI-free major and trace element abundances used in multiple precursor mass change calculations (Maclean, 1990) with least altered samples indicated by shading. Values below the detection limit have been replaced with a value equal to half of the detection limit.

Sample ID	11CPM-040	11CPM-041	11CPM-042	11CPM-044	11CPM-045	11CPM-046	11CPM-047	11CPM-048	11CPM-050
SWIR Min.[1]	Ill.pheng.	Ill.pheng.	Muscovite	Ill.pheng.	NULL	Muscovite	Ill.pheng.	Ill.pheng.	Ill.pheng.
Strat. unit	2	2	3.3	3.2	3.2	3.2	3.2	3.2	3.1
SiO_2 *	67.56	68.01	66.96	69.52	69.09	52.69	64.74	65.64	65.36
Al_2O_3 *	16.66	16.46	16.89	15.43	15.87	17.25	16.83	17.10	17.05
Fe_2O_3 *	4.60	3.77	7.54	4.14	4.31	22.56	4.86	4.88	4.73
MnO *	0.06	0.09	0.08	0.41	0.17	0.06	0.12	0.12	0.12
MgO *	2.45	1.88	2.26	2.09	2.23	0.97	1.95	1.52	1.70
CaO *	1.38	2.66	0.29	1.13	1.19	0.64	3.03	2.27	2.87
Na_2O *	2.94	3.40	0.10	3.27	2.52	0.24	3.90	3.32	2.40
K_2O *	3.71	3.15	4.99	3.40	3.97	4.90	3.89	4.48	5.10
TiO_2 *	0.51	0.49	0.73	0.53	0.56	0.56	0.61	0.61	0.58
P_2O_5 *	0.12	0.07	0.15	0.07	0.09	0.12	0.08	0.06	0.10
TOTAL *	100	100	100	100	100	100	100	100	100
Ni #	2.57	2.57	8.38	2.57	5.45	2.57	2.57	2.57	2.57
Co #	3.73	3.72	10.27	3.58	4.20	3.35	2.99	2.58	3.51
Sc #	6.00	6.00	10.00	6.00	7.00	5.00	7.00	7.00	6.00
V #	19.98	20.31	54.30	19.23	22.37	14.89	13.22	15.13	18.37
Cu #	37.21	16.36	270.45	20.68	13.78	8153.45	11.85	5.84	6.18
Pb #	4.16	16.64	17.18	40.85	15.09	982.87	10.99	8.75	9.88
Zn #	68.55	75.91	74.72	93.42	73.89	98856.15	218.52	180.42	68.61
As #	6.52	7.70	47.35	15.30	25.45	445.59	11.70	11.73	14.32
Sb #	0.26	0.29	1.47	0.56	0.96	12.29	2.19	2.37	2.97
Li #	7.48	8.27	1.99	5.26	6.92	1.66	3.70	2.34	2.37
Rb #	235.73	212.27	3067.57	1311.00	7848.07	2106.18	264.58	200.85	163.39
Ba #	1150.05	375.81	648.84	1312.56	1809.72	11335.56	2025.55	1158.85	385.10
Sr #	136.34	144.65	6.38	41.75	78.99	22.29	89.03	68.03	52.78
Tl #	1.25	1.21	13.69	1.99	5.46	5.27	1.82	1.66	0.85
Ta #	0.48	0.48	0.34	0.41	0.43	0.30	0.44	0.42	0.39
Nb #	8.31	7.91	6.08	7.10	7.32	5.47	7.94	7.81	7.25
Hf #	5.37	5.51	4.13	4.44	4.61	3.55	5.10	4.68	4.41
Zr #	212.14	209.22	164.36	182.48	189.29	139.90	198.43	196.69	187.47
Y #	20.28	21.72	14.34	14.70	16.58	4.38	21.58	15.93	23.54
Th #	5.06	6.20	3.25	4.32	4.40	1.09	4.45	2.94	4.66
U #	1.76	2.52	2.30	1.86	1.94	1.75	1.68	1.40	1.55
La #	10.90	15.59	10.35	9.30	9.17	3.00	8.49	6.54	9.31
Ce #	22.69	28.67	21.00	20.90	20.90	5.47	14.75	12.16	16.65
Pr #	3.04	3.77	2.69	2.42	2.43	0.77	2.47	1.74	2.86
Nd #	13.23	17.31	13.17	11.02	10.88	2.97	10.62	7.13	12.04
Sm #	6.24	6.84	5.27	4.78	5.38	1.42	2.80	1.96	3.04
Eu #	1.53	1.59	1.33	1.12	1.29	0.34	0.79	0.56	0.83
Gd #	4.22	4.80	3.57	3.09	3.53	0.83	3.12	2.19	3.36
Tb #	0.78	0.83	0.68	0.58	0.67	0.16	0.55	0.40	0.61
Dy #	4.54	4.64	3.45	3.16	3.58	0.86	3.73	2.70	4.17
Ho #	0.89	0.90	0.70	0.59	0.69	0.17	0.79	0.58	0.90
Er #	2.58	2.70	1.92	1.76	1.90	0.63	2.46	1.89	2.76
Tm #	0.49	0.51	0.34	0.37	0.35	0.18	0.43	0.32	0.44
Yb #	2.94	3.05	2.13	1.92	2.07	0.71	2.91	2.09	3.06
Lu #	0.48	0.55	0.35	0.30	0.35	0.12	0.45	0.31	0.47

[1] Dominant alteration mineral identified by near infrared-short wave infrared (NIR-SWIR) spectroscopy.

* wt%; ICP-OES

\# ppm; ICP-MS Least altered sample used to fit an approximate fractionation curve

Table A2-1 (continued) LOI-free major and trace element abundances used in multiple precursor mass change calculations (Maclean, 1990) with least altered samples indicated by shading. Values below the detection limit have been replaced with a value equal to half of the detection limit.

Sample ID	11CPM-051	11CPM-052	11CPM-053	11CPM-054	11CPM-055	11CPM-056	11CPM-057	11CPM-058	11CPM-059	11CPM-060
SWIR Min.[1]	Ill.pheng.	Ill.pheng.	Aspectral	Aspectral	MgChl	Phengite	Phengite	Ill.pheng.	Ill.pheng.	Muscovite
Strat. unit	3.1	3.1	3.1	2	2	4.3	4.3	4.3	4.3	4.3
SiO_2 *	63.83	66.10	72.06	50.31	49.05	67.43	59.32	68.15	61.23	67.19
Al_2O_3 *	18.12	15.56	13.35	17.97	15.79	16.62	17.23	16.52	17.81	17.06
Fe_2O_3 *	4.50	4.57	3.75	9.28	7.61	5.57	13.61	6.39	11.26	7.87
MnO *	0.13	0.15	0.07	0.16	0.19	0.20	0.25	0.08	0.05	0.04
MgO *	1.70	1.76	1.32	9.37	6.36	3.10	2.44	2.77	3.27	1.95
CaO *	2.80	4.72	2.31	5.15	14.51	0.40	0.88	0.23	0.24	0.22
Na_2O *	4.40	2.22	6.12	4.16	4.71	2.63	0.17	0.11	0.17	0.15
K_2O *	3.81	4.28	0.49	2.20	1.02	3.16	5.33	5.03	5.19	4.75
TiO_2 *	0.60	0.53	0.45	1.04	0.52	0.71	0.65	0.60	0.66	0.63
P_2O_5 *	0.11	0.13	0.09	0.36	0.23	0.17	0.12	0.13	0.14	0.14
TOTAL *	100	100	100	100	100	100	100	100	100	100
Ni #	2.57	2.57	2.57	43.79	50.02	8.45	2.57	2.57	2.57	2.57
Co #	4.09	3.58	3.66	30.49	22.06	3.37	3.98	3.54	3.57	4.92
Sc #	7.00	6.00	5.00	32.00	29.00	9.00	9.00	7.00	8.00	8.00
V #	19.42	17.71	14.21	235.18	188.63	18.36	12.45	16.28	16.99	17.11
Cu #	6.54	7.34	15.80	99.91	93.68	240.96	42.88	678.67	1607.51	81.69
Pb #	11.02	9.14	10.18	5.40	4.41	18.92	42.80	25.08	14.90	6.61
Zn #	70.45	65.55	76.18	81.77	54.20	72.22	148.86	946.57	287.86	33.11
As #	10.44	6.42	7.09	16.22	28.86	13.89	52.96	25.44	21.33	20.45
Sb #	2.02	1.48	0.77	0.10	0.10	0.37	1.05	0.56	0.49	2.01
Li #	4.16	15.58	5.42	21.89	9.07	4.74	3.78	2.85	1.87	2.19
Rb #	411.52	205.91	25.42	318.41	91.97	70.93	474.63	137.25	306.05	121.74
Ba #	252.77	248.94	184.75	369.05	267.47	268.59	1288.68	1089.84	1122.95	1411.04
Sr #	67.97	64.31	67.63	223.30	224.04	24.80	7.02	6.38	2.08	2.08
Tl #	0.91	0.71	0.04	0.51	0.11	0.78	3.30	1.30	1.55	0.89
Ta #	0.46	0.42	0.37	0.18	0.07	0.42	0.42	0.41	0.43	0.43
Nb #	8.26	7.50	6.05	2.90	1.05	8.01	7.62	7.44	7.56	7.92
Hf #	5.42	4.73	3.95	2.14	0.86	4.91	5.19	4.65	4.83	4.99
Zr #	214.19	193.80	157.46	68.01	27.37	198.50	190.60	186.60	187.55	200.16
Y #	15.10	25.20	17.82	16.79	12.84	8.07	19.85	8.97	9.17	5.90
Th #	3.15	5.19	4.04	1.79	1.11	0.63	3.99	2.41	2.04	1.46
U #	1.81	1.63	2.00	0.73	0.29	1.45	2.36	1.72	1.53	1.71
La #	6.54	12.17	8.55	6.60	5.26	2.78	12.66	5.16	5.57	1.92
Ce #	18.45	20.58	16.37	16.35	10.66	5.96	25.85	11.32	10.15	3.91
Pr #	1.77	3.50	2.14	2.34	1.42	0.78	3.54	1.56	1.48	0.66
Nd #	7.61	14.24	8.78	10.83	6.27	3.22	14.81	6.45	5.86	2.63
Sm #	1.92	3.46	2.09	3.05	1.68	0.86	3.54	1.54	1.41	0.74
Eu #	0.57	0.96	0.56	0.96	0.59	0.22	0.79	0.48	0.27	0.16
Gd #	2.23	3.71	2.26	2.92	2.01	1.00	3.49	1.64	1.47	0.80
Tb #	0.39	0.64	0.42	0.52	0.35	0.18	0.62	0.28	0.25	0.17
Dy #	2.47	4.34	2.78	3.21	2.26	1.30	3.92	1.89	1.74	1.32
Ho #	0.51	0.90	0.60	0.66	0.47	0.29	0.84	0.39	0.38	0.30
Er #	1.69	2.77	1.97	1.87	1.46	0.99	2.67	1.29	1.27	1.06
Tm #	0.28	0.51	0.35	0.27	0.25	0.19	0.44	0.25	0.25	0.21
Yb #	1.92	3.19	2.33	1.83	1.39	1.36	3.02	1.42	1.35	1.30
Lu #	0.31	0.49	0.39	0.27	0.21	0.20	0.44	0.21	0.21	0.19

[1] Dominant alteration mineral identified by near infrared-short wave infrared (NIR-SWIR) spectroscopy.

* wt%; ICP-OES

\# ppm; ICP-MS Least altered sample used to fit an approximate fractionation curve

Table A2-1 (continued) LOI-free major and trace element abundances used in multiple precursor mass change calculations (Maclean, 1990) with least altered samples indicated by shading. Values below the detection limit have been replaced with a value equal to half of the detection limit.

Sample ID	11CPM-062	11CPM-063	11CPM-065	11CPM-066	11CPM-067	11CPM-078	11CPM-080	11CPM-084	11CPM-087	11CPM-088
SWIR Min.[1]	Muscovite	FeMgChl	FeMgChl	MgChl	Aspectral	Ill.musc.	Ill.pheng.	FeChl	Ill.pheng.	FeMgChl
Strat. unit	4.3	2	2	2	2	4.2	3.3	2	4.3	4.3
SiO_2 *	54.95	48.06	28.82	49.88	51.05	68.26	63.80	65.29	74.98	63.94
Al_2O_3 *	16.97	21.45	21.97	16.15	17.55	14.53	16.47	16.33	12.61	17.10
Fe_2O_3 *	21.03	16.31	32.32	9.15	9.26	4.02	6.00	4.00	2.60	4.54
MnO *	0.02	0.20	0.32	0.35	0.19	0.29	0.21	0.12	0.09	0.20
MgO *	0.90	8.07	12.76	13.15	9.21	0.97	3.28	1.16	0.76	3.76
CaO *	0.17	0.46	0.79	7.88	6.10	2.30	3.05	8.02	1.97	0.51
Na_2O *	0.17	1.48	0.09	2.36	4.24	0.81	2.76	3.82	1.74	2.49
K_2O *	5.12	2.92	1.51	0.16	1.17	8.18	3.43	0.58	4.67	6.69
TiO_2 *	0.62	0.83	0.90	0.68	0.80	0.53	0.76	0.56	0.47	0.62
P_2O_5 *	0.07	0.22	0.53	0.25	0.45	0.13	0.23	0.11	0.11	0.16
TOTAL *	100	100	100	100	100	100	100	100	100	100
Ni #	40.39	39.54	111.09	276.32	148.85	2.57	5.15	2.57	2.57	2.57
Co #	27.15	28.35	25.06	37.68	32.23	3.95	10.32	3.27	2.00	3.67
Sc #	33.00	32.00	36.00	36.00	34.00	7.00	14.00	7.00	6.00	8.00
V #	223.48	267.34	251.02	201.65	224.40	13.12	88.55	20.43	14.80	18.68
Cu #	835.18	189.68	462.69	9.14	98.97	93.34	5.87	15.44	202.62	70.17
Pb #	33.02	3.20	11.60	2.04	3.62	24.07	12.70	15.27	4.86	6.46
Zn #	107.67	53.55	162.50	137.50	78.88	3005.80	150.68	81.18	24.13	164.80
As #	57.65	3.24	28.73	1.65	5.95	10.31	1.75	12.91	1.35	2.11
Sb #	1.15	0.10	0.10	0.10	0.30	0.70	0.23	0.51	0.27	0.25
Li #	1.05	5.80	12.49	16.88	13.93	4.39	9.22	3.26	2.32	7.77
Rb #	520.41	157.40	99.28	120.39	223.10	927.76	208.24	184.67	280.69	158.26
Ba #	437.45	1332.16	312.97	196.98	448.57	1142.99	121.32	102.80	1702.01	1518.82
Sr #	2.08	11.01	9.49	92.97	198.75	29.03	30.61	165.12	23.02	54.62
Tl #	3.91	0.42	0.30	0.15	0.53	1.71	0.63	0.32	0.92	0.81
Ta #	0.07	0.09	0.16	0.11	0.13	0.32	0.31	0.40	0.31	0.43
Nb #	1.26	1.69	2.96	2.00	2.44	6.74	5.18	7.28	5.94	8.13
Hf #	1.14	1.47	2.00	1.55	1.64	4.34	3.53	4.57	3.55	4.86
Zr #	34.89	49.42	65.71	45.18	58.05	162.78	141.71	181.84	145.98	200.81
Y #	0.81	11.97	14.59	12.76	15.59	22.17	22.46	24.97	15.79	7.66
Th #	0.14	1.33	2.37	1.55	1.64	3.81	2.93	5.28	2.98	0.84
U #	0.33	1.07	0.92	0.49	0.85	1.73	1.12	1.89	1.13	1.20
La #	0.38	4.29	5.80	7.57	7.96	8.68	9.13	13.00	5.64	4.30
Ce #	0.65	9.75	13.73	16.00	18.09	17.21	14.57	28.61	12.57	8.86
Pr #	0.14	1.38	2.18	2.15	2.46	2.72	2.76	3.37	1.80	1.16
Nd #	0.56	6.36	10.01	9.36	11.15	11.99	12.08	13.68	7.33	4.61
Sm #	0.18	1.74	2.59	2.41	2.70	3.20	3.14	3.52	1.99	1.12
Eu #	0.04	0.65	0.40	0.77	0.92	0.81	0.97	0.99	0.61	0.28
Gd #	0.18	2.16	3.00	2.60	3.03	3.25	3.56	3.83	2.19	1.15
Tb #	0.04	0.36	0.41	0.41	0.49	0.58	0.59	0.67	0.39	0.21
Dy #	0.22	2.37	2.70	2.59	2.93	3.81	3.97	4.37	2.82	1.41
Ho #	0.05	0.51	0.54	0.49	0.60	0.86	0.83	0.94	0.59	0.32
Er #	0.20	1.48	1.72	1.39	1.65	2.64	2.58	2.88	1.83	1.07
Tm #	0.04	0.28	0.29	0.22	0.26	0.45	0.43	0.46	0.30	0.20
Yb #	0.11	1.48	1.70	1.33	1.58	2.96	2.71	3.06	2.01	1.19
Lu #	0.02	0.22	0.26	0.20	0.23	0.45	0.43	0.47	0.31	0.17

[1] Dominant alteration mineral identified by near infrared-short wave infrared (NIR-SWIR) spectroscopy.

* wt%; ICP-OES

\# ppm; ICP-MS Least altered sample used to fit an approximate fractionation curve

Table A2-1 (continued) LOI-free major and trace element abundances used in multiple precursor mass change calculations (Maclean, 1990) with least altered samples indicated by shading. Values below the detection limit have been replaced with a value equal to half of the detection limit.

Sample ID	11CPM-089	11CPM-090	11CPM-091	11CPM-095	11CPM-097	11CPM-099	11CPM-101	11CPM-102	11CPM-103	11CPM-104
SWIR Min.[1]	Ill.pheng.	Ill.pheng.	FeMgChl	Aspectral	MgChl	Ill.pheng.	FeMgChl	Ill.pheng.	Muscovite	Ill.musc.
Strat. unit	4.2	3.2	3.1	2	6.1	4.2	4.2	4.4	4.1	4.2
SiO_2 *	65.48	63.78	64.46	51.58	41.55	62.44	64.03	64.78	57.57	68.78
Al_2O_3 *	16.45	17.52	17.20	17.13	12.29	20.21	16.90	17.31	17.39	11.06
Fe_2O_3 *	5.12	5.30	5.66	8.69	11.59	4.85	5.50	5.43	17.01	14.69
MnO *	0.19	0.15	0.22	0.14	0.24	0.06	0.21	0.22	0.02	0.01
MgO *	2.96	2.98	3.90	7.40	22.52	2.51	3.28	4.57	1.05	0.59
CaO *	1.63	1.03	0.55	7.98	10.68	0.49	2.25	0.39	0.38	0.41
Na_2O *	4.27	3.19	3.30	5.21	0.20	0.56	3.43	4.52	0.15	0.12
K_2O *	2.96	5.12	3.76	0.95	0.04	7.97	3.44	1.85	5.47	3.43
TiO_2 *	0.71	0.73	0.73	0.64	0.74	0.73	0.73	0.72	0.68	0.62
P_2O_5 *	0.23	0.22	0.23	0.27	0.17	0.17	0.23	0.22	0.28	0.29
TOTAL *	100	100	100	100	100	100	100	100	100	100
Ni #	2.57	2.57	2.57	52.63	801.03	2.57	5.67	2.57	47.60	13.68
Co #	6.54	6.12	6.71	34.11	72.44	3.19	7.08	6.44	34.82	50.90
Sc #	11.00	11.00	11.00	33.00	28.00	11.00	12.00	11.00	33.00	15.00
V #	96.58	54.35	56.18	213.78	172.91	15.16	63.24	55.66	249.24	174.44
Cu #	1.97	1.97	1.97	125.48	55.49	5.07	634.49	1.97	80.74	16.15
Pb #	6.91	11.00	17.30	4.54	6.34	17.96	7.08	2.67	11.03	4.26
Zn #	109.76	132.02	175.75	65.92	81.45	110.21	83.86	142.10	70.44	17.59
As #	1.47	5.58	3.70	10.85	11.11	3.09	1.65	1.47	122.94	15.38
Sb #	0.10	0.10	0.10	0.10	0.10	0.71	0.23	0.10	2.37	0.10
Li #	5.15	4.97	6.76	32.98	68.77	3.78	3.94	5.13	0.84	1.69
Rb #	402.26	233.82	89.29	119.08	58.80	566.61	372.14	114.28	583.79	193.60
Ba #	1581.49	334.90	286.76	475.02	66.03	103.48	539.29	481.12	455.91	391.84
Sr #	63.64	18.84	53.52	399.99	62.90	7.62	31.91	58.55	2.08	2.08
Tl #	0.65	0.89	0.66	0.04	0.04	1.60	1.12	0.26	13.72	0.34
Ta #	0.32	0.36	0.34	0.26	0.12	0.49	0.32	0.36	0.13	0.15
Nb #	5.70	6.23	5.93	5.19	2.27	9.15	5.78	6.18	4.30	3.20
Hf #	3.99	4.21	3.94	1.33	1.56	5.89	3.89	4.29	1.29	1.46
Zr #	159.54	170.60	164.82	43.63	45.73	233.89	158.96	174.29	43.93	52.38
Y #	17.28	8.31	8.03	13.72	13.17	5.44	22.69	9.97	1.17	0.60
Th #	2.48	0.86	0.86	1.98	1.81	1.30	3.10	0.82	0.17	0.17
U #	1.02	0.69	1.05	0.74	0.42	1.17	0.90	0.99	1.41	0.44
La #	6.96	3.30	2.75	7.00	11.29	2.08	9.04	4.14	0.44	0.26
Ce #	10.65	6.52	6.57	15.08	22.94	6.26	15.04	6.86	0.85	0.35
Pr #	2.03	0.90	0.85	2.05	2.82	0.79	2.98	1.01	0.16	0.13
Nd #	8.97	3.98	3.52	9.16	12.10	3.50	13.15	4.14	0.70	0.25
Sm #	2.15	1.18	0.93	2.48	2.84	0.88	3.47	1.07	0.18	0.18
Eu #	0.73	0.37	0.26	0.82	0.85	0.21	1.09	0.35	0.04	0.04
Gd #	2.56	1.21	1.01	2.67	2.85	1.00	3.63	1.33	0.26	0.08
Tb #	0.47	0.22	0.19	0.43	0.45	0.21	0.61	0.24	0.05	0.02
Dy #	2.95	1.46	1.49	2.57	2.61	1.32	3.96	1.65	0.36	0.07
Ho #	0.63	0.32	0.33	0.52	0.50	0.29	0.84	0.37	0.09	0.02
Er #	2.02	1.05	1.09	1.47	1.45	1.02	2.62	1.25	0.25	0.16
Tm #	0.33	0.20	0.22	0.24	0.22	0.18	0.51	0.26	0.05	0.07
Yb #	2.21	1.33	1.36	1.40	1.33	1.23	2.92	1.71	0.28	0.11
Lu #	0.35	0.20	0.21	0.21	0.20	0.19	0.43	0.26	0.02	0.02

[1] Dominant alteration mineral identified by near infrared-short wave infrared (NIR-SWIR) spectroscopy.

* wt%; ICP-OES

\# ppm; ICP-MS Least altered sample used to fit an approximate fractionation curve

Table A2-1 (continued) LOI-free major and trace element abundances used in multiple precursor mass change calculations (Maclean, 1990) with least altered samples indicated by shading. Values below the detection limit have been replaced with a value equal to half of the detection limit.

Sample ID	11CPM-105	11CPM-106	11CPM-108	11CPM-110	11CPM-111	11CPM-114	11CPM-116	11CPM-121	11CPM-122	11CPM-123
SWIR Min.[1]	FeMgChl	Aspectral	Ill.pheng.	FeMgChl	FeMgChl	Ill.pheng.	Aspectral	Ill.pheng.	FeMgChl	Ill.musc.
Strat. unit	4.2	2	4.6	4.6	3.4	3.4	2	4.2	4.2	4.2
SiO_2 *	52.99	69.38	65.13	61.14	65.28	63.16	54.68	70.25	73.56	71.76
Al_2O_3 *	16.73	15.28	16.88	16.81	16.17	17.11	14.50	15.32	14.95	18.43
Fe_2O_3 *	8.59	2.94	4.07	6.89	5.36	5.36	7.32	4.67	3.13	2.95
MnO *	0.53	0.05	0.23	0.37	0.51	0.13	0.14	0.08	0.04	0.01
MgO *	6.70	1.48	1.36	3.44	2.11	2.98	5.60	2.50	3.47	0.53
CaO *	6.82	1.44	2.36	2.94	0.74	2.88	9.66	0.62	0.20	0.15
Na_2O *	5.22	5.78	2.44	0.17	3.18	4.71	4.06	2.79	0.41	0.28
K_2O *	1.49	3.10	6.76	7.25	5.73	2.75	3.30	2.92	3.62	5.05
TiO_2 *	0.64	0.44	0.61	0.77	0.69	0.71	0.53	0.66	0.50	0.73
P_2O_5 *	0.28	0.12	0.18	0.22	0.23	0.21	0.21	0.18	0.12	0.10
TOTAL *	100	100	100	100	100	100	100	100	100	100
Ni #	44.93	2.57	2.57	7.51	2.57	5.55	76.95	18.76	2.57	27.24
Co #	32.35	3.56	2.93	4.35	4.93	7.39	25.74	6.29	2.47	2.15
Sc #	29.00	5.00	9.00	15.00	12.00	11.00	29.00	11.00	7.00	11.00
V #	197.77	17.84	12.84	89.49	68.54	65.82	189.15	41.54	21.05	17.24
Cu #	128.77	22.51	20.23	1.97	1.97	1.97	132.19	11.29	5.02	10.22
Pb #	31.27	15.44	22.01	9.67	16.78	8.98	3.42	4.11	0.79	0.91
Zn #	94.28	51.73	80.83	167.48	142.35	106.88	192.96	122.68	28.49	33.88
As #	26.80	15.18	15.87	1.53	4.77	1.77	28.44	4.00	3.42	3.67
Sb #	0.90	0.48	0.36	0.10	0.23	0.33	0.22	0.26	0.10	0.34
Li #	10.05	2.74	3.20	5.51	4.93	5.85	0.39	0.39	0.39	380.54
Rb #	131.52	506.21	540.78	345.70	1124.04	280.18	893.87	116.99	1377.67	535.41
Ba #	283.48	750.70	1048.24	1127.76	915.11	218.91	470.92	417.95	609.12	251.23
Sr #	145.61	56.55	31.77	35.45	34.10	49.40	182.15	19.05	9.22	2.08
Tl #	1.29	0.71	1.26	1.23	1.56	0.55	0.70	0.32	0.83	0.67
Ta #	0.22	0.23	0.21	0.28	0.22	0.31	0.14	0.38	0.33	0.45
Nb #	4.87	7.20	7.79	5.01	5.57	5.60	3.05	7.43	7.87	9.24
Hf #	1.25	5.00	5.05	3.69	3.90	3.83	1.21	4.69	5.29	6.04
Zr #	40.93	188.96	191.87	142.83	155.14	158.71	39.27	187.71	204.67	222.04
Y #	13.62	7.25	27.69	17.20	9.65	24.53	11.56	7.37	23.22	0.96
Th #	1.83	2.73	3.69	2.29	1.66	3.76	1.51	0.45	3.53	0.24
U #	0.52	1.74	1.39	0.73	0.90	1.32	0.53	0.86	1.34	0.26
La #	7.15	6.03	9.86	5.50	6.43	10.26	6.31	3.34	10.25	0.50
Ce #	15.02	12.91	17.68	9.79	11.79	14.14	13.48	7.06	27.30	0.74
Pr #	2.15	1.46	2.93	1.73	1.60	3.18	1.80	0.93	3.66	0.15
Nd #	9.33	5.38	11.63	7.37	6.49	13.48	9.57	3.02	16.67	1.01
Sm #	2.54	1.26	3.13	2.02	1.60	3.46	2.45	0.72	4.77	0.18
Eu #	0.85	0.35	1.01	0.72	0.51	1.02	0.85	0.04	0.33	0.04
Gd #	2.76	1.28	3.67	2.35	1.52	3.67	2.52	1.47	3.21	0.42
Tb #	0.43	0.23	0.63	0.41	0.29	0.65	0.33	0.20	0.65	0.12
Dy #	2.55	1.33	4.41	2.95	1.76	4.13	2.20	1.26	4.18	0.54
Ho #	0.53	0.28	0.93	0.61	0.38	0.90	0.45	0.27	0.98	0.06
Er #	1.57	0.78	3.05	1.99	1.18	2.87	1.13	0.96	3.04	0.28
Tm #	0.29	0.17	0.52	0.35	0.21	0.50	0.20	0.18	0.57	0.16
Yb #	1.43	0.99	3.39	2.16	1.35	2.94	0.91	1.25	3.81	0.11
Lu #	0.20	0.15	0.52	0.35	0.22	0.46	0.19	0.18	0.61	0.02

[1] Dominant alteration mineral identified by near infrared-short wave infrared (NIR-SWIR) spectroscopy.

* wt%; ICP-OES

\# ppm; ICP-MS Least altered sample used to fit an approximate fractionation curve

Table A2-1 (continued) LOI-free major and trace element abundances used in multiple precursor mass change calculations (Maclean, 1990) with least altered samples indicated by shading. Values below the detection limit have been replaced with a value equal to half of the detection limit.

Sample ID	11CPM-124	11CPM-130	11CPM-131	11CPM-133	11CPM-134	11CPM-136	11CPM-137	11CPM-138	11CPM-139	11CPM-141
SWIR Min.[1]	FeMgChl	Aspectral	Aspectral	FeMgChl	FeMgChl	Phengite	FeMgChl	MgChl	FeMgChl	MgChl
Strat. unit	4.1	7.1	7.1	6.1	6.1	6.1	6.1	6.1	6.1	6.1
SiO_2 *	55.98	54.95	55.29	49.22	51.09	57.70	46.57	56.44	49.03	50.23
Al_2O_3 *	19.65	17.67	16.55	16.26	17.81	16.67	19.79	17.90	18.60	17.75
Fe_2O_3 *	7.69	10.88	9.33	10.51	9.54	11.60	10.49	10.03	10.93	10.61
MnO *	0.13	0.19	0.11	0.16	0.15	0.56	0.22	0.50	0.26	0.45
MgO *	4.71	4.50	2.22	8.87	6.32	4.18	15.72	6.67	9.26	14.90
CaO *	3.66	4.02	7.36	9.76	8.93	0.99	2.01	0.77	6.18	1.05
Na_2O *	5.17	5.37	5.33	3.21	4.99	0.13	3.48	5.54	4.54	2.53
K_2O *	1.64	0.56	1.58	0.74	0.14	7.06	0.41	1.18	0.07	1.50
TiO_2 *	1.18	1.41	1.46	1.03	0.75	0.92	0.96	0.68	0.77	0.76
P_2O_5 *	0.20	0.43	0.77	0.26	0.29	0.19	0.36	0.29	0.36	0.21
TOTAL *	100	100	100	100	100	100	100	100	100	100
Ni #	24.61	25.54	56.88	72.81	128.04	75.87	40.49	54.89	99.39	97.39
Co #	21.64	25.84	12.98	38.69	29.23	22.68	24.79	30.01	28.79	26.38
Sc #	18.00	23.00	21.00	43.00	33.00	31.00	29.00	31.00	31.00	33.00
V #	142.77	277.14	301.75	290.33	242.34	283.32	294.72	226.12	364.41	238.65
Cu #	22.51	32.53	36.19	125.52	195.04	389.85	56.42	18.65	31.30	58.51
Pb #	2.24	6.58	8.06	9.22	4.62	11.94	49.73	28.55	7.52	6.87
Zn #	81.65	124.50	125.18	90.29	340.24	356.49	142.78	350.71	154.20	307.17
As #	4.17	51.58	43.60	20.05	13.90	21.22	5.06	23.03	7.53	12.53
Sb #	0.10	0.25	0.10	1.60	0.96	0.10	0.23	0.10	0.20	0.27
Li #	8.13	14.86	7.15	27.38	14.72	12.74	27.26	11.51	12.98	26.20
Rb #	263.63	155.69	362.02	533.00	45.78	937.40	33.27	728.73	21.17	265.67
Ba #	2838.54	169.66	265.08	234.55	36.45	3105.86	74.81	187.32	309.12	1380.82
Sr #	335.11	382.68	289.58	136.61	185.04	30.17	160.03	85.64	180.38	97.71
Tl #	0.22	0.04	0.43	0.48	0.04	1.60	0.10	0.62	0.04	0.80
Ta #	0.29	0.17	0.16	0.34	0.10	0.14	0.20	0.28	0.10	0.16
Nb #	6.06	4.39	3.95	6.71	2.46	2.03	3.87	4.83	2.99	3.38
Hf #	3.61	2.38	1.96	2.82	1.22	2.08	1.91	1.66	1.78	1.48
Zr #	145.29	99.96	76.39	78.93	55.28	59.96	78.66	47.54	53.71	53.75
Y #	18.77	28.04	30.55	19.32	16.98	15.72	21.08	6.96	16.98	14.90
Th #	3.40	2.15	1.89	5.34	1.85	1.54	2.71	1.26	2.15	1.95
U #	1.25	0.79	3.57	1.46	0.61	0.51	1.01	0.78	0.86	0.56
La #	10.30	10.53	11.94	12.29	8.83	4.43	11.51	5.43	9.88	7.35
Ce #	22.58	26.78	28.55	28.19	18.62	11.31	24.98	14.40	22.05	16.88
Pr #	3.42	3.46	3.68	3.80	2.34	1.83	3.51	1.45	2.95	2.22
Nd #	15.25	16.27	18.17	16.27	11.61	6.44	14.19	6.72	12.79	10.71
Sm #	3.59	4.99	5.12	4.41	3.24	2.62	4.35	2.16	3.35	2.99
Eu #	1.06	1.31	1.67	1.30	0.82	0.31	1.09	0.25	1.15	0.74
Gd #	3.35	4.34	5.23	3.75	2.93	2.47	4.42	1.45	3.23	2.76
Tb #	0.52	0.80	0.83	0.64	0.51	0.50	0.61	0.33	0.50	0.47
Dy #	3.64	5.44	6.16	3.60	3.28	3.10	4.23	1.81	2.96	2.96
Ho #	0.76	1.09	1.08	0.79	0.70	0.70	0.72	0.28	0.70	0.58
Er #	2.31	2.59	3.07	2.43	1.79	2.12	2.55	1.13	1.74	1.37
Tm #	0.46	0.54	0.48	0.37	0.35	0.44	0.37	0.18	0.27	0.28
Yb #	1.86	3.27	2.65	2.47	1.62	2.00	2.35	1.17	1.84	1.53
Lu #	0.22	0.40	0.39	0.24	0.25	0.31	0.39	0.10	0.31	0.26

[1] Dominant alteration mineral identified by near infrared-short wave infrared (NIR-SWIR) spectroscopy.

* wt%; ICP-OES

\# ppm; ICP-MS Least altered sample used to fit an approximate fractionation curve

Table A2-1 (continued) LOI-free major and trace element abundances used in multiple precursor mass change calculations (Maclean, 1990) with least altered samples indicated by shading. Values below the detection limit have been replaced with a value equal to half of the detection limit.

Sample ID	11CPM-143	11CPM-144	11CPM-145	11CPM-146	11CPM-147	11CPM-148
SWIR Min.[1]	Ill.pheng.	FeMgChl	Ill.pheng.	MgChl	FeMgChl	Aspectral
Strat. unit	2	2	2	2	2	6.1
SiO_2 *	61.98	54.78	61.61	51.48	51.41	55.44
Al_2O_3 *	15.20	18.54	16.04	17.85	17.32	18.28
Fe_2O_3 *	8.95	10.27	7.73	9.59	9.53	10.09
MnO *	0.36	0.35	0.32	0.60	0.16	0.22
MgO *	4.09	7.57	3.48	7.08	7.37	4.58
CaO *	2.07	1.18	2.91	5.59	7.15	2.19
Na_2O *	1.72	4.70	5.65	6.50	4.70	6.38
K_2O *	4.58	1.45	1.16	0.22	1.33	1.40
TiO_2 *	0.83	0.89	0.83	0.86	0.85	0.92
P_2O_5 *	0.22	0.28	0.27	0.23	0.19	0.51
TOTAL *	100	100	100	100	100	100
Ni #	124.83	46.70	28.83	36.41	64.36	48.91
Co #	16.97	23.89	20.82	29.81	29.09	26.47
Sc #	20.00	27.00	24.00	33.00	32.00	20.00
V #	172.33	217.66	191.45	243.91	239.26	208.48
Cu #	82.78	52.72	123.68	107.66	75.85	75.66
Pb #	74.48	11.69	13.62	19.28	5.78	5.20
Zn #	303.38	404.14	657.86	775.92	106.67	134.80
As #	54.46	10.77	12.34	10.86	5.18	14.02
Sb #	7.33	0.85	1.70	0.79	3.20	0.43
Li #	8.02	15.53	12.22	16.80	12.04	23.78
Rb #	984.31	188.37	129.63	361.30	424.60	372.18
Ba #	745.97	359.18	596.75	51.66	63.56	622.77
Sr #	111.15	90.61	131.44	162.33	148.90	214.70
Tl #	2.44	0.30	1.31	0.47	0.50	0.33
Ta #	0.31	0.23	0.28	0.17	0.29	0.24
Nb #	4.24	4.39	4.48	2.39	2.54	5.68
Hf #	2.81	2.45	2.59	2.47	1.66	3.48
Zr #	94.17	91.73	97.97	60.23	56.34	112.19
Y #	11.52	19.48	19.98	17.84	17.91	22.60
Th #	1.21	2.49	2.67	1.88	1.60	2.71
U #	0.47	0.76	1.02	0.74	0.34	1.14
La #	3.81	8.37	7.15	6.49	6.61	8.35
Ce #	7.83	19.56	15.80	14.85	14.71	18.51
Pr #	1.21	2.54	2.23	2.18	2.07	2.73
Nd #	6.06	10.99	10.36	9.21	9.16	13.32
Sm #	1.61	2.33	3.27	2.90	2.68	3.20
Eu #	0.72	0.77	0.84	1.08	1.02	1.09
Gd #	2.03	3.41	3.28	3.13	3.10	3.75
Tb #	0.42	0.56	0.60	0.59	0.52	0.67
Dy #	1.96	3.73	3.79	3.43	3.17	4.32
Ho #	0.49	0.76	0.82	0.67	0.71	0.87
Er #	1.21	2.27	2.68	2.19	2.01	2.49
Tm #	0.23	0.37	0.48	0.41	0.42	0.39
Yb #	1.37	2.08	2.58	2.08	2.52	2.24
Lu #	0.23	0.34	0.37	0.34	0.30	0.38

[1] Dominant alteration mineral identified by near infrared-short wave infrared (NIR-SWIR) spectroscopy.

* wt%; ICP-OES

\# ppm; ICP-MS

Least altered sample used to fit an approximate fractionation curve

Table A2-2 Calculated fractionation curve equations approximated from the best-fit line through least altered samples on mobile element vs Zr diagrams

Element	Fractionation Curve
SiO_2	$= 41.6489e^{0.00286764[Zr]}$
Al_2O_3	$= 0.0152591[Zr]+17.1356$
Fe_2O_3	$= 11.8084e^{-0.00762916[Zr]}$
MnO	$= 0.182423e^{-0.00429148[Zr]}$
MgO	$= 13.454e^{-0.0149791[Zr]}$
CaO	$= 14.0505e^{-0.0146278[Zr]}$
Na_2O	$= 5.06713e^{-0.00253787[Zr]}$
K_2O	$= 0.669766e^{0.0101107[Zr]}$
TiO_2	$= 0.742178e^{-0.0023268[Zr]}$
P_2O_5	$= 0.374516e^{-0.00826063[Zr]}$
Ni	$= 224.895e^{-0.0235932[Zr]}$
Co	$= 76.408e^{-0.0209066[Zr]}$
Sc	$= 57.6729e^{-0.0123707[Zr]}$
V	$= 607.746e^{-0.0217368[Zr]}$
Cu	$= 61.9559e^{-0.0130237[Zr]}$
Pb	$= 5.12848e^{0.00208805[Zr]}$
Zn	$= 66.3636e^{-0.00179842[Zr]}$
As	$= 15.0333e^{-0.00531002[Zr]}$
Sb	$= 0.0796477e^{0.0100478[Zr]}$
Li	$= 29.688e^{-0.01433[Zr]}$
Rb	$= 72.0886e^{0.00195935[Zr]}$
Ba	$= 308.621e^{0.0044467[Zr]}$
Sr	$= 421.239e^{-0.0097883[Zr]}$
Tl	$= 0.147498e^{0.00924354[Zr]}$
Ta	$= 0.0642078e^{0.0102979[Zr]}$
Nb	$= 1.15585e^{0.0107962[Zr]}$
Hf	$= 1.02407e^{0.00870041[Zr]}$
Y	$= 6.2237e\text{-}^{0.00193017[Zr]}$
Th	$= 1.24817e0^{.00430439[Zr]}$
U	$= 0.236506e^{0.0115809[Zr]}$
La	$= 6.00654e^{0.000636462[Zr]}$
Ce	$= 14.0076e^{-0.000263797[Zr]}$
Pr	$= 1.99871e^{-0.000692446[Zr]}$
Nd	$= 9.09812e^{-0.000959659[Zr]}$
Sm	$= 2.45727e^{-0.000457096[Zr]}$
Eu	$= 0.922913e^{-0.00256522[Zr]}$
Gd	$= 2.88195e^{-0.00158999[Zr]}$
Tb	$= 0.479169e^{-0.00145212[Zr]}$
Dy	$= 2.97029e^{-0.00137724[Zr]}$
Ho	$= 0.616371e^{-0.00138418[Zr]}$
Er	$= 1.76673e^{-0.00100835[Zr]}$
Tm	$= 0.267076e^{0.000000000881255[Zr]}$
Yb	$= 1.52877e^{0.000638851[Zr]}$
Lu	$= 0.235914e^{0.00072182[Zr]}$

Table A2-3 Absolute mass change values calculated using the Maclean (1990) multiple precursor method, where mass change equals reconstituted values (LOI-free untreated data multiplied by Zr enrichment factors) minus the calculated precursor values. Additional steps described in text.

Sample ID	10CPM-004a	10CPM-004b	10CPM-005	10CPM-009	10CPM-010a	10CPM-010b	10CPM-012	10CPM-021	10CPM-023
SWIR Min.[1]	Ill.pheng.	Ill.pheng.	FeMgChl	Ill.pheng.	Phengite	Aspectral	Ill.pheng.	Aspectral	Ill.pheng.
Strat. unit	5.5	5.5	5.5	5.6	5.6	5.6	6.1	5.6	6.1
ΔSiO_2 *	-3.07	-13.81	-4.19	-14.54	-2.42	0.73	-6.17	-6.83	-3.35
ΔAl_2O_3 *	-0.78	-0.24	-0.86	-0.54	-0.50	-0.61	-1.34	-0.37	-1.74
ΔFe_2O_3 *	-0.40	0.10	-0.32	0.16	0.15	-0.16	0.86	0.70	-0.64
ΔMnO *	0.02	0.01	0.01	-0.03	-0.05	-0.08	0.01	-0.03	0.02
ΔMgO *	-0.41	0.61	-0.34	1.10	0.74	-0.85	1.12	0.85	-1.86
ΔCaO *	-0.22	-0.05	-0.75	-0.62	-0.95	-1.01	-1.72	-0.61	13.12
ΔNa_2O *	-0.17	-2.56	-3.37	-0.73	-3.22	-3.25	-2.96	-0.62	1.95
ΔK_2O *	0.32	1.80	7.29	1.83	4.82	6.91	3.42	0.12	0.04
ΔTiO_2 *	-0.09	-0.07	0.08	0.03	-0.04	-0.02	-0.01	-0.03	0.29
ΔP_2O_5 *	0.00	0.01	0.05	0.04	0.02	0.00	0.03	0.03	0.33
ΔTOTAL *	-4.80	-14.22	-2.41	-13.28	-1.45	1.64	-6.75	-6.78	8.15
ΔNi #	1.66	-0.49	-2.37	-1.33	-0.90	-1.20	-30.72	-0.65	-30.99
ΔCo #	0.72	0.38	-0.05	0.05	1.32	2.73	6.41	2.53	12.48
ΔSc #	-2.63	-0.52	1.05	1.24	0.46	0.32	-5.50	0.48	-4.80
ΔV #	-5.97	-0.45	-5.85	0.18	24.22	-5.58	-4.37	5.98	195.11
ΔCu #	-5.24	-3.70	330.17	-4.58	4.75	-4.52	9.08	-3.93	-22.78
ΔPb #	5.52	1.27	12.42	-2.02	37.34	14.99	-0.02	-3.06	3.29
ΔZn #	4.61	4.84	-30.73	-33.92	-28.56	-44.49	-18.79	-35.57	-38.17
ΔAs #	-1.73	-3.97	-4.54	-5.33	-3.21	4.32	-6.48	-2.61	6.64
ΔSb #	-0.04	-0.03	-0.31	-0.38	-0.27	-0.35	-0.04	-0.21	0.16
ΔLi #	-0.97	-0.36	-1.29	0.87	2.47	-1.52	35.96	2.27	-1.20
ΔRb #	12.80	85.98	59.42	-36.41	79.58	104.00	18.07	-5.29	-28.38
ΔBa #	425.74	268.18	1801.18	737.48	2823.76	904.50	757.96	317.65	214.78
ΔSr #	55.36	12.29	33.92	20.96	25.31	-9.51	233.49	20.16	219.36
ΔTl #	0.41	1.34	0.79	0.02	0.27	0.76	0.13	-0.17	-0.10
ΔTa #	0.11	0.00	0.04	0.01	0.05	0.01	0.03	0.01	0.03
ΔNb #	1.22	-0.09	0.67	0.08	-0.16	0.11	0.57	-0.32	0.62
ΔHf #	0.45	-0.15	0.20	0.08	0.45	0.48	0.04	0.07	0.31
ΔZr #	0.00	0.00	0.00	0.00	0.00	0.00	0.00	0.00	0.00
ΔY #	5.18	4.49	-2.95	-3.21	3.73	-9.03	-0.65	-0.22	10.53
ΔTh #	1.47	0.96	-0.64	-1.69	1.28	-2.29	0.38	-0.94	0.49
ΔU #	0.22	-0.21	0.06	-0.29	-0.39	-0.56	0.55	-0.22	5.41
ΔLa #	5.55	2.36	-1.65	-1.44	-1.45	-4.58	-0.16	0.80	3.50
ΔCe #	10.14	5.83	-4.19	-6.68	-3.89	-11.20	-0.07	-4.59	7.12
ΔPr #	1.38	0.66	-0.35	-0.44	0.01	-1.11	-0.03	0.00	1.12
ΔNd #	5.13	2.03	-1.79	-2.72	-0.49	-5.25	0.17	-0.66	5.38
ΔSm #	0.52	-0.04	-0.88	-1.01	-0.45	-1.74	-0.07	-0.70	1.29
ΔEu #	0.05	0.00	-0.25	-0.29	-0.27	-0.47	-0.06	-0.16	0.43
ΔGd #	0.60	0.12	-0.71	-0.85	0.03	-1.64	0.08	-0.47	2.02
ΔTb #	0.08	0.06	-0.12	-0.16	0.01	-0.31	-0.05	-0.07	0.26
ΔDy #	0.86	0.68	-0.69	-0.99	0.48	-1.90	-0.15	-0.31	1.88
ΔHo #	0.20	0.16	-0.11	-0.19	0.14	-0.39	-0.01	-0.05	0.39
ΔEr #	0.63	0.61	-0.21	-0.51	0.54	-1.12	-0.07	-0.04	1.18
ΔTm #	0.10	0.09	-0.05	-0.07	0.08	-0.18	0.05	-0.06	0.17
ΔYb #	0.94	0.79	-0.14	-0.55	0.75	-1.37	0.09	-0.36	1.07
ΔLu #	0.12	0.12	-0.02	-0.07	0.14	-0.22	0.01	-0.04	0.16

[1] Dominant alteration mineral identified by near infrared-short wave infrared (NIR-SWIR) spectroscopy.

* wt%; ICP-OES

\# ppm; ICP-MS Least altered sample used to fit an approximate fractionation curve

Table A2-3 (continued) Absolute mass change values calculated using the Maclean (1990) multiple precursor method, where mass change equals reconstituted values (LOI-free untreated data multiplied by Zr enrichment factors) minus the calculated precursor values. Additional steps described in text.

Sample ID	10CPM-025	10CPM-029	10CPM-032	10CPM-036b	10CPM-038	10CPM-041	10CPM-044	10CPM-052	10CPM-059	10CPM-062
SWIR Min.[1]	Aspectral	Aspectral	Ill.pheng.	Phengite	Ill.pheng.	Aspectral	Ill.musc.	Ill.pheng.	MgChl	Aspectral
Strat. unit	5.5	2	2	6.1	2	6.1	6.1	6.1	2	2
ΔSiO_2 *	-10.34	-5.19	4.26	-16.50	-12.65	-4.59	-5.38	4.32	13.51	4.92
ΔAl_2O_3 *	-0.67	-1.79	-1.73	-1.83	-1.83	-1.49	-1.84	-1.27	1.58	-1.00
ΔFe_2O_3 *	1.03	1.45	0.17	1.60	5.68	2.00	2.63	0.23	1.74	-1.34
ΔMnO *	-0.02	-0.01	-0.03	0.02	0.07	-0.05	-0.01	0.00	0.03	-0.01
ΔMgO *	1.03	-2.63	-2.48	1.17	1.19	0.25	-0.94	2.52	0.35	-2.29
ΔCaO *	0.45	4.15	2.73	-0.49	1.13	-4.19	1.12	1.07	0.35	3.17
ΔNa_2O *	-3.34	2.42	2.77	0.08	-0.25	-3.25	-0.58	-0.64	3.30	0.62
ΔK_2O *	2.82	-1.05	-1.30	-1.19	0.47	5.18	0.50	0.30	-5.45	-0.17
ΔTiO_2 *	-0.02	0.34	0.28	0.48	0.70	0.20	0.48	-0.04	0.02	-0.14
ΔP_2O_5 *	0.01	0.12	0.09	0.31	0.27	0.13	0.43	-0.04	0.01	-0.08
ΔTOTAL *	-9.06	-2.19	4.75	-16.35	-5.23	-5.81	-3.59	6.45	15.42	3.68
ΔNi #	-1.68	-11.01	-16.60	-14.73	-9.07	-17.34	-28.86	34.52	2.39	-27.01
ΔCo #	2.03	10.20	0.79	9.36	20.31	2.65	15.36	9.66	2.08	-12.66
ΔSc #	0.28	4.62	0.61	2.63	8.80	0.04	0.69	11.06	4.40	-8.24
ΔV #	-7.14	167.57	154.35	109.77	272.96	73.84	183.23	3.45	3.33	-58.53
ΔCu #	-4.93	-21.36	-23.13	-15.06	-15.04	56.03	-18.98	75.02	-0.03	30.85
ΔPb #	58.47	-1.03	-2.31	0.28	-0.69	-0.50	2.22	-1.52	12.14	0.91
ΔZn #	53.45	-16.28	-54.33	-30.71	-33.12	40.36	-18.36	-24.76	13.23	-14.45
ΔAs #	27.54	1.58	11.58	9.17	54.58	-3.87	13.94	7.36	0.79	-3.44
ΔSb #	0.20	0.06	-0.05	0.02	-0.12	0.12	0.52	0.13	-0.61	-0.01
ΔLi #	-0.21	-5.49	-4.43	29.34	15.40	25.84	9.59	24.93	-0.34	-4.34
ΔRb #	81.34	-71.47	-53.58	-51.37	-18.86	866.86	14.61	-36.18	-49.37	-48.45
ΔBa #	-207.18	-364.52	-336.95	-19.47	1205.56	91.65	70.39	257.58	184.63	-26.49
ΔSr #	72.17	95.68	128.36	256.78	188.58	116.53	283.74	442.18	115.10	322.89
ΔTl #	0.66	-0.13	-0.14	-0.22	-0.06	0.63	0.08	-0.01	-1.23	-0.09
ΔTa #	0.07	0.02	0.01	0.08	0.03	-0.02	0.06	0.06	-0.36	-0.02
ΔNb #	0.60	0.19	0.11	1.82	0.72	0.35	1.00	1.32	-8.34	-0.23
ΔHf #	0.56	0.42	0.46	0.57	0.33	0.16	0.55	0.08	-1.93	-0.11
ΔZr #	0.00	0.00	0.00	0.00	0.00	0.00	0.00	0.00	0.00	0.00
ΔY #	13.48	7.09	5.05	15.12	16.36	1.54	10.47	0.12	-3.11	-1.15
ΔTh #	1.98	-0.09	-0.19	0.23	0.84	-0.04	0.11	0.41	-0.81	-0.03
ΔU #	0.39	0.31	0.11	0.25	-0.13	0.20	0.38	0.01	-2.90	-0.08
ΔLa #	15.27	1.01	0.17	1.31	6.08	-0.57	1.67	0.39	1.25	0.07
ΔCe #	30.36	4.22	2.78	7.84	18.64	1.30	7.89	0.16	10.76	-2.24
ΔPr #	3.74	0.56	0.31	1.00	2.08	-0.17	0.96	0.08	0.37	-0.25
ΔNd #	13.98	2.99	1.56	5.44	9.67	0.20	4.96	0.44	1.47	-1.31
ΔSm #	2.91	0.75	0.42	1.78	2.26	0.28	1.39	0.07	-0.34	-0.40
ΔEu #	0.64	0.27	0.19	0.58	0.76	0.10	0.48	0.01	-0.06	-0.10
ΔGd #	2.77	1.34	0.90	2.35	2.80	0.31	2.06	0.17	-0.15	-0.18
ΔTb #	0.35	0.15	0.15	0.41	0.42	0.06	0.28	0.00	-0.04	-0.07
ΔDy #	2.42	1.25	1.23	2.85	2.92	0.12	1.96	0.17	-0.10	-0.32
ΔHo #	0.52	0.29	0.22	0.56	0.58	0.11	0.39	0.01	-0.02	-0.05
ΔEr #	1.71	0.87	0.57	1.62	1.69	0.05	1.21	0.04	-0.19	-0.08
ΔTm #	0.26	0.17	0.09	0.22	0.25	0.06	0.17	0.03	-0.09	0.00
ΔYb #	1.73	1.00	0.69	1.54	1.70	-0.15	1.18	0.02	-0.56	-0.14
ΔLu #	0.31	0.16	0.11	0.20	0.24	0.06	0.16	0.00	-0.09	0.00

[1] Dominant alteration mineral identified by near infrared-short wave infrared (NIR-SWIR) spectroscopy.

* wt%; ICP-OES

\# ppm; ICP-MS Least altered sample used to fit an approximate fractionation curve

Table A2-3 (continued) Absolute mass change values calculated using the Maclean (1990) multiple precursor method, where mass change equals reconstituted values (LOI-free untreated data multiplied by Zr enrichment factors) minus the calculated precursor values. Additional steps described in text.

Sample ID	10CPM-064	10CPM-065	10CPM-069	10CPM-071	10CPM-073	10CPM-074	10CPM-075	10CPM-076	10CPM-078	10CPM-083
SWIR Min.[1]	FeMgChl	FeMgChl	MgChl	MgChl	Ill.pheng.	FeMgChl	Phengite	FeMgChl	Ill.pheng.	FeMgChl
Strat. unit	2	4.6	2	6.1	6.1	4.6	4.6	4.6	2	4.6
ΔSiO_2 *	3.42	-6.44	-3.74	-6.34	-0.53	0.56	5.71	-2.80	-1.00	11.60
ΔAl_2O_3 *	-1.06	-0.72	-0.95	-1.71	-1.82	-0.18	-0.60	-0.53	-1.34	-0.65
ΔFe_2O_3 *	-2.91	1.08	-1.69	1.09	3.31	4.08	0.05	-0.58	0.89	0.16
ΔMnO *	-0.04	0.00	-0.05	0.03	0.24	-0.04	0.03	0.00	0.10	-0.03
ΔMgO *	-3.50	-0.02	-3.53	0.34	-0.70	-0.31	-0.19	-0.54	3.69	0.08
ΔCaO *	2.47	-0.61	-2.85	-0.25	3.18	-0.39	-0.21	-0.82	3.36	-0.90
ΔNa_2O *	0.92	1.50	-0.40	0.50	-0.07	1.59	2.10	-0.58	-1.68	1.95
ΔK_2O *	-0.22	-0.53	-0.11	-1.36	-0.69	-2.00	-1.66	2.79	-0.07	-1.27
ΔTiO_2 *	-0.15	-0.01	-0.19	0.08	0.66	0.08	-0.01	0.04	-0.02	-0.03
ΔP_2O_5 *	-0.11	0.04	-0.14	-0.03	0.13	0.01	0.05	0.04	0.11	0.02
$\Delta TOTAL$ *	-1.18	-5.72	-13.64	-7.64	3.72	3.40	5.26	-2.99	4.03	10.92
ΔNi #	-10.94	-1.81	-47.46	-2.75	-15.34	0.10	-1.05	-1.05	316.66	-1.09
ΔCo #	-8.87	1.14	-10.27	4.34	4.60	1.61	1.20	1.02	25.13	0.36
ΔSc #	-10.73	-0.59	-7.59	4.49	4.09	0.69	-0.43	0.25	2.75	0.85
ΔV #	-76.43	1.08	-107.00	84.10	189.42	6.89	-0.63	4.72	40.49	-2.76
ΔCu #	30.46	19.91	-37.07	-3.01	24.83	4.73	-4.39	9.72	59.05	10.53
ΔPb #	1.56	2.24	1.80	-3.39	3.83	84.63	4.47	6.61	-1.55	47.23
ΔZn #	-29.35	165.10	-21.23	267.97	331.34	-19.55	-15.11	720.70	-4.92	345.34
ΔAs #	-8.59	20.33	8.92	-3.89	1.96	126.20	20.61	1.38	-3.99	0.22
ΔSb #	-0.02	-0.05	-0.03	0.07	0.64	33.04	3.61	-0.24	0.16	0.12
ΔLi #	-9.85	0.33	-5.99	6.03	7.76	0.13	1.89	-0.76	6.05	3.44
ΔRb #	-64.47	-48.22	-47.27	-79.23	-44.47	-26.90	-53.99	-0.89	-35.37	-51.67
ΔBa #	64.38	436.18	-52.04	-342.12	871.27	8351.53	414.45	677.29	-21.99	119.94
ΔSr #	265.17	52.08	252.93	182.42	86.59	179.62	164.35	5.78	201.68	47.77
ΔTl #	-0.10	0.29	-0.08	-0.14	-0.09	19.94	1.24	0.32	0.10	0.06
ΔTa #	-0.01	0.04	-0.02	0.03	0.03	0.02	0.02	0.02	0.02	0.05
ΔNb #	-0.29	0.35	-0.28	0.50	0.28	-0.48	0.35	0.19	0.41	0.74
ΔHf #	-0.19	0.38	-0.10	0.25	0.73	-0.19	0.24	0.00	0.49	0.21
ΔZr #	0.00	0.00	0.00	0.00	0.00	0.00	0.00	0.00	0.00	0.00
ΔY #	-2.60	-4.17	-2.57	1.31	11.97	-2.19	-7.01	-9.03	-0.81	1.61
ΔTh #	-0.13	-0.28	-0.17	0.26	0.13	0.12	-0.71	-2.24	0.33	-1.33
ΔU #	0.04	-0.04	-0.17	-0.04	0.10	-0.06	0.16	-0.20	0.18	-0.11
ΔLa #	-1.79	-0.60	-1.69	0.01	2.07	-3.73	-2.27	-5.26	1.17	-0.48
ΔCe #	-3.94	-2.18	-2.95	1.19	4.70	-8.28	-3.77	-10.69	2.25	-4.99
ΔPr #	-0.52	-0.31	-0.49	0.09	0.69	-0.96	-0.59	-1.42	0.26	-0.26
ΔNd #	-1.99	-2.06	-2.30	0.20	4.12	-4.46	-3.42	-6.33	1.17	-1.71
ΔSm #	-0.57	-0.99	-0.48	0.18	1.37	-1.39	-1.22	-2.09	0.09	-0.79
ΔEu #	-0.19	-0.23	-0.20	0.15	0.58	-0.17	-0.33	-0.55	0.06	-0.15
ΔGd #	-0.37	-0.86	-0.53	0.28	2.23	-1.04	-1.22	-1.81	0.13	-0.46
ΔTb #	-0.08	-0.14	-0.06	0.03	0.30	-0.16	-0.20	-0.31	-0.01	-0.06
ΔDy #	-0.32	-0.88	-0.37	0.28	2.36	-0.76	-1.32	-1.88	0.01	-0.32
ΔHo #	-0.08	-0.17	-0.09	0.05	0.52	-0.12	-0.25	-0.39	-0.01	-0.05
ΔEr #	-0.16	-0.50	-0.18	0.19	1.37	-0.30	-0.75	-1.09	-0.07	-0.11
ΔTm #	-0.03	-0.11	-0.02	0.03	0.20	-0.04	-0.11	-0.17	-0.01	-0.04
ΔYb #	-0.12	-0.51	-0.12	0.22	1.38	-0.34	-1.03	-1.17	-0.02	-0.25
ΔLu #	-0.03	-0.09	-0.02	0.04	0.24	-0.02	-0.15	-0.18	0.01	-0.05

[1] Dominant alteration mineral identified by near infrared-short wave infrared (NIR-SWIR) spectroscopy.

* wt%; ICP-OES

\# ppm; ICP-MS

Least altered sample used to fit an approximate fractionation curve

Table A2-3 (continued) Absolute mass change values calculated using the Maclean (1990) multiple precursor method, where mass change equals reconstituted values (LOI-free untreated data multiplied by Zr enrichment factors) minus the calculated precursor values. Additional steps described in text.

Sample ID	10CPM-084	10CPM-086	10CPM-090	10CPM-093	10CPM-095	10CPM-098b	10CPM-102	10CPM-105	10CPM-106	10CPM-108
SWIR Min.[1]	FeChl	Aspectral	Aspectral	Ill.pheng.	Ill.pheng.	FeChl	Ill.pheng.	FeMgChl	Ill.pheng.	FeMgChl
Strat. unit	4.6	4.6	4.6	4.3	4.3	4.4	4.1	4.4	4.1	4.1
ΔSiO_2 *	-5.88	-14.21	14.05	-10.33	-0.70	-3.28	10.44	-1.32	-11.56	5.87
ΔAl_2O_3 *	-0.93	-0.10	-0.30	-0.68	-0.58	-1.78	-1.53	-1.45	-1.73	-1.68
ΔFe_2O_3 *	-0.64	0.83	-0.67	0.42	0.10	0.57	0.02	0.83	1.48	-1.04
ΔMnO *	-0.01	-0.01	-0.04	0.00	0.01	0.51	0.20	0.50	0.50	0.15
ΔMgO *	0.39	0.71	-0.58	1.03	0.62	-0.87	-0.71	-0.09	0.86	-3.45
ΔCaO *	-1.20	-0.20	-0.11	0.01	-0.36	-2.04	-2.01	-1.15	-1.91	-4.18
ΔNa_2O *	-0.76	1.80	4.48	1.55	0.29	-3.18	-3.83	-0.60	-1.58	-4.53
ΔK_2O *	3.31	-1.37	-4.26	-2.39	-0.54	5.27	7.49	1.85	1.67	8.28
ΔTiO_2 *	-0.01	0.03	0.05	-0.01	0.02	0.08	0.01	0.06	0.22	0.09
ΔP_2O_5 *	0.02	0.05	0.05	0.06	0.02	0.18	0.18	0.17	0.21	0.09
$\Delta TOTAL$ *	-5.71	-12.48	12.67	-10.35	-1.13	-4.53	10.26	-1.19	-11.85	-0.40
ΔNi #	-2.79	-0.15	0.05	-1.75	-1.16	-15.18	-7.96	10.20	-1.55	-22.29
ΔCo #	-0.70	2.44	-0.17	2.22	0.53	1.68	-0.36	0.08	20.47	3.54
ΔSc #	-0.47	1.67	0.92	0.15	1.21	-4.68	-2.91	-2.15	0.83	-2.76
ΔV #	-5.67	4.65	2.57	14.10	0.06	31.82	18.44	25.48	98.69	66.65
ΔCu #	-5.90	-3.33	-3.34	-0.53	-4.47	42.65	15.67	-8.92	-12.39	178.70
ΔPb #	-4.94	3.27	0.11	5.66	6.59	307.21	1013.73	18.56	25.36	31.85
ΔZn #	100.68	8.78	-17.82	-7.40	7.35	2198.62	240.86	90.81	171.37	3226.31
ΔAs #	-2.55	-1.08	-3.30	0.36	0.10	-1.37	31.03	2.75	2.39	34.27
ΔSb #	-0.17	-0.46	-0.40	-0.35	-0.36	-0.14	0.28	0.79	-0.06	0.93
ΔLi #	3.63	1.83	-0.45	7.43	3.32	3.74	1.97	-1.87	1.27	-7.49
ΔRb #	-55.96	-8.02	-99.52	-48.30	-14.46	-34.19	94.81	-49.11	-54.45	92.03
ΔBa #	-170.28	619.70	-615.88	-76.88	178.95	1176.63	3219.53	-2.98	617.31	3354.72
ΔSr #	3.73	78.78	44.74	169.71	83.40	19.86	27.37	28.51	30.67	19.98
ΔTl #	0.16	-0.32	-0.77	-0.29	-0.09	0.62	1.67	0.29	0.50	2.26
ΔTa #	0.03	-0.05	-0.04	0.03	0.00	0.06	0.07	0.06	0.05	0.07
ΔNb #	0.89	-0.40	0.22	0.28	0.36	0.78	0.62	0.55	0.85	1.84
ΔHf #	0.42	0.00	-0.01	0.19	0.20	0.33	0.53	0.30	0.24	0.29
ΔZr #	0.00	0.00	0.00	0.00	0.00	0.00	0.00	0.00	0.00	0.00
ΔY #	-5.95	6.24	-9.56	-4.55	-3.63	-6.38	-1.45	-7.36	-3.78	-1.66
ΔTh #	-2.09	-0.50	-1.85	0.01	-1.47	-1.19	-0.18	-1.63	-1.02	-0.20
ΔU #	-0.29	-0.21	0.18	0.09	-0.22	0.16	-0.05	-0.11	0.44	0.33
ΔLa #	-4.16	2.91	-5.10	-2.10	-3.02	-3.77	1.46	-4.51	-2.67	-1.79
ΔCe #	-10.80	0.13	-8.29	0.02	-7.83	-9.91	0.14	-11.30	-4.83	-5.12
ΔPr #	-1.19	0.57	-1.34	-0.38	-0.91	-1.16	0.24	-1.29	-0.68	-0.57
ΔNd #	-5.31	1.80	-5.65	-2.33	-3.98	-5.51	0.67	-6.01	-3.12	-2.37
ΔSm #	-1.66	0.12	-2.06	-1.01	-1.34	-1.53	-0.30	-1.69	-0.94	-0.61
ΔEu #	-0.45	0.08	-0.47	-0.27	-0.28	-0.50	-0.18	-0.45	-0.27	-0.35
ΔGd #	-1.50	0.68	-1.79	-0.90	-0.98	-1.52	-0.31	-1.59	-0.75	-0.42
ΔTb #	-0.25	0.11	-0.31	-0.14	-0.16	-0.24	-0.06	-0.26	-0.13	-0.05
ΔDy #	-1.53	0.71	-1.88	-0.86	-0.86	-1.45	-0.29	-1.64	-0.69	-0.24
ΔHo #	-0.30	0.17	-0.39	-0.16	-0.15	-0.29	-0.03	-0.31	-0.15	-0.06
ΔEr #	-0.83	0.44	-1.17	-0.42	-0.39	-0.80	-0.11	-0.85	-0.41	-0.14
ΔTm #	-0.14	0.03	-0.18	-0.05	-0.08	-0.12	-0.03	-0.11	-0.05	-0.04
ΔYb #	-1.06	0.34	-1.38	-0.48	-0.48	-0.79	0.04	-0.86	-0.30	-0.09
ΔLu #	-0.16	0.05	-0.21	-0.08	-0.06	-0.12	0.02	-0.11	-0.06	-0.01

[1] Dominant alteration mineral identified by near infrared-short wave infrared (NIR-SWIR) spectroscopy.

* wt%; ICP-OES

\# ppm; ICP-MS Least altered sample used to fit an approximate fractionation curve

Table A2-3 (continued) Absolute mass change values calculated using the Maclean (1990) multiple precursor method, where mass change equals reconstituted values (LOI-free untreated data multiplied by Zr enrichment factors) minus the calculated precursor values. Additional steps described in text.

Sample ID	10CPM-109	10CPM-113b	10CPM-114	10CPM-116a	10CPM-120	10CPM-128	10CPM-129	10CPM-137	10CPM-139
SWIR Min.[1]	FeMgChl	Muscovite	Ill.pheng.	Phengite	Phengite	Aspectral	FeMgChl	Ill.pheng.	Ill.pheng.
Strat. unit	4.3	4.4	4.4	**4.3**	**6.1**	7.1	6.1	2	3.4
ΔSiO_2 *	-12.20	10.71	58.84	**274.54**	**-16.06**	-30.30	-8.20	-5.47	2.24
ΔAl_2O_3 *	-1.15	-0.77	-0.24	**-1.75**	**-1.49**	-1.15	-1.65	-1.70	-0.30
ΔFe_2O_3 *	1.33	-0.14	0.82	**1300.68**	**0.85**	4.64	2.09	7.13	0.34
ΔMnO *	0.05	-0.08	-0.07	**0.85**	**0.02**	-0.01	0.04	-0.01	-0.01
ΔMgO *	0.92	-1.09	-0.36	**-0.88**	**1.08**	1.27	-2.18	-1.87	-0.01
ΔCaO *	-1.38	-0.99	-0.87	**-0.64**	**0.66**	17.18	-2.40	5.03	-0.56
ΔNa_2O *	-0.68	-2.61	-3.12	**-0.83**	**2.97**	0.09	1.27	-2.87	-0.32
ΔK_2O *	0.09	7.47	0.13	**0.41**	**-2.65**	-1.57	-0.77	-1.29	-1.08
ΔTiO_2 *	0.06	-0.02	-0.04	**-0.15**	**0.01**	0.29	0.80	0.40	-0.01
ΔP_2O_5 *	0.07	0.02	-0.07	**0.32**	**0.29**	0.11	0.52	-0.08	0.02
ΔTOTAL *	-12.87	12.49	55.01	**1572.56**	**-14.33**	-9.46	-10.47	-0.72	0.32
ΔNi #	-4.35	-1.54	1.28	**118.54**	**10.77**	146.85	-30.85	-33.01	-0.26
ΔCo #	2.06	0.77	-0.64	**12.21**	**8.19**	26.65	-1.12	8.19	0.78
ΔSc #	0.52	-1.73	-1.03	**-6.27**	**6.59**	17.19	-6.51	9.55	0.19
ΔV #	22.83	-7.61	-4.66	**-25.96**	**131.60**	110.24	21.67	352.41	2.90
ΔCu #	-7.11	1500.65	93.35	**84558.05**	**21.63**	10.98	-25.24	96.14	-3.57
ΔPb #	-3.16	6.12	0.31	**13348.90**	**-1.39**	0.81	-1.08	-0.14	0.30
ΔZn #	19.31	-44.61	184.78	**24207.24**	**-23.00**	-39.41	-37.17	-30.86	-14.93
ΔAs #	-4.68	19.85	2.81	**19557.06**	**3.92**	18.27	-6.37	2.05	2.09
ΔSb #	-0.27	0.07	0.72	**321.56**	**0.86**	1.24	0.05	0.47	1.28
ΔLi #	3.77	-2.30	0.93	**11.33**	**5.99**	30.52	8.85	-3.94	-0.81
ΔRb #	-25.09	114.00	239.89	**18.63**	**-81.55**	2.11	-17.86	-65.99	27.02
ΔBa #	-87.56	4134.15	-284.77	**38669.13**	**-371.43**	-424.41	-144.83	-307.40	-499.72
ΔSr #	13.16	-6.29	-8.08	**1211.72**	**115.03**	97.19	190.23	291.36	83.07
ΔTl #	0.11	2.02	0.72	**374.24**	**-0.46**	-0.22	-0.10	-0.23	-0.04
ΔTa #	0.02	0.03	0.01	**0.13**	**0.25**	0.26	0.06	0.03	-0.11
ΔNb #	0.07	0.47	0.01	**3.03**	**5.09**	5.43	1.15	-0.12	-0.41
ΔHf #	0.03	-0.12	0.36	**-0.85**	**-0.03**	0.40	0.10	0.35	-0.20
ΔZr #	0.00	0.00	0.00	**0.00**	**0.00**	0.00	0.00	0.00	0.00
ΔY #	-4.07	-11.46	3.84	**1.79**	**3.56**	1.15	3.97	15.17	5.87
ΔTh #	-1.24	-2.51	2.16	**1.50**	**7.08**	3.99	1.72	0.93	0.72
ΔU #	-0.35	0.11	0.57	**4.50**	**1.38**	1.70	-0.05	0.05	-0.16
ΔLa #	-1.26	-6.37	-0.89	**7.94**	**18.13**	7.26	6.91	0.51	3.30
ΔCe #	-6.75	-13.20	-0.54	**9.98**	**38.72**	27.88	12.81	6.33	4.72
ΔPr #	-0.40	-1.63	-0.11	**1.83**	**4.85**	2.69	1.94	0.80	0.86
ΔNd #	-2.26	-7.47	-1.22	**5.37**	**19.50**	10.80	8.18	4.16	4.34
ΔSm #	-1.12	-2.07	-0.50	**0.67**	**3.16**	1.73	1.36	1.47	0.71
ΔEu #	-0.30	-0.56	-0.28	**-0.03**	**0.71**	0.47	0.36	0.52	0.26
ΔGd #	-0.93	-2.12	-0.48	**-1.08**	**1.93**	1.14	1.24	2.18	1.58
ΔTb #	-0.18	-0.35	0.01	**-0.07**	**0.17**	0.10	0.14	0.37	0.18
ΔDy #	-0.96	-2.28	0.51	**0.46**	**0.72**	0.41	0.85	2.79	1.08
ΔHo #	-0.20	-0.47	0.16	**0.14**	**0.06**	0.02	0.16	0.58	0.22
ΔEr #	-0.47	-1.42	0.63	**-0.41**	**0.16**	-0.07	0.38	1.76	0.56
ΔTm #	-0.08	-0.19	0.12	**0.73**	**0.00**	-0.05	0.08	0.28	0.06
ΔYb #	-0.51	-1.58	0.97	**0.20**	**-0.11**	-0.26	0.42	2.01	0.30
ΔLu #	-0.08	-0.24	0.18	**0.08**	**-0.01**	-0.05	0.03	0.28	0.06

[1] Dominant alteration mineral identified by near infrared-short wave infrared (NIR-SWIR) spectroscopy.

* wt%; ICP-OES

\# ppm; ICP-MS Least altered sample used to fit an approximate fractionation curve

Table A2-3 (continued) Absolute mass change values calculated using the Maclean (1990) multiple precursor method, where mass change equals reconstituted values (LOI-free untreated data multiplied by Zr enrichment factors) minus the calculated precursor values. Additional steps described in text.

Sample ID	10CPM-140a	10CPM-140d	10CPM-140e	10CPM-140f	10CPM-141	10CPM-146	10CPM-156	10CPM-159	10CPM-163a
SWIR Min.[1]	Phengite	Aspectral	Ill.pheng.	Ill.pheng.	Aspectral	Phengite	Ill.pheng.	Phengite	Aspectral
Strat. unit	3.2	3.2	3.2	3.2	3.2	6.1	2	5.5	5.5
ΔSiO_2 *	30.33	93.88	395.29	-20.98	-11.72	-14.44	-6.84	-0.82	11.61
ΔAl_2O_3 *	-0.65	-1.77	-1.80	-0.68	-0.39	-1.82	-1.82	-0.23	-0.64
ΔFe_2O_3 *	2.48	825.84	855.72	0.16	0.85	2.53	4.50	-1.42	0.01
ΔMnO *	-0.08	0.16	0.26	-0.04	0.01	-0.04	0.00	-0.06	-0.01
ΔMgO *	0.14	-3.02	-3.94	1.54	0.33	0.61	-2.22	-0.38	0.02
ΔCaO *	-1.14	-4.62	-4.08	-0.04	-0.10	-1.97	0.74	-0.77	-0.03
ΔNa_2O *	-3.32	-3.59	1.29	-0.14	1.08	0.00	1.56	-2.84	2.12
ΔK_2O *	0.73	2.50	0.23	-1.45	-1.95	-0.38	0.12	4.02	-2.44
ΔTiO_2 *	0.01	-0.38	-0.49	-0.12	-0.04	0.34	0.70	-0.06	-0.01
ΔP_2O_5 *	-0.08	0.55	0.80	0.00	0.03	0.44	0.25	0.01	0.00
$\Delta TOTAL$ *	28.42	909.55	1243.30	-21.75	-11.88	-14.72	-3.01	-2.54	10.63
ΔNi #	-0.64	-14.72	-2.41	6.96	1.83	-26.75	-20.74	-0.17	-1.05
ΔCo #	3.77	-8.41	-3.73	3.94	2.39	12.99	13.63	-0.72	0.47
ΔSc #	-1.79	-18.48	-15.65	0.01	-0.81	-2.08	2.63	-0.77	-0.24
ΔV #	8.23	-46.38	-92.09	19.34	6.76	136.66	274.18	6.96	-3.79
ΔCu #	45.78	407870.91	718849.01	317.13	46.88	48.75	43.85	13.44	8.73
ΔPb #	39.70	3426.00	12048.04	11.79	3.21	1.37	0.80	34.87	4.05
ΔZn #	46.15	26369.63	112176.80	209.44	22.52	-19.36	-17.81	33.63	-2.60
ΔAs #	18.77	3216.49	6224.76	22.91	3.14	4.78	-0.75	13.98	-0.22
ΔSb #	2.65	71.92	97.62	1.60	0.10	0.00	-0.08	0.94	-0.07
ΔLi #	1.01	-6.57	-4.67	7.93	3.21	14.17	-5.79	-0.83	1.87
ΔRb #	80.12	5.85	-55.68	-41.42	-35.00	-47.92	-45.77	141.45	-19.32
ΔBa #	3674.99	9694.23	37927.90	36.90	-237.00	-30.91	-1.29	734.79	421.55
ΔSr #	42.32	1489.32	2766.76	104.83	102.03	351.19	127.42	9.71	167.69
ΔTl #	4.31	369.41	219.06	1.55	-0.15	-0.11	-0.04	1.02	-0.30
ΔTa #	0.07	0.07	0.13	0.02	0.02	0.05	0.03	0.05	0.03
ΔNb #	0.35	1.11	3.13	-0.18	-0.32	0.99	0.55	0.03	0.07
ΔHf #	0.42	-0.81	-0.52	0.10	-0.27	0.23	0.59	0.20	0.78
ΔZr #	0.00	0.00	0.00	0.00	0.00	0.00	0.00	0.00	0.00
ΔY #	1.92	-2.80	-5.94	0.16	-7.25	6.49	11.87	-5.75	-8.31
ΔTh #	1.72	1.22	0.55	-0.59	-1.83	-0.30	-0.20	-1.51	-0.50
ΔU #	0.86	22.17	4.93	-0.12	0.16	0.24	1.21	-0.35	-0.14
ΔLa #	7.22	16.12	2.96	-2.58	-3.94	0.45	2.42	-3.52	-0.14
ΔCe #	12.11	21.89	1.85	-6.05	-8.97	4.16	5.80	-7.95	1.49
ΔPr #	1.42	2.64	0.39	-0.63	-1.15	0.46	1.06	-0.93	-0.29
ΔNd #	4.87	7.77	-5.10	-2.95	-5.40	2.54	5.38	-4.16	-1.80
ΔSm #	0.04	1.46	0.05	-0.96	-1.65	0.71	1.53	-1.42	-0.88
ΔEu #	-0.06	-0.36	-0.22	-0.18	-0.46	0.32	0.57	-0.38	-0.27
ΔGd #	-0.13	-0.35	-1.48	-0.51	-1.54	1.46	2.42	-1.18	-1.08
ΔTb #	-0.05	0.07	-0.16	-0.05	-0.27	0.17	0.35	-0.23	-0.19
ΔDy #	-0.02	-0.16	-1.73	-0.23	-1.70	1.34	2.23	-1.31	-1.36
ΔHo #	0.08	-0.15	-0.29	-0.03	-0.35	0.27	0.47	-0.25	-0.29
ΔEr #	0.44	-0.03	-0.70	0.08	-1.02	0.79	1.43	-0.73	-0.94
ΔTm #	0.06	0.34	0.40	-0.01	-0.17	0.12	0.25	-0.14	-0.18
ΔYb #	0.66	-0.49	-0.13	0.11	-1.20	0.73	1.30	-0.85	-1.18
ΔLu #	0.12	-0.05	0.02	0.02	-0.20	0.10	0.21	-0.12	-0.19

[1] Dominant alteration mineral identified by near infrared-short wave infrared (NIR-SWIR) spectroscopy.

* wt%; ICP-OES

\# ppm; ICP-MS Least altered sample used to fit an approximate fractionation curve

Table A2-3 (continued) Absolute mass change values calculated using the Maclean (1990) multiple precursor method, where mass change equals reconstituted values (LOI-free untreated data multiplied by Zr enrichment factors) minus the calculated precursor values. Additional steps described in text.

Sample ID	10CPM-163b	10CPM-166a	10CPM-166b	10CPM-167	10CPM-168a	10CPM-172	10CPM-175	10CPM-176	10CPM-178
SWIR Min.[1]	Phengite	Kaolinite WX	Ill.pheng.	Ill.pheng.	Phengite	FeMgChl	FeMgChl	FeMgChl	FeMgChl
Strat. unit	5.5	6.1	6.1	4.6	4.6	4.2	7.1	7.1	7.1
ΔSiO_2 *	18.13	35.36	-10.69	-14.02	-7.48	1.81	-2.20	-8.10	-18.37
ΔAl_2O_3 *	-0.33	-1.81	-1.78	-0.57	-0.53	-0.55	-0.71	-1.81	-1.79
ΔFe_2O_3 *	0.05	5.83	7.40	0.84	-0.52	0.67	0.83	1.31	2.28
ΔMnO *	-0.04	0.12	0.50	0.09	-0.01	-0.02	0.05	0.06	0.02
ΔMgO *	-0.57	2.27	2.47	1.09	-0.08	0.76	0.01	4.54	4.33
ΔCaO *	-0.55	6.55	7.15	-0.71	-0.69	-0.84	-0.79	7.86	4.91
ΔNa_2O *	4.18	-1.66	-4.27	-0.92	1.17	1.94	0.85	-1.89	-2.14
ΔK_2O *	-4.13	0.40	-0.07	0.05	-0.14	-1.89	-0.40	-0.32	-1.98
ΔTiO_2 *	0.02	0.54	0.68	0.03	0.03	0.01	0.02	0.24	0.28
ΔP_2O_5 *	0.02	0.45	0.10	0.04	0.05	0.04	0.01	0.05	0.05
ΔTOTAL *	16.79	48.05	1.49	-14.08	-8.19	1.94	-2.32	1.95	-12.40
ΔNi #	0.07	-15.45	-12.55	-1.46	-1.15	-0.95	-1.66	75.47	110.79
ΔCo #	0.90	11.15	28.53	0.36	0.37	1.14	1.22	23.18	20.85
ΔSc #	1.08	0.39	4.44	0.21	0.83	0.56	0.68	17.70	12.62
ΔV #	-1.22	102.61	248.08	2.53	1.07	-4.02	0.08	163.86	160.42
ΔCu #	2.14	5.35	12.56	18.22	123.61	-0.91	0.26	77.97	51.32
ΔPb #	7.06	-1.06	6.71	562.21	3.48	8.68	6.58	0.39	-2.82
ΔZn #	-2.91	14.34	77.54	887.63	-26.54	10.81	17.68	-12.91	-24.28
ΔAs #	1.96	4.23	86.67	2.92	-1.10	-1.25	-1.23	2.80	8.63
ΔSb #	-0.12	3.27	7.53	-0.20	-0.38	-0.36	-0.24	0.10	-0.15
ΔLi #	-1.67	18.67	16.09	3.46	-2.01	0.39	1.29	27.07	44.71
ΔRb #	-93.51	9.54	-41.89	-19.98	-71.36	-65.10	-30.01	-42.09	-62.28
ΔBa #	-484.45	1294.78	585.76	-177.80	1804.27	-133.19	-98.61	-215.83	-432.12
ΔSr #	142.51	142.91	70.62	19.44	23.13	57.86	31.12	330.63	300.15
ΔTl #	-0.76	0.40	-0.04	-0.05	-0.18	-0.36	-0.03	-0.15	-0.31
ΔTa #	-0.02	0.03	0.02	0.05	0.03	0.03	0.01	0.14	0.11
ΔNb #	-0.30	0.73	0.79	-0.03	0.00	0.34	0.39	3.27	1.68
ΔHf #	0.13	0.84	0.36	-0.10	0.00	0.18	0.34	0.42	1.13
ΔZr #	0.00	0.00	0.00	0.00	0.00	0.00	0.00	0.00	0.00
ΔY #	-5.15	15.60	9.71	-3.44	-9.36	-4.75	-4.35	3.02	4.24
ΔTh #	-0.56	0.28	-0.10	-1.54	-2.10	-0.52	-1.59	3.62	2.19
ΔU #	-0.48	0.23	0.52	-0.18	-0.44	0.04	-0.35	1.32	0.24
ΔLa #	-1.63	5.74	0.90	-1.62	-5.45	-2.08	-2.61	5.64	7.16
ΔCe #	1.83	15.02	3.00	-7.43	-10.61	0.06	-8.23	13.50	17.44
ΔPr #	-0.37	2.00	0.59	-0.68	-1.41	-0.55	-0.64	2.03	2.20
ΔNd #	-2.18	8.72	3.43	-3.02	-6.42	-2.46	-3.46	8.59	8.65
ΔSm #	-0.92	2.50	0.95	-1.13	-1.83	-0.89	-1.26	1.53	1.46
ΔEu #	-0.34	0.82	0.42	-0.35	-0.55	-0.29	-0.29	0.33	0.43
ΔGd #	-0.82	3.01	1.50	-0.88	-1.76	-0.80	-1.00	1.12	1.26
ΔTb #	-0.16	0.46	0.27	-0.17	-0.30	-0.14	-0.16	0.13	0.12
ΔDy #	-0.85	2.79	1.93	-0.93	-1.83	-0.72	-0.95	0.85	0.80
ΔHo #	-0.17	0.65	0.38	-0.19	-0.38	-0.14	-0.18	0.14	0.17
ΔEr #	-0.49	1.98	1.19	-0.58	-1.07	-0.40	-0.50	0.31	0.40
ΔTm #	-0.07	0.29	0.19	-0.12	-0.18	-0.07	-0.09	0.07	0.05
ΔYb #	-0.76	1.76	1.18	-0.73	-1.24	-0.52	-0.70	0.32	0.26
ΔLu #	-0.12	0.25	0.15	-0.12	-0.21	-0.10	-0.10	0.03	0.06

[1] Dominant alteration mineral identified by near infrared-short wave infrared (NIR-SWIR) spectroscopy.

* wt%; ICP-OES

\# ppm; ICP-MS

Least altered sample used to fit an approximate fractionation curve

Table A2-3 (continued) Absolute mass change values calculated using the Maclean (1990) multiple precursor method, where mass change equals reconstituted values (LOI-free untreated data multiplied by Zr enrichment factors) minus the calculated precursor values. Additional steps described in text.

Sample ID	10CPM-181	10CPM-185	10CPM-190	10CPM-191	10CPM-193	10CPM-194	10CPM-195	10CPM-198	10CPM-199	10CPM-200
SWIR Min.[1]	Ill.pheng.	Phengite	Ill.pheng.	FeMgChl	Aspectral	MgChl	MgChl	MgChl	Ill.pheng.	Ill.pheng.
Strat. unit	7.1	7.1	3.2	3.1	7.1	7.1	7.1	2	1.2	1.1
ΔSiO_2 *	-6.91	-4.04	-14.75	-5.87	-8.51	-0.29	-6.41	4.17	-15.01	-16.45
ΔAl_2O_3 *	-1.84	-1.46	-0.56	-0.51	-1.55	-1.27	-1.58	-1.11	0.35	-0.05
ΔFe_2O_3 *	3.11	0.86	-0.11	0.70	0.24	2.66	-1.16	-1.69	0.69	0.01
ΔMnO *	0.01	0.01	0.01	0.06	0.03	0.01	-0.02	-0.05	0.01	0.00
ΔMgO *	6.00	-0.74	0.05	1.00	1.08	0.10	-0.80	-3.72	0.35	-0.02
ΔCaO *	4.01	7.25	0.33	-0.53	1.60	3.30	16.13	-0.31	-0.24	0.18
ΔNa_2O *	-1.11	-3.30	-1.83	2.03	-2.04	-1.59	-0.02	1.43	-0.54	0.04
ΔK_2O *	-1.39	-1.16	1.27	-2.73	0.77	0.19	-0.42	-0.72	1.12	0.81
ΔTiO_2 *	0.24	0.11	0.03	-0.03	0.15	0.11	0.19	-0.10	-0.13	-0.17
ΔP_2O_5 *	0.01	-0.10	0.02	0.04	-0.08	-0.11	-0.02	-0.06	0.01	0.02
ΔTOTAL *	2.13	-2.58	-15.53	-5.84	-8.30	3.11	5.90	-2.16	-13.40	-15.63
ΔNi #	76.12	-23.02	-1.44	1.50	-2.29	-6.68	105.02	-53.46	0.60	-0.12
ΔCo #	23.91	4.06	-0.04	1.71	12.51	1.97	4.65	-10.97	1.40	0.72
ΔSc #	19.99	4.38	1.00	-0.82	8.47	3.44	1.95	-7.47	-0.01	-1.83
ΔV #	190.26	78.74	-0.24	2.20	115.12	67.67	62.68	-39.71	5.26	-0.10
ΔCu #	114.83	71.27	-1.70	33.87	74.80	147.18	0.33	128.05	1.72	-0.21
ΔPb #	-1.77	-1.90	0.61	15.12	-1.44	-1.01	-3.82	-1.89	0.19	3.84
ΔZn #	-31.41	-26.02	-15.28	476.69	-22.10	-29.14	-34.30	-36.04	6.90	-10.08
ΔAs #	20.63	34.44	-3.60	14.76	1.79	9.17	-3.02	38.90	6.40	1.84
ΔSb #	1.12	0.82	-0.38	0.46	0.12	-0.02	0.10	-0.02	-0.26	0.15
ΔLi #	24.07	15.14	0.56	3.20	25.56	22.52	15.27	-6.80	0.08	-1.50
ΔRb #	-65.46	-69.84	11.01	-77.94	8.92	-29.20	-54.65	-52.52	94.86	31.90
ΔBa #	-234.12	-329.38	99.28	522.81	-51.38	-231.24	-252.48	-217.85	108.09	265.97
ΔSr #	420.17	99.63	7.19	54.17	282.03	388.16	218.40	94.15	22.25	49.57
ΔTl #	-0.15	-0.20	0.45	-0.30	0.01	-0.07	-0.13	-0.10	0.09	-0.11
ΔTa #	0.15	0.04	0.02	0.04	0.02	0.01	0.02	0.01	-0.06	0.00
ΔNb #	2.89	0.76	-0.04	-0.46	0.45	0.06	0.33	-0.12	-3.01	-1.90
ΔHf #	0.44	0.54	0.13	0.00	0.46	-0.01	0.16	0.40	-0.59	-0.16
ΔZr #	0.00	0.00	0.00	0.00	0.00	0.00	0.00	0.00	0.00	0.00
ΔY #	1.46	3.38	1.85	-7.79	0.85	-0.09	1.45	-1.38	-6.17	-8.49
ΔTh #	2.38	1.61	-0.04	-1.22	0.87	0.37	1.15	-0.20	-2.00	-2.09
ΔU #	0.70	0.19	-0.35	0.40	0.57	0.21	1.72	-0.07	-0.94	-0.42
ΔLa #	8.10	6.39	-0.57	-2.90	3.31	2.04	2.66	-1.67	-3.51	-4.98
ΔCe #	18.78	11.68	-4.11	-6.13	7.51	3.83	5.68	-3.80	-9.38	-9.97
ΔPr #	2.62	1.65	0.24	-0.88	0.95	0.46	0.74	-0.47	-0.83	-1.31
ΔNd #	11.45	5.90	1.31	-4.43	3.58	1.82	3.37	-1.80	-3.96	-5.87
ΔSm #	1.74	0.97	-0.05	-1.49	0.59	0.17	0.46	-0.41	-1.44	-1.89
ΔEu #	0.41	0.23	-0.01	-0.38	0.14	0.07	0.18	-0.13	-0.36	-0.49
ΔGd #	1.08	0.81	0.16	-1.49	0.34	0.09	0.61	-0.22	-1.31	-1.71
ΔTb #	0.08	0.10	-0.01	-0.25	0.04	-0.02	0.06	-0.06	-0.23	-0.29
ΔDy #	0.54	0.69	0.12	-1.47	0.37	0.19	0.39	-0.20	-1.35	-1.78
ΔHo #	0.05	0.14	0.07	-0.29	0.06	0.02	0.07	-0.02	-0.26	-0.37
ΔEr #	0.15	0.36	0.47	-0.89	0.18	0.07	0.10	-0.04	-0.76	-1.02
ΔTm #	0.03	0.02	0.06	-0.15	0.01	0.01	0.01	-0.01	-0.14	-0.19
ΔYb #	-0.01	0.41	0.60	-1.09	0.30	0.08	0.19	0.05	-0.88	-1.19
ΔLu #	0.02	0.07	0.12	-0.17	0.02	-0.01	0.01	0.03	-0.15	-0.19

[1] Dominant alteration mineral identified by near infrared-short wave infrared (NIR-SWIR) spectroscopy.

* $wt^{0}{}_{0}$; ICP-OES

\# ppm; ICP-MS Least altered sample used to fit an approximate fractionation curve

Table A2-3 (continued) Absolute mass change values calculated using the Maclean (1990) multiple precursor method, where mass change equals reconstituted values (LOI-free untreated data multiplied by Zr enrichment factors) minus the calculated precursor values. Additional steps described in text.

Sample ID	10CPM-202b	10CPM-206	10CPM-207	10CPM-208	10CPM-209b	11CPM-003	11CPM-004	11CPM-006	11CPM-007
SWIR Min.[1]	MgChl	Aspectral	Aspectral	Kaolinite WX	Aspectral	Phengite	Aspectral	Ill.pheng.	Ill.pheng.
Strat. unit	2	4.1	4.3	1.1	6.1	3.2	3.3	3.1	3.1
ΔSiO_2 *	-6.68	93.48	2066.49	13.85	-3.33	-9.52	-0.14	-24.95	-4.74
ΔAl_2O_3 *	-1.79	-1.63	-1.85	-0.08	-1.83	-0.68	-1.14	-0.81	-0.54
ΔFe_2O_3 *	2.88	40.73	6031.43	0.13	1.50	0.96	8.18	0.20	0.15
ΔMnO *	0.07	-0.10	3.50	-0.05	-0.03	0.00	-0.06	0.01	-0.02
ΔMgO *	7.59	-4.97	-0.21	-0.26	-1.72	0.49	1.95	0.13	0.66
ΔCaO *	2.43	-5.93	3.12	-0.62	5.72	0.74	-1.31	0.99	0.53
ΔNa_2O *	-0.96	-4.35	-2.07	-3.05	2.87	-0.06	-2.80	-0.43	-0.86
ΔK_2O *	0.58	9.04	1.75	-3.18	-1.54	-0.50	1.12	-0.50	0.01
ΔTiO_2 *	0.18	0.07	0.54	-0.19	0.63	0.01	0.05	-0.04	-0.04
ΔP_2O_5 *	0.02	-0.17	1.01	-0.01	0.14	0.00	0.03	0.03	-0.03
ΔTOTAL *	4.31	126.18	8103.71	6.52	2.39	-8.55	5.88	-25.36	-4.89
ΔNi #	222.39	-13.37	184.60	3.85	-24.53	-1.70	18.40	253.03	-1.12
ΔCo #	30.15	85.30	3790.21	1.38	-1.33	0.65	7.19	1.01	0.84
ΔSc #	8.51	-8.56	145.38	-2.08	0.23	0.30	-0.57	-1.53	-0.86
ΔV #	98.06	28.45	56.32	1.38	133.61	-3.93	52.46	1.04	3.14
ΔCu #	69.09	207.62	97159.78	20.51	-19.66	2.72	1664.88	6.15	4.89
ΔPb #	3.81	188.81	216384.75	21.54	-0.33	0.63	163.02	-0.51	-0.29
ΔZn #	-6.71	68.36	18420.06	-19.81	-53.23	-2.95	1737.61	16.17	2.76
ΔAs #	41.20	262.17	74202.33	57.35	-5.60	-4.61	337.25	5.43	1.99
ΔSb #	0.03	6.16	3307.54	7.03	0.30	-0.20	123.73	0.28	-0.22
ΔLi #	26.78	-8.03	23.94	19.06	-5.20	3.79	8.66	1.70	0.91
ΔRb #	22.23	90.28	364.21	-18.01	-77.75	-32.25	-2.31	-58.55	6.65
ΔBa #	1328.39	7444.16	921572.18	3208.17	-373.62	-340.30	1202.70	-483.74	-138.80
ΔSr #	193.74	42.98	8497.74	285.68	151.97	20.13	38.45	38.77	102.80
ΔTl #	0.18	19.21	463.99	-0.24	-0.27	0.00	4.06	0.28	0.02
ΔTa #	0.10	0.06	1.48	-0.04	0.05	0.00	0.02	-0.04	0.00
ΔNb #	0.97	1.80	9.22	-2.05	0.35	1.04	1.79	0.33	-0.20
ΔHf #	1.00	-0.04	6.76	-0.27	0.38	-0.03	-0.20	-0.28	-0.04
ΔZr #	0.00	0.00	0.00	0.00	0.00	0.00	0.00	0.00	0.00
ΔY #	1.26	-12.85	20.03	-3.75	4.58	9.21	12.48	1.96	1.13
ΔTh #	2.15	-1.36	5.54	0.25	-0.18	1.17	1.87	0.47	1.61
ΔU #	0.65	0.12	10.81	-0.33	0.09	-0.35	-0.04	-0.21	0.09
ΔLa #	9.17	-4.44	17.43	0.88	2.70	3.33	8.22	0.11	2.52
ΔCe #	23.85	-12.38	36.37	3.69	8.10	5.85	23.07	-1.78	7.04
ΔPr #	3.09	-1.01	3.87	0.21	1.03	1.21	2.34	0.12	0.83
ΔNd #	13.07	-0.02	12.17	0.22	5.45	5.06	9.37	-0.33	2.76
ΔSm #	2.17	-1.98	12.41	-0.63	1.22	1.10	2.19	-0.29	0.28
ΔEu #	0.54	-0.70	2.55	-0.25	0.52	0.29	0.64	-0.12	0.02
ΔGd #	1.44	-2.43	4.07	-0.75	1.16	1.16	2.19	-0.14	0.30
ΔTb #	0.13	-0.39	1.22	-0.13	0.14	0.26	0.46	0.00	0.07
ΔDy #	0.59	-2.12	3.12	-0.69	1.02	1.72	2.47	0.15	0.33
ΔHo #	0.04	-0.52	1.10	-0.14	0.17	0.35	0.59	0.05	0.05
ΔEr #	0.06	-1.50	4.13	-0.43	0.56	1.16	1.60	0.24	0.07
ΔTm #	-0.03	-0.18	1.37	-0.06	0.09	0.16	0.24	0.04	0.00
ΔYb #	-0.03	-1.34	7.40	-0.55	0.70	1.25	1.96	0.30	0.25
ΔLu #	0.01	-0.20	1.39	-0.08	0.11	0.19	0.20	0.04	0.02

[1] Dominant alteration mineral identified by near infrared-short wave infrared (NIR-SWIR) spectroscopy.

* wt%; ICP-OES

\# ppm; ICP-MS Least altered sample used to fit an approximate fractionation curve

Table A2-3 (continued) Absolute mass change values calculated using the Maclean (1990) multiple precursor method, where mass change equals reconstituted values (LOI-free untreated data multiplied by Zr enrichment factors) minus the calculated precursor values. Additional steps described in text.

Sample ID	11CPM-008	11CPM-009	11CPM-010	11CPM-011	11CPM-012	11CPM-013	11CPM-014	11CPM-015	11CPM-016	11CPM-017
SWIR Min.[1]	Ill.pheng.	Ill.musc.	Ill.pheng.	FeMgChl	MgChl	FeMgChl	Phengite	Ill.pheng.	Phengite	Phengite
Strat. unit	3.1	3.1	3.1	2	2	2	4.4	4.4	4.3	4.3
ΔSiO_2 *	-14.03	3.77	-21.92	-7.41	-16.01	1.46	-8.77	-5.22	-2.75	-20.37
ΔAl_2O_3 *	-0.65	-0.69	0.72	-1.68	-1.85	-1.04	0.23	-0.95	-1.58	-0.78
ΔFe_2O_3 *	0.33	-0.53	1.57	0.23	2.48	0.16	0.97	1.56	3.28	1.91
ΔMnO *	0.00	-0.02	0.03	0.00	-0.01	0.02	0.64	0.38	0.14	0.08
ΔMgO *	0.54	-0.06	1.13	1.84	2.92	-0.28	2.61	0.45	-0.58	3.43
ΔCaO *	0.90	0.23	1.55	-1.29	0.65	2.59	5.41	-0.07	-2.05	0.06
ΔNa_2O *	-1.17	0.47	0.15	-0.32	-1.96	-1.53	0.62	-1.27	-4.00	-3.00
ΔK_2O *	0.36	-1.39	-2.74	0.33	1.58	1.64	-0.28	1.34	2.83	0.46
ΔTiO_2 *	-0.04	-0.07	0.04	0.19	0.23	-0.11	0.05	0.06	0.02	-0.05
ΔP_2O_5 *	-0.02	-0.02	0.00	0.01	0.02	-0.13	0.03	0.08	-0.01	-0.04
ΔTOTAL *	-13.79	1.69	-19.47	-8.11	-11.95	2.78	1.52	-3.65	-4.71	-18.29
ΔNi #	-1.75	5.75	0.89	2.63	6.79	-55.80	0.82	-2.85	2.09	-2.37
ΔCo #	0.60	0.67	2.20	10.59	11.58	-4.60	3.08	3.66	6.71	0.89
ΔSc #	-0.90	-0.98	1.96	7.39	12.27	-8.06	1.52	-0.40	0.16	-2.49
ΔV #	1.03	-0.93	10.43	71.69	141.59	-61.97	8.78	25.37	45.53	1.85
ΔCu #	2.21	23.30	3.11	65.48	81.36	110.96	7.40	24.60	198.11	17.66
ΔPb #	-1.19	4.35	1.64	3.93	0.22	-0.53	34.57	4.19	362.60	12.36
ΔZn #	0.19	31.40	4.72	13.24	4.97	-5.73	21.60	48.66	3321.49	368.87
ΔAs #	0.13	8.57	4.99	2.27	3.37	5.15	4.49	1.79	31.40	3.80
ΔSb #	-0.20	2.90	0.09	0.18	0.65	1.84	-0.35	-0.30	0.48	-0.14
ΔLi #	-1.78	-1.47	-0.91	18.45	17.08	0.14	3.50	-0.58	-0.43	3.75
ΔRb #	-30.11	-70.64	20.46	-24.01	85.46	20.36	2.32	25.91	-22.66	66.22
ΔBa #	-261.53	-350.96	-588.57	-149.51	-19.99	-285.45	-171.28	-195.87	86.63	664.04
ΔSr #	128.37	128.42	157.96	186.34	130.33	140.33	345.52	47.97	-0.84	13.46
ΔTl #	0.03	-0.37	-0.40	0.10	0.59	0.26	0.31	0.94	2.06	0.79
ΔTa #	0.02	0.01	-0.19	0.02	0.12	0.10	-0.03	-0.02	0.03	0.00
ΔNb #	0.08	-0.07	-3.26	0.76	1.05	2.64	-1.26	-0.31	0.70	-0.03
ΔHf #	-0.21	-0.01	-1.88	-0.03	0.49	-0.18	-0.17	-0.29	0.08	-0.18
ΔZr #	0.00	0.00	0.00	0.00	0.00	0.00	0.00	0.00	0.00	0.00
ΔY #	2.47	-0.80	3.18	0.64	6.73	-2.78	21.46	-0.21	-3.41	6.39
ΔTh #	1.03	0.60	1.56	-0.21	0.47	0.28	4.45	0.54	-0.06	2.14
ΔU #	-0.05	0.43	-1.00	0.23	0.43	0.18	0.48	-0.25	0.39	0.20
ΔLa #	1.18	1.85	2.67	-1.38	2.00	0.19	14.25	1.93	-1.63	2.21
ΔCe #	4.71	1.21	9.93	0.24	8.16	-0.55	37.33	3.37	-2.71	7.28
ΔPr #	0.43	0.15	0.95	0.03	1.12	-0.14	4.41	0.69	-0.40	0.72
ΔNd #	1.31	0.09	3.36	0.04	5.82	-0.76	16.92	2.47	-2.13	2.27
ΔSm #	-0.01	-0.34	0.49	0.14	1.45	-0.25	3.88	0.15	-0.81	0.29
ΔEu #	0.00	-0.08	0.19	0.06	0.45	-0.12	1.69	0.18	-0.34	-0.15
ΔGd #	0.19	-0.16	0.72	0.20	1.66	-0.32	4.67	0.29	-0.81	0.34
ΔTb #	0.03	-0.05	0.10	0.06	0.24	-0.04	0.73	0.02	-0.09	0.10
ΔDy #	0.43	-0.24	0.63	0.34	1.82	-0.37	4.49	0.08	-0.42	1.02
ΔHo #	0.06	-0.05	0.16	0.10	0.33	-0.11	0.85	0.02	-0.10	0.24
ΔEr #	0.31	-0.08	0.38	0.28	1.02	-0.30	2.84	0.12	-0.12	0.85
ΔTm #	0.06	0.00	0.02	0.05	0.19	-0.04	0.46	0.09	0.01	0.11
ΔYb #	0.27	-0.18	0.19	0.19	0.87	-0.22	2.83	-0.12	-0.14	0.86
ΔLu #	0.04	0.01	0.05	0.02	0.11	-0.02	0.42	-0.01	-0.04	0.14

[1] Dominant alteration mineral identified by near infrared-short wave infrared (NIR-SWIR) spectroscopy.

* wt%; ICP-OES

\# ppm; ICP-MS Least altered sample used to fit an approximate fractionation curve

Table A2-3 (continued) Absolute mass change values calculated using the Maclean (1990) multiple precursor method, where mass change equals reconstituted values (LOI-free untreated data multiplied by Zr enrichment factors) minus the calculated precursor values. Additional steps described in text.

Sample ID	11CPM-018	11CPM-019	11CPM-020	11CPM-021	11CPM-022	11CPM-024	11CPM-025	11CPM-026	11CPM-027	11CPM-028
SWIR Min.[1]	Muscovite	Ill.musc.	Phengite	Phengite	Phengite	FeChl	FeChl	Aspectral	Ankerite	Ill.pheng.
Strat. unit	4.2	3.2	3.1	3.1	3.1	4.5	4.4	4.4	4.3	4.3
ΔSiO_2 *	-1.72	-7.66	-7.79	3.03	-12.03	-6.60	-6.75	-8.03	-9.92	-14.51
ΔAl_2O_3 *	-0.96	-0.68	-0.60	-0.57	-0.63	-0.23	-0.76	-0.87	-0.72	-0.90
ΔFe_2O_3 *	8.07	6.99	1.13	0.06	1.19	3.53	0.79	-1.28	2.76	1.85
ΔMnO *	0.38	-0.06	0.01	-0.03	0.07	0.13	0.01	-0.03	0.05	0.09
ΔMgO *	-1.08	-0.06	0.09	-0.48	0.96	0.88	-0.54	-0.83	-0.06	0.52
ΔCaO *	-7.49	-0.90	-0.64	-0.84	-0.91	-0.59	0.36	0.10	2.47	1.18
ΔNa_2O *	-4.44	-3.31	-1.52	-3.18	-2.99	-2.17	0.09	-0.46	-0.89	-1.88
ΔK_2O *	2.40	0.59	2.82	6.55	4.23	1.22	0.85	2.69	2.36	2.06
ΔTiO_2 *	-0.01	-0.03	-0.03	-0.04	0.00	0.04	0.01	0.00	0.01	0.00
ΔP_2O_5 *	-0.16	-0.03	-0.01	0.01	-0.01	-0.01	0.00	-0.02	0.15	-0.02
$\Delta TOTAL$ *	-4.99	-5.15	-6.55	4.51	-10.12	-3.80	-5.95	-8.73	-3.78	-11.61
ΔNi #	-36.19	-1.61	2.49	-0.99	2.13	6.17	-1.99	-2.54	-1.73	-2.78
ΔCo #	2.79	3.23	1.46	1.39	2.35	0.55	-2.22	-2.17	11.47	0.36
ΔSc #	1.14	-1.32	-1.14	-0.40	0.35	2.05	0.19	-0.44	-0.42	-0.81
ΔV #	-79.14	0.56	2.02	1.32	18.55	0.22	-14.61	-6.52	-4.05	-6.61
ΔCu #	780.97	67.02	15.69	33.24	33.12	56.08	-1.42	0.00	86.92	2.54
ΔPb #	19.44	-0.49	154.12	413.18	15.79	35.93	-1.74	-3.88	31.84	-3.36
ΔZn #	193.89	-8.60	263.13	463.16	563.09	183.11	-45.34	-26.38	0.01	5.05
ΔAs #	1.30	23.38	21.96	47.22	6.06	10.75	-5.57	-1.22	0.75	-5.18
ΔSb #	0.31	4.40	0.96	0.82	-0.12	-0.32	-0.33	-0.10	0.03	-0.22
ΔLi #	-9.92	-0.92	-1.50	-1.40	3.29	7.73	1.91	-0.71	0.34	2.10
ΔRb #	10.64	-43.59	189.86	151.95	31.94	240.22	44.82	42.68	16.04	77.46
ΔBa #	200.30	-58.71	747.04	1769.58	2265.54	-19.59	243.11	518.86	2146.46	350.29
ΔSr #	16.37	-1.57	6.34	9.80	30.79	25.04	7.97	13.09	57.33	29.54
ΔTl #	1.41	0.33	2.29	2.54	0.84	0.27	0.17	0.24	0.30	0.43
ΔTa #	-0.04	0.00	-0.02	0.00	-0.01	-0.03	0.03	0.02	0.06	0.01
ΔNb #	-0.32	-0.04	-0.13	-0.18	-0.05	-0.65	-0.04	-0.06	-0.04	0.10
ΔHf #	-0.23	-0.50	-0.25	-0.37	-0.22	-0.54	0.28	0.15	0.37	-0.15
ΔZr #	0.00	0.00	0.00	0.00	0.00	0.00	0.00	0.00	0.00	0.00
ΔY #	-2.97	-2.62	-5.36	-5.45	0.48	6.96	1.87	-5.56	28.77	11.51
ΔTh #	-0.64	-0.10	-1.28	-1.01	0.37	-0.15	-0.28	-1.14	2.36	1.55
ΔU #	-0.04	-0.11	-0.44	-0.30	-0.06	-0.57	-0.36	-0.02	1.06	-0.16
ΔLa #	-1.99	-1.29	-3.61	-3.41	-0.31	7.07	-1.83	-3.85	7.36	2.99
ΔCe #	-5.20	-2.19	-7.20	-7.64	0.74	12.96	-3.27	-5.38	17.12	9.10
ΔPr #	-0.68	-0.23	-0.96	-0.77	0.08	1.38	-0.28	-0.96	2.46	1.16
ΔNd #	-3.04	-1.77	-4.48	-3.98	-0.38	4.63	-0.10	-3.89	12.83	6.95
ΔSm #	-0.69	-0.78	-1.48	-1.19	-0.33	0.44	1.29	-0.32	7.80	4.39
ΔEu #	-0.16	-0.32	-0.29	-0.36	-0.22	0.06	0.41	-0.16	1.81	0.95
ΔGd #	-0.53	-0.81	-1.28	-1.17	-0.39	0.73	0.49	-0.93	5.38	2.06
ΔTb #	-0.09	-0.09	-0.19	-0.20	-0.07	0.10	0.12	-0.11	1.05	0.53
ΔDy #	-0.46	-0.48	-1.15	-1.10	-0.05	0.99	0.61	-0.92	5.74	2.65
ΔHo #	-0.09	-0.07	-0.21	-0.20	0.04	0.19	0.14	-0.19	1.09	0.51
ΔEr #	-0.18	-0.11	-0.64	-0.56	0.25	0.60	0.33	-0.53	3.09	1.44
ΔTm #	0.00	0.00	-0.09	-0.06	0.09	0.10	0.06	-0.06	0.55	0.22
ΔYb #	-0.10	-0.11	-0.53	-0.60	0.36	0.84	0.41	-0.52	4.00	1.65
ΔLu #	-0.04	-0.01	-0.07	-0.09	0.06	0.09	0.09	-0.10	0.67	0.22

[1] Dominant alteration mineral identified by near infrared-short wave infrared (NIR-SWIR) spectroscopy.

* wt%; ICP-OES

\# ppm; ICP-MS Least altered sample used to fit an approximate fractionation curve

Table A2-3 (continued) Absolute mass change values calculated using the Maclean (1990) multiple precursor method, where mass change equals reconstituted values (LOI-free untreated data multiplied by Zr enrichment factors) minus the calculated precursor values. Additional steps described in text.

Sample ID	11CPM-029	11CPM-030	11CPM-031	11CPM-032	11CPM-033	11CPM-034	11CPM-035	11CPM-037	11CPM-038	11CPM-039
SWIR Min.[1]	NULL	Aspectral	Ill.pheng.	FeMgChl	NULL	Ill.musc.	Muscovite	Ill.musc.	FeMgChl	Aspectral
Strat. unit	4.2	4.3	4.3	4.3	3.3	3.3	3.3	3.2	3.2	2
ΔSiO_2 *	2.62	-11.06	-9.67	-15.24	-21.19	-21.69	-19.60	-28.71	-9.28	-19.12
ΔAl_2O_3 *	-0.74	-0.51	-0.90	-1.37	-1.77	-1.27	-1.48	-1.40	-1.81	-1.46
ΔFe_2O_3 *	0.05	0.78	0.06	0.92	0.78	0.20	3.42	3.10	0.13	1.09
ΔMnO *	0.03	0.05	0.02	0.01	-0.07	0.08	-0.06	-0.09	0.03	-0.05
ΔMgO *	-0.26	0.48	1.28	3.15	-3.19	2.09	-0.90	-0.99	1.89	1.58
ΔCaO *	0.41	-0.03	-0.34	1.36	-4.44	-1.11	-1.69	-1.92	0.61	-1.39
ΔNa_2O *	0.59	-0.17	-0.27	1.51	-3.16	-3.64	-3.73	-3.79	1.35	-2.33
ΔK_2O *	0.79	1.50	-0.15	-1.74	1.80	0.67	1.21	1.66	-1.95	0.29
ΔTiO_2 *	-0.01	0.02	0.11	0.10	0.20	0.07	0.09	0.07	0.08	0.05
ΔP_2O_5 *	-0.01	-0.02	0.00	0.05	-0.20	0.01	0.22	-0.07	-0.01	-0.05
ΔTOTAL *	3.46	-8.96	-9.87	-11.24	-31.23	-24.59	-22.51	-32.14	-8.96	-21.38
ΔNi #	-1.63	-1.13	8.71	25.27	-15.61	-5.62	-3.87	1.57	-8.18	31.34
ΔCo #	-1.07	-0.97	0.82	14.61	4.52	1.60	3.47	5.55	-1.32	14.92
ΔSc #	0.01	0.81	0.23	5.58	3.57	0.06	-0.43	-0.49	2.31	6.19
ΔV #	-5.85	0.66	-3.76	85.93	-58.45	32.14	36.05	-8.38	49.88	79.88
ΔCu #	8.35	0.26	1.03	23.76	34.99	0.52	1457.75	1168.65	-8.66	27.08
ΔPb #	-4.51	-4.58	-0.22	2.78	24.13	8.15	434.62	19.45	0.03	0.70
ΔZn #	6.02	-6.48	-9.67	16.85	32.17	80.94	1745.52	113.20	6.43	20.85
ΔAs #	-4.67	-3.60	-3.68	9.81	4.19	2.52	29.60	12.96	-5.53	6.97
ΔSb #	-0.19	-0.38	-0.31	0.09	0.50	0.43	1.39	0.38	0.12	0.55
ΔLi #	0.36	1.85	2.69	10.42	-5.61	5.78	-1.49	-2.46	10.84	9.13
ΔRb #	-4.94	-4.23	143.49	-29.14	5.79	174.34	84.99	298.61	-83.06	280.68
ΔBa #	1135.39	617.71	-49.46	3494.08	-95.41	-117.39	433.18	-253.37	-7.88	228.91
ΔSr #	37.20	21.09	14.24	405.71	-3.56	6.32	0.60	-9.12	344.65	44.14
ΔTl #	-0.05	-0.06	0.22	-0.19	3.35	2.41	3.88	1.13	-0.35	0.65
ΔTa #	0.00	-0.03	0.02	0.00	0.02	0.00	0.01	0.04	0.03	0.01
ΔNb #	-0.21	-0.70	0.00	-0.88	0.14	-0.37	0.10	0.01	-0.26	-0.33
ΔHf #	-0.32	-0.45	0.45	0.17	0.05	0.06	0.20	0.11	0.33	0.46
ΔZr #	0.00	0.00	0.00	0.00	0.00	0.00	0.00	0.00	0.00	0.00
ΔY #	-0.95	-2.18	7.21	4.76	-11.43	4.62	-1.32	-8.96	-0.52	-1.58
ΔTh #	-0.06	-1.28	0.73	3.23	-0.92	0.95	-0.67	-1.22	2.35	-0.23
ΔU #	-0.26	-0.30	-0.06	0.94	0.67	0.88	0.96	-0.99	0.80	-0.38
ΔLa #	-1.87	-2.14	3.94	9.92	-5.08	2.88	2.22	0.47	6.90	-0.14
ΔCe #	-3.25	-3.59	9.16	34.15	-7.53	8.62	3.08	14.30	23.58	0.23
ΔPr #	-0.40	-0.58	1.07	3.65	-1.37	0.83	0.31	0.54	2.67	-0.18
ΔNd #	-1.26	-2.05	5.66	19.46	-5.91	4.67	2.19	2.53	13.11	-0.48
ΔSm #	1.03	0.33	4.22	7.84	-0.88	3.37	1.86	2.51	5.63	1.10
ΔEu #	0.23	0.01	1.02	1.96	-0.23	0.95	0.34	0.10	1.53	0.38
ΔGd #	0.01	-0.46	2.23	2.90	-1.55	1.48	0.26	-0.07	2.06	0.34
ΔTb #	0.02	-0.01	0.40	0.40	-0.23	0.34	0.08	-0.07	0.22	0.08
ΔDy #	-0.12	-0.34	1.70	1.45	-1.62	1.54	0.02	-1.03	0.57	0.28
ΔHo #	-0.05	-0.07	0.29	0.14	-0.37	0.26	-0.03	-0.27	0.01	0.01
ΔEr #	-0.23	-0.30	0.74	0.19	-1.12	0.61	-0.30	-0.89	-0.12	-0.09
ΔTm #	-0.02	-0.02	0.09	0.03	-0.17	0.09	-0.01	-0.07	0.02	-0.02
ΔYb #	-0.20	-0.22	0.78	-0.02	-1.02	0.60	-0.21	-1.00	-0.28	-0.11
ΔLu #	-0.03	-0.06	0.11	-0.01	-0.17	0.09	-0.02	-0.15	-0.06	0.00

[1] Dominant alteration mineral identified by near infrared-short wave infrared (NIR-SWIR) spectroscopy.

* wt%; ICP-OES

\# ppm; ICP-MS Least altered sample used to fit an approximate fractionation curve

Table A2-3 (continued) Absolute mass change values calculated using the Maclean (1990) multiple precursor method, where mass change equals reconstituted values (LOI-free untreated data multiplied by Zr enrichment factors) minus the calculated precursor values. Additional steps described in text.

Sample ID	11CPM-040	11CPM-041	11CPM-042	11CPM-044	11CPM-045	11CPM-046	11CPM-047	11CPM-048	11CPM-050
SWIR Min.[1]	Ill.pheng.	Ill.pheng.	Muscovite	Ill.pheng.	NULL	Muscovite	Ill.pheng.	Ill.pheng.	Ill.pheng.
Strat. unit	2	2	3.3	3.2	3.2	3.2	3.2	3.2	3.1
ΔSiO_2 *	-13.93	-12.77	-9.25	-5.76	-8.15	-19.06	-15.24	-14.82	-13.90
ΔAl_2O_3 *	-0.36	-0.37	-1.24	-0.64	-0.61	-1.61	-0.65	-0.74	-0.89
ΔFe_2O_3 *	0.95	0.28	2.43	0.56	0.65	14.86	0.86	0.71	0.42
ΔMnO *	-0.03	0.00	-0.04	0.30	0.06	-0.06	0.01	0.01	0.00
ΔMgO *	1.22	0.74	0.34	0.89	0.99	-1.47	0.61	0.15	0.19
ΔCaO *	0.19	1.32	-1.56	-0.13	-0.08	-1.98	1.42	0.66	1.06
ΔNa_2O *	-0.74	-0.30	-3.71	-0.34	-1.10	-3.88	-0.06	-0.65	-1.50
ΔK_2O *	-1.16	-1.60	1.26	-0.77	-0.38	1.75	-0.60	-0.01	0.76
ΔTiO_2 *	-0.06	-0.07	0.07	-0.02	0.00	-0.12	0.00	-0.01	-0.04
ΔP_2O_5 *	0.02	-0.02	0.01	-0.03	-0.02	-0.04	-0.03	-0.04	-0.02
ΔTOTAL *	-13.90	-12.79	-11.69	-5.94	-8.63	-11.62	-13.69	-14.76	-13.92
ΔNi #	-0.81	-0.80	0.08	-1.50	1.18	-9.89	-1.74	-2.11	-2.78
ΔCo #	1.53	1.56	5.40	1.26	1.78	-2.80	0.45	-0.10	0.40
ΔSc #	-0.85	-0.80	-0.74	-1.26	-0.39	-8.07	-0.89	-1.28	-2.67
ΔV #	5.74	6.20	22.05	3.52	6.28	-28.19	-3.28	-2.99	-2.40
ΔCu #	26.30	8.51	229.49	12.83	6.08	7193.78	3.57	-2.00	-2.25
ΔPb #	-3.93	7.01	8.23	31.08	6.43	862.04	2.15	0.18	1.32
ΔZn #	11.24	18.40	14.87	39.13	18.89	87317.68	139.83	104.71	9.41
ΔAs #	-0.09	1.01	34.86	8.35	17.25	386.02	4.04	3.83	5.95
ΔSb #	-0.28	-0.25	0.96	0.08	0.42	10.59	1.45	1.59	2.15
ΔLi #	4.27	5.04	-1.95	2.41	3.83	-3.58	0.64	-0.69	-0.90
ΔRb #	99.86	82.05	2613.31	1132.21	7069.46	1769.63	127.52	71.09	41.75
ΔBa #	294.91	-366.95	-15.47	572.54	987.58	9483.75	1087.29	337.39	-301.02
ΔSr #	105.99	114.74	-6.63	27.62	60.55	6.92	65.18	46.25	33.55
ΔTl #	0.28	0.26	11.53	1.15	4.26	4.20	0.85	0.72	0.08
ΔTa #	-0.01	0.00	0.01	0.01	0.01	0.04	0.01	0.00	0.00
ΔNb #	-1.15	-1.39	-0.17	-0.70	-0.79	0.44	-0.49	-0.41	-0.36
ΔHf #	-0.39	-0.20	0.03	-0.38	-0.40	0.13	-0.14	-0.41	-0.37
ΔZr #	0.00	0.00	0.00	0.00	0.00	0.00	0.00	0.00	0.00
ΔY #	6.06	7.53	0.40	2.18	3.53	-8.91	6.97	1.84	8.38
ΔTh #	1.62	2.67	0.54	1.45	1.39	-1.16	1.23	-0.06	1.51
ΔU #	-0.45	0.24	0.76	0.02	0.02	0.56	-0.27	-0.46	-0.20
ΔLa #	2.64	6.85	2.55	2.05	1.67	-3.85	0.63	-1.11	1.36
ΔCe #	6.19	11.65	5.06	6.27	5.71	-8.72	-0.66	-3.04	0.91
ΔPr #	0.86	1.53	0.57	0.50	0.45	-1.15	0.36	-0.30	0.67
ΔNd #	3.76	7.46	3.72	2.65	2.23	-5.46	1.45	-1.67	2.57
ΔSm #	3.11	3.70	2.35	2.22	2.65	-1.07	0.14	-0.61	0.33
ΔEu #	0.74	0.81	0.54	0.46	0.59	-0.37	0.09	-0.12	0.10
ΔGd #	1.48	2.03	0.86	0.71	1.04	-1.63	0.50	-0.34	0.66
ΔTb #	0.30	0.36	0.21	0.17	0.24	-0.26	0.10	-0.03	0.15
ΔDy #	1.60	1.74	0.61	0.63	0.93	-1.75	0.87	-0.06	1.21
ΔHo #	0.29	0.31	0.11	0.07	0.15	-0.37	0.20	0.01	0.28
ΔEr #	0.75	0.88	0.17	0.17	0.25	-1.00	0.64	0.12	0.87
ΔTm #	0.15	0.17	0.03	0.08	0.05	-0.11	0.10	0.00	0.11
ΔYb #	0.81	0.94	0.20	0.10	0.18	-1.03	0.81	0.08	0.94
ΔLu #	0.14	0.21	0.05	0.02	0.05	-0.15	0.12	0.00	0.14

[1] Dominant alteration mineral identified by near infrared-short wave infrared (NIR-SWIR) spectroscopy.

* wt%; ICP-OES

\# ppm; ICP-MS

Least altered sample used to fit an approximate fractionation curve

Table A2-3 (continued) Absolute mass change values calculated using the Maclean (1990) multiple precursor method, where mass change equals reconstituted values (LOI-free untreated data multiplied by Zr enrichment factors) minus the calculated precursor values. Additional steps described in text.

Sample ID	11CPM-051	11CPM-052	11CPM-053	11CPM-054	11CPM-055	11CPM-056	11CPM-057	11CPM-058	11CPM-059	11CPM-060
SWIR Min.[1]	Ill.pheng.	Ill.pheng.	Aspectral	Aspectral	MgChl	Phengite	Phengite	Ill.pheng.	Ill.pheng.	Muscovite
Strat. unit	3.1	3.1	3.1	2	2	4.3	4.3	4.3	4.3	4.3
ΔSiO_2 *	-20.01	-10.65	7.29	-9.24	4.77	-12.49	-19.77	-10.25	-18.80	-13.80
ΔAl_2O_3 *	-0.64	-0.45	-0.65	-1.61	-0.68	-0.61	-0.87	-0.80	-1.02	-0.67
ΔFe_2O_3 *	0.28	1.13	0.74	0.24	-1.80	1.57	7.95	2.12	5.48	3.34
ΔMnO *	0.01	0.05	-0.01	-0.01	0.03	0.09	0.11	-0.03	-0.06	-0.05
ΔMgO *	0.29	0.68	0.36	2.54	-2.35	1.65	0.82	1.25	1.31	0.57
ΔCaO *	1.05	3.31	1.31	-1.66	5.77	-0.81	-0.64	-1.12	-1.35	-1.03
ΔNa_2O *	0.10	-1.26	3.23	-1.02	0.08	-1.11	-3.41	-3.42	-3.51	-3.31
ΔK_2O *	-0.92	-0.27	-3.43	0.62	0.15	-1.26	0.88	0.70	0.85	0.12
ΔTiO_2 *	-0.04	-0.01	-0.03	0.23	-0.18	0.10	0.02	-0.01	-0.01	0.01
ΔP_2O_5 *	-0.01	0.03	0.01	0.08	-0.06	0.06	0.00	0.01	0.00	0.02
ΔTOTAL *	-19.89	-7.44	8.81	-9.85	5.73	-12.81	-14.92	-11.54	-17.11	-14.80
ΔNi #	-1.87	-0.89	-1.15	-13.46	-60.74	3.58	-2.72	-2.30	-3.61	-1.83
ΔCo #	1.16	1.52	1.86	6.28	-18.40	0.89	0.81	0.71	0.00	2.03
ΔSc #	-1.30	-0.72	-1.49	1.83	-9.66	1.07	-0.10	-1.29	-1.80	-0.18
ΔV #	0.97	4.08	0.80	51.71	-124.56	1.89	-7.31	-2.41	-6.63	-0.34
ΔCu #	-1.39	0.80	10.54	62.19	56.55	203.59	28.99	593.13	1324.28	62.88
ΔPb #	1.49	1.00	3.74	-0.96	-0.79	9.14	29.22	14.95	5.26	-1.69
ΔZn #	7.69	12.61	34.13	14.28	-5.69	14.36	77.07	788.01	188.43	-20.63
ΔAs #	2.32	0.14	1.66	3.77	17.62	6.11	38.70	16.25	11.10	11.34
ΔSb #	1.17	0.89	0.39	-0.06	0.00	-0.13	0.49	0.08	0.03	1.27
ΔLi #	0.79	12.15	3.35	7.40	-10.02	1.65	0.31	-0.27	-1.65	-0.71
ΔRb #	228.77	88.14	-73.19	205.76	20.94	-39.35	304.77	21.80	155.93	3.03
ΔBa #	-459.40	-454.81	-460.13	-72.65	-68.21	-432.10	461.68	321.09	314.72	543.39
ΔSr #	42.80	48.05	61.93	186.89	221.53	10.01	-5.89	-6.15	-10.29	-9.90
ΔTl #	0.01	-0.12	-0.68	0.20	-0.08	-0.05	2.15	0.47	0.66	0.04
ΔTa #	-0.01	-0.02	0.03	0.04	-0.01	-0.02	0.02	0.01	0.04	-0.01
ΔNb #	-0.75	-1.07	-0.77	0.37	-0.47	-0.50	-0.17	-0.29	0.07	-0.54
ΔHf #	-0.21	-0.50	-0.25	0.18	-0.41	-0.34	0.22	-0.19	0.04	-0.26
ΔZr #	0.00	0.00	0.00	0.00	0.00	0.00	0.00	0.00	0.00	0.00
ΔY #	0.45	11.85	7.74	0.72	-1.77	-4.58	5.02	-3.86	-4.42	-6.65
ΔTh #	-0.09	2.10	1.79	-0.01	-0.24	-2.08	0.89	-0.41	-0.75	-1.36
ΔU #	-0.28	-0.38	0.46	0.18	-0.02	-0.49	0.46	-0.08	-0.16	-0.25
ΔLa #	-1.46	4.53	2.60	-0.30	-0.56	-4.28	4.11	-2.11	-2.01	-5.06
ΔCe #	1.39	5.69	4.42	0.96	-2.63	-8.19	8.57	-3.40	-5.03	-10.06
ΔPr #	-0.36	1.47	0.55	0.19	-0.46	-1.09	1.23	-0.40	-0.57	-1.21
ΔNd #	-1.62	5.52	1.84	1.19	-2.22	-4.90	4.81	-2.06	-2.98	-5.48
ΔSm #	-0.73	0.94	0.00	0.36	-0.65	-1.52	0.73	-0.92	-1.12	-1.64
ΔEu #	-0.14	0.31	0.01	0.08	-0.23	-0.40	0.06	-0.18	-0.40	-0.46
ΔGd #	-0.41	1.27	0.26	0.02	-0.63	-1.32	0.74	-0.77	-1.03	-1.52
ΔTb #	-0.06	0.22	0.08	0.03	-0.09	-0.22	0.15	-0.13	-0.18	-0.23
ΔDy #	-0.37	1.70	0.68	0.16	-0.46	-1.21	0.96	-0.69	-0.96	-1.22
ΔHo #	-0.08	0.35	0.17	0.03	-0.10	-0.23	0.22	-0.15	-0.18	-0.23
ΔEr #	-0.13	1.09	0.66	0.02	-0.17	-0.62	0.77	-0.35	-0.46	-0.58
ΔTm #	-0.05	0.20	0.11	-0.03	0.00	-0.11	0.10	-0.05	-0.06	-0.09
ΔYb #	-0.17	1.24	0.83	0.06	-0.09	-0.52	0.87	-0.44	-0.57	-0.60
ΔLu #	-0.02	0.19	0.16	0.00	-0.02	-0.09	0.11	-0.08	-0.09	-0.10

[1] Dominant alteration mineral identified by near infrared-short wave infrared (NIR-SWIR) spectroscopy.

* wt%; ICP-OES

\# ppm; ICP-MS Least altered sample used to fit an approximate fractionation curve

Table A2-3 (continued) Absolute mass change values calculated using the Maclean (1990) multiple precursor method, where mass change equals reconstituted values (LOI-free untreated data multiplied by Zr enrichment factors) minus the calculated precursor values. Additional steps described in text.

Sample ID	11CPM-062	11CPM-063	11CPM-065	11CPM-066	11CPM-067	11CPM-078	11CPM-080	11CPM-084	11CPM-087	11CPM-088
SWIR Min.[1]	Muscovite	FeMgChl	FeMgChl	MgChl	Aspectral	Ill.musc.	Ill.pheng.	FeChl	Ill.pheng.	FeMgChl
Strat. unit	4.3	2	2	2	2	4.2	3.3	2	4.3	4.3
ΔSiO_2 *	5.43	-12.25	-30.38	-0.43	-5.53	-1.67	-7.86	-11.77	15.74	-16.71
ΔAl_2O_3 *	-0.88	-1.02	-1.35	-1.27	-1.47	-0.83	-1.51	-0.85	-0.72	-0.67
ΔFe_2O_3 *	11.01	3.21	15.32	0.35	0.08	0.47	0.71	-0.01	-0.42	0.50
ΔMnO *	-0.14	-0.01	0.08	0.19	0.02	0.20	0.08	0.01	0.01	0.08
ΔMgO *	-7.61	-1.84	2.53	6.10	2.02	-0.25	0.91	-0.20	-0.26	2.10
ΔCaO *	-8.81	-8.18	-6.84	0.29	-1.29	0.97	0.51	5.83	1.02	-0.78
ΔNa_2O *	-4.73	-3.74	-4.78	-2.46	-0.88	-2.72	-1.46	-0.12	-1.45	-1.32
ΔK_2O *	4.02	1.21	-0.06	-0.99	-0.17	4.53	0.40	-3.17	1.52	1.75
ΔTiO_2 *	-0.12	-0.08	-0.05	-0.03	0.03	-0.01	0.09	-0.03	0.01	0.01
ΔP_2O_5 *	-0.23	-0.12	0.12	-0.02	0.16	0.03	0.08	0.00	0.03	0.04
ΔTOTAL *	-2.08	-22.83	-25.40	1.74	-7.03	0.73	-8.04	-10.30	15.51	-15.00
ΔNi #	-60.89	-60.94	12.13	205.09	75.43	-2.11	-5.66	-2.49	-1.24	-1.82
ΔCo #	-10.82	-12.55	-8.72	9.11	5.24	1.50	4.48	0.41	0.06	0.96
ΔSc #	-5.48	-11.29	-4.59	3.97	2.03	-0.54	1.37	-1.39	-0.23	-0.18
ΔV #	-70.35	-58.98	-22.13	-18.61	20.58	-4.00	45.67	0.79	1.54	1.00
ΔCu #	778.14	108.67	312.45	-24.75	61.33	86.70	-5.95	6.45	227.15	52.94
ΔPb #	26.83	-3.08	2.97	-3.57	-2.37	17.02	4.95	6.49	-1.68	-1.83
ΔZn #	43.03	-20.64	60.46	78.79	13.11	2978.23	86.07	23.33	-21.13	91.26
ΔAs #	43.91	-9.78	9.84	-10.10	-5.76	4.09	-5.92	5.26	-4.58	-4.28
ΔSb #	1.01	-0.04	-0.06	-0.02	0.14	0.29	-0.08	0.05	-0.12	-0.23
ΔLi #	-17.17	-12.71	-5.39	1.81	-0.75	1.59	3.89	0.06	0.03	4.03
ΔRb #	432.53	43.78	-5.29	43.60	127.28	835.10	98.44	66.42	223.91	33.80
ΔBa #	69.11	662.35	-150.31	-178.21	24.70	511.46	-439.36	-545.22	1312.73	631.74
ΔSr #	-13.15	-6.58	-7.68	79.74	170.15	17.42	15.53	136.28	14.87	34.76
ΔTl #	3.63	0.11	-0.01	-0.07	0.25	1.05	0.09	-0.38	0.36	-0.03
ΔTa #	-0.02	-0.03	0.01	0.01	0.01	-0.03	0.04	0.01	-0.01	-0.01
ΔNb #	-0.44	-0.44	0.25	0.14	0.20	0.00	0.04	-0.19	-0.28	-0.39
ΔHf #	-0.26	-0.29	-0.08	0.05	-0.11	0.11	0.06	-0.13	-0.34	-0.39
ΔZr #	0.00	0.00	0.00	0.00	0.00	0.00	0.00	0.00	0.00	0.00
ΔY #	-14.40	-5.84	-3.87	-1.86	-0.13	10.51	8.04	10.56	6.52	-5.16
ΔTh #	-1.31	-0.44	0.23	0.06	-0.05	1.31	0.51	2.22	0.86	-1.89
ΔU #	-0.03	0.46	0.27	0.10	0.35	0.16	-0.04	0.13	-0.36	-0.69
ΔLa #	-5.77	-2.84	-1.87	1.52	1.18	2.08	1.87	5.00	-0.17	-3.04
ΔCe #	-13.25	-6.34	-3.58	2.44	3.01	3.92	-0.14	12.25	1.12	-5.86
ΔPr #	-1.81	-0.88	-0.31	0.25	0.36	0.96	0.71	1.24	0.30	-0.79
ΔNd #	-8.26	-3.86	-1.21	0.82	1.73	4.30	3.08	4.49	0.73	-3.81
ΔSm #	-2.24	-1.07	-0.47	0.05	0.11	0.94	0.57	0.88	0.02	-1.32
ΔEu #	-0.81	-0.34	-0.52	-0.04	0.05	0.21	0.23	0.28	0.11	-0.36
ΔGd #	-2.55	-1.05	-0.43	-0.03	0.17	1.05	0.93	1.21	0.33	-1.22
ΔTb #	-0.42	-0.18	-0.14	-0.03	0.01	0.21	0.15	0.22	0.08	-0.20
ΔDy #	-2.62	-0.99	-0.76	-0.15	-0.03	1.47	1.17	1.55	0.90	-1.15
ΔHo #	-0.54	-0.19	-0.17	-0.08	-0.01	0.38	0.25	0.35	0.19	-0.21
ΔEr #	-1.51	-0.56	-0.40	-0.27	-0.14	1.16	0.82	1.08	0.62	-0.58
ΔTm #	-0.23	-0.05	-0.05	-0.04	-0.03	0.18	0.13	0.14	0.08	-0.10
ΔYb #	-1.45	-0.42	-0.31	-0.22	-0.11	1.28	0.83	1.05	0.62	-0.69
ΔLu #	-0.22	-0.07	-0.05	-0.04	-0.03	0.19	0.14	0.16	0.09	-0.12

[1] Dominant alteration mineral identified by near infrared-short wave infrared (NIR-SWIR) spectroscopy.

* wt%; ICP-OES

\# ppm; ICP-MS

Least altered sample used to fit an approximate fractionation curve

Table A2-3 (continued) Absolute mass change values calculated using the Maclean (1990) multiple precursor method, where mass change equals reconstituted values (LOI-free untreated data multiplied by Zr enrichment factors) minus the calculated precursor values. Additional steps described in text.

Sample ID	11CPM-089	11CPM-090	11CPM-091	11CPM-095	11CPM-097	11CPM-099	11CPM-101	11CPM-102	11CPM-103	11CPM-104
SWIR Min.[1]	Ill.pheng.	Ill.pheng.	FeMgChl	Aspectral	MgChl	Ill.pheng.	FeMgChl	Ill.pheng.	Muscovite	Ill.musc.
Strat. unit	4.2	3.2	3.1	2	6.1	4.2	4.2	4.4	4.1	4.2
ΔSiO_2 *	-8.92	-14.09	-12.15	-0.60	0.45	-25.87	-11.11	-13.32	4.43	41.83
ΔAl_2O_3 *	-1.25	-1.24	-1.28	-1.15	-1.60	-0.72	-1.32	-1.15	-1.14	-1.79
ΔFe_2O_3 *	0.41	0.29	0.62	-0.80	7.11	0.07	0.49	0.60	6.95	13.86
ΔMnO *	0.06	0.02	0.08	-0.03	0.16	-0.05	0.08	0.08	-0.14	-0.13
ΔMgO *	1.02	0.89	1.68	-0.54	23.74	0.68	1.13	2.38	-6.71	-3.97
ΔCaO *	-0.35	-0.94	-1.40	-0.45	7.72	-0.90	0.05	-1.36	-7.80	-4.57
ΔNa_2O *	0.07	-1.08	-0.96	0.15	-4.51	-3.07	-0.82	0.14	-4.74	-4.47
ΔK_2O *	-0.45	1.21	0.18	-0.18	-1.31	1.88	0.02	-1.69	4.09	3.36
ΔTiO_2 *	0.07	0.05	0.06	-0.10	0.26	0.00	0.06	0.05	-0.07	0.20
ΔP_2O_5 *	0.09	0.06	0.07	-0.02	-0.03	0.02	0.08	0.07	-0.02	0.19
ΔTOTAL *	-9.24	-14.83	-13.10	-3.73	31.99	-27.94	-11.33	-14.20	-5.14	44.51
ΔNi #	-5.05	-5.11	-5.43	-32.82	1003.11	-2.36	-3.06	-4.40	-38.98	-17.93
ΔCo #	2.23	1.55	2.01	1.09	73.98	0.05	2.27	2.17	1.06	57.86
ΔSc #	0.37	-0.19	-0.25	-2.53	9.62	0.76	0.55	0.37	-3.14	-0.93
ΔV #	61.54	20.46	21.80	-38.09	64.56	-4.66	27.69	24.21	-9.22	134.83
ΔCu #	-7.61	-7.66	-7.88	84.95	45.01	-3.24	552.71	-7.14	40.59	0.22
ΔPb #	-0.67	2.42	8.12	-1.23	2.55	5.65	-0.61	-4.72	4.87	0.15
ΔZn #	48.46	61.34	101.43	1.93	47.97	30.41	22.85	71.21	5.25	-32.50
ΔAs #	-5.63	-2.20	-3.81	-1.58	3.75	-3.92	-5.65	-5.53	104.58	12.17
ΔSb #	-0.25	-0.26	-0.25	-0.03	-0.01	0.08	-0.12	-0.27	2.13	-0.03
ΔLi #	0.95	0.53	2.06	15.49	78.27	0.07	-0.45	0.92	-15.54	-7.59
ΔRb #	269.34	103.31	-17.85	36.37	-3.53	308.02	234.96	1.42	475.58	196.16
ΔBa #	847.75	-303.64	-334.28	85.31	-316.48	-578.44	-99.41	-187.29	61.04	134.14
ΔSr #	45.49	3.79	34.20	370.12	68.58	-6.23	15.93	38.08	-13.00	-11.01
ΔTl #	0.03	0.19	0.02	-0.18	-0.20	0.45	0.45	-0.36	12.80	0.19
ΔTa #	0.01	0.02	0.01	0.15	0.04	-0.01	0.01	0.01	0.02	0.08
ΔNb #	-0.35	-0.24	-0.27	3.18	0.78	-0.54	-0.17	-0.51	2.27	2.01
ΔHf #	0.01	-0.04	-0.14	-0.20	0.33	-0.19	-0.04	-0.08	-0.25	0.13
ΔZr #	0.00	0.00	0.00	0.00	0.00	0.00	0.00	0.00	0.00	0.00
ΔY #	3.41	-5.18	-5.33	-1.75	2.94	-7.80	7.76	-3.60	-13.86	-13.15
ΔTh #	-0.08	-1.60	-1.56	0.41	0.77	-1.64	0.46	-1.67	-1.33	-1.48
ΔU #	-0.34	-0.68	-0.33	0.33	0.08	-0.82	-0.41	-0.49	0.95	0.07
ΔLa #	-0.27	-3.78	-4.19	0.57	8.66	-5.19	1.45	-3.05	-5.75	-5.93
ΔCe #	-3.82	-7.93	-7.78	0.66	16.49	-8.89	-0.16	-7.58	-13.05	-13.22
ΔPr #	0.03	-1.04	-1.07	0.03	1.81	-1.21	0.83	-0.94	-1.79	-1.71
ΔNd #	0.22	-4.52	-4.87	0.08	7.38	-5.22	3.71	-4.33	-8.08	-8.10
ΔSm #	-0.35	-1.29	-1.49	-0.02	1.36	-1.64	0.77	-1.38	-2.24	-2.11
ΔEu #	0.03	-0.32	-0.41	-0.04	0.33	-0.45	0.32	-0.33	-0.79	-0.70
ΔGd #	0.03	-1.26	-1.42	-0.13	1.14	-1.48	0.92	-1.13	-2.45	-2.44
ΔTb #	0.04	-0.20	-0.22	-0.04	0.15	-0.22	0.15	-0.18	-0.40	-0.40
ΔDy #	0.24	-1.19	-1.14	-0.33	0.71	-1.40	1.07	-1.00	-2.46	-2.58
ΔHo #	0.07	-0.23	-0.22	-0.08	0.09	-0.28	0.24	-0.18	-0.50	-0.53
ΔEr #	0.31	-0.63	-0.58	-0.28	0.25	-0.76	0.79	-0.45	-1.46	-1.41
ΔTm #	0.03	-0.10	-0.08	-0.04	0.02	-0.14	0.18	-0.05	-0.22	-0.17
ΔYb #	0.33	-0.54	-0.49	-0.22	0.17	-0.82	0.92	-0.21	-1.30	-1.45
ΔLu #	0.06	-0.09	-0.08	-0.04	0.02	-0.13	0.12	-0.04	-0.22	-0.22

[1] Dominant alteration mineral identified by near infrared-short wave infrared (NIR-SWIR) spectroscopy.

* wt%; ICP-OES

\# ppm; ICP-MS Least altered sample used to fit an approximate fractionation curve

Table A2-3 (continued) Absolute mass change values calculated using the Maclean (1990) multiple precursor method, where mass change equals reconstituted values (LOI-free untreated data multiplied by Zr enrichment factors) minus the calculated precursor values. Additional steps described in text.

Sample ID	11CPM-105	11CPM-106	11CPM-108	11CPM-110	11CPM-111	11CPM-114	11CPM-116	11CPM-121	11CPM-122	11CPM-123
SWIR Min.[1]	FeMgChl	Aspectral	Ill.pheng.	FeMgChl	FeMgChl	Ill.pheng.	Aspectral	Ill.pheng.	FeMgChl	Ill.musc.
Strat. unit	4.2	2	4.6	4.6	3.4	3.4	2	4.2	4.2	4.2
ΔSiO_2 *	2.44	-6.28	-14.28	-11.18	-7.85	-12.28	11.20	-5.40	-3.24	-15.04
ΔAl_2O_3 *	-1.10	-0.48	-0.78	-1.53	-1.27	-1.35	-1.23	-0.51	-0.06	-0.57
ΔFe_2O_3 *	-0.77	-0.36	0.01	1.35	0.67	0.25	-0.73	1.23	0.27	-0.93
ΔMnO *	0.36	-0.04	0.10	0.22	0.37	0.00	-0.01	-0.01	-0.04	-0.08
ΔMgO *	-1.21	0.44	0.00	0.95	0.24	0.79	-1.06	1.37	2.55	-0.61
ΔCaO *	-1.56	0.29	0.73	0.31	-1.19	0.53	3.10	-0.51	-0.64	-1.03
ΔNa_2O *	0.28	2.12	-1.39	-3.87	-0.88	0.25	-0.26	-0.72	-2.73	-3.16
ΔK_2O *	0.40	-1.27	2.07	3.83	2.20	-0.58	2.62	-1.40	-1.36	-0.10
ΔTiO_2 *	-0.09	-0.09	-0.01	0.09	0.06	0.04	-0.11	0.12	0.00	0.06
ΔP_2O_5 *	-0.01	0.03	0.05	0.06	0.08	0.06	-0.04	0.08	0.04	-0.01
ΔTOTAL *	-1.27	-5.64	-13.50	-9.77	-7.56	-12.28	13.48	-5.74	-5.21	-21.47
ΔNi #	-42.33	-0.93	-2.26	-3.98	-5.26	-3.56	8.73	14.22	0.12	17.72
ΔCo #	-0.89	1.52	0.16	-1.24	0.75	2.32	-0.89	4.04	1.02	-0.31
ΔSc #	-6.35	-1.64	0.38	1.82	1.31	-0.66	-0.32	3.91	1.40	1.97
ΔV #	-57.25	4.23	-5.37	43.83	36.45	28.26	-16.04	26.17	11.00	-0.19
ΔCu #	90.52	15.16	10.37	-9.79	-7.75	-8.38	115.33	4.46	-0.19	1.63
ΔPb #	25.29	7.13	11.79	2.01	8.59	1.02	-1.75	-3.55	-6.94	-6.67
ΔZn #	31.37	0.65	20.68	98.48	80.31	42.09	157.72	67.36	-19.81	-21.89
ΔAs #	14.33	8.49	7.50	-6.20	-2.61	-5.63	20.41	-2.10	-2.12	-3.07
ΔSb #	0.77	-0.02	-0.11	-0.20	-0.12	-0.03	0.13	-0.23	-0.46	-0.19
ΔLi #	-6.72	0.28	0.02	0.29	0.75	1.09	-15.23	-1.98	-1.47	296.41
ΔRb #	51.82	375.42	368.00	219.12	943.56	151.07	935.70	8.31	1200.51	319.03
ΔBa #	-89.50	26.40	261.19	470.15	261.96	-381.14	158.15	-283.87	-153.90	-472.86
ΔSr #	128.75	41.86	15.71	19.33	19.22	30.93	191.82	6.43	-2.42	-9.95
ΔTl #	1.06	-0.10	0.41	0.62	0.89	-0.05	0.57	-0.46	-0.10	-0.21
ΔTa #	0.12	-0.19	-0.17	0.01	-0.08	0.00	0.06	-0.04	-0.16	-0.03
ΔNb #	3.02	-1.13	-0.20	-0.13	-0.29	-0.28	1.59	-0.80	-1.93	-0.34
ΔHf #	-0.22	-0.11	0.03	0.19	0.04	-0.08	-0.14	-0.35	-0.52	0.07
ΔZr #	0.00	0.00	0.00	0.00	0.00	0.00	0.00	0.00	0.00	0.00
ΔY #	-1.56	-4.66	12.18	2.87	-3.38	9.12	-1.77	-4.58	10.85	-10.83
ΔTh #	0.32	-0.11	0.64	-0.11	-0.78	1.03	0.20	-2.25	0.47	-2.46
ΔU #	0.14	-0.22	-0.41	-0.39	-0.41	-0.03	0.21	-1.02	-0.97	-1.58
ΔLa #	0.90	-1.04	1.85	-1.56	-0.64	2.44	0.98	-3.57	2.92	-6.32
ΔCe #	0.97	-1.18	1.89	-4.71	-2.59	-1.10	1.45	-6.71	12.57	-12.80
ΔPr #	0.18	-0.39	0.75	-0.27	-0.33	0.97	0.10	-0.89	1.72	-1.65
ΔNd #	0.46	-2.59	2.30	-1.39	-1.93	3.86	2.14	-4.83	8.25	-6.90
ΔSm #	0.10	-1.08	0.43	-0.49	-0.82	0.73	0.37	-1.59	2.27	-2.13
ΔEu #	0.01	-0.25	0.27	-0.01	-0.17	0.25	0.14	-0.55	-0.25	-0.56
ΔGd #	0.02	-0.96	0.96	-0.23	-0.89	0.91	0.17	-0.79	0.93	-1.85
ΔTb #	-0.03	-0.15	0.17	-0.03	-0.12	0.18	-0.07	-0.18	0.25	-0.28
ΔDy #	-0.29	-1.07	1.45	0.17	-0.81	1.17	-0.30	-1.14	1.69	-1.91
ΔHo #	-0.06	-0.22	0.31	0.03	-0.15	0.28	-0.07	-0.23	0.46	-0.44
ΔEr #	-0.15	-0.74	1.14	0.24	-0.44	0.98	-0.41	-0.57	1.43	-1.26
ΔTm #	0.02	-0.11	0.18	0.05	-0.08	0.17	-0.04	-0.10	0.27	-0.15
ΔYb #	-0.16	-0.78	1.23	0.29	-0.43	0.91	-0.54	-0.53	1.88	-1.62
ΔLu #	-0.05	-0.13	0.18	0.06	-0.06	0.14	-0.03	-0.10	0.31	-0.25

[1] Dominant alteration mineral identified by near infrared-short wave infrared (NIR-SWIR) spectroscopy.

* wt%; ICP-OES

\# ppm; ICP-MS Least altered sample used to fit an approximate fractionation curve

Table A2-3 (continued) Absolute mass change values calculated using the Maclean (1990) multiple precursor method, where mass change equals reconstituted values (LOI-free untreated data multiplied by Zr enrichment factors) minus the calculated precursor values. Additional steps described in text.

Sample ID	11CPM-124	11CPM-130	11CPM-131	11CPM-133	11CPM-134	11CPM-136	11CPM-137	11CPM-138	11CPM-139	11CPM-141
SWIR Min.[1]	FeMgChl	Aspectral	Aspectral	FeMgChl	FeMgChl	Phengite	FeMgChl	MgChl	FeMgChl	MgChl
Strat. unit	4.1	7.1	7.1	6.1	6.1	6.1	6.1	6.1	6.1	6.1
ΔSiO_2 *	-20.33	-11.06	-3.73	-9.61	-5.35	2.24	-17.21	1.27	-8.24	-5.66
ΔAl_2O_3 *	-1.73	-1.85	-1.78	-1.81	-1.39	-1.56	-1.66	-1.20	-1.31	-1.36
ΔFe_2O_3 *	0.52	3.03	1.56	3.03	0.06	3.01	0.58	0.15	0.77	1.03
ΔMnO *	-0.02	0.03	-0.05	0.01	-0.03	0.39	0.02	0.30	0.07	0.26
ΔMgO *	0.97	0.07	-2.80	4.00	-1.01	-2.07	7.16	-1.36	1.03	6.82
ΔCaO *	-0.09	-0.67	1.81	4.54	0.95	-5.59	-4.42	-7.24	-2.12	-6.39
ΔNa_2O *	-0.17	0.28	0.48	-1.49	-0.25	-4.66	-1.91	0.23	-0.84	-2.51
ΔK_2O *	-1.07	-1.35	-0.04	-0.91	-1.09	5.55	-1.08	-0.03	-1.10	0.19
ΔTiO_2 *	0.29	0.59	0.72	0.32	-0.03	0.19	0.08	-0.09	-0.04	-0.01
ΔP_2O_5 *	0.00	0.18	0.52	0.03	0.00	-0.07	0.05	-0.01	0.05	-0.07
ΔTOTAL *	-21.63	-10.74	-3.30	-1.88	-8.13	-2.58	-18.38	-7.99	-11.75	-7.71
ΔNi #	3.97	-4.60	15.64	35.26	49.76	17.24	-16.40	-29.63	14.22	20.11
ΔCo #	9.89	11.23	-3.76	22.83	0.43	-0.43	0.27	-3.01	-2.95	-2.74
ΔSc #	0.01	1.40	-2.82	20.06	-0.45	2.20	-2.39	-5.05	-4.73	-0.77
ΔV #	60.75	159.99	169.79	171.98	21.11	105.31	90.03	-26.82	104.71	13.51
ΔCu #	3.58	9.65	11.32	100.56	147.20	350.86	19.20	-17.89	-5.79	21.53
ΔPb #	-4.75	-0.31	1.81	3.02	-1.46	5.84	34.73	20.65	0.97	0.65
ΔZn #	9.92	54.60	62.94	30.85	252.00	287.56	57.41	261.33	75.15	222.79
ΔAs #	-4.94	36.68	32.01	9.71	1.29	9.65	-6.56	9.27	-5.04	0.01
ΔSb #	-0.17	0.03	-0.07	1.40	0.75	-0.05	0.04	-0.03	0.05	0.12
ΔLi #	0.57	5.00	-3.39	17.08	-0.82	-0.44	10.42	-5.27	-3.60	9.60
ΔRb #	116.51	53.11	266.76	439.06	-37.57	832.42	-54.60	591.94	-60.42	165.74
ΔBa #	1712.61	-307.48	-172.29	-205.36	-353.33	2625.69	-349.53	-202.54	-108.23	889.57
ΔSr #	249.62	327.92	265.96	120.07	155.28	14.90	116.29	63.88	144.39	75.43
ΔTl #	-0.25	-0.30	0.12	0.17	-0.20	1.31	-0.19	0.35	-0.19	0.51
ΔTa #	0.02	-0.01	0.02	0.19	-0.02	0.02	0.04	0.16	-0.02	0.04
ΔNb #	0.80	0.89	1.25	3.92	0.26	-0.19	0.85	2.59	0.71	1.14
ΔHf #	0.07	-0.10	-0.05	0.76	-0.47	0.32	-0.23	0.03	0.02	-0.21
ΔZr #	0.00	0.00	0.00	0.00	0.00	0.00	0.00	0.00	0.00	0.00
ΔY #	1.69	11.37	15.47	4.99	0.89	0.82	2.87	-8.51	0.18	-0.99
ΔTh #	0.63	0.09	0.11	3.50	0.15	-0.10	0.57	-0.35	0.37	0.25
ΔU #	0.10	0.04	2.90	0.85	0.13	0.03	0.33	0.33	0.35	0.10
ΔLa #	1.61	3.04	5.25	5.75	1.91	-1.92	3.14	-1.18	2.53	0.58
ΔCe #	4.10	10.22	13.87	13.93	3.28	-2.77	6.62	-0.60	5.63	1.75
ΔPr #	0.83	1.21	1.66	1.83	0.22	-0.14	0.95	-0.60	0.67	0.12
ΔNd #	3.80	6.17	9.10	7.52	2.00	-2.33	3.03	-2.54	2.59	1.21
ΔSm #	0.48	2.09	2.58	1.96	0.58	0.16	1.16	-0.42	0.55	0.36
ΔEu #	0.14	0.44	0.85	0.52	-0.06	-0.49	0.11	-0.59	0.20	-0.13
ΔGd #	0.22	1.37	2.49	1.13	0.03	-0.22	1.01	-1.35	0.18	-0.12
ΔTb #	0.00	0.29	0.37	0.20	0.02	0.05	0.06	-0.15	-0.01	-0.01
ΔDy #	0.31	2.23	3.27	0.86	0.24	0.28	0.73	-1.13	-0.17	-0.04
ΔHo #	0.07	0.43	0.49	0.22	0.07	0.11	0.02	-0.32	0.04	-0.04
ΔEr #	0.24	0.70	1.33	0.75	-0.03	0.40	0.43	-0.65	-0.15	-0.42
ΔTm #	0.09	0.21	0.20	0.09	0.05	0.16	0.03	-0.10	-0.03	-0.01
ΔYb #	-0.19	1.30	0.96	0.82	-0.09	0.36	0.33	-0.50	0.05	-0.17
ΔLu #	-0.08	0.11	0.13	-0.01	-0.02	0.06	0.07	-0.15	0.03	0.00

[1] Dominant alteration mineral identified by near infrared-short wave infrared (NIR-SWIR) spectroscopy.

* wt%; ICP-OES

\# ppm; ICP-MS Least altered sample used to fit an approximate fractionation curve

Table A2-3 (continued) Absolute mass change values calculated using the Maclean (1990) multiple precursor method, where mass change equals reconstituted values (LOI-free untreated data multiplied by Zr enrichment factors) minus the calculated precursor values. Additional steps described in text.

Sample ID	11CPM-143	11CPM-144	11CPM-145	11CPM-146	11CPM-147	11CPM-148
SWIR Min.[1]	Ill.pheng.	FeMgChl	Ill.pheng.	MgChl	FeMgChl	Aspectral
Strat. unit	2	2	2	2	2	6.1
ΔSiO_2 *	2.36	-11.09	-1.06	-6.22	-4.34	-13.82
ΔAl_2O_3 *	-1.84	-1.82	-1.85	-1.49	-1.45	-1.85
ΔFe_2O_3 *	2.93	1.62	1.20	0.29	0.41	2.31
ΔMnO *	0.23	0.15	0.18	0.39	-0.01	0.05
ΔMgO *	0.69	1.91	-0.19	0.02	0.34	0.37
ΔCaO *	-1.67	-3.93	-1.03	-1.76	-0.30	-1.97
ΔNa_2O *	-2.65	-0.58	1.08	1.13	-0.39	1.04
ΔK_2O *	2.72	-0.41	-0.84	-1.07	0.00	-0.78
ΔTiO_2 *	0.19	0.07	0.14	0.07	0.09	0.12
ΔP_2O_5 *	0.04	0.02	0.07	-0.05	-0.08	0.25
ΔTOTAL *	3.01	-14.05	-2.29	-8.70	-5.73	-14.28
ΔNi #	105.77	5.13	4.67	-28.21	-3.56	18.67
ΔCo #	7.42	5.83	10.02	3.01	2.25	12.46
ΔSc #	3.23	1.46	5.80	0.92	0.27	-0.41
ΔV #	103.72	77.57	111.20	38.77	34.00	103.58
ΔCu #	67.75	23.12	103.04	68.02	40.49	47.15
ΔPb #	70.44	4.00	7.05	11.85	-0.28	-1.81
ΔZn #	256.76	289.77	586.93	648.29	40.25	59.73
ΔAs #	47.12	-0.63	3.01	-1.31	-6.46	3.00
ΔSb #	7.34	0.55	1.45	0.58	2.88	0.16
ΔLi #	0.87	3.76	4.41	1.84	-2.52	12.90
ΔRb #	926.72	77.77	39.70	249.57	320.30	232.01
ΔBa #	293.33	-129.50	110.71	-346.95	-330.92	60.54
ΔSr #	101.04	63.95	114.94	133.62	125.73	170.57
ΔTl #	2.15	-0.05	0.92	0.18	0.23	-0.08
ΔTa #	0.14	0.05	0.10	0.04	0.16	0.03
ΔNb #	1.07	1.07	1.13	0.09	0.34	1.60
ΔHf #	0.51	0.07	0.18	0.60	-0.06	0.62
ΔZr #	0.00	0.00	0.00	0.00	0.00	0.00
ΔY #	-1.59	2.81	6.04	1.70	2.24	5.90
ΔTh #	-0.65	0.39	0.72	0.13	-0.06	0.43
ΔU #	-0.24	0.06	0.28	0.23	-0.12	0.26
ΔLa #	-2.46	0.88	0.60	-0.30	0.02	0.77
ΔCe #	-5.59	3.09	1.78	-0.25	0.06	2.21
ΔPr #	-0.62	0.29	0.31	0.07	0.02	0.47
ΔNd #	-2.05	1.01	1.82	-0.22	-0.01	3.12
ΔSm #	-0.69	-0.37	0.84	0.25	0.13	0.39
ΔEu #	0.02	-0.09	0.10	0.18	0.16	0.21
ΔGd #	-0.38	0.39	0.73	0.22	0.27	0.74
ΔTb #	0.02	0.05	0.17	0.10	0.05	0.16
ΔDy #	-0.58	0.54	1.10	0.38	0.23	1.10
ΔHo #	-0.03	0.10	0.26	0.04	0.10	0.21
ΔEr #	-0.36	0.32	1.01	0.33	0.22	0.53
ΔTm #	-0.03	0.05	0.20	0.11	0.13	0.06
ΔYb #	-0.22	0.18	0.90	0.32	0.79	0.29
ΔLu #	-0.02	0.04	0.11	0.06	0.04	0.07

[1] Dominant alteration mineral identified by near infrared-short wave infrared (NIR-SWIR) spectroscopy.

* wt%; ICP-OES

\# ppm; ICP-MS Least altered sample used to fit an approximate fractionation curve

Appendix III: 2D Visualizations of Mass Change Data

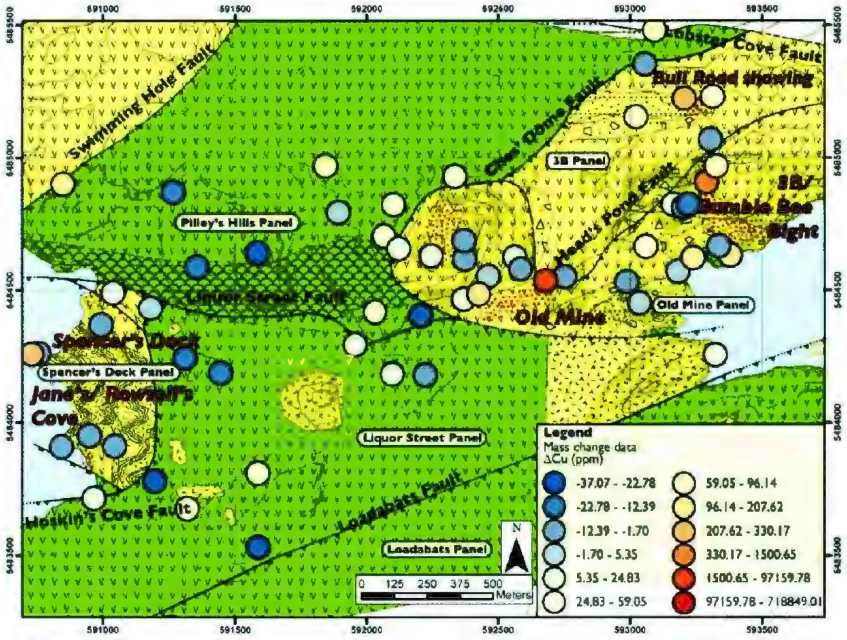

Figure A3-1 2D visualization of Cu mass change on a geological map of the Pilley's Island VMS district. Rock unit descriptions and legend of geology provided in figures within text.

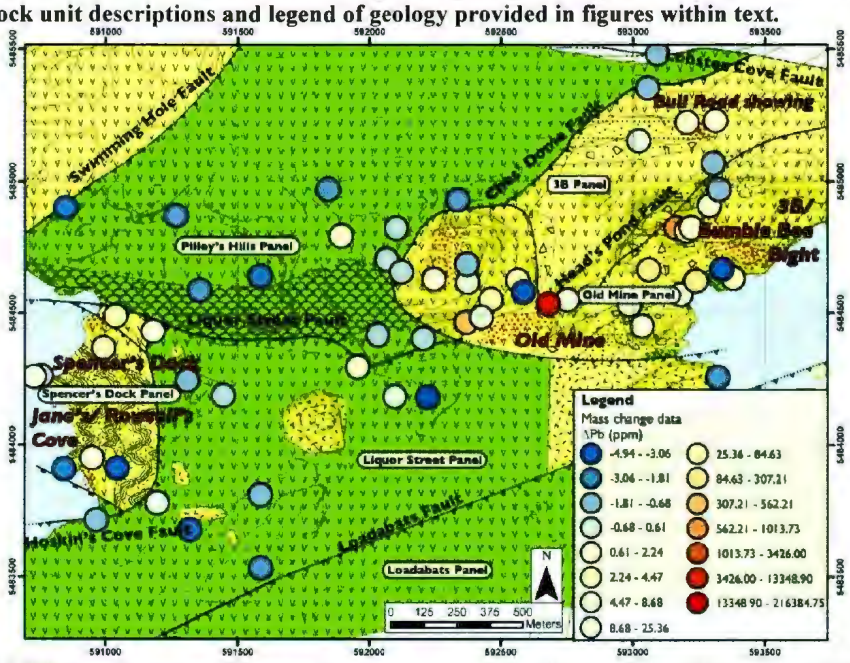

Figure A3-2 2D visualization of Pb mass change on a geological map of the Pilley's Island VMS district. Rock unit descriptions and legend of geology provided in figures within text.

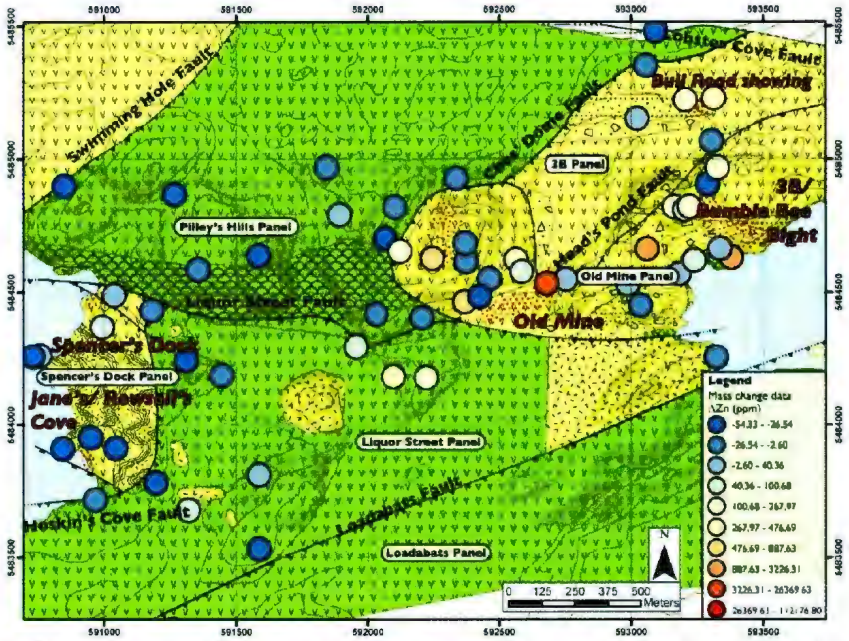

Figure A3-3 2D visualization of Zn mass change on a geological map of the Pilley's Island VMS district. Rock unit descriptions and legend of geology provided in figures within text.

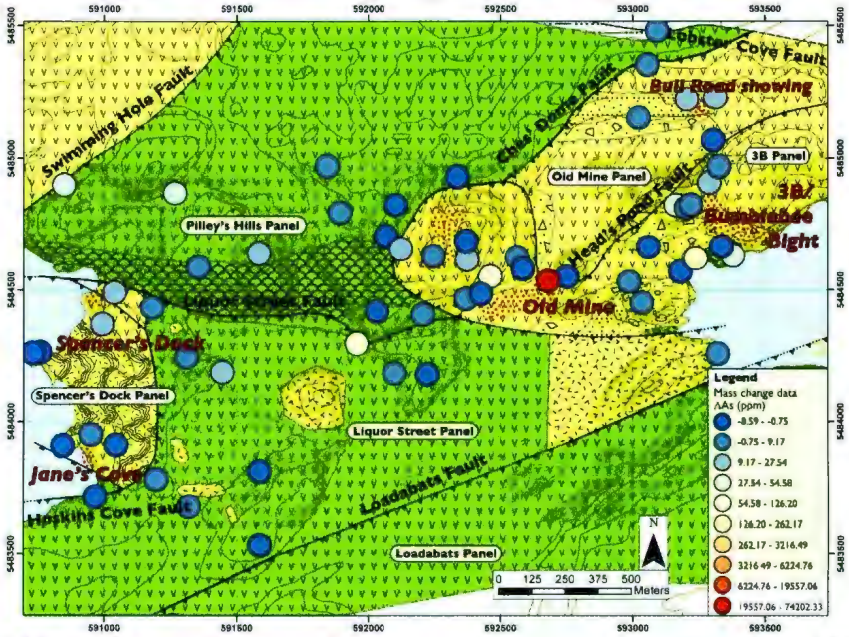

Figure A3-4 2D visualization of As mass change on a geological map of the Pilley's Island VMS district. Rock unit descriptions and legend of geology provided in figures within text.

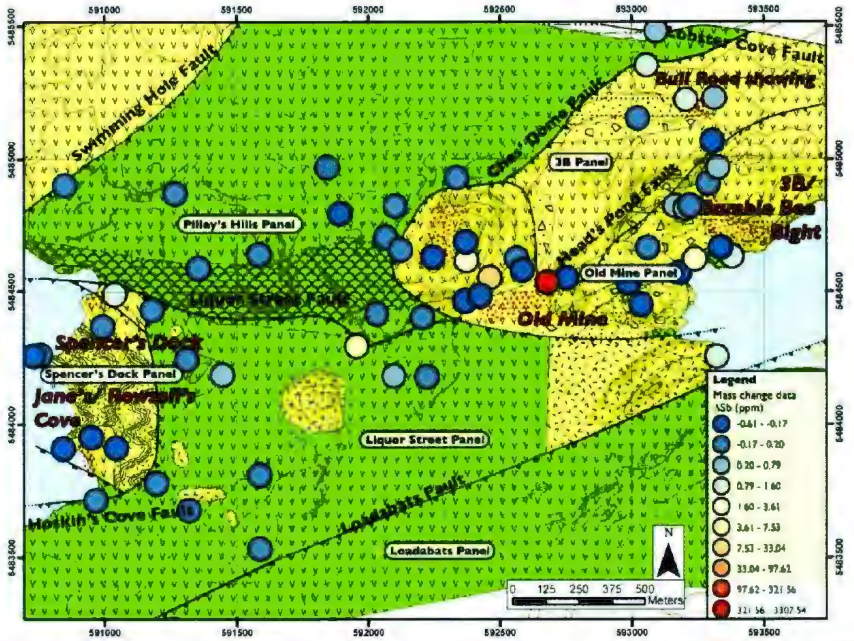

Figure A3-5 2D visualization of Sb mass change on a geological map of the Pilley's Island VMS district. Rock unit descriptions and legend of geology provided in figures within text.

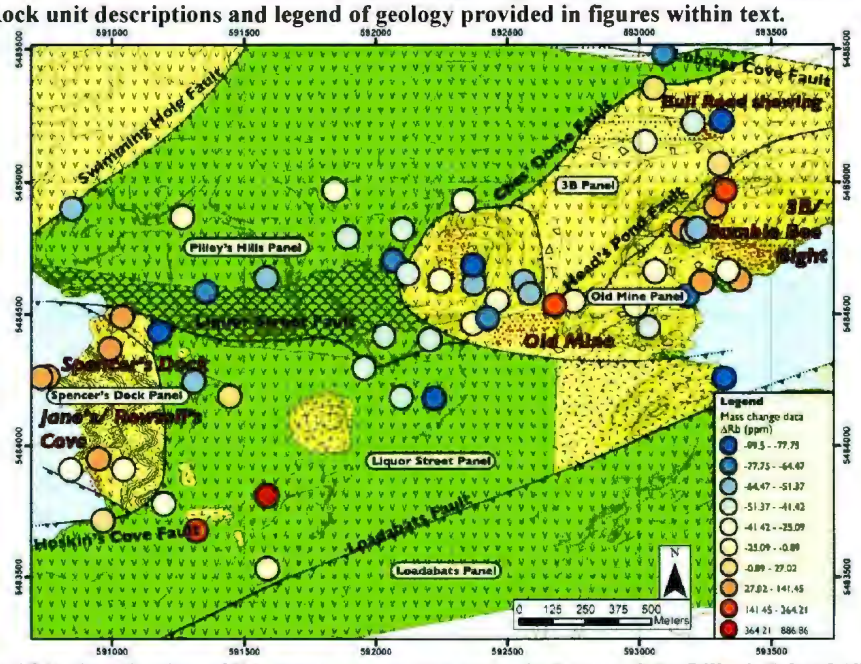

Figure A3-6 2D visualization of Rb mass change on a geological map of the Pilley's Island VMS district. Rock unit descriptions and legend of geology provided in figures within text.

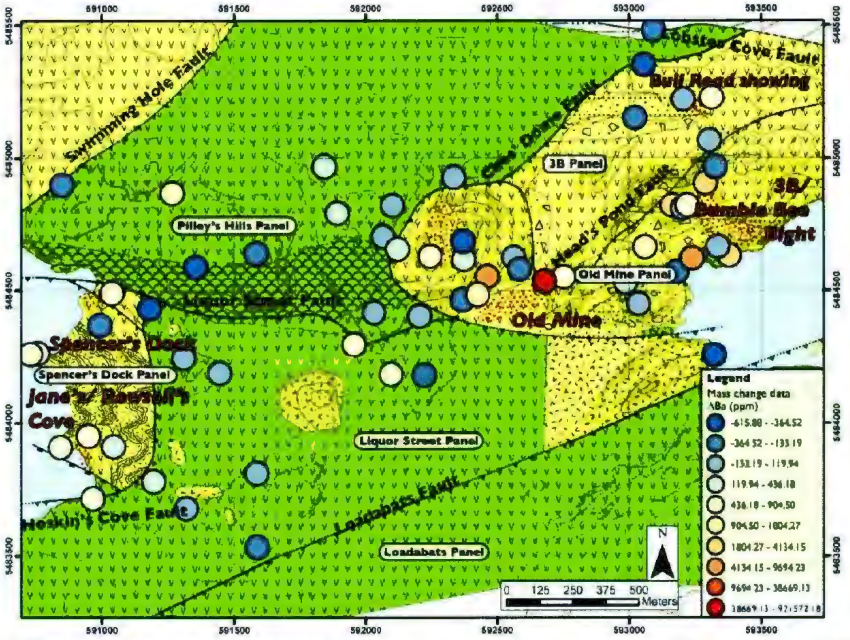

Figure A3-7 2D visualization of Ba mass change on a geological map of the Pilley's Island VMS district. Rock unit descriptions and legend of geology provided in figures within text.

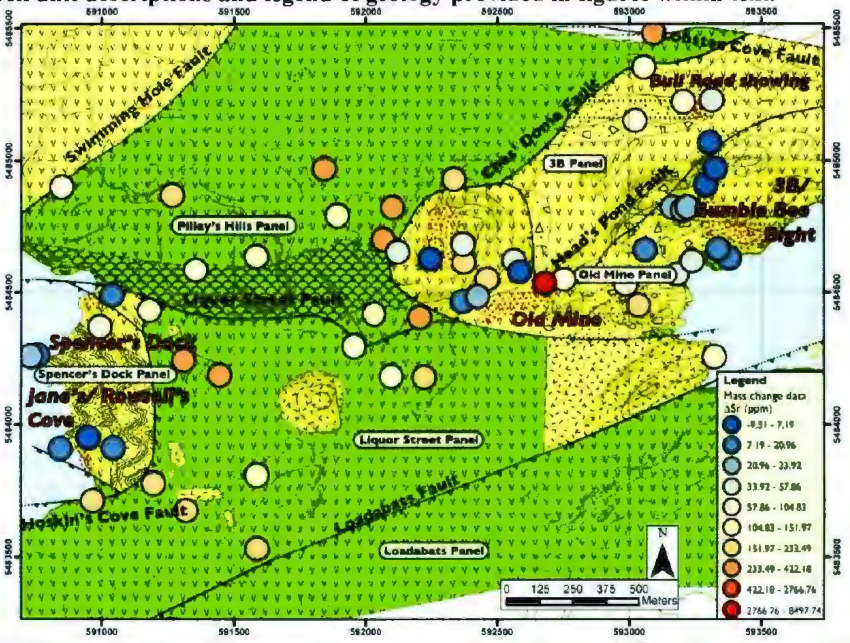

Figure A3-8 2D visualization of Sr mass change on a geological map of the Pilley's Island VMS district. Rock unit descriptions and legend of geology provided in figures within text.

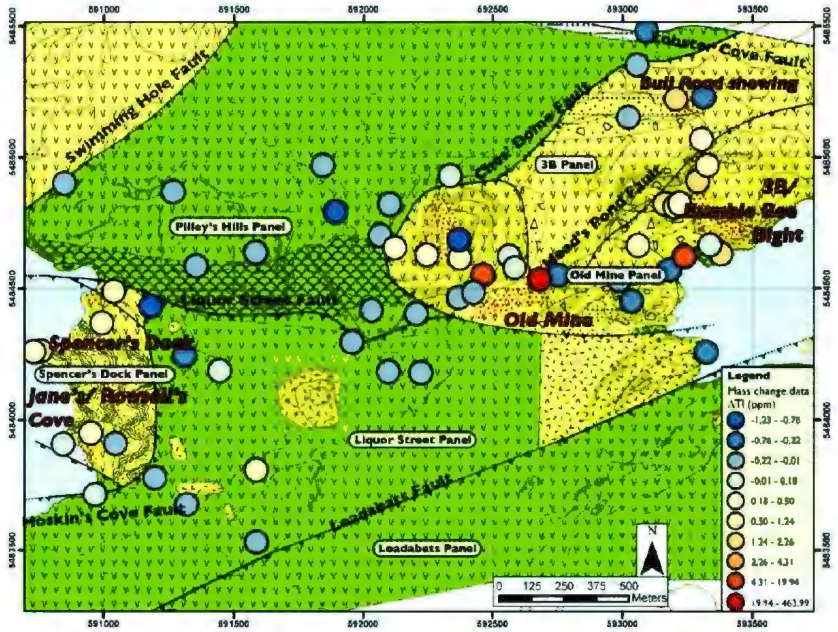

Figure A3-9 2D visualization of Tl mass change on a geological map of the Pilley's Island VMS district. Rock unit descriptions and legend of geology provided in figures within text.

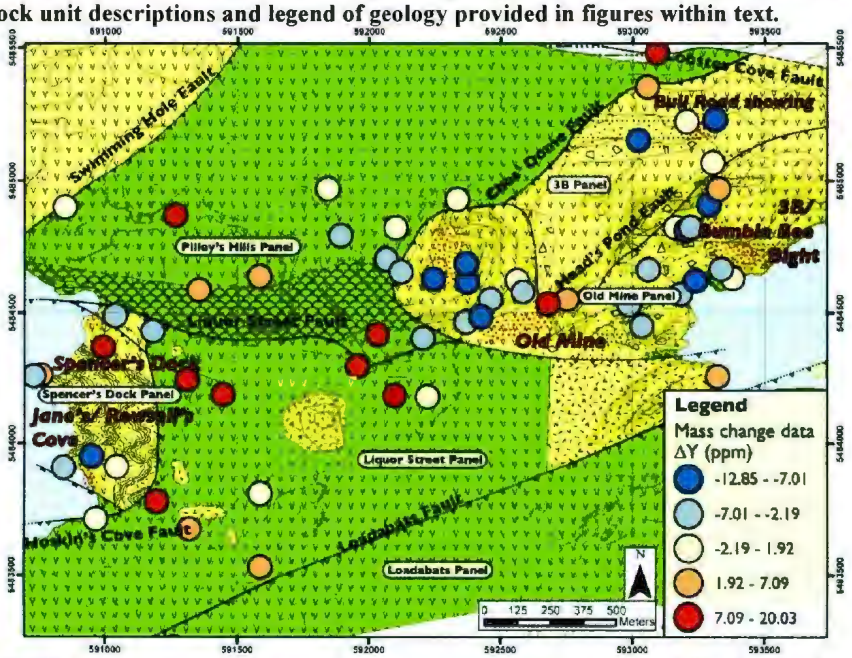

Figure A3 10 2D visualization of Y mass change on a geological map of the Pilley's Island VMS district. Rock unit descriptions and legend of geology provided in figures within text.

Appendix IV: 3D Visualizations of Mass Change Data

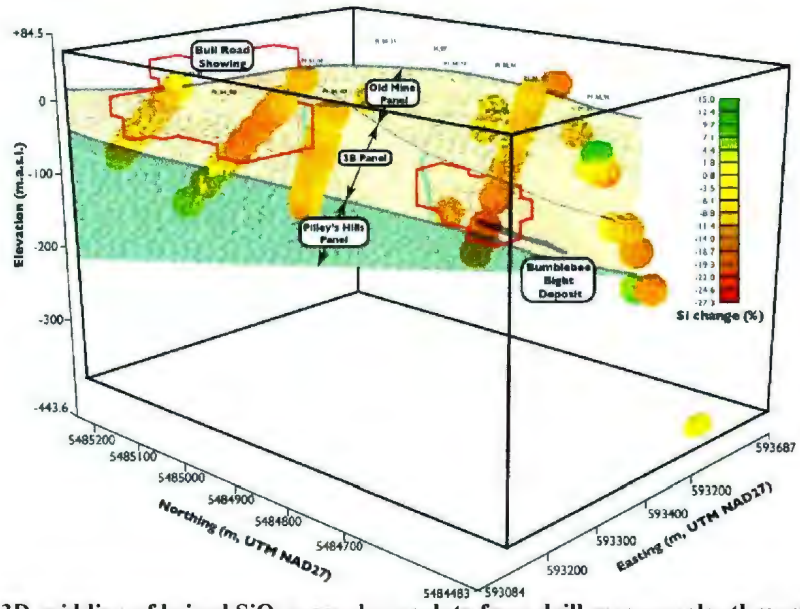

Figure A4-1 3D gridding of kriged SiO_2 mass change data from drill core samples throughout and surrounding the Bull Road showing and the Bumble Bee Bight deposit on Pilley's Island. Red wireframes represent raw, kriged Cu values greater than 400ppm.

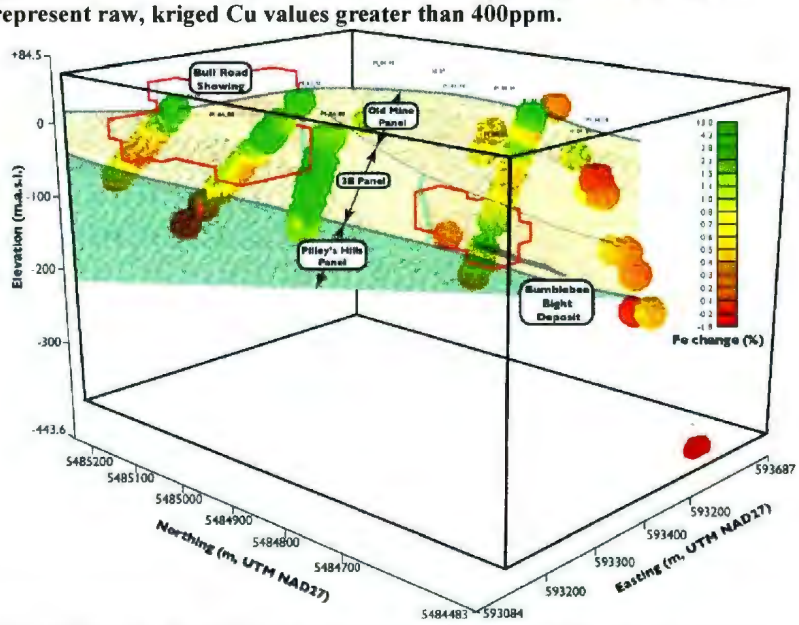

Figure A4-2 3D gridding of kriged Fe_2O_3 mass change data from drill core samples throughout and surrounding the Bull Road showing and the Bumble Bee Bight deposit on Pilley's Island. Red wireframes represent raw, kriged Cu values greater than 400ppm.

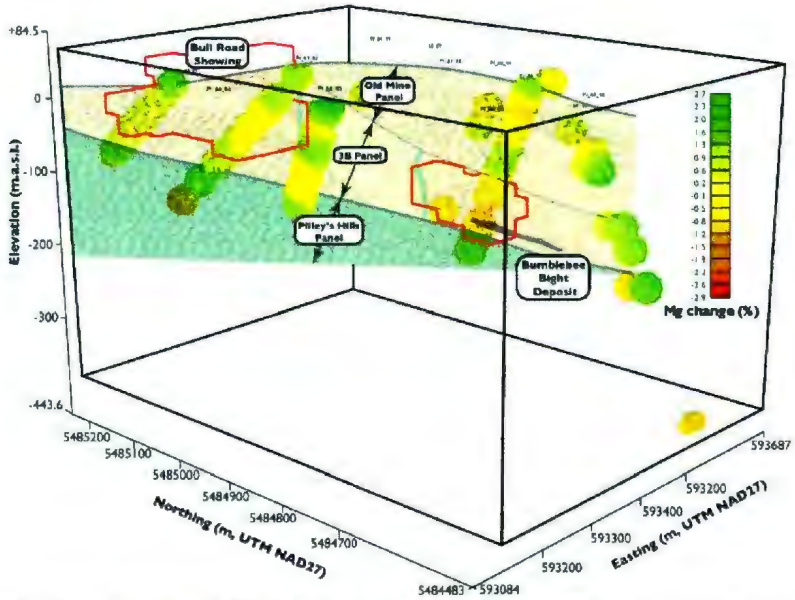

Figure A4-3 3D gridding of kriged MgO mass change data from drill core samples throughout and surrounding the Bull Road showing and the Bumble Bee Bight deposit on Pilley's Island. Red wireframes represent raw, kriged Cu values greater than 400ppm.

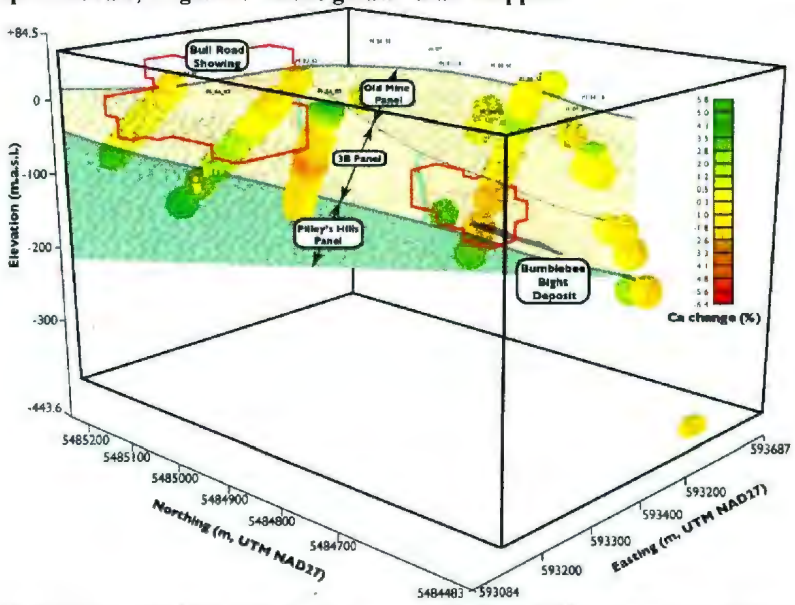

Figure A4-4 3D gridding of kriged CaO mass change data from drill core samples throughout and surrounding the Bull Road showing and the Bumble Bee Bight deposit on Pilley's Island. Red wireframes represent raw, kriged Cu values greater than 400ppm.

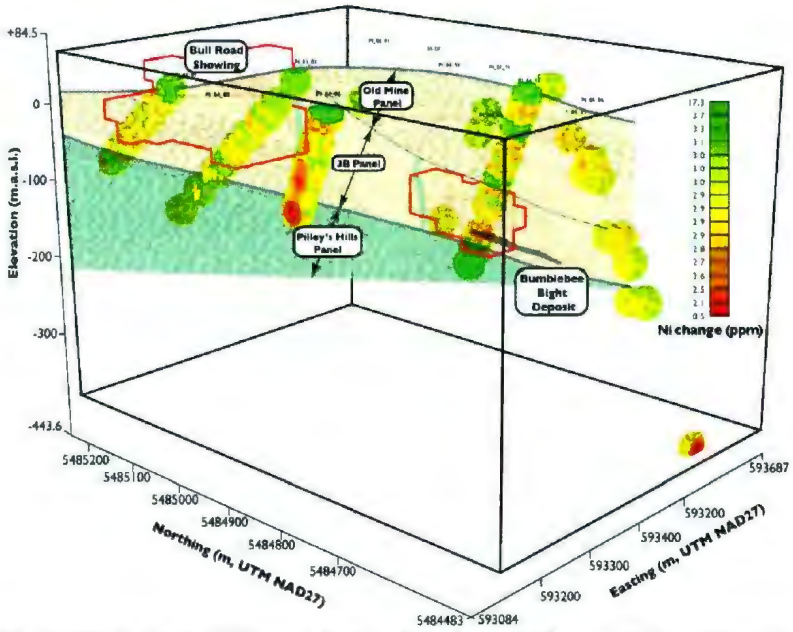

Figure A4-5 3D gridding of kriged Ni mass change data from drill core samples throughout and surrounding the Bull Road showing and the Bumble Bee Bight deposit on Pilley's Island. Red wireframes represent raw, kriged Cu values greater than 400ppm.

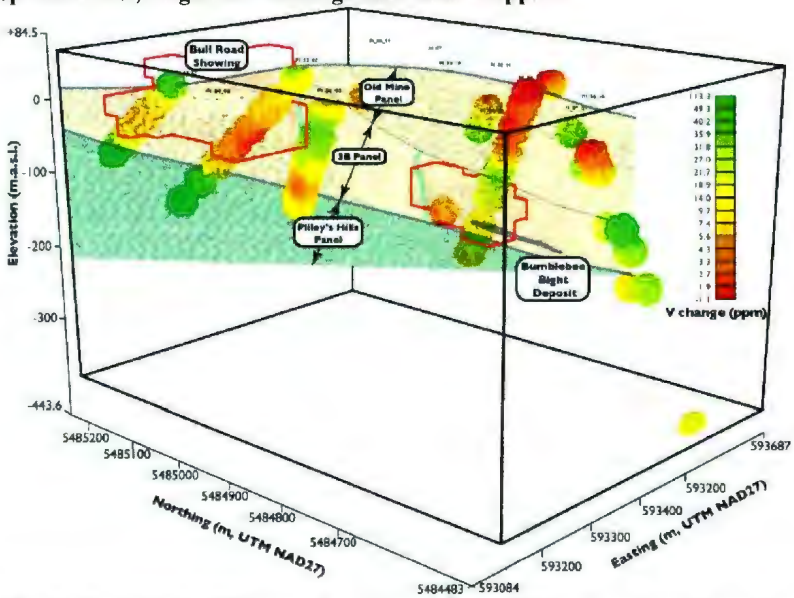

Figure A4-6 3D gridding of kriged V mass change data from drill core samples throughout and surrounding the Bull Road showing and the Bumble Bee Bight deposit on Pilley's Island. Red wireframes represent raw, kriged Cu values greater than 400ppm.

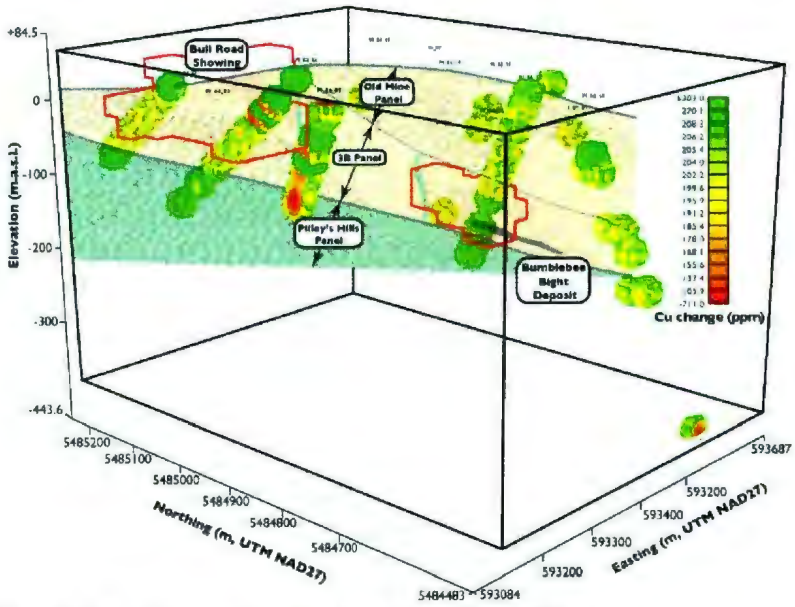

Figure A4-7 3D gridding of kriged Cu mass change data from drill core samples throughout and surrounding the Bull Road showing and the Bumble Bee Bight deposit on Pilley's Island. Red wireframes represent raw, kriged Cu values greater than 400ppm.

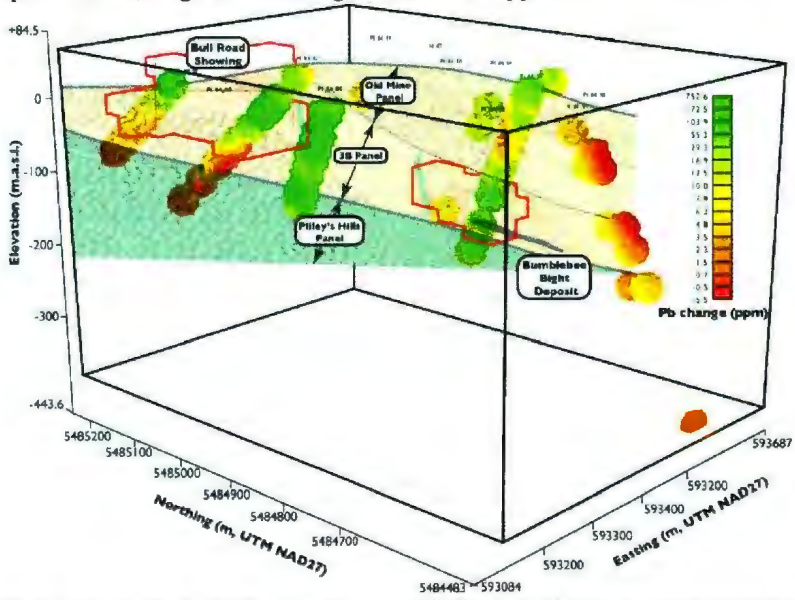

Figure A4-8 3D gridding of kriged Pb mass change data from drill core samples throughout and surrounding the Bull Road showing and the Bumble Bee Bight deposit on Pilley's Island. Red wireframes represent raw, kriged Cu values greater than 400ppm.

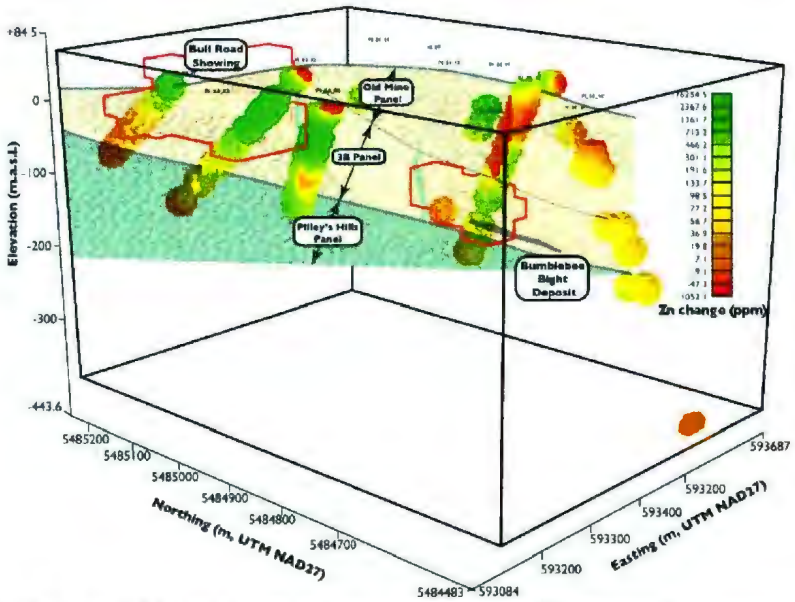

Figure A4 9 3D gridding of kriged Zn mass change data from drill core samples throughout and surrounding the Bull Road showing and the Bumble Bee Bight deposit on Pilley's Island. Red wireframes represent raw, kriged Cu values greater than 400ppm.

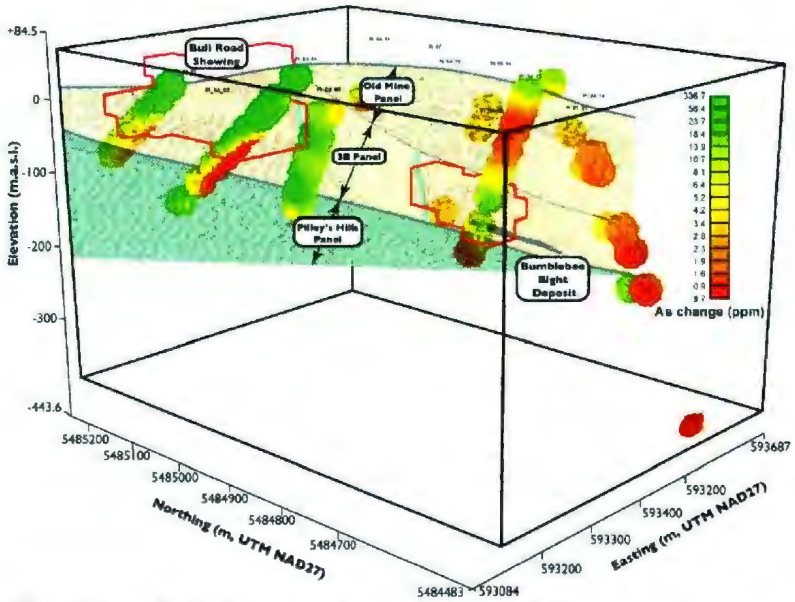

Figure A4-10 3D gridding of kriged As mass change data from drill core samples throughout and surrounding the Bull Road showing and the Bumble Bee Bight deposit on Pilley's Island. Red wireframes represent raw, kriged Cu values greater than 400ppm.

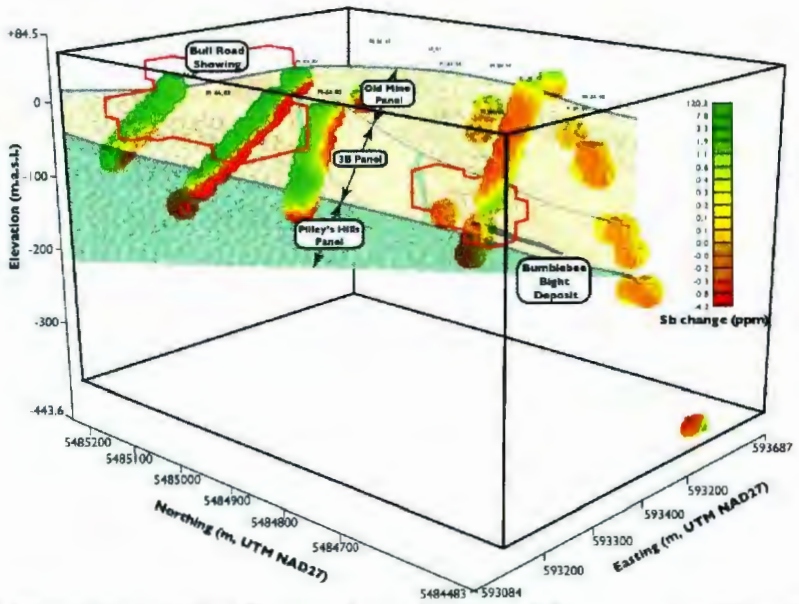

Figure A4-11 3D gridding of kriged Sb mass change data from drill core samples throughout and surrounding the Bull Road showing and the Bumble Bee Bight deposit on Pilley's Island. Red wireframes represent raw, kriged Cu values greater than 400ppm.

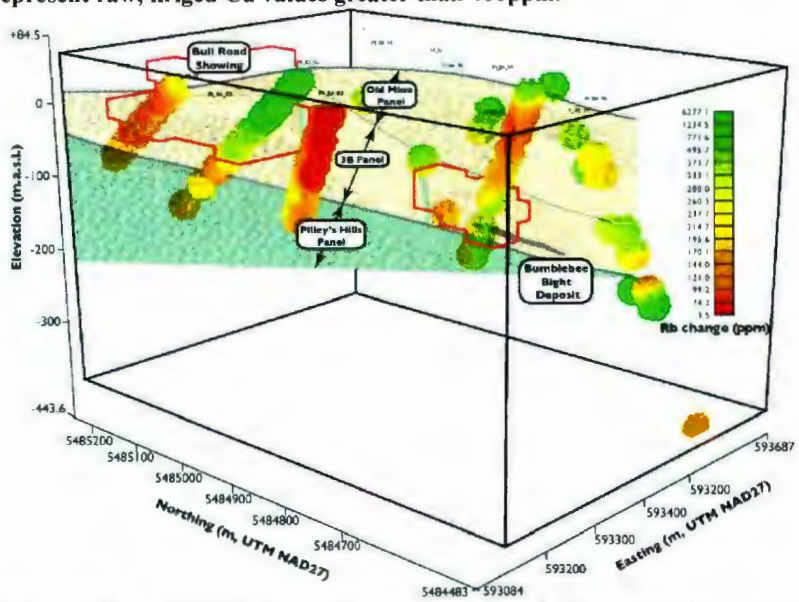

Figure A4-12 3D gridding of kriged Rb mass change data from drill core samples throughout and surrounding the Bull Road showing and the Bumble Bee Bight deposit on Pilley's Island. Red wireframes represent raw, kriged Cu values greater than 400ppm.

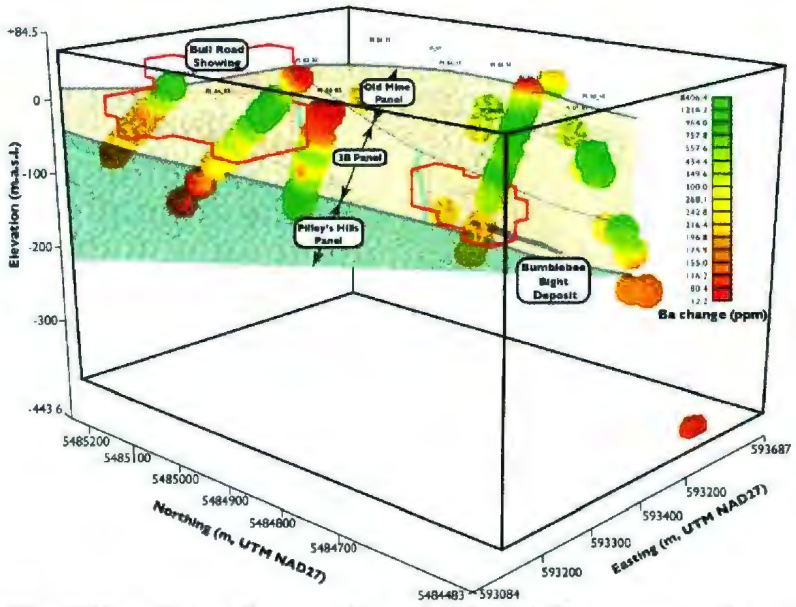

Figure A4-13 3D gridding of kriged Ba mass change data from drill core samples throughout and surrounding the Bull Road showing and the Bumble Bee Bight deposit on Pilley's Island. Red wireframes represent raw, kriged Cu values greater than 400ppm.

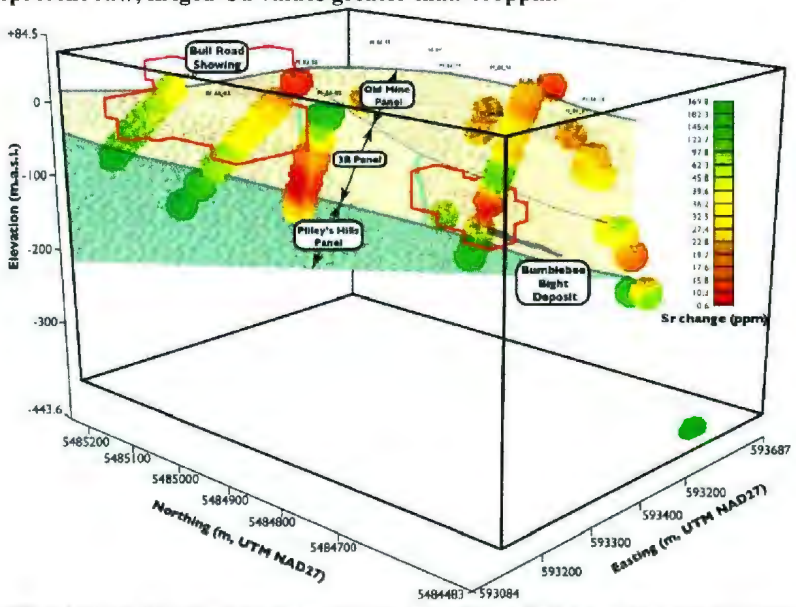

Figure A4-14 3D gridding of kriged Sr mass change data from drill core samples throughout and surrounding the Bull Road showing and the Bumble Bee Bight deposit on Pilley's Island. Red wireframes represent raw, kriged Cu values greater than 400ppm.

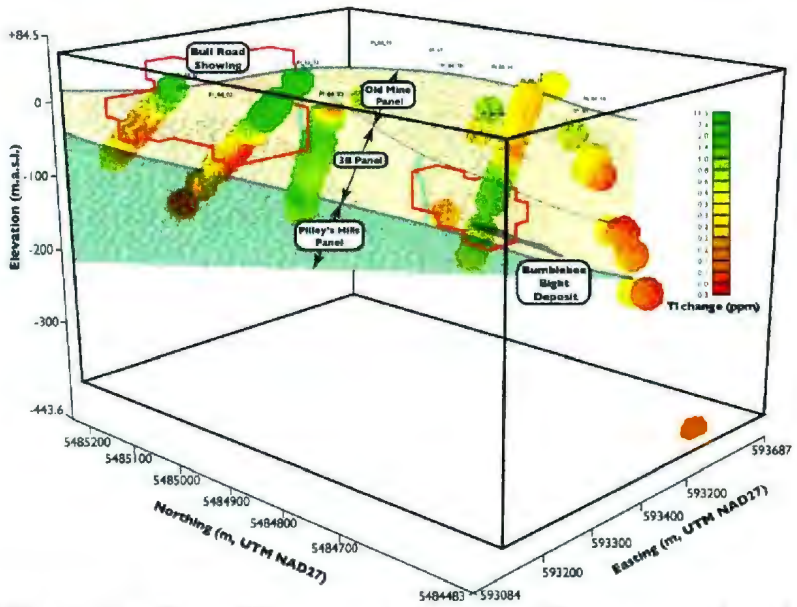

Figure A4-15 3D gridding of kriged Tl mass change data from drill core samples throughout and surrounding the Bull Road showing and the Bumble Bee Bight deposit on Pilley's Island. Red wireframes represent raw, kriged Cu values greater than 400ppm.

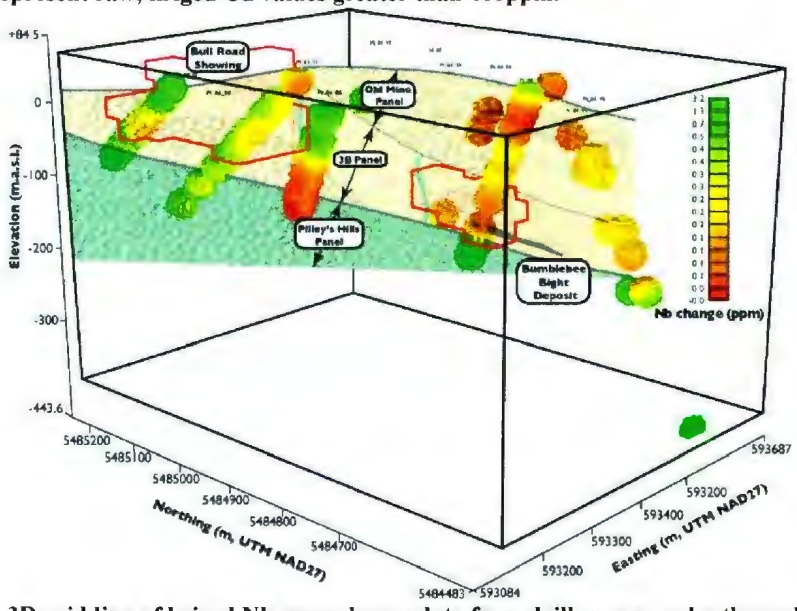

Figure A4-16 3D gridding of kriged Nb mass change data from drill core samples throughout and surrounding the Bull Road showing and the Bumble Bee Bight deposit on Pilley's Island. Red wireframes represent raw, kriged Cu values greater than 400ppm.

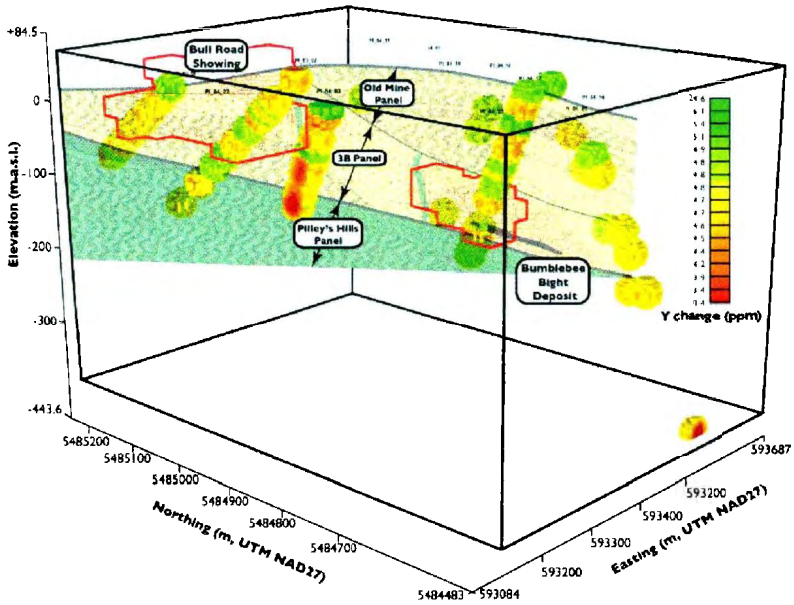

Figure A4-17 3D gridding of kriged Y mass change data from drill core samples throughout and surrounding the Bull Road showing and the Bumble Bee Bight deposit on Pilley's Island. Red wireframes represent raw, kriged Cu values greater than 400ppm.